DET KGL. DANSKE VIDENSKABERNES SELSKAB
MATEMATISK-FYSISKE MEDDELELSER, BIND XXV, NR. 1

A COMPOSITE GIANT STAR MODEL WITH ISOTHERMAL CORE

BY

ANDERS REIZ

KØBENHAVN
I KOMMISSION HOS EJNAR MUNKSGAARD
1948

Printed in Denmark.
Bianco Lunos Bogtrykkeri.

1. During the last few years a number of papers [1] have appeared dealing with the problems of energy production and evolution of main-sequence and giant stars, which start from discussions of composite stellar models consisting of isothermal cores and point-source envelopes.

GAMOW [2] in particular has considered the evolution of a star with energy production in a convective core according to the carbon cycle mechanism, and suggested that such a star, as a consequence of exhaustion of the hydrogen in the convective core, would evolve into a giant star, of very large radius for its mass, and built on a model in which the energy is produced by the carbon cycle in a sufficiently hot shell surrounding the inert core.

Although the investigations quoted above [1] would appear to throw some doubts on GAMOW's suggestion, it nevertheless seemed worth while to examine whether a model for the giant stars, characterized by a core devoid of hydrogen, might lead to sufficiently high temperatures and densities in the region immediately surrounding the core to explain the energy production in the giant stars according to the carbon cycle.

The aim of the present paper is to investigate, by numerical methods, the possibilities of a model with non-productive core to explain the energy production of giant stars. The investigation was restricted to a single giant star (*Capella A*) of specified mass, radius, and luminosity.

The problem has been simplified through the assumption that the entire energy production takes place in an infinitely narrow shell surrounding the core. This means that the total outward net-flux of energy $L(r)$ is assumed to be constant, and equal to the luminosity L, right up to the core, and zero inside the core.

The temperature of the shell in which the energy production takes place is assumed to be 20 million degrees. The choice of the value of the temperature is governed by the following considerations. The simplified model should approximate as closely as possible a model which has these properties: 1. The change of $L(r)$ with distance r from the centre throughout the envelope is given by the energy production according to the carbon cycle mechanism. 2. The particular distance r from the centre at which $L(r)$ becomes zero, coincides with the radius of the non-productive core.

It may be remarked here already that the results of the present investigations tend to show that the energy production takes place in a very narrow zone, and indicate that a repetition of the investigations with a considerably higher value of the representative temperature would be desirable[1].

2. As already mentioned the model considered is specified by given values of the mass, M, the radius R, and the luminosity L. The hydrogen content X is considered as a variable parameter. We assume that the helium content of the envelope is negligible, and that the non-hydrogen part contains the heavier elements in the relative proportions of the RUSSELL-mixture. The mean molecular weight of the envelope can then be calculated from X. With regard to the core we assume that each gram consists of X gram helium, and $1-X$ gram of the RUSSELL-mixture (no hydrogen). The mean molecular weight of the core can then also be calculated as a function of X.

We thus assume that the model is composed by an envelope with constant $L(r)$ surrounding an isothermal core, the mean molecular weights being μ_1 and μ_2, respectively. The transition from envelope to core is assumed to take place when the temperature, going inward, reaches 20 million degrees. The following question is now formulated: given mass, radius, and luminosity

[1] Note added in proof: After this paper was sent to the press calculations (to appear in Arkiv för Astronomi, Band 1:1, 1948) have been performed with a temperature of 33 million degrees as representative for the carbon cycle. The energy-output computed by means of BETHE's law from the new temperatures and densities is for $X = 0.34$, $L = 4.0 \cdot 10^{35}$ erg/sec closely agreeing with $L_{obs} = 4.5 \cdot 10^{35}$ The central conditon $M(r) = 0$ for $r = 0$ for the composite configuration is satisfied for the above hydrogen content. The representative temperature almost coincides with the theoretical value 32 million degrees derived by BETHE for Capella A (Phys. Rev., **55**, 434, 1939).

of the star, does there exist a certain value of the hydrogen content X, which is varied as a parameter, for which such a composite model can be constructed, satisfying the condition $M(r) = 0$ for $r = 0$? In fact, from our investigations it will appear that for X situated between 0.31 and 0.32, there does exist such a configuration, built up by an envelope with zones in radiative and convective equilibrium surrounding an isothermal core.

The differential equations which form the starting point are the classical ones given by EDDINGTON (cf. [5])

$$\left.\begin{aligned} \frac{dP}{dr} &= -\frac{GM(r)}{r^2}\varrho \\ P &= p_g + p_r = \frac{k}{\mu H}\varrho T + \frac{1}{3}aT^4 \\ \frac{dp_r}{dr} &= -\frac{\varkappa L(r)}{4\pi c r^2}\varrho \\ \frac{dM(r)}{dr} &= 4\pi r^2 \varrho \\ \frac{dL(r)}{dr} &= 4\pi r^2 \varrho \varepsilon(r), \end{aligned}\right\} \quad (1)$$

where the symbols used mean: r distance from the centre, P total pressure, composed by p_g, gas-pressure, and p_r, radiation-pressure, T temperature, ϱ density, $M(r)$ mass inside sphere of radius r, $L(r)$ net-flux through sphere of radius r, $\varkappa$ coefficient of opacity, μ molecular weight, G constant of gravitation, a STEFAN's constant, k BOLTZMANN's constant, H mass of the proton, c velocity of light.

Starting from the boundary values of the variables $T = T_0$, $\varrho \simeq 0$, $M(R) = M$, $L(R) = L$, the differential equations can be integrated inwards, thus giving temperature, density, and mass at any point in the configuration. As to the function $\varepsilon(r)$ expressing the energy generation per unit mass at the distance r from the centre we can make use of the formula derived by BETHE [3]; in the following calculations, however, as has already been mentioned, we make use of the approximation $L(r) = \textit{constant} = L$ in the envelope. In order to simplify the integrations the following

variables are conveniently introduced [4]

$$\left.\begin{aligned} x &= 1/r, \quad x_0 = 1/R, \quad t = 12 + \log (x - x_0) \\ y &= \log T, \quad z = \log \varrho, \quad u = M(r)/M. \end{aligned}\right\} \quad (2)$$

Substituting at the same time the expression, cf. [5],

$$\varkappa = \varkappa_0 \frac{1}{\tau} \frac{\varrho}{T^{3.5}},$$

where $$\varkappa_0 = 3.89 \cdot 10^{25} (1 - X^2).$$

X being the hydrogen abundance, the helium content being zero, the equations (1) are transformed as follows [4]:

$$\left.\begin{aligned} \frac{dy}{dt} &= \gamma \frac{x - x_0}{T} \frac{\varrho^2}{T^{6.5}} \frac{1}{\tau} \\ \frac{dz}{dt} &= \alpha \frac{x - x_0}{T} u - \frac{dy}{dt} \left\{ 1 + \delta \frac{T^3}{\varrho} \right\} \\ \frac{du}{dt} &= -\zeta \frac{x - x_0}{x^4} \varrho, \end{aligned}\right\} \quad (3)$$

which govern the variations in the variables y, z, and u in the case of radiative equilibrium. The constants α, δ, γ, and ζ are to be found in [4].[1] As to the guillotine factor τ the values given by B. Strömgren [6] have been used.

3. The integrations of the equations (3) were started using an analytical development [7] from the surface to a certain point well below the surface; from this the integrations were carried out inwards by means of standard methods until a temperature of 20 million degrees was reached. The observational data for *Capella A* on which the calculations are based are due to Kuiper [8]

$$L = 120\, L_\odot, \quad M = 4.18\, M_\odot, \quad R = 15.8\, R_\odot$$

[1] In the expression for ζ given there the factor M has dropped out in the denominator; further the constant here denoted by δ is there called β.

Table 1

	$X = 0.28$			$X = 0.30$		
t	$y = \log T$	$z = \log \varrho$	$u = \frac{M(r)}{M}$	$y = \log T$	$z = \log \varrho$	$u = \frac{M(r)}{M}$
0.0—1	5.191	4.150—10	1.000	5.179	4.107—10	1.000
.1	.290	.473	1.000	.278	.430	1.000
.2	.390	.798	1.000	.378	.754	1.000
.3	.490	5.124	1.000	.478	5.080	1.000
.4	.591	.451	0.999	.578	.407	0.999
.5	.691	.779	.996	.679	.734	.997
.6	.792	6.106	.992	.779	6.061	.993
.7	.892	.431	.984	.880	.387	.985
.8	5.990	.755	.967	5.978	.711	.970
.9—1	6.087	7.076	.937	6.074	7.032	.943
0.0	.182	.384	.886	.171	.343	.897
.1	.274	.673	.808	.263	.637	.826
.2	.362	.932	.701	.352	.902	.726
.3	.443	8.153	.570	.435	8.132	.601
.4	.514	.329	.430	.509	.320	.467
.5	.575	.461	.303	.572	.466	.340
.6	.625	.555	.201	.625	.575	.236
.7	.666	.618	.128	.670	.653	.158
.8	.700	.657	.081	.706	.707	.106
.9	.728	.682	.053	.738	.747	.074
1.0	.752	.697	.036	.764	.779	.053
.1	.772	.709	.027	.787	.807	.042
.2	.790	.720	.022	.808	.834	.036
.3	.808	.732	.019	.828	.866	.032
.4	.824	.749	.017	.848	.904	.030
.5	.840	.771	.016	.868	.951	.028
.6	.856	.800	.016	.890	9.009	.028
.7	.873	.838	.016	.912	.079	.027
.8	.892	.888	.016	.938	.164	.027
.9	.912	.950	.016	6.967	.266	.027
2.0	.935	9.026	.016	7.001	.387	.027
.1	.961	.118	.015	.040	.526	.
.2	6.992	.228	.	.085	.685	.
.3	7.028	.357	.	.137	9.863—10	.
.4	.070	.507	.	.195	0.061	.
.5	.118	.676	.	.259	.276	.
.6	.173	9.866—10	.	.329	.510	.
.7	.235	0.074	.	.401	.765	.
.8	.303	.300	.015	.475	1.044	.027

(to be continued)

Table 1 (continued).

	$X = 0.32$			$X = 0.34$		
t	$y = \log T$	$z = \log \varrho$	$u = \frac{M(r)}{M}$	$y = \log T$	$z = \log \varrho$	$u = \frac{M(r)}{M}$
0.0—1	5.168	4.065—10	1.000			
.1	.266	.388	1.000	5.255	4.348—10	1.000
.2	.366	.712	1.000	.354	.672	1.000
.3	.466	5.038	1.000	.454	.998	1.000
.4	.566	.364	0.999	.555	5.324	0.999
.5	.667	.691	.997	.655	.651	.997
.6	.767	6.018	.994	.756	.977	.994
.7	.868	.344	.986	.856	6.303	.988
.8	5.966	.668	.973	5.955	.628	.975
.9—1	6.063	.992	.948	6.052	.950	.952
0.0	.159	7.305	.906	.148	7.265	.914
.1	.253	.601	.840	.242	.565	.854
.2	.343	.873	.748	.333	.843	.768
.3	.427	8.111	.630	.418	8.089	.658
.4	.503	.309	.501	.497	.297	.533
.5	.569	.468	.376	.565	.467	.410
.6	.625	.590	.269	.624	.602	.302
.7	.672	.682	.188	.674	.706	.217
.8	.712	.750	.131	.717	.788	.156
.9	.746	.804	.095	.753	.854	.116
1.0	.775	.850	.072	.784	.913	.090
.1	.801	.893	.058	.812	.970	.074
.2	.825	.938	.050	.839	9.028	.065
.3	.848	.987	.046	.865	.093	.059
.4	.871	9.045	.043	.891	.166	.056
.5	.895	.114	.041	.919	.252	.053
.6	.921	.195	.040	.949	.351	.052
.7	.950	.292	.040	6.983	.466	.051
.8	6.982	.405	.039	7.021	.598	.050
.9	7.020	.537	.039	.064	.748	.050
2.0	.063	.687	.039	.113	9.918—1	.050
.1	.112	9.858—10	.039	.169	0.106	.049
.2	.167	0.047	.039	.230	.312	.
.3	.229	.254	.038	.298	.534	.
.4	.296	.478	.	.368	.776	.
.5	.368	.722	.	.440	1.039	.049
.6	.440	.987	.038			

(to be continued)

Table 1 (continued).

	$X = 0.38$			$X = 0.40$		
t	$y = \log T$	$z = \log \varrho$	$u = \frac{M(r)}{M}$	$y = \log T$	$z = \log \varrho$	$u = \frac{M(r)}{M}$
0.1—1	5.233	4.272—10	1.000	5.223	4.237—10	1.000
.2	.332	.596	1.000	.322	.560	1.000
.3	.432	.921	1.000	.422	.885	1.000
.4	.532	5.246	0.999	.522	5.210	0.999
.5	.632	.573	.998	.622	.537	.998
.6	.733	.900	.995	.722	.864	.996
.7	.833	6.225	.990	.822	6.190	.991
.8	5.932	.550	.979	5.922	.514	.981
.9—1	6.030	.874	.960	6.020	.839	.965
0.0	.126	7.192	.928	.116	7.158	.935
.1	.221	.497	.877	.212	.466	.888
.2	.314	.784	.803	.304	.756	.818
.3	.402	8.043	.706	.394	8.020	.726
.4	.484	.268	.591	.477	.253	.616
.5	.557	.459	.473	.552	.452	.502
.6	.621	.616	.364	.618	.619	.394
.7	.676	.744	.275	.676	.757	.302
.8	.724	.849	.207	.726	.873	.231
.9	.765	.940	.159	.769	.974	.180
1.0	.801	9.022	.127	.807	9.067	.145
.1	.833	.102	.106	.842	.156	.121
.2	.864	.184	.093	.874	.247	.106
.3	.895	.271	.084	.907	.342	.096
.4	.926	.367	.079	.941	.447	.089
.5	.960	.475	.075	6.977	.562	.085
.6	6.997	.596	.073	7.016	.691	.082
.7	7.037	.733	.071	.059	.834	.079
.8	.083	9.887—10	.070	.107	9.994—10	.078
.9	.133	0.058	.069	.159	0.170	.077
2.0	.190	.246	.068	.218	.363	.076
.1	.252	.451	.068	.281	.571	.075
.2	.319	.672	.067	.348	.796	.075
.3	.388	.912	.067			
.4	.458	1.174	.066			

(to be continued)

Table 1 (continued).

	$X = 0.42$			$X = 0.50$		
t	$y = \log T$	$z = \log \varrho$	$u = \frac{M(r)}{M}$	$y = \log T$	$z = \log \varrho$	$u = \frac{M(r)}{M}$
0.1—1	5.213	4.203—10	1.000	5.175	4.080—10	1.000
.2	.312	.526	1.000	.273	.402	1.000
.3	.411	.850	1.000	.372	.725	1.000
.4	.511	5.176	0.999	.472	5.049	0.999
.5	.611	.502	.998	.572	.374	.998
.6	.712	.828	.996	.672	.700	.997
.7	.812	6.154	.991	.772	6.026	.994
.8	5.911	.479	.982	.872	.350	.987
.9—1	6.009	.802	.966	5.971	.674	.975
0.0	.106	7.122	.939	6.067	.997	.955
.1	.201	.433	.895	.164	7.312	.922
.2	.295	.726	.831	.258	.617	.872
.3	.385	.996	.744	.352	.902	.804
.4	.469	8.235	.640	.440	8.163	.718
.5	.546	.442	.529	.524	.396	.620
.6	.615	.618	.422	.599	.603	.521
.7	.675	.767	.330	.667	.784	.429
.8	.727	.894	.257	.727	.945	.350
.9	.773	9.005	.203	.780	9.091	.286
1.0	.812	.109	.164	.827	.230	.238
.1	.849	.209	.138	.871	.362	.202
.2	.884	.309	.121	.913	.493	.176
.3	.919	.414	.109	.955	.626	.158
.4	.956	.528	.101	6.999	.763	.144
.5	6.994	.651	.096	7.044	9.908—10	.135
.6	7.036	.788	.092	.092	0.063	.128
.7	.081	9.939—10	.090	.143	.229	.123
.8	.132	0.106	.088	.200	.407	.119
.9	.187	.288	.086	.259	.599	.116
2.0	.247	.486	.085	.323	.803	.114
.1	.312	.700	.084			

(to be continued)

Table 1 (continued).

	$X = 0.70$			$X = 0.80$		
t	$y = \log T$	$z = \log \varrho$	$u = \frac{M(r)}{M}$	$y = \log T$	$z = \log \varrho$	$u = \frac{M(r)}{M}$
0.2—1	5.193	4.183—10	1.000	5.160	4.134—10	1.000
.3	.292	.503	1.000	.258	.452	1.000
.4	.390	.825	1.000	.357	.773	1.000
.5	.490	5.148	0.999	.456	5.095	0.999
.6	.589	.472	.998	.555	.418	.998
.7	.689	.796	.996	.654	.741	.997
.8	.789	6.121	.992	.754	6.065	.993
.9—1	.888	.444	.985	.853	.387	.987
0.0	5.986	.767	.973	5.952	.709	.977
.1	6.083	7.088	.954	6.048	7.031	.960
.2	.179	.404	.924	.144	.347	.933
.3	.274	.709	.881	.239	.655	.895
.4	.367	.998	.824	.333	.950	.845
.5	.458	8.268	.755	.425	8.227	.782
.6	.544	.517	.677	.513	.485	.711
.7	.624	.747	.597	.596	.725	.636
.8	.698	.959	.520	.673	.948	.562
.9	.764	9.159	.451	.743	9.158	.494
1.0	.824	.351	.391	.806	.361	.433
.1	.879	.537	.340	.865	.559	.381
.2	.933	.718	.299	.921	.752	.337
.3	6.987	9.894—10	.267	6.978	9.941—10	.301
.4	7.042	0.070	.241	7.035	0.128	.272
.5	.098	.246	.221	.094	.314	.250
.6	.156	.426	.206	.154	.502	.232
.7	.215	.611	.194	.215	.694	.217
.8	.277	.803	.184	.279	.890	.206
.9	.340	1.004	.177	.343	1.095	.196

The hydrogen abundance has been varied as follows: $X = 0.25$, 0.28, 0.30, 0.32, 0.34, 0.38, 0.40, 0.42, 0.50, 0.70, 0.80. The solutions are listed in Table 1 except for $X = 0.25$, in which case the mass was used up before arriving at the above temperature. The computations were carried out with one more figure than given in the tables. The quantities listed are supposed to be correct to the last figure.

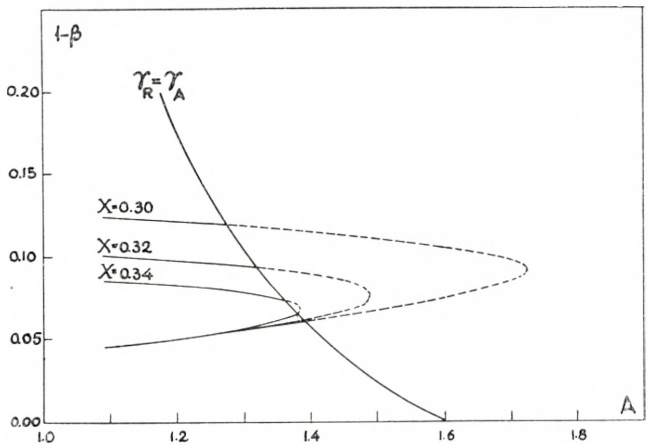

Fig. 1

4. The above-mentioned integrations have been performed on the tacit assumption that radiative equilibrium is stable. This is the case if the radiative gradient γ_R is less than the corresponding adiabatic gradient γ_A. The gradients can be written as follows [9]

$$\gamma_R = \frac{\beta}{1 - \left(1 - \frac{3}{4}\beta\right) A} \tag{4}$$

$$\gamma_A = \beta + \frac{2}{3}\frac{(4 - 3\beta)^2}{(8 - 7\beta)}, \tag{5}$$

where

$$A = \frac{\varkappa}{4\pi c G} \frac{L(r)}{M(r)} \cdot \frac{1}{(1 - \beta)} \tag{6}$$

and

$$p_g = \beta P. \tag{7}$$

An instructive picture of the conditions is obtained by plotting the quantity A against the corresponding value $(1-\beta)$ [10]. In the same diagram has been drawn the curve for which $\gamma_A = \gamma_R$, that is the limiting curve of the domain of convection. It appears that in the actual case convection is possible only for $X < 0.34$, and that the convection zones are increasing through the star for decreasing hydrogen content. It is thus concluded that it is necessary to revise the calculations, taking into account the modifications due to the convective equilibrium. In the convection zone the following differential equations are valid [9]:

$$\left.\begin{aligned} \frac{1}{P}\frac{dP}{dr} &= \gamma_A \frac{1}{\varrho}\frac{d\varrho}{dr} \\ \frac{dP}{dr} &= -\frac{GM(r)}{r^2}\varrho \\ \frac{dM(r)}{dr} &= 4\pi r^2 \varrho. \end{aligned}\right\} \tag{8}$$

Transforming these by means of the variables (2) we are left with

$$\left.\begin{aligned} \frac{dy}{dt} &= \frac{2(4-3\beta)}{3(8-7\beta)}\frac{dz}{dt} \\ \frac{dz}{dt} &= \frac{GMH}{k}\mu\frac{(x-x_0)}{T}\frac{u\beta}{\gamma_A}. \end{aligned}\right\} \tag{9}$$

The third equation remains unchanged. The integrations are thus performed by means of these equations as long as the condition $\gamma_R > \gamma_A$ is fulfilled. From the point where the convection zone is changed back into the radiative zone the corresponding differential equations are to be used until a temperature of 20 million degrees has been reached.

5. At this interface has been fitted an isothermal core devoid of hydrogen. The fitting conditions imply continuity in pressure, temperature, and mass; the density, however, has a discontinuity at the interface. The ratio of the densities on both sides of the interface is equal to the ratio of the respective molecular weights. The differential equations of the isothermal core are immediately

derived from (3) by putting $\frac{dy}{dt}$ equal to zero and changing the molecular weight μ_1 entering in the constant α to μ_2.

The integrations are now continued until the stage of non-relativistic degeneracy defined through the equality in pressure at the interface

$$\frac{k}{\mu_2 H} \varrho T = \frac{K_1}{\mu_3^{5/3}} \varrho^{5/3} \tag{10}$$

or

$$\varrho = \left(\frac{kT}{HK_1} \frac{\mu_3^{5/3}}{\mu_2} \right)^{3/2} \tag{11}$$

is reached [9, ciph. 56c]. μ_3 denotes the mean molecular weight of the degenerate core, the constant K_1 is equal to $9.91 \cdot 10^{12}$. The mean molecular weights μ_1, μ_2, and μ_3 are derived from the formulae

$$\left.\begin{aligned} \mu_1^{-1} &= 2X + n_R(1 - X) \\ \mu_2^{-1} &= \frac{3}{4}X + n_R(1 - X) \\ \mu_3^{-1} &= \frac{1}{2}X + n_R(1 - X), \end{aligned}\right\} \tag{12}$$

where the quantity n_R has been put equal to 0.54, or the value given for a completely ionized RUSSELL-mixture [11].

In the case of non-relativistic degeneracy the equation of state is given by the right member of (10), which means that the configuration is a LANE-EMDEN polytrope of index $n = 3/2$. It appears from the integrations that the density in the relevant parts of our models stays below the limit where relativistic degeneracy sets in. Before performing the actual integrations it is advisable to investigate if a fitting of a polytrope of that type is really possible. The fitting problem can be solved in a convenient way by a method due to RUSSELL [12], cf. also [5]. Defining the variables[1]

$$A = \frac{4\pi\varrho r^3}{3M(r)}, \quad B = 4\pi G \frac{\varrho^2 r^2}{P}, \tag{13}$$

[1] This variable A must not, of course, be confused with the variable A defined by means of (6).

RUSSELL in a diagram with the ordinate A and the abscissa B plots the function $A(B)$ corresponding to the E-solutions of different polytropes. In order to determine the type of solution in a certain point of a model we have only to calculate the polytropic index n and the quantities A and B. The solution will be an E-solution, an M-solution, or an F-solution according as the point (A, B) lies upon, inside, or outside the E-curve for the given polytropic index. The quantities A, B for $n = 3/2$ calculated for the hydrogen contents 0.30, 0.31, 0.32 are listed in Table 2.

Table 2.

X	A	B
0.30	0.13	4.72
0.31	0.23	7.79
0.32	0.34	11.33

It is remarked in passing that the integrations for $X = 0.31$ are based upon interpolated y, z, and u values; by means of these the numerical integrations are started at the point where the convection zone begins. The points (A, B) are plotted in the diagram (Figure 2), from which is clearly demonstrated that an E-solution does exist for an X-value between 0.31 and 0.32.

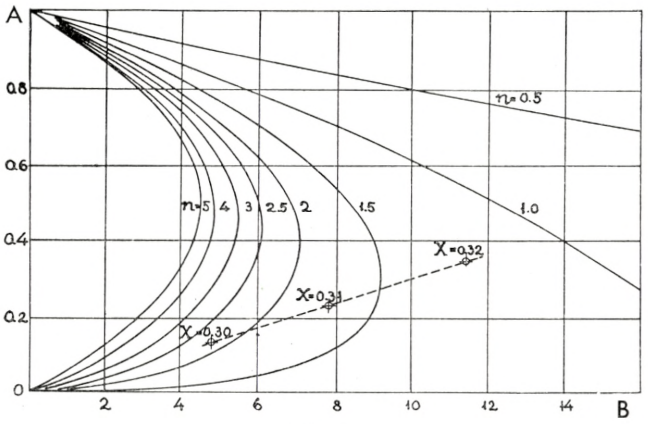

Fig. 2.

The differential equations governing the variation in z in the degenerate zone can be written as follows

Table 3.

$X = 0.30$

Zone of convective equilibrium.

t	$\log T$	$\log \varrho$	$u = \frac{M(r)}{M}$
0.70	6.668	8.654—10	0.1586
.80	.702	.715	.1063
.90	.728	.763	.0726
1.00	.749	.803	.0522
.10	.768	.839	.0400
.20	.786	.873	.0331
.30	.804	.908	.0292
.40	.824	.946	.0271
.50	.846	8.990	.0258
.60	.871	9.039	.0250
.70	.899	.096	.0246

Second zone of radiative equilibrium.

1.80	6.931	9.162—10	0.0243
.90	.962	.248	.0242
2.00	6.995	.352	.0241
.10	7.032	.475	.0240
.20	.073	.619	.0240
.30	.120	.782	.0239
.40	.174	9.966—10	.0239
.50	.234	0.168	.0239
.60	.301	.388	.0239

Isothermal zone.

t	$\log \varrho$	$u = \frac{M(r)}{M}$
2.60	0.598	0.0239
.64	.820	.0239

$X = 0.31$

Zone of convective equilibrium.

t	$\log T$	$\log \varrho$	$u = \frac{M(r)}{M}$
0.70	6.671	8.668—10	0.1731
.80	.707	.734	.1190
.90	.735	.787	.0838
1.00	.759	.832	.0620
.10	.781	.873	.0490
.20	.802	.914	.0414
.30	.824	8.956	.0370
.40	.847	9.001	.0345
.50	.874	.052	.0330

Second zone of radiative equilibrium.

1.60	6.901	9.112—10	0.0321
.70	.929	.188	.0316
.80	.959	.280	.0313
.90	6.992	.390	.0311
2.00	7.029	.518	.0310
.10	.071	9.667	.0309
.20	.120	9.834—10	.0308
.30	.174	0.022	.0308
.40	.236	.227	.0307
.50	.303	.450	.0307

Isothermal zone.

t	$\log \varrho$	$u = \frac{M(r)}{M}$
2.50	0.674	0.0307
.54	0.899	.0307

$X = 0.32$

Zone of convective equilibrium.

t	$\log T$	$\log \varrho$	$u = \frac{M(r)}{M}$
0.70	6.672	8.682—10	0.1879
.80	.711	.752	.1313
.90	.742	.810	.0946
1.00	.769	.860	.0716
.10	.793	.906	.0577
.20	.817	.951	.0494
.30	.842	8.999	.0445

Second zone of radiative equilibrium.

1.40	6.868	9.052—10	0.0417
.50	.893	.116	.0401
.60	.920	.193	.0390
.70	.949	.286	.0384
.80	6.981	.395	.0380
.90	7.018	.522	.0378
2.00	.059	.668	.0376
.10	.107	9.834—10	.0374
.20	.161	0.020	.0374
.30	.222	.223	.0373
.40	.288	.444	.0372
.50	.359	.683	.0372

Isothermal zone.

t	$\log \varrho$	$u = \frac{M(r)}{M}$
2.42	0.715	0.0372
.46	0.941	.0372

.76	1.621	.0238
.80	1.940	.0238
.84	2.289	.0237
.88	2.671	.0236
.92	3.087	.0234
.96	3.537	.0229
3.00	4.016	.0220

Degeneracy at $t = 2.974$.

3.00	3.866	0.0221
.04	4.064	.0210
.08	.221	.0197
.12	.350	.0183
.16	.459	.0170
.20	.554	.0157
.24	.638	.0145
.28	.713	.0134
.32	.782	.0124
.36	.844	.0115
.40	.903	.0108
.44	4.958	.0101
.48	5.010	.0096
.52	.061	.0091
.56	.110	.0087
3.60	.157	.0083
3.70	5.273	.0077
.80	.387	.0073
.90	.502	.0070
4.00	.619	.0068
.10	.740	.0067
.20	.864	.0066
.30	5.991	.0066
.40	6.122	.0065

.66	1.713	.0305
.70	2.037	.0304
.74	2.390	.0303
.78	2.775	.0300
.82	3.192	.0294
.86	3.637	.0283
.90	4.096	.0259

Degeneracy at $t = 2.865$.

2.88	3.793	0.0274
.92	3.998	.0252
.96	4.154	.0227
3.00	.277	.0201
.04	.376	.0175
.08	.459	.0151
.12	.528	.0129
.16	.586	.0110
.20	.637	.0094
.24	.680	.0080
.28	.719	.0068
.32	.753	.0058
.36	.784	.0051
.40	.812	.0044
.44	.838	.0039
.48	.862	.0035
.52	.885	.0032
.56	.908	.0029
.60	.930	.0027
3.70	4.984	0.0024
.80	5.040	.0022
.90	.100	.0020
4.00	.166	.0020
.10	.238	.0019
.20	.318	.0019

.58	1.755	.0369
.62	2.078	.0367
.66	2.431	.0364
.70	2.813	.0359
.74	3.223	.0349
.78	3.654	.0328
.82	4.085	.0286

Degeneracy at $t = 2.784$.

2.80	3.798	0.0312
.88	4.129	.0232
2.96	.316	.0150
3.04	.424	.0084
.12	.483	.0037
.20	.507	.0008

$$\frac{dz}{dt} = \frac{3}{5}\frac{GM}{K_1}\mu_3^{5/3}\frac{x - x_0}{\varrho^{2/3}}u, \tag{14}$$

the second equation being identical with the last one in (3). They are integrated numerically in the above three cases and the corresponding y, z, and u values are collected in Table 3. The existence of an E-solution for X between 0.31 and 0.32 is clearly exhibited. Finally it should be noted that the higher the X-value the smaller the remaining relative mass, contrary to the case of the point-source models without an isothermal core (cf. Table 1).

I gratefully acknowledge a grant from Letterstedtska Fonden, Kungl. Vetenskapsakademien, Stockholm, which made a stay at the Copenhagen Observatory possible. I am highly indebted to Professor Bengt Strömgren for encouraging me to investigate the present problem, for many helpful discussions, and for his reading of the manuscript. Thanks are also due to Professor Strömgren for the privilege of working at the Copenhagen Observatory.

References.

(1) M. Schönberg and S. Chandrasekhar, Ap. J. **96**, 161, 1942; M. Hall Harrison, Ap. J. **103**, 193, 1946; Ap. J. **105**, 322, 1947.
(2) G. Gamow, Phys. Rev. **67**, 120, 1945; G. Gamow and G. Keller, Rev. Mod. Phys. **17**, 125, 1945.
(3) Phys. Rev. **55**, 434, 1939; Ap. J. **92**, 118, 1940.
(4) B. Strömgren, Z. f. Ap. **2**, 345, 1931.
(5) S. Chandrasekhar, An introduction to the study of stellar structure, 293, 1939.
(6) Z. f. Ap. **7**, 222, 1933.
(7) Cf. Ref. (4).
(8) Ap. J. **88**, 472, 1938.
(9) H. d. Ap. **VII**, 171—180, 1936, where further references to the work of L. Biermann and others are given.
(10) H. Siedentopf, A. N. **244**, 278, 1932.
(11) Cf. Ref. (5), 260.
(12) M. N. **91**, 739, 1931.

Indleveret til Selskabet den 3. November 1947.
Færdig fra Trykkeriet den 21. September 1948.

DET KGL. DANSKE VIDENSKABERNES SELSKAB
MATEMATISK-FYSISKE MEDDELELSER, BIND XXV, NR. 2

THE MOTION OF COMET SCHWASSMANN-WACHMANN 2 IN THE YEARS 1942-1949

BY

HANS Q. RASMUSEN

KØBENHAVN
I KOMMISSION HOS EJNAR MUNKSGAARD
1948

Printed in Denmark
Bianco Lunos Bogtrykkeri

When comet Schwassmann-Wachmann 2 was rediscovered in 1941 the deviation from the calculated position appeared to be $\Delta\alpha \cos\delta = -2^{s}.2$ and $\Delta\delta = +6''$. A continuation of the calculated orbit for the years 1929—1942[1] therefore is likely to lead to an ephemeris sufficiently accurate to make it possible to find the comet in the coming apparition in 1947—48. As before account has been taken of the perturbations from Jupiter and Saturn. The computed equatorial co-ordinates for the equinox 1950.0 are given in the following table.

Table I.

0^h U. T.	x	y	z
1942 Feb. 10.....	− 1.157 275	+ 1.659 070	+ 0.710 564
Mar. 2.....	1.381 204	1.504 224	0.662 982
22.....	1.588 657	1.331 425	0.607 488
Apr. 11.....	1.777 488	1.143 014	0.544 872
May 1.....	1.946 127	0.941 597	0.476 058
21.....	2.093 577	0.729 904	0.402 052
Jun. 10.....	2.219 408	0.510 650	0.323 884
30.....	2.323 690	0.286 411	0.242 561
Jul. 20.....	2.406 905	+ 0.059 550	0.159 029
Aug. 9.....	2.469 858	− 0.167 838	+ 0.074 148
29.....	2.513 575	0.393 942	− 0.011 319
Sep. 18.....	2.539 233	0.617 239	0.096 714
Oct. 8.....	2.548 083	0.836 472	0.181 477
28.....	− 2.541 401	− 1.050 625	− 0.265 142

[1] Det Kgl. Danske Videnskabernes Selskab, Math.-fys. Medd. XIII, 16 and XIX, 3, and Publikationer og mindre Meddelelser fra Københavns Observatorium Nr. 106 and 128.

Table I (continued).

0^h U. T.	x	y	z
1942 Nov. 17	— 2.520 449	— 1.258 897	— 0.347 324
Dec. 7	2.486 448	1.460 670	0.427 716
27	2.440 560	1.655 476	0.506 069
1943 Jan. 16	2.383 882	1.842 978	0.582 191
Feb. 5	2.317 434	2.022 941	0.655 933
25	2.242 163	2.195 216	0.727 182
Mar. 17	2.158 942	2.359 722	0.795 859
Apr. 6	2.068 577	2.516 431	0.861 908
26	1.971 805	2.665 360	0.925 291
May 16	1.869 304	2.806 556	0.985 992
Jun. 5	1.761 694	2.940 097	1.044 002
25	1.649 546	3.066 072	1.099 327
Jul. 15	1.533 381	3.184 594	1.151 980
Aug. 24	1.290 875	3.399 760	1.249 352
Oct. 3	1.037 570	3.586 624	1.336 327
Nov. 12	0.776 344	3.746 263	1.413 161
Dec. 22	0.509 664	3.879 762	1.480 136
1944 Jan. 31	— 0.239 657	3.988 178	1.537 544
Mar. 11	+ 0.031 825	4.072 527	1.585 675
Apr. 20	0.303 150	4.133 778	1.624 814
May 30	0.572 872	4.172 849	1.655 236
Jul. 9	0.839 687	4.190 602	1.677 203
Aug. 18	1.102 412	4.187 854	1.690 965
Sep. 27	1.359 959	4.165 372	1.696 760
Nov. 6	1.611 314	4.123 877	1.694 812
Dec. 16	1.855 524	4.064 056	1.685 332
1945 Jan. 25	2.091 678	3.986 560	1.668 523
Mar. 6	2.318 895	3.892 008	1.644 576
Apr. 15	2.536 319	3.780 996	1.613 674
May 25	2.743 098	3.654 099	1.575 992
Jul. 4	2.938 384	3.511 877	1.531 702
Aug. 13	3.121 321	3.354 882	1.480 969
Sep. 22	3.291 033	3.183 663	1.423 957
Nov. 1	+ 3.446 621	— 2.998 772	— 1.360 829

Table I (continued).

0^h U. T.	x	y	z
1945 Dec. 11	+ 3.587 150	— 2.800 772	— 1.291 753
1946 Jan. 20	3.711 644	2.590 247	1.216 901
Mar. 1	3.819 073	2.367 809	1.136 451
Apr. 10	3.908 347	2.134 114	1.050 598
May 20	3.978 301	1.889 869	0.959 551
Jun. 29	4.027 691	1.635 858	0.863 544
Aug. 8	4.055 178	1.372 955	0.762 843
Sep. 17	4.059 316	1.102 155	0.657 751
Oct. 27	4.038 545	0.824 602	0.548 628
Dec. 6	3.991 175	0.541 634	0.435 896
1947 Jan. 15	3.915 380	— 0.254 827	0.320 066
Feb. 24	3.809 194	+ 0.033 932	0.201 762
Apr. 5	3.670 514	0.322 368	— 0.081 749
May 15	3.497 118	0.607 710	+ 0.039 020
Jun. 24	3.286 708	0.886 562	0.159 355
Aug. 3	3.036 994	1.154 733	0.277 752
Sep. 12	2.745 853	1.407 044	0.392 320
Oct. 2	2.584 186	1.525 306	0.447 442
22	2.411 572	1.637 099	0.500 666
Nov. 11	2.227 930	1.741 393	0.551 595
Dec. 1	2.033 272	1.837 061	0.599 792
21	1.827 723	1.922 871	0.644 768
1948 Jan. 10	1.611 559	1.997 491	0.685 992
30	1.385 240	2.059 496	0.722 882
Feb. 19	1.149 454	2.107 390	0.754 818
Mar. 10	0.905 155	2.139 630	0.781 146
30	0.653 609	2.154 677	0.801 195
Apr. 19	0.396 427	2.151 055	0.814 301
May 9	+ 0.135 585	2.127 427	0.819 832
29	— 0.126 576	2.082 693	0.817 229
Jun. 18	0.387 383	2.016 090	0.806 043
Jul. 8	0.643 902	1.927 290	0.785 981
28	0.893 052	1.816 479	0.756 943
Aug. 17	— 1.131 740	+ 1.684 415	+ 0.719 047

Table I (continued).

0^h U. T.	x	y	z
1948 Sep. 6.....	— 1.357 031	+ 1.532 417	+ 0.672 641
26.....	1.566 300	1.362 321	0.618 292
Oct. 16.....	1.757 369	1.176 382	0.556 754
Nov. 5.....	1.928 595	0.977 142	0.488 922
25.....	2.078 909	0.767 284	0.415 780
Dec. 15.....	2.207 801	0.549 494	0.338 343
1949 Jan. 4.....	2.315 242	0.326 345	0.257 612
24.....	— 2.401 660	+ 0.100 208	+ 0.174 532

From these co-ordinates the following ephemeris was deduced and cabled to the Yerkes Observatory on Oct. 17:

0^h U. T.	α 1947.0	δ 1947.0
1947 Oct. 18.....	$2^h\ 36^m.0$	+ 9° 27′
22.....	2 33.2	+ 9 11
26.....	2 30.2	+ 8 54
30.....	2 27.0	+ 8 36

The comet was rediscovered by Van Biesbroeck on Oct. 20, and by Jeffers on Oct. 24. The last observation gave the following residuals:

		$\Delta\alpha \cos\delta$	$\Delta\delta$
1947 Oct.	24.41048	+ $1^s.49$	+ $8''.2$
	24.47645	+ 1.40	+ 8.4

In the first part of 1949 the comet will be well placed for observation, and the following ephemeris is deduced from the rectangular co-ordinates:

Table II.

0^h U. T.	α 1950.0	δ 1950.0	Δ	r
1948 Nov. 25	$12^h\ 3^m.4$	$+1^\circ\ 31'$	2.533	2.254
29	9.8	0 55	2.499	2.263
Dec. 3	16.1	+ 0 21	2.464	2.272
7	22.2	— 0 12	2.428	2.281
11	28.1	0 44	2.392	2.290
15	33.9	1 13	2.356	2.300
19	39.4	1 42	2.317	2.310
23	44.7	2 8	2.279	2.320
27	49.8	2 32	2.241	2.331
31	54.6	2 55	2.202	2.341
1949 Jan. 4	12 59.2	3 16	2.164	2.352
8	13 3.4	3 34	2.125	2.363
12	7.4	3 50	2.086	2.375
16	11.1	4 4	2.048	2.386
20	14.4	4 15	2.010	2.398
24	17.4	4 24	1.972	2.410
28	19.9	4 30	1.935	2.422
Feb. 1	22.1	4 34	1.900	2.435
5	23.9	4 35	1.865	2.447
9	25.3	4 34	1.832	2.461
13	26.2	4 30	1.800	2.473
17	26.7	4 23	1.770	2.486
21	26.8	4 14	1.743	2.499
25	26.4	4 2	1.718	2.512
Mar. 1	25.6	3 48	1.695	2.526
5	24.4	3 32	1.676	2.539
9	22.8	3 14	1.660	2.553
13	20.8	2 55	1.647	2.567
17	18.5	2 34	1.638	2.581
21	16.0	2 13	1.633	2.595
25	13.2	1 51	1.632	2.609
29	10.3	1 29	1.635	2.623
Apr. 2	7.2	1 8	1.642	2.638
6	13 4.2	— 0 47	1.654	2.652

Table II (continued).

0^h U. T.	α 1950.0	δ 1950.0	Δ	r
1949 Apr. 10	$13^h\ 1^m.2$	$-0^\circ\ 28'$	1.671	2.667
14	12 58.3	− 0 10	1.691	2.681
18	55.6	+ 0 6	1.716	2.696
22	53.0	0 20	1.745	2.711
26	50.7	0 32	1.778	2.725
30	48.7	0 41	1.815	2.740
May 4	12 47.0	+ 0 48	1.855	2.755

The co-ordinates and velocities for 1949 January 4.0 U.T. lead to the following elements:

Epoch and osculation 1949 Jan. 4.0 U.T.

$$\left.\begin{aligned} T &= 1948\ \text{Aug.}\ 23.5770\ \text{U.T.} \\ M &= 20^\circ.1512 \\ \omega &= 358.1003 \\ \Omega &= 126.0201 \\ i &= 3.7239 \\ e &= 0.383651 \\ a &= 3.49212 \\ \mu &= 0.1510324 \end{aligned}\right\} \ 1950.0$$

$$\left.\begin{aligned} P_x &= -0.560986 & Q_x &= -0.826157 \\ P_y &= +0.760332 & Q_y &= -0.539306 \\ P_z &= +0.327400 & Q_z &= -0.163137 \end{aligned}\right\} \ 1950.0$$

The ephemeris of course can also be computed by means of these elements, but it is far easier to deduce the ephemeris from the rectangular co-ordinates for every 20th day and then interpolate to every 4th day, as has been done in this case.

The perturbed co-ordinates of comet Schwassmann-Wachmann 2 based on elements from 1929 Feb. 18 have now been computed for 20 years, during which time the comet has made three revolutions.

The differences between computation and observations are less than one minute of arc, and undoubtedly the orbit will not deviate particularly much from the observations even if the same elements are used for a few more revolutions. After 270 intervals, however, the perturbations are somewhat uncertain, so that the good accordance may partly be due to chance. At any rate an improvement of the orbit by means of the observed positions cannot be obtained without computing perturbations of higher accuracy.

I am indebted to the Carlsberg Foundation for having placed at my disposal the calculating-machine used in this investigation.

Værslevgaarden, May 1948.

Indleveret til Selskabet den 7. Juni 1948.
Færdig fra Trykkeriet den 6. September 1948.

DET KGL. DANSKE VIDENSKABERNES SELSKAB
MATEMATISK-FYSISKE MEDDELELSER, BIND XXV, NR. 3

STUDIES ON THE ORIGIN OF THE SOLAR SYSTEM

BY

D. TER HAAR

KØBENHAVN
I KOMMISSION HOS EJNAR MUNKSGAARD
1948

TABLE OF CONTENTS

Printed in Denmark
Bianco Lunos Bogtrykkeri

INTRODUCTION

In this introduction, we shall give in Part A a statement of the problem of the origin of the solar system and of the facts which have to be explained. In Part B, we shall take a necessarily short survey of sundry theories which have been proposed, together with reasons why we feel that they cannot be accepted as final solutions of this fascinating problem.

A. Statement of the Problem.

The nearest neighbours of our earth in the universe are the moon, the sun and the other members of the solar system. The sun and the moon are by far the brightest objects in the sky and the other members of the solar system are also among the brightest. It is not, therefore, surprising that astronomers throughout the ages have devoted special attention to the solar system.

Moreover, the system shews so many regularities in its dynamic and physical properties that its formation was certainly not due to chance. The fact alone that the direction of orbital motion of all planets and asteroids is the same is sufficient to establish this.

Before we discuss some of the theories advanced as to the origin of the system, we shall point out some of these regularities.

The solar system consists of the sun, nine large planets, twenty-eight satellites belonging to six of these planets, more than 1500 asteroids, and the comets and meteors. We shall center our attention on the large planets and only speak occasionally about the other bodies.

The regularities shewn by the solar system may be divided into a few groups:

A. The first group is that of the orbital regularities (cf. Table I). Apart from the common direction of orbital motion, the eccentricities of the orbits are small and the orbital planes are practically

coincident. Also, the rotation of the sun is in the same direction and its equator is only slightly inclined to the planetary orbits.

B. The second striking feature is that the mean distances of the planets from the sun very closely obey the so-called Titius-Bode law. If the mean distance of the n-th planet from the sun is denoted by r_n and if we count the group of the asteroids as one of the planets, we have:

$$r_n = a + b \cdot 2^n,$$

where $a = 0.4$ A. U. and $b = 0.3$ A. U.

We may remark here that orbital regularities and laws for distances, comparable to the Titius-Bode law, are also found for the satellite systems (compare Tables II, III, IV, V).

C. The next group is the fact that the planets can be divided into two groups. The inner planets which form the first group have relatively small masses, high specific densities, low rotational velocities, and few satellites. The outer planets, which form the second group, have large masses, low specific densities, a relatively fast rotation, and large satellite systems[1].

If a theory is able to withstand the attacks of serious criticism, it ought to be able to explain the above-mentioned facts. However, there are more features of the solar system which have to be considered. We may call the reader's attention to a few of these.

Between Mars and Jupiter, there is no other planet, but the system of asteroids, estimated by Baade to contain about 30000 bodies, of which only less than 2000 have been observed up to now. The total mass of the asteroid system is extremely small (about 0.0003 times the mass of the earth).

Saturn possesses a ring system.

The outer satellites of Jupiter and Saturn have retrogade motions.

The inclination of the equatorial plane to the orbital plane is increasing in the series of the outer planets. Also some orbits of satellites are much inclined to the equatorial plane of their primaries.

Pluto, as we have already remarked, does not fit in with the other outer planets.

[1] We leave Pluto out of this discussion. Pluto's orbit has a large eccentricity, and the planet itself is small and dense.

D. Finally, the distribution of the angular momentum in the solar system has proved to be a stumbling block for many theories. As it is, the sun, although possessing more than 99 per cent. of the mass of the system, possesses only 2 per cent. of its angular momentum. The puzzle is why the sun has so little angular momentum.

We may, perhaps, point out here the difficulties inherent in this distribution of the angular momentum.

If the origin of the solar system has to be ascribed to a catastrophe of some kind, this accident in itself could have been able to transfer angular momentum to the material which would condense subsequently into the planets.

If, however, one tries to build up a theory starting from the sun, perhaps surrounded by a gas cloud, it is difficult to understand how this distribution came about. If the sun had been surrounded from the beginning by a gas cloud, the difficulty is to understand why the angular momentum per unit mass in this gas cloud should be so much larger than the angular momentum per unit mass in the sun. If, on the other hand, the system started from the sun alone, with the material for the planets being provided for instance by eruptions from the sun, one certainly would expect the angular momentum per unit mass to be about the same for the solar as for the planetary material.

Fouché, in 1884, was the first to point out the extraordinary character of the actual distribution of the angular momentum.

We shall see how this question has played a great role in the evaluation of sundry theories.

The origin of the asteroids will not be discussed here. The generally accepted explanation involves the breaking up of a larger body. According to recent work of Brown (1), this process might also have given rise to the meteorites.

We shall also not enter extensively into a discussion of the irregularities mentioned above. As far as the satellite systems are concerned, the great resemblance between them and the planetary system seems to point to a formation of the satellite systems analogous to the formation of the planetary system itself, even though the distribution of the angular momentum is not quite so extreme as in the case of the planetary system (2).

The ring system of Saturn is probably due to the fact that its

distance from Saturn is less than the limit of Roche, inside which no satellite is stable against a tidal action of the mother planet. To understand this qualitatively, imagine a satellite brought nearer and nearer to its primary. The tidal forces increase, but the gravitational forces of the satellite itself on its matter remain the same. And so at a certain moment, the satellite, if liquid, would break in two and so forth until the fragments would be so small that surface tension keeps them together. If the density of the planet were the same as that of the satellite, the critical distance at which the breaking up would begin would be 2.44 times the planet's radius, as shown by Roche in 1850. Since the ring system of Saturn lies completely inside this limit, it seems reasonable to accept the thesis that these rings are the remains of a satellite, broken up during its formation.

It has been established that the age of the solar system is of the order of 2 to 3.10^9 years by different, independent indications such as, for instance, the lead content of rocks, where the lead is the end product of a radioactive family and thus has a different atomic weight (206.0) from that of the familiar lead (207.1). Another determination of the age of the universe can be obtained from the redshift of extragalactic nebulae, giving the same result[1].

The sun is radiating at present at a rate of 4.10^{33} erg per sec, which corresponds to a loss of mass of 4.10^{12} g sec^{-1}. If the sun had radiated energy at the present rate during the 3.10^9 years of its probable existence, it should only have lost 0.0001 of its mass. We shall assume in the present paper that during the process, leading to the solar system as we find it at present, the physical state of the sun was as we observe it at present. It is possible that we neglect vital processes by this assumption.

B. Survey of Theories about the Origin of the Solar System.

We can only report here very incompletely on the various theories. For further details, and a detailed criticism of the older theories, we therefore refer the reader to the original papers and to the many textbooks written on this subject, especially the volumes by Russell, Dugan, and Stewart (3), Nölke (4), and Russell (5).

[1] Compare the considerations of Bok (39) and Unsöld (40).

In general it is possible to divide all theories into two groups, according to the question whether or not the author has assumed an interaction with other celestial bodies as an important factor in the development of the solar system. In the first case, we have an open system and, using the term introduced by Belot, we can call these theories dualistic (sometimes the adjective "catastrophic" is used). In the other case, we have to deal with a closed system and the theories are called monistic or uniformitarian.

I. Monistic theories: 1. Descartes' theory. The first theory proposed in modern times is that of Descartes, advanced in 1644. At that time, observational data were scarce and only the sun, 6 planets and 7 satellites (the moon, 4 Jovian and 2 Saturnian satellites) had been observed. Also Newton's law of gravitation, which was to be published in 1665, was still unknown. It is thus more surprising that Descartes was able to formulate a theory which could explain many of the observational data than that his theory had to be abandoned after Newton's severe criticism.

Descartes started from a large whirl of matter in which 14 large bodies were floating as pieces of wood in a river. As can be seen in actual whirls carrying pieces of wood, the larger bodies have a tendency to collect around them the smaller ones and in the same way the sun became surrounded by the 6 planets, while the earth, Jupiter and Saturn got respectively 1, 4, and 2 satellites. Since the movement in the inner regions of a whirl is faster than in the outer regions, one could also understand that the rotation of the inner planets was faster than that of the outer ones.

The great historical significance of this theory is that it was the first attempt to explain the observational data, starting from some simple hypothesis. As soon as Newton had found his gravitational law, it was, however, possible to shew that this theory could not be maintained.

Newton himself believed that God had created the solar system in its present state and that He would look after it if its future were endangered by mutual perturbations of the planets. His influence on his fellow-scientists was so large that the cosmogonical theories of Buffon and Kant remained practically unnoticed. This only changed when Laplace arrived with his theory.— Laplace who wrote about Newton: "Je ne puis m'empêcher d'ob-

server combien Newton s'est écarté sur ce point de la méthode dont il a fait ailleurs de si heureuses applications."

2. KANT's theory. In 1755, IMMANUEL KANT in his "Allgemeine Naturgeschichte und Theorie des Himmels" gave a qualitative cosmogony, which was ultimately worked out more quantitatively by Du Ligondès in 1897.

Kant started his treatise by answering the theological objections to the proposal of a cosmogony by remarking that the laws of nature are created by God, so that it is not lack of reverence when we try to find out the effects to which their action leads.

Kant's idea is to start from a nebula in the centre of which the sun is placed. Due to gravitational forces the rest of the matter will rotate around the sun. Under the influence of mutual collisions, the nebula will pass into a disc, where all particles are rotating in circles around the sun. The next step is that there is a tendency of the matter in the disc to condense into some large bodies which become the planets. Since this condensation takes place gradually, the first result will again be a rotating nebula, but now on a smaller scale, from which the satellite systems ensue. The larger the planet, the larger its gravitational attraction, and the larger the number of satellites.

Kant also shews that the rotation of the planets around their axes will be in the same direction as their rotation around the sun. To understand this, we have to consider a particle moving in the same orbit as and behind the planet. Under the influence of the attraction of the planet, its velocity will increase and thus also the centrifugal force. The result is that it will move outwards and that if it collides it will give to the planet an angular momentum of the right direction.

Kant was able to explain the first group of regularities, mentioned in part A. He did not attempt to explain the other three. He was unaware of the difficulty of the distribution of the angular momentum, and even of the fact that angular momentum has to be preserved. The fact that the present distribution of the angular momentum was not explained in this theory was the reason why Kant's theory was not accepted as the final answer. In the following chapters we shall see that an extension of this theory seems to be able to give an explanation of C and perhaps of B.

3. LAPLACE's theory. In many textbooks and popular works,

Kant's theory is mentioned together with the theory of Laplace of 1796. The view often held is that Laplace put Kant's ideas into scientific terms. As we shall see, this is far from correct. The theories are widely different. Moreover, Laplace when writing his popular book "Exposition du Système du Monde" was unaware of the existence of Kant's theory.

Laplace's idea was to start from a situation where the sun is surrounded by a hot gaseous atmosphere. This nebular atmosphere was gradually cooling and thus contracting. As it contracted, the rotational velocity necessarily increased by the preservation of angular momentum, and thus also the centrifugal force at the equator. Ultimately this force became larger than the gravitational force and a ring of matter was flung into space.

This process was repeated, giving rise to a system of concentric rings from which by a process not further explained the planets derived. Finally, the remains constituted the sun.

Laplace can easily explain A and perhaps B, but the crucial point here is again D. In fact, if all the mass and angular momentum of our solar system was concentrated in even as small a volume as that of the present sun, the centrifugal force at its equator would only be about five per cent. of gravity and it would be far from any danger of breaking up.

This failure to explain D alone suffices to disprove Laplace's theory. Another difficulty, which can only be overcome quite artificially, is that the Laplacian rings have no tendency to condense into planets (they might form a swarm of asteroids but not larger bodies). The only explanation is to suppose that the actual condensation should have begun already before the throwing off of the rings.

Faye's theory of 1885 was essentially the same as Laplace's and is also unable to explain D.

4. Birkeland's theory (6); Berlage's theories (7): In 1912, Birkeland gave a sketch of a theory in which the solar magnetic moment and the particles emitted by the sun played a role. His idea was that through the strong magnetic field of the sun the charged particles, which are for the most part emitted from the equatorial regions, should spiral down towards limiting circles. The radii of these circles would depend on the ratio of the charge to the mass of the particles.

Birkeland is thus able to explain both A and B. The problem D is not a problem in this case either, since, as shewn by Alfvén, due to currents in the surrounding matter evoked by the sun's magnetic field transfer of angular momentum from the sun to the surrounding matter is possible. The time needed for this transfer is small (10^5 years) as compared with the age of the solar system.

Nevertheless, this theory could not be maintained since the solar magnetic field is not strong enough to produce the desired effect. The orbits of the emitted particles are only slightly curved and they all leave the regions of the solar system.

Birkeland was the first author to consider electromagnetic effects. After him, Berlage, inspired by his ideas, tried to account for many features of the solar system by taking the solar electric field into account. Berlage's theories met with the same fate as Birkeland's. They remained practically unobserved. For instance, Alfvén who in 1942 again investigated the possible influence of the solar magnetic field does not mention either of them.

In his first theory Berlage assumed that the sun emits negatively charged solid particles and positively charged ions. Their emission is a consequence of the fact that radiation pressure on them exceeds gravitation. The result is a space charge around the sun and a positive charge of the sun itself.

The next assumption is that the sun, as in the theory of Kant, is surrounded by a gaseous disc. If we now roughly calculate the equilibrium position of an ion in the disc under the influence of the space charge, solar charge and solar gravitational field (Berlage neglects the centrifugal force), it can be shewn that for each ion there exists an equilibrium distance which increases with decreasing atomic number of the ions.

The result is that in the disc there will be formed concentric rings of ions, their radii depending on the ion in question.

These ion rings will act as the initial nuclei for condensation, and afterwards each of these rings will condense ultimately into one planet, as in Laplace's theory.

Since to each of these ion rings is ascribed a certain isotope of one of the elements, Berlage is able to estimate the masses of the planets. Also he finds decreasing densities of the planets with increasing distance from the sun, which—assuming that Jupiter

and Saturn possess a heavy nucleus surrounded by a lighter atmosphere (Jeffreys)—is in agreement with observation.

The distance of the rings from the sun can be shewn to correspond to the Titius-Bode law.

We see that Berlage is able to explain here A, B and C: he does not attempt an explanation of D. This theory will not, however, stand criticism. Apart from the fact that it can easily be shewn that in the way Berlage suggests enough matter can never be collected to build up, for instance, Jupiter there is the fact that the basic assumption that the sun should emit negatively charged solid particles is shewn to be wrong by observation.

This was the reason why Berlage himself left this theory for a second attempt where he now used the fact that the sun emits positive ions and electrons. Considering the effect of space charge, radiation pressure and gravitation on the charged particles, but still neglecting centrifugal forces due to rotation, Berlage is able to calculate the electric field strength in the neighbourhood of the sun. It then appears that this field is of a periodic character. This means that there are concentric spheres on the surface of which the field strength is equal to zero.

If we now consider the gaseous disc which is again supposed to be surrounding the sun, we see that since the atoms will all be ionized for part of their life matter will be concentrated on the circles where the disc is intersecting the spheres of zero field strength. In this way Berlage now gets his rings of matter. The rest of the condensation then takes place in the same unexplained way as in Laplace's theory.

This theory explains A and B, but has to leave C and D unexplained. Berlage himself sees as a serious deficiency of this attempt that it is unable to explain the satellite systems. Another serious objection is that the degree of ionization in the gaseous disc will be so low that electrostatic effects are negligible (compare Chapter II, Section B).

In his latest theory, Berlage has completely left all electromagnetic considerations and considers in detail the history of a gaseous system which may be found around the sun. He thus follows Kant. First of all, he shews that this system will assume the form of a disc. He also gives an expression for the density in the plane of the disc as a function of the distance from the sun.

After that Berlage looks for a possibility that this disc may condense spontaneously into rings. Afterwards these rings have to condense into the planets. For that purpose he investigates whether a slightly different density function might be stable. This means that for this new density function, the total mass, angular momentum, and energy are the same as before, but the kinetic energy of the system is larger than initially. Berlage really finds such a tendency to form rings.

In this way he can explain A and B. His reasoning is, however, very loose as, for instance, his assumptions about the temperature distribution and the laminar motion in the disc. Also his assertion that rings will be formed does not rest on a firm foundation. Finally, there is still the difficulty of the condensation of the rings into planets which we met already in the discussion of Laplace's theory.

5. ALFVÉN's theory (8). The Swedish physicist Alfvén has given a very interesting theory in a series of three papers, taking into account the magnetic forces on ionized matter.

His reasons for advancing this theory are the following. To begin with, the force exerted by the sun's magnetic moment on ionized matter can be much larger than the gravitational force on the same matter. For instance, on a proton moving in the earth's orbit with the earth's velocity, the first force exceeds the second by a factor 60.000. In the second place, ALFVÉN has shewn in an earlier paper (9) that transfer of angular momentum from the sun to a surrounding ion cloud is possible. The rotating magnetic moment of the sun evokes currents in the cloud and an effect similar to that braking a metal between a magnet's poles takes place. This transfer of angular momentum can take place in an appreciable amount in as short a period as 10^5 years. In this way, D does not present any difficulty.

Now, Alfvén's idea about the formation of the outer planets is the following. Suppose that in its journey through space, the sun meets an interstellar gas cloud and becomes surrounded by it. If we may neglect the rotation and velocity of the cloud with respect to the sun, the atoms in the cloud will start falling towards the sun, and their kinetic energy will increase during that fall. Eventually this kinetic energy will become so large that ioniza-ion by collisions can take place.

The idea is now that collisions are so frequent that this ionization indeed takes place. Once an ion is formed, the movement towards the sun is stopped and the ion has to move along the magnetic lines of force until it reaches an equilibrium position. Alfvén shews that this equilibrium position is situated in the equatorial plane of the sun.

Assuming now that the ions are moving uniformly towards the sun and are all ionized at the same distance from the sun, and considering in detail the subsequent movement of the ions towards their equilibrium position in the equatorial plane, he gets the mass distribution in the equatorial plane. Alfvén takes the fact that this mass distribution agrees roughly with the mass distribution in the series of the outer planets as a support of his theory.

In this way Alfvén is able to account for the outer planets. This mechanism is, however, unable to explain the origin of the inner planets because even in the most favourable case the distance from the sun at which ionization occurs will be by far larger than the mean distance of Mercury from the sun. Also, one should expect from this mechanism to find lower densities for the inner than for the outer planets but the densities of the inner planets are higher than those of the outer ones.

Alfvén without any detail suggests the following process. The sun in its travel through space should have met an interstellar smoke cloud consisting of solid particles. Through the strong radiation of the sun those particles will sublimate as soon as they have come near enough. The resulting atoms become ionized but at a shorter distance from the sun.

Instead of the Titius-Bode law, Alfvén introduces a diagram where the ratios of the masses and of the distances from the primary are connected. His explanation of this diagram, however, seems to be extremely weak, and it does not seem to be possible to get the same result by valid reasoning.

But also his original idea is unable to stand a critical scrutiny. In the case of a gaseous cloud surrounding the sun from the beginning electromagnetic forces will not play any role at all because of the absence of ionization in the cloud (cf. chapter II, section B).

As far as Alfvén's suggestion about the heating up of an interstellar gas cloud is concerned, the atoms will certainly not save

up their energy until they reach the immediate vicinity of the sun. It can easily be shewn that their mean free path is by far too small. However, one could imagine that the whole cloud was heated up while contracting. Apart from the fact that one has to assume zero angular momentum of the cloud around the sun, and the fact that the energy gained seems to be emitted by radiation before ionization takes place, it seems that the desired object still is not attained. Ionization will start all over the cloud, and since ions cannot approach the sun, only a very small fraction of the gas cloud, insufficient to form the planets, will be available for further condensation.

6. Von Weizsäcker's theory (10). In a paper, dedicated to Sommerfeld on the occasion of his 75th birthday, von Weizsäcker has advanced a new theory about the origin of the solar system. The greatest importance of this theory is in the fact that it provides us with a definite scheme for further calculations[1].

His theory can be divided into different parts, corresponding to the different stages in the development of the solar system. First, he discusses the formation of a gaseous disc around the sun, secondly, the formation of a system of vortices in this disc, finally, the condensation process, and the satellite systems.

The first part is practically identical with the similar parts in Kant's or Berlage's theory. The disc is supposed to contain about one tenth of the solar mass, and the over all density will be about 10^{13} atoms per cm^3.

The second part is the most interesting, but probably also the weakest point in this theory. Supposing that the orbits of mass elements in the disc may be assumed to be Keplerian, von Weizsäcker shews that a system of vortices can be built up from these Keplerian orbits. In fig. 1, we see such a configuration.

Von Weizsäcker is led to such a configuration for two reasons. The first is that gravitational forces are by far the most important forces in the disc. The second is that in a system of vortices, as shewn in fig. 1, the energy dissipation will be small. In the large vortices the dissipation will be negligible in a first approximation. However, along those circles where the rings of vortices meet there will be large viscous stresses. These will presumably

[1] It will be seen that the present paper is to a large extent a clarification and extension of von Weizsäcker's ideas.

give rise to secondary eddies on the circles separating the main vortices. These eddies are called the "roller bearing" eddies. They will probably regulate the whole system. However, energy will be dissipated in these "roller bearings". Conditions for condensation will be more favourable in these secondary eddies (compare Chapter IV), and so we may expect the planets to be formed at distances from the sun corresponding to the radii of

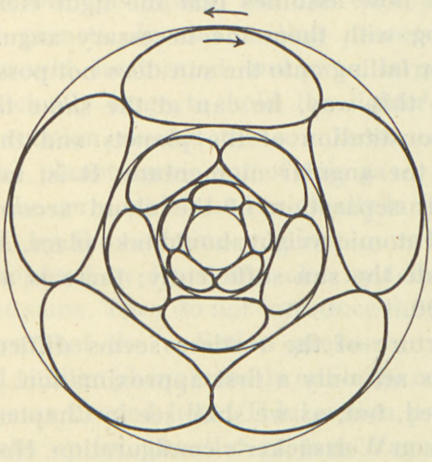

Figure 1. The outer arrow indicates the direction of rotation of the whole disc, while the inner arrow indicates the direction of rotation in the vortices. The sun is in the centre of the whole system.

the circles separating the main vortices. Now, von Weizsäcker gives reasons to believe that the number of large vortices in each ring is constant. This means that the ratio of two consecutive radii will be constant, thus giving us the Titius-Bode law for the distances of the planets from the sun (neglecting the constant term).

Another consequence of the condensation into planets in the "roller bearings" is that we will get a counter-clockwise rotation of the planets if the whole system is rotating in a counter-clockwise direction, in agreement with observation. The rotation in the large vortices is in the opposite clockwise direction.

During their formation and immediately thereafter the planets will be surrounded by extended atmospheres. In these atmospheres the satellite systems will be formed. Von Weizsäcker does not, however, enter into an extensive discussion of this question.

Due to the dissipation of energy, the disc will disappear

gradually. Von Weizsäcker estimates its lifetime to lie between 10^7 and 10^8 years, which is of the same order of magnitude as the period necessary to build up bodies of the size of the planets.

Von Weizsäcker has given an explanation of A, B, and C. He also gives an explanation of D in the following way. The dissipation of the gaseous system is accompanied by a flow of atoms into interstellar space and a simultaneous flow of matter to the sun. He now assumes that the light elements leave the system, carrying with them the necessary angular momentum, while the matter falling onto the sun does not possess any angular momentum. In this way, he can at the same time explain the difference in constitution of the planets and the sun, and the distribution of the angular momentum. It is, however, difficult to see why this separation of the cloud according to angular momentum and atomic weight should take place. Also, this process cannot decelerate the sun sufficiently; there is a discrepancy of a factor 100.000.

Also his picture of the vortices seems difficult to maintain: Keplerian orbits are only a first approximation. Hydrodynamics has to be applied, but, as we shall see in Chapter III, it is as yet unable to give von Weizsäcker's configuration. However, the main merit of this theory is that it has revived again Kant's theory and that it has drawn attention to the importance of hydrodynamical considerations.. In the following chapters we shall see that a slightly different attack seems to give a reasonable explanation of A, C, and perhaps B, while D has as yet to remain unexplained.

II. Dualistic Theories: 1. Buffon, Chamberlin-Moulton, Jeffreys, Jeans. Ten years before Kant published his theory a dualistic theory had been advanced by Buffon. In those days fantastic ideas about comets were common and Buffon therefore proposed the collision of the sun and a comet as the source of our solar system. (Buffon estimated the mass of the comet of 1680 as 28000 times the earth's mass.)

Through the collision matter was torn out of the sun which matter later condensed into planets. The rotation of the sun might also have been caused by the collision.

Modern tidal and collision theories have the same foundation the only difference being that another star, instead of a comet, is the foreign body which produces the material.

Chamberlin and Moulton proposed that as a second star was passing the sun in a hyperbolic orbit by tidal action and eruptions material for the planets was provided. The first heavier eruptions would provide the material for the outer and the secondary eruptions that for the terrestrial planets.

After the second star had departed the gaseous matter would cool and condense. Part of it had fallen back on the sun and part of it escaped into open space, but the rest could be used for building up the planets. In the cooling process liquid drops (planetesimals) would be formed and even larger solid cores which were sufficiently large to hold the lighter gases. In the course of their rotation around the sun those cores swept up matter and so the planets grew out of this gas.

The orbits of the cores which had originally large eccentricities are "ironed out" by the resisting medium.

The theory proposed by Jeans and also by Jeffreys in his first paper is about the same. They do not introduce the solar eruptions since it is known that the radiation pressure responsible for prominences and similar phenomena is not large enough to cause eruptions as large as needed here. Tidal action produced a filament which breaks up into smaller gaseous fragments. In those fragments condensation takes place into liquid bodies and so on to planets.

The small eccentricities are again brought about by the resisting medium.

These theories have the advantage that they are able at first sight to explain the distribution of the angular momentum (D) without difficulty. They do not attempt to explain either B or C while for A they use the resisting medium.

The first difficulty lies in the explanation of the planetary rotation. The explanation put forward by Chamberlin is not convincing and therefore Jeffreys assumed later that it was not a close encounter, but an actual collision which took place. Taking into account the viscosity of the resulting ribbon torn out of the sun, he could then shew that rotation of the right order of magnitude would ensue.

The next and greater difficulty is as Nölke has shown the influence of the resisting medium. It seems to be doubtful whether this medium really can bring about the small eccentricities.

Another difficulty is the formation of the satellite systems. Although the original idea was that tidal forces caused by the sun were responsible for them, Jeans himself shewed that this notion would not work. In Jeffreys' later theory it is perhaps more easily explained, since (quoting Russell) "almost anything may have happened in the period of wild turbulence, which included the formation of the ribbon and its segregation into separate bodies."

Also, if the material comes from the sun, it will be extremely hot and the danger exists that it may fly away into open space before beginning to condense, as was pointed out by SPITZER (11).

Finally, the explanation of D is not as easy as it seems. At first sight one would think that during the collision sufficient angular momentum may have been imparted to the filament. RUSSELL (5) has shown, however, that this transfer of angular momentum by the second star is not an easy job and that, if it was possible at all, which he doubts, one would expect large inner and small outer planets.

Russell also deals with some other hypotheses to save these theories, but ends his monograph by saying that we are as yet no wiser about the origin of the solar system than we were when Newton found his law of gravitation, a point of view shared by Nölke.

2. Binary hypotheses; LYTTLETON (12, 13), HOYLE (14). During the last decade, several theories have been proposed involving the assumption that the sun was originally a member of a binary or multiple system.

The first theory of Lyttleson assumes that the binary companion of the sun undergoes a close encounter with a third star, similar to the encounter assumed in Jeffreys' theory. The encounter results in a disruption of the binary system and the production of a gaseous filament which may produce the planets. Although Luyten's manifold criticism does not seem to be valid, the formation of satellite systems and the small eccentricities, together with SPITZER's objection (11) seem to be too large stumbling blocks.

In his second theory, Lyttleton starts from a triple star. The separation of the two companions of the sun will decrease as part of the evolution of a binary system. The two stars will finally combine into one mass. This mass will, however, break

up because of rotational instability. After this fission the two parts will leave the system producing a situation similar to that met in Lyttleton's first theory. The same objections apply, therefore, to this theory.

The last development in this direction is given by Hoyle. According to Hoyle, a supernova outburst of the second component will account for the breaking up of the binary system and for the material from which the planets are formed. It seems, however, that this theory meets the same difficulties.

In his last paper, Hoyle considers the condensation process in detail and arrives at estimates of the original rotational periods of the planets. His reasoning develops along lines parallel to those which will be discussed in Chapter IV. It seems, however, that he arrives at wrong conclusions because he neglects the exhaustion of the gaseous system and all hydrodynamical effects. His proof of the direct rotation of the planets is essentially the same as that given by Kant or Alfvén.

III. Final Remarks: We have not included all theories in our survey. Manyof them as, for instance, those by Arrhenius and See are merely variations on themes discussed here. Other theories like the "Welteislehre" by Hörbiger-Fauth, which has been dealt with conclusively by Nölke (4), or the recent theory by Haldane (15) who seems to drive the consequences of the expanding universe rather far need not to be taken seriously.

However, there exists one recent theory which seems to be, at present anyhow, only an outline of a theory but which must be mentioned briefly. It is Whipple's attempt (16) to produce a planetary system from a large smoke cloud. He starts from a smoke and gas cloud with a radius of about 30000 A. U. containing about one solar mass. The contraction of this cloud should produce both the sun and the planetary system.

The original cloud is assumed to possess negligible angular momentum so as to account for the low angular momentum of the sun. The planets are assumed to be formed in a stream in the cloud so that those initial condensations which have to develop into the planets have already from the beginning the necessary angular momentum. The solution of D is thus put into the theory from the beginning. The planets (or better the condensations

which will later form the planets) will now spiral towards the sun because their accretion of matter of zero angular momentum.

Whipple gives a rather half-hearted explanation of A, but does not attempt to explain B or C. Furthermore, his discussion of the planetary rotations seems to be difficult to follow and lacks quantitative evaluation. Altogether, there seems to be very little reason as yet to accept this theory as a final solution.

Recapitulating, we can say that there seems at present to be no theory which can explain satisfactorily the various properties of our solar system. Especially the differences between the outer and the inner planets and the present distribution of the angular momentum seem to have presented unsurmountable difficulties.

Dr. L. Spitzer has kindly drawn my attention to the recent papers by A. Gasser (Helv. Phys. Acta, *18*, 226, 1945), J. Sourek (Memoirs and Observations Czechoslov. Astron. Soc., Nr. 7, 1946), A. C. Banerji, Proc. Nat. Inst. Sc. India, *8*, 173, 1942) and G. Armellini (Rendic. Reale Accad. d'Italia, serie 7, vol. *4*, no. 11). It has not, however, been possible to include these in the review in this introduction.

Chapter I.

Summary.

In view of the fact that as yet no acceptable solution for the origin of the solar system appears to exist, it seems justifiable to investigate again a few aspects of this old question. There are several reasons why this should be done. First of all, it seems that as yet no sufficient attention has been paid to the physical properties of a gaseous system from which the planets should condense. Secondly, up to now nobody seems to have drawn any conclusions from the remark of JEFFREYS (17) that the initial steps in the condensation process will be the same as in the case of a supersaturated vapour. HOYLE (14) has discussed this problem rather extensively, but his discussion lacks quantitative reasoning and he neglects a few important aspects of the problem and therefore arrives at the wrong conclusions. Finally, in an as yet unpublished paper which was dedicated to Prof. Niels Bohr on the occasion of his sixtieth birtday[1], VON WEIZSÄCKER (18) has set forth new ideas about cosmogonies which might be used for a discussion of the origin of the solar system. Our discussion will, however, run along lines slightly different from those of von Weizsäcker's own theory (10) about the origin of the solar system, because of the difficulties encountered there.

Before discussing the new ideas which we wish to present in the present paper and the reasons why we are discussing just those points which we shall look into, we shall briefly discuss this second paper by von Weizsäcker.

Von Weizsäcker starts from a situation in which the universe

[1] I wish to express my sincere thanks to Prof. Bohr for giving me an opportunity to see this manuscript. This paper has in the meantime been published.

is filled with gas. The composition of this gas is supposed to be roughly the same as that of the sun or of the interstellar gas, i.e., mainly hydrogen. Also there is a velocity distribution which may be described apart from its fluctuations as the expansion of the universe. The origin of these velocities and of the distribution of the elements in the gas are not discussed and are supposed to belong to earlier periods. Now, von Weizsäcker investigates the development of this gaseous system. Because of its large dimensions, turbulence will be present. The consequence is that there will be regions of higher density. Matter entering such denser regions will lose the energy gained in the gravitational field because of viscous interaction and will be captured. In this way we shall get conglomerations of matter. These conglomerations are the first stage of galaxies.

In such a proto-galaxy, the same process will start afresh on a smaller scale, and the condensations will now be the proto-stars. The next step should be the formation of planets in the gaseous system doomed to become a star, and the last step might be the formation of the satellite systems.

The formation of the star from the gaseous rotating system will be accompanied by the dissipation of the system. The rotation is due to the whirling movement of the matter, and we may expect the linear velocities at the outskirts of the system to be of the order of magnitude of the turbulent velocities. Due to the concentration of matter in the centre, the outer parts will try to move with velocities given by Kepler's third law. This means that different parts of the system will move with different velocities and viscous stresses will result. These forces try to accelerate the outer parts and decelerate the inner parts of the system in an attempt to bring about a uniform rotation like that of a rigid body. Also these viscous forces entail a loss of energy. So we have a situation where there is at the same time a dissipation of energy and a transfer of angular momentum from the inside to the outside of the system. Von Weizsäcker assumes that these two processes are possible because mass with higher than average angular momentum disappears into interstellar space while at the same time the rest of the mass with low angular momentum will become concentrated in the centre of the system thus providing us with the necessary energy. In this way we get a slowly rotating central

mass (the star) surrounded by a faster rotating surrounding gaseous cloud. This implies that although in the initial stages the rotational velocities in the centre were much higher than at the outskirts the second stage presents us with a slowly rotating star and a faster rotating gaseous cloud. As soon as the density in the cloud is below a certain limit the rotational velocities in the cloud will be determined by the central mass and follow the third Keplerian law.

The equilibrium shape of such a rotating gaseous cloud will be a lens shape or disc. In this disc there will still be turbulence. However, it is still the question whether the configuration of vortices will really be as regular as the one given by von Weizsäcker.

Accompanying the disappearance of the solar gaseous envelope, condensation will take place in it. There will be many centres of condensation and during the lifetime of the disc these condensations will grow to become as large as the present planets. Together with their formation the planets will become surrounded by extended atmospheres. The evolution of these atmospheres will probably be analogous to the evolution of the solar envelope. In this way we have a mechanism for the formation of the satellite systems.

Now, the question discussed in the present paper is in how far this qualitative scheme may account for the various properties of the solar system. Before starting to discuss the various aspects of the problem quantitatively we shall give a brief survey of the contents of the following chapters.

In Chapter II we shall first of all discuss the shape of the solar gaseous envelope. We shall try to take into account the dissipation of the disc by assuming this disc shape to vary slowly. After that we shall discuss the various physical properties of this disc. The most important property is the temperature in the disc since the temperature is important in determining the shape of the disc. First, it is shewn that ionization in the disc is negligible. As was first shewn by Eddington (19), ionization by stellar (or solar) radiation will result in a much higher temperature of the gaseous system because the electrons will leave the atom with kinetic energies corresponding to the surface temperature of the star. These high velocity electrons will, by interactions with the gas

atoms, set up a high temperature. Then, we have to calculate the optical depth of the disc in order to determine whether much radiation energy is captured in the disc. This, however, appears not to be the case. After that, we can determine the temperature in the disc. This temperature ranges from 75°K in the neighbourhood of Neptune, to 700°K in the vicinity of Mercury.

Next, it is shewn that the radiation density will be approximately a diluted Planck radiation, that radiation pressure can be neglected, and that there will be no appreciable separation of elements, due to either gravitational separation, thermal difffusion, or other sources. Finally, we compute the densities of various molecules in the disc.

In this way, we have a more or less definite physical picture of the disc.

In Chapter III we shall discuss the hydrodynamical aspects of a gaseous disc in general.

We shall try to estimate the lifetime of the disc, and the transfer of angular momentum, not necessarily due to a flow of matter, from the central body to the disc during the lifetime of the disc. We shall also discuss the question whether it is possible to explain the Titius-Bode law.

In Chapter IV the condensation process is discussed. This discussion will resemble very closely the discussion of HOYLE (14) or VON WEIZSÄCKER (10) but some new features will be revealed. We shall discuss the three stages in the condensation process. These are the formation of condensation nuclei, the growth of these nuclei, and finally the stage of rapid gravitational capture.

In Chapter V we shall apply the results of Chapters II to IV to the solar envelope. We shall see that we are now able to explain the differences between the outer and the inner planets as far as mass and density are concerned.

In Chapter VI we shall discuss the satellite systems and the rotations of the planets. It will be seen that we can divide the satellites into two groups which we shall call the "regular" and the "irregular" satellites. It is proposed that the "regular" satellites are formed out of the planetary envelopes. The "irregular" satellites, however, are supposedly captured by the planets.

If we now compare the results of the present paper with the requirements of a successful theory discussed in the introduction

we see that we have been able to explain some hitherto unexplained points of the group C, and, possibly, shed some light on the difficulties connected with the explanation of B and D.

We have been able to account for the fact that the planets fall into two definite groups (C) by looking carefully into the condensation process.

Although the Titius-Bode law (B) has still to remain unexplained there seem to be indications that a thorough investigation of the hydrodynamical problems connected with the evolution of gaseous systems, such as we have studied here, might give a clue to this property of the solar system.

A regular system of vortices would at the same time give us an easy explanation of the circular orbits. The direct rotation of all the planets in one plane follows immediately from the fact that the condensation takes place in a rotating disc.

The present distribution of the angular momentum (D) still cannot be explained but some indications are given as to the direction in which the solution might possibly be found.

We have not discussed at all the way in which the sun should have been formed from an original nebula. This formation may have an important bearing on the explanation of the present distribution of the angular momentum but falls outside the scope of the present paper.

Altogether, the present paper gives a program for future investigations of many points rather than a complete solution.

Chapter II.

Physical Properties of the Solar Envelope.

We shall consider here a gaseous system in the centre of which the sun is situated. The radiation of the sun is assumed to be the radiation of a black body of 6000°K. The dimensions of the sun are supposed to be the same as at present ($r_0 = 7.10^{10}$ cm). The constitution of the envelope will be assumed to be about the same as the constitution of the sun, i. e., mainly hydrogen and helium, corresponding to a mean molecular weight of about 3.

A. Shape of the envelope. In this section we shall follow VON WEIZSÄCKER (10) with a few alterations. We shall start from the equations of motion:

$$\text{grad } U + \frac{1}{\varrho} \text{ grad } p - \omega^2 \vec{s} = 0, \tag{2.1}$$

where U is the gravitational potential energy, ϱ the density of the gas, p its pressure, and ω its angular velocity. Finally, $\vec{s}$ is the vectorial distance from the rotational axis (z-axis).

We take for U:

$$U = -\frac{\gamma M_0}{r}, \tag{2.2}$$

where γ is the gravitational constant, M_0 the solar mass (we neglect the gravitational action of the gaseous envelope), and r the distance from the centre of the sun.

For the pressure we use the ideal gas law:

$$p = \varrho RT, \tag{2.3}$$

where R is the gas constant per gr., and T the absolute temperature.

For this temperature we shall use:

$$T = a \cdot r^{-\frac{1}{2}}, \tag{2.4}$$

which follows if the temperature is determined by an equilibrium between the absorbed solar radiation, and emitted black body radiation by the gas. In the next sections of this chapter we shall derive this formula for the temperature.

Combining equations (2.3) and (2.4), we have

$$p = b \varrho r^{-\frac{1}{2}}. \tag{2.5}$$

Normalizing b so that $T = 6000°$ for $r = 7.10^{10}$ cm (solar radius), we get: $b = 4.10^{16}\,\mathrm{cm}^{\frac{5}{2}}\,\mathrm{sec}^{-2}$. [1]

Introducing:

$$b \log \frac{\varrho}{\varrho_0} = \sigma, \tag{2.6}$$

where ϱ_0 is an arbitrary constant, and writing equation (2.1) out in the two directions parallel and perpendicular to the rotational axis, we have

$$\frac{\partial \varrho}{\partial z} = \left(-\frac{\gamma M_0}{r^3} + \frac{b}{2 r^{\frac{5}{2}}} \right) r^{\frac{1}{2}} z, \tag{2.7}$$

$$\frac{\partial \sigma}{\partial s} = \left(\omega^2 - \frac{\gamma M_0}{r^3} + \frac{b}{2 r^{\frac{5}{2}}} \right) r^{\frac{1}{2}} s. \tag{2.8}$$

Equation (2.7) can be solved, and gives us

$$\sigma = \frac{2 \gamma M_0}{r^{\frac{1}{2}}} + \frac{b}{2} \log r + \tau(s), \tag{2.9}$$

where τ is independent of z, and has to be solved from the following equation, obtained by substituting equation (2.9) into equation (2.8):

$$\frac{d\tau}{ds} = \omega^2 r^{\frac{1}{2}} s. \tag{2.10}$$

[1] Von Weizsäcker's normalization giving 300° K. for $r = 10^{13}$ cm (mean distance of Venus from the sun) is derived from the observational data about Venus' temperature. The surface temperature of Venus is, however, lower than the equilibrium temperature required here by a factor 1.4 because of the fact that the sun can only heat up that part of the surface which faces the sun.

Since τ is independent of z we have for the case of equilibrium:

$$\omega^2 = f(s)\, r^{-\frac{1}{2}} = \mu^2 \frac{\gamma M_0}{s^3}\left(\frac{s}{r}\right)^{\frac{1}{2}}, \tag{2.11}$$

where μ is still a function of s.

Now, the pressure gradient is everywhere in the system small compared with the gravitational force (even for $r = 10^{15}$, the term with b in equation (2.8) is only about 1/200 of the gravitational term). It seems therefore to be permissible to neglect in equation (2.1) the term $\partial p/\partial s$, and determine ω from the equation:

$$\frac{\partial U}{\partial s} \approx \omega^2 s,$$

or

$$\omega^2 \approx \frac{\gamma M_0}{r^3}, \tag{2.12}$$

which corresponds to Kepler's third law.

We might try to take into account the dissipation of the disc, which will result in a steep density gradient, and therefore a steep pressure gradient. (Von Weizsäcker here introduces an artificial boundary.) One way of introducing this is by putting

$$\mu^2 = 1 - a \cdot s, \tag{2.13}^1$$

where a may increase with time. As long as a^{-1} is large as compared with the dimensions of the solar system, equation (2.12) will approximately be valid in the equatorial plane of the sun.

Using equations (2.6), (2.9), (2.10), (2.11), and (2.13), we get for the density in the envelope:

$$\varrho = \varrho_0 \left(\frac{r}{r_0}\right)^{\frac{1}{2}} \cdot e^{\varkappa\left(\frac{1}{\sqrt{r}} - \frac{1}{\sqrt{s}}\right) - \varkappa a \sqrt{s}}, \tag{2.14}$$

where $\varkappa$ is given by

$$\varkappa = \frac{2\gamma M_0}{b} = 10^{10}\ \mathrm{cm}^{\frac{1}{2}}. \tag{2.15}$$

We see from equation (2.14) that the density falls off rapidly in directions perpendicular to the equatorial plane. If we take

[1] Any μ^2, decreasing with increasing s, will give a slowly decreasing density in the equatorial plane. Equation (2.13) is one of the simplest ways of introducing such a decreasing μ^2.

for the height of the disc the distance over which the density is decreased by a factor 2, we get for this height h:

$$\frac{h}{r} = 2\sqrt{\log 2} \cdot \left(\frac{r}{\varkappa^2}\right)^{\frac{1}{4}} \sim \frac{1}{30}. \qquad (2.16)^1$$

The density in the equatorial plane decreases because of the term with $\varkappa a \sqrt{s}$ in the exponential. Since $\varkappa^2$ is very large compared with the dimensions of the solar system, it is possible to find values of a such that $\varkappa a \sqrt{s}$ is large as compared with one, and still a^{-1} large as compared with the dimensions of the solar system. In this way, we should have an appreciable decrease in density in the equatorial plane, thus getting for the shape of our envelope a lens shape.

The density in the equatorial plane can be written in the form:

$$\varrho = \varrho_m \left(\frac{s}{s_m}\right)^{\frac{1}{2}} e^{1-\left(\frac{s}{s_m}\right)^{\frac{1}{2}}} \qquad (2.17)$$

where ϱ_m is the maximum density in the disc, and s_m the distance from the sun where that maximum density is attained. We find s_m from:

$$s_m = (\varkappa a)^{-2}. \qquad (2.18)$$

The advantage of the density function given by equation (2.14) over the one given by von Weizsäcker lies in the fact that it is now no longer necessary to introduce an artificial boundary as was done by von Weizsäcker.

In using equation (2.17), we shall often assume:

$$\varrho_m = 2.10^{16} \text{ atoms per cm}^3; \; s_m = 1{,}6.10^{12} \text{ cm}, \qquad (2.19)$$

corresponding to a total mass of the system of about one tenth of the solar mass. The value of s_m is taken so that we can expect a maximum planetary mass in the approximate neighbourhood of Jupiter (cf. Chapter V, Section B).

B. Degree of ionization. There are two possible causes for ionization, viz., the solar radiation or the collisions between the atoms. In order to get an idea about the degree of ionization due

[1] Strictly speaking h/r depends on r but only as $r^{1/4}$. The value given in equation (2.16) is an average value for the disc.

to the solar radiation, we may suppose for a moment that we have to deal with a spherical gaseous envelope with a density of about 10^{16} hydrogen atoms per cm^3. This certainly will give us an upper limit since there is a possibility of the loss of energy by oblique emission from the disc which possibility is not present in the case of a sphere.

Using STRÖMGREN's equation (20):

$$^{10}\log S_0 = -0.44 - 4.51\,\theta + \frac{1}{2}\,^{10}\log T + \frac{2}{3}\,^{10}\log R - \frac{2}{3}\,^{10}\log N, \quad (2.20)$$

where S_0: radius of the sphere containing the H II region (i. e., the region where the hydrogen is ionized), in parsecs (1 pc = 3.10^{18} cm);

R: radius of the central star, in solar radii;

T: temperature of the central star;

θ: $\frac{5040^\circ}{T}$;

N: number of hydrogen atoms per cm^3.

Using $T = 6000^\circ$, $N = 10^{16}\,cm^{-3}$, we get from equation (2.20):

$$S_0 = 3.10^5 \text{ cm},$$

which is even far less than the solar radius. This means, of course, that we may safely assume all the hydrogen in the disc to be neutral. Since the ionization potentials of oxygen and nitrogen are larger than that of hydrogen they will also be neutral.

The next element is carbon. We then have the equation:

$$\left.\begin{aligned} ^{10}\log S_0 = -6.17 - \frac{1}{3}\,^{10}\log a - \frac{1}{3}\,\theta\chi + \frac{1}{2}\,^{10}\log T + \\ + \frac{2}{3}\,^{10}\log R - \frac{2}{3}\,^{10}\log N, \end{aligned}\right\} \quad (2.21)$$

where a is the absorption coefficient at the absorption edge, and χ the ionizational potential. Using $a_C = a_H\,(\chi_H/\chi_C)^3 = 10^{-17}\,cm^2$ (cf. (21)), $\chi = 11{,}22$ ev, we get:

$$S_0 = 10^8 \text{ cm}.$$

We shall finally investigate Mg, Na, K. Their abundance and ionization potentials decrease in this order. Using again equation

(2.21), we get the following table, where for the absorption coefficients of Na and K we use the values given by RUDKJÖBING (21) and LAWRENCE and EDLEFSEN (22), and for Mg:

$$a_{Mg} = a_{Na}(\chi_{Na}/\chi_{Mg})^3:$$

Table 2. I.

	Mg	Na	K
Abundance relative to hydrogen	3.10^{-5}	3.10^{-6}	10^{-6}
Absolute abundance	3.10^{11}	3.10^{10}	10^{10}
Ionization potential in electrovolts	7.61	5,12	4,32
a in cm^2	5.10^{-20}	$1{,}6.10^{-19}$	3.10^{-20}
S_0 in cm	7.10^{10}	3.10^{12}	7.10^{12}

We see that the only element which might be ionized would be potassium. We have not, however, taken into account that the effect of recombination processes leading to excited states, followed practically always by cascading to the ground state, will decrease the degree of ionization as pointed out by STRÖMGREN (20). Furthermore, the fact that the radiation emitted after the recombination can leave the disc obliquely also diminishes the degree of ionization.

One might be afraid that the radiation density in the ultraviolet might be higher than corresponding to a black body radiation of 6000°. Recent V-2 rocket experiments (23) show, however, that the radiation density in the ultraviolet follows a black body radiation of 3800° more closely than one of 6000°.[1] This factor also shows that we have overestimated the degree of ionization. Using equation (2.21) with T = 3800°, we get for K for instance:

$$S_0 = 10^{12} \text{ cm},$$

which is far less than the mean distance of Mercury from the sun.

Altogether, it seems safe to conclude that the ionization due to the solar radiation is certainly absent in the region of the major planets and almost certain also in the region of the inner planets.

The next step is to investigate the degree of ionization due to collisions between the atoms, i. e., the ionization equilibrium of

[1] This may no longer be true in the far ultraviolet.

the different elements at temperatures ranging from 700° K to 75° K. We use the normal Saha equation:

$$\frac{n_{A^+} n_{el}}{n_A} = q \left(\frac{2\pi\, mkT}{h^2} \right)^{\frac{3}{2}} e^{-\chi / kT}, \qquad (2.22)$$

where q is a weight factor, m the electron mass, A^+ the ion, and A the neutral atom.

Even for potassium (low density, low ionization potential), at 700° K (highest temperature), only one atom in 10^{10} is ionized. Hence, we can safely conclude that this source of ionization can also be neglected.

Since the solar radiation is unable to ionize even potassium, we may safely assume that the highly diluted radiation from other stars is also unable to produce any appreciable amouni of ionization except, perhaps, in a very thin boundary layer.

C. Optical depth; temperature of the disc. If the intensity of the radiation passing through matter is decreased by a factor $e^{-\tau}$, τ is called the optical depth of this matter. It is difficult to estimate accurately the optical depth of the disc since we ought to take into account the fact that the scattered radiation can leave the disc obliquely so that the radiation has not to pass all the mass before leaving the system.

We may, perhaps, obtain an estimate by smoothing out all matter in the disc over a sphere around the sun with the same linear dimensions as the disc. We obtain an upper and lower limit for this optical depth by considering two cases, viz. either a density varying according to equation (2.17), or a constant density.

The selective absorption starts at 4.3 eV (ionization potential of K) and the maximum intensity of the solar radiation occurs for 2.6 eV. Therefore, we may treat the scattering as Rayleigh scattering on H atoms.

The total optical depth τ is given by:

$$\tau = \int \delta\, \varrho(r)\, dr, \qquad (2.23)$$

where δ is the cross section for Rayleigh scattering ($\delta = 10^{-27}\,\mathrm{cm}^2$), and $\varrho(r)$ is the number of hydrogen atoms per cm^3.

The lower limit is obtained by putting $\varrho\ (r)$ as constant. This density will be about 3.10^{10} cm^{-3} for a total mass in the disc of about 0.1 M_0. Then we get:

$$\tau = \delta\, l\, \varrho \simeq 0.03,$$

where l is the total path ($l \sim 10^{15}$ cm).

For the upper limit we use equation (2.17) for the density, with $\varrho_m \sim 10^{14}$, corresponding to a smoothing out of the total mass over the sphere. We then get:

$$\tau \sim 2.$$

The actual τ, giving us an estimate of the total scattering of light in the disc, will probably be somewhat smaller than unity, which means that the disc is rather transparent and that we may assume that the energy which a gas volume receives from the sun will be proportional to the inverse square of the distance from the sun.

We can then calculate the temperature in the way already indicated in Section A. The sun is considered to be the only source of energy. Equilibrium reigns if every gas volume in the disc emits as much energy as it absorbs. If temperature equilibrium should exist, the total energy emitted by a gas volume would be proportional to T^4 (Stefan-Boltzmann's law), which should still be valid for a H and He atmosphere because of the principle of detailed balancing. Since the energy received from the sun will be proportional to r^{-2}, we have:

$$T = a \cdot r^{-\frac{1}{2}}. \qquad (2.4)$$

Normalizing T to 6000° for $r = 7.10^{10}$ cm (solar radius), we get the following table for the temperatures of the cloud at the present position of the planets:

Table 2. II.

Mercury	Venus	Earth	Mars	Jupiter	Saturn	Uranus	Neptune
650°K	480°K	400°K	330°K	170°K	130°K	90°K	75°K

These temperatures may be lower limits in the neighbourhood of the inner planets (ionization of potassium giving rise to high

energy electrons), while the temperatures in the regions of the outer planets may be regarded as upper limits since there will be a decrease in the intensity of solar radiation due to the Rayleigh scattering. This might perhaps give rise to a factor two, Table 2. II giving too high values[1].

D. Radiative conditions: seperation of elements. If we could completely neglect absorption in the disc, the radiation would be a diluted black body radiation, in as far as we may treat the solar radiation as a black body radiation. This means the energy density corresponding to a certain frequency (or energy) is given by the well-known Planck formula multiplied by a factor g, the so-called dilution factor:

$$\varrho(\nu) = g \cdot \frac{8\pi h \nu^3}{c^3} \cdot \left(e^{\frac{h\nu}{kT}} - 1 \right)^{-1}.$$

The dilution factor g is given by

$$g = \left(\frac{r_0}{r} \right)^2, \tag{2.24}$$

where r_0 is the solar radius and r the distance from the sun.

However, there will be an appreciable absorption in the ultraviolet region ($h\nu > 4.32$ eV). For those wavelengths the dilution factor may well be as small as 10^{-12}—10^{-16}. In the rest of the spectrum, the dilution factor will probably be given by equation (2.24), perhaps with an additional factor of the order $^1/_2$ corresponding to the loss of scattered light (see Section C).

Since the disc is chiefly made up of hydrogen, and since Baade and Pauli (24) have shown that for hydrogen, at the surface of the sun, the radiation pressure is negligible as compared with the gravitational force, we may safely neglect the radiation pressure, the more so since the radiation pressure will presumably decrease more rapidly (due to the absorption) than the gravitational force. If there were no absorption both would decrease as the inverse square of the distance from the sun.

In the next chapter we shall see that all particles are part of

[1] Dr. L. Spitzer has kindly pointed out to me that the opacity of the disc might be larger than calculated in the beginning of this section, due to the absorption and scattering by small solid particles.

the turbulent motion in the disc so that it is difficult to imagine a process separating the different elements. The gravitational separation discussed by EDDINGTON (25), e. g., will not take place since the centrifugal potential will balance the gravitational potential (cf., e. g., equation (2.12)). Other effects such as thermal diffusion, are very small and, as remarked before, will probably be annihilated by turbulence. Even if this should not be the case, it can be shown that this should only slightly affect the ratio of the heavier elements to hydrogen, and since anyhow hydrogen is the main element and the ratios in question uncertain, it seems that we may neglect all separation effects.

E. Molecular densities. As the last feature in the disc, we want to give a list of approximate densities of various compounds in the disc. Of course these densities vary from point to point, due to the different pressure and temperature, but in order to get a picture, we may take a density of the hydrogen of 10^{16} at cm^{-3} and a temperature of a few hundred degrees Kelvin.

We are far removed from an equilibrium situation, since the temperature of the radiation is different from the temperature in the disc and the radiation is diluted. It seems therefore dangerous to use the (quasi) equilibrium formulae of either SWINGS and ROSENFELD (26) or ROSSELAND (27). We have instead to look into the different possible processes, as was done for the interstellar space by KRAMERS and the present author (28)[1].

As an example we may discuss the case of CH and use the same considerations as in BAN 371. The numerical constants are, however, different. We now have: $T_g \sim 400°$, $T_{\text{rad}} \sim 6000°$, g as given in Section D. (We shall use the same notation as in BAN 371 and refer to that paper for this notation).

The first processes which are of interest are the radiation captures (processes α and η). The number of these processes is given by

$$N_\alpha = Q_{\text{rad}}\, \varrho_C \varrho_H, \quad N_\eta = Q'_{\text{rad}}\, \varrho_C \varrho_H, \tag{2.25}$$

where Q_{rad} is given by

$$Q_{\text{rad}} = 4\pi f \int_0^\infty A(r)\, r^2\, e^{-\frac{U(r)}{kT}} \left[F\left(\sqrt{-\frac{U'(r)}{kT}} \right) - F\left(\sqrt{-\frac{U(r)}{kT}} \right) \right] dr, \tag{2.26}$$

[1] We quote this paper in the following as BAN 371.

where

$$F(x) = \frac{4}{\sqrt{\pi}} \int_0^x e^{-x^2} x^2 \, dx. \tag{2.27}$$

$U(r)$ and $U'(r)$ are the potential energy curves of the molecule in the two electronic states between which the radiative transition can take place ($U(r)$ is an excited state and $U'(r)$ the ground state). The transition probability at a certain distance r is given by $A(r)$ and f is the probability that the upper state is realized when the two atoms meet.

In the case in which we are interested, the temperatures are so low that we can replace $F(x)$ by

$$F(x) = 1 - \frac{2}{\sqrt{\pi}} x \cdot e^{-x^2}, \tag{2.28}$$

and since $U'(r)/kT \ll U(r)/kT < 0$, we can write with fair accuracy instead of equation (2.26):

$$Q_{\text{rad}} = \frac{4\pi f}{\sqrt{kT}} \int_0^\infty A(r) \, r^2 \sqrt{-U(r)} \, dr. \tag{2.29}$$

We see that for low temperatures Q_{rad} is inversely proportional to the square root of the temperature since the integral is independent of T.

In the case of CH, we get from equation (2.29) by numerical integration for $T = 400°$:

$$Q_{\text{rad}} \simeq 2.10^{-17} \text{ cm}^3 \text{ sec}^{-1}. \tag{2.30}$$

For CN, numerical integration gives us:

$$Q_{\text{rad}} \simeq 10^{-17} \text{ cm}^3 \text{ sec}^{-1}. \tag{2.31}$$

We have assumed that three body collisions can be neglected as a means for the formation of molecules. For a density of 10^{16} hydrogen atoms per cm^3, we get for the Q corresponding to that process:

$$Q \sim 10^{-18} \text{ cm}^3 \text{ sec}^{-1}. \tag{2.32}$$

For the rate of formation of those molecules which cannot

be formed through a radiation capture accompanied by an electronic transition, we can use equation (2.32).

Larger molecules will be assumed to be formed by radiation capture, and we shall use for the capture cross sections (cf. BAN 371):

$$Q_{3\text{-}at}\ 10^{-16}\ \mathrm{cm^3\ sec^{-1}};\quad Q_{n\text{-}at} = 10^{-19+n}\ \mathrm{cm^3\ sec^{-1}}. \qquad (2.33)$$

For the processes involved in the CH equilibrium, we get the following table (we refer to BAN 371 for the meaning of the various processes):

Table 2. III.

$N_\alpha = 4.10^{-17}\ \varrho_{C^+}\ \varrho_H$;	$N_\beta = 2.10^{-12}\ \varrho_{el}\ \varrho_{CH^+}$;	N_γ = negligible
N_δ = negligible ;	N_ε = negligible ;	$N_\zeta = 2.10^{-13}\ \varrho_{el}\ \varrho_{CH^+}$
$N_\eta = 2.10^{-17}\ \varrho_C\ \varrho_H$;	$N_\vartheta = 10^{-16}\ \varrho_H\ \varrho_{CH}$;	$N_{\vartheta'} = 10^{-16}\ \varrho_H\ \varrho_{CH^+}$

(We have taken here $T = 100°$ K.)

Since $\varrho_{el} \sim \varrho_{C^+} \sim 0$, we see that the only processes of any importance are η and ϑ (i. e., radiation captures leading to CH, resp. CH_2), for the determination of ϱ_{CH}. The concentration of CH^+ will be negligible.

By equalizing N_η and N_ϑ we finally get:

$$\varrho_{CH} \sim 2.10^{14}\ \mathrm{cm^{-3}}.$$

For a few other compounds we get the following densities, using the above values for the formation cross sections. We want to stress that all values in Table 2. IV are very uncertain and may well be higher or lower by a few powers of ten.

Table 2. IV.

H_2 : 10^{15} cm^{-3}	CH : 2.10^{14} cm^{-3}	CH_4 : 2.10^{13} cm^{-3}	C_4H_{10} : 2.10^{10}
H_2O : 10^{12}	CN : 10^{11}	NH_3: 10^{13}	O_2 : 10^{10}
HCN : 10^{10}	CO_2 : 10^7	C_2 : 10^{10}	SiC : 10^8
BaO : 10^5	SO_2 : 2.10^4	CO : 10^{10}	NO : 10^{10}

Chapter III.

Hydrodynamical Properties of a Gaseous Disc.

In this chapter, we shall be interested in the evolution of a gaseous disc in the centre of which a large mass is concentrated. We saw in Chapter II, Section A, that the angular velocities in the disc follow Kepler's third law closely. We shall assume that we may use equation (2.12) for the velocities in the disc.

We shall treat the problem as a two dimensional problem, i. e., we shall neglect all effects in directions perpendicular to the plane of the disc. For the height of the disc we shall assume:

$$h = ar, \quad a \sim 1/15 \tag{3.1}$$

in accordance with equation (2.16).

The density in the disc may be given by equation (2.17). We shall here use ϱ measured in g cm^{-3}.

In the disc we have a velocity gradient and an energy gradient. The energy content per unit mass is given by:

$$\varepsilon = -\frac{\gamma M_0}{2r}, \tag{3.2}$$

giving the energy of matter, moving in a Keplerian orbit round a mass M_0 at a distance r. The kinetic energy $\left(\frac{3}{2}\frac{\varrho}{m}kT\right)$ may be neglected with respect to ε, given by equation (3.2).

In Chapter I we saw that due to the velocity gradient in the disc viscous stresses will be set up which together with the escape of matter at the boundaries in the course of time may bring about a profound transformation of the disc. This transformation of the disc is accompanied by three phenomena, viz.,

a loss of mechanical energy, a flow of matter from the disc, partly to the sun in the centre and partly to interstellar space, and finally a transfer of angular momentum in outward direction. In this chapter we shall try to estimate the rate at which the various processes take place.

A. Dissipation of energy. We can use here the formula given for instance by LAMB (29) for the dissipation of mechanical energy due to viscous forces. We have the equation:

$$\delta E = \int \eta \, s^2 \left(\frac{d\omega}{ds}\right)^2 dx \, dy \, dz,$$

where η is the viscosity coefficient and where we have assumed that the velocity is everywhere in the plane of the disc and perpendicular to the radius vector. The angular velocity will still depend on the distance from the sun in the way given by equation (2.12).

If we now consider a ring of height h, radius s, and thickness ds, we see that the total loss of energy per sec in that ring is given by:

$$\delta E = 2\pi h s^3 \eta \left(\frac{d\omega}{ds}\right)^2 ds, \tag{3.3}$$

and the total loss of energy in the disc is given by:

$$\frac{dE}{dt} = \int_{r_0}^{s_0} \delta E = \frac{9}{2} \pi \alpha \eta \gamma M_0 \log \frac{s_0}{r_0}, \tag{3.4}$$

where r_0 is the solar radius, s_0 the radius of the disc, and where we have supposed η to be constant throughout the disc.

In the case of laminar motion, η is the normal viscosity coefficient, but in the case where the motion is turbulent, we can still use the above equations. The quantity η is then, however, defined by the equation:

$$\eta \simeq \frac{1}{3} \varrho \, v \lambda, \tag{3.5}$$

where λ is the mean free path or the so-called "mixing length".

B. Lifetime of the disc. We see that we have a steady loss of mechanical energy in the disc. The energy for this dissipation

process is provided by matter falling towards the centre and so gaining gravitational energy.

We can estimate the total amount of energy available by assuming that a fraction β of each volume element in the disc falls onto the central body and that the rest of the mass disappears into space. In section D we shall see that β is given by:

$$\beta = r_0/s. \tag{3.6}$$

For the total energy available, we now get, using equations (3.2) and (3.6):

$$E_0 = -\int \varrho \frac{\gamma M_0}{2s} 2\pi s h ds + \int \varrho \beta(s) \frac{\gamma M_0}{r_0} 2\pi s h ds$$

$$\simeq \int_{r_0}^{s_0} \varrho \frac{\gamma M_0}{2s} 2\pi s h ds = \frac{\gamma M_0 M}{60 s_m},$$

where M is the total mass in the disc and s_m the distance at which the maximum density in the disc occurs.

The lifetime of the disc, τ, will now be determined by dividing E_0 by dE/dt of equation (3.4), and in this way we get:

$$\tau^{-1} = 90\pi\alpha \frac{\varrho v \lambda s_m}{M} \log \frac{s_0}{r_0}. \tag{3.7}$$

The derivation of equation (3.6) is very tentative. Thus β might easily be larger, giving rise to an estimate of τ larger than that given by equation (3.7) by, say, a factor 10 or 100.

C. Transfer of angular momentum. Due to the velocity gradient there will be a transport of momentum through any area perpendicular to the radius vector. This transport of momentum will be accompanied by a transport of angular momentum and energy. Those three quantities are given by:

$$\delta P = s\eta \frac{d\omega}{ds}, \quad \delta\theta = -s^2\eta \frac{d\omega}{ds}, \quad \delta E = -s^2\omega\eta \frac{d\omega}{ds}. \tag{3.8}$$

The total transport of angular momentum per sec through a cylinder of height h and radius s will be given by:

$$\frac{d\theta}{dt} = -2\pi h s^3 \eta \frac{d\omega}{ds} = 3\pi\alpha\eta s^{\frac{3}{2}} \sqrt{\gamma M_0}. \tag{3.9}$$

We are especially interested in the angular momentum transferred from the central body during the lifetime of the disc. If in equation (3.9) we put s equal to r_0, we get the transfer of angular momentum per sec in a situation where the velocities are perpendicular to the radius vector and given by equation (2.12). As soon as the central body is slowed down, the velocity pattern in the neighbourhood of the central body will become changed and it is difficult to predict exactly what will happen.

In order to get an idea of the magnitude of the transfer, we might compare $d\theta/dt$ for $s = r_0$ with θ_0/τ, where θ_0 is the angular momentum of the central body in the case where its angular velocity corresponds to Kepler's third law:

$$\frac{\tau \dfrac{d\theta_0}{dt}}{\theta_0} \sim \frac{0.0003\, M}{M_0}, \tag{3.10}$$

where we have used $s_0/r_0 \sim 10^4$, and $\theta_0 = \dfrac{\omega_0 M_0 r_0^2}{5} = \dfrac{1}{5} M_0 \sqrt{r_0 \gamma M_0}$.

Although the above-mentioned phenomenon of transfer of angular momentum will slow down the solar rotation, it is clear at first sight from (3.10) that this can hardly account for the present slow rotation (present $\theta \sim 0.005\ \theta_0$).

The present slow rotation of the sun has perhaps to be explained by an investigation of the earlier steps in the process leading to the formation of the sun. This investigation, however, falls outside the scope of the present paper.

D. Estimation of the increase of the solar mass during the dissipation process. Before discussing the possibility of a regular system of vortices, we wish to look into the question of the dissipation of the disc. We shall try to estimate the quantity $\beta(s)$, i. e., the fraction of the mass which will fall onto the sun. In order to calculate this rigorously one should have to solve the hydrodynamical equations, preferably with the terms involving the viscosity. Also, one should have to consider a velocity component different from zero in the direction of the radius vector. These calculations should give us at the same time the transfer of angular momentum and, perhaps, the formation of a regular system of vortices.

However, we can try to get a first estimate of the magnitude of β in the following way.

If we consider a cylindrical ring with height h, between the radii s and $s + ds$, this ring will lose per sec angular momentum at the rate:

$$\delta\theta = \frac{d}{ds}\left(2\pi hs^3 \eta \frac{d\omega}{ds}\right) ds = \frac{9}{2}\pi a\eta \sqrt{\gamma M_0 s}\, ds.$$

The total angular momentum of the ring is given by:

$$\theta = 2\pi hs^3 \varrho\omega\, ds = 2\pi a\varrho \sqrt{\gamma M_0 s^5}\, ds.$$

If a kind of over all equilibrium in the disc should reign, this loss of angular momentum would correspond to a loss of mass given by:

$$\frac{\delta m}{m} = \frac{\delta\theta}{\theta},$$

where m is the mass of the ring, and given by:

$$m = 2\pi hs\varrho\, ds.$$

The energy loss per sec is given by equation (3.3):

$$\delta E_1 = 2\pi hs^3 \eta \left(\frac{d\omega}{ds}\right)^2 ds = \frac{9}{2}\pi a\eta \frac{\gamma M_0}{s} ds, \qquad (3.3)$$

and if a fraction β of the original mass of the ring falls onto the sun, this loss of energy is compensated by the gain of energy by this matter, again assuming a quasi equilibrium situation throughout the disc:

$$\delta E_2 = \beta\, \delta m \frac{\gamma M_0}{r_0} = \beta \frac{\delta\theta}{\theta} m \frac{\gamma M_0}{r_0}. \qquad (3.11)$$

Putting $\delta E_1 = \delta E_2$ we can determine β, and in this way we get:

$$\beta(s) = r_0/s. \qquad (3.6)$$

The total mass which will fall onto the sun is now given by:

$$\beta M = \int_{r_0}^{s_0} 2\pi hs \varrho\beta(s)\, ds = \frac{r_0}{5 s_m} M. \qquad (3.12)$$

The reasoning in this section is only tentative. It would be desirable to complement it by a direct estimate of the amount of matter which escapes from the boundaries of the disc.

E. Possibility of regular systems of vortices. We saw that VON WEIZSÄCKER (10) introduced a regular system of vortices in his theory and that he was able in that way to explain the Titius-Bode law. In this section we should like to look very briefly into this question.

Of course one cannot use von Weizsäcker's treatment since the mean free path in the disc is far too small to allow for unperturbed Keplerian orbits. However, one might hope to be able to deduce from the hydrodynamical equations a similar set of rings of vortices.

The first important point is that, as we already saw in the previous chapter, gravitational forces are by far the most important. They are not only more important than the pressure gradient, but also than the viscous forces. (Reynold's number $(= \frac{\varrho v l}{\eta}$, where l is a length of the order of the dimensions of the system), which measures the ratio of the inertial forces to the viscous forces is very large in our disc). This might give rise to systems like the one pictured by von Weizsäcker (cf. p. 15).

The system which we consider is different from the common hydrodynamical systems because of the absence of a wall. But the fact that the mean free path increases with decreasing density may have the same effect as a wall. And also it might be that during the development of the gaseous system which will become a galaxy the other turbulence elements may have acted somewhat restrainingly on the whirl which would develop into the sun and the solar system. We are thus tempted to compare this with normal hydrodynamical systems although we are aware of the danger attached to this procedure. There are, however, some signs that this might not be as far from the actual truth as one might fear.

The idea is to assume for a moment that due to the preponderance of the gravitational force regular systems of vortices might be set up. Now, we can assume that the distance between two circles separating the various rings of vortices will be given by the mean size of the turbulence elements. In this way we might arrive at an estimate of the size of the turbulent elements in the solar envelope and in the planetary atmospheres from the differences of the observed mean distances of the successive planets (satellites) from the central body since these planets and satellites will probably have been formed on the circles separating the main vortices, as we shall see in the next chapter. In Table 3. I we have collected the data for the sun, Jupiter, Saturn, and Uranus, using only the data of the "regular" satellites (see Chapter VI). In the second row we have taken the observed planets and satellites only and in deriving the values for the last row we have assumed that due to some unknown reason there are gaps, corresponding in the series of the planets, e. g., to the asteroids. Finally, we assumed that the size of the turbulence elements is proportional to the distance from the primary:

$$l = a \cdot r, \tag{3.13}$$

and the values given in Table 3. I. are the mean values of a. If r_n is the mean distance of the n-th body from the centre, $l = r_n - r_{n-1}$, and $2r = r_n + r_{n-1}$.

Table 3. I.

	Sun	Jupiter	Saturn	Uranus
Mean value of a for "regular" satellites	0.56	0.56	0.42	0.36
Mean value of a with assumed gaps. The number of gaps is inserted between brackets	0.50 (1)	0.45 (1)	0.33 (2)	0.28 (1)

We may compare this with VON KÁRMÁN's formula (30) for the mean size of a turbulence element. This was first done by TUOMINEN (31), who shewed that the Titius-Bode law for the planets follows within a factor 2 from the size of vortices given

by equation (3.14). He did not, however, compare the planets with the satellites. We shall follow his argumentation here with a few alterations.

Von Kármán had remarked that for the cases which he investigates the mean size of the turbulence elements is given by:

$$l = k_0 \left| \frac{dv/ds}{d^2v/ds^2} \right|, \tag{3.14}$$

with a constant k_0 (~ 0.4). If the velocity is given by equation (2.12), we get for the size of the turbulence elements:

$$l \sim 0.27\, r. \tag{3.15}$$

If we now look at Table 3.I., we see one striking point, viz., that a is decreasing with decreasing mass of the primary, i. e., with decreasing influence of the gravitational force and that a approaches the value of equation (3.15). This might prove to be an important point in a discussion of the hydrodynamical properties of the disc and the planetary envelopes.

We want to point out a few more points connected with these regular systems of vortices.

The first is that the energy dissipation in such a regular system might be less than in the case of an irregular turbulent situation. In this way, we should get a longer lifetime than that corresponding to an energy loss, calculated under the assumption that we may use equations (3.4) and (3.5) with a λ equal to the dimensions of the vortices. This might amount to as much as a few powers of ten. There are also other indications that the lifetime of the disc might well have been much longer as we shall see in Chapter V. This might then also be an indication that regular systems of vortices have once been established. In order to bring about a regular series for the distances of the planets or satellites it is not necessary that the system remained the same during the whole lifetime of the disc. As was already shewn by von Weizsäcker it is only necessary that these regular systems lasted for about 10 years, which is of the order of magnitude of the period of rotation of the outer parts of the disc. In that period the condensation products become so large that they

can no longer be displaced appreciably by turbulence in the disc.

The second point is that we can easily calculate the velocities on the outskirts of the large vortices which will form the systems of vortices. These velocities will be the turbulent velocities, and we may take for those the mean fluctuations of the velocities in a gas kinetic system with a velocity gradient as was done also by PRANDTL (32) in a similar case.

If v is the mean velocity given by equation (2.12), we have for the turbulence velocity u:

$$u = \lambda \left| \frac{dv}{ds} \right|, \tag{3.16}$$

where λ should be the mixing length which is equal to the mean size of the vortices and given by equation (3.14).

We see that u decreases with increasing distance from the central body which means that if the large vortices are rotating themselves in a counter-clockwise direction the motion in these vortices will be clockwise.

Between the rings of large vortices there will be large viscous stresses along the circles separating the main vortices. We may therefore here expect secondary eddies like the "roller bearing" eddies of von Weizsäcker. Those "roller bearings" will again show direct (counter-clockwise) rotation. Since the planets will probably be formed in those "roller bearings", as we shall see in the next chapter, we are here presented with an explanation of their direct rotation. It is a tempting thought to assume that the size of the "roller bearings" will be determined by the fact that the velocities at the outside will be equal to the turbulent velocities given by equation (3.16). This would mean that we should be able to determine in that way the size of the planetary atmospheres since the velocities in these atmospheres are determined by Kepler's third law (cf. Chapter II, Section A). We may remark here that the considerations of this paragraph also remain valid if there should not be a regular system of large vortices.

Finally, we may remark that the size of the large vortices will

only on an average be proportional to the distance from the sun, i. e., that equation (3.13) will only approximately be fulfilled. We should therefore expect rather than be disappointed by the fact that the Titius-Bode law or similar laws for the satellite systems do not hold rigorously from planet to planet or from satellite to satellite.

Chapter IV.

The Condensation Process.

Condensation processes in astrophysics can be divided into two different phases. The first phase is the formation of nuclei on which the further condensation can easily take place. The second phase is this subsequent growth of the nuclei. These nuclei will grow in the beginning because impinging atoms or particles will stick to them, but later this growth will be much more rapid because of the possibility of gravitational capture,

A. Formation of nuclei for condensation. We shall use here a model given in an earlier paper (33), in the following quoted as BAN 361.

If we want to investigate the possibilities of condensation, it seems to be a fair approximation to treat the condensed particles as heteropolar crystals. We are interested in the condensation in a gas with density ϱ and kinetic energy corresponding to a temperature T_1, while the radiation density is assumed to be a diluted black body radiation with temperature T_2 and dilution factor g.

The first question to be investigated is the temperature of the condensed particles. We can find this temperature from the energy balance.

In as much as there are only slight deviations from harmonic binding between the atoms in the crystal, the particles will emit and absorb radiation practically as one large harmonic oscillator, and only the fundamental frequency contributes. If ω is the frequency of the oscillator and $kT \ll h\omega$, we have for the emitted and absorbed energy of the particle

$$E_{abs} = \frac{\pi\varepsilon^2}{M}\varrho(\omega), \quad E_{em} = \frac{8\pi^2 h\omega^3\varepsilon^2}{Mc^3}\cdot e^{-\frac{h\omega}{kT}}, \tag{4.1}$$

where M and ε are the mass and charge of the oscillator, and $\varrho(\omega)$ the radiation density. If the particle, which is assumed to be small compared with the wavelength of light considered, consists of i atoms, we have: $\varepsilon = i \cdot e$ (e is an effective charge), $M = i \cdot m$ (m: mass of one atom), $T = T_i$ (temperature of a particle consisting of i atoms), and $\omega = \omega_0$ (fundamental frequency).

On the other hand, we have energy conveyed to and from the particles by colliding atoms which do not stick to the surface. As was pointed out in BAN 361, these are mainly hydrogen atoms. The energies in question are given by:

$$E_{\text{on}} = c_1 \sigma \varrho v i^{\frac{2}{3}} k T_1, \quad E_{\text{off}} = c_2 \sigma \varrho v i^{\frac{2}{3}} k T_i, \tag{4.2}$$

where c_1 and c_2 are numerical constants of the order 1, σ the surface of one atom, v the mean velocity of the colliding atoms, and ϱ their density.

We have now the following equilibrium condition:

$$E_{\text{on}} + E_{\text{abs}} = E_{\text{off}} + E_{\text{em}} \tag{4.3}$$

or

$$A \varrho T_1 i^{\frac{2}{3}} + B g i \left(e^{\frac{h\omega_0}{kT_2}} - 1 \right)^{-1} = C \varrho T_i i^{\frac{2}{3}} + D i e^{-\frac{h\omega_0}{kT_i}}. \tag{4.4}$$

For given values of ϱ, T_1, T_2, and g, we can determine from equation (4.4) the temperatures of the particles, T_i.

Inserting numerical values, we have (cf. BAN 361):

$$\left.\begin{aligned} &A \sim C \sim 4.10^{-26} \text{ erg degree}^{-1} \text{ cm}^3; \\ &B \sim D \sim 2.10^{-13} \text{ erg}; \quad \frac{h\omega_0}{k} \sim 1400^\circ. \end{aligned}\right\} \tag{4.5}$$

In all cases, the term with A is large as compared with that with B, but according to whether the term with C is small or large as compared with that with D, we have the following two cases:

(α) $C \ll D$, which will be realized in interstellar space, where we have low gas densities and low radiation density.

(β) $C \gg D$, which will be realized in all other cases in astrophysics such as condensation in nova shells, condensation in the corona, or condensation in a gaseous disc such as we consider in the present paper.

In case α, equation (4.3) reduces to

$$E_{on} = E_{em},$$

or

$$T_i = \frac{a}{\log(bi)}. \tag{4.6}$$

In case β, equation (4.3) reduces to

$$E_{on} = E_{off},$$

or

$$T_i = T_1. \tag{4.7}$$

The formation of nuclei can now be calculated in the way first indicated by BECKER and DOERING (34).

The main feature of the condensation is that in order to get an appreciable precipitation it is necessary that the vapour pressure of large particles is less than the pressure in the gas because in that case there will be more atoms condensing on than evaporating from the particles.

In case β, which is also the normal case in chemistry (where we have $T_1 = T_2$, $g = 1$), the vapour pressure of the particles will decrease with increasing size due to the influence of surface free energy. Finally it reaches the value of the saturated pressure for infinite size at the temperature present. Thus, if this saturated vapour pressure is smaller than the pressure of the gas, we can expect condensation. This is the well-known phenomenon of precipitation (or condensation) in a supersaturated vapour.

In case α, the decrease of vapour pressure with increasing size is due to the decreasing temperature (cf. equation (4.6))[1]. There are two possibilities, viz. that the temperature is already low enough for particles consisting of only a few atoms in which case the rate of precipitation depends only on the rate of formation of molecules of, say, 10 atoms because smaller particles cannot be considered to behave like crystals. If we denote the rate of precipitation by j, we have:

$$j \sim K\varrho^n, \tag{4.8}$$

[1] This case has been extensively discussed in BAN 361. We only give the main results here, and refer the reader to BAN 361 for details.

where n lies between 2 and 10 and depends on the number of atoms for which the capture in the "crystal" is difficult; K is a numerical constant.

This possibility is realized for extremely low densities. In that case, the energy conveyed to the particles will be very small so that their temperature will be low enough to allow for an easy condensation.

For higher densities which are still so low that we are in case α, the temperature of the small particles will be higher than corresponding to a vapour pressure equal to the gas pressure. However, the temperatures of larger particles will be low enough. However, since the temperature of the particles increases with increasing density (cf. equations (4.4) and (4.6)), the critical size, i. e., the size for which the temperature corresponds exactly to a vapour pressure equal to the gas pressure, will increase with increasing density. The rate of precipitation will correspondingly decrease:

$$j \sim K \varrho^a e^{-b \varrho^s}. \tag{4.9}$$

The so-called characteristic density, i. e., the density at which the transition between the two above-mentioned possibilities occurs and which also marks a maximum in j, is much lower than the density marking the transition from α to β.

In case β there will only be appreciable condensation if there is a state of supersaturation, i. e., if the gas pressure is higher than the saturated vapour pressure.

The vapour pressure of a crystal is given by:

$$p_v = \frac{m^{\frac{3}{2}} (kT)^{\frac{5}{2}}}{h^3} e^{-\chi/kT}, \tag{4.10}$$

where m and χ are the mass and sublimation heat (in ergs) of an atom of the crystal. If the density of the gas is ϱ atoms per cm^3, its pressure is given by the ideal gas law

$$p_g = \varrho kT. \tag{4.11}$$

The necessary condition for condensation is now

$$p_g \geq p_v \text{ or } e^{\chi/kT} \geq \left(\frac{mkT}{h^2}\right)^{\frac{3}{2}} \cdot \frac{1}{\varrho}. \tag{4.12}$$

For a given temperature and density we have a critical sublimation heat χ determined by equation (4.12) with the equal sign. Compounds with a larger sublimation heat will condense, those with a smaller sublimation heat will not condense.

From equation (4.12) with the equal sign we can calculate χ for different values of T and ϱ, and we get the following table. We have given χ in eV and (between brackets) in Cal/mole.

Table 4. I.
Values of the critical sublimation heat.

ϱ	50°	100°	200°	400°	1000°	10000°
10^{10}	0.14	0.29	0.60	1.25	3.23	35
	(3.3)	(6.8)	(14)	(29)	(75)	(810)
10^{12}	0.12	0.25	0.53	1.09	2.84	31
	(2.8)	(5.8)	(12)	(25)	(65)	(720)
10^{14}	0.10	0.21	0.45	0.93	2.44	27
	(2.4)	(4.9)	(10)	(21)	(56)	(630)
10^{16}	0.08	0.17	0.37	0.77	2.04	23
	(1.9)	(4.0)	(8)	(18)	(47)	(540)

We see from Table 4. I, and equation (4.12) that χ depends only slightly on ϱ, but is mainly determined by T.

In the next table we have for comparison collected the sublimation heats (in Cal/mole) for a number of inorganic and organic substances, and also their specific densities, σ.

Table 4. II.

Compound	χ	σ	Compound	χ	σ	Compound	χ	σ
CO	1.9	0.9	HNO_3	8?	2?	Mg	34	1.7
CH_4	2.3	0.5	SO_2	8.5	2	Ba	41	3.5
NO	3.8	1.6	HCN	8.5	1?	Ca	43	1.5
N_2O	5.8	1.6	H_2O	11.3	0.9	BaO	90	5.7
C_2H_6	6?	0.9?	N_2O_4	12.6	2.0	Fe	97	7.9
CO_2	6.3	1.6	NO_2	13	1.5	C	125	3.5
C_4H_{10}	7?	0.9	SO_3	12—16	2.4	Si	large	2.3
NH_3	7.5	0.8	K	21.8	0.9	SiO_2	large	2.3
$(CN)_2$	7.8	1.4?	Na	26	1.0	SiC	large	3.2

Comparing Tables 4. I and 4. II, and remembering that the temperature in the corona or nova shells is at least a few thousand degrees, we may safely conclude that in those cases there will be no condensation. This does not, however, exclude the possibility of the presence of molecules (cf. (35)). We also see that it is necessary to have a temperature which is at most 1000° in order to have an appreciable condensation. This is another difficulty encountered by theories like the one proposed by HOYLE (14).

B. Second and final stages of the condensation. After the first stage, the formation of nuclei for condensation, there are two more stages. The second stage is the normal condensation where the particles grow because impinging molecules stick to them. The final stage is that of the gravitational capture.

We may draw attention here to the fact that as soon as there is a state of supersaturation the nuclei will be formed in sufficient number (34), so that it is not necessary to consider that stage of the condensation process in any more detail.

The second stage closely resembles the process proposed by LINDBLAD (36) for the formation of interstellar smoke particles. For the sake of simplicity we shall assume that the particles are spherical with radius r and specific density ϱ_0.

If the density of the matter impinging on the particle and sticking to it is denoted by ϱ_1, and their mean relative velocity by v_1, we have for the increase of mass per sec:

$$\frac{dm}{dt} = 4\pi r^2 \cdot \frac{v_1}{4} \varrho_1 . \tag{4.13}$$

Since

$$m = \frac{4}{3} \pi \varrho_0 r^3 , \tag{4.14}$$

we have

$$r(-r_0) = \frac{\varrho_1}{\varrho_0} \frac{v_1}{4} t. \tag{4.15}$$

This is correct as long as gravitational effects can be neglected. If, however, we have reached the last stage, we get a much faster growth[1].

We can introduce a distance R (by Chandrasekhar called the

[1] For an extensive discussion of this stage of the condensation, we may refer to a paper by EAKIN and MCCREA (37).

"gravitational radius") such that the gravitational energy of matter at that distance from the centre of the particle is equal to its kinetic energy:

$$R = \frac{2\gamma m}{v_2^2}, \tag{4.16}$$

where v_2 is the mean velocity of the matter in the system and m again the mass of the growing particle.

The cross section for gravitational capture is now $\pi\delta^2 R^2$, where δ is of the order of magnitude 0.1. For the growth of the particle we have now

$$\frac{dm}{dt} = 4\pi\delta^2 R^2 \frac{v_2}{4}\varrho_2, \tag{4.17}$$

or, using equation (4.16):

$$\frac{dr}{dt} = \beta r^4, \quad \beta = \frac{16\pi^2}{9}\delta^2\frac{\gamma^2\varrho_0\varrho_2}{v_2^3}, \tag{4.18}$$

with the solution:

$$r^3 = \frac{1}{3(\varepsilon - \beta t)},$$

where ε is an integration constant to be determined by $r = r_{\text{crit}}$ for $t = 0$. The quantity r_{crit} is the radius of a particle for which the gravitational cross section $\pi\delta^2 R^2$ equals the geometric cross section πr^2:

$$r_{\text{crit}}^2 = \frac{3v_2^2}{8\pi\gamma\delta\varrho_0}. \tag{4.20}$$

If there should be no exhaustion of the gas, the lumps would become infinitely large in a finite time, given by:

$$t_\infty = t_{\text{crit}} + \frac{\varepsilon}{\beta} = \frac{4}{3}t_{\text{crit}}, \tag{4.21}$$

where t_{crit} is the time necessary to reach dimensions of the order r_{crit}, and given by (cf. equation (4.15)):

$$t_{\text{crit}} = \frac{4\varrho_0}{\varrho_1 v_1}\cdot r_{crit} = \frac{v_2}{v_1\varrho_1}\left(\frac{6\varrho_0}{\pi\gamma\delta}\right)^{\frac{1}{2}}. \tag{4.22}$$

As we mentioned in the previous chapter, condensation is more likely to take place in the "roller bearings" than in the large vortices, as was first shewn by von Weizsäcker, whose reasoning we follow here in the form presented by CHANDRASEKHAR (10). This preference for the "roller bearings" is due to the fact that the mean free path for larger particles is greater than the size of the "roller bearings". The mean free path is in this case defined as the distance travelled through by the particle before its loss of momentum is of the same order of magnitude as its original momentum. This means that these particles will no longer be carried along by the "roller bearings" even though the large vortices are able to carry them along. Therefore the number of collisions between such particles and gas atoms or smaller condensation products will be enhanced in the "roller bearings".

The mean free path of a particle can be estimated in the following way. If ϱ_1 is the gas density, m the mass of the particle (for m we have equation (4.14)), r its radius and u_s its velocity relative to the medium, we have for the loss of momentum in an interval dt:

$$m du_s = -\pi r^2 \varrho_1 u_s^2 \, dt. \tag{4.23}$$

Using the definition of the mean free path, λ_p given above, we get for λ_p:

$$\lambda_p = \frac{m_s u_s}{\pi r^2 \varrho_1 u_s^2} \cdot u_s = \frac{4}{3} \frac{\varrho_0}{\varrho_1} r, \tag{4.24}$$

which gives us with $\varrho_0 = 3 \text{ g cm}^{-3}$, $\varrho_1 = 10^{-5} \text{ g cm}^{-3}$:

$$\lambda_p = 4.10^9 \, r. \tag{4.25}$$

As long as λ_p is smaller than the size of a vortex, this vortex will carry the particle along. We see that hence there will be a range of particle sizes such that the large vortices can carry them along, but such that the "roller bearings" can no longer carry them along. Therefore, the probability of finding a condensation product is largest at the "roller bearing" circles in the regular system of vortices—if such a system has ever existed. It has not been proved that only *one* planet is formed on each circle. We may, perhaps, be allowed, as far as that is concerned, to express an optimism similar to VON WEIZSÄCKER'S (10).

The time necessary to reach such dimensions that even the largest vortex is unable to move the particle essentially is found by combining equations (4.15) and (4.25).

As soon as the last stage, i. e. the stage of the gravitational capture, is attained, the bodies will collect an atmosphere around them. We can estimate the dimensions of these atmospheres in two different ways. Either in the way indicated at the end of the previous chapter, viz. that the velocities on the outskirts of the atmosphere should be equal to the turbulent velocities, or by using for the radius of the atmosphere the "gravitational radius". In formula we have, using equation (3.16) for the turbulent velocities and putting $a = {}^1/_2$ in equation (3.15),

$$R_1 = 16\, s \frac{M}{M_0} = 7.10^8\, m\bar{s} \tag{4.26}$$

or

$$R_2 = \frac{2\gamma M}{v_2^2} = 2\, s \frac{M}{M_0} = 10^8\, m\bar{s}, \tag{4.27}$$

where M and m are the planet's mass in grams and in the earth's mass as unit, and $\bar{s}$ its distance from the sun in astronomical units. For v_2 we have used again equation (2.12). We see that both equations, apart from a factor 8, give the same result. In the following chapters we shall use equation (4.26).

Chapter V.

The Planetary System.

In this and the next chapter we shall try to apply the results of the foregoing chapters to the solar system and the satellite systems of the major planets.

A. Densities of the planets. In Chapter II we saw that the temperature in the disc decreased with increasing distance from the sun. If we assume that the planets were formed at essentially those distances from the sun at which they are observed now, each planet corresponds to a certain temperature, as shewn in Table 2. II. According to the previous chapter, however, a given temperature corresponds to a certain critical sublimation heat given by equation (4.12). So we can assign to each planet a sublimation heat telling us which compounds will have taken part in the initial condensation process leading to dimensions of r_{crit} (see previous chapter). In Table 5. I we have given these sublimation heats. We have taken an average density of 10^{12} at· cm^{-3}. [1] Of course, we should for every compound calculate its density in the disc (cf. Chapter II, Section E) and investigate whether its sublimation heat is higher or lower than the critical sublimation heat for that density and the given temperature. So we should find for each temperature which compounds would

Table 5. I.

	Mercury	Venus	Earth	Mars	Jupiter	Saturn	Uranus	Neptune
T.....	650°	480°	400°	330°	170°	130°	90°	75°
χ in Cal/mole	42	30	25	20	10	8	5	4

[1] This corresponds to about 0.1 per cent. of the gas condensing, and an average density of 10^{14} at cm^{-3} in the disc.

condense at the given temperature. Fortunately, however, the critical sublimation heat does not depend very strongly on the density, as we saw in Chapter IV, so that we can calculate the sublimation heats for an average density and we need not worry about the variation of density for various substances.

If we compare this table with the sublimation heats given in Table 4. II, we see that while in the outer regions compounds like HCN, H_2O, NH_3 can condense, in the regions of the inner planets only metals and other inorganic compounds can condense. This has two consequences. The inorganic compounds are less frequent and are heavier. Therefore, the first stage of the condensation will end in heavy bodies in the inner regions and lighter bodies in the regions of the outer planets. Since the dimensions of the inner planets are hardly larger than r_{crit}, we can expect higher densities for the inner planets than for the outer planets. The initial condensation stage brings this difference about, and the gravitational capture, practically only acting in the case of the outer planets, accentuates this difference. The dimensions of the inner planets are only just larger than r_{crit}, which is given by Equation (4.20), and gives us:

$$r_{crit} = \sqrt{\frac{3\,v_2^2}{8\,\pi\gamma\delta\varrho_0}} \sim 10^9\,\mathrm{cm}, \tag{5.1}$$

with $\delta \sim 0.1$, $\varrho_0 \sim 3\ \mathrm{g\ cm^{-3}}$, $v_2 \sim 10^6\ \mathrm{cm\ sec^{-1}}$ (corresponding to Jupiter's distance from the sun). We see from this equation that, indeed, gravitational capture can only have played a minor part in the growth of the inner planets.

It seems even possible to account for the smaller differences in densities of the various planets, as was also shewn by Brown (1). We shall not, however, enter into this question here.

B. Masses of the planets. The second consequence of the condensation picture is that there will be more condensation nuclei per cm^3 in the regions of the outer planets than in the inner regions because there are more compounds which can condense. This means that a greater fraction of the gas will take part in the condensation in the outer regions. This again is accentuated by the fact that gravitational capture has played a part in the building up of the outer planets. If we postpone for

a moment the discussion of the problem why this gravitational capture has not been active in the case of the inner planets, we can try to estimate the masses of the planets under the assumption that a larger fraction of the matter took part in the building up of the major planets than in the case of the inner planets.

For the mass of the n-th planet we may write:

$$M_n = \Delta_n \varrho(r_n) A_n h_n, \tag{5.2}$$

where Δ_n: fraction of the gas taking part in the condensation process;

r_n : mean distance of the planet from the sun;

$\varrho(r)$: gas density in the disc, given by equation (2.17);

A_n : area in the disc, involved in the building up of the planet; we may take $A_n = c \cdot r_n^2$ (c will be of the order of magnitude one);

h_n : height of the disc at a distance r_n; h_n is given by equation (3.1).

Equation (5.2) can now be written in the following form:

$$M_n = A \Delta_n \varrho(r_n) r_n^3 = B \Delta_n r_n^{\frac{7}{2}} e^{-(r_n/s_m)^{\frac{1}{2}}}, \tag{5.3}$$

where A and B are constants. We now, for the sake of simplicity, take Δ to be constant throughout the regions of the inner planets, and also constant throughout the regions of the outer planets. For the ratio of Δ in the two regions we shall take 100, which takes into account the fact that gravitational capture has played a part in the formation of the outer planets, and the fact that lighter elements are more abundant than the heavier elements. We then get Table 5. II.

We see that the general agreement is quite good, especially in view of the fact that we have simplified the problem very much. We could probably get an even better agreement by a variation of s_m and the ratio of the Δ_n's in the two parts of the planetary system, but it does not seem worth while to do that. The only point is that the condensation picture presents us with a mass distribution in the solar system which agrees as well with the observational data as we can expect from necessarily rough considerations.

Table 5. II.

	$\frac{A_n}{A_{\text{earth}}}$	$\frac{\varrho}{\varrho_{\text{earth}}}$	$\frac{r_n}{r_{\text{earth}}}$	$\frac{M_{\text{calc}}}{M_{\text{earth}}}$	$\frac{M_{\text{obs}}}{M_{\text{earth}}}$
Mercury..	1	1.9	0.4	0.11	0.05
Venus....	1	1.4	0.7	0.5	0.8
Earth....	1	1	1	1	1
Mars.....	1	0.6	1.5	2.1	0.1
Jupiter...	100	0.045	5	640	318
Saturn ..	100	0.005	10	450	95
Uranus...	100	$1{,}4.10^{-4}$	19	100	15
Neptune..	100	6.10^{-6}	30	16	17
(Pluto....	100	6.10^{-7}	40	4	0.9)

The only serious disagreement seems to be a too small mass of Mars and the absence of a planet in the neighbourhood of the asteroids. We shall return to this point at the end of this paper.

There are, however, a few points which we still have to examine before we can accept the above considerations as giving us really an estimate of the planetary masses. These are the following:

(a) How great has the density to be in the disc in order to provide us with sufficient mass for the planets?
(b) What is the lifetime of the disc, and how does it compare with t_{crit}?
(c) Why has the gravitational capture not played a role in the building-up process of the inner planets?

(a) If we assume that a fraction 10^{-4} has taken part in the building-up process of the inner planets and a fraction 10^{-2} in the building-up process of the outer planets, we have the following conditions, if there has been enough mass available to build up the inner, respectively the outer planets:

$$10^{-4} \int_{r_0}^{s_{\text{Mars}}} \varrho \, 2\pi s \cdot h ds \geq 10^{28} \text{ g.},$$

and

$$10^{-2} \int_{s_{\text{Jup}}}^{\infty} \varrho \, 2\pi s \cdot h ds \leq 2.10^{30} \text{ g.}$$

Using equations (2.17) and (3.1), we get for the maximum density ϱ_m the condition:

$$\varrho_m \geq 7.10^{15} \text{ at cm}^{-3} \text{ and } \varrho_m \geq 3.10^{16} \text{ at cm}^{-3}.$$

This tallies very well with our assumption of $\varrho_m = 2.10^{16}$ at·cm^{-3}, corresponding to a total mass of the gaseous disc of about one tenth of the solar mass at the stage where equation (2.17) is valid.

(b) From equations (3.7) and (4.22), we can calculate the lifetime of the disc and t_{crit}.

If we should assume a laminar motion in the disc, equation (3.7) would give us:

$$\tau = 3.10^{14} \text{ years},$$

which is obviously by far too large.

Even if we take into account the uncertainties involved in the derivation of equation (3.7), it will stay too large. We should in that case expect still to see the remnants of the disc at the present time.

However, if we assume turbulence, equation (3.7) presents us with a lifetime given by:

$$\tau \sim \frac{10^{11}}{\varrho v \lambda} \text{yrs} \sim 10^2 \text{ yrs}, \tag{5.4}$$

where we used $\eta = \frac{1}{3} \varrho v \lambda$, $\varrho \sim 10^{-9}$ g cm^{-3}, $v \sim 10^6$ cm sec^{-1}, $\lambda \sim 10^{12}$ cm.

On the other hand, t_{crit} as given by equation (4.22) gives us:

$$t_{\text{crit}} = \frac{v_2}{v_1 \varrho_1} \left(\frac{6 \varrho_0}{\pi \gamma \delta} \right)^{\frac{1}{2}} \sim \frac{10^{-3}}{\varrho_1 \Delta} \text{ yrs} \sim 10^8 \text{ yrs}, \tag{5.5}$$

with $\Delta \sim 10^{-2}$, $\varrho \sim 10^{-9}$ g cm^{-3}.

Before looking into this question more carefully, and taking into account the change of t_{crit} with distance from the sun, we see immediately that t_{crit} is much larger than τ. This means that the lifetime of the disc should be too short to allow for even the building-up of the inner planets. We may remark here that these considerations are not restricted to the gaseous disc which we are considering, but may also play an important part in the discussion of whatsoever other theory one wants to propose.

If, however, some kind of regular system of vortices has existed, the dissipation of energy might well have been far less, perhaps even so much less that τ in that case should have been of the same order of magnitude as t_{crit}. In that case, it will not be unreasonable to assume a density distribution like the one given by equation (2.17) for the estimate of the planetary masses. The last part of the growth of the planets which is at the same time the part of the rapid growth happened just at a time when the dissipation of the envelope began to be felt. That dissipation, which will be strongest on the outskirts of the system is taken into account by the decreasing density given by equation (2.17).

(c) If we compare the ratio of τ and t_{crit} for the different planets, we get

$$\frac{t_{crit}}{\tau} \sim c \cdot \frac{v\lambda}{\Delta}. \tag{5.6}$$

Now, v is proportional to $s^{-\frac{1}{2}}$, λ to s (cf. Equation (3.14)) so that the numerator increases by a factor of the order 5 from the inner to the outer planets. The denominator, however, increases by a factor of the order 100. This means that it is possible that t_{crit} can be of the same order of magnitude as τ in the regions of the inner planets while being appreciably smaller in the regions of the outer planets. This entails that it is very possible that the size of the inner planets was restricted to r_{crit} because of the dissipation of the disc before they could grow larger. But the outer planets grew faster and were able to grow beyond the critical dimensions until also there the supply of matter ran out.

We are quite aware of the fact that the above considerations are very incomplete but in view of the many uncertain factors entering, it seems hardly worth while to start a more detailed investigation. It is, for instance, easy to see from equation (4.17), taking into account the decrease of ϱ with time ($\varrho \sim e^{-t/\tau}$), that if $t_{crit} > \tau$, the condensation products will not reach even the critical dimensions. However, if $\tau > t_{crit}$, the growth of the bodies can go on until all matter is used up. A change in the ratio t_{crit}/τ of only a few per cent. changes the picture completely in the region where that ratio is about 1. It also seems to be very dificult to take the exhaustion of the gas due to the condensation process itself adequately into account.

Chapter VI.

The Satellite Systems.

In this chapter we shall discuss the properties of the satellite systems and the rotational periods of the planets.

We want to stress the point that we cannot expect here a too close agreement with observational data. On the one hand, the observational data are not too accurate, and on the other, the situation in the planetary atmospheres will have been even more complicated than in the solar envelope. For instance, the fact that the dimensions of the atmospheres are of the same order of magnitude as the height of the disc will cause our two dimensional considerations to be certainly only rough approximations.

A. "Regular" and "irregular" satellites. If we look into the data about the satellites of the solar system (see Tables II—V), we see that we can divide them into two groups. The first group is made up of the first five Jovian satellites, the first eight Saturnian satellites, the four Uranian satellites, and Triton, Neptune's satellite. This group has orbits which are all approximately in the equatorial plane of the primary and whose eccentricities are small. We shall call these satellites the "regular" satellites.

The second group, that of the "irregular" satellites, consists of the moon, the two Martian satellites, the six outer Jovian satellites, and the outermost Saturnian satellite. Apart from the Martian satellites, the "irregular" satellites have orbital planes, highly inclined to the equatorial plane of the primary, and great orbital eccentricities[1].

We shall show here that there is also another difference between the two groups, viz., that the "regular" satellites may have been formed inside the planetary atmospheres. The "ir-

[1] We follow von Weizsäcker's classification (10). The origin of the moon is a problem lying outside the scope of the present paper. The Martian satellites are perhaps wrongly classified. See, however, the discussion on p. 68.

regular" satellites, however, are probably condensation products captured at a later stage by the planets.

In order to prove the probability of this point, we have collected the next table. In the first row we have the mean distances of the outermost "regular" satellite. In the second row we have inserted the radius of the planetary atmosphere as given by equation (4.26). In the third row we have inserted the mean distances of the first "irregular" satellite. Finally, in the last row, we have given the ratio between the radius of the atmosphere and the radius of the planet itself.

Table 6. I.

	Mercury	Venus	Earth	Mars	Jupiter	Saturn	Uranus	Neptune
s_{regul} in cm.	..	..	..	..	2.10^{11}	4.10^{11}	6.10^{10}	4.10^{10}
R_1 in cm ...	10^7	4.10^8	7.10^8	10^8	12.10^{11}	7.10^{11}	2.10^{11}	4.10^{11}
s_{irr} in cm ...	..	..	4.10^{10}	9.10^9	12.10^{11}	13.10^{11}	..	..
R_1/R_{plan} ...	0.06	0.6	1.1	0.3	170	120	80	160

We see that, indeed, the values of the second row are everywhere between those of the first and third row in agreement with our assumption of the origin of the "regular" and "irregular" satellites.

We note here finally that for the mean distances of the "regular" satellites from their primaries exponential laws like the Titius-Bode law seem to exist:

$$r_n = r_0 \varepsilon^n. \tag{6.1}$$

The value of ε decreases from 1.78 for Jupiter to 1.44 for Uranus. The value for the solar system is 1.86 if we exclude Pluto as an "irregular" planet. We have commented on these exponential laws in Chapter III and shall not discuss them here.

B. Densities and masses of the satellites. Since all satellites are smaller than the critical dimensions, gravitational capture has not played a role in their building-up process. Since (apart from the moon) all satellites are formed in the regions of the outer planets, we should expect densities of the satellites lower than those of the inner planets, but higher than those of

the outer planets, since the outer planets have been able to pick up light gases during the stage of gravitational capture. This agrees within the observational uncertainties with the observed data.

We shall not estimate here the masses of the satellites in the same way as we have done in the case of the planets. We can, however, use equation (5.2) the other way round, and try to find the density function in the original planetary atmosphere from the observed masses of the satellites. We take the fraction of the matter taking part in the condensation, A, to be constant in each atmosphere.

The result is that we find a density function resembling very closely the density distribution in the solar envelope, i. e., a function with a maximum at a distance from the primary equal to about 10 planetary radii. However, it is impossible to arrive at any more definite conclusions.

We may draw the reader's attention to one more point connected with the condensation process of the satellites, viz. that we have to assume that the building-up process of the satellites started before the planets with their atmospheres were left in the regions of the solar system like islands in an empty space. The lifetime of the planetary atmospheres as given by equation (3.7) is at least 100 times smaller than the lifetime of the solar envelope, but the dimensions of the satellites are of the same order of magnitude as the critical dimensions so that we see that they could not have been formed during the time when the atmospheres were left to themselves.

This means that we have to imagine the following picture of the complete solar system, accepting for a moment the idea of regular systems of vortices. In the initial stages of the process, when the central mass had just become of the order of magnitude of the present solar mass, the concentration of matter in our galaxy in the neighbourhood of the solar envelope was still large enough to regulate to some extent the motion in the solar envelope. The result was a regular system of vortices, and between them "roller bearings". Originally these "roller bearings" were probably much smaller than the large vortices. However, after the planets had grown considerably they could keep larger gas masses around them. In that way the planetary atmospheres

started. In the first stages of their development, there was still a disc of matter present which in its turn regulated the motion in the planetary atmospheres, resulting in a regular system of vortices in these atmospheres. In the "secondary roller bearings" the satellites started to grow.

Finally the whole disc started to disappear, and we were left with the system as we observe it at present. Of course, as soon as the dimensions of the atmospheres had become so small that there was no longer any turbulence, the planets were able to retain the atmospheres. These atmospheres are the ones we can observe now. Their lifetime is much longer than the probable age of the solar system.

C. Rotational periods of the planets. We have seen that there are so many features which are the same for the planetary system and the systems of the "regular" satellites that it seemed unavoidable not to arrive at the conclusion that their origin was analogous. These features were the nearly circular orbits lying practically in the equatorial plane of the primary, the distribution of mass in the system, viz. the largest bodies in the middle of the system, and exponential laws for the mean distances from the primary. Also the ratio of the total mass of the planetary system, respectively satellite systems to the sun, respectively mother planets, is about constant, i. e. about one thousandth. The question we are interested in now is why the outer planets have still a fairly rapid rotation while the sun is rotating so slowly.

Before considering the outer planets, we shall devote a few sentences to the inner planets. There are two reasons why we should expect low rotational velocities for the inner planets. First, they have had practically no atmospheres around them during their growth (see Table 6. I). This means that the interaction with the gas in the disc could not have followed a regular pattern. Secondly, the tidal action of the sun has been much larger for the inner planets than for the outer planets, as was shewn by STRATTON (38). This easily accounts for the fact that Mercury's rotational period is equal to its period around the sun.

Altogether it seems that the low rotational velocities of the inner planets constitute no serious difficulty. It is not, perhaps, irrelevant that the earth with the highest rotational velocity has also had the largest atmosphere.

In the case of the outer planets tidal action seems to have been negligible. We want to investigate how the atmospheres of the outer planets could have influenced their rotation. At the beginning, the large vortices will have supplied angular momentum to the planetary atmospheres. The result was probably that the angular velocities in these atmospheres corresponded to Kepler's third law (cf. Chapter II, Section A). In particular, the rotational velocities of the planets will have been given by that law.

However, as soon as the disc started to dissipate, the same process started for the planetary atmospheres, and the planets were decelerated because of the transfer of angular momentum accompanying the dissipation.

In the next table, we have inserted the rotational periods corresponding to Kepler's third law, the observed rotational periods, and the percentage change in angular momentum from the first to the second:

Table 6. II.

	T_{Kepl}	T_{obs}	$d\theta/\theta$
Jupiter	3 hrs	10 hrs	0.70
Saturn	4 hrs	10 hrs	0.60
Uranus	3 hrs	11 hrs	0.73
Neptune	2 hrs	12 hrs	0.83

We see that though the rotations of the planets are still fairly fast, they probably must have been slowed down considerably.

Final remarks.

In the last two chapters we saw that we could explain the differences between the outer and the inner planets as far as mass, density, and rotational velocities are concerned by looking carefully into the condensation process. This then presents us with an explanation of group C.

There are also indications given in Chapters III and V that the motion in the disc has once shewn regularities which might easily account for both the orbital regularities (A) and the exponential laws like the Titius-Bode law (B).

We have not entered into a discussion of the many irregularities which can be observed in the solar system. Some of them have been commented upon by VON WEIZSÄCKER (10). For instance, the fact that the eccentricity of Mercury's orbit is so large may well have been due to the regularity of the vortex system being disturbed in the immediate neighbourhood of the sun.

We want to remark here that there is one point which seems to deserve a thorough investigation. It is the fact that Mars is so much smaller than the earth, that Mars has only two very small satellites, and that instead of another planet between Mars and Jupiter we find the asteroids which together possess only a very small mass. This is an especially interesting point since there is also other evidence that in that neighbourhood some catastrophe has occurred. Recent investigations by BROWN (1) indicate that the meteorites might be the remnants of a planet of the size of Mars which was broken up by some unspecified process.

A question which might be asked is how much chance is there to find a planetary system surrounding a certain star. It seems that planetary systems will be much more frequent than corresponding to e. g. Jeans' tidal theory. However, there are still a few requirements which have to be met. One of them is

that the temperature of the central star has to be below a certain value. Otherwise condensation will be out of the question. This can, for instance, be seen from equation (5.6). If the temperature in the disc is much higher than in the disc considered in this paper, the fraction of the gas taking part in the condensation will be much smaller and t_{crit} will be larger than the lifetime of the disc, thus leaving us without condensation products. A higher temperature of the central star results not only in higher temperatures in the disc because of greater energy output, but also in a higher temperature because of a higher degree of ionization.

Although the actual figures given by Jeans in the following quotation will not be the right ones if the theory given in this paper should be correct, we still think that this quotation will give us an adequate ending for this paper:

"The contrast between the slowness of cosmogonic events and the rapidity with which events on our earth move leads to some interesting reflections. Let us suppose that civilisation on earth is 10000 years old. If each planetary system in the universe contains 10 planets, and life and civilisation appear in due course on each, the civilisations appear at an average rate of one per 500 million years. It follows that we should probably have to visit 50000 galaxies before finding a civilisation as young as our own. And as we have only studied cosmogony for some 200 years, we should have to search through about 25 million galaxies, if they exist, before encountering cosmogonists as primitive as ourselves. We may well be the most ignorant cosmogonists in the whole of space."

I should like to express my sincere thanks to the many physicists and astronomers whose advice and criticism have helped me so much during my investigations of this subject. In particular, I want to express my thanks to Profs. N. Bohr, J. M. Burgers, H. A. Kramers, J. H. Oort, F. J. M. Stratton, and B. Strömgren, and to Dr. A. Pais for their many helpful suggestions. I also want to express my thanks to the Rask-Ørsted-Foundation for a grant which made my stay in Copenhagen possible.

København, Universitetets Institut for teoretisk Fysik.
Purdue University, Department of Physics.

Observational data[1].

Earth's mass: $5.975 \cdot 10^{27}$ g.
Moon's mass: $7.35 \cdot 10^{25}$ g.
Sun's mass: $1.992 \cdot 10^{33}$ g.
Sun's mean radius: $6.965 \cdot 10^{10}$ cm.
Sun's rotational period (at the equator): 24.65 days.

Table I.
Elements of the planetary system.

	Mercury	Venus	Earth	Mars	Jupiter	Saturn	Uranus	Neptune	Pluto
Mean dist. from sun in 10^{12} cm.	5.8	10.8	15.0	22.8	77.9	143	287	450	591
Sidereal period	88 d	225 d	365 d	687 d	12 y	29 y	84 y	165 y	249 y
Eccentricity ..	0.206	0.007	0.017	0.093	0.048	0.056	0.047	0.009	0.247
Inclination of orbital plane to ecliptic.....	7°0′	3°24′	0°	1°51′	1°18′	2°29′	0°46′	1°47′	17°19′
Mass in earth's mass as unit..	0.05	0.8	1	0.1	318	95	15	17	0.9
Density in g cm^{-3}	4.1	4.9	5.5	3.9	1.3	0.7	1.3	1.6	5.5
Rad. in 10^8 cm.	2.5	6.2	6.4	3.4	69.8	57.6	25.5	25.0	6.4
Number of satellites	..	..	1	2	11	9 + rings	4	1	..
Inclination of equator to orbital plane ...	..	..	23°	25°	3°	26°	98°	141°	..
Axial rotational period.....	88 d	..	24 h	25 h	10 h	10 h	11 h	12 h[2]	..
	inner or terrestrial planets				outer or major planets				

[1] All data are taken from RUSSELL, DUGAN, STEWART (3).
[2] I am indebted to Prof. Lundmark for giving me his new data about Neptune's rotational period before publication.

Table II.
Jupiter's satellites.

	5	Io	Europa	Ganymede	Callisto	6	7	10	11	8	9
Mean dist. from Jup. in 10^{10} cm	1.8	4.2	6.7	11	19	115	118	118	225	235	237
Mean dist. in planetary radii	2.5	5,9	9.4	15	26	161	165	165	315	330	332
Inclination of orbit to Jup.'s equat. plane	27′	1′	28′	11′	15′	181°	243°	82°	232°	208°	61°
Eccentricity	0.0028	0.0000	0.0003	0.0015	0.0075	0.16	0.21	0.08	0.21	0.38	0.27
Mass (moon = 1)	..	0.99	0.64	2.11	1.32	..	..	..	..	..	..
Density in g cm^{-3}	..	2.7	2.9	2.2	1.3	..	..	..	..	..	..

Table III.
Saturn's satellites.

	Mimas	Enceladus	Tethys	Dione	Rhea	Titan	Hyperion	Iapetus	Phoebe
Mean dist. from Sat. in 10^{10} cm	1.9	2.4	2.9	3.8	5.3	12	15	36	130
Mean dist. from Sat. in planetary radii	3.11	3.99	4.94	6.33	8.84	20.5	24.8	59.7	217
Inclination of orbit to Sat's equat. plane	1°31′	1′	1°5′	0′	21′	18′	17′-56′	14°	149°
Eccentricity	0.0201	0.0044	0.0000	0.0022	0.0010	0.0289	0.1043	0.0283	0.166
Mass (moon = 1)	0.0005	0.001	0.009	0.014	0.03	1.9	< 0.0006	0.019	..
Density in g cm^{-3}	0.8?	1.3?	1.0?	1.5?	1.0?	3.6?	1.3?	1.2?	..

Table IV.
Uranus' satellites.

	Ariel	Umbriel	Titania	Oberon
Mean distance from Uranus in 10^{10} cm	1.9	2.7	4.4	5.9
Mean distance from Uranus in planetary radii	7.4	10	17	22
Inclination of orbit to Uranus' equatorial plane	0°	0°	0′	0′
Eccentricity	0.007	0.008	0.023	0.010

Table V.
Other satellites.

	Moon	Phobos	Deimos	Triton
Mean distance from primary in 10^{10} cm	3.8	0.9	2.4	3.5
Mean distance from primary in planetary radii	60	2.8	6.9	14
Inclination of orbit to primary's equatorial plane	$\sim$ 20°	1°	2°	20°
Eccentricity	0.055	0.021	0.003	0.000
Mass (moon = 1)	1	extremely small		1.8
Density in g cm^{-3}	3.34	..	..	2.8

References.

(1) H. S. Brown, Astrophys. Journ., in the press.
(2) R. A. Lyttleton, M.N.R.A.S., **98**, 634, 1938.
(3) H. N. Russell, R. S. Dugan, J. Q. Stewart, Astronomy I, revised edition, New York 1945.
(4) F. Nölke, Das Problem der Entwicklung unseres Planetsystems, Berlin 1919.
(5) H. N. Russell, The solar system and its origin, New York 1935.
(6) K. Birkeland, C. R., **155**, 892, 1912.
(7) H. P. Berlage Jr., Ergänzungsband zu Gerlands Beiträge zur Geophysik **17**, 1927; Proc. Koninkl. Ned. Acad. Wet., Amsterdam, **33**, 614, 719, 1930; **35**, 553, 1932; **37**, 221, 1934; **38**, 857, 1935; **43**, 532, 557, 1940.
(8) H. Alfvén, Stockholms Observatoriums Annaler, **14**, nrs 2, 5, 9, 1942—1946.
(9) H. Alfvén, Arkiv f. Astr., Mat och Fys., **28** A, nr. 6, 1942.
(10) C. F. von Weizsäcker, Zs. f. Astroph, **22**, 319, 1944. S. Chandrasekhar, Rev. Mod. Phys., **18**, 94, 1946.
(11) L. Spitzer, Astroph. Journ., **90**, 675, 1939.
(12) R. A. Lyttleton, M.N.R.A.S., **96**, 559, 1936; **98**, 536, 1938.
(13) R. A. Lyttleton, M.N.R.A.S., **101**, 216, 1941.
(14) F. Hoyle, Proc. Camb. Phil. Soc., **40**, 256, 1944; M.N.R.A.S., **105**, 175, 1945; **106**, 406, 1947.
(15) J. B. S. Haldane, Nature, **155**, 133, 1945.
(16) F. L. Whipple, Paper read before the A.A.A.S. on Dec. 27th 1947.
(17) H. Jeffreys, Nature, **153**, 140, 1944.
(18) C. F. von Weizsäcker, Zs. f. Astroph., **24**, 181, 1947.
(19) A. S. Eddington, Internal Constitution of Stars, Cambridge 1926, Ch. XIII.
(20) B. Strömgren, Astroph. Journ., **89**, 526, 1939.
(21) M. Rudkjöbing, Kgl. Danske Vid. Selsk., Mat.-fys. Medd., **18**, nr. 2, 1940.
(22) E. O. Lawrence, N. E. Edlefsen, Phys. Rev., **34**, 1056, 1929.
(23) R. Tousey, Paper read before the Am. Phys. Soc., Dec. 29th 1947.
(24) W. Baade, W. Pauli Jr., Naturwissenschaften, **15**, 49, 1927.
(25) A. S. Eddington, Internal constitution of the stars, Cambridge 1926, Ch. X.

(26) P. Swings, L. Rosenfeld, Astroph. Journ., **86**, 483, 1937.
(27) S. Rosseland, Theoretical Astrophysics, Oxford 1936, Ch. XXII.
(28) H. A. Kramers, D. ter Haar, B.A.N., **10**, 137, 1946 (nr. 371).
(29) H. Lamb, Hydrodynamics, Cambridge 1932, 6th edition, p. 580.
(30) Th. von Kármán, Göttinger Nachrichten, **1930**, 58.
(31) J. Tuominen, Ann. d'Astroph., in the press.
(32) L. Prandtl, Abriss d. Strömungslehre, Braunschweig 1931, p. 93.
(33) D. ter Haar, B.A.N., **10**, 1, 1943 (nr. 361); Astroph. Journ. **100**, 288, 1944.
(34) R. Becker, W. Döring, Ann. d. Phys., (V) **24**, 719, 1935.
(35) D. ter Haar, M.N.R.A.S., **106**, 283, 1947.
(36) B. Lindblad, Nature, **135**, 133, 1935.
(37) W. C. H. Eakin, W. H. McCrea, Proc. Roy. Irish Acad., **46**, 91, 1940.
(38) F. J. M. Stratton, M.N.R.A.S., **66**, 374, 1906.
(39) B. J. Bok, M.N.R.A.S., **106**, 61, 1946.
(40) A. Unsöld, Zs. f. Astroph., **24**, 278, 1948.

Indleveret til Selskabet den 29. April 1948.
Færdig fra Trykkeriet den 30. August 1948.

DET KGL. DANSKE VIDENSKABERNES SELSKAB
MATEMATISK-FYSISKE MEDDELELSER, BIND XXV, NR. 4

ON THE INTRODUCTION OF MEASURES IN INFINITE PRODUCT SETS

BY

ERIK SPARRE ANDERSEN
AND
BØRGE JESSEN

KØBENHAVN
I KOMMISSION HOS EJNAR MUNKSGAARD
1948

Printed in Denmark
Bianco Lunos Bogtrykkeri

1. **Introduction.** It is shown that an important theorem on the introduction of measures in a real space of an infinite number of dimensions cannot be extended to abstract sets. From the theory of product measures in abstract product sets follows that the extension is valid in the case, where, in the terminology of the theory of probability, the coordinates are independent. It will be shown by an example that the extension need not be possible when the coordinates are dependent.

2. **Formulation of the result.** Let I denote an infinite set of indices i, and let there for every $i \in I$ be given a non-empty set E_i and a Borel field $\mathfrak{F}_i$ of sub-sets of E_i such that $E_i \in \mathfrak{F}_i$. By $E = (E_i)$ we denote the product of the sets E_i, consisting of all symbols $x = (x_i)$ where $x_i \in E_i$ for every $i \in I$. The elements x_i are called the coordinates of x. The smallest Borel field in E, which for every i and every $A_i \in \mathfrak{F}_i$ contains the set of all x for which $x_i \in A_i$, will be denoted by $\mathfrak{F} = (\mathfrak{F}_i)$.

For an arbitrary finite sub-set $I' = \{i_1, \cdots, i_n\}$ of I we may consider the corresponding partial product $E' = (E_{i_1}, \cdots, E_{i_n})$ with elements $x' = (x_{i_1}, \cdots, x_{i_n})$ and in E' the smallest Borel field $\mathfrak{F}' = (\mathfrak{F}_{i_1}, \cdots, \mathfrak{F}_{i_n})$ which for every $i \in I'$ and every $A_i \in \mathfrak{F}_i$ contains the set of all x' for which $x_i \in A_i$.

For an arbitrary $x \in E$ the element $x' \in E'$ for which the coordinates are equal to the corresponding coordinates of x is called the projection of x on E'. The set of all x for which the projection x' belongs to a set A' in E' will be denoted by $\{x' \in A'\}$; it is called the cylinder with base A' in E'. It belongs to $\mathfrak{F}$ if and only if A' belongs to $\mathfrak{F}'$.

Our problem is now the following:

Let there for every finite partial product E' of E be given a measure μ' defined on the system of all cylinders of $\mathfrak{F}$ with base in E' and with $\mu'(E') = 1$. Suppose that any two of these measures coincide in the common part of their domains, so that a set function λ is defined on the system of all cylinders of $\mathfrak{F}$ with base in some finite partial product by placing $\lambda(A) = \mu'(A)$ when A is a cylinder with base in E'. Is it then possible to extend λ to a measure defined on $\mathfrak{F}$?

It is clear that the domain of λ is a field and that λ is additive. Since $\mathfrak{F}$ is the smallest Borel field containing the domain of λ, a necessary and sufficient condition that λ may be extended to a measure defined on $\mathfrak{F}$ is that λ is completely additive. The extension is then unique.

3. Two important cases are known in which the answer is affirmative.

The one is the case where each E_i is the real axis $-\infty < x_i < +\infty$ and $\mathfrak{F}_i$ is the system of Borel sets on E_i. Then E is the real space whose dimension is the cardinal number of I, and $\mathfrak{F}$ is (by definition) the system of Borel sets in E. The explicit formulation of the possibility of the extension under these conditions is due to Kolmogoroff [9, pp. 24—30]; essentially, the result goes back to Daniell [3], [4].

The other is the case where there is given a measure μ_i in every E_i with domain $\mathfrak{F}_i$ such that $\mu_i(E_i) = 1$ and where $\mu'(A)$ for a set of the type $A = \{x_{i_1} \varepsilon A_{i_1}\} \cdots \{x_{i_n} \varepsilon A_{i_n}\}$, where $A_{i_1} \varepsilon \mathfrak{F}_{i_1}$, $\cdots$, $A_{i_n} \varepsilon \mathfrak{F}_{i_n}$, is equal to the product $\mu_{i_1}(A_{i_1}) \cdots \mu_{i_n}(A_{i_n})$. By this condition the measures μ' are uniquely determined. The extension of λ to $\mathfrak{F}$ is the product measure $\mu = (\mu_i)$ generated by the measures μ_i. Proofs of this result, which has first been formulated by Łomnicki and Ulam [10], have been given by von Neumann [11, pp. 105—129] and Jessen [7], cf. Sparre Andersen and Jessen [2, pp. 18—22]. The latter proof has also been found by Kakutani [8].

These examples make it natural to expect that the answer is always affirmative. Attempts to prove that it is so have been made by Doob [6, pp. 90—93], who considers the case with

equal E_i and equal $\mathfrak{F}_i$, and, independently, by Sparre Andersen [1]. That these proofs are incomplete has been pointed out in Sparre Andersen and Jessen [2, p. 22]. We shall now prove by the construction of an example that actually the theorem fails. More explicitly we shall prove:

For an arbitrary infinite set I there exists a case with equal E_i and equal $\mathfrak{F}_i$ for which the answer to the problem is negative.

In the terminology of the theory of probability this means, that the case of dependent variables cannot be treated for abstract variables in the same manner as for unrestricted real variables. Professor Doob has kindly pointed out, what was also known to us, that this case may be dealt with along similar lines as the case of independent variables (product measures) when conditional probability measures are supposed to exist. This question will be treated in a forthcoming paper by Doob and Jessen. That conditional probability measures need not always exist, has, as we have been informed, already been shown by Dieudonné in a paper which is about to appear [5, p. 42]. This is also seen from our example.

4. Construction of the example. Let C denote a circle of length 1 and let m^* denote the exterior (linear) Lebesgue measure on C. Let C be divided in Hausdorff's manner into disjoint sets $\cdots, C_{-1}, C_0, C_1, \cdots$ which are congruent by rotation. For each $i \in I$ we take $E_i = C - C_j$ for some $j = j(i)$ and choose as $\mathfrak{F}_i$ the system of all sets which are the common part of E_i and a Borel set on C. We suppose, as we may since I is infinite, that every integer j occurs as value of $j(i)$ for at least one i. With this choice the sets E_i are not actually equal, but they are congruent, which amounts to the same; if by rotation we make the E_i equal, the $\mathfrak{F}_i$ will also be equal.

The product $E = (E_i)$ is a sub-set of the torus-space $Q = (Q_i)$, where all $Q_i = C$. Similarly, for an arbitrary finite sub-set $I' = \{i_1, \cdots, i_n\}$ of I the partial product E' is a sub-set of the torus-space $Q' = (Q_{i_1}, \cdots, Q_{i_n})$.

A point $x = (t, \cdots, t)$ on the 'diagonal' of Q' will belong to E' if and only if t belongs to the set $D' = (C - C_{j(i_1)}) \cdots$

$(C - C_{j(i_n)}) = C - (C_{j(i_1)} + \cdots + C_{j(i_n)})$ on C. Since C contains an infinite number of disjoint sets congruent to $C_{j(i_1)} + \cdots + C_{j(i_n)}$ we have $m^*(D') = 1$.

We now consider a cylinder $A = \{x' \varepsilon A'\}$ with base $A' \varepsilon \mathfrak{F}'$ in E'. The base A' is the common part of E' and a Borel set in Q'. Hence the set $S_{A'}$ of points t on C for which the corresponding point $x' = (t, \cdots, t)$ on the diagonal of Q' belongs to A' is the common part of D' and a Borel set on C. We may therefore define a measure μ' on the system of these cylinders A by placing $\mu'(A) = m^*(S_{A'})$. Plainly $\mu'(E) = 1$.

We shall now prove that any two of these measures coincide in the common part of their domains. It will be sufficient to prove that if μ_0' is the measure corresponding to a sub-set $I_0' = \{i_1, \cdots, i_n, i_{n+1}, \cdots, i_{n_0}\} \supset I'$ then μ' is a contraction of μ_0'. To see this it is sufficient to notice that when a cylinder $\{x' \varepsilon A'\}$ with base in E' is considered as a cylinder $\{x_0' \varepsilon A_0'\}$ with base in the partial product E_0' corresponding to I_0' then the set $S_{A'}$ is replaced by a set $S_{A_0'} \subseteq S_{A'}$. Hence $\mu_0'(A) \leqq \mu'(A)$. If this inequality is applied to the complementary set $E - A$ we obtain, since $\mu_0'(E) = \mu'(E)$, the opposite inequality $\mu_0'(A) \geqq \mu'(A)$. Hence $\mu_0'(A) = \mu'(A)$.

Finally we shall prove that the set-function λ defined by the measures μ' cannot be extended to a measure defined on $\mathfrak{F}$. To see this we consider for every finite partial product E' the cylinder $A = \{x' \varepsilon A'\}$ whose base A' consists of all $x' \varepsilon E'$ which do not lie on the diagonal of Q' (this set A' belongs to $\mathfrak{F}'$ since it is the common part of E' and a Borel set in Q'). Then $S_{A'}$ is empty so that $\lambda(A) = \mu'(A) = 0$. Let $i_1, i_2, \cdots$ be a sequence of elements of I such that the numbers $j(i_1), j(i_2), \cdots$ are *all* integers, and let A_n be the set A formed, in the manner just explained, for $I' = \{i_1, \cdots, i_n\}$. Then the sets $A_1, A_2, \cdots$ will cover E, since for any element $x = (x_i)$ of E the coordinates $x_{i_1}, x_{i_2}, \cdots$ cannot all be equal. Consequently λ is not completely additive.

5. The idea of the above example may briefly be described as follows: We choose $E = (E_i)$ as a sub-set of the torus-space $Q = (Q_i)$ choosing the sets E_i in such a manner that any finite partial product E' of E contains a set of exterior linear Lebesgue measure 1 on the diagonal of the corresponding partial product

Q' of Q whereas there exists an enumerable partial product E'' of E (corresponding to the indices $i_1, i_2, \cdots$) which contains no points on the diagonal of the corresponding partial product Q'' of Q. The first property makes it possible to define the measures μ' by 'projection' on E' of an equidistribution of unit mass on the diagonal of Q, and the second property prevents the complete additivity of the corresponding set-function λ, since by projection on Q'' the whole mass falls outside E''.

References.

[1] E. Sparre Andersen. Indhold og Maal i Produktmængder. Mat. Tidsskr. B 1944, pp. 19—23.

[2] E. Sparre Andersen and B. Jessen. Some limit theorems on integrals in an abstract set. D. Kgl. Danske Vidensk. Selskab, Mat.-fys. Medd. 22, no. 14 (1946).

[3] P. J. Daniell. Integrals in an infinite number of dimensions. Ann. af Math. (2) 20 (1918—19), pp. 281—288.

[4] P. J. Daniell. Functions of limited variation in an infinite number of dimensions. Ann. of Math. (2) 21 (1919—20), pp. 30—38.

[5] J. Dieudonné. Sur le théorème de Lebesgue-Nikodym III. Ann. Univ. Grenoble (2) 23 (1947—48), pp. 25—53.

[6] J. L. Doob. Stochastic processes with an integral-valued parameter. Trans. Amer. Math. Soc. 44 (1938), pp. 87—150.

[7] B. Jessen. Abstrakt Maal- og Integralteori 4. Mat. Tidsskr. B 1939, pp. 7—21.

[8] S. Kakutani. Notes on infinite product measure spaces I. Proc. Imp. Acad. Tokyo 19 (1943), pp. 148—151.

[9] A. Kolmogoroff. Grundbegriffe der Wahrscheinlichkeitsrechnung. Berlin 1933.

[10] Z. Łomnicki and S. Ulam. Sur la théorie de la mesure dans les espaces combinatoires et son application au calcul des probabilités I. Variables indépendantes. Fund. Math. 23 (1934), pp. 237—278.

[11] J. von Neumann. Functional operators. First volume. Notes on lectures given at The Institute for Advanced Study, Princeton 1933—34.

Indleveret til Selskabet den 28. Juni 1948.
Færdig fra Trykkeriet den 31. August 1948.

DET KGL. DANSKE VIDENSKABERNES SELSKAB
MATEMATISK-FYSISKE MEDDELELSER, BIND XXV, NR. 5

SOME LIMIT THEOREMS ON SET-FUNCTIONS

BY

ERIK SPARRE ANDERSEN

AND

BØRGE JESSEN

KØBENHAVN
I KOMMISSION HOS EJNAR MUNKSGAARD
1948

Printed in Denmark
Bianco Lunos Bogtrykkeri

1. Introduction. In a recent paper [1] we have considered two limit theorems on set-functions in an abstract set. The first theorem is a generalization of the theorem on differentiation on a net, the net being replaced by an increasing sequence of σ-fields. The second theorem is a sort of counterpart of the first, the sequence of σ-fields being now decreasing. The theorems had presented themselves as generalizations of known theorems on integration of functions of infinitely many variables.

When publishing our paper we were not aware that essentially equivalent results had already been published by Doob [2], though in a form in which the close connection with the known results on functions of infinitely many variables is less apparent. There is, however, the difference, that while Doob considers point-functions, which amounts to assume the set-functions continuous with respect to the given measures, we have, in the first theorem, made this assumption only for the contractions to the σ-fields of the sequence, whereas the set-function itself was allowed to contain a singular part.

The object of the present paper is to prove generalizations of the two theorems, in which no assumptions regarding continuity of the set-functions with respect to the measures are made. Thus we obtain two theorems which are completely analogous. For this purpose only slight changes in the former proofs are required, but for the convenience of the reader we give the proofs in detail. Actually the generalization makes the proofs more conspicuous.

2. Derivative of a set-function with respect to a measure. In addition to the definitions and theorems stated at the beginning of [1] we shall use the following fundamental theorem:

Let E be a set containing at least one element, and μ a mea-

sure in E with domain $\mathfrak{F}$, such that $E \in \mathfrak{F}$ and $\mu(E) = 1$. Then to any bounded, completely additive set-function φ with domain $\mathfrak{F}$ there exists a μ-integrable function f with $[f] = E$ such that the μ-continuous part φ_c of φ is the indefinite integral of f, i. e.

$$\varphi_c(A) = \int_A f(x)\,\mu(dE)$$

for any $A \in \mathfrak{F}$, and that the positive and negative parts of the μ-singular part φ_s of φ for any $A \in \mathfrak{F}$ are determined by

$$\varphi_s^+(A) = \varphi(A\,[f = +\infty]) \quad \text{and} \quad \varphi_s^-(A) = \varphi(A\,[f = -\infty]).$$

Any such function f will be called a *derivative of φ with respect to μ*.

It is easily seen that if f_0 is a derivative of φ with respect to μ then a μ-measurable function f is a derivative of φ with respect to μ if and only if $\mu([f \neq f_0]) = 0$ and $\varphi(A) = 0$ for any sub-set $A \in \mathfrak{F}$ of $[f \neq f_0]$.

A μ-measurable function f is a derivative of φ with respect to μ if and only if it satisfies the following conditions: For an arbitrary (finite) number a we have $\varphi(A) \leqq a\mu(A)$ for any sub-set $A \in \mathfrak{F}$ of $[f \leqq a]$ and $\varphi(A) \geqq a\mu(A)$ for any sub-set $A \in \mathfrak{F}$ of $[f \geqq a]$.

The necessity of the first condition is plain, for since $A\,[f = +\infty] = 0$ we have

$$\varphi(A) = \int_A f(x)\,\mu(dE) + \varphi(A\,[f = -\infty]) \leqq \int_A a\mu(dE) + 0 = a\mu(A).$$

The necessity of the second condition is proved analogously.

The sufficiency of the conditions is well known from the proof of the above mentioned theorem.

3. The two limit theorems. Let E be a set containing at least one element, and μ a measure in E with domain $\mathfrak{F}$, such that $E \in \mathfrak{F}$ and $\mu(E) = 1$. Let φ be a bounded, completely additive set-function with domain $\mathfrak{F}$.

Let $\mathfrak{F}_1, \mathfrak{F}_2, \cdots$ be a sequence of σ-fields contained in $\mathfrak{F}$, such

that $E \in \mathfrak{F}_n$ for all n. Let μ_n and φ_n denote the contractions of μ and φ to $\mathfrak{F}_n$, and let f_n denote a derivative of φ_n with respect to μ_n.

The first limit theorem now states:

If $\mathfrak{F}_1 \subseteq \mathfrak{F}_2 \subseteq \cdots$ *then the functions*

$$\underline{f} = \liminf_n f_n \quad \textit{and} \quad \overline{f} = \limsup_n f_n$$

are derivatives of φ' *with respect to* μ', *where* μ' *and* φ' *are the contractions of* μ *and* φ *to the smallest* σ*-field* $\mathfrak{F}'$ *containing all* $\mathfrak{F}_n$.

In the particular case in which φ_n for every n is μ_n-continuous, this theorem is equivalent to the first limit theorem of our previous paper [1].

The second limit theorem states:

If $\mathfrak{F}_1 \supseteq \mathfrak{F}_2 \supseteq \cdots$ *then the functions*

$$\underline{f} = \liminf_n f_n \quad \textit{and} \quad \overline{f} = \limsup_n f_n$$

are derivatives of φ' *with respect to* μ', *where* μ' *and* φ' *are the contractions of* μ *and* φ *to the largest* σ*-field* $\mathfrak{F}'$ *contained in all* $\mathfrak{F}_n$.

In the particular case in which φ is μ-continuous, and hence φ_n for every n is μ_n-continuous, this theorem is equivalent to the second limit theorem of [1].

4. Proof of the first limit theorem. Since $\underline{f}$ and $\overline{f}$ evidently are μ'-measurable it will according to § 2 be sufficient to prove the inequalities

$$\varphi(HA) \leqq a\mu(HA) \quad \text{and} \quad \varphi(KA) \geqq a\mu(KA)$$

for any $A \in \mathfrak{F}'$, when $H = [\underline{f} \leqq a]$ and $K = [\overline{f} \geqq a]$ for an arbitrary number a.[1]

In order to prove the first inequality we put

[1] For if A is a sub-set of $[\underline{f} \leq a]$ or $[\overline{f} \leq a]$ we have $HA = A$, and if A is a sub-set of $[\underline{f} \geq a]$ or $[\overline{f} \geq a]$ we have $KA = A$.

$$H_n = [\inf_p f_{n+p} < a_n]$$

and

$$H_{np} = \begin{cases} [f_{n+1} < a_n] \text{ for } p = 1 \\ [f_{n+1} \geqq a_n, \cdots, f_{n+p-1} \geqq a_n, f_{n+p} < a_n] \text{ for } p > 1, \end{cases}$$

where $a_1, a_2, \cdots$ denotes a (strictly) decreasing sequence of numbers converging towards a. Then $H_{np} \in \mathfrak{F}_{n+p}$ and $H_{np} \subseteq [f_{n+p} < a_n]$. Clearly (for a given n) no two of the sets H_{np} have elements in common, and $H_n = \sum_p H_{np}$. Further $H_1 \supseteq H_2 \supseteq \cdots$ and $H = \mathfrak{D}_n H_n$. Now, if A belongs to the field $\mathfrak{G} = \mathfrak{S}_n \mathfrak{F}_n$, we shall have $A \in \mathfrak{F}_n$ for all $n \geqq$ (some) n_0; hence $H_{np} A \in \mathfrak{F}_{n+p}$ for $n \geqq n_0$ and all p. We therefore have

$$\varphi(H_n A) = \sum_p \varphi(H_{np} A) = \sum_p \varphi_{n+p}(H_{np} A)$$

$$\leqq \sum_p a_n \mu_{n+p}(H_{np} A) = \sum_p a_n \mu(H_{np} A) = a_n \mu(H_n A).$$

Since $H_1 A \supseteq H_2 A \supseteq \cdots$ and $HA = \mathfrak{D}_n H_n A$, we have $\mu(HA) = \lim_n \mu(H_n A)$ and $\varphi(HA) = \lim_n \varphi(H_n A)$. We therefore obtain $\varphi(HA) \leqq a\,\mu(HA)$.

We now define a set-function $\varkappa$ on $\mathfrak{F}'$ by placing

$$\varkappa(A) = a\,\mu(HA) - \varphi(HA).$$

Clearly $\varkappa$ is bounded and completely additive. Moreover, since $\varphi(HA) \leqq a\,\mu(HA)$ for $A \in \mathfrak{G}$, the contraction of $\varkappa$ to $\mathfrak{G}$ is non-negative. Since $\mathfrak{F}'$ is the smallest σ-field containing $\mathfrak{G}$ this implies that the set-function $\varkappa$ itself is non-negative, i. e. the inequality $\varphi(HA) \leqq a\,\mu(HA)$ is valid for all $A \in \mathfrak{F}'$.

The inequality $\varphi(KA) \geqq a\,\mu(KA)$ is proved analogously.

5. Corollaries of the first limit theorem. If in particular $\mathfrak{F}' = \mathfrak{F}$, we have $\mu' = \mu$ and $\varphi' = \varphi$, so that the first limit theorem contains statements about the set-function φ itself.

Even if $\mathfrak{F}' \subset \mathfrak{F}$, we may, however, by means of the following general remark concerning derivatives, under a certain additional assumption, deduce results regarding the set-function φ.

Let E, μ, $\mathfrak{F}$, and φ be as in § 2, and let μ' and φ' denote the contractions of μ and φ to a σ-field $\mathfrak{F}' \subset \mathfrak{F}$, such that $E \in \mathfrak{F}'$.

Let f' denote a derivative of φ' with respect to μ'. Suppose, that *to any set* $A \in \mathfrak{F}$ *there exist sets* $B \in \mathfrak{F}'$ *and* $C \in \mathfrak{F}'$ *such that* $B \subseteq A \subseteq C$ *and* $\mu(C-B) = 0$. *Then*

(i) *if* φ *is non-negative* f' *is also a derivative of* φ *with respect to* μ;

(ii) *in any case the indefinite integral of* f' *with respect to* μ *is the* μ*-continuous part of* φ.

Proof. (i) Let $A \in \mathfrak{F}$, and let B and C be corresponding sets according to the assumption. On placing $H = [f' \leqq a]$ and $K = [f' \geqq a]$ we have

$$\varphi(HA) \leqq \varphi(HC) \leqq a\,\mu(HC) = a\,\mu(HA)$$

and

$$\varphi(KA) \geqq \varphi(KB) \geqq a\,\mu(KB) = a\,\mu(KA).$$

(ii) The statement follows easily by application of (i) to the set-functions φ^+ and $-\varphi^-$.

Our assumption does not imply that f' for an arbitrary φ is a derivative of φ with respect to μ. This is shown by the following example:[1]

Let $\mathfrak{F}$ consist of all sub-sets of a set E of three elements a, b, and c, and let $\mu(\{a\}) = 1$, $\mu(\{b\}) = \mu(\{c\}) = 0$, and $\varphi(\{a\}) = 0$, $\varphi(\{b\}) = 1$, $\varphi(\{c\}) = -1$. Let $\mathfrak{F}'$ consist of all sets containing either both or none of the elements b and c. Then the function $f' = 0$ is a derivative of φ' with respect to μ', but not of φ with respect to μ.

6. Proof of the second limit theorem. In this case $\mathfrak{F}' = \mathfrak{D}_n \mathfrak{F}_n$ Since $\underline{f}$ and $\overline{f}$ are μ_n-measurable for all n, they are μ'-measurable; according to § 2 it is therefore sufficient to prove the inequalities

$$\varphi(HA) \leqq a\mu(HA) \quad \text{and} \quad \varphi(KA) \geqq a\mu(KA)$$

for any $A \in \mathfrak{F}'$, when $H = [\inf_n f_n < a]$ and $K = [\sup_n f_n > a]$ for an arbitrary number a.[2]

[1] A corresponding example in our previous paper ([1], pp. 12—13) is wrong as it stands. The above example shows how it may be rectified.

[2] For if A is a sub-set of $[\underline{f} \leq a]$ or $[\overline{f} \leq a]$, it is a sub-set of $[\inf_n f_n < a + \varepsilon]$ for any $\varepsilon > 0$, hence $\varphi(A) \leqq (a+\varepsilon)\,\mu(A)$ and consequently $\varphi(A) \leqq a\,\mu(A)$. Similarly, if A is a sub-set of $[\underline{f} \geq a]$ or $[\overline{f} \geq a]$, it is a sub-set of $[\sup_n f_n > a - \varepsilon]$ for any $\varepsilon > 0$, hence $\varphi(A) \geqq (a-\varepsilon)\,\mu(A)$ and consequently $\varphi(A) \geqq a\,\mu(A)$.

In order to prove the first inequality it is sufficient to prove that if for an arbitrary n we put

$$H_n = [\min_{p \leq n} f_p < a]$$

we have $\varphi(H_n A) \leq a\mu(H_n A)$ for any $A \in \mathfrak{F}'$. For $H_1 \subset H_2 \subset \cdots$ and $H = \mathop{\mathfrak{S}}_n H_n$. Hence $\mu(HA) = \lim_n \mu(H_n A)$ and $\varphi(HA) = \lim_n \varphi(H_n A)$.

To prove the inequality $\varphi(H_n A) \leq a\mu(H_n A)$ we put

$$H_{np} = \begin{cases} [f_p < a,\ f_{p+1} \geq a,\ \cdots,\ f_n \geq a] \text{ for } p < n \\ [f_n < a] \text{ for } p = n. \end{cases}$$

Then $H_{np} \in \mathfrak{F}_p$ and $H_{np} \subseteq [f_p < a]$. Moreover $H_n = \sum_{p \leq n} H_{np}$. Since $A \in \mathfrak{F}_p$ for any p this implies

$$\begin{aligned} \varphi(H_n A) &= \sum_{p \leq n} \varphi(H_{np} A) = \sum_{p \leq n} \varphi_p(H_{np} A) \\ &< \sum_{p \leq n} a\mu_p(H_{np} A) = \sum_{p \leq n} a\mu(H_{np} A) = a\mu(H_n A). \end{aligned}$$

The inequality $\varphi(KA) \geq a\mu(KA)$ is proved analogously.

References.

[1] E. Sparre Andersen and B. Jessen. Some limit theorems on integrals in an abstract set. D. Kgl. Danske Vidensk. Selskab, Mat.-fys. Medd. 22, no. 14 (1946).

[2] J. L. Doob. Regularity properties of certain families of chance variables. Trans. Amer. Math. Soc. 47 (1940), pp. 455—486.

Indleveret til Selskabet den 16. August 1948.
Færdig fra Trykkeriet den 23. Oktober 1948.

DET KGL. DANSKE VIDENSKABERNES SELSKAB
MATEMATISK-FYSISKE MEDDELELSER, BIND XXV, NR. 6

ON THE CONVERGENCE PROBLEM FOR DIRICHLET SERIES

BY

HARALD BOHR

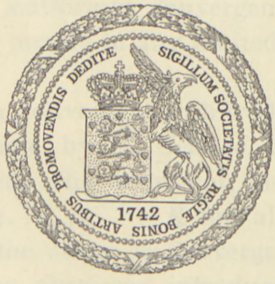

KØBENHAVN
I KOMMISSION HOS EJNAR MUNKSGAARD
1949

Printed in Denmark
Bianco Lunos Bogtrykkeri

Introduction.

Let $\sum_1^\infty a_n n^{-s}$ be a Dirichlet series in the complex variable $s = \sigma + it$. With such a series are connected several values of the abscissa σ which are characteristic for the series in question.

Firstly, as $|a_n n^{-s}| = |a_n| n^{-\sigma}$, it is evident that there exists an "abscissa of absolute convergence" σ_A $(-\infty \leqq \sigma_A \leqq \infty)$ such that the series is absolutely convergent for $\sigma > \sigma_A$ but not for $\sigma < \sigma_A$.

Secondly, as first proved by JENSEN, the series also possesses an "abscissa of convergence" σ_C, i. e. there exists a number σ_C such that the series is convergent for $\sigma > \sigma_C$, divergent for $\sigma < \sigma_C$. Between σ_A and σ_C we have the relation $0 \leqq \sigma_A - \sigma_C \leqq 1$. For any $\varepsilon > 0$, $K > 0$ the series is uniformly convergent in $\sigma > \sigma_C + \varepsilon$, $|s| < K$; hence the series represents in its half-plane of convergence $\sigma > \sigma_C$ an analytic function $f(s)$.

Thirdly we have the "abscissa of uniform convergence" σ_U, introduced by the author as the g. l. b. of the abscissae σ_0 for which the series is uniformly convergent in the whole half-plane $\sigma > \sigma_0$ (and not merely in any limited part of it). Obviously $\sigma_C \leqq \sigma_U \leqq \sigma_A$.

Finally it is often convenient to introduce a fourth abscissa, which we shall denote by σ^*, defined as the g. l. b. of the abscissae σ_0 for which the terms of the series $\sum a_n n^{-(\sigma_0 + it)}$ remain bounded (i. e. $|a_n| n^{-\sigma_0} < K$ for all n). Except for the special cases where the series is convergent everywhere or nowhere (where all the abscissae introduced are either $-\infty$ or $+\infty$ respectively) the abscissa σ^* may also be defined as the—certainly existing—smallest number σ for which $a_n n^{-\sigma} = O(n^\delta)$ for every $\delta > 0$. Evidently $\sigma_C \geqq \sigma^*$ and $\sigma_A \leqq \sigma^* + 1$.

There is no real difficulty in giving explicit expressions for the four abscissae, introduced above, in terms of the coefficients a_n of the series. As regards σ^*, it follows immediately from the definition of this number that

$$\sigma^* = \overline{\lim_{n\to\infty}} \frac{\log|a_n|}{\log n},$$

and for the three abscissae of convergence one finds by partial summation, in case the series is divergent for $s = 0$, the well-known expressions

$$\sigma_C = \overline{\lim} \frac{\log|S_n|}{\log n}, \qquad \sigma_A = \overline{\lim} \frac{\log A_n}{\log n}, \qquad \sigma_U = \overline{\lim} \frac{\log U_n}{\log n}$$

where

$$S_n = \sum_{\nu=1}^{n} a_\nu, \qquad A_n = \sum_{\nu=1}^{n} |a_\nu|, \qquad U_n = \underset{-\infty<t<\infty}{\text{l. u. b.}} \left| \sum_{\nu=1}^{n} a_\nu \nu^{-it} \right|.$$

In the following we shall, however, use only a simple consequence of the expression for σ_C, viz., if for some $\alpha > 0$ the partial sum $S_n = a_1 + \cdots + a_n$ is *not* $o(n^\alpha)$ for $n \to \infty$, then the abscissa of convergence σ_C is certainly $\geqq \alpha$.

While the four numbers σ_A, σ_C, σ_U, σ^* are defined directly from the series itself, there are some other abscissae, important for the theory of Dirichlet series, which are determined in a more indirect manner, namely from the behaviour of the analytic function $f(s)$ given by the series in its half-plane of convergence. We shall mention three such numbers, viz.

ω = g. l. b. of those σ_0 such that $f(s)$ is regular and bounded in $\sigma > \sigma_0$,

ω_1 = g. l. b. of those σ_0 such that $f(s)$ is regular and $O(|t|^\varepsilon)$ in $\sigma > \sigma_0$ for any $\varepsilon > 0$,

Ω = g. l. b. of those σ_0 such that $f(s)$ is regular and of finite order in $\sigma > \sigma_0$, i. e. $= O(|t|^K)$ for some value of $K = K(\sigma_0)$.

Obviously $\omega \geqq \omega_1 \geqq \Omega$.

By the "convergence-problem" for Dirichlet series is understood the problem of finding relations between the properties of the series $\sum a_n n^{-s}$ as such—especially the values of the different abscissae of convergence—and the properties of the analytic function $f(s)$ defined by the series.

Only in the case of the abscissa of uniform convergence do we have a simple and general solution of the problem; in fact, as proved by the author, we have for every Dirichlet series the relation

$$\sigma_U = \omega,$$

i. e. the series is uniformly convergent just so far to the left as the function $f(s)$ represented by the series remains regular and bounded.

In the case of the abscissa of absolute convergence the problem of characterizing the abscissa σ_A has turned out to be in the main a problem of discussing the possible values of $\sigma_A - \sigma_U$, i. e. of $\sigma_A - \omega$, and this latter problem has in turn, as shown by the author, an intimate relation with problems from the theory of power series in infinitely many variables. In this way it was found that the difference $\sigma_A - \sigma_U$ (which evidently is $\leqq 1$) is always $\leqq \frac{1}{2}$ and, as proved by HILLE and BOHNENBLUST, that this upper bound $\frac{1}{2}$ can not be diminished.

The problem of determining, or rather estimating, the abscissa of convergence σ_C itself by means of analytical properties of the function $f(s)$ was first attacked by LANDAU who by his researches opened the whole field of investigations in question. Starting from the well-known fact that $f(s) = O(|t|)$ for $\sigma > \sigma_C + \varepsilon$, which so to speak limits the extension of the half-plane of convergence, he proved the other way round that if the order of magnitude of $f(s)$ is known in a certain half-plane $\sigma > \eta$ one may conclude that the half-plane of convergence cannot be too small. LANDAU's estimation of σ_C was sharpened and generalized first by SCHNEE, who proved among other things that σ_C is always $\leqq \omega_1$, and later on by LANDAU himself. The best result, obtained by these successive improvements, is stated in the following theorem[1], the "LANDAU-SCHNEE theorem":

L.-S. Theorem. *For the Dirichlet series* $\sum a_n n^{-s}$ *let the abscissa* σ^* *be* $\leqq 0$, *i. e. let* $a_n = O(n^\delta)$ *for every* $\delta > 0$, *so that the series is certainly absolutely convergent for* $\sigma > 1$. *Further we assume*

[1] See e. g. E. LANDAU, Handbuch der Lehre von der Verteilung der Primzahlen, Leipzig und Berlin 1909, p. 853 and 857.

the existence of two constants $\eta < 1$ *and* $k \geqq 0$ *such that the function* $f(s)$ *defined by the series is regular for* $\sigma > \eta$ *and*

$$f(s) = O(|t|^{k+\varepsilon}) \quad \text{for} \quad \sigma > \eta + \varepsilon .$$

Then the series is convergent beyond the line $\sigma = 1$, *namely at any rate for*

$$\sigma > \operatorname{Min}\left\{\frac{\eta+k}{1+k},\quad \eta+k\right\}.$$

In other words, under the above conditions the abscissa of convergence satisfies the relation

$$\sigma_C \leqq \frac{\eta+k}{1+k} \quad \text{if} \quad \eta+k \geqq 0$$

and

$$\sigma_C \leqq \eta+k \quad \text{if} \quad \eta+k \leqq 0 .$$

When applying the L.-S. theorem to the classical Dirichlet series occurring in the analytical theory of numbers, such as the zeta-series with alternating signs $\sum (-1)^{n-1} n^{-s}$, the results obtained come out to be rather far from the real truth, i. e. the values obtained as an upper bound for σ_C are far too big. This might indicate that the theorem could be improved, i. e. that the number $\operatorname{Min}\left\{\frac{\eta+k}{1+k},\ \eta+k\right\}$ could be replaced by a smaller one. From an earlier investigation by the author, carried out with a somewhat different purpose, it can, however, be concluded that this is not always the case; in fact, from the study of a certain artificially constructed Dirichlet series of the "gap type", it may be shown that in the special cases $0 \leqq k \leqq 1$, $\eta = -k$, the L.-S. theorem cannot be improved. Recently, I have taken the whole question up for a renewed investigation and by generalizing my earlier construction I have proved that the L.-S. theorem is in the very strictest sense, i. e. for every pair of values (η, k) with $\eta < 1$, $k \geqq 0$, the best possible one. In fact the following theorem holds.

Theorem 1. *For any given pair of values* (η, k) *with* $\eta < 1$, $k \geqq 0$, *there exists a Dirichlet series* $\sum a_n n^{-s}$ *with* $\sigma^* \leqq 0$ *for which the function* $f(s)$ *represented by the series is regular in*

$\sigma > \eta$ and, for any $\varepsilon > 0$, is $O(|t|^{k+\varepsilon})$ in $\sigma > \eta + \varepsilon$ and such that the value of the abscissa of convergence σ_C is given exactly by the equation

$$\sigma_C = \text{Min}\left\{\frac{\eta + k}{1 + k},\ \eta + k\right\}.$$

By means of trivial transformations (s being replaced by $s + s_0$) it is easily seen that we may confine ourselves to consider the case $\eta + k \geqq 0$, $\sigma^* = 0$, i.e. to prove the

Theorem 1a. *Let (η, k) be an arbitrary point in the domain determined by $\eta < 1$, $k \geqq 0$, $\eta + k \geqq 0$. Then there exists a Dirichlet series $f(s) = \sum a_n n^{-s}$ with $\sigma^* = 0$, with $f(s)$ regular in $\sigma > \eta$ and $O(|t|^{k+\varepsilon})$ in $\sigma > \eta + \varepsilon$, such that its abscissa of convergence σ_C is just the point $\frac{\eta + k}{1 + k}$ ($\geqq 0$ and < 1), i.e. the point in which the line connecting the two points (η, k) and $(1, -1)$ cuts the axis of abscissae.*

For a Dirichlet series we introduce in the usual way the LINDELÖF μ-function $\mu = \mu(\sigma)$ $(\Omega < \sigma < \infty)$ defined for each $\sigma_0 > \Omega$ as the g.l.b. of the values of l such that

$$f(\sigma_0 + it) = O(|t|^l)$$

or, what amounts to the same thing, that

$$f(\sigma + it) = O(|t|^l) \quad \text{for} \quad \sigma \geqq \sigma_0 \quad (\text{or } \sigma > \sigma_0).$$

The μ-function is a continuous convex function in $\Omega < \sigma < \infty$ and is equal to zero for sufficiently large values of σ, at any rate for $\sigma > \sigma_A$. By help of the μ-function the L.-S. theorem, in the case $\eta + k \geqq 0$, $\sigma^* = 0$, may easily be shown[1] to be equivalent with the following theorem.

Other form of the L.-S. theorem. *Let α be an arbitrary number in the interval $0 \leqq \alpha < 1$, and let $f(s) = \sum a_n n^{-s}$ be a Dirichlet series with $\sigma^* = 0$ and $\sigma_C = \alpha$. Then the μ-function*

[1] Compare K. GRANDJOT, Ueber das absolute Konvergenzproblem der Dirichletschen Reihen, Dissertation, Göttingen 1922.

attached to $f(s)$ will in the whole interval $\sigma > \Omega$ satisfy the condition

$$\mu(\sigma) \geqq M_\alpha(\sigma)$$

where $M_\alpha(\sigma)$ is the simple convex function characterizing the broken line which consists of two half-lines meeting in the point $(\alpha, 0)$, namely of the part of the axis of abscissae to the right of $\sigma = \alpha$ and of the prolongation of the segment from the point $(1, -1)$ to the point $(\alpha, 0)$ beyond this latter point, i. e.

$$M_\alpha(\sigma) = \begin{cases} 0 & \text{for} \quad \sigma \geqq \alpha \\ \dfrac{\sigma - \alpha}{\alpha - 1} & \text{for} \quad \Omega \leqq \sigma \leqq \alpha. \end{cases}$$

Furthermore, using this form of the L.-S. theorem it is readily seen that our theorem 1 a (i. e. the theorem 1) is certainly true if the following theorem holds good.

Theorem 2. *For any α in the interval $0 \leqq \alpha < 1$ there exists a Dirichlet series $f(s) = \sum a_n n^{-s}$ with $\sigma^* = 0$ and $\sigma_C = \alpha$, such that $\Omega = -\infty$ and the μ-function attached to $f(s)$ is given by*

$$\mu(\sigma) = M_\alpha(\sigma) = \begin{cases} 0 & \text{for} \quad \sigma \geqq \alpha \\ \dfrac{\sigma - \alpha}{\alpha - 1} & \text{for} \quad \sigma \leqq \alpha. \end{cases}$$

The main object of the present paper is to prove this theorem 2. I may add, however, that the types of Dirichlet series constructed below may also be used to illustrate various points in the theory of CESARO-summability of the Dirichlet series $\sum a_n n^{-s}$ as developed independently by M. RIESZ and the author. I may return to these summability problems in a later paper; here I shall only recall one of the most striking results of this theory, viz. the relation

$$\sigma_S = \Omega$$

where σ_S denotes the g. l. b. of those σ_0 for which the series is C-summable of some order in the half-plane $\sigma > \sigma_0$. Thus σ_S like σ_U (but in contrast to σ_C and σ_A) can be fully determined by means of simple characteristic properties of the function $f(s)$ represented by the series.

The paper is divided into two sections. In § 1 we prove our theorem 2 for the special case $\alpha = 0$, and in § 2 we treat the general and somewhat more difficult case $0 < \alpha < 1$.

Added remark. After having completed this paper, containing, for an arbitrarily given α in the interval $0 \leqq \alpha < 1$, the construction of a Dirichlet series $\sum a_n n^{-s}$ satisfying the conditions of theorem 2, I became aware that quite a similar problem had already been treated and solved in an interesting paper by NEDER[1] who used a method of construction which shows characteristic relationship with that applied by the author. The results of NEDER, however, do not cover the results of this paper. In order to explain the connection between the results I have for a moment to consider not only the "ordinary" Dirichlet series $\sum a_n n^{-s} = \sum a_n e^{-s \log n}$, with which we exclusively deal in the present paper, but also the "general" Dirichlet series $\sum a_n e^{-\lambda_n s}$ where $0 < \lambda_1 < \lambda_2 < \cdots$ is an arbitrary increasing sequence tending to ∞. For a certain class of such general Dirichlet series we have, as well known, a theorem quite similar to (and including) the L.-S. theorem mentioned above. In fact, if the λ_n-sequence satisfies, for a positive finite l and any $\delta > 0$, the condition

$$(*) \qquad \frac{1}{\lambda_{n+1} - \lambda_n} = O\left(e^{\lambda_n (l+\delta)}\right),$$

introduced by the author (and shown to be the widest class for which theorems of the type in question hold), then the L.-S. theorem in the second formulation is still valid when only α runs through the interval $0 \leqq \alpha < l$ (instead of the interval $0 \leqq \alpha < 1$) and the dominator $1 - \alpha$ in the expression for $M_\alpha(\sigma)$ is replaced by $l - \alpha$. Now, the problem treated and solved by NEDER was just to prove the converse of this last theorem concerning the general class of Dirichlet series $\sum a_n e^{-\lambda_n s}$ satisfying the condition (*), say with $l = 1$, namely to each $0 \leqq \alpha < 1$ to construct a series $\sum a_n e^{-\lambda_n s}$ of the type in question with $\sigma^* = 0$, $\sigma_C = \alpha$ and its μ-function given by $\mu(\sigma) = M_\alpha(\sigma)$. If

[1] L. NEDER, Ueber Umkehrungen der Konvergenzsätze für Dirichletsche Reihen, Berichte der Akademie der Wissenschaften zu Leipzig, Math.-Phys. Klasse, Bd. LXXIV, 1922.

this had been done for an *arbitrarily given* sequence of exponents satisfying (*), for $l = 1$, NEDER's results would obviously have contained our theorem 2. But this was not the case; in fact, NEDER only proved that for any α in $0 \leqq \alpha < 1$ there exists *some* sequence $\lambda_1, \lambda_2, \cdots$ satisfying (*) for $l = 1$ and a corresponding Dirichlet series $\sum a_n e^{-\lambda_n s}$ with $\sigma^* = 0$, $\sigma_C = \alpha$ and $\mu(\sigma) = M_\alpha(\sigma)$; indeed, he just faciliated his construction by choosing an "artificial" sequence λ_n especially suited for his purpose, namely a sequence which—in contrast to the sequence $\lambda_n = \log n$—is composed by parts of different arithmetical progressions.

In this connection it may be emphasized that many problems concerning Dirichlet series essentially depend on the special character of the sequence λ_n of exponents. Thus, to mention an interesting example, nearly related to the problem in question, it has been proved by NEDER in his paper quoted above that there exists a general Dirichlet series $\sum a_n e^{-\lambda_n s}$, with exponents satisfying (*) for $l = 1$, such that $\sigma_C = 0$, $\sigma_A = 1$ and $\mu(\sigma) = \frac{1}{2} - \sigma$ for $\sigma \leqq \frac{1}{2}$, while it is an open problem whether there exists a Dirichlet series of the ordinary type $\sum a_n n^{-s}$ with the same properties. [Only under the assumption of the so-called LINDELÖF hypothesis—which certainly holds good if the RIEMANN hypothesis does—we possess, as emphasized by GRANDJOT, such an example, namely the series $\zeta(s)\,(1 - 2^{1-s}) = \sum (-1)^{n+1} n^{-s}$].

§ 1. The case $\alpha = 0$.

In this section we shall prove theorem 2 in the special case $\alpha = 0$, i.e. we shall construct a Dirichlet series $f(s) = \sum a_n n^{-s}$ with $\sigma^* = 0$, $\sigma_C = 0$ and $\Omega = -\infty$ such that the μ-function is given by

$$\mu(\sigma) = \begin{cases} 0 \text{ for } \sigma \geqq 0 \\ -\sigma \text{ for } \sigma \leqq 0. \end{cases}$$

The idea of the construction, namely to build a gap-series containing differences of higher and higher order, has been used previously by the author[1].

[1] H. BOHR, Bidrag til de Dirichlet'ske Rækkers Theori, Habilitationsskrift, København 1910.

Let $p_1 < p_2 < p_3 \cdots$ be a sequence of positive integers which increases so rapidly that $p_{m+1} > p_m + m$ and that the infinite series

$$\sum_{m=1}^{\infty} 2^m p_m^{-\varepsilon}$$

converges for every $\varepsilon > 0$.

We consider the Dirichlet series

$$\sum_{n=1}^{\infty} a_n n^{-s} = p_1^{-s} - (p_1+1)^{-s} + p_2^{-s} - 2(p_2+1)^{-s} + (p_2+2)^{-s} + \cdots$$

the terms of which consist of groups of 2, 3, $\cdots$ elements such that the m^{th} group is given by

$$p_m^{-s} - \binom{m}{1}(p_m+1)^{-s} + \binom{m}{2}(p_m+2)^{-s} - \cdots + (-1)^m (p_m+m)^{-s}$$

and where, on account of the inequality $p_{m+1} > p_m + m$, the groups do not overlap. Applying the usual terminology for differences of 1^{st} and higher order, i. e.

$$\Delta u_p = u_p - u_{p+1}, \quad \Delta^2 u_p = u_p - 2u_{p+1} + u_{p+2}, \quad \cdots$$

$$\Delta^m u_p = u_p - \binom{m}{1} u_{p+1} + \binom{m}{2} u_{p+2} - \cdots + (-1)^m u_{p+m}, \quad \cdots$$

we may write our Dirichlet series, with its terms in groups, in the form

$$f(s) = \sum_{n=1}^{\infty} a_n n^{-s} = \sum_{m=1}^{\infty} \Delta^m (p_m^{-s}).$$

For these differences we shall have to use, besides the general trivial estimations

$$|\Delta^m u_p| \leqq |u_p| + \binom{m}{1} |u_{p+1}| + \cdots + |u_{p+m}| \leqq 2^m \cdot \operatorname*{Max}_{p \leqq \nu \leqq p+m} |u_\nu|$$

and, for $1 \leqq h < m$,

$$|\Delta^m u_p| = |\Delta^{m-h} \Delta^h u_p| \leqq 2^{m-h} \cdot \operatorname*{Max}_{p \leqq \nu \leqq p+m-h} |\Delta^h u_\nu|,$$

the special, well-known, integral-representation for $u_p = p^{-s}$ ($p \geqq 1$, s arbitrary complex)

$$\Delta^h(p^{-s}) = (-1)^h \int_p^{p+1} dx_1 \int_{x_1}^{x_1+1} dx_2 \cdots \int_{x_{h-1}}^{x_{h-1}+1} \frac{d^h}{dx_h^h}(x_h^{-s})\, dx_h =$$

$$s(s+1)\cdots(s+h-1) \int_p^{p+1} dx_1 \cdots \int_{x_{h-1}}^{x_{h-1}+1} x_h^{-s-h} dx_h$$

which, in case $\sigma + h > 0$, immediately gives the inequality

$$|\Delta^h(p^{-s})| \leqq |s| \cdot |s+1| \cdots |s+h-1| \cdot p^{-\sigma-h}.$$

We shall now show that our series $f(s) = \sum a_n n^{-s} = \sum \Delta^m(p_m^{-s})$ has all the properties stated.

Firstly we have $\sigma^* = 0$. On the one hand σ^* is certainly $\geqq 0$, as a_n does not tend to zero for $n \to \infty$ (e. g. $a_n = 1$ for $n = p_m$). On the other hand $a_n = O(n^\varepsilon)$ for each $\varepsilon > 0$; in fact since $2^m p_m^{-\varepsilon} \to 0$, we have for each n for which $a_n \neq 0$, i. e. for $n = p_m + \nu\ (0 \leqq \nu \leqq m)$ and m sufficiently large

$$|a_n| = \left|(-1)^\nu \binom{m}{\nu}\right| \leqq 2^m = \left(2^m p_m^{-\varepsilon}\right) p_m^\varepsilon < p_m^\varepsilon \leqq n^\varepsilon.$$

Secondly we have $\sigma_C = 0$. As $\sigma_C \geqq \sigma^* = 0$ we need only show that the series is convergent for $\sigma > 0$. We shall see that it is even absolutely convergent for $\sigma > 0$, and thus not only $\sigma_C = 0$ but also $\sigma_A = 0$. In fact for each $\sigma > 0$ the sum of the numerical values of the terms in the group $\Delta^m(p_m^{-s})$ is equal to

$$\sum_{\nu=0}^{m} \binom{m}{\nu} (p_m + \nu)^{-\sigma} \leqq p_m^{-\sigma} \sum_{\nu=0}^{m} \binom{m}{\nu} = 2^m p_m^{-\sigma},$$

and the series $\sum 2^m p_m^{-\sigma}$ is convergent for $\sigma > 0$.

Thirdly we have $\Omega = -\infty$, i. e. the function $f(s)$ defined by the series in the half-plane of convergence $\sigma > 0$ is an integral function and of finite order in each half-plane $\sigma > \sigma_0$. To this purpose we consider, for an arbitrary fixed positive integer h, the half-plane $\sigma > -h$ and in this half-plane estimate

the group of terms $\Delta^m(p_m^{-s})$ for each $m>h$. By help of the estimations indicated above we get, for $\sigma>-h$, $m>h$

$$|\Delta^m(p_m^{-s})| \leqq 2^{m-h}\cdot \operatorname*{Max}_{p_m \leqq \nu \leqq p_m+m-h} |\Delta^h(\nu^{-s})|$$

$$\leqq 2^{m-h}|s||s+1|\cdots|s+h-1|\cdot \operatorname*{Max}_{p_m \leqq \nu \leqq p_m+m-h} \nu^{-\sigma-h} = 2^{m-h}|s|\cdots|s+h-1|p_m^{-\sigma-h}.$$

Writing

$$f(s) = \sum_{m=1}^{\infty} \Delta^m(p_m^{-s}) = \sum_{m=1}^{h} \Delta^m(p_m^{-s}) + \sum_{m=h+1}^{\infty} \Delta^m(p_m^{-s}) = f_1(s)+f_2(s),$$

the finite sum $f_1(s) = \sum_{m=1}^{h}$ is evidently an integral function bounded in every half-plane $\sigma>\sigma_0$, while the series $f_2(s) = \sum_{m=h+1}^{\infty}$ is majorized in the half-plane $\sigma>-h+\varepsilon$ by the convergent series

$$2^{-h}|s|\cdots|s+h-1|\sum_{m=h+1}^{\infty} 2^m p_m^{-\varepsilon}.$$

Hence $f_2(s)$ is analytic in $\sigma>-h+\varepsilon$ (the series being uniformly convergent in $\sigma>-h+\varepsilon$, $|s|<K$) and $= O(|t|^h)$ for $|t|\to\infty$, uniformly in $-h+\varepsilon<\sigma<2$ and hence also in $-h+\varepsilon<\sigma<\infty$. Therefore $f(s)=f_1(s)+f_2(s)$ is regular and $= O(|t|^h)$ in $\sigma>-h+\varepsilon$. Thus $\Omega \leqq -h+\varepsilon$ for each h, i. e. $\Omega = -\infty$.

Finally we have to consider the μ-function $\mu(\sigma)$, defined for all σ. As $\sigma_A = 0$ we have immediately $\mu(\sigma) = 0$ for $\sigma>0$ and hence, as $\mu(\sigma)$ is a continuous function,

$$\mu(\sigma) = 0 \quad \text{for} \quad \sigma \geqq 0.$$

We shall show that $\mu(\sigma) = -\sigma$ for $\sigma \leqq 0$. We apply the L.-S. theorem in its second form. Since for our series $f(s) = \sum a_n n^{-s}$ we have $\sigma^* = 0$, $\sigma_C = 0$ and $\Omega = -\infty$, the theorem (for $\alpha = 0$) states that $\mu(\sigma)$ is certainly $\geqq M_0(\sigma) = -\sigma$ for $\sigma \leqq 0$; thus, in order to prove that $\mu(\sigma) = -\sigma$ for $\sigma \leqq 0$, we have only to show that

$$\mu(\sigma) \leqq -\sigma \quad \text{for} \quad \sigma \leqq 0.$$

As $\mu(\sigma)$ is convex, and $\mu(0) = 0$, it suffices to prove that

$$\mu(-h) \leqq h \quad \text{for} \quad h = 1, 2, 3, \cdots.$$

This, however, follows immediately from the above relation, holding for an arbitrary positive integer h,

$$f(s) = O(|t|^h) \quad \text{in} \quad \sigma > -h + \varepsilon$$

which shows that $\mu(\sigma) \leqq h$ for $\sigma > -h$ and hence also, by reason of continuity, $\mu(-h) \leqq h$.

§ 2. The case $0 < \alpha < 1$.

In this last section we shall prove theorem 2 in the general case, i. e. for an arbitrary α in the interval $0 < \alpha < 1$. We have to prove the existence of a Dirichlet series $f(s) = \sum a_n n^{-s}$ with $\sigma^* = 0$, $\sigma_C = \alpha$, $\Omega = -\infty$ and the μ-function

$$\mu(\sigma) = \begin{cases} 0 & \text{for} \quad \sigma \geqq \alpha \\ \dfrac{\sigma - \alpha}{\alpha - 1} & \text{for} \quad \sigma \leqq \alpha. \end{cases}$$

As in the case $\alpha = 0$ we start from a rapidly increasing sequence of positive integers $p_1 < p_2 \cdots$. But now—in order that $\sum a_n n^{-s}$ shall converge only for $\sigma > \alpha$, and not for $\sigma > 0$—we must take care that the partial sums $S_n = a_1 + \cdots + a_n$ are not for all values of n too small compared with n but, roughly speaking, for some large n's are of the order of magnitude n^α. To this end we introduce, besides the numbers $p_1, p_2, \cdots$, other numbers $q_1, q_2, \cdots$ such that q_m is of the order p_m^α, and choose $a_n = 1$ for the values of n between p_m and $p_m + q_m$. Specifically, we choose the positive integers $(1 <) p_1 < p_2 \cdots$; $q_1, q_2, \cdots$ such that

$$p_m^\alpha < q_m < 2 p_m^\alpha, \qquad p_{m+1} > p_m + (m+1) q_m - 1$$

and (as in § 1) such that

$$\sum_{m=1}^{\infty} 2^m p_m^{-\varepsilon}$$

converges for every $\varepsilon > 0$.

The Dirichlet series to be constructed is based on the same idea as that of § 1 but is of a somewhat more complicated structure. Instead of the differences $\Delta^m(p^{-s})$ we have now to use differences $\Delta_q^m(p^{-s})$ with a "span" q (where q tends to infinity together with p), defined in the usual manner by

$$\Delta_q u_p = u_p - u_{p+q},\ \Delta_q^2 u_p = u_p - 2u_{p+q} + u_{p+2q},\ \cdots$$

$$\Delta_q^m u_p = u_p - \binom{m}{1} u_{p+q} + \binom{m}{2} u_{p+2q} - \cdots + (-1)^m u_{p+mq},\ \cdots.$$

For these differences we have for $1 \leqq h < m$ the trivial estimation

$$\left|\Delta_q^m u_p\right| = \left|\Delta_q^{m-h}\Delta_q^h u_p\right| = \left|\Delta_q^h u_p - \binom{m-h}{1}\Delta_q^h u_{p+q} + \cdots + (-1)^{m-h}\Delta_q^h u_{p+(m-h)q}\right|$$

$$\leqq 2^{m-h} \cdot \operatorname{Max}_{p \leqq \nu \leqq p+(m-h)q} \left|\Delta_q^h u_\nu\right|,$$

and for $p > 0$, $s = \sigma + it$ and $\sigma + h > 0$

$$\left|\Delta_q^h(p^{-s})\right| = \left|\int_p^{p+q} dx_1 \int_{x_1}^{x_1+q} dx_2 \cdots \int_{x_{h-1}}^{x_{h-1}+q} \frac{d^h}{dx_h^h}\left(x_h^{-s}\right) dx_h\right| \leqq$$

$$|s|\,|s+1| \cdots |s+h-1|\, q^h p^{-\sigma-h}.$$

In our series $\sum a_n n^{-s}$ the first group of terms is no longer (as in § 1) of the simple form $p_1^{-s} - (p_1+1)^{-s} = \Delta(p_1^{-s})$ but of the form

$$p_1^{-s} + (p_1+1)^{-s} + \cdots + (p_1+q_1-1)^{-s} - (p_1+q_1)^{-s} - (p_1+q_1+1)^{-s} - \cdots -$$

$$(p_1+2q_1-1)^{-s} = \Delta_{q_1}(p_1^{-s}) + \Delta_{q_1}(p_1+1)^{-s} + \cdots + \Delta_{q_1}(p_1+q_1-1)^{-s}$$

and analogously for the following groups, i. e. the m^{th} group consists of the $(m+1)q_m$ terms (here not indicated in their natural order)

$$\sum_{\mu=0}^{q_m-1} \Delta_{q_m}^m (p_m+\mu)^{-s}.$$

Our Dirichlet series is then defined by

$$f(s) = \sum a_n n^{-s} = \sum_{m=1}^{\infty} \sum_{\mu=0}^{q_m-1} A_{q_m}^m (p_m+\mu)^{-s}$$

where the different groups, on account of $p_{m+1} > p_m + (m+1) q_m - 1$, do not overlap.

Firstly we have to show that $\sigma^* = 0$. As in § 1 we see immediately that σ^* is ≥ 0, as for instance $a_n = 1$ for $n = p_m$. On the other hand $a_n = O(n^\varepsilon)$ for every $\varepsilon > 0$, since for each n with $a_n \neq 0$, i.e. $n = p_m + \mu\, (0 \leq \mu < (m+1)\, q_m)$ we have for sufficiently large m (on account of $2^m p_m^{-\varepsilon} \to 0$)

$$|a_n| \leq 2^m = 2^m p_m^{-\varepsilon} p_m^{\varepsilon} < p_m^{\varepsilon} \leq n^{\varepsilon}.$$

Secondly we have $\sigma_C = \alpha$, and also $\sigma_A = \alpha$. To prove this, we first show that $\sum a_n n^{-s}$ is absolutely convergent for $\sigma > \alpha$, i.e. that $\sigma_A \leq \alpha$, and secondly that $\sigma_C \geq \alpha$. In order to prove the convergence of $\sum |a_n| n^{-\sigma}$ for $\sigma > \alpha$, we simply observe that for each $\sigma > \alpha$ the sum of the numerical values of the $(m+1)\, q_m$ terms in the group

$$\sum_{\mu=0}^{q_m-1} A_{q_m}^m (p_m+\mu)^{-s}$$

is equal to

$$\sum_{\mu=0}^{q_m-1} \sum_{\nu=0}^{m} \binom{m}{\nu} (p_m+\mu+\nu\, q_m)^{-\sigma} < p_m^{-\sigma} 2^m q_m < 2 \cdot 2^m p_m^{\alpha-\sigma}$$

and that the series $\sum 2^m p_m^{\alpha-\sigma}$ is convergent for $\sigma > \alpha$. Next, in order to show that $\sigma_C \geq \alpha$, it suffices (compare a remark in the introduction) to show that $S_n = a_1 + \cdots + a_n$ is *not* $o(n^\alpha)$. But this is certainly the case, as the assumption $S_n = o(n^\alpha)$ would imply that

$$S_{p_m-1} = o(p_m-1)^\alpha = o(p_m^\alpha), \quad S_{p_m+q_m-1} = o(p_m+q_m-1)^\alpha = o(p_m^\alpha)$$

and hence

$$S_{p_m+q_m-1} - S_{p_m-1} = o(p_m^{\alpha})$$

which contradicts the fact that $a_n = 1$ for $p_m \leqq n \leqq p_m + q_m - 1$ and thus

$$S_{p_m+q_m-1} - S_{p_m-1} = q_m > p_m^{\alpha}.$$

Thirdly, in order to prove that $\Omega = -\infty$, it suffices to show that the analytic function $f(s)$ defined by the series for $\sigma > \alpha$ for some decreasing sequence of real numbers $\sigma_h (h = 1, 2, \cdots)$ tending to $-\infty$ is regular and of finite order in $\sigma > \sigma_h + \varepsilon$. As these numbers σ_h we choose the equidistant numbers

$$\sigma_h = \alpha - h(1-\alpha) \qquad (h = 1, 2, \cdots),$$

i. e. the numbers σ_h for which the linear function $M_{\alpha}(\sigma) = \dfrac{\sigma - \alpha}{\alpha - 1} = h$. We proceed in a way analogous to that in § 1, i. e. we divide, for a fixed h, the function $f(s)$ into two parts, viz.

$$f(s) = f_1(s) + f_2(s) = \sum_{m=1}^{h} \sum_{\mu=0}^{q_m-1} A_{q_m}^{m} (p_m + \mu)^{-s} + \sum_{m=h+1}^{\infty} \sum_{\mu=0}^{q_m-1} A_{q_m}^{m} (p_m + \mu)^{-s}$$

where the finite sum $f_1(s) = \sum_{m=1}^{h}$ is obviously an integral function bounded in every half-plane $\sigma > \sigma_0$. In the second sum $f_2(s) = \sum_{m=h+1}^{\infty}$ we estimate each term for $\sigma > \sigma_h + \varepsilon$ and find for an arbitrary one of its q_m components

$$\left| A_{q_m}^{m} (p_m + \mu)^{-s} \right| \leqq 2^{m-h} \cdot \operatorname{Max}_{p_m+\mu \leqq \nu \leqq p_m+\mu+(m-h)q_m} \left| A_{q_m}^{h} \nu^{-s} \right|$$

where the right-hand side, on account of $\sigma + h > \alpha(1+h) + \varepsilon$ for $\sigma > \sigma_h + \varepsilon$, is again

$$\leqq 2^{m-h} \left| s \right| \left| s+1 \right| \cdots \left| s+h-1 \right| q_m^{h} \cdot \operatorname{Max}_{p_m+\mu \leqq \nu \leqq p_m+\mu+(m-h)q_m} \nu^{-\alpha(1+h)-\varepsilon}$$

$$\leqq 2^{m-h} \left| s \right| \cdots \left| s+h-1 \right| q_m^{h} p_m^{-\alpha(1+h)-\varepsilon}.$$

Thus for $\sigma > \sigma_h + \varepsilon$ we find for the whole m^{th} group consisting of q_m components the estimation

$$\left| \sum_{\mu=0}^{q_m-1} A_{q_m}^{m} (p_m + \mu)^{-s} \right| \leq q_m \cdot \left(2^{m-h} \left| s \right| \cdots \left| s+h-1 \right| q_m^h p_m^{-\alpha(1+h)-\varepsilon}\right)$$

which, on account of $q_m < 2 p_m^{\alpha}$, is again

$$< 2^{m+1} \left| s \right| \cdots \left| s+h-1 \right| p_m^{\alpha(1+h)-\alpha(1+h)-\varepsilon} = 2 \left| s \right| \cdots \left| s+h-1 \right| \cdot 2^m p_m^{-\varepsilon}.$$

Now, as $\sum 2^m p_m^{-\varepsilon}$ is convergent, we conclude, just as in § 1, that $f_2(s)$ and hence also $f(s) = f_1(s) + f_2(s)$, is regular and $O(|t|^h)$ in $\sigma > \sigma_h + \varepsilon$, and thus we have proved that $\Omega = -\infty$.

Finally we shall prove that the μ-function, defined for all σ, is given by

$$\mu(\sigma) = \begin{cases} 0 & \text{for } \sigma \geq \alpha \\ M_\alpha(\sigma) = \dfrac{\sigma - \alpha}{\alpha - 1} & \text{for } \sigma \leq \alpha. \end{cases}$$

That $\mu(\sigma) = 0$ for $\sigma \geq \alpha$ follows immediately from $\sigma_A = \alpha$. Since, according to the L.-S. theorem in the formulation of pag. 7, we have certainly

$$\mu(\sigma) \geq M_\alpha(\sigma) = \frac{\sigma - \alpha}{\alpha - 1} \quad \text{for } \sigma \leq \alpha$$

we need only show that

$$\mu(\sigma) \leq M_\alpha(\sigma) \quad \text{for} \quad \sigma \leq \alpha,$$

and as $\mu(\sigma)$ is convex, and $\mu(\alpha) = 0$, it suffices to show that

$$\mu(\sigma_h) \leq M_\alpha(\sigma_h) = h \quad \text{for} \quad h = 1, 2, \cdots.$$

This, however, is an immediate consequence of the relation

$$f(s) = O(|t|^h) \quad \text{for} \quad \sigma > \sigma_h + \varepsilon,$$

which shows that $\mu(\sigma) \leq h$ for $\sigma > \sigma_h$ and hence also for $\sigma = \sigma_h$.

Indleveret til Selskabet den 20. august 1948.
Færdig fra trykkeriet den 17. januar 1949.

DET KGL. DANSKE VIDENSKABERNES SELSKAB
MATEMATISK-FYSISKE MEDDELELSER, BIND XXV, NR. 7

LE SPECTRE DES NAINES BLANCHES ET LEUR DÉBIT D'ÉNERGIE

PAR

EVRY SCHATZMAN

KØBENHAVN
I KOMMISSION HOS EJNAR MUNKSGAARD
1950

Printed in Denmark
Bianco Lunos Bogtrykkeri

L'interprétation du spectre des naines blanches est profondément liée à la compréhension de leur structure interne. Le triage des éléments dans un champ de pesanteur, phénomène particulièrement important dans les naines blanches, détermine presque totalement à lui seul leur structure et l'aspect de leur spectre. On étudie donc pour commencer le triage des éléments (chapitre I). On montre comment se distribuent les éléments dans un champ de pesanteur. L'évaluation de la hauteur de mélange dans des cas variés montre que cette grandeur est peu sensible à l'état de dégénérescence du gaz d'électrons. La hauteur de mélange est toujours très petite dans les naines blanches. On voit aussi que les éléments lourds doivent avoir en général dans les régions extérieures des naines blanches une concentration extraordinairement faible, ce qui explique l'absence de raies métalliques dans le spectre.

Les densités relativement élevées qui règnent dans l'atmosphère des naines blanches exigent une étude de l'ionisation de pression dans l'hydrogène (chapitre II). On montre en particulier que l'effet Stark moléculaire semble mieux décrit aux fortes densités par les formules de Russell et Stewart que par celles de Holtsmark.

On a calculé un modèle d'atmosphère pour deux étoiles correspondant approximativement à 40 Eridani B et Van Maanen 2 (Chapitre III). On a supposé une atmosphère faite d'hydrogène pur, ainsi que l'étude du chapitre I l'a suggéré. Le calcul de l'élargissement des raies par effet Stark moléculaire montre une importante déformation du contour du fond continu sous l'influence de la pression.

Les résultats précédents permettent d'étudier la relation entre la température de couleur et la température effective dans les

naines blanches (chapitre IV). On trouve que pour une même température de couleur, la température effective est beaucoup plus élevée dans les naines blanches que dans les étoiles de la série principale. Ce fait joint aux résultats de la théorie du débit d'énergie aux grandes densités, indique pour les naines blanches des rayons plus petits et entraîne de très faibles teneurs en hydrogène.

Ce résultat est confirmé par la théorie élémentaire du débit d'énergie (Chapitre V). On peut montrer que la réaction proton — proton dans l'enveloppe d'hydrogène explique le débit d'énergie des naines blanches. Cette réaction pouvant être permise sans catastrophe astrophysique, on réconcilie ainsi les données de l'astrophysique avec la théorie des réactions nucléaires. Les réactions du cycle de Bethe semblent, en général, ne jouer qu'un rôle secondaire (un pour cent du débit d'énergie total dans 40 Eridani B).

La question de l'évolution des naines blanches reste une question ouverte que les calculs précédents ne résolvent pas. De même, la structure de Van Maanen 2, seule naine blanche présentant avec certitude des raies métalliques, présente des difficultés, car elle doit être compatible à la fois avec la théorie du débit d'énergie et la théorie du triage des éléments.

Je tiens à adresser mes remerciements les plus sincères à Monsieur le Professeur Strømgren pour son accueil si chaleureux à Copenhague, et pour les nombreuses discussions que j'ai pu avoir avec lui. Je remercie également M. Rudkjøbing pour les conversations que j'ai eues avec lui.

I. Le triage des éléments.

1. Aspect général du problème. Le problème de l'équilibre statistique dans un champ de gravitation d'un mélange de particules d'espèces différentes est un problème déjà ancien auquel des contributions très nombreuses ont été apportées.

Mentionnons tout d'abord les problèmes relatifs aux mélanges isothermes, nous réservant d'aborder plus loin la question des gaz non uniformes et des cas de dégénérescence.

Pour des éléments soumis au seul champ de pesanteur, à

l'exclusion de tout autre champ de force (électrique ou magnétique), on a simplement, en appliquant la loi de distribution de Boltzmann:

$$\varrho = \varrho_0 \, e^{-m(V-V_0)/kT} \tag{1.1}$$

qui est la loi de distribution des densités connue sous le nom de loi de Dalton.

Dans le cas d'un équilibre de dissociation produisant ou non des particules chargées, l'équilibre thermodynamique n'est pas modifié par la présence ou l'absence d'un champ. Ceci a été démontré dans le cas d'un champ de pesanteur par Gibbs (17), dans le cas d'un champ de forces électrostatiques par Milne (24). Les conséquences de la présence d'un champ de gravitation sur la séparation des charges électriques (les électrons étant plus légers que les protons) ont été données pour la première fois par Pannekoek (27), qui a évalué la charge d'origine thermique de la matière. On savait déjà par ce résultat que la charge électrique de la matière était très faible et que le champ électrique présent était assez fort pour empêcher toute séparation des charges. L'analyse de Rosseland (29) montre que la séparation des charges dans une atmosphère isotherme ne commence que lorsque le terme

$$\frac{4\,\pi\varepsilon^2 p_e}{m_e^2 g^2} \tag{1.2}$$

est petit comparé à l'unité. Dans le cas du soleil, le produit $4\,\pi\,\varepsilon^2/m^2\,g^2$ vaut $4{,}85\cdot10^{27}$. Dans le cas des naines blanches connues, g peut être 10^6 fois plus fort, et $4{,}85\cdot10^{15}$ peut être considéré comme une limite inférieure. p_e doit donc être inférieur à 10^{-16} dynes/cm^2 ou, pour une température moyenne de $2\cdot10^4$ degrés de l'atmosphère des naines blanches, le nombre d'électrons par centimètre cube doit être inférieur à $10^{-4,4}$, c-à-d. bien inférieur à la densité de l'espace interstellaire. Par une autre voie que celle de Pannekoek, Rosseland a donc montré la justesse de l'hypothèse de neutralité électrique de la matière stellaire.

Dans le cas des champs de pesanteur intenses, la séparation des éléments peut être assez considérable pour qu'on puisse

définir une hauteur de mélange de deux éléments. Ceci a été fait par l'auteur (34) dans le cas où le gaz d'électrons est dégénéré et étendu (35) au cas où le gaz d'électrons étant parfait, l'ionisation est partielle. La charge électrique lorsque le gaz d'électrons est dégénéré a été calculée également (37). Le problème du gaz isotherme peut être abordé d'une toute autre manière à partir de l'étude des gaz non-uniformes (12). Le phénomène de diffusion de pression, dû à l'existence d'un gradient de pression partielle d'un gaz mêlé à un autre est connu depuis longtemps. Le langage de la théorie des gaz non-uniformes nous amène au cas des gaz non-isothermes, qui est le cas réel des étoiles. Un bref aperçu est donné par Eddington dans I.C.S.(14), qui renvoie pour la diffusion thermique à un travail de CHAPMAN (10). La diffusion thermique qui est de très faible importance devant d'autres phénomènes est traitée par Chapman dans cet article déjà ancien sans tenir compte des phénomènes d'ionisation. EDDINGTON (l. c.) évalue qualitativement l'influence du modèle atomique utilisé, et conclut, en accord avec une confirmation personnelle de Chapman, que la diffusion thermique joue sans doute dans le même sens que la diffusion de pression. BIERMANN (3) étudie le problème de la diffusion et de l'équilibre statistique en donnant une bibliographie du sujet.

Tous ces travaux sur les gaz non-uniformes sont faits en supposant que les atomes ne transportent avec eux aucune énergie autre que cinétique de translation ou de rotation (11) et par conséquent ne tiennent pas compte de l'énergie d'ionisation. L'hypothèse de l'équilibre thermodynamique local permet d'adapter les équations valables pour une atmosphère isotherme à une atmosphère à température non-uniforme, et, par comparaison avec les formules de diffusion, de montrer l'existence d'une diffusion thermique due à l'ionisation.

D'autre part, suivant que le gaz de noyaux se trouve plongé dans un gaz d'électrons dégénéré ou parfait, le triage est déterminé, dans le premier cas par la quantité

$$\frac{A_i}{Z_i}. \tag{1.3}$$

dans le second par la quantité:

$$\frac{A_i - m_e}{Z_i + 1}.$$

Lorsque le gaz d'électrons est dégénéré, tous les éléments se comportent de la même façon devant l'hydrogène ($A_i/Z_i \simeq 2$), alors que dans le second cas, tous les éléments subissent en plus les uns par rapport aux autres un triage important.

Lorsque les phénomènes de dégénérescence apparaissent également au sein du gaz de noyaux, particulièrement avec les dégénérescences de Bose-Einstein, differents phénomènes assez curieux apparaissent. Tous ces résultats ont reçu un commencement d'application à la théorie des naines blanches (34).

A. Les gaz non-dégénérés.

2. Méthode statistique. Rappelons brièvement comment on traite le problème de l'équilibre de dissociation d'un mélange de particules d'espèces différentes. Cette méthode est inspirée de celle employée par CHANDRASEKHAR (6) à la suite de MILNE (25).

Etant donnés j éléments de charge Z_i et possédant différents degrés d'ionisation, on peut représenter les réactions d'équilibre par:

$$A_i^n + ne - \sum_n \chi_i^n \rightleftarrows A_i^0, \tag{2.1}$$

dans lequel A est l'atome d'espèce i ionisé n fois. χ_i^n est l'énergie pour ioniser le n^e électron et $\sum_n \chi_i^n$ est l'énergie nécessaire pour ioniser n fois l'atome.

Nous appelons p_{is}^n le nombre d'atomes d'espèce i, n fois ionisés, d'énergie $E_s^{in} + \sum_n \chi_i^n$ et x_{is}^n le nombre d'états possibles d'énergie $E_s^{in} + \sum_n \chi_i^n$. r_s, E_s, x_s représentent des quantités analogues pour les électrons. Pour trouver l'état le plus probable, nous astreignons les quantités p_{is}^n et r_s aux conditions suivantes:

$$\begin{cases} \sum_{ns} p_{is}^n = p_i \\ \sum_{ns} (Z_i - n)\, p_{is}^n + r_s = r \\ \sum p_{is}^n \left(E_s^{in} + \sum_n \chi_i^n \right) + E_s r_s = E \end{cases} \tag{2.2}$$

conditions relatives au nombre de particules et à l'énergie. En associant ces conditions au nombre de complexions (qu'il est inutile d'écrire) et en employant la méthode des multiplicateurs de Lagrange en multipliant les équations de condition par $\alpha_i\ \beta\ \vartheta$, on obtient:

$$(2.3)\qquad \begin{cases} p_{is}^n = x_{is}^n\, e^{-\alpha_i(Z_i-n)\beta-\vartheta(E_s^{in}+\sum\chi_i^n)} \\ r_s = x_s e^{-\beta-\vartheta E_s}. \end{cases}$$

Par intégration dans l'espace des moments, et en se rappelant que E_s^{in} contient l'énergie cinétique et l'énergie potentielle:

$$(2.4)\qquad E_s^{in} = \frac{p_s^2}{2\,m_i} + \varphi m_i - ne\psi,$$

on obtient:

$$(2.5)\qquad \begin{cases} p_i^n = g_i^n \dfrac{(2\pi m_i^n kT)^{\frac{3}{2}}}{h^3}\, e^{-\alpha_i-(Z_i-n)\beta-\vartheta\left(\varphi m_i-ne\psi+\sum\limits_n \chi_i^n\right)} \\ r = 2\dfrac{(2\pi m_e kt)^{\frac{3}{2}}}{h^3}\, e^{-\beta-\vartheta(\varphi m+e\psi)}. \end{cases}$$

On retrouve ici le résultat déjà obtenu par Gibbs et Milne c-à-d., l'indépendance de l'équation d'équilibre par rapport aux champs électriques et de pesanteur:

$$(2.6)\qquad \frac{p_i^n\, r}{p_i^{n-1}} = \frac{2\,g_i^n}{g_i^{n-1}} \frac{(2\pi m_e kT)^{\frac{3}{2}}}{h^3}\, e^{-\vartheta\chi_i^n}.$$

Comme nous sommes dans le cas d'un gaz isotherme, les α_i et β sont des constantes, et l'équation d'équilibre hydrostatique:

$$(2.7)\qquad \frac{dP}{dz} = -F\varrho$$

est une conséquence des équations écrites ci-dessus.

3. Le triage des éléments. La détermination du potentiel électrique ψ pourrait se faire en utilisant la relation de Poisson. On obtient alors les résultats bien connus relatifs à la quasi-

neutralité électrique du milieu. Il est donc plus simple de partir de cette relation pour définir ψ:

$$\sum_{in} n p_i^n = r, \tag{3.1}$$

ou, après élimination de $T^{\frac{3}{2}}$,

$$\sum_{in} n \frac{g_i^n}{2} \left(\frac{m_i^n}{m_e}\right)^{\frac{3}{2}} e^{-\alpha_i - (Z_i - n - 1)\beta - \vartheta[\varphi(m_i^n - m_e) - (n+1)e\psi] - \vartheta \Sigma \chi_i^n} = 1, \tag{3.2}$$

équation de la forme:

$$\sum_{in} n a_{in} u^{A_i^n} v^{n+1} = 1 \tag{3.3}$$

avec

$$\begin{cases} u = e^{-\vartheta \varphi H} & HA_i^n = m_i - (n+1)\, m_e \\ v = e^{\vartheta e \psi}, \end{cases} \tag{3.4}$$

m_i étant la masse de l'atome non ionisé.

Il est aisé de démontrer, comme nous l'avons déjà fait (34, paragraphe 14), que les maxima de concentration des différents éléments et de leurs ions se succèdent de bas en haut d'un récipient vertical dans l'ordre des $A_i^n/(n+1)$ décroissants, les atomes les plus ionisés ou les plus légers se trouvant en haut. Remarquons toutefois que la démonstration concerne une concentration particulière:

$$c_{in} = \frac{p_i^n}{r} \tag{3.5}$$

qui est le nombre d'atomes i ionisés n fois au nombre total de charges positives (ou négatives) libres, et non pas la masse de particules p_i^n à la masse totale. Le résultat subsiste cependant avec cette définition de la concentration.

Dans le cas d'un mélange de deux éléments, il est possible de pousser les conclusions beaucoup plus loin. Nous allons donner ici une première définition de la hauteur de mélange, identique à celle déjà utilisée (34). Nous appelons hauteur de mélange l'intervalle dans lequel les éléments 1 et 2 étant mélangés, le produit des concentration en poids $c_1 \cdot c_2$ reste supérieur

à une quantité donnée. On est assuré de définir ainsi une région où l'on trouve simultanément les concentrations les plus élevées des deux éléments. Si l'on suppose que pour une densité et une température données, l'élément 1 est essentiellement ionisé n_1 fois et l'élément 2, n_2 fois, l'équation de neutralité électrique se réduit approximativement à:

$$n_1 p_1^n + n_2 p_2^n = r. \tag{3.6}$$

La concentration en poids est alors approximativement:

$$\begin{cases} c_1 = \dfrac{m_1 p_1^{n_1}}{m_1 p_1^{n_1} + m_2 p_2^{n_2}} \\ c_2 = \dfrac{m_2 p_2^{n_2}}{m_1 p_1^{n_1} + m_2 p_2^{n_2}}. \end{cases} \tag{3.7}$$

Le produit $c_1 c_2$ est maximum pour $\dfrac{m_2 p_2^{n_2}}{m_1 p_1^{n_1}} = 1$ et prend la moitié de la valeur au maximum pour $\dfrac{m_2 p_2^{n_2}}{m_1 p_1^{n_1}} = 3 \pm \sqrt{8}$. Le système des équations (2.5) nous permet d'éliminer la variation de potentiel électrique ψ et on obtient ainsi sous une forme symétrique:

$$h = \frac{\Re T}{g} \frac{1}{2} \frac{\left(\dfrac{1}{n_1+1} + \dfrac{1}{n_2+1}\right) \log (17 + 12\sqrt{2}) + \left(\dfrac{1}{n_1+1} - \dfrac{1}{n_2+1}\right) \log \left[\dfrac{\dfrac{A_1}{n_1}\sqrt{3+\sqrt{8}} + \dfrac{A_2}{n_2}\sqrt{3-\sqrt{8}}}{\dfrac{A_1}{n_1}\sqrt{3-\sqrt{8}} + \dfrac{A_2}{n_2}\sqrt{3+\sqrt{8}}} \right]}{\left| \dfrac{A_1}{n_1+1} - \dfrac{A_2}{n_2+1} \right|}. \tag{3.8}$$

On voit ici que la grandeur caractéristique pour le phénomène de triage est la quantité $A_1/n_1 + 1$, et que, si l'on trouvait deux éléments portant la même masse par particule libre, ils ne seraient soumis à aucun triage.

Lorsque l'élément 1 est l'hydrogène et l'élément 2 un métal, et que l'on se trouve dans une région de forte ionisation, on obtient approximativement, en négligeant $1/n_2 + 1$ devant $^1/_2$:

$$(3.9) \qquad h = \frac{\Re T}{g}\frac{1}{2}\frac{\log\dfrac{(17+12\sqrt{2})^{\frac{3}{4}}\sqrt{\dfrac{A_2}{n_2}}}{\dfrac{1}{2}-\dfrac{A_2}{n_2+1}}}{}.$$

Nous avons supposé l'ionisation presque totale, donc $A_2/n_2 \simeq 2$ et

$$(3.10) \qquad h \simeq 6{,}4\cdot 10^7 \frac{T}{g}.$$

Lorsque l'ionisation est presque totale, tous les éléments se comportent de la même façon devant l'hydrogène.

Nous préciserons plus loin (§ 9) ces résultats.

4. L'atmospèhre non isotherme. Dans le cas où l'atmosphère n'est pas isotherme, l'énergie $m_i\varphi - n_i e\psi$ a une valeur purement locale, si bien qu'il faut remplacer l'expression $\dfrac{m_i\varphi - n_i e\psi}{kT}$ par

$$(4.1) \qquad \int \frac{m_i d\varphi - ne\,d\psi}{kT} = \int \frac{m_i\varphi' - ne\psi'}{kT}\,dz.$$

De plus, les grandeurs α_i et β, qui étaient des constantes dans le cas de l'atmosphère isotherme, ne le sont plus maintenant.

Le dénombrement des équations et des constantes nous permet de choisir une forme pour α_i et β; nous avons les équations:

$$(4.2) \qquad \begin{cases} \sum n_i p_i = r \\ \dfrac{dP}{dr} = -f\varrho \\ \sum_n{}' \int_\vartheta p_i^n\,dv = P_i. \end{cases}$$

Nous avons supposé ici que la température est une fonction connue de la cote, ce qui revient au même que de se donner une équation de transfert. On a donc $j+2$ relations pour déterminer les $j+2$ quantités α_i, β, $\int \dfrac{\psi' dz}{T}$. La première est une relation algébrique, la deuxième une équation différentielle et les j autres des relations numériques. Nous voyons que nous pouvons déter-

miner au plus par ce système $j+1$ constantes, et 2 fonctions, à condition que les quantités $\alpha_i \beta$ dépendent d'une fonction dépendant d'une constante. Nous prendrons, puisque cette fonction est arbitraire:

$$e^{-\alpha_i} = A_i\, u \qquad e^{-\beta} = B\, u. \tag{4.3}$$

Déterminons dans ces conditions la fonction u. L'équation d'équilibre hydrostatique, compte tenu de l'expression (2.5) des p_i^n et de r, donne:

$$\frac{T'}{T} kT \left[\sum p_i^n \frac{\sum \chi_i^n}{kT} \frac{5}{2} \left(r + \sum p_i^n \right) \right] + kT \frac{u'}{u} \left[r + \sum (Z_i - n)\, p_i^n \right] + kT \frac{u'}{u} \sum p_i^n = 0. \tag{4.4}$$

Cette expression est importante, car, lorsque l'on suppose $\chi_i^n = 0$, c-à-d. la matière totalement ionisée, cette équation se simplifie et donne:

$$\frac{u'}{u} = -\frac{5}{2} \frac{T'}{T} \tag{4.5}$$

et l'on obtient grâce à (2.5) pour tous les p_i et pour r une loi en:

$$\begin{cases} p_i \sim T^{-1} e^{-\int \frac{m_i \varphi' - Ze\psi'}{kT} dz} \\ r \sim T^{-1} e^{-\int \frac{m_e \varphi' + e\psi'}{kT} dz}, \end{cases} \tag{4.6}$$

c-à-d. un résultat parfaitement identique à celui que donnent les équations de la diffusion lorsque l'on néglige la diffusion thermique.

Dans le cas plus général où l'ionisation joue encore un rôle, on a:

$$\frac{u'}{u} = -\frac{T'}{T} \frac{\sum p_i^n \frac{\sum \chi_i^n}{kT} + \left(\sum p_i^n + r \right)}{\sum p_i^n (Z_i - n + 1) + r}. \tag{4.7}$$

Pour déterminer la fonction ψ, il est nécéssaire d'intégrer le système de deux équations (4.7) et (3.1), cette dernière étant l'équation de neutralité électrique. Evidemment, dans le cas général où (3.1) est une expression polynôme en u et $\exp \int \frac{e\psi'\, dz}{kT}$, l'intégration de ce système ne pourra pas se faire sans difficultés.

5. La diffusion d'ionisation. Considérons l'équation:

$$\frac{dP_i}{dz} = f_i \varrho_i \tag{5.1}$$

qui exprime l'équilibre des pressions partielles et qui est la seule équation à satisfaire dans le cas de l'ionisation totale.

Lorsque l'ionisation n'est pas totale, il faut ajouter un terme supplémentaire qui tienne compte de l'existence de collisions avec recombinaison et ionisation. On a immédiatement, d'après (2.5),

$$\frac{dP_i}{dz} = P_i\left[\frac{5}{2}\frac{T'}{T} + (Z_i - n + 1)\frac{u'}{u} - \frac{\varphi' m_i - ne\psi'}{kT} + \frac{1}{kT}\frac{T'}{T}\sum \chi_i^n\right]. \tag{5.2}$$

Nous avons donc un terme supplémentaire

$$\frac{T'}{T} p_i^n kT\left[\frac{5}{2} + \frac{\sum \chi_i^n}{kT} - (Z_i - n + 1)\frac{\sum p_i^n \dfrac{\sum \chi_i^n}{kT} + \dfrac{5}{2}\left(\sum p_i^n + r\right)}{\sum p_i^n (Z_i - n + r) + r}\right] \tag{5.3}$$

qui bien entendu se réduit à zéro quand $n = Z_i$, $\chi_i^n = 0$. Nous pouvons l'évaluer numériquement de la façon approximative suivante: si l'on prend $n_i = Z_i$, ce qui revient à considérer le reste atomique, on a:

$$\frac{T'}{T} p_i^n kT\left[\frac{5}{2} + \frac{\sum \chi_i^n}{kT} - \frac{5}{2} - \frac{\sum p_i^n \dfrac{\chi_i^n}{kT}}{\sum p_i^n + r}\right] \tag{5.4}$$

ou:

$$\frac{T'}{T} p_i^n \left[\sum \chi_i^n - \frac{\sum p_i^n \chi_i^n}{\sum p_i^n + r}\right]. \tag{5.5}$$

Nous arrivons donc à l'équation:

$$\frac{\partial P_i}{\partial z} - f_i \varrho_i - \delta_i \frac{1}{T}\frac{\partial T}{\partial z} = 0 \tag{5.6}$$

avec:

$$\delta_i = p_i^n\left[V_i^n - \frac{\sum p_i^n V_i^n}{\sum p_i^n + r}\right]. \tag{5.7}$$

Dans l'équation de diffusion (M.T. 14.1.1) ce coefficient figurerait avec le coefficient $1/P$:

$$(5.8) \qquad -\frac{1}{P}\frac{1}{T}\frac{\partial T}{\partial z}p_i^n\left[V_i^n-\frac{\sum p_i^n V_i^n}{\sum p_i^n+r}\right].$$

Comparons le terme

$$(5.9) \qquad -\frac{p_i^n}{P}\left[V_i^n-\frac{\sum p_i^n V_i^n}{\sum p_i^n+r}\right]$$

au coefficient k_T (M.T. 14.1.1). Si l'on suppose un élément, en équilibre avec ses produits de dissociation, l'expression (5.9) pour l'un des produits de dissociation s'écrit:

$$(5.10) \qquad -\frac{p_1}{P}\left[V-\frac{p_1 V}{p_1+p_2+p_3}\right]$$

ou:

$$(5.11) \qquad -\frac{p_1 V}{P}\frac{p_2+p_3}{p_1+p_2+p_3}$$

qui est de l'ordre de grandeur de $p_1 V/P$. Si l'on prend P égal à la pression atmosphérique, $p_1\, kT = \frac{1}{3}P$, le terme (5.9) est de l'ordre de grandeur de

$$(5.12) \qquad \frac{1}{3}\frac{V}{kT}.$$

Pour un corps dissocié à moitié, ce terme est de l'ordre de quelques unités, et par conséquent considérablement plus grand que le coefficient de diffusion thermique k_T. A l'équilibre, on a évidemment un équilibre thermodynamique local, et la mesure de la concentration d'un point à un autre ne serait qu'une mesure de l'énergie de réaction. Cette diffusion ne se manifeste que durant le passage à l'équilibre.

6. Hydrogène presque pur. L'hypothèse que les naines blanches ont une atmosphère d'hydrogène presque pur, entraîne la nécessité de traiter le cas de l'hydrogène, et de déterminer le potentiel ψ et la fonction u, afin de pouvoir les reporter dans les expressions p_i^n du nombre des autres éléments, supposé petit comparé à l'hydrogène. On a alors:

$$\frac{u'}{u} = -\frac{T'}{T}\frac{p_1\frac{\chi}{kT}+\frac{5}{2}(p_0+p_1+r)}{2p_0+p_1+r}. \tag{6.1}$$

A l'intérieur de la région d'hydrogène, χ/kT est très petit, p_0 est très petit, et par conséquent:

$$u = \text{cte}\left(\frac{1}{T}\right)^{\frac{5}{2}}, \tag{6.2}$$

d'où les nombres des différentes particules:

$$p_0 = A_0 T^{-\frac{7}{2}} e^{-\int \vartheta \varphi' m_i dz}. \tag{6.3}$$

$$p_1 = A_1 T^{-1} e^{-\int \vartheta(\varphi' m_i^1 - e\psi')dz - \frac{\chi}{kT}}. \tag{6.4}$$

$$r = BT^{-1} e^{-\int \vartheta(\varphi' m_i - e\psi')dz}. \tag{6.5}$$

La condition de neutralité électrique nous détermine ψ':

$$A_1 e^{-\int \vartheta(\varphi' m_i - e\psi')dz} = Be^{-\int \vartheta(\varphi' m_e + e\psi')dz} \tag{6.6}$$

ou:

$$\frac{A_1}{B} e^{-\int \vartheta \varphi'(m_i^1 - m_e)dz} = e^{-\int 2\vartheta e\psi' dz} \tag{6.7}$$

ou, par dérivation logarithmique:

$$\varphi'(m_i^1 - m_e) = 2e\psi'$$

$$\psi' = \frac{m_i^1 - m_e}{2e}\varphi'. \tag{6.8}$$

On en déduit la concentration d'un élément quelconque de charge Z, ionisé n fois:

$$p_i^n = A_i T^{\frac{3}{2}} T^{-\frac{5}{2}(Z-n+1)} e^{-\int \vartheta\left(m_i - \frac{nm_i}{2}\right)d\varphi} e^{-\chi/kT}. \tag{6.9}$$

Dans cette région, on a (34):

$$T = -\frac{\varphi'\frac{m_1}{2}}{\frac{17}{4}k} z \tag{6.10}$$

en prenant la surface de l'étoile pour origine, ou:

$$\frac{m_1}{2}\frac{1}{kT} = -\frac{17}{4}\frac{1}{\varphi' z}. \tag{6.11}$$

L'intégrale en exponentielle vaut:

$$\int \vartheta\left(m_i - \frac{nm_1}{2}\right)\varphi'\,dz = -\left(2\frac{m_i}{m_1} - n\right)\frac{17}{4}\log|z| \tag{6.12}$$

et puisque T est proportionnel à z:

$$p_i^n \sim T^{\frac{3}{2}-\frac{5}{2}(Z-n+1)+\frac{17}{4}\left(2\frac{A_i}{A_1}-n\right)} e^{-\sum_n \frac{\chi_i^n}{kT}}. \tag{6.13}$$

Nous avons donc un terme exponentiel qui contient l'énergie d'ionisation et un terme en T^α. Si nous supposons pour commencer que T est assez élevé pour que l'on puisse négliger les variations de $e^{-\chi/kT}$, nous n'avons à tenir compte que du terme en T^α. On a:

$$\alpha = -1 - \frac{7}{4}n - \frac{5}{2}Z + \frac{17}{2}\frac{A_i}{A_1}.$$

Ici, $A_1 = 1$ (hydrogène). On a donc:

$$\alpha = -1 - \frac{7}{4}n - \frac{5}{2}Z + \frac{17}{2}A_i.$$

Nous donnons dans le tableau I les valeurs de α pour quelques éléments.

Tableau I.

Élément	A_i	n				
		0	2	4	6	8
Hélium	4	28	24,5	..	..	..
Carbone	12	86	82,5	79	75,5	..
Azote	14	100,5	97	93,5	90	..
Oxygène	16	115	111,5	108	104,5	101
Sodium	23	167	163,5	160	156,5	153
Magnésium	24	173	169,5	166	162,5	159
Silicium	28	202	198,5	195	191,5	188
Potassium	39	283	279,5	276	272,5	269
Calcium	40	289	285,5	282	278,5	275
Fer	56	376	372,5	369	365,5	362

On ne peut manquer d'être frappé par les très grandes valeurs de cet exposant, et l'on conclut immédiatement que si aucun autre phénomène n'intervient, la concentration en éléments lourds à la surface des naines blanches doit être imperceptible.

En fait, nous savons qu'il existe dans le soleil une couche convective près de la surface. Son existence a été démontrée par UNSÖLD (49). Elle a été étudiée en particulier par BIERMANN (4), RUDKJØBING (30, 32). Il est possible que cette couche atteigne des profondeurs relativement grandes. Si une telle couche existe dans les naines blanches, elle peut être susceptible d'aller chercher les éléments lourds à une grande profondeur pour les ramener à la surface de l'étoile où ils peuvent apparaître dans le spectre. Cela semble être le cas de Van Maanen 2, comme une étude à paraître prochainement le montrera.

7. Couche de mélange. Nous avions introduit pour les couches profondes un élément moyen (34). Au voisinage de la couche de mélange, il est nécessaire d'introduire une autre approximation.

Supposant toujours que les variations dues aux termes exponentiels $exp(-\chi/kT)$ sont faibles en raison de la haute température de la couche de mélange, nous posons:

$$u = e^{-\int \vartheta \varphi' H dz} \tag{7.1}$$

$$v = e^{\int \vartheta e \psi' dz} \tag{7.2}$$

et l'équation de neutralité électrique prend la forme:

$$\sum \frac{a_i}{b} Z_i u^{A_i - A_e} v^{Z_i + 1} = 1 . \tag{7.3}$$

Nous déterminons les constantes a_i, b par un choix convenable de l'origine des coordonnées. A l'origine, nous avons $u = v = 1$. Si l'on suppose que l'hydrogène et les autres éléments pris ensemble ont une concentration respectivement égale à $^1/_2$ en ce point, on a à un facteur près, le même pour a_i et b:

$$(7.4)\qquad \begin{cases} a_i = \dfrac{1}{2}\dfrac{c_i}{m_i} \\ a_n = \dfrac{1}{2}\dfrac{1}{m_n} \\ \text{(hydrogène)} \end{cases}$$

et on en déduit b:

$$(7.5)\qquad b = \frac{1}{2}\frac{Z_n}{m_n} + \frac{1}{2}\sum \frac{Z_i c_i}{m_i}.$$

L'équation de neutralité électrique s'écrit alors:

$$(7.6)\qquad \frac{\sum \dfrac{c_i}{A_i} Z_i u^{A_i} v^{Z_i+1} + \dfrac{1}{A_n} u^{A_n} v^{Z_n+1}}{\sum c_i \dfrac{Z_i}{A_i} + \dfrac{Z_n}{A_n}} = 1.$$

Nous allons supposer maintenant que pour les éléments lourds

$$\frac{A_i}{Z_i+1} - \frac{A_j}{Z_j+1}$$

est si petit que nous pouvons le négliger. En prenant comme nouvelle variable $u^{A_1} v^{Z_1} = t$ on obtient ainsi, avec $Z_i/A_i = {}^1/_2$ et en confondant Z_i et $Z_i + 1$

$$\frac{1}{2}\sum c_i t^{Z_i/Z_1} + u\,(t^{1/Z_1} u^{-2})^2 = \frac{3}{2}$$

ou:

$$(7.7)\qquad \frac{1}{2}\sum c_i t^{Z_i/Z_1} + u^{-3} t^{2/Z_1} = \frac{3}{2},$$

d'où u:

$$(7.8)\qquad u^3 = \frac{t^{2/Z_1}}{\dfrac{3}{2} - \dfrac{1}{2}\sum c_i t^{Z_i/Z_1}}.$$

On en déduit la concentration en hydrogène x_H représentée paramétriquement en fonction de t par (7, 8) et

$$x_H = \frac{u^{-1}\, t^{1/Z_1}}{u^{-1}\, t^{1/Z_1} + \sum c_i\, t^{Z_i/Z_1}}. \tag{7.9}$$

On a de plus:

$$-\int_0^z \vartheta\varphi'\, H dz = \log_e u \tag{7.10}$$

qui donne la variation de u avec la cote.

La solution ainsi trouvée se raccorde aisément du côté de l'hydrogène à la solution (6.13) et du côté des éléments lourds à la solution approchée de non triage.

Nous avons calculé une table des variations de x_H avec la hauteur en admettant pour les éléments lourds un mélange de Russell simplifié, dont la composition est donnée dans le tableau II.

Tableau II.

Élément	Concentration
O	0,5
Mg	0,25
Si	0,0625
Ca	0,0625
Fe	0,125

On obtient ainsi les résultats donnés dans le tableau III. Les hauteurs ont été calculées pour un gaz isotherme à $T = 10^7$ degrés et dans un champ de pesanteur $g = 10^9$ c. g. s. On remarquera combien ces hauteurs sont faibles dans un si grand champ de pesanteur.

On remarquera que nous n'avons pas introduit d'hélium. La raison essentielle est que pour l'hélium, l'hypothèse $A_i/Z_i + 1 = Cte$ n'est plus valable, ou n'est plus en tout cas qu'une grossière approximation. L'introduction d'hélium compliquerait considérablement la solution, sauf si toutefois on supposait l'étoile composée d'hydrogène et d'hélium presque exclusivement.

On trouvera fig. 1, p. 20, la courbe représentative de x_H en fonction de $\log u$. Ce résultat peut être utilisé pour le calcul de la distribution de la température et du débit d'énergie, car la fonction $x(t)$ ainsi obtenue est indépendante de la température

Tableau III.

t^{1/Z_1}	$\Sigma c_i t^{Z_i/Z_1}$	$-\log_{10} u$	x_H	Z_{km} ($T=10^{7°}$ $g=10^9$ cgs)	$\frac{x_0}{1-x_H}$	$\frac{x_{Mg}}{1-x_H}$	$\frac{x_{Si}}{1-x_H}$	$\frac{x_{Fe}}{1-x_H}$
0	0	$+\infty$	1	$+\infty$	..	..	..	..
0,4	0,013	0,323	0,984	6,2	0,98	0,079		..
0,5	0,035	0,258	0,963	..	0,90	0,112	..	..
0,6	0,078	0,202	0,925	3,7	0,83	0,150	0,021	..
0,7	0,157	0,154	0,864	..	0,764	0,187	0,033	0,008
0,8	0,297	0,108	0,776	2,1	0,688	0,221	0,044	0,023
0,9	0,545	0,060	0,655	..	0,603	0,224	0,055	0,059
1,0	1,000	0,000	0,500	0	0,500	0,250	$0,062_5$	0,125
1,02	1,133	— 0,017	0,465	..	0,478	0,248	$0,063_4$	0,143
1,04	1,287	— 0,034	0,431	— 0,6	0,454	0,246	$0,064_2$	0,163
1,10	1,888	— 0,112	0,315	— 2,1	0,387	0,234	$0,064_7$	0,228
1,15	2,628	— 0,297	0,188	— 5,7	0,333	0,218	$0,063_3$	0,291
..	3	$-\infty$	0	$-\infty$	..	..	..	..

et de la densité. Pour obtenir $x(z)$ il faut en plus tenir compte de l'équation de transfert d'énergie. Les courbes de la figure 2, p. 21, représentatives de la variation de composition du mélange des éléments lourds avec la cote, montrent qu'il n'est pas légitime de remplacer le mélange des éléments lourds par un élément moyen. Nous pouvons remarquer de plus que, dès que

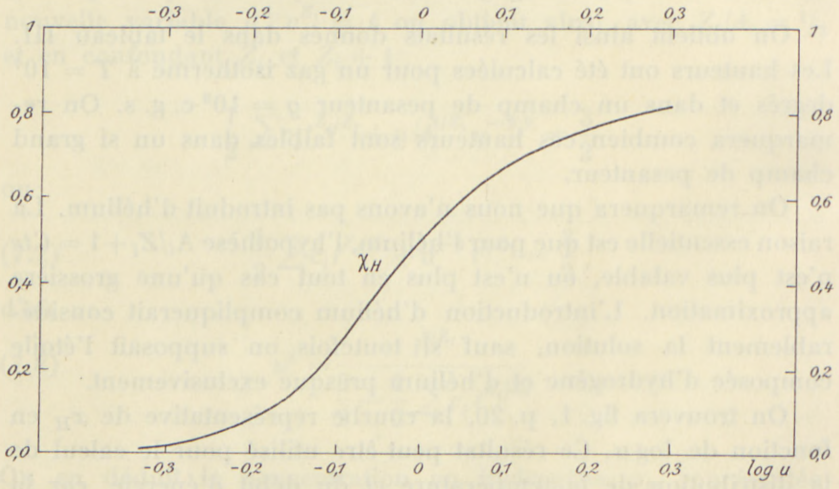

Fig. 1. Variation de la concentration x_H en hydrogène en fonction de l'altitude dans la couche de mélange.

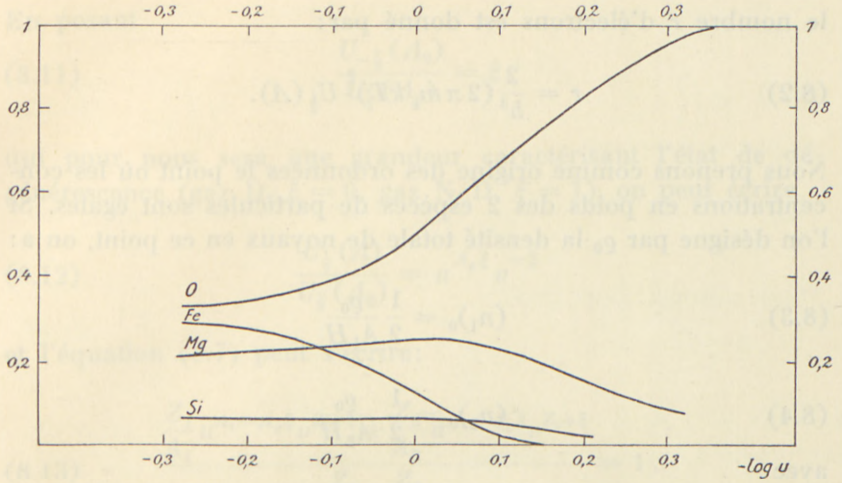

Fig. 2. Variations des concentrations [O] [Fe] [Mg] [Si] au sein du mélange d'éléments lourds. On remarquera que la concentration en oxygène croit considérablement à l'extérieur de la couche de mélange, c'est-à-dire là où la concentration en hydrogène est déjà grande.

$\log u > 0{,}2$ par exemple, seul l'oxygène est pratiquement présent, comme élément lourd. Dans le calcul du coefficient d'absorbtion et de la température il pourra être considéré comme légitime de supposer avoir affaire à un mélange d'hydrogène et d'oxygène seulement.

Ces conclusions seront appliquées plus tard à l'étude de certains modèles de naines blanches.

B. Phénomènes dûs aux dégénérescences.

8. Phénomènes dûs à la dégénérescence du gaz d'électrons. Nous allons étudier le mélange de deux espèces atomiques au voisinage de la couche de mélange, lorsque le gaz d'électrons est plus ou moins dégénéré. L'hypothèse supplémentaire d'un champ de pesanteur intense, et par conséquent d'une faible hauteur de mélange permet alors l'emploi d'un développement réduit au premier terme pour décrire l'état du gaz d'électrons. Nous supposerons le mélange isotherme.

En posant

$$U_\nu(A) = \frac{1}{\Gamma(\nu+1)} \int_0^\infty \frac{U^\nu \, du}{\frac{1}{A} e^u + 1}, \tag{8.1}$$

le nombre r d'électrons est donné par:

$$r = \frac{2}{h^3}(2\pi m_e kT)^{\frac{3}{2}} U_{\frac{1}{2}}(\Lambda). \tag{8.2}$$

Nous prenons comme origine des ordonnées le point où les concentrations en poids des 2 espèces de particules sont égales. Si l'on désigne par ϱ_0 la densité totale de noyaux en ce point, on a:

$$(n_1)_0 = \frac{1}{2}\frac{\varrho_0}{A_1 H} \tag{8.3}$$

$$(n_2)_0 = \frac{1}{2}\frac{\varrho_0}{A_2 H} \tag{8.4}$$

avec

$$H A_i = m_i, \tag{8.5}$$

m_i masse d'un noyau d'espèce i. Dans ces conditions

$$r_0 = \frac{1}{2}\frac{\varrho_0}{H}\left(\frac{Z_1}{A_1} + \frac{Z_2}{A_2}\right) \tag{8.6}$$

et l'on a, pour le quotient r/r_0, en utilisant les notations (7,1) et (7,2) pour u et v qui valent 1 pour $z = 0$:

$$\frac{r}{r_0} = \frac{U_{\frac{1}{2}}(\Lambda)}{U_{\frac{1}{2}}(\Lambda_0)} = \frac{\frac{Z_1}{A_1}u^{A_1}v^{Z_1} + \frac{Z_2}{A_2}u^{A_2}v^{Z_2}}{\frac{Z_1}{A_1} + \frac{Z_2}{A_2}}; \tag{8.7}$$

Λ_0 est défini par (8,2) et (8,6) et on a:

$$\Lambda = \Lambda_0 u^{A_e} v^{-1}. \tag{8.8}$$

En supposant que Λ ne varie pas de façon considérable, on a:

$$\log\frac{U_{\frac{1}{2}}(\Lambda)}{U_{\frac{1}{2}}(\Lambda_0)} = \log\frac{U_{\frac{1}{2}}(\Lambda_0) + \frac{\delta\Lambda}{\Lambda}U_{-\frac{1}{2}}(\Lambda_0)}{U_{\frac{1}{2}}(\Lambda_0)} \simeq \frac{\delta\Lambda}{\Lambda}\frac{U_{-\frac{1}{2}}(\Lambda_0)}{U_{\frac{1}{2}}(\Lambda_0)} \tag{8.9}$$

$$\log\frac{U_{\frac{1}{2}}(\Lambda)}{U_{\frac{1}{2}}(\Lambda_0)} \simeq \frac{U_{-\frac{1}{2}}(\Lambda_0)}{U_{\frac{1}{2}}(\Lambda)}\left(\frac{A_e}{u} - \frac{1}{v}\right). \tag{8.10}$$

En posant

$$\frac{U_{-\frac{1}{2}}(A_0)}{U_{\frac{1}{2}}(A_0)} = \xi, \tag{8.11}$$

qui pour nous sera une grandeur caractérisant l'état de dégénérescence (gaz D. $\xi = 0$, gaz N. D. $\xi = 1$), on peut écrire

$$\frac{U_{\frac{1}{2}}(A)}{U_{\frac{1}{2}}(A_0)} = u^{A_e \xi} v^{-\xi} \tag{8.12}$$

et l'équation (8.7) peut s'écrire:

$$\frac{\frac{Z_1}{A_1} u^{A_1 - A_e \xi} v^{Z_1 + \xi} + \frac{Z_2}{A_2} u^{A_2 - A_e \xi} v^{Z_2 + \xi}}{\frac{Z_1}{A_1} + \frac{Z_2}{A_2}} = 1. \tag{8.13}$$

9. Hauteur de mélange. Nous allons donner une définition plus logique et plus précise de la hauteur de mélange de la façon suivante. Dans un mélange, le nombre de particules d'espèce 1 et d'espèce 2 est:

$$n_1 = \frac{1}{2} \frac{\varrho_0}{A_1 H} u^{A_1} v^{Z_1} \tag{9.1}$$

$$n_2 = \frac{1}{2} \frac{\varrho_0}{A_2 H} u^{A_2} v^{Z_2}. \tag{9.2}$$

Nous avons à utiliser pour le calcul du débit d'énergie dans une région isotherme l'expression:

$$\int n_1 n_2 dz \tag{9.3}$$

et nous appelons hauteur de mélange h la quantité

$$h = \frac{\int n_1 n_2 dz}{\frac{1}{4} \frac{\varrho_0^2}{A_1 A_2 H^2}} = \int u^{A_1 + A_2} v^{Z_1 + Z_2} dz. \tag{9.4}$$

Nous allons transformer cette expression afin de la calculer à l'aide de (8,13), (7,1) et (7,2).

En vertu de (7,1) nous avons

$$\frac{du}{u} = -\vartheta H g dz \tag{9.5}$$

et par conséquent:

$$h = \frac{1}{\vartheta H g}\int u^{A_1+A_2} v^{Z_1+Z_2}\frac{du}{u}. \tag{9.6}$$

Nous posons, dans (8.13):

$$t = \frac{\dfrac{Z_1}{A_1}}{\dfrac{Z_1}{A_1}+\dfrac{Z_2}{A_2}} u^{A_1-A_e\xi} v^{Z_1+\xi}. \tag{9.7}$$

En posant

$$\zeta = \frac{Z_2+\xi}{Z_1+\xi}, \tag{9.8}$$

on a:

$$u^{A_2-A_e\xi-\zeta(A_1-A_e\xi)} = \frac{1-t}{t^\zeta}\frac{\dfrac{Z_1}{A_1}+\dfrac{Z_2}{A_2}}{\dfrac{Z_2}{A_2}}\left(\frac{\dfrac{Z_1}{A_1}}{\dfrac{Z_1}{A_1}+\dfrac{Z_2}{A_2}}\right)^\zeta. \tag{9.9}$$

Posons:

$$\alpha = \frac{\dfrac{Z_1}{A_1}}{\dfrac{Z_1}{A_1}+\dfrac{Z_2}{A_2}} \qquad 1-\alpha = \frac{\dfrac{Z_2}{A_2}}{\dfrac{Z_1}{A_1}+\dfrac{Z_2}{A_2}}. \tag{9.10}$$

L'intégrale que nous avons à calculer s'écrit alors, en raison de (9.7):

$$\int u^{A_1+A_2}\left(\frac{t}{\alpha}u^{-A_1+A_e\xi}\right)^{\frac{Z_1+Z_2}{Z_1+\xi}}\frac{du}{u}. \tag{9.11}$$

En posant encore:

$$A = A_2 - A_e\xi - \zeta(A_1 - A_e\xi), \tag{9.12}$$

on tire de (9.9):

$$A\frac{du}{u} = \left(-\frac{1}{1-t}-\frac{\zeta}{t}\right)dt. \tag{9.13}$$

L'intégrale (9.11) s'écrit donc:

$$(9.14)\qquad \frac{1}{A}\int_0^1 u^{A_1+A_2-(A_1-A_e\xi)\frac{Z_1+Z_2}{Z_1+\xi}}\left(\frac{t}{\alpha}\right)^{\frac{Z_1+Z_2}{Z_1+\xi}}\left(\frac{1}{1-t}+\frac{\zeta}{t}\right)dt.$$

En portant l'expression (9.9) pour $u(t)$ dans (9.14), on obtient:

$$(9.15)\qquad \frac{1}{A}\int_0^1\left(\frac{1-t}{t^\zeta}\,\frac{\alpha^\zeta}{1-\alpha}\right)^{\frac{A_1+A_2-(A_1-A_e\xi)\frac{Z_1+Z_2}{Z_1+\xi}}{A}}\left(\frac{t}{\alpha}\right)^{\frac{Z_1+Z_2}{Z_1+\xi}}\left(\frac{1}{1-t}+\frac{\zeta}{t}\right)dt.$$

En vertu de (8.13) et de (9.7), t est compris entre 0 et 1. On a donc une intégrale Eulérienne de première espèce. Le coefficient numérique dans l'intégrale (9.15) est

$$(9.16)\qquad \frac{1}{A}(1-\alpha)^{-1-\frac{2\xi(A_1+Z_1A_e)}{(Z_1+\xi)A}}\,\alpha^{-1+\frac{2Z_2A_e\xi}{(Z_1+\xi)A}}$$

et l'intégrale s'écrit:

$$(9.17)\qquad \begin{cases} \displaystyle\int_0^1 = B\left(1+2\frac{\xi(A_1+Z_1A_e)}{(Z_1+\xi)A},\ 2-\frac{2Z_2A_e\xi}{(Z_1+\xi)A}\right)+ \\ \qquad\qquad \displaystyle+\zeta B\left(2+\frac{2\xi(A_1+Z_1A_e)}{(Z_1+\xi)A},\ 1-\frac{2Z_2A_e\xi}{(Z_1+\xi)A}\right). \end{cases}$$

En vertu de la relation

$$(9.18)\qquad B(m,\ n)=\frac{\Gamma(m)\,\Gamma(n)}{\Gamma(m+n)}$$

et en négligeant A_e/A, ce qui n'est incorrect que lorsque A est du même ordre de grandeur que A_e, l'expression (9.18) se simplifie beaucoup et devient:

$$(9.19)\qquad \frac{1}{2+\dfrac{2\xi(A_1+Z_1A_e)}{(Z_1+\xi)A}}\left(\frac{1}{1+\dfrac{2\xi(A_1+Z_1A_e)}{(Z_1+\xi)A}}+\zeta\right).$$

On obtient alors pour la hauteur de mélange:

$$(9.20)\quad \left\{ h = \frac{kT}{Hg}\left(\frac{1}{1-\alpha}\right)^{1+\frac{2\xi(A_1+Z_1A_e)}{(Z_1+\xi)A}} \frac{1}{\alpha}\frac{1}{2}\frac{1}{A+\frac{\xi(A_1+Z_1A_e)}{Z_1+\xi}} \left(\zeta+\frac{1}{1+\frac{2\xi(A_1+Z_1A_e)}{(Z_1+\xi)A}}\right). \right.$$

Dans le cas où $\xi = 0$ (gaz D.), (9.20) se réduit à

$$(9.21)\quad h = \frac{kT}{Hg}\frac{1}{1-\alpha}\frac{1}{\alpha}\frac{1}{2}\frac{\zeta+1}{A_2-\zeta A_1}$$

qui est à une petite différence numérique près l'expression déjà trouvée (34). La différence provient d'une meilleure évaluation de la hauteur de mélange. Pour donner une idée de l'influence de la dégénérescence sur la hauteur de mélange, nous allons calculer pour $A_2 = 24$, $A_1 = 1$, $Z_2 = 12$, $Z_1 = 1$ les variations de h avec ξ. Dans ce cas, on a:

$$(9.22)\quad \alpha = \frac{2}{3} \qquad 1-\alpha = \frac{1}{3} \qquad A = 24-\zeta.$$

On obtient le tableau IV donnant h/h_D en fonction de ξ et les valeurs correspondantes de kT/ε_0 (ε_0, énergie maximum au zéro absolu) et de ϱ/μ pour $T = 10^7$ degrés. Les tables de E. C. Stoner (46) des fonctions $U_{-1/2}$, $U_{1/2}$ et $U_{3/2}$ ont servi à dresser le tableau.

Tableau IV.

ξ	h/h_D	kT/ε_0	$\log \varrho/\mu$ ($T=10^7$ degrés)
1	0,406	∞	$-\infty$
0,8	0,466	1,06	2,246
0,6	0,522	0,55	2,67
0,4	0,617	0,294	3,08
0,2	0,745	0,151	3,51
0	1	0	∞

On voit que la dégénérescence ne modifie pas considérablement la valeur de la hauteur de mélange et que cette hauteur est plus faible dans le cas de non dégénérescence.

10. Dégénérescence dans le gaz de noyaux.

a) Statistique de Bose. Si l'on se place au zéro absolu, tous les atomes se répartissent dans un état d'énergie minimum, donc d'énergie potentielle nulle. Ceci implique pour chaque espèce

$$m_i \varphi - Z_i e \psi = 0. \tag{10.1}$$

Cette condition ne peut être satisfaite simultanément pour toutes les espèces atomiques à spin entier. Il y a donc séparation complète des éléments obéissant à la statistique de Bose et ces éléments sont superposés dans l'ordre m_i/Z_i décroissant.

b) Statistique de Bose et statistique de Fermi. La condition (10.1) détermine le potentiel électrique. Les particules obéissant à la statistique de Fermi sont alors en nombre:

$$n_1 = \frac{8\pi}{3h^3}(p_0^2 - 2 m_1 W_1)^{\frac{3}{2}} \tag{10.2}$$

et le nombre d'électrons est:

$$n_e = \frac{8\pi}{3h^3}(p_e^2 - 2 m_e W_e)^{\frac{3}{2}} \tag{10.3}$$

avec

$$\left\{ \begin{aligned} W_1 &= m_1 \varphi - Z_1 e \psi \\ &= \left(m_1 - Z_1 \frac{m_i}{Z_i}\right) \varphi \\ W_e &= \left(m_e + \frac{m_i}{Z_i}\right) \varphi . \end{aligned} \right. \tag{10.4}$$

Le nombre n_i des particules obéissant à la statistique de Bose est donné par la condition de neutralité électrique (une seule espèce à la fois):

$$(10.5)\quad \begin{cases} Z_i n_i + Z_1 \dfrac{8\pi}{3h^3}\left(p_0^2 - 2m_1\left(m_1 - Z_1\dfrac{m_i}{Z_i}\right)\varphi\right)^{\frac{3}{2}} = \\ \\ = \dfrac{8\pi}{3h^3}\left(p_e^2 - 2m_e\left(m_e + \dfrac{m_i}{Z_i}\right)\varphi\right)^{\frac{3}{2}}. \end{cases}$$

Les constantes p_0 et p_e sont déterminées par les conditions relatives au nombre total de particules i et 1 en présence. Le nombre de particules d'espèce 1 subit une discontinuité chaque fois que l'on passe d'une espèce i à une autre, en raison du changement de potentiel électrique. Il peut enfin y avoir une région de pur hydrogène et dans ce cas la relation entre les potentiels est donnée par:

$$(10.6)\quad Z_1\frac{8\pi}{3h^3}\left(p_0^2 - 2m_1(m_1\varphi - Z_1 e\psi)\right)^{\frac{3}{2}} = \frac{8\pi}{3h^3}\left(p_e^2 - 2m_e(m_e\varphi + e\psi)\right)^{\frac{3}{2}}.$$

A travers chaque surface de discontinuité de la densité on doit avoir continuité de la pression. Cette condition peut être satisfaite en supposant que les potentiels φ et ψ subissent une discontinuité. Si l'on a p éléments obéissant à la statistique de Bose, de l'hydrogène et des électrons, on a p équations de continuité pour la pression, $p+1$ conditions pour le nombre de particules déterminant les $p+1$ constantes présentes dans les potentiels et les positions des p surfaces de discontinuité.

Traitons plus simplement le cas d'un seul élément. L'équation (10.5) est la seule à être satisfaite, tant que $n_i \neq 0$. Lorsque n_i s'annule, seule l'équation (10.6) est satisfaite. Nous supposerons que p_e^2 étant très grand devant $m_e W_e$, le nombre d'électrons est sensiblement constant:

$$(10.7)\quad Z_i n_i + Z_1\frac{8\pi}{3h^3}\left(p_0^2 - 2m_1\left(m_1 - Z_1\frac{m_i}{Z_i}\right)\varphi\right)^{\frac{3}{2}} = r.$$

Calculons sur quelle hauteur $Z_i n_i$ varie de 0 à r/Z_i. L'équation

$$(10.8)\quad Z_1\frac{8\pi}{3h^3}\left(p_0^2 - 2m_1\left(m_1 - Z_1\frac{m_i}{Z_i}\right)\varphi\right)^{\frac{3}{2}} = r - Z_i n_i$$

donne les deux équations suivantes

$$(10.9)\quad \begin{cases} p_0^2 - 2\,m_1\left(m_1 - Z_1\dfrac{m_i}{Z_i}\right)\varphi = \left(\dfrac{r\,h^3}{8\,\pi\,Z_i}\right)^{\frac{2}{3}} \\ p_0^2 = 0 \end{cases}$$

en prenant pour origine $\varphi = 0$ quand $p_0 = 0$ (pas de protons). On a ainsi:

$$(10.10)\qquad hg = \frac{1}{2\,m_1\left(Z_1\dfrac{m_i}{Z_i} - m_1\right)}\left(\frac{3\,r\,h^3}{8\,\pi\,Z_i}\right)^{\frac{2}{3}}$$

ou numériquement:

$$(10.11)\qquad h = [9.814]\,\frac{\varrho^{-\frac{2}{3}}}{g\left(\dfrac{A_i}{Z_i} - 1\right)}.$$

Nous avons déjà donné (44) l'expression de la hauteur de mélange pour un gaz dégénéré de protons et un gaz parfait de noyaux. On avait trouvé:

$$(10.12)\qquad h = [9.923]\,\frac{\varrho^{-\frac{2}{3}}}{g\left(\dfrac{A_i}{Z_i} - 1\right)}.$$

On voit, que lorsque l'un des gaz de noyaux est un gaz de Fermi, la hauteur de mélange est déterminée par lui, en raison de la grande énergie d'agitation des noyaux du gaz de Fermi.

II. L'ionisation de l'hydrogène.

I. Introduction.

1. L'étude de l'état de l'hydrogène aux densités relativement élevées est absolument essentielle pour les naines blanches. D'abord parce que l'atmosphère des naines blanches est constituée d'hydrogène pur. Ensuite parce que l'on atteint très rapidement, pour de faibles profondeurs optiques, des densités considérables.

Alors que d'ordinaire, à des températures de 30.000 degrés, on a seulement des densités de 10^{14} ou 10^{15} ions positifs hydrogène

par unité de volume, dans le cas des naines blanches ce sont facilement des densités de 10^{18} ou 10^{20}. Il n'est pas possible alors de tenir compte d'une manière arbitrairement simple de l'ionisation de pression, par exemple en coupant la somme d'états en un point convenable. D'autre part, la méthode des volumes exclus (15) (16) ne donne que des résultats extrêmement grossiers, et a le tort de ne donner aucune indication sur l'état des atomes neutres.

Une méthode parfaitement correcte, tant du point de vue de l'ionisation que du calcul du coefficient d'absorption et de la conductibilité serait la suivante: placer les protons en des points déterminés distribués au hasard dans une enceinte close, déterminer tous les niveaux d'énergie possibles pour les électrons, distribuer ces électrons parmi les niveaux d'énergie en accord avec la température du gaz, à l'aide des fonctions d'onde obtenues, calculer l'énergie potentielle des protons en fonction de leurs coordonnées et l'utiliser pour trouver à l'aide de l'équation de Schrödinger leur mouvement. Cette méthode est en fait celle qui est utilisée dans les théories du corps solide, mais elle est essentiellement simplifiée par le fait que les atomes ne sont pas distribués parfaitement au hasard, mais au voisinage des nœuds d'un réseau. Il est donc nécessaire d'employer ici une théorie statistique pour arriver à un résultat.

Le principe de la théorie statistique est le suivant: étant donné un atome supposé à l'état neutre, il est soumis à un certain champ électrique, et l'on a à déterminer la probabilité $W(F)\,dF$ que ce champ soit compris entre les valeurs F et $F + dF$. Sous l'influence de ce champ, les niveaux sont perturbés, et pour les grandes valeurs du nombre quantique principal n, cette perturbation peut être assez forte pour empêcher les états d'exister. On a donc un nombre moyen $NW(F)\,dF$ d'atomes soumis au champ F et dont l'énergie d'ionisation est plus faible que celle des atomes en l'absence de champ. Il est alors possible de dénombrer les états d'énergie E des électrons, en prenant pour origine des énergies celle des électrons libres de vitesse nulle. En conséquence, les électrons libres ont des énergies positives, les électrons liés des énergies négatives.

Cette théorie est linéaire, car elle ne tient compte que de la valeur du champ électrique F au point considéré, et non pas

des valeurs grad F, grad grad F etc. ... En d'autres termes, les dimensions de l'atome sont supposées négligeables devant l'hétérogénéité du champ. Mise à part l'extrême complication qu'implique l'introduction de ces grandeurs, nous serons amenés, pour dégager les faits essentiels, à d'autres simplifications plus importantes que celle du champ uniforme.

Cette théorie a un caractère de première approximation, car nous supposerons que le champ F ne modifie que d'une quantité négligeable les niveaux d'énergie et les probabilités de transition, bien que nous tenions compte de la destruction des états par les champs intenses. Il serait évidemment plus correct de tenir compte individuellement des états séparés par le champ, mais il ne semble pas que l'introduction de cette complication soit justifiée.

Mrowka (26) a essayé de traiter le problème de l'élargissement des raies spectrales par la mécanique ondulatoire. Mais sa théorie suppose que seule l'action des atomes neutres est à considérer et que la température est assez basse pour que tous les atomes d'hydrogène soient dans l'état fondamental. Il s'agit donc d'un cas extrêmement différent de celui que nous nous proposons d'étudier.

II. État de l'hydrogène.

2. Dénombrement des états. Ionisation. Nous supposerons un volume où se trouvent N_1 ions positifs N_e électrons et N_0 atomes neutres par cm^3.

Un atome neutre, de nombre quantique principal n, placé dans un champ F est susceptible d'avoir $2n$—1 niveaux d'énergie. Soit x le nombre quantique «électrique», nous avons $2n$—1 niveaux d'énergie $-E_{nx}(F)$ avec $-(n-1) < x < n-1$. Le poids statistique de chacun de ces états est g_{nx}. Soit $W(F)$ la probabilité pour que le champ soit compris entre F et $F + dF$. Pour les fortes valeurs de F les niveaux sont détruits, alors $g_{nx} = 0$. Comme nous avons fait choix pour origine des énergies des électrons de vitesse nulle, nous dénombrons les états de la façon suivante.

Il y a N_1 protons et $N_1\, g_{nx}\, W(F)\, dF$ états possibles d'énergie E_{nx}. Le nombre d'électrons liés dans ces niveaux est:

$$(2.1) \qquad dn_1 = N_1 g_{nx} W(F)\, dF \frac{1}{1 + e^{-\vartheta E_{nx} - \alpha}}$$

où $\vartheta = 1/kT$ et α est une constante déterminée de la façon suivante.

Le nombre total d'électrons est:

$$(2.2) \qquad N_e + N_0 = \int dn_0 + \int_0^\infty \frac{8\pi p^2 dp}{h^3} \frac{1}{1 + e^{\frac{p^2}{2mkT} - \alpha}}.$$

Le nombre total d'électrons libres est donné par la seconde intégrale et le nombre total d'électrons liés par la première:

$$(2.3) \qquad N_0 = N_1 \sum_{n,x} \int_0^\infty \frac{g_{nx} W(F)\, dF}{1 + e^{-\vartheta E_{nx} - \alpha}}$$

$$(2.4) \qquad N_e = \int \frac{8\pi p^2 dp}{h^3} \frac{1}{1 + e^{\vartheta \frac{p^2}{2m} - \alpha}}.$$

Lorsqu'on est loin des conditions de dégénérescence, on a plus simplement:

$$(2.5) \qquad N_e = 2 \frac{(2\pi m_e kT)^{\frac{3}{2}}}{h^3} e^{\alpha}$$

$$(2.6) \qquad N_0 = N_1 \sum_{n,x} \int_0^\infty g_{nx} W(F)\, e^{\vartheta E_{nx}} dF \cdot e^{\alpha};$$

par élimination de e^{α}, on obtient une expression analogue à celle de Saha:

$$(2.7) \qquad \frac{N_e N_1}{N_0} = \frac{2 \cdot (2\pi mkT)^{\frac{3}{2}}}{h^3} \frac{1}{\sum_{nx} \int_0^\infty g_{nx} W(F)\, e^{\vartheta E_{nx}} dF}$$

où la somme au dénominateur du second membre est l'équivalent de l'habituelle somme d'états et se ramène à celle-ci lorsque la densité tendant vers zéro, le champ F devient extrêmement faible et sans influence sur les niveaux.

3. En réalité, pour un niveau nx donné, l'intégrale n'est pas prise jusqu'à l'infini, mais seulement jusqu'à la valeur du champ F qui détruit l'état nx. On doit donc écrire pour la somme Σ:

$$\sum\nolimits' = \sum_{nx} \int_0^{F_{nx}} g_{nx} W(F)\, dF e^{\vartheta E_{nx}}. \tag{3.1}$$

La détermination de F_{nx} est donc essentielle à la poursuite du calcul. Nous suivrons pour cela une méthode très analogue à celle de PANNEKOEK (28). Cette méthode est la suivante. Dans le champ F, l'atome d'hydrogène subit une destruction spontanée analogue à la radioactivité α, l'électron franchissant la barrière de potentiel à l'intérieur de laquelle il se trouve enfermé. Cette destruction s'opère avec une durée de vie δ donnée par LANCZOS (23)

$$\delta = \frac{\pi e^2}{h a_0} \frac{e^{-2I_2}}{2I_1} = 2{,}066 \cdot 10^{16} \frac{e^{-2I_2}}{2I_1} \tag{3.2}$$

où I_1 et I_2 sont reliés aux intégrales elliptiques complètes de première et deuxième espèce. Lorsque cette durée de vie δ est plus courte qu'un temps α lié à la durée de vie de l'atome effectuant des transitions spontanées (de l'ordre de 10^{-8} sec.), nous dirons avec Pannekoek que l'état a cessé d'exister. La valeur de α peut être choisie arbitrairement sans changer considérablement les résultats en raison de la présence dans δ d'une exponentielle variant très rapidement. Nous avons pris ici $\alpha = 10^{-8}$ sec.

Le système de Lanczos, reproduit par Pannekeok est le suivant:

$$\left\{\begin{array}{ll} \varepsilon = \dfrac{2a_0^2}{e} F n^3 & \tau = 8\gamma_2 n\varepsilon = \sin^2\varphi \\[2ex] k = \operatorname{tg}\dfrac{1}{2}\varphi & k' = \sqrt{1-k^2} \\[2ex] z = 3\varepsilon I_2 = 2\cos\dfrac{\varphi}{2}\cdot E' - 2\sin\varphi \sin\dfrac{\varphi}{2}\cdot K' & \\[2ex] \dfrac{2I_1}{n^2} = 2\cos\dfrac{\varphi}{2}(K-E) & \end{array}\right. \tag{3.3}$$

dans lequel K et E sont les fonctions elliptiques complètes de première et seconde espèce de module k et K', E' les mêmes de

module k'. γ_2 représente la fraction rouge du réseau de raies Stark détruite par le champ F.

Les fonctions $z = 3\,\varepsilon I_2$ et $y = \log \frac{\varepsilon I_1}{n^2}$ ont été tabulées par Pannekoek (28). Comme nous supposons la différence $E_{nx} - E_n$ petite devant E_n, nous pouvons définir la disparition des états dans le champ F par la condition $\gamma_2 = {}^1/_2$.

La relation $\delta = \alpha$ qui peut s'écrire:

$$(3.4) \qquad 16{,}01 - 2 \cdot 0{,}4343 \frac{z}{3\,\varepsilon} - y + \log \frac{\varepsilon}{n^2} = \log \alpha$$

ou

$$(3.5) \qquad 16{,}01 - \log \alpha - y + \log \tau - \log 4\,n - \log n^2 = \frac{z}{3{,}454} \frac{4\,n}{\tau}$$

nous détermine complètement τ_n. On en déduit ensuite:

$$(3.6) \qquad \tau_n = 4\,n \frac{2\,a_0^2}{e} F n^3,$$

d'où:

$$(3.7) \qquad F = \frac{\tau_n}{4{,}68\ 10^{-7} n^4} = 2{,}14 \cdot 10^6 \frac{\tau_n}{n^4}.$$

Le résultat est donné dans le tableau I.

Tableau I.

n	$\log \tau_n$	$\log F_n$	$\log N_1^{2/3} \frac{F_n}{F_0}$	Destruction des états pour $\log N_1$	Recouvrement des raies pour $\log N_1$
1	$\bar{1}{,}356$	5,686	14,588	21,873	23,257
2	$\bar{1}{,}583$	4,709	13,611	20,417	21,000
3	$\bar{1}{,}695$	4,117	13,019	19,529	19,678
4	$\bar{1}{,}764$	3,686	12,588	18,883	18,742
5	$\bar{1}{,}810$	3,344	12,246	18,370	18,014
6	$\bar{1}{,}842$	3,059	11,961	17,943	17,421
7	$\bar{1}{,}866$	2,815	11,717	17,577	16,919
8	$\bar{1}{,}883$	2,601	11,503	17,254	16,483
9	$\bar{1}{,}899$	2,411	11,313	16,972	16,103
10	$\bar{1}{,}911$	2,241	11,143	16,715	15,757
11	$\bar{1}{,}920$	2,085	10,987	16,480	15,447
12	$\bar{1}{,}927$	1,941	10,843	16,268	15,164
13	$\bar{1}{,}935$	1,810	10,712	16,069	14,904

τ est une fonction lentement variable de n alors que le dénominateur contenant n^4 croît très rapidement.

Lorsque k tend vers 1, k' tend vers zéro, $z \cong \frac{5\sqrt{2}}{3\pi} k'^4$ et on a

$$4\,n^3 \cong [7{,}86] \log_e \frac{4}{k'}, \tag{3.8}$$

ce qui entraîne de très grandes valeurs de n (n de l'ordre de 300).

4. Il est nécessaire maintenant de préciser la fonction de distribution $W(F)\,dF$. Cette fonction est évidemment donnée — en principe — par une méthode de champ self-consistent. Chaque proton est entouré d'électrons libres qui font plus ou moins écran à sa charge. En d'autres termes, la théorie de Holtsmark (18) qui ne considère que des ions et des électrons ponctuels n'est sans doute pas correcte et cette conclusion a déjà été tirée par Verwej (51) de ses résultats relatifs aux contours de raies. Il semble bien que pour la théorie de l'ionisation, la théorie de Holtsmark ne convienne absolument pas et par contre que la théorie de Russell et Stewart (33) donne simplement des résultats conformes à la théorie des volumes exclus et d'ailleurs de façon plus simple.

La loi de probabilité $W(F)\,dF$ — que nous écrivons ici $W(\beta)\,d\beta$ en utilisant le champ normal

$$F_0 = 2{,}61\; e\; N_1^{2/3} \tag{4.1}$$

et la notation

$$\beta = \frac{F}{F_0} \tag{4.2}$$

est une fonction transcendante nouvelle de β

$$W(\beta) = \frac{2}{\pi\beta} \int_0^\infty v \sin ve^{-\left(\frac{v}{\beta}\right)^{3/2}} dv, \tag{4.3}$$

qui, pour les faibles valeurs de β, admet un développement dont le premier terme nous suffit:

$$W(\beta) = \frac{4}{3\pi}\beta^2. \tag{4.4}$$

Si nous supposons la densité d'ions N_1 très élevée (par exemple 10^{22}), le champ normal F_0 est très intense et la destruction des états a lieu même pour de très faibles valeurs de β. Si de plus, et uniquement pour la commodité de notre argumentation, nous supposons la température assez élevée pour que les exponentielles

$$e^{\vartheta E_{nx}} \tag{4.5}$$

se réduisent à l'unité, la somme Σ devient:

$$\sum = \sum_n 2n^2 \int_0^{\beta_n} \frac{4}{3\pi} \beta^2 d\beta \tag{4.6}$$

ou, en tenant compte des équations (3.7) (4.2) (4.4):

$$\sum = \sum_n \frac{1}{2\pi (4{,}68 \cdot 10^{-7} F_0)^3} \frac{\tau_n^3}{n^{10}}. \tag{4.7}$$

Cette somme est évidemment convergente et même très rapidement, mais nous remarquerons en raison de la valeur (4.1) du champ normal qu'elle est inversement proportionnelle à N_1^2, N_1 nombre d'ions positifs. On conclut de la relation (2.7) avec $N_e = N_1$ que:

$$N_0 = \frac{1}{2\pi} \frac{\sum \frac{\tau_n^3}{n^{10}}}{(4{,}68 \cdot 10^{-7} \cdot 2{,}61\, e)^3} \cdot \frac{h^3}{2(2\pi mkT)^{\frac{3}{2}}} \tag{4.8}$$

c. à. d. que, à température constante, N_0 serait constant pour les grandes densités. Ce résultat n'aurait en soi rien d'absurde, mais le calcul numérique de N_0 nous donne:

$$N_0 = \frac{[28{,}566]}{T^{\frac{3}{2}}}. \tag{4.9}$$

La valeur exagérément élevée de N_0 ainsi obtenue est en contradiction absolue avec toutes les indications de la théorie des volumes exclus qui indique une décroissance extrêmement rapide du nombre d'atomes neutres avec les densité croissantes.

Il a paru que ce résultat provenait de l'emploi de la théorie de Holtsmark, de préférence à une autre. Nous avons donc essayé la théorie de Russell et Stewart (33). Russell et Stewart,

exprimant que dans la sphère de rayon x, $x + dx$ se trouve un ion positif, et que cet ion, le plus proche de l'atome considéré, est aussi le seul à agir, obtiennent la fonction de distribution:

$$W(\beta)\,d\beta = \frac{1{,}50}{\beta^{\frac{5}{2}}} e^{-\beta^{-\frac{3}{2}}} d\beta \tag{4.10}$$

qui est identique à la fonction de Holtsmark pour les grandes valeurs de β ($\beta > 50$ par exemple) mais qui en diffère très considérablement (en puissances de 10) quand β est très petit. Si nous supposons comme précédemment que la densité N_1 est élevée, et la température aussi, nous avons à utiliser l'intégrale

$$\int_0^{\beta_n} W(\beta)\,d\beta = e^{-\beta_n^{-\frac{3}{2}}}, \tag{4.11}$$

ce qui donne pour la somme Σ:

$$\sum\nolimits' = \sum_n 2\,n^2 \exp -(4{,}68 \cdot 10^{-7} F_0)^{\frac{3}{2}} \frac{n^6}{\tau_n^{\frac{3}{2}}}. \tag{4.12}$$

Elle contient ainsi des exponentielles dont la valeur numérique est:

$$\exp -[\overline{23},151]\, N_1 \frac{n^6}{\tau_n^{\frac{3}{2}}}. \tag{4.13}$$

Le terme qui figure ici en exponentielle est tout à fait analogue au terme élémentaire que l'on obtient par la méthode des volumes exclus sous la forme donnée par Fermi (15). Une différence très importante est que le coefficient numérique est beaucoup plus grand. Pour donner un ordre de grandeur, l'exposant vaut 1 pour $n = 2$ lorsque $N_1 = [20{,}43]$, alors que la méthode des volumes exclus introduit pour le même résultat une valeur $N_1 = [23{,}1]$. Autrement dit l'effet Stark linéaire détruit les états stationnaires bien avant que se produisent des collisions au sens classique du terme. On trouvera dans le tableau I les densités pour lesquelles se produit la destruction des états quantiques (colonne 5). Ces valeurs correspondent aux densités pour lesquelles le champ normal (équation 4.1) est égal au champ F_n (colonne 4). On les comparera aux densités déduites de la for-

mule d'Inglis et Teller (équation 12.1) pour lesquelles se produit le recouvrement des raies (colonne 6).

C'est cet accord entre le résultat de la théorie des volumes exclus et l'emploi de la théorie statistique de Russell Stewart qui nous fait conclure à une impossibilité très réelle d'obtenir des résultats complètement corrects par la théorie de Holtsmark. Il serait en particulier intéressant de voir comment l'emploi de la fonction (4.10) modifierait les résultats de VERWEJ (51), particulièrement dans la partie centrale de ses profils de raies.

5. On pourrait chercher à améliorer la théorie de Holtsmark, mais les difficultés qui se présentent sont très grandes. Dans le but de montrer de quelle nature sont ces difficultés, nous allons tout d'abord rappeler de quelle nature est la méthode de Holtsmark.

Etant donnée à l'origine des coordonnées une particule, on veut mesurer le champ dans lequel elle est placée. Si l'on appelle $1, 2, \cdots n \cdots$ les différentes particules agissantes, chacune produisant un champ de composantes $X_i Y_i Z_i$, le champ à l'origine a pour composantes

$$(5.1) \quad \begin{cases} X_0 = \Sigma X_i \\ Y_0 = \Sigma Y_i \\ Z_0 = \Sigma Z_i . \end{cases}$$

Si l'on appelle $dx_{1i} \cdots dx_{\nu i}$ la probabilité d'avoir une particule au point de coordonnées $x_{1i} \cdots x_{\nu i}$, la probabilité d'avoir un champ compris entre X_0, $X_0 + dX_0$, Y_0, $Y_0 + dY_0$, Z_0, $Z_0 + dZ_0$ est donnée par

$$(5.2) \quad W(X_0 Y_0 Z_0) = \frac{1}{V_N} \int \cdots \int \sigma_1 \cdots \sigma_N \, dx_{11} \cdots dx_{\nu N},$$

l'intégrale multiple portant sur le volume où les conditions

$$(5.3) \quad \begin{cases} X_0 < X < X_0 + dX_0 \\ \cdots \\ \cdots \end{cases}$$

sont satisfaites et V_N étant obtenu par intégration sur le volume total:

$$V_N = \int \cdots \int \sigma_1 \cdots \sigma_N \, dx_{11} \cdots dx_{\nu N}. \tag{5.4}$$

Afin d'étendre l'intégrale (5.2) à tout l'espace, Holtsmark introduit des facteurs de Dirichlet:

$$\left\{ \begin{aligned} H(X) &= \frac{1}{\pi} \int_{-\infty}^{+\infty} \frac{\sin \alpha\xi}{\xi} e^{i\delta\xi} \, d\xi \\ H(Y) &= \frac{1}{\pi} \int_{-\infty}^{+\infty} \frac{\sin \beta\eta}{\eta} e^{i\varepsilon\eta} \, d\eta \\ H(Z) &= \frac{1}{\pi} \int_{-\infty}^{+\infty} \frac{\sin \gamma\zeta}{\zeta} e^{i\chi\zeta} \, d\zeta \end{aligned} \right. \tag{5.5}$$

avec les valeurs suivantes de α, β, γ, δ, ε, χ:

$$\left\{ \begin{aligned} \alpha &= \frac{1}{2} dX_0 & \delta &= \sum_1^N X_n - X_0 \\ \beta &= \frac{1}{2} dY_0 & \varepsilon &= \sum_1^N Y_n - Y_0 \\ \gamma &= \frac{1}{2} dZ_0 & \chi &= \sum_1^N Z_n - Z_0 . \end{aligned} \right. \tag{5.6}$$

Les intégrales (5.5) valent 1 ou 0 suivant que les inégalités suivantes sont satisfaites ou non:

$$-\alpha < \delta < \alpha \qquad -\beta < \varepsilon < \beta \qquad -\gamma < \chi < \gamma. \tag{5.7}$$

Comme α, β, γ sont des infiniments petits, Holtsmark écrit:

$$H(X) = \frac{dX_0}{2\pi} \int_{-\infty}^{+\infty} e^{i(\Sigma X_n - X_0)} \, d\xi; \tag{5.8}$$

d'où, pour W:

$$\left\{ \begin{aligned} W(X_0 Y_0 Z_0) \, dX_0 \, dY_0 \, dZ_0 &= \frac{1}{8\pi^3} dX_0 \, dY_0 \, dZ_0 \iiint_{-\infty}^{+\infty} d\xi \, d\eta \, d\zeta \, e^{-i(\xi X_0 + \eta Y_0 + \zeta Z_0)} \\ & \frac{1}{V_n} \underbrace{\int \cdots \int}_{W_n} \sigma_1 \cdots \sigma_N \, e^{i(\xi \Sigma X_n + \eta \Sigma Y_n + \zeta \Sigma Z_n)} \, dx_{11} \cdots dx_{\nu N}. \end{aligned} \right. \tag{5.9}$$

Nous introduirons ici une hypothèse différente de celle de Holtsmark: nous supposerons que les particules $1, 2, \cdots N$ ne sont identiques qu'en moyenne, et nous conserverons jusqu'à nouvel ordre l'indice i.

Nous avons en tout cas, comme Holtsmark:

$$V_N = V^N, \tag{5.10}$$

ce qui implique l'identité et l'indépendance des probabilités $\sigma_1 \cdots \sigma_N$. Nous avons à calculer l'intégrale type:

$$J_i = \frac{1}{V}\int_V \cdots \int e^{i(\xi X_i + \eta Y_i + \zeta Z_i)}\, \sigma_i\, dx_{i1} \cdots dx_{i\nu}. \tag{5.11}$$

Si l'on suppose que la force $X_i\, Y_i\, Z_i$ agit suivant le rayon vecteur r_i, on peut écrire, en prenant pour $\xi\, \eta\, \zeta$ les composantes d'un vecteur $\vec{s}$ faisant un angle θ avec le rayon vecteur r_i:

$$J_i = \frac{1}{V}\underbrace{\int \cdots \int}_{V} e^{i(\vec{s}\cdot\vec{f}_i)}\, \sigma_i\, dx_{1i} \cdots dx_{\nu i}. \tag{5.12}$$

Nous avons évidemment

$$\sigma_i\, dx_{1i} \cdots dx_{\nu i} = r_i^2\, dr_i \sin\theta_i\, d\theta_i\, d\varphi_i \tag{5.13}$$

et l'on a en limitant l'intégration à une sphère de rayon R:

$$J_i = \frac{1}{\frac{4}{3}\pi R^3}\int_0^R r_i^2\, dr_i \int_0^{\pi} d\theta_i \int_0^{2\pi} d\varphi_i\, e^{i(\vec{s}\cdot\vec{f}_i)}. \tag{5.14}$$

Posons $f_i = \frac{e}{r^2}\, g_i(r)$ avec $g_i = 1$ quand $r \to 0$.

On a:

$$\vec{s}\cdot\vec{f}_i = -\frac{e g_i}{r_i^2}\, \varrho \cos\theta; \tag{5.15}$$

posons

$$e\,\varrho\cos\theta\,\frac{g_i}{r_i^2} = \varrho\, w_2\, \frac{g_i}{r_i^2} \tag{5.16}$$

et prenons comme nouvelle variable

$$\frac{\varrho\, w_2}{r_i^2} = u \tag{5.17}$$

on a alors:

$$J_i = \frac{3}{4\pi R^3} \iint \sin\theta\, d\theta\, d\varphi\, \frac{(\varrho\, w_2)^{\frac{3}{2}}}{2} \int_\alpha^\infty e^{iug_i(u)}\, u^{-\frac{5}{2}}\, du \tag{5.18}$$

avec $\alpha = \dfrac{\varrho\, w_2}{R^2}$.

On a donc:

$$J_i = \frac{3}{4\pi} \iint \sin\theta\, d\theta\, d\varphi\, \frac{\alpha^{\frac{3}{2}}}{2} \int_\alpha^\infty e^{iug_i(u)}\, u^{-\frac{5}{2}}\, du. \tag{5.19}$$

La deuxième intégrale peut s'intégrer par parties:

$$\begin{cases} \displaystyle\int_\alpha^\infty e^{iug_i(u)}\, u^{-\frac{5}{2}}\, du = \frac{2}{3}\alpha^{-\frac{3}{2}} e^{i\alpha g_i(\alpha)} + \frac{4}{3} i\alpha^{-\frac{1}{2}} e^{i\alpha g_i(\alpha)} \left(g_i(\alpha) + \alpha g_i'(\alpha)\right) \\ \qquad\qquad + \dfrac{4}{3}\displaystyle\int_0^\infty u^{-\frac{1}{2}} e^{iug_i(u)} \left(2ig_i' + iug_i'' - (g_i + ug_i')^2\right) du \\ \qquad\qquad + \cdots; \end{cases} \tag{5.20}$$

comme α est très petit (R grand) on peut développer les exponentielles et on obtient:

$$\frac{2}{3}\alpha^{-\frac{3}{2}} + i\alpha^{-\frac{1}{2}}\left(2g_i + \frac{4}{3}\alpha g_i'\right) + \frac{4}{3}\int_0^\infty u^{-\frac{1}{2}} e^{iug_i(u)} \left(2ig_i' + iug_i'' - (g_i + ug_i')^2\right) du. \tag{5.21}$$

On obtient alors pour J_i:

$$\begin{cases} J_i = \dfrac{1}{4\pi}\displaystyle\int d\Omega \left[1 + i\alpha\,(3g_i + 2\alpha g_i') + \right. \\ \qquad \left. + 2\alpha^{\frac{3}{2}} \displaystyle\int_0^\infty u^{-\frac{1}{2}} e^{iug_i(u)} \left(2ig_i' + iug_i'' - (g_i + ug_i')^2\right)\right] du \\ \qquad = 1 + i\displaystyle\int \frac{d\Omega}{4\pi}\alpha\,(3g_i + 2\alpha g_i') + \\ \qquad + \dfrac{1}{4\pi}\displaystyle\int 2\alpha^{\frac{3}{2}}\, d\Omega \int_0^\infty u^{-\frac{1}{2}} e^{iug_i(u)} \left(2ig_i' + iug_i'' - (g_i + ug_i')^2\right) du, \end{cases} \tag{5.22}$$

g_i étant une fonction paire par sa définition même, $\alpha g_i'$ est aussi une fonction paire et la première intégrale disparaît. La deuxième intégrale nous fournit une fonction compliquée de ϱ:

$$(5.23)\quad \left\{ \begin{aligned} J_i &= 1 + \frac{2\pi}{4\pi} 2 \cdot \frac{\varrho^{\frac{3}{2}}}{R^3} e^{\frac{3}{2}} \int_0^{\pi} (\cos\theta)^{\frac{3}{2}} \sin\theta \, d\theta \int_0^{\infty} u^{-\frac{1}{2}} e^{iug_i(u)} \\ &\quad (2ig_i' + iug_i'' - (g_i + ug_i')^2)\, du. \end{aligned} \right.$$

En raison du fait que $\frac{4}{3}\pi R^3 n = N$, nombre de particules actives dans le volume considéré, on a pour le produit πJ_i:

$$(5.24)\quad \pi J_i = \exp\left\{ \frac{8\pi n}{3} e^{\frac{3}{2}} \varrho^{\frac{3}{2}} \frac{1}{N} \sum_1^N{}_i \int_0^{\pi} (\cos\theta)^{\frac{3}{2}} \sin\theta \, d\theta \int_0^{\infty} u^{-\frac{1}{2}} e^{iug_i(u)} H_i(u)\, du \right\};$$

la somme $\frac{1}{N}\sum_1^N$ a la signification d'une moyenne étendue à toutes les fonctions possibles $g_i(r)$.

Holtsmark suppose toutes ces fonctions g_i identiques à 1 et obtient ainsi le champ dû aux ions:

$$(5.25)\qquad J^N = \exp\left[-4{,}21\, n\varrho^{\frac{3}{2}} e^{\frac{3}{2}}\right]$$

et par conséquent la fonction W:

$$(5.26)\qquad W = \frac{1}{4\pi^2} \int_0^{\infty} \varrho^2 d\varrho \, e^{-4{,}21\, n\varrho^{\frac{3}{2}} e^{\frac{3}{2}}} \frac{2}{\varrho F_0} \sin(\varrho F_0)$$

où F_0 est l'intensité du champ de composantes $X_0\ Y_0\ Z_0$.

6. Nous voyons donc par l'expression (5.24) que si une moyenne peut se définir, elle ne s'obtient pas sans calculs d'une extrême complication, comportant 4 intégrales successives portant respectivement sur u, θ, (i), et enfin ϱ. Il semble donc indispensable de faire une première simplification en supposant toutes les fonctions g_i identiques. On a alors:

$$(6.1)\quad W\, dX_0\, dY_0\, dZ_0 = dX_0\, dY_0\, dZ_0 \iiint \sin\theta \, d\theta \, d\varphi \varrho^2 d\varrho \, e^{-iF_0 \varrho \cos\theta} \exp\left[K(\varrho)\right],$$

ce qui donne:

$$W(X_0\,Y_0\,Z_0) = \frac{1}{4\pi^2}\int_0^\infty \varrho^2\, d\varrho\, \frac{2\sin \varrho F_0}{\varrho F_0} \exp\left[K(\varrho)\right], \tag{6.2}$$

avec pour $K(\varrho)$:

$$K(\varrho) = \frac{8\pi n}{3} e^{\frac{3}{2}} \varrho^{\frac{3}{2}} \int_0^{\pi} (\cos\theta)^{\frac{3}{2}} \sin\theta\, d\theta \int_0^\infty u^{-\frac{1}{2}} e^{iug(u)} H(u)\, du, \tag{6.3}$$

avec

$$H(u) = 2ig' + iug'' - (g + ug')^2 \tag{6.4}$$

$$g(u) = g\left(\sqrt{\frac{\varrho w_2}{u}}\right). \tag{6.5}$$

On voit, par la nature des fonctions écrites que même les fonctions g les plus simples conduisent tout de même — en général — à des fonctions $K(\varrho)$ d'une extrême complication. En particulier, nous voyons qu'il serait possible, au moins en principe, de résoudre le système de deux équations intégrales successives (6.2) et (6.3) et d'obtenir la fonction $g(r)$ donnant la loi de probabilité de Russell Stewart.

Les équations (5.24) et (6.2) en particulier nous montrent de quelle nature sont les difficultés d'une méthode statistique de champ self-consistent pour des atomes distribués au hasard.

Il serait possible d'adjoindre aux conditions (5.1) une condition exprimant que l'intégration se fait le long d'une surface d'énergie constante. Mais alors la séparation (5.11) des différentes variables est impossible, ce qui rend le calcul impraticable.

Nous voyons donc de quelle nature sont les difficultés d'amélioration de la théorie de Holtsmark. Il paraît ainsi plus sage de s'en tenir à une théorie au sens physique évident, analytiquement simple et donnant des résultats, pour les faibles densités conformes à la théorie de Holtsmark et pour les grandes densités conformes à la théorie des volumes exclus, autrement dit, la théorie de Russell et Stewart.

7. Tables d'ionisation. Calculons tout d'abord la contribution à la somme Σ des termes pour n grand. On a à calculer:

$$\sigma_n = \sum_n^\infty n^2 e^{-\beta_n^{-\frac{3}{2}}} \tag{7.1}$$

car, en raison de la valeur élevée de n, le terme $e^{\vartheta E}$ peut être pris égal à l'unité.

On a:

$$\beta = 2{,}14 \cdot 10^6 \frac{\tau}{n^4} \frac{1}{F_0} \tag{7.2}$$

et en vertu de (3.7) et (3.8) nous supposerons τ sensiblement constant. On a alors

$$n^2 = \left(\frac{2{,}14 \cdot 10^6 \tau}{F_0}\right)^{\frac{1}{2}} \frac{1}{\sqrt{\beta}} \tag{7.3}$$

et nous remplacerons la somme (7.1) par une intégrale:

$$\sigma_n = \int_n^\infty n^2 dn\, e^{-\beta_n^{-\frac{3}{2}}}. \tag{7.4}$$

On a:

$$n^2 dn = \frac{1}{3} d(n^3) \tag{7.5}$$

$$= -\left(\frac{2{,}14 \cdot 10^6 \tau}{F_0}\right)^{\frac{3}{4}} \frac{1}{4} \beta^{-\frac{7}{4}} d\beta. \tag{7.6}$$

La somme (7,1) devient alors:

$$\sigma_n = \left(\frac{2{,}14 \cdot 10^6 \tau}{F_0}\right)^{\frac{3}{4}} \frac{1}{4} \int_0^{\beta_n} \beta^{-\frac{7}{4}} d\beta\, e^{-\beta^{-\frac{3}{2}}} \tag{7.7}$$

$$= \left(\frac{2.14 \cdot 10^6 \tau}{F_0}\right)^{\frac{3}{4}} \frac{1}{4} \frac{4}{3} \int_0^{\beta_n} d\left(\beta^{-\frac{3}{4}}\right) e^{-\beta^{-\frac{3}{2}}}. \tag{7.8}$$

Pour β petit, on peut réduire l'intégrale dans (7.8) au premier terme du développement asymptotique. On a alors:

$$\sigma_n = \left(\frac{2{,}14 \cdot 10^6 \tau}{F_0}\right)^{\frac{3}{4}} \frac{1}{3} \frac{e^{-\beta^{-\frac{3}{2}}}}{2\beta^{-\frac{3}{4}}} \tag{7.9}$$

et, en vertu de (7.3), on obtient:

$$\sigma_n = \frac{n^3}{6} \frac{e^{-\beta_n^{-\frac{3}{2}}}}{\beta_n^{-\frac{3}{2}}}. \tag{7.10}$$

La table suivante nous montre la contribution σ_n pour $n = 13$ en fonction de la densité. On voit que pour des densités même relativement faibles, la contribution à la somme Σ des termes pour $n > 13$ devient tout à fait négligeable.

Tableau II.

Log N_1	$\beta^{-\frac{3}{2}}$	σ_{13}
15	0,0857	4217,1
16	0,857	181,59
17	8,57	0,0085

8. Méthode de calcul. Pour calculer les intégrales

$$\int_0^{\beta_n} e^{\vartheta W_n} W(\beta)\, d\beta \tag{8.1}$$

on procède de la façon suivante. On a:

$$W_n = E_n - E_F, \tag{8.2}$$

E_n étant l'énergie d'ionisation en l'absence de champ de l'état n, E_F étant l'énergie d'ionisation en l'absence de champ de l'état détruit par le champ F. On a donc à calculer:

$$2 \sum_n{}' n^2 e^{\vartheta E_n} \int_0^{\beta_n} W(\beta)\, d\beta\, e^{-\vartheta E_F}. \tag{8.3}$$

On a:

$$W(\beta)\, d\beta = d\left(e^{-\beta^{-\frac{3}{2}}}\right) \tag{8.4}$$

et l'on construit la courbe $e^{-\vartheta E_F}$ en fonction de $e^{-\beta^{-\frac{3}{2}}}$. On a seulement à déterminer l'aire de cette courbe. On trouvera sur la figure 3, p. 46, les formes de cette courbe pour différentes densités et pour $\theta = 0{,}2$. On obtient ainsi pour chaque valeur de la densité N_1 et de la température $\theta = \frac{5040}{T}$ la valeur de la somme. En fait, on calcule

$$(8.5) \qquad 2 \sum_n n^2 e^{-\vartheta(E_0 - E_n)} \int_0^{\beta_n} W(\beta)\, d\beta\, e^{-\vartheta E_F}$$

qui est l'équivalent de la somme d'états. On en déduit, à l'aide

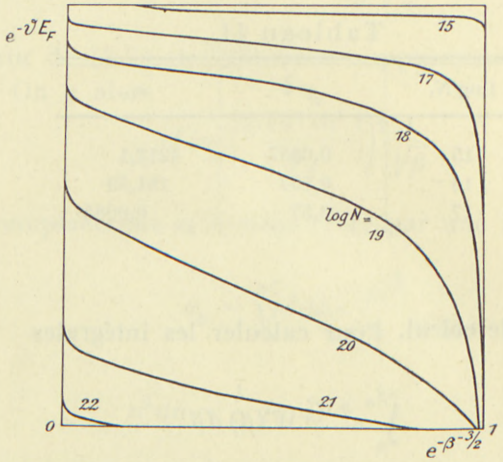

Fig. 3. Courbes pour l'intégration numérique de la formule (II 8,1).

de (2.7) N_0 en fonction de N_1 et de θ, et ensuite $N = N_1 + N_0$, donc $\varrho = NH$ en fonction de N_1 et θ, ainsi que l'ionisation:

$$(8.6) \qquad x = \frac{N_1}{N_0 + N_1}$$

en fonction de N_1 et θ. A l'aide de la table (N_1, θ) on peut finalement construire une table $x(\varrho, \theta)$ (Des tables complètes sont en cours de préparation. Les tableaux III et IV en sont extraits).

Tableau III.

x (degré d'ionisation)

$\log N_1$ / θ	15	16	17	18	19	20	21	22	23
0,2	0,999	0,999	0,993	0,953	0,754	0,387	0,226	0,393	1,000
0,1	1,000	1,000	0,999	0,997	0,987	0,946	0,848	0,828	1,000
0,05	1,000	1,000	1,000	0,999	0,998	0,991	0,974	0,954	1,000
0,02	1,000	1,000	1,000	1,000	0,999	0,998	0,996	0,990	1,000
0,01	1,000	1,000	1,000	1,000	1,000	0,999	0,999	0,997	1,000

Tableau IV.

$\bar{\chi}_{volts}$[1] (potentiel moyen d'ionisation)

θ \ log N_1	15	16	17	18	19	21	21	22	23
0,2	1,326	5,113	8,432	10,996	11,423	10,442	8,017	2,077	0,000
0,1	0,449	0,625	1,481	3,237	6,223	8,137	7,355	1,511	0,000
0,05	0,239	0,267	0,578	1,402	3,336	5,449	6,673	1,209	0,000
0,02	0,192	0,196	0,383	0,892	1,838	3,809	6,143	1,025	0,000
0,01	0,182	0,181	0,343	0,744	1,579	3,343	5,931	0,956	0,000

[1] On remarquera que $\bar{\chi}$ décroît quand la densité décroît. Cela est dû à la possibilité du peuplement des niveaux excités aux faibles densités.

9. Compressibilité adiabatique. Le calcul de la couche convective est important, comme nous l'avons vu à propos de la théorie du triage. Il est nécessaire, pour en établir les limites, de calculer le coefficient de compressibilité adiabatique. On peut remarquer que l'influence de l'ionisation sur le coefficient $(d \log T/d \log P)$ est la même, que l'ionisation ait pour origine une élévation de température ou une augmentation de pression.

En effet, si on se trouve dans une région de demi-ionisation de température, une compression adiabatique élève la température, donc le nombre d'atomes présents et l'élévation de température est moindre que celle qui se produit en l'absence d'ionisation. L'effet est le même si on se trouve dans une région d'ionisation de pression. Il faut donc s'attendre à trouver une vaste région de températures et de densités où $(d \log T/d \log P)$ est inférieur à 0,4, valeur maximum pour un gaz monoatomique.

Une transformation adiabatique est définie par

$$dE + P\,dV = 0. \tag{9.1}$$

La pression P est:

$$PV = N(1 + x)\,kT \tag{9.2}$$

et l'énergie est:

$$E = \frac{3}{2} N(1+x)\,kT - \sum n_i \chi_i \tag{9.3}$$

n_i étant le nombre de particules d'énergie $-\chi_i$. Si E_{p_i} est l'énergie de l'état de nombre quantique p_i, E_F l'énergie du niveau détruit dans le champ F, on a:

$$dn_i = \frac{N_0 g_i W(\beta)\, d\beta e^{\vartheta\chi_i}}{\sum_i \int_0^{\beta_i} g_i W(\beta)\, d\beta e^{\vartheta\chi_i}} \tag{9.4}$$

et l'équation (9.3) devient

$$E = \frac{3}{2} N(1+x) kT - N(1-x) \frac{\sum_i \int g_i W(\beta)\, d\beta e^{\vartheta\chi_i} (E_i - E_F)}{\sum_i \int g_i W(\beta)\, d\beta e^{\vartheta\chi_i}}. \tag{9.5}$$

Nous poserons de façon abrégée:

$$\overline{\chi} = \frac{\sum_i \int g_i (E_i - E_F) W(\beta)\, d\beta\, e^{\vartheta\chi_i}}{\sum_i \int g_i W(\beta)\, d\beta e^{\vartheta\chi_i}} \tag{9.6}$$

et de même:

$$\overline{\chi^2} = \frac{\sum_i \int g_i (E_i - E_F)^2 W(\beta)\, d\beta e^{\vartheta\chi_i}}{\sum_i \int g_i W(\beta) d\beta e^{\vartheta\chi_i}}. \tag{9.7}$$

Afin de pouvoir effectuer les dérivations par rapport à x, V et T dans $\overline{\chi}$, nous explicitons la fonction $W(\beta)$ en mettant en évidence comme variable le champ électrique F. On écrit alors:

$$\overline{\chi} = \frac{\sum_i \int_0^{F_i} g_i (E_i - E_F) \frac{3}{2} (2{,}61 \cdot e)^{\frac{3}{2}} \frac{Nx}{V} F^{-\frac{5}{2}}\, dF e^{-F^{-\frac{3}{2}} (2{,}61 \cdot e)^{\frac{3}{2}} \frac{Nx}{V}} e^{\vartheta (E_i - E_F)}}{\sum_i \int_0^{F} g_i \frac{3}{2} (2{,}61 \cdot e)^{\frac{3}{2}} \frac{Nx}{V} F^{-\frac{5}{2}}\, dF e^{\vartheta (E_i - E_F)}}. \tag{9.8}$$

Nous posons:

$$E = \chi N (1 - x). \tag{9.9}$$

En posant également:

(9.10) $$\bar{\chi} = \frac{S}{\Sigma}$$

(9.11) $$\boldsymbol{T} = \sum \int_0^{\beta_i} g_i (E_i - E_F)\, d\left(\beta^{-\frac{3}{2}} e^{-\beta^{-\frac{3}{2}}}\right) e^{\vartheta (E_i - E_F)}$$

(9.12) $$\Theta = \sum \int_0^{\beta_i} g_i\, d\left(\beta^{-\frac{3}{2}} e^{-\beta^{-\frac{3}{2}}}\right) e^{\vartheta (E_i - E_F)},$$

on obtient:

(9.13) $$\frac{1}{\mathfrak{E}} \frac{\partial \mathfrak{E}}{\partial x} = -\frac{dx}{1-x} + \frac{1}{S}\frac{\partial S}{\partial x} - \frac{1}{\Sigma}\frac{\partial \Sigma}{\partial x}.$$

On a:

(9.14) $$\frac{\partial S}{\partial x} = -\frac{\boldsymbol{T}}{x} \qquad \frac{\partial S}{\partial V} = \frac{\boldsymbol{T}}{V}$$

(9.15) $$\frac{\partial \Sigma}{\partial x} = -\frac{\Theta}{x} \qquad \frac{\partial \Sigma}{\partial V} = \frac{\Theta}{V} \qquad \frac{V}{\Sigma}\frac{\partial \Sigma}{\partial V} = \frac{\Theta}{\Sigma}.$$

On obtient donc

(9.16) $$\frac{\partial \mathfrak{E}}{\partial x} = -N\bar{\chi} + \frac{\mathfrak{E}}{x}\left(\frac{\Theta}{\Sigma} - \frac{\boldsymbol{T}}{S}\right).$$

On a de même:

(9.17) $$\frac{\partial \mathfrak{E}}{\partial V} = \frac{\mathfrak{E}}{V}\left(\frac{\boldsymbol{T}}{S} - \frac{\Theta}{\Sigma}\right) \qquad \frac{1}{P}\frac{\partial \mathfrak{E}}{\partial V} = \frac{1-x}{1+x}\frac{\bar{\chi}}{kT}\left(\frac{\boldsymbol{T}}{S} - \frac{\Theta}{\Sigma}\right).$$

On a enfin:

(9.18) $$\frac{1}{\bar{\chi}}\frac{\partial \bar{\chi}}{\partial T} = -\frac{1}{kT^2}\frac{\overline{\chi^2}}{\bar{\chi}} + \frac{1}{kT^2}\bar{\chi}$$

ou

(9.19) $$\frac{\partial \bar{\chi}}{\partial T} = -\frac{1}{kT^2}(\overline{\chi^2} - \bar{\chi}^2).$$

Différentions (9.5), (9.2) et l'équation d'équilibre (2.7). On obtient ainsi le système d'équations différentielles:

(9.20) $$dE = N(1+x)\frac{3}{2}kT\frac{dT}{T} + N\cdot\frac{3}{2}kT\,dx - \frac{\partial \mathfrak{E}}{\partial x}dx - \frac{\partial \mathfrak{E}}{\partial V}dV - \frac{\partial \mathfrak{E}}{\partial T}dT$$

(9.21) $$\frac{dP}{P} = \frac{dx}{1+x} + \frac{dT}{T} - \frac{dV}{V}$$

$$(9.22)\quad -\frac{dV}{V}+\frac{2\,dx}{x}+\frac{dx}{1-x}=\frac{3}{2}\frac{dT}{T}-\frac{1}{\Sigma}\frac{\partial\Sigma}{\partial x}dx-\frac{1}{\Sigma}\frac{\partial\Sigma}{\partial T}dT-\frac{1}{\Sigma}\frac{\partial\Sigma}{\partial V}dV$$

auquel il faut adjoindre (9.1) qui permet d'éliminer dE. On obtient alors le système:

$$(9.23)\quad \left(\frac{\partial\mathfrak{E}}{\partial V}-P\right)dV=\left(\frac{3}{2}\frac{PV}{T}-\frac{\partial\mathfrak{E}}{\partial T}\right)dT+\left(\frac{3}{2}\frac{PV}{1+x}-\frac{\partial\mathfrak{E}}{\partial x}\right)dx$$

$$(9.24)\quad \frac{dP}{P}=\frac{dx}{1+x}+\frac{dT}{T}-\frac{dV}{V}$$

$$(9.25)\quad \left(-\frac{1}{V}+\frac{1}{\Sigma}\frac{\partial\Sigma}{\partial V}\right)dV+dx\left(\frac{2}{x}+\frac{1}{1-x}+\frac{1}{\Sigma}\frac{\partial\Sigma}{\partial x}\right)=\frac{dT}{T}\left(\frac{3}{2}-\frac{T}{\Sigma}\frac{\partial\Sigma}{\partial T}\right).$$

On tire dV de l'équation (9.24) et on obtient:

$$(9.26)\quad \begin{cases} -\left(\dfrac{\partial\mathfrak{E}}{\partial V}-P\right)V\dfrac{dP}{P}=dT\left(\dfrac{3}{2}\dfrac{PV}{T}-\dfrac{\partial\mathfrak{E}}{\partial T}-\dfrac{V}{T}\left(\dfrac{\partial\mathfrak{E}}{\partial V}-P\right)\right)+ \\ \qquad +dx\left(\dfrac{3}{2}\dfrac{PV}{1+x}-\dfrac{\partial\mathfrak{E}}{\partial x}\left(\dfrac{V}{1+x}\dfrac{\partial E}{\partial V}-P\right)\right) \end{cases}$$

$$(9.27)\quad \begin{cases} -\left(-\dfrac{1}{V}+\dfrac{1}{\Sigma}\dfrac{\partial\Sigma}{\partial V}\right)V\dfrac{dP}{P}=\dfrac{dT}{T}\left(\dfrac{3}{2}-\dfrac{T}{\Sigma}\dfrac{\partial\Sigma}{\partial T}-V\left(-\dfrac{1}{V}+\dfrac{1}{\Sigma}\dfrac{\partial\Sigma}{\partial V}\right)\right)- \\ \quad -dx\left(\dfrac{2}{x}+\dfrac{1}{1-x}+\dfrac{1}{\Sigma}\dfrac{\partial\Sigma}{\partial x}+V\left(-\dfrac{1}{V}+\dfrac{1}{\Sigma}\dfrac{\partial\Sigma}{\partial V}\right)\dfrac{1}{1+x}\right). \end{cases}$$

On élimine maintenant dx entre ces deux équations. Groupons auparavant les termes identiques

$$(9.28)\quad \begin{cases} -\left(\dfrac{\partial\mathfrak{E}}{\partial V}-P\right)V\dfrac{dP}{P}=dT\left(\dfrac{5}{2}\dfrac{PV}{T}-\dfrac{\partial\mathfrak{E}}{\partial T}-\dfrac{V}{T}\dfrac{\partial\mathfrak{E}}{\partial V}\right)+ \\ \qquad +dx\left(\dfrac{5}{2}\dfrac{PV}{1+x}-\dfrac{\partial\mathfrak{E}}{\partial x}-\dfrac{V}{1+x}\dfrac{\partial\mathfrak{E}}{\partial V}\right) \end{cases}$$

$$(9.29)\quad \begin{cases} -\left(-\dfrac{1}{V}+\dfrac{1}{\Sigma}\dfrac{\partial\Sigma}{\partial V}\right)V\dfrac{dP}{P}=\dfrac{dT}{T}\left(\dfrac{5}{2}-\dfrac{V}{\Sigma}\dfrac{\partial\Sigma}{\partial V}-\dfrac{T}{\Sigma}\dfrac{\partial\Sigma}{\partial T}\right)- \\ \qquad -dx\left(\dfrac{2}{x(1-x^2)}+\dfrac{1}{\Sigma}\dfrac{\partial\Sigma}{\partial x}+\dfrac{V}{1+x}\dfrac{1}{\Sigma}\dfrac{\partial\Sigma}{\partial V}\right). \end{cases}$$

Par élimination de dx on obtient:

$$(9.30)\qquad \frac{d\log T}{d\log P}=\frac{V\left[-\left(\frac{\partial \mathfrak{E}}{\partial V}-P\right)\left(\frac{2}{x(1-x^2)}+\frac{1}{\Sigma}\frac{\partial \Sigma}{\partial x}+\frac{V}{1+x}\frac{1}{\Sigma}\frac{\partial \Sigma}{\partial V}\right)+\left(\frac{1}{V}-\frac{1}{\Sigma}\frac{\partial \Sigma}{\partial V}\right)\left(\frac{5}{2}\frac{PV}{1+x}-\frac{\partial \mathfrak{E}}{\partial x}-\frac{V}{1+x}\frac{\partial \mathfrak{E}}{\partial V}\right)\right.}{\left(\frac{5}{2}-\frac{V}{\Sigma}\frac{\partial \Sigma}{\partial V}-\frac{T}{\Sigma}\frac{\partial \Sigma}{\partial T}\right)\left(\frac{5}{2}\frac{PV}{1+x}-\frac{\partial \mathfrak{E}}{\partial x}-\frac{V}{1+x}\frac{\partial \mathfrak{E}}{\partial V}\right)+\left(\frac{5}{2}PV-T\frac{\partial \mathfrak{E}}{\partial T}-V\frac{\partial \mathfrak{E}}{\partial V}\right)\left(\frac{2}{x(1-x^2)}+\frac{1}{\Sigma}\frac{\partial \Sigma}{\partial x}+\frac{V}{1+x}\frac{1}{\Sigma}\frac{\partial \Sigma}{\partial V}\right)}.$$

En divisant haut et bas par $PV/x\,(1-x^2)$, on obtient l'expression suivante:

$$(9.31)\qquad \frac{d\log T}{d\log P}=\frac{\left(1-\frac{1}{P}\frac{\partial \mathfrak{E}}{\partial V}\right)\left(2+x(1-x^2)\frac{1}{\Sigma}\frac{\partial \Sigma}{\partial x}+x(1-x)\frac{V}{\Sigma}\frac{\partial \Sigma}{\partial V}\right)+\left(1-\frac{V}{\Sigma}\frac{\partial \Sigma}{\partial V}\right)x(1-x)\left(\frac{5}{2}-\frac{1+x}{PV}\frac{\partial \mathfrak{E}}{\partial x}-\frac{1}{P}\frac{\partial \mathfrak{E}}{\partial V}\right)}{\left(2+x(1-x)\frac{V}{\Sigma}\frac{\partial \Sigma}{\partial V}+x(1-x^2)\frac{1}{\Sigma}\frac{\partial \Sigma}{\partial x}\right)\left(\frac{5}{2}-\frac{T}{PV}\frac{\partial \mathfrak{E}}{\partial T}-\frac{1}{P}\frac{\partial \mathfrak{E}}{\partial V}\right)+x(1-x)\left(\frac{5}{2}-\frac{V}{\Sigma}\frac{\partial \Sigma}{\partial V}-\frac{T}{\Sigma}\frac{\partial \Sigma}{\partial T}\right)\left(\frac{5}{2}-\frac{1+x}{PV}\frac{\partial \mathfrak{E}}{\partial x}-\frac{1}{P}\frac{\partial \mathfrak{E}}{\partial V}\right)};$$

à l'aide des notations (9.9) et suivantes on obtient:

$$(9.32)\qquad \begin{cases}\dfrac{d\log T}{d\log P}= \\ \dfrac{\left(1-\dfrac{1-x}{1+x}\dfrac{\bar{\chi}}{kT}\left(\dfrac{\boldsymbol{T}}{S}-\dfrac{\Theta}{\Sigma}\right)\right)\left(2-(1-x^2)\dfrac{\Theta}{\Sigma}+x(1-x)\dfrac{\Theta}{\Sigma}\right)+\left(1-\dfrac{\Theta}{\Sigma}\right)(1-x)\,x\left(\dfrac{5}{2}+\dfrac{\bar{\chi}}{kT}-\dfrac{\bar{\chi}}{kT}\dfrac{1-x}{x(1+x)}\left(\dfrac{\Theta}{\Sigma}-\dfrac{\boldsymbol{T}}{S}\right)\right)}{\left(2+x(1-x)\dfrac{\Theta}{\Sigma}-(1-x^2)\dfrac{\Theta}{\Sigma}\right)\left(\dfrac{5}{2}+\dfrac{1-x}{1+x}\dfrac{\bar{\chi}}{kT}\left(\dfrac{\Theta}{\Sigma}-\dfrac{\boldsymbol{T}}{S}\right)-\dfrac{1-x\overline{\chi^2}-\bar{\chi}^2}{1+x\,(kT^2)}\right)+x(1-x)\left(\dfrac{5}{2}-\dfrac{\Theta}{\Sigma}\dfrac{\bar{\chi}}{kT}\right)\left(\dfrac{5}{2}+\dfrac{\bar{\chi}}{kT}-\dfrac{\bar{\chi}}{kT}\dfrac{1-x}{x(1+x)}\left(\dfrac{\Theta}{\Sigma}-\dfrac{\boldsymbol{T}}{S}\right)\right)}.\end{cases}$$

Après de petites réductions, on obtient:

$$(9.33)\quad \frac{d\log T}{d\log P}=\frac{\left(1-\frac{1-x}{1+x}\frac{\bar{\chi}}{kT}\left(\frac{\boldsymbol{T}}{S}-\frac{\Theta}{\Sigma}\right)\right)\left(2-(1-x)\frac{\Theta}{\Sigma}\right)+\left(1-\frac{\Theta}{\Sigma}\right)x(1-x)\left(\frac{5}{2}+\frac{\bar{\chi}}{kT}-\frac{\bar{\chi}}{kT}\frac{1-x}{x(1+x)}\left(\frac{\Theta}{\Sigma}-\frac{\boldsymbol{T}}{S}\right)\right)}{\left(\frac{5}{2}+\frac{1-x}{1+x}\frac{\bar{\chi}}{kT}\left(\frac{\Theta}{\Sigma}-\frac{\boldsymbol{T}}{S}\right)-\frac{1-x}{1+x}\frac{\overline{\chi^2}-\bar{\chi}^2}{(kT)^2}\right)\left(2-(1-x)\frac{\Theta}{\Sigma}\right)+x(1-x)\left(\frac{5}{2}+\frac{\bar{\chi}}{kT}-\frac{\Theta}{\Sigma}\right)\left(\frac{5}{2}+\frac{\bar{\chi}}{kT}-\frac{\bar{\chi}}{kT}\frac{1-x}{x(1+x)}\left(\frac{\Theta}{\Sigma}-\frac{\boldsymbol{T}}{S}\right)\right)};$$

ou, en cherchant à se rapprocher de la forme habituelle

$$(9.34)\quad \frac{d\log T}{d\log P}=\frac{2+x(1-x)\left(\frac{5}{2}+\frac{\bar{\chi}}{kT}\right)\left(1-\frac{\Theta}{\Sigma}\right)+(1-x)\frac{\bar{\chi}}{kT}\left(\frac{\Theta}{\Sigma}-\frac{\boldsymbol{T}}{S}\right)}{5+x(1-x)\left(\frac{5}{2}+\frac{\bar{\chi}}{kT}\right)\left(\frac{5}{2}+\frac{\bar{\chi}}{kT}-\frac{\Theta}{\Sigma}\right)+\left(\frac{\Theta}{\Sigma}-\frac{\boldsymbol{T}}{S}\right)\frac{\bar{\chi}}{kT}\frac{1-x}{1+x}\left[2-(1-x)\left(\frac{5}{2}+\frac{\bar{\chi}}{kT}\right)\right]+\frac{\overline{\chi^2}-\bar{\chi}^2}{(kT)^2}\frac{1-x}{1+x}\left[(1-x)\frac{\Theta}{\Sigma}-2\right]}.$$

Pour une dilution infinie, $\Theta\to 0$, $\boldsymbol{T}\to 0$, $(\overline{\chi^2}-\bar{\chi}^2)\to 0$ et on retrouve l'expression classique donnée par Unsöld (50):

$$(9.35)\quad \frac{d\log T}{d\log P}=\frac{2+x(1-x)\left(\frac{5}{2}+\frac{\bar{\chi}}{kT}\right)}{5+x(1-x)\left(\frac{5}{2}+\frac{\chi}{kT}\right)^2}.$$

On a calculé en fonction de N_1 et T, $\bar{\chi}$, Θ, $\boldsymbol{T}$ et $\overline{\chi^2}$. On obtient ainsi finalement le tableau de $d\log T/d\log P$ en fonction de P et T (Voir l'appendice p. 98).

C. Coefficient d'absorption.

10. Méthode de calcul. Représentons l'énergie de l'électron en nous servant de la variable parabolique η. Pour un certain état initial en l'absence de champ, l'énergie potentielle a la forme représentée sur la figure 4, p. 53. Pour produire l'ionisation, il faut effectivement une énergie supérieure à ε.

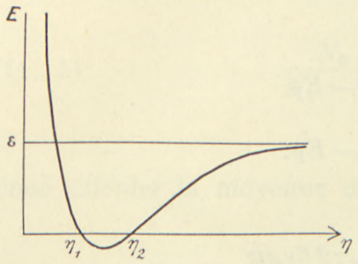

Fig. 4. Energie de l'électron en l'absence de champ électrique en fonction de la variable parabolique η.

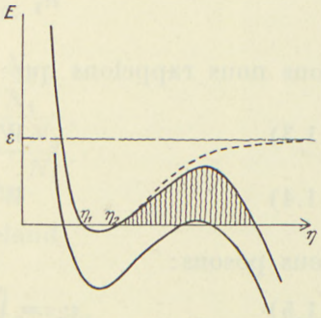

Fig. 5. Energie de l'électron en présence d'un champ électrique en fonction de la variable parabolique η.

Dans le cas où il y a un champ (fig. 5, p. 53) l'électron a à franchir la barrière de potentiel hachurée et, en toute rigueur, le potentiel d'ionisation est égal à la hauteur de la barrière de potentiel, hauteur inférieure à ε. Nous supposerons que le champ est assez faible pour que les fonctions d'onde diffèrent de quantités négligeables des fonctions d'onde en l'absence de champ, et par conséquent la force de l'oscillateur est la même qu'en l'absence de champ. Mais en raison de l'abaissement de la barrière de potentiel, nous supposerons que l'ionisation se produit pour une énergie plus faible et par conséquent que l'atome a un spectre continu s'étendant plus loin dans le rouge qu'en l'absence de champ. Cette simplification est légitime puisque nous utilisons la première approximation pour décrire l'atome perturbé par le champ, et bien entendu elle ne peut s'appliquer qu'à l'hydrogène qui seul présente l'effet Stark linéaire.

11. Calcul du coefficient d'absorption. Le coefficient d'absorption dans le spectre continu d'un atome dans l'état p est:

$$(11.1) \qquad \varkappa_\nu = \frac{1}{p^2}\frac{64\pi^4}{3\sqrt{3}}\frac{me^{10}}{ch^6}\frac{1}{p^3}\frac{1}{\nu^3}.$$

Nous supposons ici le facteur de Gaunt égal à l'unité. Nous nous reportons au nombre d'atomes dans l'état fondamental:

$$(11.2) \qquad \frac{dn_p}{n_1} = \frac{p^2 W(F)\, e^{\vartheta W_p}\, dF}{\int_0^{F_1} W(F)\, e^{\vartheta W_1}\, dF}.$$

Nous nous rappelons que:

$$(11.3) \qquad W_p = E_p - E_F$$

$$(11.4) \qquad W_1 = E_1 - E_F.$$

Nous posons:

$$(11.5) \qquad \gamma_p = \int_0^{F_p} W(F)\, e^{-\vartheta E_F} dF.$$

Nous posons comme Unsöld (50) $\vartheta E_p = u_p$. On a alors la contribution des atomes dans l'état p en sommant pour tous les niveaux qui sont susceptibles d'absorber la fréquence ν_1, soit de F_ν, à F_p, F_ν pouvant être nul si $h\nu > E_p$. On a donc:

$$(11.6) \qquad \varkappa_\nu = \frac{1}{H}\frac{64\pi^4}{3\sqrt{3}}\frac{me^{10}}{ch^3}\frac{1}{k^3T^3}\frac{e^{-u_1}}{\gamma_1}\frac{1}{u^3}\int_{F_\nu}^{F_p}\frac{e^{u_p}}{p^3} W(F)\, e^{-u_F} dF.$$

On trouve de même pour la contribution des électrons libres:

$$(11.7) \qquad \varkappa_\nu = \frac{1}{H}\frac{64\pi^4}{3\sqrt{3}}\frac{me^{10}}{ch_3}\frac{1}{k^3T^3}\frac{e^{-u_1}}{\gamma_1}\frac{1}{u^3}\frac{1}{2u_1},$$

d'où pour le coefficient d'absorption:

$$(11.8) \qquad \varkappa_\nu = \frac{1}{H}\frac{64\pi^4}{3\sqrt{3}}\frac{me^{10}}{ch^3}\frac{1}{k^3T^3}\frac{e^{-u_1}}{\gamma_1}\frac{1}{u^3}\left\{\frac{1}{2u_1} + \sum_p \frac{e^{u_p}}{p^3}\int_{F_\nu}^{F_p} W(F)\, e^{-u_F} dF\right\}.$$

Le coefficient d'absorption par gramme de matière s'obtient en multipliant (11.8) par la concentration en atomes neutres par gramme d'hydrogène. En vertu de l'équation (2.7) que nous écrivons

$$\frac{N_e N_1}{N_0} = 2 \frac{(2\pi mkT)^{\frac{3}{2}}}{h^3} \frac{e^{-\vartheta E_1}}{\sum 2 p^2 \gamma_p e^{-\vartheta E_p}} \tag{11.9}$$

et de

$$N_e = N_1, \tag{11.10}$$

on obtient N_1 en fonction de N_0 et T. Nous avons donc à multiplier le coefficient obtenu (11,8) par:

$$\frac{N_0}{N_1 + N_0} = \frac{\frac{N_0}{N_1}}{1 + \frac{N_0}{N_1}}. \tag{11.11}$$

Pour calculer la moyenne de Rosseland

$$\frac{1}{\bar{\varkappa}} = \frac{15}{4\pi^3} \int_0^\infty \frac{1}{\chi_\nu} \frac{u^4 e^{-u} du}{(1 - e^{-u})^3}. \tag{11.12}$$

on a à faire intervenir l'intégrale:

$$\int_0^\infty \frac{u^7 e^{-u} du}{(1 - e^{-u})^3 \left(\frac{1}{2 u_1} + \sum_p \frac{e^{u_p}}{p^3} \int_{F_\nu}^{F_p} W(F) e^{-u_F} dF \right)}. \tag{11.13}$$

En utilisant la notation (11.5), on peut écrire:

$$\int_0^\infty \frac{u^7 e^{-u} du}{(1 - e^{-u})^3 \left(\frac{1}{2 u_1} + \sum_p \frac{e^{u_p}}{p^3} (\gamma_p - \gamma_\nu) \right)} \tag{11.14}$$

et l'on a:

$$\begin{cases} h\nu < E_p & \gamma_\nu = \int_0^{(Wp = h\nu)} W(F) e^{-u_F} dF \\ h\nu > E_p & \gamma_\nu = 0; \end{cases} \tag{11.15}$$

pour les très faibles densités, le coefficient d'absorption se réduit à sa valeur usuelle, et pour les grandes densités au coefficient d'absorption des électrons libres en présence des protons.

La diffusion de J. J. Thomson pour de l'hydrogène pur donne un coefficient d'absorption

$$\varkappa_e = 0{,}38 \tag{11.16}$$

qui est petit devant le coefficient d'absorption de l'hydrogène en raison des grandes densités considérées, mais ceci n'est vrai que pour les naines blanches.

12. Influence de l'élargissement des raies. Sous l'influence de l'effet Stark linéaire, les raies s'élargissent au point de se recouvrir complètement. Le coefficient d'absorption se raccorde alors de façon continue au fond continu d'au-delà de la discontinuité de Balmer. Nous verrons dans le chapitre III comment calculer alors le coefficient moyen d'absorption. Nous allons seulement comparer ici les deux effets: ionisation de pression et recouvrement des raies.

a) Recouvrement des raies. Le coefficient de $1/\nu^3$ dans le coefficient d'absorption est pris constant jusqu'à une fréquence définie par le nombre quantique m de la dernière raie visible (Inglis et Teller (19)):

$$m = \frac{[3{,}101]}{N_1^{2/15}}. \tag{12.1}$$

b) Ionisation de pression. Le coefficient de $1/\nu^3$ est pris constant jusqu'à une fréquence définie par le nombre quantique n de la première raie ionisée par effet Stark moléculaire:

$$n = \frac{[3{,}808]\,\tau^{\frac{1}{4}}}{N_1^{1/6}} \tag{12.2}$$

qui est pratiquement toujours plus grand que m, l'égalité ne se produisant que pour $\log N_1 = 19{,}2$ $n = 3{,}5$, mais alors la formule simplifiée (12.1) d' Inglis et Teller, obtenue pour des nombres quantiques élevés, n'est certainement plus valable (voir tableau I, p. 34).

III. Un modèle d'atmosphère pour les naines blanches.

A. Introduction.

1. Nous avons étudié dans la première partie le triage des éléments dans un champ de gravitation. Dans le champ de pesanteur extrêmement intense des naines blanches la séparation de l'hydrogène est quasi-totale. Il semble donc possible de constituer un modèle de naine blanche d'une couche d'hydrogène pur entourant un noyau d'éléments lourds (34). Un tel modèle semble bien expliquer le débit d'énergie des naines blanches et paraît s'accorder avec les traits principaux qui se manifestent dans leur spectre (41), si bien que la théorie de la structure interne doit rester à la base d'une théorie du spectre.

2. Rappelons ce résultat essentiel de l'observation des naines blanches que toutes sauf deux — Van Maanen 2 et Sirius B — n'ont pas de raies métalliques dans leur spectre. Le spectre très difficile à prendre de Sirius B ne m'est pas connu, mais Kuiper a publié (22) des enregistrements du spectre de Van Maanen 2. On ne peut manquer d'être frappé par la largeur considérable des raies *H* et *K* de *Ca* II, due sans doute à l'élargissement par chocs, et en même temps par l'absence des raies de l'hydrogène. Cette absence de raies métalliques dans le spectre des naines blanches est manifestement une conséquence du triage des éléments et à nos yeux constitue une preuve suffisante de ce phénomène.

3. Pour une même profondeur optique, la densité d'une atmosphère est, très approximativement proportionnelle à l'intensité du champ de pesanteur, si bien que l'on atteint, très près de la surface, des densités déjà élevées. A ces densités tous les effets de pression deviennent considérables. Nous avons mentionné plus haut la grande largeur des raies métalliques dans la seule naine blanche où on les observe. L'élargissement des raies de l'hydrogène est bien connu et semble relié à l'effet Stark moléculaire.

4. Verwej (51) a fait la théorie de l'élargissement des raies de l'hydrogène par effet Stark moléculaire, en s'appuyant sur la théorie de Holtsmark (18) et il semble bien, comme l'a montré Kuiper (22), qu'elle n'est valable que pour les ailes des raies. Notons que Verwej n'a pas tenu compte de l'élargissement par choc des raies du réseau Stark. Il n'est pas impossible que l'introduction de l'élargissement par chocs modifie assez fortement au voisinage du centre les profils calculés par Verwej.

5. Mentionnons les idées de Blackett (5) sur le champ magnétique des corps en rotation et leurs conséquences pour la théorie du spectre des naines blanches. Il semble bien (41) qu'il n'est pas nécessaire d'introduire de champ magnétique intense pour expliquer le spectre des naines blanches. Nous considérons ce résultat comme n'étant pas dirigé contre la théorie de Blackett mais comme une preuve supplémentaire (39) d'une origine distincte pour les naines blanches et pour les étoiles de la série principale.

6. Il ressort des critiques de Chandrasekhar (8) et de Kourganoff (20) que non seulement la moyenne de Rosseland n'est pas adaptée au traitement des problèmes d'atmosphère, mais qu'il n'existe aucune moyenne permettant de traiter rigoureusement les problèmes d'atmosphères. C'est seulement en raison de la complication des méthodes à employer pour le calcul d'une atmosphère que nous nous sommes trouvés réduits à employer la moyenne de Rosseland. L'expérience des autres étoiles montrant qu'elle donnait à bien des égards des résultats satisfaisants, il a semblé que pour le premier calcul d'atmosphère de naine blanche on ne pouvait exiger plus.

B. Le modèle d'atmosphère.

7. **Stabilité de l'ion négatif hydrogène.** Deux méthodes différentes donnent des résultats cohérents pour la stabilité de l'ion négatif hydrogène à l'égard des collisions. Il est ainsi possible de déterminer le «volume» de l'ion négatif à introduire dans la théorie des volumes exclus ou de tout autre analogue. On peut

déterminer les conditions d'utilisation des formules usuelles et des tables déjà connues et leurs limites d'application aux atmosphères de naines blanches.

Nous devons en effet nous attendre à une très grande fragilité de H^- en raison à la fois de son gros volume et de son bas potentiel d'ionisation. Nous pouvons décrire la destruction de H^- au cours d'une collision soit comme une ionisation par choc, soit comme un effet Stark moléculaire. Si l'effet Stark, dans le cas des systèmes à plusieurs électrons ne produit pas d'effet du premier ordre, il est néammoins capable d'amener la destruction des effets stationnaires par abaissement de la barrière de potentiel. Il s'agit là de deux phénomènes indépendants, l'un faisant intervenir la symétrie des fonctions d'onde, l'autre la transparence d'une barrière de potentiel. On peut alors faire soit un calcul de section de choc par la méthode de J. J. Thomson ou tout autre plus éprouvée, soit un calcul d'effet Stark. Les deux résultats concordent. En effet, la première méthode nous montre que H^- a la même fragilité dans une collision que l'état $n \cong 5$ de l'hydrogène neutre. L'autre également très approchée est basée sur l'idée que l'ionisation se produit lorsque la variation de potentiel électrique à travers le domaine de l'atome est du même ordre de grandeur que le potentiel d'ionisation. Dans ce cas, la difficulté est de choisir le rayon de l'atome, ce qui est particulièrement délicat, puisque dans H^- la densité électronique $(\psi\psi^*)$ varie très lentement. Un calcul précis est difficile à mener en raison de la difficulté de transposer la méthode de champ self-consistent de Hartree en coordonnées paraboliques. Une évaluation grossière légitime l'assimilation de la fragilité de l'ion négatif hydrogène à celle de l'état $n \cong 5$ de l'hydrogène neutre.

8. Un tel calcul approché n'a de sens que parce qu'il permet d'évaluer grossièrement le maximum de concentration de l'ion négatif et de déterminer les conditions dans lesquelles l'absorption due à l'ion négatif est négligeable comparée à celle de l'hydrogène. Le principe du calcul est le suivant: nous modifions légérement l'équation de Saha pour l'ion négatif afin de tenir compte de l'ionisation de pression de l'ion négatif. Nous avons les deux équations d'equilibre pour H^+ et H^-:

$$\frac{N_e N_1}{N_0} = \frac{(2\pi mkT)^{\frac{3}{2}}}{h^3} e^{-\vartheta E_0} \tag{8.1}$$

$$\frac{N_e N_0}{N^-} = 2\frac{(2\pi mkT)^{\frac{3}{2}}}{h^3} 2e^{-\vartheta J} e^{\alpha N_0}; \tag{8.2}$$

avec la valeur de α obtenue au § 7:

$$\log_{10}\alpha = \overline{19},65. \tag{8.3}$$

Nous devons ajouter à ces deux équations la relation:

$$N_1 = N_e + N^- \tag{8.4}$$

qui exprime que les électrons ne proviennent que de l'hydrogène. Si l'on prend N_1 comme paramètre, on trouve que, pour une température donnée, le nombre d'ions négatifs N^- passe par un maximum pour

$$\alpha N_1 = 3 + \varepsilon, \tag{8.5}$$

ε étant une quantité très petite dont la première approximation est:

$$\varepsilon = \frac{18\, e^{-3}}{\alpha^2 g + 6\, e^{-3}} \tag{8.6}$$

où g représente

$$g = 2\frac{(2\pi mkT)^3}{h^6} e^{-\vartheta(E_0+J)}. \tag{8.7}$$

En posant $\theta = \frac{5040}{T}$ on obtient la valeur approximative suivante pour $N^-_{\max}$:

$$N^-_{\max} = \frac{[24,113]}{T^3} 10^{14,31\,\theta}. \tag{8.8}$$

On peut alors aisément calculer le rapport de l'absorption due à l'ion négatif à celle due à l'hydrogène lorsque N^- est maximum. On trouve les résultats contenus dans le tableau I.

Ce rapport est très grand, mais il correspond à des valeurs si élevées de la pression qu'elles ne se rencontrent pas dans l'atmosphère des naines blanches connues. Nous voyons qu'il

Tableau I.

θ	$\log(\chi_H^-/\chi_H)_{max}$
0.3	3.90
0.4	3.65
0.5	3.59
0.6	4.13
0.7	4.53

faut reprendre les tables de STRÖMGREN (48) pour le coefficient d'absorption, mais en supposant l'absorption due à l'hydrogène pur et en tenant compte à la fois de l'ion négatif et de l'hydrogène neutre.

9. Absorption par l'hydrogène moléculaire. Lorsque la densité croît et devient un peu élevée, la probabilité qu'une absorption ait lieu par collision triple d'un photon et de deux atomes devient appréciable.

CRITCHFIELD (13) donne une évaluation grossière de la section de choc:

$$\sigma = 10^{-17}(4\cdot 10^{-24} n)^2, \tag{9.1}$$

le coefficient d'absorption par gramme étant

$$\varkappa = \frac{n\sigma}{\varrho}, \tag{9.2}$$

n étant le nombre d'atomes neutres par gramme. Dans les conditions où n devient notable, n est pratiquement égal au nombre d'atomes d'hydrogène présent et on a:

$$\varkappa_{\text{coll. triples}} = 16\cdot 10^{-65}\frac{n_H^3}{\varrho}. \tag{9.3}$$

On en déduit la relation suivante qui donne $p_e(\theta)$ le long de la courbe

$$\varkappa_{\text{coll. triples}} = \bar{\varkappa}_H, \tag{9.4}$$

$$p_e\theta\frac{1-x}{x} = \bar{\chi}_H[7{,}85], \tag{9.5}$$

d'où le tableau II.

Tableau II.

θ	$\log p_e$
0.4	8.7
0.5	7.2
0.6	4.68
0.7	4.25

On trouvera sur la figure 6, p. 63, différentes courbes, montrant dans le diagramme θ, $\log p_e$ les régions de différents coefficients d'absorption. Une courbe limite indique pour quelle valeur de p_e la pression totale

$$P = \frac{p_e\left(1 + \frac{2N_{H^+}}{N_H}\right)}{\frac{N_{H^+}}{N_H} - \frac{N_{H^-}}{N_H}} \tag{9.6}$$

devient infinie (car $N_{H^+} = N_{H^-}$ lorsque tous les électrons ont été absorbés par l'ion négatif). Bien entendu, il n'est pas question de dresser des tables si loin, l'ionisation de pression (§ 8) intervenant bien avant.

10. Formation des molécules[1]. L'énergie de formation de la molécule H^2 est 4.46 électron-volts. Elle peut donc certainement se former assez facilement quand la presson augmente. En appliquant la relation de Saha

$$\frac{[H]^2}{[H_2]} = \frac{2}{2^{\frac{3}{2}}} \frac{(2\pi HkT)^{\frac{3}{2}}}{h^3} e^{-10{,}26\,\theta} \tag{10.1}$$

et en tenant compte de la relation

$$\log \frac{[H^+]}{[H]} = -0{,}48 - 13{,}56 \cdot \theta + \frac{5}{2} \log T - \log p_e, \tag{10.2}$$

on obtient aisément $\log \frac{[H_2]}{[H]}$ en fonction de la pression électronique et de la température:

(1) M. R. Wildt a bien voulu faire remarquer à l'auteur que ces résultats doivent être sensiblement modifiés, en raison de la valeur élevée de la somme d'états de la molécule d'hydrogène. Le nombre de molécules d'hydrogène n'est sans doute pas négligeable, mais leur effet ne peut pas encore être calculé en raison de notre ignorance des coefficients d'absorption. (Note ajoutée à la correction des épreures).

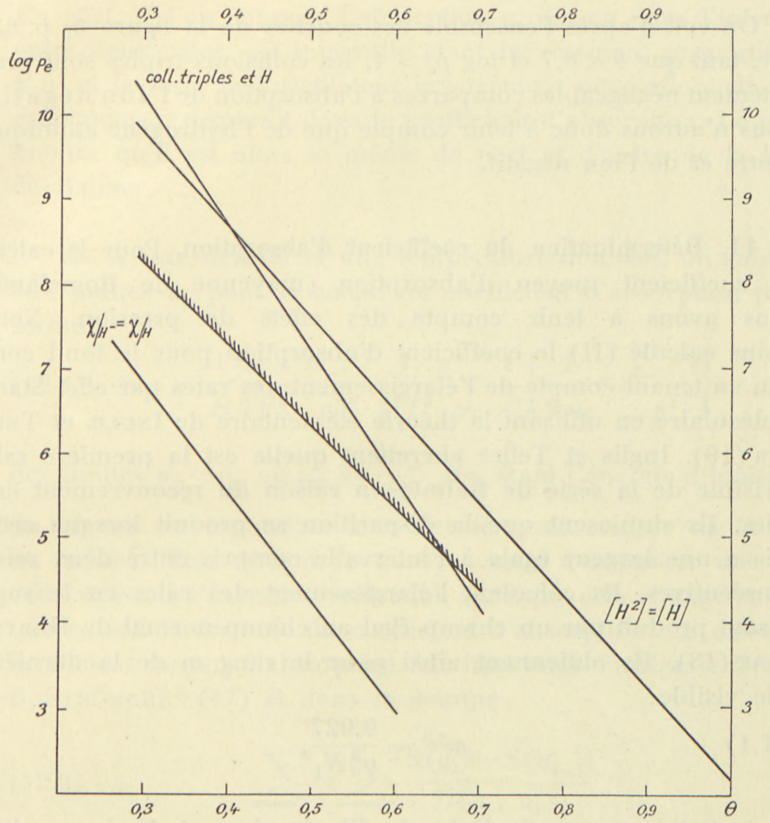

Fig. 6. Domaine d'application des différentes approximations relatives au coefficient d'absorption. On remarquera que dans le domaine des températures étudiées les collisions triples ne contribuent pas de façon sensible à l'absorption.

$$(10.3) \qquad \log \frac{[H_2]}{[H]} = -22{,}31 + 18{,}0\,\theta + 5 \log \theta + 2 \log p_e;$$

ce logarithme est égal à zéro (nombre égal) pour des valeurs de θ et de p_e données dans le tableau III.

Tableau III.

θ	$\log p_e$
0.3	9.77
0.4	8.55
0.5	7.41
0.6	6.31
1	2.15

On voit d'après l'ensemble des courbes de la figure 6, p. 63, que, tant que $\theta < 0{,}7$ et $\log p_e > 4$, les collisions triples sont parfaitement négligeables comparées à l'absorption de l'ion négatif. Nous n'aurons donc à tenir compte que de l'hydrogène atomique neutre et de l'ion négatif.

11. Détermination du coefficient d'absorption. Pour le calcul du coefficient moyen d'absorption (moyenne de Rosseland) nous avons à tenir compte des effets de pression. Nous avons calculé (II) le coefficient d'absorption pour le fond continu en tenant compte de l'élargissement des raies par effet Stark moléculaire en utilisant la théorie élémentaire de INGLIS et TELLER (19). Inglis et Teller cherchent quelle est la première raie invisible de la série de Balmer en raison du recouvrement des raies. Ils supposent que la disparition se produit lorsque cette raie a une largeur égale à l'intervalle compris entre deux raies consécutives. Ils calculent l'élargissement des raies en le supposant produit par un champ égal au champ normal de HOLTSMARK (18). Ils obtiennent ainsi pour le rang m de la dernière raie visible:

$$m^{7,5} = \frac{0{,}027}{a_0^3 N_1}, \tag{11.1}$$

où a_0 est le rayon de Bohr de l'hydrogène et N_1 le nombre d'ions par cm^3. En pratique, nous prendrons pour N_1 seulement le nombre de protons par cm^3, l'élargissement dû aux électrons étant négligeable. Numériquement, la formule (11.1) donne:

$$m = \frac{[3{,}101]}{N_1^{2/15}} \tag{11.2}$$

et le tableau p. 34 donne les valeurs de N_1 correspondant aux 10 premières valeurs de m.

Les valeurs de N_1 sont de l'ordre de ce que l'on observe dans l'atmosphère des naines blanches.

Dans le domaine où les raies de Balmer se recouvrent, tout se passe comme si l'on avait un coefficient d'absorption continu inversement proportionnel au cube de la fréquence et prolongeant de façon continue le coefficient d'au-delà la limite de Balmer.

En effet, si l'on suppose l'absorption uniforme dans l'intervalle entre deux raies, cet intervalle étant inversement proportionnel à n^3 et la force de l'oscillateur inversement proportionnelle à n^3 également, n disparait dans le coefficient d'absorption. Le calcul montre qu'il est alors le même de part et d'autre de la limite de Balmer.

12. A une densité et une température données, on substitue aux limites u_p pour le calcul du coefficient d'absorption par la formule

$$(12.1) \qquad \varkappa_H = \frac{1}{H}\frac{64\pi^4}{3\sqrt{3}}\frac{m_e e^{10}}{ch^3}\frac{1}{k^3T^3}\frac{e^{-u_1}}{\gamma_1}\frac{1}{u^3}\left\{\frac{1}{2u_1}+\frac{\sum e^{u_p}}{p^3}\right\},$$

des limites $u_p - u_m$ où $u_m = \frac{h\nu_m}{kT}$, $h\nu_m$ étant l'énergie d'ionisation du niveau correspondant à la dernière raie visible de la série de Balmer. Cela revient en quelque sorte à supposer une nouvelle valeur à l'énergie d'ionisation sans que cela change en quoi que ce soit la formule du coefficient d'absorption. Le calcul du coefficient moyen d'absorption fait intervenir l'intégrale $S(u)$ de B. Strömgren (47) et dans la somme

$$(12.2) \qquad \sum = \sum_i \frac{S(u_i) - S(u_{i+1})}{D(u_i,\ u_{i+1}}$$

les quantités $D(u_i,\ u_{i+1})$ gardent les mêmes valeurs, mais les limites u_i sont modifiées de quantités u_m. Calculons la modification qui est apportée à la somme (12.2) en supposant les u_m petits devant u_i. On a:

$$S(u) = \frac{15}{4\pi^4}\int_0^u \frac{u^7 e^{2u}}{(e^u-1)^3}$$

$$S(u+h) = S(u) + hS'(u)$$

et par conséquent

$$(12.3) \qquad \Delta\sum = \sum_i \frac{h(S'(u_i) - S'(u_{i+1}))}{D(u_i,\ u_{i+1})}$$

avec $h = \frac{h\nu_m}{kT}$ et

Tableau IV ($\log \bar{\varkappa}$)

Log P.....	4,6	4,8	5,0	5,2	5,4	5,6	5,8	6,0	6,2	6,4
0,30	1,79	1,98	2,18	2,37	2,54	2,71	2,88	3,03	3,14	3,29
0,32	1,96	2,15	2,33	2,51	2,67	2,82	2,96	3,08	3,19	3,28
0,34	2,12	2,29	2,46	2,61	2,74	2,87	2,98	3,08	3,17	3,24
0,36	2,23	2,37	2,52	2,66	2,77	2,86	2,94	3,00	3,07	3,14
0,38	2,30	2,42	2,52	2,64	2,73	2,79	2,86	2,92	2,98	3,04
0,40	2,31	2,41	2,50	2,58	2,65	2,70	2,74	2,80	2,86	2,91
0,42	..	2,35	2,40	2,46	2,52	2,57	2,61	2,66	2,71	2,76
0,44	..	..	2,29	2,35	2,40	2,44	2,48	2,53	2,58	2,63
0,46	..	..	..	2,21	2,26	2,31	2,35	2,40	2,45	2,51
0,48	..	..	..	..	2,09	2,14	2,19	2,25	2,31	2,37
0,50	..	..	..	..	..	..	2,04	2,10	2,16	2,22
0,52	..	..	..	..	..	..	..	..	..	..
0,54	..	..	..	..	..	..	..	..	..	..
0,56	..	..	..	..	..	..	..	..	..	..
0,58	..	..	..	..	..	..	..	..	..	..
0,60	..	..	..	..	..	..	..	..	..	..

(12.4) $$S'(u) = \frac{15}{4\pi^4} \frac{u^7 e^{2u}}{(e^u - 1)^3}.$$

La quantité u_m est égale à u_1/m^2. m étant dans 40 Eridani B de l'ordre de 8 à 10, u_m est de l'ordre de $u_1/50$ à $u_1/100$. u_1 étant de l'ordre de 10, u_m est de l'ordre de 0,2 à 0,1. $S'(u)$ atteint son maximum au voisinage de $u = 7$ et ce maximum vaut 29,6. Calculons effectivement la variation $\Delta\left(\frac{1}{\varkappa}\right)$ pour $\theta = 0{,}4$. On trouve

(12.5) $$\Delta(\Sigma) = 0{,}12 \cdot 24 = 2{,}9,$$

alors que $\Sigma = 73{,}5$. L'erreur relative $\frac{\Delta\Sigma}{\Sigma} = 0{,}04$ est très petite et nous voyons que malgré le déplacement des limites d'absorption il est cependant encore légitime (38) de se servir des tables déjà existantes de la moyenne de Rosseland pour l'hydrogène pur.

Tableau IV (suite).

6,4	6,6	6,8	7,0	7,2	7,4	7,6	7,8	8,0	8,2	..... Log P
3,29	3,40	3,50	3,58	3,67	3,75	3,83	3,90	3,98	..	 0,30
3,28	3,37	3,45	3,52	3,60	3,67	3,73	3,80	3,86	3,94	 0,32
3,24	3,31	3,38	3,45	3,52	3,58	3,64	3,70	3,76	3,82	 0,34
3,14	3,22	3,28	3,35	3,42	3,49	3,55	3,62	3,68	3,74	 0,36
3,04	3,10	3,15	3,21	3,28	3,35	3,42	3,49	3,57	3,63	 0,38
2,91	2,96	3,01	3,07	3,13	3,20	3,27	3,35	3,43	3,50	 0,40
2,76	2,82	2,89	2,95	3,01	3,07	3,13	3,20	3,28	3,36	 0,42
2,63	2,69	2,75	2,82	2,88	2,95	3,02	3,10	3,18	3,26	 0,44
2,51	2,57	2,63	2,69	2,77	2,84	2,92	2,99	3,07	3,15	 0,46
2,37	2,44	2,50	2,59	2,65	2,73	2,80	2,88	2,96	3,04	 0,48
2,22	2,29	2,36	2,44	2,52	2,60	2,69	2,77	2,85	2,94	 0,50
..	..	..	..	..	..	..	..	..	..	 0,52
..	..	..	..	..	..	..	..	..	..	 0,54
..	..	..	..	..	..	..	..	..	..	 0,56
..	..	..	..	..	..	..	..	..	..	 0,58
..	..	..	..	..	..	..	..	..	..	 0,60

13. Le calcul du modèle d'atmosphère ne diffère pas dans ces conditions du calcul de Bengt Strömgren (48) si ce n'est dans l'emploi du coefficient d'absorption pour l'hydrogène pur.

On emploie simultanément les formules suivantes:

équation d'équilibre hydrostatique:

$$\frac{dp}{dz} = -g\varrho; \tag{13.1}$$

équation de transfert

$$d\tau = -\bar{\varkappa}\varrho\, dh; \tag{13.2}$$

équation standard reliant la profondeur optique et la température (approximation de Milne Eddington pour le corps gris)

$$T^4 = T_e^4\left(\frac{1}{2} + \frac{3}{4}\tau\right) \tag{13.3}$$

ou

$$T^4 = T_0^4\left(1+\frac{3}{2}\tau\right). \tag{13.4}$$

En éliminant dh on a ainsi à résoudre:

$$\frac{d\tau}{d\log p} = \frac{1}{g\log e}\bar{\varkappa}p. \tag{13.5}$$

L'intégration est faite en utilisant la méthode indiquée par Strömgren (48). Toutefois nous n'avons pas cru utile de faire un calcul aussi précis.

Nous avons calculé $\log\bar{\varkappa}$ en fonction de θ et de $\log p$ (Tableau IV contenant partiellement les tables de Strömgren) pour l'hydrogène pur.

Nous n'avons calculé jusqu'à présent que deux modèles d'atmosphères, correspondant respectivement aux conditions approximatives de 40 Eri B et de Van Maanen 2 (tableau VI). Nous avons pris:

pour 40 Eridiani B $\theta_0 = 0{,}45$ $\log g = 7{,}69$
pour Van Maanen 2 $\theta_0 = 0{,}50$ $\log g = 10{,}00.$

Pour 40 Eridani B les valeurs de $\bar{\varkappa}$ utilisées étaient déduites d'une table préliminaire et différaient légèrement de celles données dans le tableau IV.

14. Couche convective. Nous calculons à l'aide de la formule d'Unsöld (50) pour l'hydrogène pur:

$$\frac{d\log T}{d\log p} = \frac{2+x(1-x)\left(\frac{5}{2}+u_1\right)}{5+x(1-x)\left(\frac{5}{2}+u_1\right)^2} \tag{14.1}$$

la valeur de la compressibilité adiabatique. On trouve dans le tableau VI les valeurs de $(d\log T/d\log P)_{\text{ad}}$ et $(d\log T/d\log P)_{\text{rad}}$. La comparaison entre ces deux séries de valeurs permet de trouver la profondeur optique de la limite supérieure de la zone convective. On trouve

(14.2) Pour 40 Eridani B, $\tau = 0{,}14$
(14.3) Pour Van Maanen 2, $\tau = 0{,}43.$

Nous n'avons pas encore cherché à déterminer de limite inférieure de la zone convective.

Tableau V

τ	θ	$\log p$	$\log \overline{z}$	$\left(\frac{d\log T}{d\log P}\right)_{ad}$	$\left(\frac{d\log T}{d\log P}\right)_{rad}$	$\log N_1$
			Modèle pour une étoile du type de 40 Eridani B			
0	0,45	3,4	1,57	0,092	0	15,10
0,0009	0,4498	3,6	1,69	0,089	0	15,26
0,0027	0,4495	3,8	1,80	0,085	0	15,41
0,0064	0,4489	4	1,89	0,083	0,005	15,55
0,0110	0,4482	4,2	1,96	0,083	0,014	15,66
0,0248	0,4458	4,4	2,04	0,085	0,025	15,79
0,0517	0,4412	4,6	2,11	0,087	0,040	15,93
0,1019	0,4344	4,8	2,19	0,090	0,065	16,09
0,2063	0,421	5,0	2,31	0,094	0,140	16,29
0,473	0,395	5,2	2,51	0,100	0,235	16,51
1,061	0,355	5,4	2,70	0,106	..	16,80
2,083	0,316	5,6	2,78	..	..	16,98
3,559	0,284	5,8	..	..	..	..
			Modèle pour une étoile du type de Van Maanen 2			
..	0,50	5	1,85	0,11	0	15,71
0,007	0,50	5,2	1,89	0,13	0	15,82
0,0013	0,50	5,4	1,94	0,14	0	15,92
0,0023	0,50	5,6	1,99	0,15	0	16,02
0,0041	0,50	5,8	2,04	0,17	0	16,12
0,0072	0,50	6	2,10	0,19	0,011	16,23
0,013	0,4975	6,2	2,18	0,21	0,013	16,34
0,024	0,4955	6,4	2,25	0,22	0,018	16,45
0,044	0,4915	6,6	2,35	0,24	0,029	16,59
0,085	0,485	6,8	2,47	0,24	0,055	16,74
0,170	0,473	7	2,61	0,25	0,113	16,92
0,356	0,450	7,2	2,83	0,25	0,215	17,18
0,843	0,408	7,4	3,15	0,20	0,395	17,48
2,46	0,340	7,6	3,64	0,17	..	18,13

C. Répartition spectrale de l'énergie.

15. Le fond continu. Le calcul du fond continu ne présente pas de difficultés spéciales. La répartition spectrale de l'énergie à la surface est donnée par:

$$\frac{1}{2}\frac{F_\nu}{\pi} = \int_0^\infty B_\nu(\tau_\nu)\, K_2(\tau_\nu)\, d\tau_\nu \qquad (15.1)$$

et l'on emploie une formule d'approximation (quadrature numérique à trois termes)

$$(15.2)\quad \begin{cases} \dfrac{F_\nu}{\pi} = 0{,}76689\, B_\nu\,(\tau_\nu = 0{,}287) \\ \qquad + 0{,}22652\, B_\nu\,(\tau_\nu = 1{,}81436) \\ \qquad + 0{,}006591\, B_\nu\,(\tau_\nu = 5{,}385). \end{cases}$$

La profondeur optique est donnée par

$$(15.3)\quad d\tau_\nu = -\varkappa'_\nu \varrho\, dx$$

à quoi l'on joint

$$(15.4)\quad dx = -\frac{dp}{g\varrho},$$

d'où

$$(15.5)\quad \tau_\nu = \frac{1}{g \log_{10} e} \int_0^p \varkappa'_\nu(\tau, \theta)\, \frac{d \log_{10} p}{p}.$$

Ici, $\varkappa'_\nu$ est le coefficient d'absorption réduit pour tenir compte de l'émission induite. En fait, $\varkappa'_\nu$ est dans le cas qui nous occupe très peu différent de $\varkappa_\nu$ et nous ne tiendrons pas compte de la différence.

Lorsque l'on atteint, pour une longueur d'onde donnée une région où les raies se recouvrent en raison de l'augmentation de pression, le coefficient d'absorption devient plus grand. $B\nu$ possède en ce point une discontinuité de sa dérivée, ce qui ne gêne

Tableau VI.

Répartition de l'energie dans le spectre continu d'une étoile du type de 40 Eridani B.

λ	$\log \frac{F_\nu}{F_{3000}}$	λ	$\log \frac{F_\nu}{F_{3000}}$
3000	0,0	3897	0,170
3200	0,022	3947	0,199
3400	0,034	3997	0,207
3600	0,047	4200	0,195
3647	0,049	4400	0,185
3747	0,052	4600	0,167
3797	0,064	4800	0,150
3847	0,117	5000	0,138

pas pour l'emploi de la formule d'intégration numérique à 3 termes de Gauss. Afin de tenir compte de la dispersion du prisme, les valeurs trouvées en utilisant les tables de $B(\nu, \theta)$ sont multipliées par un terme proportionnel à λ^2. On obtient ainsi le tableau VI donnant le logarithme du flux, exprimé en unités arbitraires en fonction de la longueur d'onde.

16. La superposititon des raies. La distance entre deux raies Stark dans la série de Balmer, séparées par un champ électrique d'intensité F_{cgs}, est:

$$\Delta\lambda_0 = 0{,}00256\, F_{cgs} \left(\frac{n^2}{n^2-4}\right)^2 \tag{16.1}$$

et la distance séparant les deux raies extrêmes est, mesurée en cette unité:

$$\Delta\lambda = [n(n-1)+2]\, \Delta\lambda_0, \tag{16.2}$$

Par ailleurs, la théorie de Rudkjøbing (31) permet de calculer l'élargissement des raies dû aux collisions. La constante d'amortissement exprimée en unités de $2\pi\nu$ est:

$$\gamma = \frac{\sqrt{2}}{\pi^{\frac{3}{2}}} \frac{h^2}{m^{\frac{3}{2}}} \frac{N_e}{\sqrt{kT}} \int_0^\infty \sum_l (2l+1) \sin^2 (\nu_1 - \nu_2)_{l,E}\, e^{-E/kT}\, d\left(\frac{E}{kT}\right). \tag{16.3}$$

Afin de comparer cette expression avec la valeur $\Delta\lambda$ que nous venons de trouver, nous pouvons remplacer l'intégrale par l'unité. On a alors numériquement:

$$\gamma \cong 10^{-4,46} \frac{N_e}{\sqrt{T}} \tag{16.4}$$

On trouve alors que l'élargissement des raies par collision est plus important que l'effet Stark moléculaire, tant que

$$N_1 < [15{,}360]\, T^{\frac{3}{2}}. \tag{16.6}$$

Tant que cette inégalité est satisfaite (ce qui est d'ailleurs le cas de 40 Eridani B) l'hypotèse simplificatrice de Pannekoek que l'énergie de la raie est uniformément répartie sur toute sa largeur est une approximation satisfaisante.

Nous voyons, au seul énoncé de l'importance considérable de cet effet, que le calcul de VERWEJ (51) du profil des raies devrait être repris en tenant compte de l'amortissement par chocs. On devrait s'attendre à voir le profil des raies s'adoucir considérablement et sans doute verrait- on disparaître le ou les pics centraux que Verwej a obtenu pour les forts champs de pesanteur.

17. Méthode de calcul. Le calcul a été effectué d'après les calculs de PANNEKOEK (28). Pannekoek a étudié l'intensité des raies d'émission. Il ressort de son travail que le phénomène prépondérant est le phénomène de recouvrement des raies, le phénomène de dissolution étant beaucoup moins important.

a) Le coefficient d'absorption en un point situé à une distance $\Delta\lambda$ du centre de la raie est donné par:

$$[2{,}549]\left(\frac{n^2}{n_2-4}\right)^2 f\frac{1}{SF_0}\int_0^\infty \frac{W(\beta)}{\beta}\,d\beta \tag{17.1}$$

où S, qui donne l'étendue en ångströms du réseau de raies Stark est donné par

$$S = 0{,}00256\,[n(n-1)+2]\left(\frac{n^2}{n^2-4}\right)^2 \tag{17.2}$$

avec

$$\Delta\lambda_0 = SF_0, \tag{17.3}$$

F_0 étant le champ moléculaire moyen.

Si $\Delta\lambda$ est la distance fixe au centre de la raie où l'on mesure l'intensité et $\Delta\lambda_0$ l'élargissement moyen, on a:

$$\beta = \frac{\Delta\lambda}{\Delta\lambda_0}, \tag{17.4}$$

$W(\beta)\,d\beta$ est ici la fonction de distribution de HOLTSMARK (18) telle qu'il en a été fait mention au chapitre II;

f est la force de l'oscillateur telle qu'elle est donnée par BETHE (12) et reproduite par UNSÖLD (50).

b) On calcule en un point situé à mi-distance de deux raies voisines la contribution de 2 raies (ou 4) élargies (1 ou 2 de chaque côté). On calcule ainsi le coefficient d'absorption par gramme d'hydrogène dans l'état quantique $n = 2$ en fonction du nombre N_1 de protons par cm^3.

Pour chaque modèle d'atmosphère envisagé, on calcule le coefficient d'absorption k_ν par gramme de matière et l'on ajoute l_ν au coefficient k_ν déjà trouvé pour le fond continu. Lorsque l'on atteint la région où l'effet de pression fait disparaître les raies dans le continu, on ne tient plus compte que du coefficient d'absorption k_ν du continu.

Le tableau VIII donne le coefficient d'absorption entre deux raies consécutives en fonction de log N_1 par gramme d'hydrogène dans l'état $n = 2$.

On a calculé de cette manière l'intensité pour les longueurs d'onde 3862 3930 4036 pour 40 Eridani B et 3930 4036 4221 4601 pour Van Maanen 2 correspondant respectivement aux points situés à mi-distance des raies $\zeta\eta$, $\varepsilon\zeta$, $\delta\varepsilon$, et $\varepsilon\zeta$, $\delta\varepsilon$, $\gamma\delta$, $\beta\gamma$.

Le tableau IX donne les valeurs de s, f et $q = [2{,}549]\left(\frac{n^2}{n^2-4}\right)^2 \frac{f}{s}$ en fonction de n. Le tableau X donne les valeurs de l'intensité relative rapportée à $\lambda = 3000$ Å.

Tableau VIII.

log l_ν par gramme d'hydrogène dans l'état $n = 2$.

log N_1	4801 log $l_\nu = 8 +$	4221 log $l_\nu = 8 +$	4036 log $l_\nu = 8 +$	3930 log $l_\nu = 8 +$	3862 log $l_\nu = 8 +$
15,0	$\bar{5}$,613	$\bar{4}$,19	$\bar{4}$,69	$\bar{3}$,22	$\bar{3}$,86
15,2	$\bar{5}$,82	$\bar{4}$,41	$\bar{4}$,97	$\bar{3}$,44	$\bar{2}$,05
15,4	$\bar{4}$,03	$\bar{4}$,64	$\bar{3}$,17	$\bar{3}$,64	$\bar{2}$,29
15,6	$\bar{4}$,23	$\bar{4}$,84	$\bar{3}$,36	$\bar{3}$,87	$\bar{2}$,53
15,8	$\bar{4}$,43	$\bar{3}$,02	$\bar{3}$,56	$\bar{2}$,06	$\bar{2}$,78
16,0	$\bar{4}$,64	$\bar{3}$,22	$\bar{3}$,79	$\bar{2}$,33	$\bar{2}$,99
16,2	$\bar{4}$,89	$\bar{3}$,42	$\bar{2}$,00	$\bar{2}$,56	$\bar{1}$,17
16,4	$\bar{3}$,08	$\bar{3}$,66	$\bar{2}$,26	$\bar{2}$,84	$\bar{1}$,21
16,6	$\bar{3}$,26	$\bar{3}$,94	$\bar{2}$,52	$\bar{2}$,97	$\bar{1}$,23
16,8	$\bar{3}$,46	$\bar{2}$,18	$\bar{2}$,73	$\bar{1}$,03	$\bar{1}$,17
17,0	$\bar{3}$,67	$\bar{2}$,31	$\bar{2}$,91	$\bar{1}$,04	$\bar{1}$,11
17,2	$\bar{3}$,90	$\bar{2}$,57	$\bar{1}$,02	$\bar{1}$,00	..
17,4	$\bar{2}$,10	$\bar{2}$,80	$\bar{1}$,05	$\bar{2}$,93	..
17,6	$\bar{2}$,34	$\bar{2}$,97	$\bar{1}$,02	..	..
1,78	$\bar{2}$,60	$\bar{1}$,08	$\bar{2}$,97	..	..
18,0	$\bar{2}$,83	$\bar{1}$,08	..	..	..
18,2	$\bar{1}$,03	$\bar{1}$,04	..	..	..

Tableau IX.

n	s	log s	log f	log q
4	0,06369	$\bar{2}$,804	$\bar{1}$,076	1,875
5	0,07980	$\bar{2}$,902	$\bar{2}$,647	1,348
6	0,1037	$\bar{1}$,0156	$\bar{2}$,327	0,979
7	0,1336	$\bar{1}$,1257	$\bar{2}$,087	0,810
8	0,1690	$\bar{1}$,2279	$\bar{3}$,903	0,509
9	0,2095	$\bar{1}$,3211	$\bar{3}$,681	0,274

Tableau X.

40 Eridani B			Van Maanen 2		
raies n $n+1$	λ	$\log \frac{F}{F_{3000}}$	raies n $n+1$	λ	$\log \frac{F}{F_{3000}}$
9			8		
	3862	0,081		3862	..
8			7		
	3930	0,103		3930	0,131
7			6		
	4036	0,147		4036	0,152
6			5		
	4221	..		4221	0,171
5			4		
	4601	..		4601	0,184
4					

18. Comparaison avec l'observation. Nous limitons les comparaisons au fond continu pour les raisons suivantes. Nous avons défini le fond continu au milieu de deux raies consécutives de la série de Balmer (§ 17b), le coefficient d'absorption étant lui-même défini par l'approximation de Pannekoek (Equation 17.1), suffisante ici. Mais comme nous l'avons brièvement indiqué à la fin du paragraphe 16, le calcul du contour des raies de l'hydrogène exigerait que l'on reprenne le travail de Verwej en le modifiant pour tenir compte de l'amortissement par chocs. Il faudrait en particulier évaluer l'intégrale de Rudkjøbing (second membre de 16.3) pour chacune des raies du réseau Stark des raies de l'hydrogène, calcul qui se trouve au-delà des limites que nous nous sommes fixées.

Kuiper (22) a donné le contour du fond continu pour 40 Eridani B et Van Maanen 2. Il ne s'agit que d'un microphoto-

gramme, et par conséquent on n'a que les densités photographiques. On trouve fig. 7, p. 75, les contours théoriques pour des étoiles de température et de gravité voisines. On voit que la ressemblance est frappante. Il ne fait aucun doute pour nous que la disparition des raies de Balmer dans les naines blanches

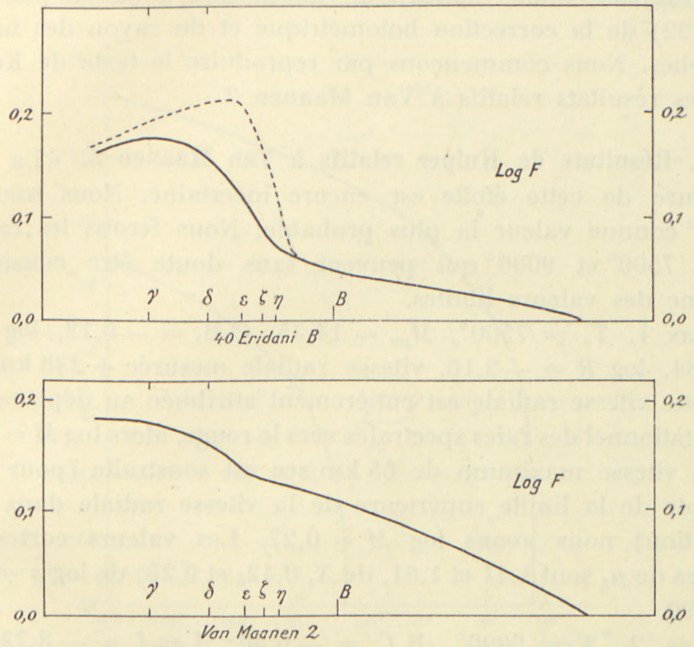

Fig. 7. Courbes représentatives du flux sortant pour 40 Eridani B et pour Van Maanen 2.

est effectivement due à l'élargissement des raies par effet Stark moléculaire.

On a tracé le fond continu pour 40 Eridani B dans les deux cas 1°) on néglige, et, 2°) on tient compte du recouvrement des raies par élargissement au-delà de leur largeur moyenne. On notera l'influence considérable du recouvrement même très loin des raies mélangées (par exemple entre H_β et H_γ). Il apparaît dès lors contestable que l'intensité mesurée par Kuiper entre H_β et H_γ pour 40 Eri B soit celle du fond continu. Il ne semble donc pas possible de relier de façon simple la grandeur de la discontinuité de Balmer au nombre d'atomes d'hydrogène présents dans l'état $n = 2$.

IV. Température effective et rayon des naines blanches.

1. L'étude de la répartition spectrale de l'énergie faite en troisième partie nous amène à une analyse détaillée, à la lumière des résultats connu maintenant, de la détermination par KUIPER (22) de la correction bolométrique et du rayon des naines blanches. Nous commençons par reproduire le texte de Kuiper sur les résultats relatifs à Van Maanen 2.

2. Résultats de Kuiper relatifs à Van Maanen 2. «La température de cette étoile est encore incertaine. Nous trouvons 8200° comme valeur la plus probable. Nous ferons les calculs pour 7500° et 9000° qui peuvent sans doute être considérés comme des valeurs limites.

Cas 1. $T_e = 7500°$, $M_{pv} = 14{,}35$, C.B. $= -0{,}12$, $\log L = -3{,}84$, $\log R = -2{,}16$, vitesse radiale mesurée $+ 238$ km/sec. Si cette vitesse radiale est entièrement attribuée au déplacement gravitationnel des raies spectrales vers le rouge, alors $\log M = 0{,}41$. Si la vitesse maximum de 65 km/sec est soustraite (pour tenir compte de la limite supérieure de la vitesse radiale dans cette direction) nous avons $\log M = 0{,}27$. Les valeurs correspondantes de μ_e sont 1,41 et 1,61, de X, $0{,}42_5$ et 0,25; de $\log \bar{\varrho} = 7{,}04$ et 6,90.

Cas 2. $T_e = 9000°$. B.C. $= -0{,}40$; $\log L = -3{,}73$, $\log R = -2{,}26$. Les deux hypothèses sur la vitesse radiale donnent $\log M = 0{,}31$, ou 0,17; $\mu_e = 1{,}60$ ou 1,85; $X = 0{,}26$ ou $0{,}09_5$, $\log \bar{\varrho} = 7{,}24$ ou 7,10. On voit sur la figure 8, p. 77, l'emplacement des 4 solutions discutées. Dans la direction verticale, elles peuvent représenter les cas limites; la ligne de gauche correspondant à $V_{rad} = +65$ km est très probablement une ligne limite.

Mais la vitesse radiale véritable pourrait être négative et de 200 à 300 km/sec, doublant par conséquent le déplacement gravitationnel vers le rouge, entraînant ainsi une augmentation de 0,3 du logarithme de M. Mais même dans ce cas extrême, il semble difficile d'amener l'étoile entre les deux lignes pointillées de la figure 1[1], comme il serait nécessaire si l'équation d'état $P = K\varrho^{\frac{5}{3}}$ était applicable. Il semble plus important de poser

(1) du texte de Kniper.

la question de la température effective qui définit la position en ordonnées. La coordonnée horizontale pourra à la longue être déterminée par la variation séculaire du mouvement propre qui permettra de connaître la vitesse radiale exacte.».

On remarquera que la principale question abordée dans ce texte est celle de la position de Van Maanen 2 dans le diagramme

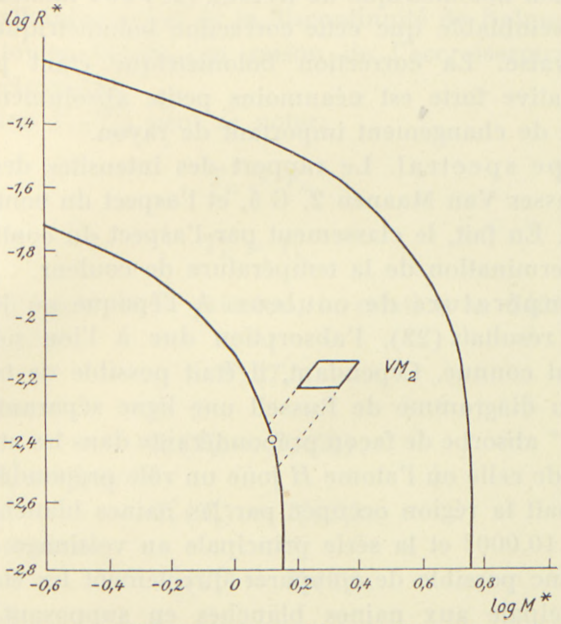

Fig. 8. Diagramme log M^* log R^*. La position de Van Maanen 2 telle qu'elle a été donnée par KUIPER est indiquée par le parallélogramme. Les lignes pointillées, courbes à vitesse radiale constante, indiquent les positions extrêmes de Van Maanen 2. Le cercle sur la courbe inférieure indique la position qui a été choisie pour Vann Maanen 2 en conclusion de la discussion de la discussion du chapitre IV.

de la fig. 1 par rapport aux deux lignes pointillées. Cette question était particulièrement importante en 1939 au moment du «Colloque des Astrophysiciens» en raison de la controverse sur l'équation d'état de la matière dégénérée. En fait, nous verrons que les nouveaux résultats que nous indiquons sont nettement favorables à la théorie de Chandrasekhar.

Nous ne nous attarderons pas sur la question de la vitesse radiale de Van Maanen 2, qui ne prête pas à de longues discussions, mais nous examinerons de très près la question de la température effective de Van Maanen 2.

3. Température effective de Van Maanen 2 et correction bolométrique. Ces deux grandeurs sont déterminées par le type spectral. Faisons tout d'abord quelques remarques préliminaires:

a) La correction bolométrique C.B., dans ce domaine de températures n'est pas sujette à des erreurs considérables. Bien qu'il soit douteux qu'on puisse appliquer directement les tables de correction bolométrique de KUIPER (21) aux naines blanches, il est vraisemblable que cette correction bolométrique n'est pas très mauvaise. La correction bolométrique étant petite, une erreur relative forte est néanmoins petite absolument et n'entraîne pas de changement important de rayon.

b) Type spectral. Le rapport des intensités des raies du fer fait classer Van Maanen 2, G 5, et l'aspect du continu la fait classer a6. En fait, le classement par l'aspect du continu repose sur la détermination de la température de couleur.

c) Température de couleur. A l'époque où Kuiper publiait ses résultats (22), l'absorption due à l'ion négatif était encore mal connue. Cependant, il était possible de tracer dans le plan du diagramme de Russell une ligne séparant la région où l'ion H^- absorbe de façon prépondérante dans les atmosphères stellaires, de celle où l'atome H joue un rôle prépondérant. Cette ligne coupait la région occupée par les naines blanches au voisinage de 10.000° et la série principale au voisinage de 7.000°. Il était donc possible de comparer directement les étoiles de la série principale aux naines blanches en supposant pour $T_{\text{eff}} < 7.000°$ l'absorption due uniquement à H^- et pour $T_{\text{eff}} > 10.000°$ l'absorption due uniquement à H. Cette hypothèse d'un absorbant unique permettait d'espérer l'absence de tout phénomène dû à la magnitude absolue. De plus l'estimation de la discontinuité de Balmer devait corroborer ce premier résultat.

Deux circonstances permettent de douter du résultat. La première soulignée par Kuiper est que Van Maanen 2 se trouve justement dans la région A—F où la méthode de comparaison employée n'est pas applicable. La deuxième est que Kuiper n'a pas tenu compte de la déformation du spectre par le recouvrement des raies de l'hydrogène. Cette déformation se manifeste de deux façons, d'une part par une diminution de la discontinuité de Balmer, d'autre part, par une diminution de la température de couleur.

En effet, l'abaissement du fond continu par recouvrement des raies est d'autant plus marqué que l'on se rapproche de la discontinuité de Balmer, ce qui correspond à un abaissement de la température de couleur et à un affaiblissement de la discontinuité de Balmer. La discontinuité de Balmer et la température de couleur sont donc plus petites que celles que l'on observerait dans une étoile de la série principale de même température effective. L'affaiblissement de la discontinuité de Balmer se produirait de toutes façons, en raison de l'accroissement de la pression électronique.

La relation $T_e(T_c)$ peut se noter:

$$T_{c_1} > T_{c_2}$$

entraîne

$$T_{e_1} > T_{e_2}.$$

Sous l'influence de la pression, la relation se déforme. On avait la fonction

$$T_c(T_e),$$

on a maintenant

$$T'_c(T_e) < T_c(T_e).$$

Cherchons T'_e tel que

$$T'_c(T'_e) = T_c(T_e).$$

Comme on a alors

$$T'_c(T'_e) = T'_c(T_e),$$

on en déduit

$$T'_e > T_e.$$

La déformation du fond continu par recouvrement des raies fait qu'à une même température de couleur correspond une température effective plus élevée dans les naines blanches que dans les étoiles de la série principale, et cet effet est d'autant plus grand que la gravité (donc la pression) est plus forte.

Nous voyons donc que même sans mettre en doute la relation entre la correction bolométrique et la température effective, il est nécessaire de se méfier de la valeur de la correction bolométrique adoptée par Kuiper, car il est hors de doute que la température effective adoptée est trop faible. Nous donnons ici les valeurs de $\log R$ pour différentes valeurs de T_{eff}.

On a:

$$L = 4\,\pi\,R^2\,\sigma\,T_e^4$$

ou numériquement:

$$L^* = [18{,}536]\;R^{*2}\;T_e^4$$

Le tableau I donne la relation entre la température effective et les différentes grandeurs relatives à l'étoile.

Tableau I.

T_e	B.C.	M_{Bol}	log L^*	log R^*
7.500	— 0,10	14,25	— 3,84	— 2,15
8.000	— 0,20	14,14	— 3,80	— 2,19
8.500	— 0,32	14,03	— 3,75	— 2,22
9.000	— 0,42	13,93	— 3,71	— 2,25
9.500	— 0,52	13,83	— 3,67	— 2,27
10.000	— 0,62	13,73	— 3,63	— 2,30
10.500	— 0,72	13,63	— 3,59	— 2,32
11.000	— 0,82	13,53	— 3,55	— 2,34
12.000	— 1	13,35	— 3,48	— 2,38
13.000	— 1,2	13,15	— 3,40	— 2,41
15.000	— 1,52	12,83	— 3,27	— 2,47

On a noté ici L^* et R^* pour la luminosité et le rayon exprimé en unités de soleil afin de les distinguer de L et R en C.G.S.

Les valeurs limites de log R^*, point de rencontre des droites $V = 65$ km et $V = 0$ avec la courbe limite log M^*; log R^*, sont:

$$\log R^* = -2{,}33 \text{ et } \log R^* = -2{,}45$$

correspondant respectivement aux températures effectives

$$T_e = 10.700° \text{ et } T_e = 14.200.$$

Le modèle d'atmosphère que nous avons calculé pour Van Maanen 2 nous permet une estimation du rôle de l'élargissement des raies. On a approximativement:

$$\log_{10} \frac{F_{4000}}{F_{4600}} = 0{,}10 \pm 0{,}03$$

d'où, d'après les définitions données dans (9)

$$\Phi = 1{,}47 \pm 0{,}2$$

ou

$$\theta'_c = 0{,}49 \pm 0{,}07.$$

La température de couleur θ_c, définie de la même façon, correspondant à $\theta_0 = 0{,}50$, et $\theta_e = 0{,}42$ pour une étoile de la série principale, est approximativement (9)

$$\theta_c = 0{,}22.$$

On a donc

$$\theta_c = \theta'_c - 0{,}27 \mp 0{,}07.$$

Dans le cas de Van Maanen 2, classée avec

$$\theta'_c = 0{,}46,$$

on déduit

$$\theta_{c_{\mathrm{VM}2}} = 0{,}19 \pm 0{,}07,$$

d'où

$$\theta'_{e_{\mathrm{VM}2}} = 0{,}40 \pm 0{,}05,$$

ou

$$T'_{e_{\mathrm{VM}2}} = 12 \cdot 500^\circ \pm 1000^\circ = T_{e_{\mathrm{VM}2}} + 4300^\circ.$$

Sans attacher une trop grande valeur à l'exactitude de la correction apportée à la détermination de T'_e, on voit toutefois qu'elle est certainement considérable et a le signe indiqué. Il est donc parfaitement possible que Van Maanen 2 se trouve beaucoup plus près de la courbe $\mu_e = 2$ qu'il n'avait été supposé (34).

4. Le rayon des naines blanches et la théorie du débit d'énergie aux grandes densités. L'énormité du facteur d'accélération (44) nécessite une révision des résultats antérieurement donnés (34) concernant Van Maanen 2 et conduit à des conclusions analogues à celles du paragraphe précédent.

On trouvera dans le tableau II pour différentes densités et pour la température de $4{,}7 \cdot 10^6$ degrés les facteurs d'accélération correspondant à la réaction $^{12}C + {}^1H$.

Tableau II.

$\log(\varrho/\mu_e)$	$\log A$
5,102	5,06
6,102	9,87
7,102	16,01
8,102	28,15

En supposant la hauteur de mélange donnée par la formule (34)

$$h = 1{,}5 \cdot 10^8 \frac{T}{g},$$

on obtient pour la luminosité

$$L = [25{,}815]\, A\, \eta^2 \frac{(\Phi^2 y_0^2 - 1)^3}{-\Phi' y_0^4}$$

en supposant la concentration en ^{12}C approximativement égale à 1 % au sein du mélange d'éléments lourds.

Différentes valeurs de la luminosité ont été calculées pour $1/y_0^2 = 0{,}01$ qui correspond approximativement au rayon de Van Maanen 2, et pour différentes valeurs de η, rayon réduit (7). Les calculs ont été faits également pour d'autres valeurs de T (tableau III).

Tableau III.

T	η	$\log A$	$\log L/L_{VM2}$
$4{,}7 \cdot 10^6$	4	13	7
$4{,}7 \cdot 10^6$	4,5	11,6	5,3
$3 \cdot 10^6$	4,5	16	5,3

Les valeurs de la densité sont donc encore assez élevées pour entraîner des facteurs d'accélération énormes. Il est donc nécessaire de supposer que Van Maanen 2 est entourée d'une très mince couche d'hydrogène, si l'on veut éviter de telles difficultés.

5. Influence du triage des éléments. Il pourrait sembler possible que le triage des éléments dans Van Maanen 2 réduise la concentration de ^{12}C et ^{14}N dans la couche de mélange dans

de telles proportions que le débit d'énergie s'en trouve fortement réduit. Une formule approximative, déjà utilisée par ailleurs (36) donne un facteur:

$$C_N \text{ moyen } / \; C_N \text{ dû au triage } = 500.$$

Bien que déjà élevé, ce facteur est néanmoins trop petit pour combler l'écart observé. La conclusion s'impose: Van Maanen 2, semblable en cela à la plupart des autres naines blanches connues, a une très petite teneur en hydrogène.

V. Théorie élémentaire du débit d'énergie des naines blanches.

1. Généralités. Nous avons longuement insisté dans la première partie sur la définition de la couche de mélange. Nous avons montré que sa hauteur variait légèrement suivant la dégénérescence du gaz d'électrons. En moyenne, on peut prendre (34):

$$h = 1{,}5 \cdot 10^8 \frac{T}{g}. \tag{1.1}$$

Elle varie, suivant les naines blanches, de quelques centièmes à quelques millièmes du rayon. Nous basons la théorie simplifiée que nous présentons ici sur l'hypothèse que la couche de mélange est infiniment mince et se réduit à une surface S de séparation entre l'hydrogène et les noyaux lourds.

Il n'est pas inutile de préciser que si nous négligeons l'épaisseur de la couche de mélange dans notre description de la structure des naines blanches, c'est à ce seul point de vue que nous la négligeons, car nous tenons compte exactement des sources d'énergie qui s'y trouvent accumulées (réactions du cycle de Bethe) comme on peut le voir plus loin.

La réaction proton-proton est supposée jouer un rôle essentiel et la vitesse de réaction est donnée par la formule calculée par Bethe et Critchfield (2). La production d'énergie dans la couche de mélange est donnée par:

$$L_B = [40{,}286]\, T^{\frac{1}{3}} \quad \exp\left(-\frac{15250}{T^{\frac{1}{3}}}\right) \frac{r^2 \varrho^2}{g} (c_N)_R \tag{1.2}$$

où ϱ est la densité à l'intérieur de la surface S, $(c_N)_R$ la concentration en azote au sein du mélange d'éléments lourds, T la température en degrés, L_B le débit d'énergie en ergs.

Le coefficient d'absorption du gaz non dégénéré de protons et d'électrons est

$$\chi = [22{,}870]\ \varrho\ T^{-3{,}5} \tag{1.3}$$

car, aux densités considérées, l'absorption par les électrons libres est négligeable (diffusion Thomson).

2. Les limites de la théorie élémentaire. Lorsque l'épaisseur de la couche de mélange n'est plus négligeable, la théorie n'est certainement plus applicable. La théorie qui est donnée ici n'est pas valable en toute généralité pour toutes les naines blanches. Elle ne peut sans doute être appliquée qu'aux naines blanches ne présentant pas de raies métalliques dans leur spectre, les autres ayant une structure légérement différente.

Certains résultats antérieurs (34) (39) deviennent entièrement différents.

Une partie des résultats présentés ici ont déjà été annoncés (40), (41), (42), (43), (45). Nous allons les exposer ici avec quelques détails.

3. La réaction proton-proton. Cette réaction avait été supposée interdite (39) dans le but d'expliquer l'épaisse couche d'hydrogène de Van Maanen 2. L'étude théorique du spectre et des réactions nucléaires conduisent au même résultat et permettent de conclure qu'il est impossible que Van Maanen 2 ait une couche d'hydrogène épaisse.

Ceci nous montre en particulier que Van Maanen 2 a un très petit rayon et se place donc très loin de la ligne correspondant dans la figure 8 à l'équation d'état $P = K\varrho^{\frac{5}{3}}$. On confirme ainsi la théorie de la dégénérescence de Stoner et Anderson et les résultats de Chandrasekhar.

Il n'y a donc plus aucune raison de supposer la réaction

$$^1H + {}^1H = {}^2D + \varepsilon^+$$

interdite (au sens des règles de sélection) et il est possible d'utiliser la formule de Bethe et Critchfield (2):

$$\varepsilon = 410\, \varrho\, X^2\, \tau^2\, e^{-\tau},$$

avec

$$\tau = \frac{33{,}8}{T^{\frac{1}{3}}} \qquad T \text{ en millions de degrés}$$

et tout calcul du débit d'énergie doit se faire en utilisant ces valeurs numériques.

4. Les bases de la théorie simplifiée. Nous devons rappeler certaines formules qui ont été déjà données (34).

On calcule le modèle pour la couche extérieure mince d'hydrogène en supposant la gravité et le rayon pratiquement constants dans toute cette couche. On obtient ainsi les relations suivantes entre la température et la densité d'une part et la profondeur géométrique comptée à partir de la surface d'autre part:

$$T = [6{,}434]\frac{M^*}{R^*}\frac{\Delta R}{R}, \tag{4.1}$$

$$\varrho = [0{,}116]\, R^{*-\frac{13}{4}} L^{*-\frac{1}{2}} M^{*\frac{15}{4}} \left(\frac{\Delta R}{R}\right)^{\frac{13}{4}}. \tag{4.2}$$

Ces formules supposent la dégénérescence négligeable. La condition de la dégénérescence:

$$\frac{R\varrho T}{\bar{\mu}} = K \varrho^{\frac{5}{3}} \mu_e^{-\frac{5}{3}} \tag{4.3}$$

conduit à une limite différente pour $\frac{\Delta R}{R}$ suivant que l'on admet que la dégénérescence apparaît dans l'hydrogène ($\mu_e = 1$, $\bar{\mu} = \frac{1}{2}$) ou dans le noyau d'éléments lourds ($\mu_e = 2$). L'épaisseur non dégénérée maximum de l'hydrogène est donnée par

$$\frac{\Delta R}{R} < [1{,}351]\, R^* L^{*\frac{2}{7}} M^{*-\frac{9}{7}}. \tag{4.4}$$

Tous les calculs faits en supposant la couche d'hydrogène non dégénérée doivent conduire à une valeur de $\frac{\Delta R}{R}$ inférieure à cette quantité.

5. Les éléments de la théorie du débit d'énérgie. La réaction proton-proton a lieu évidemment dans un domaine d'une certaine épaisseur. Comme nous supposons la couche de mélange infiniment mince, nous calculons la réaction (a) en supposant l'hydrogène pur, (b) en supposant que la température décroît si rapidement dans la couche d'hydrogène que la production d'énergie a lieu dans une couche infiniment mince.

La production d'énergie est donnée par:

$$L^* = \frac{R_\odot^3}{L_\odot} \int 4\pi R^{*2} \varrho \varepsilon \, dr^* \tag{5.1}$$

$$L^* = 4\pi R^{*2} 410 \frac{R_\odot^3}{L_\odot} \int \varrho^2 \tau^2 e^{-\tau} dr^* . \tag{5.2}$$

Nous introduisons les expressions (4,1) et (4,2) pour la température et la densité, ce qui correspond à l'hypothèse (b). De plus nous avons:

$$\tau = \frac{B}{[2{,}145]} \left(\frac{M^*}{R^*}\right)^{-\frac{1}{3}} \left(\frac{\Delta R}{R}\right)^{-\frac{1}{3}} \tag{5.3}$$

$$\tau_0 = \frac{B}{[2{,}145]} \left(\frac{M^*}{R^*}\right)^{-\frac{1}{3}} \tag{5.4}$$

$$\frac{\Delta R}{R} = \left(\frac{\tau_0}{\tau}\right)^3 . \tag{5,5}$$

On obtient ainsi

$$L^* = 4\pi R^{*3} 410 \frac{R_\odot^3}{L_\odot} \varrho_0^2 \, 3 \, \tau_0^{\frac{4\,5}{2}} \int_\tau^\infty \tau^{-\frac{4\,3}{2}} e^{-\tau} d\tau \tag{5.6}$$

où l'on a

$$\varrho = \varrho_0 \left(\frac{\Delta R}{R}\right)^{\frac{13}{4}}. \tag{5.7}$$

On remplace l'intégrale par le premier terme de son développement asymptotique:

$$L^* = 12\pi R^{*3} \cdot 410 \frac{R_\odot^3}{L_\odot} \varrho_0^2 \tau_0^{\frac{45}{2}} \frac{e^{-\tau}}{\frac{41}{2}\tau^{\frac{41}{2}}}. \tag{5.8}$$

On obtient ainsi l'expression numérique [1]:

$$L^{*2} = [4{,}824]\, R^{*-\frac{17}{6}} M^{*\frac{41}{6}} \left(\frac{\Delta R}{R}\right)^{\frac{41}{6}} e^{-[1{,}384]\left(\frac{E^*}{M^*}\right)^{\frac{1}{3}}\left(\frac{\Delta R}{R}\right)^{-\frac{1}{3}}} \tag{5.9}$$

ou

$$L^* = [2{,}412]\, R^{*-\frac{17}{12}} M^{*\frac{41}{12}} \left(\frac{\Delta R}{R}\right)^{\frac{41}{12}} e^{-[1{,}083]\left(\frac{R^*}{M^*}\right)^{\frac{1}{3}}\left(\frac{\Delta R}{R}\right)^{-\frac{1}{3}}}. \tag{5.10}$$

On peut poser:

$$L^* = \lambda \left(\frac{\Delta R}{R}\right)^{\frac{41}{12}} e^{-\mu\left(\frac{\Delta R}{R}\right)^{-\frac{1}{3}}}; \tag{5.11}$$

les coefficients λ et μ sont donnés dans la table I.

Table I.

$1/y_0^2$	$\log \lambda$	μ
0	..	..
0,01	6,47	1,56
0,02	6,25	1,73
0,05	5,89	2,00
0,1	5,57	2,27
0,2	5,11	2,65
0,3	4,74	2,96
0,4	4,38	3,29
0,5	4,02	3,65
0,6	3,62	4,07
0,8	2,58	5,44

[1] On peut faire un calcul analogue en supposant que la réaction se produit dans une région à température constante. On trouve une expression de même forme, avec un facteur numérique très légèrement différent.

Si la concentration en hydrogène est:

$$(5.12)\quad X = \frac{\text{masse de la couche extérieure d'hydrogène}}{\text{masse de l'étoile}},$$

on a:

$$(5.13)\quad X = [\bar{1},812]\, R^{*-\frac{1}{4}} L^{*-\frac{1}{2}} M^{*\frac{11}{4}} \left(\frac{\Delta R}{R}\right)^{\frac{17}{4}}$$

qui devient à l'aide de (10,10)

$$(5.14)\quad X = [\bar{2},609]\, R^{*\frac{11}{24}} M^{*\frac{25}{24}} \left(\frac{\Delta R}{R}\right)^{\frac{61}{24}} e^{\frac{\mu}{2}\left(\frac{\Delta R}{R}\right)^{-\frac{1}{3}}}.$$

6. Eléments de la théorie. Dégénérescences. Lorsque la dégénérescence apparaît dans la couche d'hydrogène, le calcul doit être modifié.

Dans ce cas, on suppose la température centrale égale à:

$$(6.1)\quad T = [7,79]\left(\frac{L^*}{M^*}\right)^{\frac{2}{7}}$$

et constante dans toute la région dégénérée. Le débit d'énergie est alors dans la région dégénérée:

$$(6.2)\quad L^* = 4\pi R^{*2} \frac{R_\odot^2}{L_\odot} 410\, \tau^2 e^{-\tau} \frac{5}{3} \frac{K}{g} \int_D^{\varrho} \varrho^{\frac{5}{3}}\, d\varrho$$

où g est la gravité, $K = [12,996]$ et

$$(6.3)\quad \tau = [0,927]\left(\frac{M^*}{L^*}\right)^{\frac{2}{21}}.$$

La teneur en hydrogène est:

$$(6.4)\quad \begin{cases} MX = \int 4\pi r^2 \varrho\, dr \\ \qquad = 4\pi R^2 \int \varrho\, dr, \end{cases}$$

or

$$(6.5)\quad \varrho\, dr = -\frac{dP}{g},$$

d'où

$$MX = 4\pi R^2 \frac{P}{g}. \tag{6.6}$$

La pression est $P = K\varrho^{\frac{5}{3}}$. On en déduit:

$$X = [0{,}043]\frac{R^{*4}}{M^{*2}}\varrho^{\frac{5}{3}}, \tag{6.7}$$

formule valable dans la région de dégénérescence.

La production d'énergie est égale à la somme de l'énergie produite dans la région dégénérée et de l'énergie produite dans la région non dégénérée. On obtient ainsi:

$$\left\{\begin{aligned} L^* &= [5{,}157]\, L^{*-\frac{4}{21}} R^{*-\frac{12}{5}} M^{*\frac{251}{105}} e^{-\tau}\left(X^{\frac{8}{5}} - X_0^{\frac{8}{5}}\right) \\ &\quad + [14{,}064]\frac{R^{*4}}{M^{*\frac{41}{21}}} L^{*\frac{20}{21}} e^{-\tau}. \end{aligned}\right. \tag{6.8}$$

Avec la définition que nous avons prise pour l'apparition de la dégénérescence, on a:

$$L_{ND} = \frac{4\pi K}{G}\frac{102}{164}\,410\,\frac{R^4}{M}\tau^2 e^{-\tau}\varrho^{\frac{8}{3}} \tag{6,9}$$

$$L_0 = \frac{4\pi K}{G}\frac{5}{8}\,410\,\frac{R^4}{M}\tau^2 e^{-\tau}\varrho^{\frac{8}{3}} \tag{6.10}$$

où L_0 est l'énergie qui serait produite par la masse d'hydrogène non dégénérée MX_0 si toute cette masse était dégénérée. On a pratiquement $L_{ND} = L_0$, d'où:

$$L^* = [5{,}157]\, L^{*-\frac{4}{21}} R^{*-\frac{12}{5}} M^{*\frac{251}{105}} e^{-\tau} X^{\frac{8}{5}}. \tag{6,11}$$

Cette expression est valable quelle que soit la masse d'hydrogène dégénérée.

On trouvera dans le tableau II les coefficients en fonction de $1/y_0^2$.

Tableau II.

$1/y_0^2$	$[0{,}927]\, M^{*\frac{2}{21}}$	$5{,}157 + \log R^* - \frac{12}{5} M^{*\frac{251}{105}}$
0		
0,01	8,70	11,552
0,02	8,68	11,266
0,05	8,61	10,770
0,1	8,50	10,391
0,2	8,35	9,900
0,3	8,20	9,554
0,4	8,07	9,223
0,5	7,92	8,907
0,6	7,76	8,572
0,8	7,31	7,657
1		

Ce calcul cesse d'être valable quand la région d'hydrogène dégénéré occupe une épaisseur nulle. Le cas se présente lorsque

$$\frac{\Delta R}{R} = [1{,}354]\, R^* L^{*\frac{2}{7}} M^{*-\frac{9}{7}}. \tag{6.12}$$

On a alors

$$L^{*\frac{1}{42}} = [7{,}032]\, R^{*2} M^{*-\frac{41}{42}} e^{-[0{,}630]\left(\frac{M^*}{L^*}\right)^{\frac{2}{21}}}. \tag{6.13}$$

A cette relation correspond une courbe limite dans le plan L^*, M^* (fig. 9). D'un côté, les naines blanches ont leur couche d'hydrogène entièrement non-dégénérée, de l'autre, elle est partiellement dégénérée.

Tableau III.

$\log M^*$	$\log L^*$
0,140	+ 0,25
0,125	— 0,50
0,085	— 1,30
0,035	— 1,80
— 0,053	— 2,38
— 0,131	— 2,75
— 0,213	— 3,10
— 0,297	— 3,50
— 0,391	— 3,80
— 0,657	— 4,60

Le tableau III donne les points de la courbe $L^*(M^*)$ limite. Ces valeurs ont été déterminées en résolvant (6.13) à l'aide d'une abaque à points alignés, et ne sont pas données avec une grande précision.

7. Analyse de 40 Eridani B. Nous prenons pour 40 Eridani B les valeurs suivantes:

$$\log L^* = -2{,}1 \quad \log R^* = -1{,}8 \quad \log M^* = -0{,}35.$$

La formule (5.10) donne:

$$\frac{\Delta R}{R} = 0{,}15. \tag{7.1}$$

La condition (4.4) donne

$$\frac{\Delta R}{R} \leqq 0{,}25. \tag{7.2}$$

La condition (4,4) est satisfaite. 40 Eri B s'explique donc entièrement par la réaction proton-proton. La formule (4.1) donne la température qui règne dans la couche de mélange:

$$T = 11{,}46 \cdot 10^6 \text{ degrés}. \tag{7.3}$$

La hauteur de mélange rapportée au rayon est:

$$\frac{h}{R} = 0{,}022. \tag{7.4}$$

Elle est très petite comparée à l'épaisseur de la couche d'hydrogène.

Calculons à titre de comparaison la production d'énergie par les réactions du cycle de Bethe. La formule (1.2) nous donne le débit d'énergie dans la couche mixte.

La densité est [(34), 199]:

$$\varrho = [1{,}377]\, R^{*-2{,}55} M^{*2{,}85} L^{*0{,}3} \left(\frac{\Delta R}{R}\right)^{2{,}55} \tag{7.5}$$

d'où:

$$\log \varrho = 3{,}490. \tag{7.6}$$

En prenant $(c_N)_R = 10^{-2}$, on obtient

$$\log L_B = 29{,}4, \tag{7.7}$$

soit environ

$$L_B = 10^{-2} L_H \tag{7.8}$$

Le débit d'énergie par les réactions du cycle du carbone est négligeable. La luminosité de 40 Eridani B est entièrement due aux réactions proton-proton et suivantes.

Ce résultat, en parfait accord avec tout ce que la physique nucléaire nous apprend sur la réaction proton-proton, est à la fois une preuve de l'exactitude de la théorie de la réaction proton-proton et une explication sans défaut, au moins en principe, de l'origine du débit d'énergie des naines blanches.

8. Influence des réactions du cycle du carbone. Pour les naines blanches les plus chaudes les réactions du cycle du carbone peuvent devenir importantes.

Le débit d'énergie dû aux réactions du cycle du carbone est:

$$L_c^* = [14{,}778]\, T^{\frac{1}{3}} \exp\left(\frac{15250}{T^{\frac{1}{3}}}\right) \frac{R^{*4}}{GM^*} \varrho_{\text{core}}^2, \tag{8.1}$$

avec

$$\varrho_c = 2\, \varrho_H, \tag{8.2}$$

où ϱ_H est donné par (4,2)[1]. On en déduit:

$$L_c^* = [22{,}788] \frac{R^{*4}}{M^*} R^{*-\frac{13}{2}} M^{*\frac{15}{2}} \left(\frac{\Delta R}{R}\right)^{\frac{13}{2}} T^{\frac{1}{3}} \exp\left(-\frac{15250}{T^{\frac{1}{3}}}\right) L^{*-1}; \tag{8.3}$$

comme

$$L^* = L_c^* + L_H^*, \tag{8.4}$$

(1) En fait, il faudrait prendre suivant les cas (4.2) ou (7.5). Le calcul montre que le résultat est insensible à la formule employée.

on a

$$(8.5)\quad \begin{cases} L^{*2} = [24{,}933]\dfrac{R^{*4}}{M^*} R^{*-\frac{13}{2}} M^{*\frac{15}{2}} \left(\dfrac{\Delta R}{R}\right)^{\frac{13}{2}} \left(\dfrac{M^*}{R^*}\right)^{\frac{1}{3}} \left(\dfrac{\Delta R}{R}\right)^{\frac{1}{3}} \exp\left(\dfrac{15250}{T^{\frac{1}{3}}}\right) \\ \qquad + [4{,}824]\, R^{*-\frac{17}{6}} M^{*\frac{41}{6}} \left(\dfrac{\Delta R}{R}\right)^{\frac{41}{6}} \exp\left(-\dfrac{3380}{T^{\frac{1}{3}}}\right). \end{cases}$$

L'égalité $L_c = L_H$ se produit pour

$$(8.6)\qquad T = 16{,}9 \cdot 10^6 \text{ degrés.}$$

Ceci correspond à

$$(8.7)\qquad \frac{\Delta R}{R} = \frac{R^*}{M^*}[0{,}795].$$

On en déduit $L^*(M^*)$ le long de la courbe

$$(8.8)\qquad L^* = [2{,}69]\, R^{*2}.$$

On calcule de même les courbes le long desquelles $\dfrac{L_B}{L_H} = \xi$. Elles sont de la forme $L^* = Cte\, R^{*2}$ et le coefficient Cte est donné dans le tableau IV.

Tableau IV.

ξ	log Cte
10^{-2}	1,54
10^{-1}	1,93
1	2,42
10	3,15
100	4,04

Il faut arrêter cette courbe à la courbe limite déjà calculée, lieu d'apparition de la dégénérescence dans l'hydrogène. On trouve ainsi que pour Sirius B, $L_C = L_H$. On a alors

$$(8.9)\qquad T = 16{,}8 \cdot 10^6 \text{ degrés}$$

$$(8.10)\qquad \frac{\Delta R}{R} = 0{,}05.$$

La condition (9.4) donne

$$\frac{\Delta R}{R} < 0{,}064. \tag{8.11}$$

Cette condition est donc satisfaite par la valeur (8.10). On a de plus $h = 0{,}00667$.

Dans le cas où les réactions proton-proton se produisent dans une région d'hydrogène où le gaz d'électrons est dégénéré, un calcul analogue donne une autre courbe limite. L'égalité entre les deux termes L_H et L_c donne

$$\left\{\begin{aligned} \frac{L^*}{2} &= [5{,}157]\, R^{-\frac{12}{5}} M^{\frac{251}{105}} X^{\frac{8}{5}} L^{*-\frac{4}{21}} \exp - [0{,}927] \left(\frac{M^*}{L^*}\right)^{\frac{2}{21}} \\ &= [24{,}500]\, R^{-\frac{4}{5}} M^{\frac{7}{5}} X^{\frac{6}{5}} \left(\frac{L}{M}\right)^{\frac{2}{21}} \exp - [1{,}586] \left(\frac{M^*}{L^*}\right)^{\frac{2}{21}}. \end{aligned}\right. \tag{8.12}$$

On en tire X

$$X^{\frac{2}{5}} = [19{,}343]\, R^{*\frac{8}{5}} M^{*-\frac{114}{105}} L^{*\frac{6}{21}} \exp - [1{,}478] \left(\frac{M^*}{L^*}\right)^{\frac{2}{21}}$$

et finalement la relation:

$$\frac{1}{21} \log L^* + 55{,}8 \left(\frac{M^*}{L^*}\right)^{\frac{2}{21}} = 82{,}530 + 4 \log R^* - \frac{205}{105} \log M^*,$$

ou

$$\left(\frac{M^*}{L^*}\right)^{\frac{2}{21}} = 1{,}480 + 0{,}0718 \log R^* - 0{,}0380 \log M^* - 0{,}00085 \log L^*. \tag{8.14}$$

Cette relation a été calculée numériquement pour quelques valeurs de M^*. Les points obtenus se trouvent au-dessus de la courbe d'apparition de la dégénérescence dans l'hydrogène.

On trouve ainsi pour AC 70°8247, avec

$$\log L^* = -1{,}67 \qquad \log M^* = 0{,}12 \qquad \log R^* = -2{,}41,$$

que

$$L_c^* \cong \frac{1}{2} L_H^* \cong \frac{1}{3} L^*,$$

ce qui correspond à la position de AC 70°8247 au voisinage de la courbe qui vient d'être calculée.

9. Les courbes à teneur en hydrogène X = Constante. On a calculé pour les différentes masses, à l'aide de la représentation paramétrique $\frac{\Delta R}{R}$, L^* et X. Par interpolations graphiques, on a obtenu les courbes de la figure 9, p. 95. On a également calculé le lieu des points où $L_B/L_H = 0{,}01\,;\ 0{,}1\,;\ 1\,;\ 10$, et on a marqué sur ces courbes les points log $X = \bar{4}{,}6$ à $\bar{5}{,}4$ de 0,2 en 0,2. On a procédé de même dans la région dégénérée (tableaux V, VI et VII).

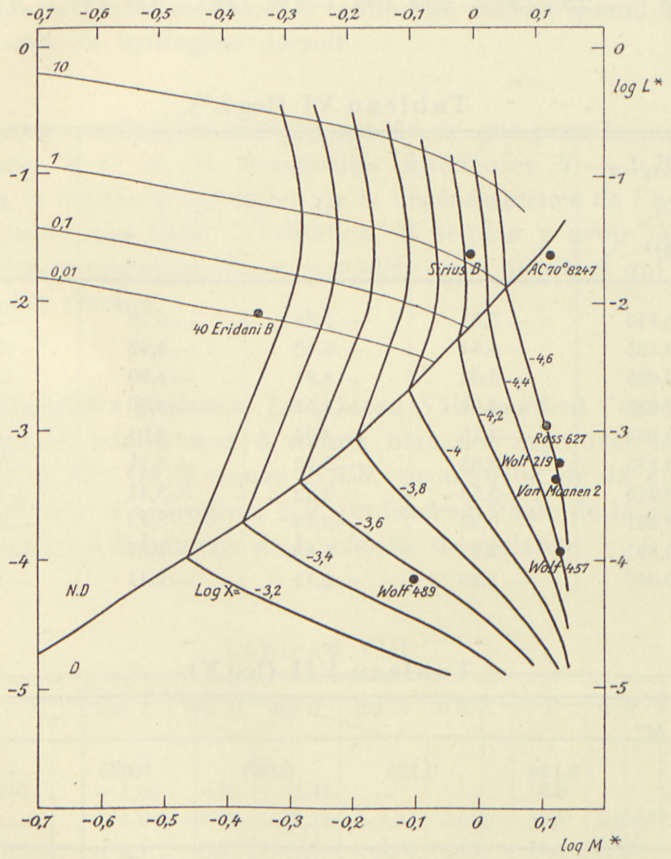

Fig. 9. Diagramme Masse-Débit d'énergie (log M^*, log L^*). On a tracé les courbes X = *Cte* et la courbe d'apparition de la dégénérescence dans l'hydrogène. On a tracé également les courbes indiquant la contribution des réactions du cycle du carbone par rapport à la réaction proton-proton dans les naines blanches les plus brillantes. On a marqué la position des principales naines blanches connues. On remarquera ainsi la faible contribution des réactions du cycle du carbone dans 40 Eridani B (0,01) et leur légère prépondérance dans Sirius B.

Tableau V.

Région non dégénérée, log X et log L^*.

log M^*	— 0,391		— 0,297		— 0,213		— 0,131		— 0,053	
log $\frac{\Delta R}{R}$	log L^*	log X	log L^*	log X	log L^*	log X	log L^*	log X	log L^*	log X
— 1,5	— 7,09	$\bar{4}$,34	— 6,12	$\bar{4}$,15	— 5,25	$\bar{5}$,96	— 4,64	$\bar{5}$,79	— 3,65	$\bar{5}$,63
— 1	— 3,61	$\bar{4}$,73	— 2,82	$\bar{4}$,62	— 2,12	$\bar{4}$,51	— 1,45	$\bar{4}$,42	— 0,79	$\bar{4}$,32
— 0,9	— 2,99	$\bar{4}$,85	— 2,23	$\bar{4}$,75	— 1,55	$\bar{4}$,65	— 0,91	$\bar{4}$,57	— 0,26	$\bar{4}$,48
— 0,8	— 2,37	$\bar{4}$,97	— 2,58	$\bar{4}$,89	— 0,99	$\bar{4}$,80	— 0,37	$\bar{4}$,76	+ 0,26	$\bar{4}$,65

Tableau VI (log L^*).

L_B/L_H / log M^*	0,01	0,1	1	10
0,140	— 5,91	— 5,80	— 5,79	— 5,88
0,125	— 5,54	— 5,43	— 5,42	— 5,51
0,085	— 5,02	— 4,91	— 4,90	— 4,99
0,035	— 4,62	— 4,51	— 4,50	— 4,59
— 0,053	— 4,15	— 4,04	— 4,03	— 4,12
— 0,133	— 3,83	— 3,72	— 3,71	— 3,80
— 0,213	— 3,53	— 3,42	— 3,41	— 3,50
— 0,297	— 0,25	— 3,14	— 3,13	— 3,22
— 0,391	— 2,97	— 2,80	— 2,85	— 2,94
— 0,657	— 2,23	— 2,12	— 2,11	— 2,20

Tableau VII (log X).

log M^* / log L^*	0,140	0,125	0,085	0,035	— 0,053
— 1	— 5,02	— 4,83	— 4,56	— 4,37	— 4,08
— 2	— 5,04	— 4,85	— 4,59	— 4,40	— 4,15
— 3	— 4,90	— 4,71	— 4,46	— 4,28	— 4,05
— 5	— 4,52	— 4,33	— 4,09	— 3,94	— 3,72
— 5	— 3,88	— 3,69	— 3,46	— 3,32	— 3,13

Dans la partie supérieure du diagramme (p. 95), les courbes se raccordent à celles qui avaient déjà été calculées (34). Mais dans sa partie inférieure le diagramme est très différent.

On remarquera
que dans la partie supérieure, la luminosité croît quand la teneur en hydrogène décroît,
que dans la partie inférieure, la luminosité croît quand la teneur en hydrogène décroît,
que dans la partie médiane, la luminosité décroît quand la teneur en hydrogène décroît.

On sera particulièrement frappé de ce que pour les masses inférieures à $\odot$ et les luminosités inférieures à $-1{,}7\ L\odot$ environ, la courbe d'apparition de la dégénérescence de l'hydrogène semble une limite d'évolution. Il semble y avoir là une contradiction essentielle dans le modèle ainsi décrit, et qui n'est pas encore résolue.

10. Résultats généraux. Le tableau VIII contient l'ensemble des résultats relatifs aux 8 naines blanches marquées sur la figure 9, p. 95. On y trouve $\Delta R/R$, profondeur de la couche non dégénérée d'hydrogène, z/R, profondeur totale de la couche d'hydrogène, h/R hauteur de la couche de mélange.

Tableau VIII.

Etoile	log L	log M	log R	log X	$\Delta R/R$	T	h/R	z/R
A C 70°8247 ...	—1,67	0,12	—2,41	..	..	18,9	..	..
Sirius B	—1,6	—0,01	—2,11	—4,3	0,050	16,8	0,0067	..
O_2 Eri B	—2,1	—0,35	—1,8	—3,05	0,15	11,5	0,022	..
Ross 627	—3,00	0,11	—2,34	—4,6	..	..	..	..
Wolf 219	—3,28	0,13	—2,48	—4,7	..	..	..	..
V. M. 2.....	—3,4	0,125	—2,41	—4,57	0,0072	6,02	0,0014	0,031
Wolf 457.....	—3,96	0,13	—2,47	—4,4	..	..	..	..
Wolf 489.....	—4,16	—0,11	—1,98	—3,55	..	..	..	..

Conclusions.

11. Il semble bien que la théorie du débit d'énergie des naines blanches puisse se faire sans contradiction avec la physique nucléaire. Cependant, d'autres difficultés surgissent inévitablement.

a) Nous avons déjà signalé une difficulté relativement à l'évolution des naines blanches.

b) La couche d'hydrogène expliquant le débit d'énergie de Van Maanen 2, bien que mince, est cependant 20 fois plus épaisse que la couche de mélange. Il semble indispensable, si on veut expliquer la présence des raies métalliques dans l'atmosphère de Van Maanen 2 de modifier notre conception de la structure des naines blanches. En fait, il ne s'agit pas exactement d'une structure différente, mais d'une structure plus complexe, avec des couches convectives multiples dans les régions extérieures de Van Maanen 2. C'est ce que nous nous proposons d'étudier prochainement.

Appendice.

Valeurs de $d\log T / d\log P$ en fonction de la densité et de la température (Voir p. 47 et suivantes).

	log N_e								
θ	15	16	17	18	19	20	21	22	23
0.01	0.400	0.400	0.400	0.400	0.400	0.400	0.400	0.400	0.4
0.02	0.4	0.4	0.4	0.4	0.4	0.4	0.399	0.398	0.4
0.05	0.4	0.4	0.4	0.4	0.4	0.397	0.389	0.388	0.4
0.1	0.4	0.4	0.4	0.399	0.394	0.366	0.325	0.339	0.4
0.2	0.4	0.4	0.392	0.317	0.225	0.169	0.123	0.167	0.4

Institut d'Astrophysique de Paris et Observatoire de l'Université de Copenhague.

Bibliographie.

1. Bethe, Handbuch der Physik, **24**, 2.
2. Bethe and Crietchfield, Phys. Rev., **54**, 248, 1938.
3. Biermann, A. N., **263**, 185, 1937.
4. — **264**, 361, 1937.
5. Blackett, Nature, **159**, 658, 1947.
6. Chandrasekhar, M. N., **91**, 446, 1931.
7. — Stellar Structures.
8. — Ap. J., **101**, 328, 1945.
9. Chandrasekhar and Münch, A. J., **104**, 446, 1946.
10. Chapman, M. N., **77**, 539, 1917.
11. Chapman and Cowling, Mathematical Theory and non-uniform Gases, Chapitre 7.
12. — — M.T., Chapitre 14.
13. Critchfield, Ap. J., **96**, 1, 1942.
14. Eddington, Internal Constitution of the Stars.
15. Fermi, Zts. f. Phys., **36**, 383, 1926.
16. Fowler, Phil. Mag. **1**, 863, 1926.
17. Gibbs, Collected Papers, Thermodynamics, pp. 144, 171.
18. Holtsmark, Ann. d. Phys., **58**, 577, 1919.
19. Inglis and Teller, Ap. J., **90**, 439, 1939.
20. Kourganoff, Communication faite aimablement à l'auteur.
21. Kuiper, Ap. J., **88**, 429, 1938.
22. — White Dwarfs, Actualités scientiflques et Industrielles, 903, Hermann, Paris.
23. Lanczos, Zts. f. Phys., **68**, 204, 1931.
24. Milne, Proc. Camb. Phil. Soc., XXII, 493, 1924.
25. — M. N., **90**, 769, 1930.
26. Mrowka, Ann. d. Phys., **16**, 756, 1932.
27. Pannekoek, B. A. I. N., **19**, 1932.
28. — M. N., **98**, 694, 1938.
29. Rosseland, M. N., **84**, 729, 1924.
30. Rudkjøbing, Zts. f. Astr., **21**, 254, 1942.
21. — Festskrift til N. E. Nørlund, **1**, 161, Kbh. 1945.
32. — Annales d'Astrophysique, **9**, 17, 1946.
33. Russell and Stewart, Ap. J., **59**, 197, 1924.

34. Schatzman, Annales d'Astrophysique, **8**, 143, 1945.
35. — C. R., **222**, 479, 1946[1].
36. — Ann. d'Astr., **9**, 199, 1946.
37. — C. R., **224**, 31, 1947.
38. — C. R., **225**, 1060, 1474.
39. — Ann. d. Astr., **10**, 93, 1947.
40. — C. R., **225**, 867, 1947.
41. — Nature, **161**, 61, 1948.
42. — C. R., **226**, 67, 1948.
43. — Ap. J., **107**, 110, 1948[2].
44. — Journal de Physique et le Radium **IX**, 46, 1948.
45. — Ann. d'Astr. **10**, 341, 1947.
46. Stoner, Phil. Trans. Roy. Sos. A., **237**, 67, 1938.
47. Strömgren, Zs. f. Astr., **4**, 118, 1932.
48. — Publ. Kbhv. Observatorium. Nr. 138.
49. Unsöld, Zts. f. Astr., **1**, 138, 1931; **2**, 209, 1931.
50. — Phys. d. Sternatmosphären.
51. Verwej, Proc. K. Akad. Wetens. Amsterdam, **38**, 1935, No. 5.

[1] Cette note comporte à la fin des conclusions inexactes.

[2] Cette note comporte une petite erreur numérique qui ne change aucune des conclusions. Dans l'équation 7 p. 111, au lieu du coefficient $10^{2\cdot91}$, lire $10^{2\cdot41}$.

Indleveret til selskabet den 14. maj 1948.
Færdig fra trykkeriet den 13. januar 1950.

DET KGL. DANSKE VIDENSKABERNES SELSKAB
MATEMATISK-FYSISKE MEDDELELSER, BIND XXV, NR. 8

ON THE PROOFS OF THE FUNDAMENTAL THEOREM ON ALMOST PERIODIC FUNCTIONS

BY

BØRGE JESSEN

KØBENHAVN
I KOMMISSION HOS EJNAR MUNKSGAARD
1949

Printed in Denmark.
Bianco Lunos Bogtrykkeri

1. Introduction. The fundamental theorem of the theory of almost periodic functions states that any almost periodic function $f(x)$ with the Fourier series

$$f(x) \sim \sum a(\lambda)\, e^{i\lambda x}, \text{ where } a(\lambda) = M\{f(x)\, e^{-i\lambda x}\},$$

satisfies the Parseval equation

$$M\{|f(x)|^2\} = \Sigma |a(\lambda)|^2.$$

Many proofs of this theorem have been given. Among them the proof of Weyl [6] is, perhaps, the one which leads most directly to the goal. It depends on a systematic use of the process of convolution and on the methods of the theory of integral equations. Another proof, depending on the general theory of Fourier integrals, is due to Wiener [7]; it has been given a particularly simple form by Bochner [2, pp. 81—82].

Though these proofs give a clear insight in the whole theory, the more elementary proofs are not without interest. Among them the original proof of Bohr [3] is interesting by its crudeness. Its idea is to consider for every positive T the periodic function with the period T which coincides with $f(x)$ in the interval $(0, T)$, and to use Parseval's equation for this function. By making $T \to \infty$, one obtains the theorem. The passage to the limit is, however, of a complicated nature, and the whole proof is very long.

A considerable simplification was obtained by de la Vallée Poussin [5], who used the same idea together with the convolution process to prove the uniqueness theorem, which states that if $a(\lambda) = 0$ for all λ, then $f(x)$ vanishes identically. From this theorem Parseval's equation follows by a simple application of the convolution process. Since $f(x)$ vanishes identically if and

only if $M\{|f(x)|^2\} = 0$, the proof of the uniqueness theorem amounts to a proof of Parseval's equation in the particular case where $a(\lambda) = 0$ for all λ. A simplification of de la Vallée Poussins proof has been given by M. Riesz [4].

It seems very natural to base a proof of the fundamental theorem on almost periodic functions on the corresponding theorem on periodic functions. It must, however, be mentioned, that the periodic function with the period T which coincides with $f(x)$ in the interval $(0, T)$ will generally be discontinuous in the points nT, so that it is not a special case of the theorem on almost periodic functions, which is used. Moreover, the periodic functions will generally not approximate $f(x)$ outside the interval $(0, T)$.

The truth is that actually it complicates matters to introduce this periodic function. As will be shown in the following pages, the proofs take a simpler form if, instead of the Fourier series of the periodic function with the period T, we consider the Fourier integral of the function $f_T(x)$ which coincides with $f(x)$ in the interval $(0, T)$ and is 0 elsewhere. Naturally, for large T this Fourier integral does not differ much from the Fourier series of the periodic function.

All we shall need on Fourier integrals is, that if $F(x)$ is a function, which is continuous in a certain closed interval and is 0 outside this interval, and if

$$\int_{-\infty}^{\infty} F(x)\, e^{-i\lambda x}\, dx = A(\lambda),$$

then in analogy to Parseval's equation

$$\int_{-\infty}^{\infty} |F(x)|^2\, dx = \frac{1}{2\pi} \int_{-\infty}^{\infty} |A(\lambda)|^2\, d\lambda.$$

Thus our proofs are more elementary than the proof of Wiener referred to above, with which they have no connection.

Our proof of the Parseval equation follows step by step Bohr's proof. The main simplifications are in the beginning. In the later part a simplification in the exposition has been ob-

tained by the use of a function introduced by Wiener [7, p. 495], connected with Bochner's translation function [1, p. 136].

In our proof of the uniqueness theorem we use de la Vallée Poussin's main lemma, which actually concerns the Fourier integral of the function $f_T(x)$. The simplification is in the remainder of the proof, where we avoid the artifice of choosing T as a fine translation number.

2. Proof of the Parseval equation. The inequality obtained from Parseval's equation by replacing $=$ by $\geq$ being an easy consequence of Bessel's formula, it is sufficient to prove the inequality obtained by replacing $=$ by $\leq$.

For an arbitrary $T>0$ consider the function

$$\frac{1}{T}\int_0^T f(x)\, e^{-i\lambda x}\, dx = \frac{1}{T}\int_{-\infty}^{\infty} f_T(x)\, e^{-i\lambda x}\, dx = a_T(\lambda).$$

Then

$$\frac{1}{T}\int_0^T |f(x)|^2\, dx = \frac{1}{T}\int_{-\infty}^{\infty} |f_T(x)|^2\, dx = \frac{T}{2\pi}\int_{-\infty}^{\infty} |a_T(\lambda)|^2\, d\lambda.$$

It is therefore sufficient to prove:

To every $\delta > 0$ there exists a $T_0 > 0$ such that

$$\frac{T}{2\pi}\int_{-\infty}^{\infty} |a_T(\lambda)|^2\, d\lambda < \Sigma |a(\lambda)|^2 + \delta \quad \text{for} \quad T > T_0.$$

3. We begin by proving

Lemma 1. *To every λ_0 and every $\delta > 0$ correspond an $\omega > 0$ and a $T_0 > 0$ such that*

$$\frac{T}{2\pi}\int_{\lambda_0-\omega}^{\lambda_0+\omega} |a_T(\lambda)|^2\, d\lambda < |a(\lambda_0)|^2 + \delta \quad \text{for} \quad T > T_0.$$

Proof. If $f(x)$ is replaced by $f(x)\, e^{-i\lambda_0 x}$ the function $a_T(\lambda)$ is replaced by $a_T(\lambda+\lambda_0)$. It is therefore sufficient to consider the case $\lambda_0 = 0$.

(i) $a(0) = 0$, i. e. $M\{f(x)\} = 0$. — On placing for a given $c > 0$

$$\Phi(x) = \frac{1}{c}\int_x^{x+c} f_T(y)\,dy$$

we have by a simple computation

$$\frac{1}{T}\int_{-\infty}^{\infty} \Phi(x)\, e^{-i\lambda x}\,dx = a_T(\lambda)\,\frac{e^{i\lambda c}-1}{i\lambda c};$$

hence

$$\frac{1}{T}\int_{-\infty}^{\infty} |\Phi(x)|^2\,dx = \frac{T}{2\pi}\int_{-\infty}^{\infty} |a_T(\lambda)|^2 \left|\frac{e^{i\lambda c}-1}{i\lambda c}\right|^2 d\lambda.$$

Since $\frac{1}{c}\int_x^{x+c} f(y)\,dy$ converges uniformly in x towards $M\{f(x)\}$ as $c \to \infty$ there exists to every $\varepsilon > 0$ a $c = c(\varepsilon)$, such that when $T > c$ then $|\Phi(x)| \leq \varepsilon$ in the interval $(0,\ T-c)$. In the intervals $(-c,\ 0)$ and $(T-c,\ T)$ we have $|\Phi(x)| \leq G = \sup|f(x)|$. Outside the interval $(-c,\ T)$ we have $\Phi(x) = 0$. Hence

$$\frac{1}{T}\int_{-\infty}^{\infty} |\Phi(x)|^2\,dx \leq \varepsilon^2 + \frac{2\,c\,G^2}{T}$$

and consequently

$$\frac{T}{2\pi}\int_{-\infty}^{\infty} |a_T(\lambda)|^2 \left|\frac{e^{i\lambda c}-1}{i\lambda c}\right|^2 d\lambda \leq 2\,\varepsilon^2 \quad \text{for} \quad T > T_0 = \frac{2\,c\,G^2}{\varepsilon^2}.$$

For $|\lambda| <$ (some) $\omega = \omega(c)$ we have

$$\left|\frac{e^{i\lambda c}-1}{i\lambda c}\right| > \frac{1}{2}.$$

Hence

$$\frac{T}{2\pi}\int_{-\omega}^{\omega} |a_T(\lambda)|^2\,d\lambda \leq 4\cdot 2\,\varepsilon^2 = 8\,\varepsilon^2 \quad \text{for} \quad T > T_0.$$

(ii) $a(0) = a \neq 0$. — On placing $f(x) = a + h(x)$ we obtain a corresponding decomposition of $a_T(x)$ in two terms:

$$a_T(\lambda) = b_T(\lambda) + c_T(\lambda).$$

Hereby

$$\frac{1}{T}\int_0^T |a|^2\,dx = |a|^2 = \frac{T}{2\pi}\int_{-\infty}^{\infty} |b_T(\lambda)|^2\,d\lambda.$$

Hence by the triangle inequality we have for every $\omega > 0$

$$\left[\frac{T}{2\pi}\int_{-\omega}^{\omega} |a_T(\lambda)|^2\,d\lambda\right]^{\frac{1}{2}} \leqq |a| + \left[\frac{T}{2\pi}\int_{-\omega}^{\omega} |c_T(\lambda)|^2\,d\lambda\right]^{\frac{1}{2}}.$$

Let $\varepsilon > 0$ be chosen such that $(|a|+3\varepsilon)^2 < |a|^2 + \delta$, and next by (i), since $M\{h(x)\} = 0$, the numbers ω and T_0 such that

$$\frac{T}{2\pi}\int_{-\omega}^{\omega} |c_T(\lambda)|^2\,d\lambda < 9\varepsilon^2 \quad \text{for} \quad T > T_0.$$

Then

$$\frac{T}{2\pi}\int_{-\omega}^{\omega} |a_T(\lambda)|^2\,d\lambda \leqq |a|^2 + \delta \quad \text{for} \quad T > T_0.$$

4. On account of Lemma 1 it is, in order to prove the Parseval equation, sufficient to prove the following

Lemma 2. *To every $\delta > 0$ there exists a finite set of numbers $\lambda_1, \cdots, \lambda_M$ such that for every $\omega > 0$*

$$\frac{T}{2\pi}\int_{\substack{|\lambda-\lambda_1| \geqq \omega \\ \cdots \\ |\lambda-\lambda_M| \geqq \omega}} |a_T(\lambda)|^2\,d\lambda < \delta \quad \textit{for} \quad T > (\textit{some})\ T_0(\omega).$$

We shall reduce this lemma to a lemma on the translation function

$$e(\tau) = \sup_x |f(x+\tau) - f(x)|.$$

On placing for a given $\tau > 0$

$$\psi_\tau(x) = f_T(x+\tau) - f_T(x)$$

we have

$$\frac{1}{T}\int_{-\infty}^{\infty} \psi_\tau(x)\, e^{-i\lambda x}\,dx = a_T(\lambda)\,(e^{i\lambda\tau} - 1);$$

hence

$$\frac{1}{T}\int_{-\infty}^{\infty}|\psi_\tau(x)|^2\,dx = \frac{T}{2\pi}\int_{-\infty}^{\infty}|a_T(\lambda)|^2|e^{i\lambda\tau}-1|^2\,d\lambda.$$

Now $|\psi_\tau(x)| \leq e(\tau)$ if the points x and $x+\tau$ both lie in the interval $(0, T)$, and $|\psi_\tau(x)| \leq G$ if one of the points lie in $(0, T)$, whereas $\psi_\tau(x) = 0$ if both points lie outside $(0, T)$. Hence

$$\frac{1}{T}\int_{-\infty}^{\infty}|\psi_\tau(x)|^2\,dx \leq e(\tau)^2 + \frac{2\tau G^2}{T}$$

and consequently

$$\frac{T}{2\pi}\int_{-\infty}^{\infty}|a_T(\lambda)|^2|e^{i\lambda\tau}-1|^2\,d\lambda \leq 2\varepsilon^2 \quad \text{if} \quad e(\tau) \leq \varepsilon \quad \text{and} \quad T > \frac{2\tau G^2}{\varepsilon^2}.$$

On placing

$$\varphi(\tau) = \begin{cases} \varepsilon - e(\tau) & \text{when } e(\tau) \leq \varepsilon \\ 0 & \text{when } e(\tau) > \varepsilon \end{cases}$$

we therefore obtain for every $X > 0$

$$\frac{T}{2\pi}\int_{-\infty}^{\infty}|a_T(\lambda)|^2\left(\frac{1}{X}\int_0^X|e^{i\lambda\tau}-1|^2\varphi(\tau)\,d\tau\right)d\lambda \leq 2\varepsilon^2\frac{1}{X}\int_0^X\varphi(\tau)\,d\tau$$

$$\text{for} \quad T > \frac{2X G^2}{\varepsilon^2}.$$

In order to prove Lemma 2 it is therefore sufficient to prove

Lemma 3. *To every $\varepsilon > 0$ there exists a finite set of numbers $\lambda_1, \cdots, \lambda_M$ such that for every $\omega > 0$ there exists an $X > 0$ for which*

$$\frac{1}{X}\int_0^X|e^{i\lambda\tau}-1|^2\varphi(\tau)\,d\tau > \frac{1}{17}\frac{1}{X}\int_0^X\varphi(\tau)\,d\tau$$

when $|\lambda-\lambda_1| > \omega, \cdots, |\lambda-\lambda_M| \geq \omega$.

5. Translation numbers of $f(x)$ belonging to a given $\varrho > 0$, i. e. numbers τ for which $e(\tau) \leq \varrho$, will be denoted throughout by $\tau(\varrho)$. We shall first prove

Lemma 4. *For every $\varrho > 0$ the set S of numbers λ for which $|e^{i\lambda t} - 1| \leq 1$ for all $t = \tau(\varrho) > 0$ is finite.*

If S consist of the numbers $\lambda_1, \cdots, \lambda_M$, there exists to every $\omega > 0$ an $A > 0$, such that if $|\lambda - \lambda_1| \geq \omega, \cdots, |\lambda - \lambda_M| \geq \omega$, then $|e^{i\lambda t} - 1| > 1$ for some positive $t = \tau(\varrho) < A$.

Proof. By the uniform continuity of $f(x)$ there exists an $\eta > 0$ such that any positive $\tau < \eta$ is a $\tau(\varrho)$. Hence, if $|\lambda| > \pi/3\,\eta$ there exists a positive $t = \tau(\varrho) < \eta$ for which $|e^{i\lambda t} - 1| > 1$. Thus S belongs to the interval $|\lambda| \leq \pi/3\,\eta$.

If λ' and λ'' both belong to S, i. e. if $|\lambda' t| \leq \pi/3 \mod 2\pi$ and $|\lambda'' t| \leq \pi/3 \mod 2\pi$ for all $t = \tau(\varrho) > 0$, we have $|\lambda' - \lambda''|\, t \leq 2\pi/3 \mod 2\pi$ for all $t = \tau(\varrho) > 0$. In particular, the interval $2\pi/3\,|\lambda' - \lambda''| < t < 4\pi/3\,|\lambda' - \lambda''|$ of length $2\pi/3\,|\lambda' - \lambda''|$ will contain no $\tau(\varrho)$. Since every interval of a certain length $l = l(\varrho)$ contains a $\tau(\varrho)$, we obtain $|\lambda' - \lambda''| \geq 2\pi/3\,l$. Hence S is finite.

Let now $\omega > 0$ be chosen, and consider the closed bounded set of numbers λ for which $|\lambda - \lambda_1| \geq \omega, \cdots, |\lambda - \lambda_M| \geq \omega$, $|\lambda| \leq \pi/3\,\eta$. This set is covered by the open sets U_t defined by an inequality $|e^{i\lambda t} - 1| > 1$ for a $t = \tau(\varrho) > 0$. Hence, by Borel's theorem, it is covered by a finite number of these sets, say by $U_{t_1}, \cdots, U_{t_n}$. As number A may then be used any number larger than the numbers $\eta, t_1, \cdots, t_n$.

6. We now turn to the proof of Lemma 3.

The translation function $e(\tau)$ being almost periodic, so is the function $\varphi(\tau)$. Since $\varphi(\tau)$ is non-negative and not identically zero, we have

$$M\{\varphi(\tau)\} = m > 0.$$

In Lemma 4 let $\varrho = \frac{1}{2}\,m$. Then the lemma gives numbers $\lambda_1, \cdots, \lambda_M$ and, when $\omega > 0$ is chosen, a number $A > 0$.

If $|\lambda - \lambda_1| \geq \omega, \cdots, |\lambda - \lambda_M| \geq \omega$, there exists a positive $t = \tau(\varrho) < A$ such that $|e^{i\lambda t} - 1| > 1$. For $X > A$ we have

$$\frac{1}{X}\int_0^X |e^{i\lambda\tau} - 1|^2\,\varphi(\tau)\,d\tau \geq \frac{1}{2X}\int_0^{X-A} \left[|e^{i\lambda\tau} - 1|^2\,\varphi(\tau) + |e^{i\lambda(\tau+t)} - 1|^2\,\varphi(\tau+t)\right] d\tau.$$

Now, since $|\lambda t| > \pi/3 \mod 2\pi$, the relations $|\lambda\tau| \leq \pi/6 \mod 2\pi$ and $|\lambda(\tau + t)| \leq \pi/6 \mod 2\pi$ cannot be valid together, i. e. we have for every τ

$$\max\{|e^{i\lambda\tau}-1|^2, |e^{i\lambda(\tau+t)}-1|^2\} > |e^{i\pi/6}-1|^2 > \tfrac{1}{4}.$$

Moreover, since t is a $\tau(\varrho)$, we have $e(\tau+t) \leqq e(\tau)+\varrho$, and consequently

$$\varphi(\tau+t) \geqq \varphi(\tau)-\varrho.$$

Hence we obtain

$$\frac{1}{X}\int_0^X |e^{i\lambda\tau}-1|^2 \varphi(\tau)\, d\tau \geqq \frac{1}{2X}\int_0^{X-A} \tfrac{1}{4}[\varphi(\tau)-\varrho]\, d\tau.$$

Here the right hand side converges for $X\to\infty$ towards $\frac{1}{8}(m-\varrho) = \frac{1}{16}m$. The right hand side of the inequality in Lemma 3 converges for $X\to\infty$ towards $\frac{1}{17}m$. Hence the latter inequality is valid for some X and the proof is completed.

7. Proof of the uniqueness theorem. The main lemma in de la Vallée Poussin's proof states that when $a(\lambda) = 0$ for all λ, then $a_T(\lambda) \to 0$ uniformly in λ as $T\to\infty$. Starting from this lemma the proof may by completed as follows.

For a given $\varepsilon > 0$ let $T_0 > 0$ be chosen such that $|a_T(\lambda)| \leqq \varepsilon$ for all λ when $T > T_0$. For $U > T > T_0$ consider the function

$$g_{TU}(x) = \frac{1}{T}\int_{-\infty}^{\infty} f_U(x+t)\overline{f_T(t)}\, dt = \frac{1}{T}\int_0^T f_U(x+t)\overline{f(t)}\, dt.$$

Plainly, $g_{TU}(x)$ vanishes outside the interval $(-T, U)$ and coincides in the interval $(0, U-T)$ with the almost periodic function

$$g_T(x) = \frac{1}{T}\int_0^T f(x+t)\overline{f(t)}\, dt.$$

By a simple calculation

$$\int_{-\infty}^{\infty} g_{TU}(x)\, e^{-i\lambda x}\, dx = U a_U(\lambda)\overline{a_T(\lambda)}.$$

Hence

$$\frac{1}{U}\int_0^{U-T} |g_T(x)|^2\, dx \leqq \frac{1}{U}\int_{-\infty}^{\infty} |g_{TU}(x)|^2\, dx = \frac{U}{2\pi}\int_{-\infty}^{\infty} |a_U(\lambda)|^2 |a_T(\lambda)|^2\, d\lambda$$

$$\leqq \varepsilon^2 \frac{U}{2\pi}\int_{-\infty}^{\infty} |a_U(\lambda)|^2\, d\lambda = \varepsilon^2 \frac{1}{U}\int_0^U |f(x)|^2\, dx \leqq \varepsilon^2 G^2.$$

For $U \to \infty$ this gives

$$M\{|g_T(x)|^2\} \leqq \varepsilon^2 G^2.$$

For $T \to \infty$ the function $g_T(x)$ converges uniformly in x towards the convolution

$$g(x) = \underset{t}{M}\{f(x+t)\,\overline{f(t)}\}.$$

Hence

$$M\{|g(x)|^2\} \leqq \varepsilon^2 G^2.$$

Since this is true for all $\varepsilon > 0$, we have $M\{|g(x)|^2\} = 0$, which implies $g(x) \equiv 0$. In particular $g(0) = M\{|f(x)|^2\} = 0$, and hence $f(x) \equiv 0$.

8. Another variant of the proof of the uniqueness theorem. It may be remarked that a slight change in the above proof permits us to replace the use of Parseval's formula for Fourier integrals by Parseval's formula for periodic functions, which may be formulated as follows:

If $F(x)$ is continuous in a closed interval of length $\leqq P$ and is 0 outside this interval, and if

$$\int_{-\infty}^{\infty} F(x)\, e^{-i\lambda x}\, dx = A(\lambda),$$

then

$$\int_{-\infty}^{\infty} |F(x)|^2\, dx = \frac{1}{P} \sum_{n=-\infty}^{\infty} \left| A\left(\frac{2\pi}{P} n\right)\right|^2.$$

Applying this formula to the function $g_{TU}(x)$, which vanishes outside the interval $(-T, U)$, and using that $f_U(x)$ also vanishes outside this interval we obtain

$$\int_0^{U-T} |g_T(x)|^2\, dx \leqq \int_{-\infty}^{\infty} |g_{TU}(x)|^2\, dx = \frac{1}{T+U} \sum_{n=-\infty}^{\infty} U^2 \left| a_U\left(\frac{2\pi}{T+U} n\right)\right|^2 \left| a_T\left(\frac{2\pi}{T+U} n\right)\right|^2$$

$$\leqq \varepsilon^2 \frac{1}{T+U} \sum_{n=-\infty}^{\infty} U^2 \left| a_U\left(\frac{2\pi}{T+U} n\right)\right|^2 = \varepsilon^2 \int_{-\infty}^{\infty} |f_U(x)|^2\, dx \leqq \varepsilon^2 U G^2,$$

and the proof is completed as before.

References.

[1] S. Bochner. Beiträge zur Theorie der fastperiodischen Funktionen I. Math. Ann. 96 (1926), pp. 119—147.
[2] — Vorlesungen über Fouriersche Integrale. Leipzig 1932.
[3] H. Bohr. Zur Theorie der fastperiodischen Funktionen I. Acta math. 45 (1924), pp. 29—127.
[4] M. Riesz. Eine Bemerkung über den Eindeutigkeitssatz der Theorie der fastperiodischen Funktionen. Mat. Tidsskrift B 1934, pp. 11—13.
[5] C. de la Vallée Poussin. Sur les fonctions presque périodiques de H. Bohr. Ann. Soc. Sci. Bruxelles 47_2 (1927), pp. 141—158; 48_1 (1928), pp. 56—57.
[6] H. Weyl. Integralgleichungen und fastperiodische Funktionen. Math. Ann. 97 (1926), pp. 338—356.
[7] N. Wiener. The spectrum of an arbitrary function. Proc. London Math. Soc. (2) 27 (1928), pp. 483—496.

Indleveret til Selskabet den 29. november 1948.
Færdig fra trykkeriet den 30. Maj 1949.

DET KGL. DANSKE VIDENSKABERNES SELSKAB
MATEMATISK-FYSISKE MEDDELELSER, BIND XXV, NR. 9

ON THE UNIQUENESS OF THE POTENTIAL IN A SCHRÖDINGER EQUATION FOR A GIVEN ASYMPTOTIC PHASE

BY

N. LEVINSON

KØBENHAVN
I KOMMISSION HOS EJNAR MUNKSGAARD
1949

Printed in Denmark.
Bianco Lunos Bogtrykkeri.

1. The solution $y(x, \lambda)$ of the differential equation

$$y'' + (\lambda^2 - P(x))\, y = 0 \tag{1.0}$$

with initial values

$$y(0, \lambda) = 0, \quad y'(0, \lambda) = 1, \tag{1.1}$$

will, in case $P(x)$ is small enough for large x, and in case $\lambda = u \neq 0$ where u is real, satisfy

$$\lim_{x \to \infty} \left[y(x, u) - \frac{A(u)}{u} \sin(ux - \Phi(u)) \right] = 0 \tag{1.2}$$

where $A(u)$ and $\Phi(u)$ are continuous function of u, $0 < u < \infty$. The function $\Phi(u)$ is the asymptotic phase.

The problem of determining the potential $P(x)$ from $\Phi(u)$ arises in physics. Recently C. E. Fröberg, [1], has given various approximate procedures for calculating $P(x)$ from $\Phi(u)$ based on the variation of constants formula or on one or more iterations of this formula. He treats the equation $y'' - \frac{l(l+1)}{x^2} y + (\lambda^2 - (Px))\, y = 0$ where l is an integer. The equation (1.0) is the case $l = 0$. Fröberg observes that his method need not of course be convergent. Indeed the question arises as to whether $\Phi(u)$ determines $P(x)$ uniquely at all. We shall show that with suitable hypotheses this is indeed the case. We shall also see that $\Phi(u)$ determines $A(u)$ in (1.2) uniquely and conversely. The theory we shall develop for (1.0) can be carried over to more general cases. (See note on p. 27 for the case $l > 0$.)

Theorem I. *If $P(x)$ is piecewise continuous (or more generally if $P(x)$ is Lebesgue measurable), if*

(1.3) $$P(x) \geqq 0$$

and

(1.4) $$\int_0^\infty x\,|P(x)|\,dx < \infty\,,$$

then (1.2) *is valid where* $A(u)$ *and* $\Phi(u)$ *are continuous functions of* u. *There is no other potential function* $Q(x)$ *satisfying the same hypothesis as* $P(x)$ *with an identical phase function* $\Phi(u)$. *Moreover* $\Phi(u)$ *determines* $A(u)$ *uniquely and conversely.*

The condition (1.3) can be modified. However, without (1.3) it is possible for (1.0) to have discrete characteristic values $\lambda_k = iv_k$, $k = 1, 2, \cdots$, where the v_k are real. Associated with each $\lambda_k = iv_k$ there is exactly one characteristic function $y(x, \lambda_k)$ which for large x is $O(e^{-v_k x})$. If we assume

(1.5) $$\int_1^\infty x^2\,|P(x)|\,dx < \infty$$

in place of (1.3) then we shall find that there are at most a finite number of characteristic values, $\lambda_k = iv_k$, and with $v_k \neq 0$.

We shall see that under the hypothesis of Theorem II, if

$$\Phi(\infty) - \Phi(+0) < \pi,$$

then there are no discrete characteristic values. (In fact we shall find that we always have either $\Phi(\infty) = \Phi(+0) + m\pi$ or $\Phi(\infty) = \Phi(+0) + \left(m + \frac{1}{2}\right)\pi$ where m is the number of characteristic values in $v > 0$, i. e. with $\lambda^2 < 0$). We now have the following result.

Theorem II. *If* $P(x)$ *is real and measureable and if*

(1.6) $$\int_0^1 x\,|P(x)|\,dx + \int_1^\infty x^2\,|P(x)|\,dx < \infty$$

then (1.2) *is valid. If there are no discrete characteristic values, i. e., if* $\Phi(\infty) - \Phi(+0) < \pi$, *then there is no potential function* $Q(x)$ *different from* $P(x)$ *satisfying* (1.6) *and with the same phase function* $\Phi(u)$. *Moreover* $\Phi(u)$ *determines* $A(u)$ *uniquely and conversely.*

In case $P(x)$ satisfies

$$\int_0^1 |P(x)|\,dx < \infty \tag{1.7}$$

which is a stricter requirement at $x = 0$ than (1.4) or (1.6) it is possible to consider initial values of the form

$$y(0, \lambda) = \sin\alpha, \quad y'(0, \lambda) = \cos\alpha. \tag{1.8}$$

In this case we could dispense with some of the lemmas we require for Theorems I and II and use known results [2, § 5.3 and Chapter VI] in their place. The methods used here will carry over to cover (1.8) with the assumption (1.7). However, in practise the condition

$$\int_0^1 x\,|P(x)|\,dx < \infty$$

is much more useful than (1.7) and we shall carry out our proofs for this case.

We shall see in the course of our proof that the spectral representation of a function $f(x)$ involves the integral

$$\frac{1}{\pi}\int_{-\infty}^{\infty}\frac{u^2}{A^2(u)}\,y(x, u)\,du\int_0^{\infty} y(\xi, u)\,f(\xi)\,d\xi.$$

Thus we see that the weight function in this integral $u^2/A^2(u)$ determines $A(u)$, and therefore from theorems I and II also $\Phi(u)$. Thus the weight function $u^2/A^2(u)$ can arise from one $P(x)$ only.

In the course of our proof we shall also get the following relationship valid for any function $f(x)$ in $L^2(0, \infty)$,

$$\int_0^{\infty}|f(x)|^2\,dx = \frac{1}{\pi}\int_{-\infty}^{\infty}\frac{u^2}{A^2(u)}\,du\left|\int_0^{\infty} y(x, u)\,f(x)\,dx\right|^2. \tag{1.9}$$

We shall see that there is a function of $\lambda = u + iv$, $F(\lambda)$, analytic for $v > 0$ and continuous for $v \geqq 0$ such that for real

$\lambda = u$ we have $F(u) = A(u)\, e^{i\Phi(u)}$. We shall see that the behavior of $F(\lambda)$ as $\lambda \to 0$ is of concern to us and for this reason we need requirement (1.3) in Theorem I and

$$\int_1^\infty x^2 |P(x)|\, dx < \infty$$

in Theorem II.

2. Here we shall show that $\Phi(u)$ determines $A(u)$ and conversely under the hypothesis of Theorem I. Actually we shall use only (1.4) except to show that $F(0) \neq 0$ where we need (1.3). Thus most of § 2 will be available to us to prove Theorem II as well.

We shall require the following results. We shall use K to denote positive constants which depend on $P(x)$ only. We recall $\lambda = u + iv$.

Lemma 2.0. *If $P(x)$ satisfies* (1.4) *then there is a solution $y(x, \lambda)$ of* (1.0) *satisfying* (1.1) *which for any x is an entire function of λ and which for all λ satisfies*

$$|y(x, \lambda)| \leqq \frac{Kxe^{|v|x}}{1 + |\lambda| x}, \quad 0 \leqq x < \infty. \tag{2.0}$$

As $|\lambda| \to \infty$

$$y(x, \lambda) = \frac{\sin \lambda x}{\lambda} + o\left(\frac{e^{|v|x}}{|\lambda|}\right) \tag{2.1}$$

uniformly in x, $0 \leqq x < \infty$. Moreover $y(x, \lambda)$ is an even function of λ.

Lemma 2.1. *If $P(x)$ satisfies* (1.4) *then for $v \geqq 0$ there is a solution of* (1.0), *$y_1(x, \lambda)$ which for each x is an analytic function of λ for $v > 0$ and continuous for $v \geqq 0$ and satisfies*

$$|y_1(x, \lambda)| \leqq Ke^{-vx}, \quad 0 \leqq x < \infty \tag{2.2}$$

and

$$|y_1(x, \lambda) - e^{i\lambda x}| \leqq \frac{Ke^{-vx}}{|\lambda|} \int_x^\infty |P(\xi)|\, d\xi. \tag{2.3}$$

For $v \leqq 0$ there exists a function $y_2(x, \lambda)$ similarly related to $e^{-i\lambda x}$ for large x or $|\lambda|$.

We shall prove these lemmas in § 5. It is clear that for $\lambda = u$, $y_1(x, u)$ and $y_2(x, u)$ by (2.3) are independent solutions of (1.0) for large x. Since they are independent for large x, they are independent for all x, $0 \leqq x < \infty$. From (2.0) we have

$$|y(x, \lambda)| \leqq Kxe^{|v|x}. \tag{2.4}$$

We also have, as can be verified by substitution into (1.0), the "variation of constants" formula

$$y(x, \lambda) = \frac{\sin \lambda x}{\lambda} + \frac{1}{\lambda}\int_0^x \sin \lambda (x-\xi)\, P(\xi)\, y(\xi, \lambda)\, d\xi. \tag{2.5}$$

Here the right side exists because of (2.4). We see from (2.5), by use of (2.4), that for $\lambda = u \neq 0$ we have as $x \to \infty$

$$\begin{cases} y(x, u) = \dfrac{\sin ux}{u}\left(1 + \displaystyle\int_0^\infty \cos u\xi\, P(\xi)\, y(\xi, u)\, d\xi\right) \\ \qquad\qquad + \dfrac{\cos ux}{u}\displaystyle\int_0^\infty \sin u\xi\, P(\xi)\, y(\xi, u)\, d\xi + o(1). \end{cases} \tag{2.6}$$

Or as $x \to \infty$

$$y(x, u) = \frac{A(u)}{u} \sin (ux - \Phi(u)) + o(1)$$

where if

$$F(u) = 1 + \int_0^\infty e^{iu\xi}\, P(\xi)\, y(\xi, u)\, d\xi$$

then by (2.6)

$$A(u) = |F(u)|, \quad \Phi(u) = \arg F(u).$$

Since $y(x, u)$ is an even function of u, $A(u)$ is an even function. From (1.4) and (2.4) we see that

$$F(\lambda) = 1 + \int_0^\infty e^{i\lambda\xi}\, P(\xi)\, y(\xi, \lambda)\, d\xi \tag{2.7}$$

is an analytic function of λ for $v > 0$ and is continuous for $v \geqq 0$. The properties of $F(\lambda)$ are given in the following lemma.

Lemma 2.2. *If $P(x)$ is real and satisfies* (1.4) *then $F(\lambda)$ defined in* (2.7) *is analytic in the half-plane $v > 0$ and continuous for $v \geq 0$. In $v \geq 0$ it can vanish only for values of λ for which $u = 0$. If $\lambda_k = iv_k$, $v_k > 0$, is a root of $F(\lambda) = 0$ then $y(x, iv_k)$ is a characteristic solution of* (1.0) *satisfying, for some $C_k \neq 0$,*

$$y(x, iv_k) = C_k y_1(x, iv_k) \to 0 \text{ as } x \to \infty . \tag{2.8}$$

For large $|\lambda|$ we have

$$F(\lambda) = 1 + o(1) \tag{2.9}$$

uniformly for $0 \leq \arg \lambda \leq \pi$.

The proof of lemma 2.2 is given in § 5.

For $v > 0$ we have the following relationship for $e^{i\lambda x} y(x, \lambda)$ as $x \to \infty$. From (2.5) we have

$$\left\{ \begin{aligned} e^{i\lambda x} y(x, \lambda) &= e^{i\lambda x} \frac{\sin \lambda x}{\lambda} \\ &+ \frac{1}{\lambda} \int_0^x \sin \lambda (x - \xi)\, e^{i\lambda (x-\xi)} P(\xi)\, y(\xi, \lambda)\, e^{i\lambda \xi}\, d\xi . \end{aligned} \right.$$

Letting $x \to \infty$ and using (2.4) we get

$$\lim_{x \to \infty} e^{i\lambda x} y(x, \lambda) = -\frac{F(\lambda)}{2i\lambda} . \tag{2.10}$$

We shall now introduce the hypothesis $P(x) \geq 0$ and show that in this case $F(iv) \neq 0$ for $v \geq 0$. We have

$$F(iv) = 1 + \int_0^\infty e^{-v\xi} P(\xi)\, y(\xi, iv)\, d\xi . \tag{2.11}$$

Since $y'' = (v_1^2 + P)\, y$, $y(0, iv_1) = 0$ and $y'(0, iv_1) = 1$ we see that $y'' \geq 0$ and thus $y' \geq 1$ and $y \geq 0$. In (2.11) this yields $F(iv) \geq 1$.

Since $F(\lambda) \neq 0$ for $v \geq 0$ and since $F(\lambda) = 1 + o(1)$ as $|\lambda| \to \infty$ uniformly for $0 \leq \arg \lambda \leq \pi$, wee see that $g(\lambda) = \log F(\lambda)$ is analytic for $v > 0$ and continuous for $v \geq 0$ and moreover we can choose $g(\lambda)$ so that

$$g(\lambda) = o(1) \quad \text{as} \quad |\lambda| \to \infty \tag{2.12}$$

uniformly for $0 \leq \arg \lambda \leq \pi$. Applying Cauchy's theorem over a semi-circle of radius R with center at $\lambda = 0$ and diameter on the real axis and letting $R \to \infty$ we find by use of (2.12) that

$$g(\lambda) = \lim_{R \to \infty} \frac{1}{2\pi i} \int_{-R}^{R} \frac{g(\sigma)}{\sigma - \lambda} d\sigma \tag{2.13}$$

where σ is real and $\lambda = u + iv$, $v > 0$. In the same way if $\overline{\lambda} = u - iv$, $v > 0$ then

$$0 = \lim_{R \to \infty} \frac{1}{2\pi i} \int_{-R}^{R} \frac{g(\sigma)}{\sigma - \overline{\lambda}} d\sigma. \tag{2.14}$$

Taking the conjugate of the latter formula and adding to (2.13) we find

$$g(\lambda) = \lim_{R \to \infty} \frac{1}{\pi} \int_{-R}^{R} \frac{\operatorname{Im} g(\sigma)}{\sigma - \lambda} d\sigma.$$

Or since $\operatorname{Im} g(\sigma) = \Phi(\sigma)$

$$\log F(\lambda) = \lim_{R \to \infty} \frac{1}{\pi} \int_{-R}^{R} \frac{\Phi(\sigma)}{\sigma - \lambda} d\sigma. \tag{2.15}$$

Thus we see that $\Phi(u)$ determines $F(\lambda)$ and in particular then, $\Phi(u)$ determines

$$A(u) = \lim_{v \to +0} |F(u + iv)|.$$

We observe that $\Phi(u)$ is an odd function of u. By subtracting the conjugate of (2.14) from (2.13) and using the fact that $A(u)$ is even we get for $v > 0$

$$\log F(\lambda) = \frac{2\lambda}{\pi i} \int_{0}^{\infty} \frac{\log A(\sigma)}{\sigma^2 - \lambda^2} d\sigma.$$

Thus $A(u)$ determines $F(\lambda)$ and in particular then determines

$$\Phi(u) = \lim_{v \to +0} \operatorname{Im} \log F(u+iv).$$

3. We now assume that there is another differential equation with $P(x)$ replaced by $Q(x)$ where $Q(x)$ satisfies the same hypothesis as $P(x)$ in Theorem I and where the asymptotic phase is again $\Phi(u)$. The equation is

$$z'' + (\lambda^2 - Q(x))\, z = 0. \tag{3.0}$$

Since the asymptotic phase of $z(x, u)$ is $\Phi(u)$, its asymptotic amplitude is $A(u)/u$. Thus

$$z(x, u) = \frac{A(u)}{u} \sin(ux - \Phi(u)) + o(1) \tag{3.1}$$

as $x \to \infty$ where $z(0, u) = 0$ and $z'(0, u) = 1$. There are also two solutions of (3.0), $z_1(x, \lambda)$ and $z_2(x, \lambda)$ satisfying the same conditions as y_1 and y_2 in Lemma 2.1.

Returning to $y(x, u)$ where $u \neq 0$ we have since y_1 and y_2 are independent solutions.

$$y(x, u) = C_1(u)\, y_1(x, u) + C_2(u)\, y_2(x, u).$$

Letting $x \to \infty$ we have

$$\frac{A(u)}{u} \sin(ux - \Phi(u)) = C_1(u)\, e^{iux} + C_2(u)\, e^{-iux} + o(1).$$

From this we see that indeed the term $o(1)$ is zero and that

$$C_1(u) = \frac{A(u)\, e^{-i\Phi(u)}}{2iu}, \quad C_2(u) = -\frac{A(u)\, e^{i\Phi(u)}}{2iu}.$$

Thus

$$y(x, u) = \frac{A(u)}{2iu}\left[y_1(x, u)\, e^{-i\Phi(u)} - y_2(x,u)\, e^{i\Phi(u)}\right]. \tag{3.2}$$

In exactly the same way we see that (3.1) implies

$$z(x, u) = \frac{A(u)}{2iu}\left[z_1(x, u)\, e^{-i\Phi(u)} - z_2(x, u)\, e^{i\Phi(u)}\right]. \tag{3.3}$$

Let $f(x)$ be a real differentiable function which vanishes for

x near zero and for large x. Let $\max(|f(x)|+|f'(x)|) = M$. (These requirements on $f(x)$ are somewhat more severe than is actually necessary for our argument.) We now consider the following pseudo-Green's function integrals of $f(x)$,

$$(3.4)\qquad \begin{cases} H_1(x,\lambda) = \dfrac{\lambda}{F(\lambda)}\, y(x,\lambda)\displaystyle\int_x^\infty z_1(\xi,\lambda)\, f(\xi)\, d\xi \\ H_2(x,\lambda) = \dfrac{\lambda}{F(\lambda)}\, z_1(x,\lambda)\displaystyle\int_0^x y(\xi,\lambda)\, f(\xi)\, d\xi. \end{cases}$$

Clearly for each x, $H_j, j = 1, 2$, is analytic in λ in the upper half-plane $v > 0$ and continuous for $v \geqq 0$. Thus if c is the semi-circle of radius R, $\lambda = Re^{i\theta}$, $0 \leqq \theta \leqq \pi$, then for any x, $0 < x < \infty$, Cauchy's theorem yields

$$(3.5)\qquad \int_c H_j(x,\lambda)\, d\lambda + \int_{-R}^{R} H_j(x,u)\, du = 0.$$

Let $\delta > 0$ and let

$$J_1 = \int_x^\infty z_1(\xi,\lambda)\, f(\xi)\, d\xi = \left(\int_x^{x+\delta} + \int_{x+\delta}^\infty\right) z_1(\xi,\lambda)\, f(\xi)\, d\xi.$$

Using (2.3) we get since $\displaystyle\int_x^\infty |P(\xi)|\, d\xi \leqq \int_x^\infty \xi\, |P(\xi)|\, d\xi/x$,

$$\left| J_1 - \int_x^{x+\delta} e^{i\lambda\xi} f(\xi)\, d\xi \right| \leqq \frac{Ke^{-vx}}{|\lambda| x} \int_x^{x+\delta} |f(\xi)|\, d\xi + \frac{KMe^{-(x+\delta)v}}{|\lambda|}\left(1 + \frac{1}{x}\right).$$

Integrating by parts we have

$$\left| \int_x^{x+\delta} e^{i\lambda\xi} f(\xi)\, d\xi + \frac{e^{i\lambda x} f(x)}{i\lambda} \right| \leqq \frac{M\delta e^{-vx}}{|\lambda|} + \frac{Me^{-(x+\delta)v}}{|\lambda|}.$$

Thus

$$(3.6)\qquad \left| J_1 + \frac{e^{i\lambda x} f(x)}{i\lambda} \right| \leqq \frac{KMe^{-vx}}{|\lambda|}\left(\delta + e^{-\delta v}\right)\left(1 + \frac{1}{x}\right).$$

Therefore for large $|\lambda| = R$, using (2.1) (2.9) and (3.6)

$$\left| \int_c \frac{\lambda\, y(x,\lambda)}{F(\lambda)}\, d\lambda \int_x^\infty z_1(\xi,\lambda)\, f(\xi)\, d\xi + \frac{f(x)}{i} \int_c \frac{y(x,\lambda)\, e^{i\lambda x}}{F(\lambda)}\, d\lambda \right|$$
$$\leqq KM\left(\delta + \frac{1}{R\delta}\right)\left(1 + \frac{1}{x}\right).$$

If $\delta = R^{-1/2}$ we have uniformly in x for any closed interval of x interior to the open interval $(0, \infty)$,

$$\lim_{R\to\infty} \int_c \frac{\lambda\, y(x,\lambda)}{F(\lambda)}\, d\lambda \int_x^\infty z_1(\xi,\lambda)\, f(\xi)\, d\xi = -\frac{1}{2}\pi i f(x).$$

Using this in (3.5) with $j = 1$ we have

$$(3.7) \qquad f(x) = \frac{2}{\pi i} \lim_{R\to\infty} \int_{-R}^{R} \frac{u\, y(x,u)}{F(u)}\, du \int_x^\infty z_1(\xi,u)\, f(\xi)\, d\xi.$$

We also have the following result.

Lemma 3.0. *For any* $x > 0$,

$$\frac{\lambda z_1(x,\lambda)}{F(\lambda)} \int_0^x y(\xi,\lambda)\, f(\xi)\, d\xi = -\frac{f(x)}{2\lambda} + J_2(x,\lambda)$$

where uniformly for any closed interval of x *interior to the open interval* $(0, \infty)$

$$\lim_{R\to\infty} \int_c |J_2(x,\lambda)|\, |d\lambda| = 0.$$

The proof of this lemma is given in § 5.

Using Lemma 3.0 we have

$$(3.8) \qquad \lim_{R\to\infty} \int_c \frac{\lambda z_1(x,\lambda)}{F(\lambda)}\, d\lambda \int_0^x y(\xi,\lambda)\, f(\xi)\, d\xi = -\frac{1}{2}\pi i f(x).$$

Using (3.8) in (3.5) with $j = 2$ we have

$$(3.9) \qquad f(x) = \frac{2}{\pi i} \lim_{R\to\infty} \int_{-R}^{R} \frac{u z_1(x,u)}{F(u)}\, du \int_0^x y(\xi,u)\, f(\xi)\, d\xi.$$

Since $\bar{z}_1(x, u)$ is a solution of (3.0), $\bar{z}_1(x, u) = C_1 z_1(x, u) + C_2 z_2(x, u)$. Letting $x \to \infty$ we see that $\bar{z}_1(x, u) = z_2(x, u)$. Taking the conjugate of (3.7) and (3.9) we have therefore

$$(3.10)\quad f(x) = -\frac{2}{\pi i} \lim_{R\to\infty} \int_{-R}^{R} \frac{u y(x, u)}{\overline{F}(u)}\, du \int_x^\infty z_2(\xi, u) f(\xi)\, d\xi,$$

$$(3.11)\quad f(x) = -\frac{2}{\pi i} \lim_{R\to\infty} \int_{-R}^{R} \frac{u z_2(x, u)}{\overline{F}(u)}\, du \int_0^x y(\xi, u) f(\xi)\, d\xi.$$

Since by (3.3)

$$z(x, u) = \frac{A^2(u)}{2iu}\left(\frac{z_1(x, u}{F(u)} - \frac{z_2(x, u)}{\overline{F}(u)}\right)$$

we have by adding (3.7) and (3.10)

$$(3.12)\quad f(x) = \lim_{R\to\infty} \frac{2}{\pi} \int_{-R}^{R} \frac{u^2 y(x, u)}{A^2(u)}\, du \int_x^\infty z(\xi, u) f(\xi)\, d\xi.$$

In the same way (3.9) and (3.11) give

$$(3.13)\quad f(x) = \lim_{R\to\infty} \frac{2}{\pi} \int_{-R}^{R} \frac{u^2 z(x, u)}{A^2(u)}\, du \int_0^x y(\xi, u) f(\xi)\, d\xi.$$

Interchanging the role of y and z we get instead of (3.12)

$$f(x) = \lim_{R\to\infty} \frac{2}{\pi} \int_{-R}^{R} \frac{u^2 z(x, u)}{A^2(u)}\, du \int_x^\infty y(\xi, u) f(\xi)\, d\xi.$$

Combining the above with (3.13) we have

$$(3.14)\quad f(x) = \lim_{R\to\infty} \frac{1}{\pi} \int_{-R}^{R} \frac{u^2 du}{A^2(u)} z(x, u) \int_0^\infty y(\xi, u) f(\xi)\, d\xi.$$

Since the convergence above is uniform except near $x = 0$ and $x = \infty$ where $f(x)$ vanishes we have

$$(3.15)\quad \int_0^\infty f^2(x)\, dx = \lim_{R\to\infty} \frac{1}{\pi} \int_{-R}^{R} \frac{u^2 du}{A^2(u)} \int_0^\infty z(x, u) f(x)\, dx \int_0^\infty y(\xi, u) f(\xi)\, d\xi.$$

The derivation of (3.15) is certainly valid if z is replaced by y. Thus

$$(3.16) \qquad \int_0^\infty f^2(x)\,dx = \lim_{R\to\infty} \frac{1}{\pi} \int_{-R}^{R} \frac{u^2 du}{A^2(u)} \left(\int_0^\infty y(x,u) f(x)\,dx \right)^2$$

and the corresponding result with y replaced by z. Combining we get

$$\frac{1}{\pi} \int_{-\infty}^{\infty} \frac{u^2}{A^2(u)}\,du \left(\int_0^\infty y(x,u) f(x)\,dx - \int_0^\infty z(x,u) f(x)\,dx \right)^2 = 0.$$

Thus

$$(3.17) \qquad \int_0^\infty y(x,u) f(x)\,dx = \int_0^\infty z(x,u) f(x)\,dx.$$

For any fixed u let us suppose $z(x,u) \neq y(x,u)$ at $x = x_1 > 0$. Let us suppose then that $y(x_1,u) - z(x_1,u) > 0$ for some u. Since $y(x,u)$ and $z(x,u)$ are differentiable they are continuous and we must have for small $\delta > 0$, where $x_1 - \delta > 0$,

$$y(x,u) - z(x,u) > 0, \quad |x - x_1| \leqq \delta.$$

Choose $f(x) > 0$ for $|x - x_1| < \delta$ and $f(x) = 0$ for $|x - x_1| \geqq \delta$. Then clearly for the value of u in question

$$\int_0^\infty [y(x,u) - z(x,u)] f(x)\,dx > 0$$

which contradicts (3.17). The same argument applies of course if $z - y > 0$ and we see then that $y(x,u) = z(x,u)$. Therefore from the differential equations for y and z we get

$$(3.18) \qquad y(x,u)\,[P(x) - Q(x)] = 0.$$

(In case $P(x)$ or $Q(x)$ are discontinuous (3.18) holds almost everywhere.) Since $y(x,u)$ vanishes only for isolated values of x and since xP and xQ are integrable we have $P(x) = Q(x)$ almost everywhere which proves Theorem I.

4. Here we no longer assume $P(x) \geqq 0$ but rather that $\int_1^\infty x^2 |P(x)|\,dx < \infty$ and proceed to prove Theorem II. Lemma 2.2

is valid but the argument in § 2 which follows it can of course no longer be used. Now we shall show that either $F(0) \neq 0$ or else that near $\lambda = 0$ and for $v \geqq 0$

$$F(\lambda) = \alpha\lambda + o(|\lambda|) \text{ where } \alpha \neq 0. \tag{4.0}$$

Since $F(\lambda) \to 1$ for large $|\lambda|$ and is analytic for $v > 0$ and since the zeros of $F(\lambda)$ all lie on the line $u = 0$ we see that *either* $F(0) \neq 0$ *or* (4.0) *implies that there are at most a finite number of zeros of* $F(\lambda)$ *in the upper half-plane.*

With $F(0) = 0$ we also have

$$F(\lambda) = \int_0^\infty e^{i\lambda x} y(\lambda, x) P(x)\, dx - \int_0^\infty y(x, 0) P(x)\, dx. \tag{4.1}$$

Thus

$$\begin{cases} F(\lambda) = \int_0^\infty (e^{i\lambda x} - 1) y(x, 0) P(x)\, dx \\ \qquad + \int_0^\infty e^{i\lambda x} [y(x, \lambda) - y(x, 0)] P(x)\, dx = I_1 + I_2. \end{cases} \tag{4.2}$$

Here

$$I_1 = \int_0^\infty (e^{i\lambda x} - 1) y(x, 0) P(x)\, dx \tag{4.3}$$

and I_2 represents the second integral in (4.2). We have from (1.0) when $F(0) = 0$

$$y'(x, 0) = 1 + \int_0^x P(\xi) y(\xi, 0)\, d\xi = -\int_x^\infty P(\xi) y(\xi, 0)\, d\xi. \tag{4.4}$$

Or since by Lemma 2.2, $|y(x, 0)| \leqq Kx$,

$$|y'(x, 0)| \leqq K \int_x^\infty \xi |P(\xi)|\, d\xi.$$

Thus

$$\int_1^\infty |y'(x, 0)|\, dx \leqq K \int_1^\infty dx \int_x^\infty \xi |P(\xi)|\, d\xi = K \int_1^\infty \xi^2 |P(\xi)|\, d\xi < \infty.$$

From this we see that

$$|y(x, 0)| < K. \tag{4.5}$$

From (4.3)

$$\left| I_1 - i\lambda \int_0^\infty x\, y(x,0)\, P(x)\, dx \right|$$

$$\leqq \int_0^\infty | e^{i\lambda x} - 1 - i\lambda x \,|\, | y(x,0)\, P(x) |\, dx$$

$$\leqq |\lambda|^2 \int_0^{1/|\lambda|} x^2 |\, y(x,0)\, P(x) |\, dx + 3|\lambda| \int_{1/|\lambda|}^\infty x |\, y(x,0)\, P(x) |\, du,$$

wherein the last integral above we use $|e^{i\lambda x} - 1| \leqq 2$ for $v \geqq 0$ and $2 \leqq 2|\lambda| x$ for $x \geqq 1/|\lambda|$. Using (4.5) we see that as $|\lambda| \to 0$

$$I_1 - i\lambda \int_0^\infty xy(x,0)\, P(x)\, dx = o(|\lambda|). \tag{4.6}$$

Now we shall show

$$\int_0^\infty xy(x,0)\, P(x)\, dx \neq 0. \tag{4.7}$$

We have from (4.4)

$$y(x,0) = x + \int_0^x (x-\xi)\, P(\xi)\, y(\xi,0)\, d\xi. \tag{4.8}$$

If (4.7) is false and if $F(0) = 0$ then (4.8) becomes

$$y(x,0) = -x \int_x^\infty P(\xi)\, y(\xi,0)\, d\xi + \int_x^\infty \xi\, P(\xi)\, y(\xi,0)\, d\xi. \tag{4.9}$$

Let $x_1 > 1$ be large enough so

$$\int_{x_1}^\infty \xi\, |P(\xi)|\, d\xi < \frac{1}{4}.$$

Let $\max\limits_{x \geqq x_1} |y(x,0)| = m$. Then by (4.9)

$$m \leqq 2 \int_{x_1}^\infty \xi\, |P(\xi)\, y(\xi,0)|\, d\xi \leqq \frac{1}{2} m.$$

Thus $m = 0$ which is impossible and we see then that (4.7) holds. Thus from (4.6) we have as $\lambda \to 0$

$$I_1 = \alpha\lambda + o(|\lambda|) \text{ where } \alpha \neq 0. \tag{4.10}$$

We show next that $I_2 = o(|\lambda|)$ as $\lambda \to 0$. We have

$$I_2 = \int_0^\infty e^{i\lambda x} [y(x,\lambda) - y(x,0)]\, P(x)\, dx. \tag{4.11}$$

As solutions of

$$y'' - P(x)\,y = 0 \tag{4.12}$$

we have $y_3(x) = y(x, 0)$ and an independent solution $y_4(x)$ chosen so that $y_3 y_4' - y_4 y_3' = 1$. Since by (4.4), $y_3(x) - x \to 0$ as $x \to 0$ we see that a solution of (4.12) independent of y_3 is

$$y(x) = y_3(x) \int_x^{\cdot} \frac{d\xi}{y_3^2(\xi)}$$

and this is bounded as $x \to 0$. Thus y_4 is bounded as $x \to 0$. We have obviously also

$$y_4(x) = y_4(x_1) + (x - x_1)\,y_4'(x_1) + \int_{x_1}^{x} (x - \xi)\,P(\xi)\,y_4(\xi)\,d\xi.$$

If $\max_{x_1 \leqq x \leqq x_2} \left| \frac{y_4(x)}{x} \right| = m$ and if x_1 is chosen as below (4.9) then clearly for large x_2

$$m \leqq |y_4(x_1)| + |y_4'(x_1)| + m \int_{x_1}^{\infty} \xi\,|P(\xi)|\,d\xi.$$

Thus

$$\frac{3}{4} m \leqq |y_4'(x_1)| + |y_4(x_1)|$$

and we see that $|y_4(x)| \leqq Kx$ for large x. Now if

$$y'' - P(x)\,y = f(x)$$

then

$$y(x) = c_1 y_3(x) + c_2 y_4(x) - \int_0^{x} [y_3(x)\,y_4(\xi) - y_4(x)\,y_3(\xi)]\,f(\xi)\,d\xi.$$

Thus from

$$y''(x, \lambda) - P(x)\,y(x, \lambda) = -\lambda^2 y(x, \lambda)$$

we have

$$y(x, \lambda) = y_3(x) + \lambda^2 \int_0^{x} [y_3(x)\,y_4(\xi) - y_4(x)\,y_3(\xi)]\,y(\xi, \lambda)\,d\xi.$$

Thus

$$I_2 = \lambda^2 \int_0^{\infty} e^{i\lambda x} P(x)\,dx \int_0^{x} [y_3(x)\,y_4(\xi) - y_4(x)\,y_3(\xi)]\,y(\xi, \lambda)\,d\xi.$$

Or

$$|I_2| \leqq K|\lambda|^2 \int_0^\infty x|P(x)|\,dx \int_0^x |y(\xi,\lambda)|\,e^{-vx}\,d\xi.$$

Using Lemma 2.0 we have

$$|I_2| \leqq K|\lambda|^2 \int_0^\infty x|P(x)|\,dx \int_0^x \frac{\xi}{1+|\lambda|\xi}\,d\xi.$$

Thus

$$|I_2| \leqq K|\lambda|^2 \int_0^{1/|\lambda|} x|P(x)|\,dx \int_0^x \xi\,d\xi$$

$$+K|\lambda|^2 \int_{1/|\lambda|}^\infty x|P(x)|\,dx \left(\int_0^{1/|\lambda|} \xi\,d\xi + \int_{1/|\lambda|}^x \frac{d\xi}{|\lambda|} \right)$$

$$\leqq K|\lambda|^2 \int_0^{1/|\lambda|} x^3|P(x)|\,dx + K\int_{1/|\lambda|}^\infty x|P(x)|\,dx + K|\lambda| \int_{1/|\lambda|}^\infty x^2|P(x)|\,dx$$

$$\leqq K|\lambda|^{3/2} \int_0^{1/|\lambda|^{1/2}} x^2|P(x)|\,dx + K|\lambda| \int_{1/|\lambda|^{1/2}}^{1/|\lambda|} x^2|P(x)|\,dx$$

$$+2K|\lambda| \int_{1/|\lambda|}^\infty x^2|P(x)|\,dx.$$

Since $\int_0^\infty x^2|P(x)|\,dx < \infty$ we have then as $|\lambda| \to 0$

$$I_2 = o(|\lambda|).$$

Thus we have demonstrated (4.0).

Exactly as in § 2 we find that if $F(0) \neq 0$ then the formula

$$\log F(\lambda) = \lim_{R\to\infty} \frac{1}{\pi} \int_R^{-R} \frac{\Phi(\sigma)}{\sigma - \lambda}\,d\sigma$$

is valid as are the other formulae. In this case we have, since $F(\lambda) \to 1$, as $|\lambda| \to \infty$, that the total number of zeros of $F(\lambda)$

in $v > 0$ is given by $(\Phi(\infty) - \Phi(-\infty))/2\pi = (\Phi(\infty) - \Phi(0))/\pi$. Since $\Phi(+0) = \Phi(0)$ here we see that if $\Phi(\infty) - \Phi(+0) < \pi$ the total number of zeros must be zero and in fact that $\Phi(\infty) = \Phi(0)$. Since $\Phi(\infty)$ can be taken as zero we see that $\Phi(0) = 0$ and thus if $F(0) \neq 0$, $F(0) > 0$. If $F(0) = 0$, then we can work with a contour containing a small semi-circle, γ, with center at $\lambda = 0$ and radius ϱ. On γ, $\lambda = \varrho e^{i\theta}$, $0 \leqq \theta \leqq \pi$. Thus as in (2.13) $g(\lambda) = \log F(\lambda)$ is given by

$$g(\lambda) = \lim_{R \to \infty} \frac{1}{2\pi i} \left(\int_{-R}^{-\varrho} + \int_{\varrho}^{R} \right) \frac{g(\sigma)}{\sigma - \lambda} d\sigma + \frac{1}{2\pi i} \int_{\gamma} \frac{g(\sigma)}{\sigma - \lambda} d\sigma.$$

Since $g(\lambda) = \log \frac{F(\lambda)}{\lambda} + \log \lambda$ near $\lambda = 0$ we find on letting $\varrho \to 0$ that since $\frac{F(\lambda)}{\lambda} \to \alpha \neq 0$ we have

$$g(\lambda) = \lim_{R \to \infty} \frac{1}{2\pi i} \int_{-R}^{R} \frac{g(\sigma)}{\sigma - \lambda} d\sigma$$

from which all the other formulas relating F, A and Φ follow. Here we find that $\Phi(+0) - \Phi(-0) = -\pi$ and that the total number of zeros m of $F(\lambda)$ in $v > 0$ is given by

$$m = \frac{1}{2\pi} (\Phi(\infty) - \Phi(+0) + \Phi(-0) - \Phi(-\infty)) - \frac{1}{2}.$$

Since $\Phi(\infty) - \Phi(+0) = \Phi(-0) - \Phi(-\infty)$ we have $m = \frac{1}{\pi}(\Phi(\infty) - \Phi(+0)) - \frac{1}{2}$. Since $\Phi(\infty) - \Phi(+0) < \pi$ we see that $m = 0$. In fact here we must have $\Phi(\infty) = \Phi(+0) + \frac{1}{2}\pi$. Since we take $\Phi(\infty) = 0$ we have $\Phi(+0) = -\frac{1}{2}\pi$. Also $\Phi(-0) = \frac{1}{2}\pi$ and as in the other case $\Phi(u)$ is an odd function. The results of § 3 carry over without change thus establishing Theorem II.

5. Here we prove a number of lemmas. In all these lemmas we shall require only that

$$(5.0) \qquad \int_0^\infty x\,|P(x)|\,dx < \infty .$$

In the proofs of Lemmas 2.0 and 2.1 the formulas are written for the case $\lambda \neq 0$. In case $\lambda = 0$ the changes involved are obvious.

Proof of Lemma 2.0. Consider the sequence $y_n(x, \lambda)$ where $y_0(x, \lambda) = 0$ and

$$(5.1) \quad y_n(x, \lambda) = \frac{\sin \lambda x}{\lambda} + \frac{1}{\lambda}\int_0^x \sin \lambda (x-\xi)\, P(\xi)\, y_{n-1}(\xi, \lambda)\, d\xi .$$

We have if $\lambda = u + iv$, for $v \geq 0$

$$(5.2) \quad |y_1(x, \lambda) - y_0(x, \lambda)| = \left|\frac{\sin \lambda x}{\lambda}\right| = x e^{vx} \left|\frac{1 - e^{2i\lambda x}}{\lambda x}\right| .$$

Thus

$$(5.3) \qquad |y_1 - y_0| = \left|\frac{\sin \lambda x}{\lambda}\right| \leq 4\, x e^{|v|x}$$

and this is true for all λ. Using this in (5.1) we get

$$|y_2 - y_1| \leq \int_0^x \left|\frac{\sin \lambda (x-\xi)}{\lambda}\right| |P(\xi)|\, 4\, \xi e^{|v|\xi}\, d\xi .$$

Much as we found (5.3) we have

$$(5.4) \qquad \left|\frac{\sin \lambda (x-\xi)}{\lambda}\right| \leq 4\, x e^{|v|(x-\xi)}, \quad 0 \leq \xi \leq x .$$

Thus

$$|y_2 - y_1| \leq 4^2 x e^{|v|x} \int_0^x \xi\, |P(\xi)|\, d\xi .$$

If we set

$$B(x) = \int_0^x \xi\, |P(\xi)|\, d\xi < \int_0^\infty x\, |P(x)|\, dx$$

then

$$|y_2 - y_1| \leq 4^2 x e^{|v|x} B(x) .$$

Again from (5.1) we have

$$|y_3 - y_2| \leq 4^3 x e^{|v|x} \int_0^x \xi\, |P(\xi)|\, B(\xi)\, d\xi = 4^3 x e^{|v|x} \frac{(B(x))^2}{2!} .$$

Proceeding we have

$$|y_n - y_{n-1}| \leqq 4^n x e^{|v|x} \frac{(B(x))^{n-1}}{(n-1)!}.$$

Thus in any finite range of x and finite region of λ, $y_n(x, \lambda)$ converges uniformly to a limit $y(x, \lambda)$ which is therefore analytic in λ and by (5.1) satisfies

$$(5.5) \quad y(x, \lambda) = \frac{\sin \lambda x}{\lambda} + \frac{1}{\lambda} \int_0^x \sin \lambda (x - \xi) P(\xi) y(\xi, \lambda) d\xi.$$

From (5.5) we see easily that $y(x, \lambda)$ is a solution of (1.0) and satisfies

$$y(0, \lambda) = 0, \quad y'(0, \lambda) = 1.$$

Let

$$(5.6) \qquad M(x, \lambda) = \frac{1}{x} |y(x, \lambda)| (1 + |\lambda| x) e^{-|v|x}.$$

From (5.2) we have easily by considering separately $|\lambda x| \leqq 1$ and $|\lambda x| > 1$,

$$\left| \frac{\sin \lambda x}{\lambda} \right| \leqq \frac{8 x e^{|v|x}}{1 + |\lambda| x}.$$

Using this in (5.5) we have

$$\frac{x M(x, \lambda) e^{|v|x}}{1 + |\lambda| x} \leqq \frac{8 x e^{|v|x}}{1 + |\lambda| x} + 8 \int_0^x \frac{(x - \xi) e^{|v|(x-\xi)}}{1 + |\lambda| (x - \xi)} |P(\xi)| \frac{M(\xi, \lambda) \xi e^{|v|\xi}}{1 + |\lambda| \xi} d\xi.$$

Or

$$M(x, \lambda) \leqq 8 + 8 \int_0^x \xi |P(\xi)| M(\xi, \lambda) d\xi.$$

By a well known inequality this implies

$$M(x, \lambda) \leqq 8 \exp \left(8 \int_0^x \xi |P(\xi)| d\xi \right).$$

Using (5.0) we have $M(x, \lambda) \leqq K$. With (5.6) this gives

$$(5.7) \qquad |y(x, \lambda)| \leqq \frac{K x e^{|v|x}}{1 + |\lambda| x}.$$

In (5.5) this gives

$$\left| y(x,\lambda) - \frac{\sin \lambda x}{\lambda} \right| \leq \frac{K e^{|v|x}}{|\lambda|} \int_0^x \frac{|\xi|}{1+|\lambda|\xi} |P(\xi)|\, d\xi$$

$$\leq \frac{K e^{|v|x}}{|\lambda|} \left(\int_0^{1/|\lambda|^{1/2}} \xi |P(\xi)|\, d\xi + \frac{1}{|\lambda|^{1/2}} \int_{1/|\lambda|^{1/2}}^{\infty} \xi |P(\xi)|\, d\xi \right).$$

Thus as $|\lambda| \to \infty$

$$y(x,\lambda) = \frac{\sin \lambda x}{\lambda} + o\left(\frac{e^{|v|x}}{|\lambda|} \right).$$

That $y(x,\lambda)$ is an even function of λ is clear from the fact that each $y_n(x,\lambda)$ is even. The completes the proof of the lemma.

Proof of Lemma 2.1. Let $W_0(x,\lambda) = 0$ and let

$$(5.8)\quad W_n(x,\lambda) = e^{i\lambda x} - \frac{1}{\lambda} \int_x^{\infty} \sin \lambda (x-\xi)\, P(\xi)\, W_{n-1}(\xi,\lambda)\, d\xi.$$

From (5.3) for $v \geq 0$

$$\left| \frac{\sin \lambda (x-\xi)}{\lambda} \right| \leq 4 (\xi - x)\, e^{v(\xi - x)}, \quad \xi \geq x.$$

Clearly $|W_1 - W_0| \leq e^{-vx}$ and

$$|W_2(x,\lambda) - W_1(x,y)| \leq 4 \int_x^{\infty} (\xi - x)\, e^{v(\xi-x)} |P(\xi)|\, e^{-v\xi}\, d\xi$$

$$\leq 4\, e^{-vx} \int_x^{\infty} \xi |P(\xi)|\, d\xi.$$

If

$$B(x) = \int_x^{\infty} \xi |P(\xi)\, d\xi$$

then

$$|W_2 - W_1| \leq 4\, e^{-vx} B(x).$$

Again

$$|W_3 - W_2| 4^2 e^{-vx} \int_x^{\infty} \xi |P(\xi)|\, B(\xi)\, d\xi$$

$$= 4^2 e^{-vx} \frac{(B(x))^2}{2!} \leq 4^2 e^{-vx} \frac{(B(o))^2}{2!}$$

etc. Thus $W_n(x,\lambda)$ converges uniformly for $v \geq 0$ and $0 \leq x < \infty$ to a limit we denote by $y_1(x,\lambda)$. Clearly

$$|y_1(x,\lambda)| \leqq Ke^{-vx}$$

and from (5.8)

$$(5.9)\quad y_1(x,\lambda) = e^{i\lambda x} - \frac{1}{\lambda}\int_x^\infty \sin\lambda(x-\xi)\,P(\xi)\,y_1(\xi,\lambda)\,d\xi.$$

From this we have

$$(5.10)\quad |y_1(x,\lambda) - e^{i\lambda x}| \leqq \frac{Ke^{-vx}}{|\lambda|}\int_x^\infty |P(\xi)|\,d\xi.$$

This proves the lemma.

Proof of Lemma 2.2. That

$$F(\lambda) = 1 + \int_0^\infty e^{i\lambda x}\,y(x,\lambda)\,P(x)\,dx$$

is analytic for $v>0$ and continuous for $v \geqq 0$ follows from Lemma 2.0 and (5.0). That $F(\lambda) = 1 + o(1)$ uniformly in $v \geqq 0$ as $|\lambda| \to \infty$ follows from use of

$$\left|\begin{array}{l} |F(\lambda)-1| \leqq K\displaystyle\int_0^\infty \frac{\xi}{1+|\lambda|\xi}|P(\xi)|\,d\xi \\ \leqq K\displaystyle\int_0^{1/|\lambda|^{1/2}} \xi|P(\xi)|\,d\xi + \frac{K}{|\lambda|^{1/2}}\int_{1/|\lambda|^{1/2}}^\infty \xi|P(\xi)|\,d\xi. \end{array}\right.$$

For real $\lambda = u \neq 0$ we have as in (3.2)

$$y(x,u) = \frac{A(u)}{2iu}\left[y_1(x,u)\,e^{-i\Phi(u)} - y_2(x,u)\,e^{i\Phi u}\right].$$

If $F(u) = 0$ then $A(u) = 0$ and $y(x,u) = 0$ which is impossible. Thus $F(u) \neq 0$ for $u \neq 0$.

Let $F(\lambda)$ vanish for some $\lambda_1 = u_1 + iv_1$, $v_1 > 0$. For large x

$$y_3(x,\lambda_1) = -2i\lambda_1\,y_1(x,\lambda_1)\int_x^\infty \frac{d\xi}{y_1^2(\xi,\lambda_1)}$$

is a solution of (1.0). Since $y_1(x,\lambda_1) \sim e^{i\lambda_1 x}$ we have

$$y_3(x,\lambda_1) \sim e^{-i\lambda_1 x}$$

as $x \to \infty$. Moreover from (5.9) we also get

$$y_1'(x, \lambda) \sim i\lambda_1 e^{i\lambda_1 x}. \tag{5.11}$$

Since y_1 and y_3 are obviously independent

$$y(x, \lambda_1) = c_1 y_1(x, \lambda_1) + c_2 y_3(x, \lambda_1).$$

If $F(\lambda_1) = 0$ we see from (2.10) that we must have $c_2 = 0$. Thus

$$y(x, \lambda_1) = c_1 y_1(x, \lambda_1) \sim c_1 e^{i\lambda_1 x} \tag{5.12}$$

and from (5.11)

$$y'(x, \lambda_1) \sim ic_1\lambda_1 e^{i\lambda_1 x}. \tag{5.13}$$

Using a familiar argument we have that the conjugate of $y(x, \lambda_1)$, $\bar{y}(x, \lambda_1)$ is a solution of (1.0) with λ_1 replaced by $\bar{\lambda}_1 = u_1 - iv_1$. Thus

$$\begin{cases} y(x, \lambda_1)\,\bar{y}'(x, \lambda_1) - \bar{y}(x, \lambda_1)\,y'(x, \lambda_1) \\ \quad + (\bar{\lambda}_1^2 - \lambda_1^2) \int_0^x |y(x, \lambda_1)|^2\, dx = 0. \end{cases}$$

Letting $x \to \infty$ and using (5.12) and (5.13) we have

$$(\bar{\lambda}_1^2 - \lambda_1^2) \int_0^\infty |y(x, \lambda_1)|^2\, dx = 0.$$

Thus $u_1 = 0$ and $\lambda_1 = iv_1$ if $F(\lambda_1) = 0$. This completes the proof of the lemma.

We prove finally

Lemma 3.0. We have by (5.5)

$$\begin{cases} J = \dfrac{\lambda z_1(x, \lambda)}{F(\lambda)} \int_0^x y(\xi, \lambda) f(\xi)\, d\xi = \dfrac{z_1(x, \lambda)}{F(\lambda)} \int_0^x \sin\lambda\xi\, f(\xi)\, d\xi \\ \quad + \dfrac{z_1(x, \lambda)}{F(\lambda)} \int_0^x f(\xi)\, d\xi \int_0^\xi \sin\lambda(\xi - s)\, P(s)\, y(s, \lambda)\, ds = I_1 + I_2. \end{cases} \tag{5.14}$$

Clearly on integrating by parts

$$I_1 = \frac{z_1(x, \lambda)}{F(\lambda)} \left[-f(x) \frac{\cos\lambda x}{\lambda} + \frac{1}{\lambda} \int_0^x \cos\lambda\xi\, f'(\xi)\, d\xi \right].$$

Thus for large $|\lambda|$ and $v \geqq 0$ using (2.2) and (2.9)

$$\left| I_1 + \frac{z_1(x,\lambda) f(x) \cos \lambda x}{\lambda F(\lambda)} \right| \leqq \frac{K e^{-\delta v}}{|\lambda|} \int_0^{x-\delta} |f'(\xi)\, d\xi| + \frac{KM\delta}{|\lambda|}$$

where we recall $M = \max (|f(x)| + |f'(x)|)$. Or by (5.10) and the above inequality for large $|\lambda|$

$$\left\{ \begin{aligned} \left| I_1 + \frac{1}{2\lambda} f(x) \right| &\leqq \left| I_1 + \frac{1}{2\lambda F(\lambda)} f(x) \right| + \left| \frac{f(x)(F(\lambda)-1)}{2\lambda F(\lambda)} \right| \\ &\leqq \frac{KMx e^{-\delta v}}{|\lambda|} + \frac{KM\delta}{|\lambda|} + \left| \frac{f(x)(F(\lambda)-1)}{2\lambda F(\lambda)} \right| + \frac{M e^{-2vx}}{|\lambda|} \\ &\quad + \frac{KM}{|\lambda|^2} \int_0^\infty |P(\xi)\, d\xi. \end{aligned} \right. \tag{5.15}$$

For I_2 we have inverting the order of integration

$$I_2 = \frac{z_1(x,\lambda)}{F(\lambda)} \int_0^x y(s,\lambda) P(s) D(x,s,\lambda)\, ds \tag{5.16}$$

where

$$D = \int_s^x f(\xi) \sin \lambda (\xi - s)\, d\xi.$$

Integrating by parts we find

$$D = -\frac{\cos \lambda (x-s)}{\lambda} f(x) + \frac{f(s)}{\lambda} + \frac{1}{\lambda} \int_s^x \cos \lambda (\xi - s) f'(\xi)\, d\xi.$$

Thus for large $|\lambda|$

$$|D| \leqq \frac{4 M e^{v(x-s)} (x+1)}{|\lambda|}.$$

Therefore

$$|I_2| \leqq \frac{MK(x+1)}{|\lambda|} \int_0^x \frac{s}{1+|\lambda| s} |P(s)|\, ds.$$

We have easily since $|\lambda| = R$ on c

$$\int_c |I_2|\, |d\lambda| \leqq MK(x+1)\pi \int_0^x \frac{s}{1+Rs} |P(s)|\, ds.$$

Thus as $R \to \infty$

$$\int_c |I_2||d\lambda| \to 0 \tag{5.17}$$

uniformly in x over any finite interval of x. From (5.15) we also have easily for $x > 0$ that as $|\lambda| = R \to \infty$

$$\int_c \left| I_1 - \frac{f(x)}{2\lambda} \right| |d\lambda| \to 0, \tag{5.18}$$

providing we take $\delta = R^{-1/2}$, uniformly in x over any closed interval in x interior to the open interval $(0, \infty)$. But (5.17) and (5.18) complete the proof of Lemma 3.0.

In the introduction we remarked that Plancherel's theorem (1.9) holds for $f(x) \varepsilon L^2(0, \infty)$. In (3.16) we proved it for a restricted class. It is easy to exploit (3.16) to show that for any $f(x) \varepsilon L^2(0, \infty)$

$$g(u) = \underset{a \to \infty}{\text{l. i. m.}} \frac{u}{A(u)} \int_0^a f(x)\, y(x, u)\, dx$$

must exist and that

$$\int_0^\infty (g(u))^2\, du = \int_0^\infty (f(x))^2\, dx.$$

In case (1.0) has discrete characteristic values it is still the case that $\Phi(u)$ determines $F(\lambda)$. Indeed it can be shown that the zeros of $F(\lambda)$ which as we have seen occur at characteristic values $\lambda_k = i\nu_k$ are all simple. If the characteristic values are known then clearly

$$G(\lambda) = F(\lambda) \prod_{k=1}^{m} \left(\frac{1 + \dfrac{\lambda}{i\nu_k}}{1 - \dfrac{\lambda}{i\nu_k}} \right)$$

is free of zeros for $v > 0$ and thus $\log G(\lambda)$ is analytic. Moreover $|G(u)| = |F(u)|$ and

$$\arg G(u) = \arg F(u) + \sum_{k=1}^{m} \arg \left(\frac{1 + \dfrac{u}{i\nu_k}}{1 - \dfrac{u}{i\nu_k}} \right)$$

Thus $G(\lambda)$ can be found and therefore also $F(\lambda)$.

Added March 9, 1949.

The method used in proving Theorem I carries over to the equation

$$y'' + \left(u^2 - \frac{l(l+1)}{x^2} - P(x)\right) y = 0 \tag{1}$$

where l is a positive integer and $P(x)$ satisfies (1.4). Indeed if $j_l(x) = \left(\frac{\pi x}{2}\right)^{\frac{1}{2}} J_{l+\frac{1}{2}}(x)$ where $J_{l+\frac{1}{2}}(x)$ is the Bessel function then (1) has a solution $y(x, u)$ which satisfies

$$\lim_{x \to +0} \frac{y(x, u)}{j_l(x)} = 1. \tag{2}$$

(We recall that except for a constant $j_l(x)$ acts like x^{l+1} as $x \to 0$.) Moreover for any $u > 0$,

$$y(x, u) - \frac{A(u)}{u^{l+1}} \sin\left(ux - \frac{1}{2} l\pi - \Phi(u)\right) \to 0 \tag{3}$$

as $x \to \infty$. *It is indeed the case that* $\Phi(u)$ *determines* $P(x)$ *uniquely if*

$$\frac{l(l+1)}{x^2} + P(x) \geqq 0 \tag{4}$$

(and as already stated if (1.4) is satisfied). (The condition (4) has considerably wider possibilities in application than the special case $l = 0$.)

To indicate the modifications necessary for the case $l > 0$ we introduce

$$h_l(x) = \left(\frac{\pi x}{2}\right)^{\frac{1}{2}} H^{(1)}_{l+\frac{1}{2}}(x) = e^{i\left(x - \frac{1}{2} l\pi - \frac{1}{2}\pi\right)} \left[1 - \frac{l(l+1)}{2ix} + \cdots\right]$$

where $H^{(1)}_{l+\frac{1}{2}}(x)$ is a Hankel function. Clearly $h_l(ux)$ is a solution of (1) with $P \equiv 0$ as is $h_l(-ux)$. We also have

$$j_l(x) = \frac{1}{2}\left[h_l(x) - (-1)^l h_l(-x)\right]$$

and

$$k_l(x) = \frac{1}{2i}[h_l(x) + (-1)^l h_l(-x)]$$

from which it follows that

$$j_l(x) + ik_l(x) = h_l(x).$$

If

$$\begin{cases} g(x, \xi, \lambda) = j_l(\lambda\xi)\, k_l(\lambda\xi) - j_l(\lambda\xi)\, k_l(\lambda x) \\ = \dfrac{(-1)^l}{2i}[h_l(\lambda x)\, h_l(-\lambda\xi) - h_l(-\lambda x)\, h_l(\lambda\xi)], \end{cases}$$

then the "variation of constants" formula (2.5) becomes

$$(5) \qquad y(x, \lambda) = \frac{j_l(\lambda x)}{\lambda^{l+1}} - \frac{1}{\lambda}\int_0^x g(x, \xi, \lambda)\, P(\xi)\, y(\xi, \lambda)\, d\xi.$$

It is easy to show that, with $\lambda = u + iv$, and $v \geqq 0$

$$|j_l(\lambda x)| \leqq Ke^{vx}\frac{|\lambda x|^{l+1}}{(1+|\lambda x|)^{l+1}}, \quad x \leqq 0,$$

for some constant K, and also for $x \geqq \xi \geqq 0$

$$|g(x, \xi, \lambda)| \leqq Ke^{v(x-\xi)}\frac{(1+|\lambda\xi|)^l}{|\lambda\xi|^l}\frac{|\lambda x|^{l+1}}{(1+|\lambda x|)^{l+1}}.$$

Using these we get from (5) the analogue of Lemma (2.0) including (3). Here we also find for $v \geqq 0$ as a generalization of (2.7)

$$F(\lambda) = 1 - i\int_0^\infty \lambda^l y(\xi, \lambda)\, P(\xi)\, h_l(\lambda\xi)\, d\xi$$

where $A(u) = |F(u)|$ and $\Phi(u) = \arg F(u)$. Instead of (5.9) we have

$$y_1(x, \lambda) = h_l(\lambda x) + \frac{1}{\lambda}\int_x^\infty g(x, \xi, \lambda)\, P(\xi)\, y_1(\xi, \lambda)\, d\xi.$$

These indications suffice to show the changes in going from the case of Theorem I ($l = 0$) to the general case.

Added in proof: An analogue of Theorem II for $l > 0$ also holds. Interesting examples of cases where the phase does not

determine the potential (owing to the presence of discrete characteristic values, i. e. bound states) have been given by V. BARGMANN (Phys. Rev. 75 (1949) p. 301).

(This paper was written while the author was a JOHN SIMON GUGGENHEIM Memorial Fellow on leave from the Massachusetts Institute of Technology.)

Literature.

[1] FRÖBERG, C. E. Calculation of the potential from the asymptotic phase, Arkiv för Mat. Astr. och Fysik, Band 34 A, No. 28, Band 36 A, No. 11, 1948.

[2] TITCHMARSH, E. C. Eigenfunction Expansions associated with Second Order Differential Equations, Oxford 1946.

Indleveret til selskabet den 10. december 1948.
Færdig fra trykkeriet den 5. maj 1949.

DET KGL. DANSKE VIDENSKABERNES SELSKAB
MATEMATISK-FYSISKE MEDDELELSER, BIND XXV, NR. 10

EINLEITUNG IN DIE ALLGEMEINE KONGRUENZLEHRE

VON

JOHANNES HJELMSLEV

SECHSTE MITTEILUNG

KØBENHAVN
I KOMMISSION HOS EJNAR MUNKSGAARD
1949

Printed in Denmark.
Bianco Lunos Bogtrykkeri.

§ 1. Einleitung.

1. Diese sechste Mitteilung soll die allgemeine Kongruenzlehre der offenen Ebene, ohne Eindeutigkeitsaxiom und ohne Anordnungsaxiome, weiterführen.[1]

In der fünften Mitteilung wurde gezeigt, dass die Hauptsätze der euklidischen Geometrie unabhängig vom Eindeutigkeitsaxiom bestehen. In der vorliegenden Arbeit soll das entsprechende Resultat für die nicht-euklidischen Geometrien mittels einer axiomatischen Transformation erzielt werden.

Wir erinnern an das Axiomsystem wie wir es ursprünglich (Einl. I und III) aufgestellt haben (das allgemeine Axiomsystem der offenen Ebene):

I. Es gibt Punkte. Es gibt Punktmengen, welche gerade Linien (Geraden) heissen. Es gibt Transformationen, welche Bewegungen heissen. Jede Bewegung ist eine Zuordnung, bei welcher jeder Geraden und jedem auf ihr gelegenen Punkte eine Gerade und ein auf ihr gelegener Punkt umkehrbar eindeutig entspricht. Die Umkehrung einer Bewegung ist auch eine Bewegung. Die Bewegungen bilden eine Gruppe. Zwei Figuren, die durch eine Bewegung auseinander abgeleitet werden können, sollen kongruent heissen.

II. Ausser der Identität gibt es eine und nur eine Bewegung, welche alle Punkte einer geraden Linie fest lässt. Diese Bewegung heisst Spiegelung an der geraden Linie. Die Linie wird als Achse der Spiegelung bezeichnet. Jede Gerade ist die Achse einer Spiegelung. Jeder Punkt ausserhalb der Achse geht bei der Spiegelung in einen von ihm verschiedenen Punkt über.

[1] Die früher veröffentlichten Mitteilungen:
Erste Mitt. Math.-fys. Medd. VIII, 11, 1929; Zweite Mitt. ibd. X, 1, 1929; Dritte Mitt. ibd. XIX, 12, 1942; Vierte Mitt. ibd. XXII, 6, 1945; Fünfte Mitt. ibd. XXII, 13, 1945 sollen als Einl. I—V zitiert werden.

III. Eine Gerade b heisst senkrecht zu einer von ihr verschiedenen Geraden a (in Zeichen: $b \perp a$), wenn b bei der Spiegelung an a (Spiegelung a) in sich selbst übergeht. Durch jeden Punkt geht eine und nur eine Gerade b, die senkrecht zu einer gegebenen Geraden a ist; die beiden Geraden a, b haben stets einen und nur einen Punkt gemein.

IV. Wenn zwei Punkte A, B auf einer Geraden l liegen, so haben sie immer eine Spiegelungsachse m derart, dass A und B bei der Spiegelung m mit einander vertauscht werden, während l in sich selbst übergeführt wird ($l \perp m$). Diese Spiegelungsachse schneidet l in einem Punkt M, welcher als Mittelpunkt von A und B (oder von AB) auf l bezeichnet wird.

V. Zwei kongruente Punktreihen $ABC \cdots$ und $AB'C' \cdots$ auf einer oder auf zwei Geraden, mit dem gemeinsamen Punkt A, können immer durch eine Spiegelung ineinander übergeführt werden.

VI. Es gibt zwei zueinander senkrechte kongruente Geraden.

Was VI anbetrifft, verweisen wir auf die Bemerkungen in Einl. III, S. 4—7.

§ 2. Bemerkungen zum obenstehenden Axiomsystem.

2. A. Bei den meisten Anwendungen wird man durchweg voraussetzen, dass je zwei Geraden kongruent sind, d. h. dass jede Gerade in eine beliebige andere Gerade durch eine Bewegung übergehen kann, und dann spielt natürlich das Axiom VI keine Rolle.

Es dürfte aber in dieser Hinsicht Interesse haben, das folgende Beispiel einer endlichen Geometrie, wo alle Axiome I—VI gültig sind, die letztere Bedingung, dass je zwei Geraden kongruent sind, aber nicht erfüllt ist, in Erinnerung zu bringen[1]:

Unsere Geometrie umfasst 9 Punkte: $A, B, C, D, E, F, G, H, I$, welche der Anschaulichkeit halber in dem beistehenden quadratischen Schema (Fig. 1) aufgestellt sind.

Es gibt 12 Geraden, jede Gerade mit 3 Punkten:

I. 3 »waagerechte« Geraden ABC, DEF, GHI;

II. 3 »lotrechte« Geraden ADG, BEH, CFI;

[1] Dieses Beispiel einer endlichen Geometrie ist wie ich glaube zum ersten mal von T. Brodén (2. skand. Matematikerkongres 1911, S. 133) angegeben worden.

III. 3 »rechts abwärts gehende« Geraden *DHC, AEI, BFG*;

IV. 3 »links abwärts gehende« Geraden *BDI, CEG, FHA*,

Jede Gerade der Gruppe I ist senkrecht zu jeder Geraden der Gruppe II; ebenso jede Gerade der Gruppe III zu jeder Geraden der Gruppe IV. Es ergibt sich dann von selbst, was man unter Spiegelung zu verstehen hat, und es ist leicht zu sehen, dass alle Axiome I—VI erfüllt sind. Es gibt aber keine Bewegung, welche eine »waagerechte« Linie in eine »schräge Linie« überführt.

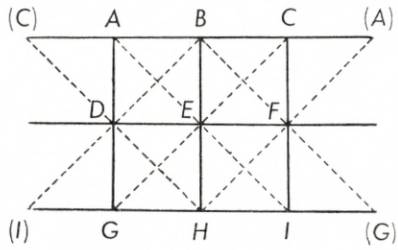

Fig. 1.

B. Unser Axiomsystem enthält keine Aussagen über die Bestimmung einer Geraden durch zwei Punkte. Wir haben früher (Einl. I, III) gelegentlich die Möglichkeit in Betracht gezogen, dass zwei Punkte ausnahmsweise keine Verbindungsgerade haben. Im folgenden soll aber diese Möglichkeit ausgeschlossen werden. Mit anderen Worten: Wir wollen stets voraussetzen, dass zwei Punkte wenigstens eine Verbindungsgerade haben.

Wir erinnern an die früher eingeführten Bezeichnungen:

Nachbarpunkte *A, B* sind zwei Punkte mit mehreren Verbindungsgeraden. Das System der beiden Punkte soll als singulärer Abstand *AB* bezeichnet werden.

Fernpunkte *A, B* sind Punkte mit einer einzigen Verbindungsgeraden. Das System der beiden Fernpunkte soll als ordinärer Abstand bezeichnet werden.

Schmieggeraden *a, b* sind zwei Geraden mit mehreren gemeinsamen Punkten. Das Geradensystem *a, b* bezeichnen wir als singulären Winkel (*a, b*).

Kreuzgeraden *a, b* sind Geraden mit einem einzigen gemeinsamen Punkt. Sie bilden einen ordinären Winkel (*a, b*).

Ferner wird auch gelegentlich von Nachbarpunkten einer Geraden (d. h. Nachbarpunkten eines Punktes dieser Geraden) gesprochen. Ebenso von Fernpunkten einer Geraden.

Ferngeraden heissen zwei Geraden, wenn alle Punkte der einen Geraden Fernpunkte der anderen Geraden sind, Nachbargeraden, wenn jeder Punkt der einen Geraden Nachbarpunkt der anderen Geraden ist.

Ein Winkel (a, b) soll fast-recht heissen, wenn das Lot von a in einem gemeinsamen Punkt der beiden Geraden Schmieggerade von b ist.

Um geläufige Ausdrücke der Elementargeometrie verwenden zu können, sprechen wir von einem Dreieck ABC mit den Seitengeraden a, b, c, wo a durch B und C, b durch C und A, c durch A und B gehen, und mit den Winkeln (b, c), (c, a), (a, b) im oben angegebenen Sinne.

Ist das Dreieck rechtwinklig $(a \perp b)$, so bezeichnen wir die Abstände AC und BC als Katheten, den Abstand AB als Hypotenuse.

C. Bei Anwendungen, wo es naturgemäss erscheint, die traditionellen Ordnungsregeln für die Punkte einer geraden Linie anzunehmen, lassen sich viele unserer Untersuchungen sehr anschaulich gestalten, wenn diese Ordnungsregeln zum allgemeinen Axiomsystem I—VI hinzugefügt werden. In der so definierten Geometrie, welche wir dann als graphische Geometrie (im weitesten Sinne) bezeichnen werden, soll dann die folgende Aussage gelten:

Je zwei Punkte A, B bestimmen eindeutig eine Strecke AB. Diese Strecke soll (wie der Abstand AB) ordinär heissen, wenn die Verbindungsgerade AB eindeutig bestimmt ist. In anderen Fällen nennen wir die Strecke singulär; die Strecke ist dann in allen Verbindungsgeraden von A und B enthalten.

In dieser Geometrie ist z. B. unmittelbar ersichtlich, dass eine Gerade l, welche durch den Schnittpunkt von zwei zueinander senkrechten Geraden (oder von zwei beliebigen Kreuzgeraden) a, b geht und Schmieggerade von einer von diesen ist, die andere eindeutig schneiden muss.

Ebenso leicht zeigt sich die folgende Tatsache. Wenn drei Geraden durch denselben Punkt gehen und eine von diesen Schmieggerade der beiden anderen ist, so sind diese letzteren Schmieggeraden voneinander.

Wenn aber die Ordnungsregeln nicht zur Verfügung stehen, lassen sich die erörterten Tatsachen in der hier vorgelegten Form nicht beweisen.

D. Die wichtigsten der früher bewiesenen einleitenden allgemeinen Sätze (Einl. I, 10—29) sollen hier zusammengestellt werden:

1°. Die Aufeinanderfolge abc von drei Spiegelungen, deren Achsen a, b, c durch denselben Punkt O gehen, kann durch eine

einzige Spiegelung ersetzt werden. Die Achse dieser Spiegelung geht durch O.

2°. Zwei zueinander senkrechte Geraden a, b durch den Punkt O bestimmen eine involutorische Bewegung ab, welche jede Gerade c durch O in sich überführt. Diese Bewegung soll als Punktspiegelung O bezeichnet werden. Sie lässt keinen von O verschiedenen Punkt fest.

3°. Die Aufeinanderfolge von 3 Spiegelungen, deren Achsen a, b, c senkrecht zu einer Geraden l sind, lässt sich durch eine einzige Spiegelung ersetzen, deren Achse ebenfalls senkrecht auf l steht.

4°. Die Aufeinanderfolge ABC von drei Punktspiegelungen an Punkten A, B, C einer Geraden l kann durch eine einzige Punktspiegelung an einem Punkt derselben Geraden ersetzt werden.

5°. Wenn A und B auf l liegen, und $r \perp l$, so ist ArB eine Spiegelung, deren Achse senkrecht auf l steht.

6°. Wenn ArB eine involutorische Bewegung darstellt, so muss das Lot von A auf r durch den Punkt B gehen.

7°. Zwei Punkte haben immer einen eindeutig bestimmten Mittelpunkt, unabhängig davon, ob die Punkte eine oder mehrere Verbindungsgeraden haben (Einl. I, 28—29).

8°. Wenn 3 Geraden a, b, c, eine involutorische Spiegelungsfolge abc bestimmen, und wenn zwei von ihnen, a, b, einen eindeutigen Schnittpunkt O haben, dann geht die dritte Gerade c notwendig durch O (Einl. III, S. 6).

9° a. Die Lote x, y welche von einem beliebigen Punkt P auf zwei Schmieggeraden gefällt werden, sind ebenfalls Schmieggeraden (Einl. I, 62).

b. Haben zwei Geraden p, q zwei gemeinsame Lote r, s (also unendlich viele), so müssen die Lote x, y, welche von einem beliebigen Punkt P auf p und q gefällt werden, (entweder ganz zusammenfallen oder) unendlich viele Punkte gemein haben. (ibid.)

10°. Ferner erinnern wir an die folgenden Hilfssätze, die früher bewiesen oder leicht beweisbar sind:

a. Ist in einem rechtwinkligen Dreieck ABC mit dem rechten Winkel C einer der beiden Winkel A, B singulär, so ist der andere fast-recht; und umgekehrt. Folgt aus Einl. I, S. 18, oder IV, S. 11, und dem obenstehenden Satz 9° a.

b. Ist eine Kathete singulär, die andre ordinär, so sind ihre Gegenwinkel singulär bez. fast-recht.

c. Sind beide Katheten ordinär, so ist keiner der Gegenwinkel singulär oder fast-recht.

d. Ist die Hypotenuse singulär, so sind beide Katheten singulär.

e. Sind in einem beliebigen Dreieck zwei Seiten ordinär, die dritte Seite aber singulär, so ist der Winkel der beiden ordinären Seiten singulär.

E. Ferner erinnern wir an die folgenden Resultate in Einl. V, S. 5—7:

Zwei Nachbarpunkte A, B bestimmen ein lineares Element (einen Strich) $S(A, B)$, d. i. die Menge der Punkte, welche in allen Geraden durch das Punktepaar A, B enthalten sind. Die Menge dieser Geraden bilden ein Schmiegbüschel $s(A, B)$.

Aus dem linearen Element $S(A, B)$ wird das ebene Element (der Fleck) $F(A, B)$ durch Drehung um einen beliebigen Punkt von $S(A, B)$ abgeleitet. $F(A, B)$ ist der Inbegriff der gemeinsamen Fixpunkte aller direkten Bewegungen mit den Fixpunkten A, B.

Jede Gerade, welche durch A oder einen anderen Punkt von $F(A, B)$ gelegt wird, schneidet $F(A, B)$ in einem Strich, welcher dem Strich $S(A, B)$ kongruent ist.

Für die innere Geometrie des Flecks $F(A, B)$ sind alle Axiome der offenen Ebene gültig, wenn wir unter »Gerade« den Durchschnitt des Flecks mit einer ursprünglichen Geraden verstehen.

F. Im allgemeinen Fall wo keine Ordnungsregeln zur Verfügung stehen, muss mit der Möglichkeit gerechnet werden, dass verschiedene Arten von Elementen im Sinne der folgenden Definition auftreten können:

Zwei Elemente sollen gleichartig oder ungleichartig heissen, je nachdem sie kongruente Elemente enthalten (speciell selbst kongruent sind) oder nicht.

Zwei singuläre Punktepaare (Abstände) sollen gleichartig heissen, wenn sie zwei kongruenten Elementen angehören. Ebenso: Zwei singuläre Winkel sind gleichartig, wenn ihre Scheitelelemente gleichartig sind.

Die Anzahl der verschiedenen Arten von singulären Abständen, bezw. Winkeln, soll immer als endlich vorausgesetzt werden.

Wenn alle Abstände gleichartig sind, was z. B. in der graphischen Ebene immer der Fall ist, soll die Ebene homogen heissen.

3. Es lässt sich ohne Schwierigkeit beweisen, dass die am Schluss des Abschnitts C für die graphische Ebene angeführten

Sätze auch für jede andere homogene Ebene Gültigkeit haben. Für nicht-homogene Ebenen verlieren sie aber ihre allgemeine Gültigkeit.

Sind je zwei Punkte unserer Ebene Nachbarpunkte, so ist die Ebene homogen. Sind nämlich A und B beliebige Punkte auf zwei zueinander senkrechten Geraden a, b mit dem Schnittpunkt C, und sind p, q zwei Geraden durch das Punktepaar A, B, so lassen sich zwei Geraden a_1, b_1 durch A, B derart bestimmen, dass

$$pq = aa_1 = bb_1,$$

woraus folgt, dass sowohl a_1 wie b_1 durch C gehen.

Da aber die Geradenpaare p, q; a, a_1; b, b_1 kongruent sind, folgt hieraus, dass die Elemente $S(A, B)$, $S(A, C)$, $S(B, C)$ gleichartig sind, d. h. die Ebene ist homogen.

4. Im folgenden soll stets vorausgesetzt werden, dass ordinäre Punktepaare vorhanden sind. Das bedeutet tatsächlich keine wesentliche Beschränkung der Untersuchung.

Sollte nämlich der Fall eintreten, dass je zwei Punkte der Ebene Nachbarpunkte sind, so folgt erstens hieraus, dass die Ebene homogen ist (3), und zweitens lässt sich dann jede Figur, welche durch eine endliche Anzahl von Punkten definiert ist, in einen zweckmässig bestimmten Fleck einbetten, und für diesen Fleck gilt dann die obenstehende Voraussetzung, dass ordinäre Punktepaare vorhanden sind.

§ 3. Allgemeine Eigenschaften der Schmieggeraden.

5. Zwei Schmieggeraden a, b durch den Punkt A (Fig. 2) haben die Lote n, n_1 in A und werden von der Transversalen $c \perp b$ in zwei verschiedenen Punkten P und Q geschnitten. Es sei ferner C ein von A verschiedener gemeinsamer Punkt der Geraden n, n_1, und die Verbindungsgerade CP werde mit c_1 bezeichnet.

Es sei nun c' diejenige Gerade durch P, welche durch die Gleichung $ac_1 = c'c$ definiert wird; c' ist dann von c verschieden, weil a und c_1 voneinander verschieden sind; die Gerade a geht nämlich nicht durch C, weil a und n nur einen Punkt gemein haben. Es folgt nun:

$$c_1 n n_1 = c_1 ab = cc'b.$$

Die Bewegung $cc'b$ ist sonach involutorisch, d. h. die Gerade c' geht durch den eindeutig bestimmten Schnittpunkt Q der Geraden b, c. Die beiden verschiedenen Geraden c, c' gehen also

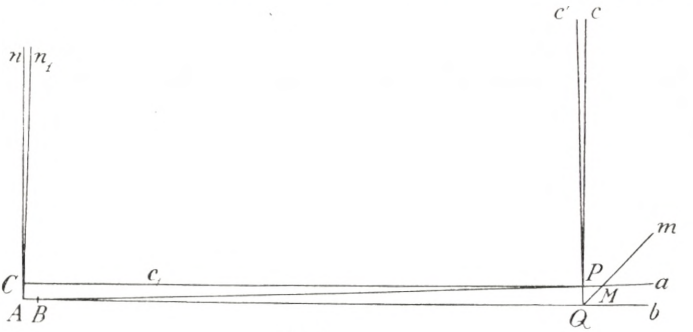

Fig. 2

durch die beiden Punkte P, Q, d. h. diese Punkte P, Q sind Nachbarpunkte.

Aus der Gleichung $ac_1 = c'c$ folgt ferner, dass a und c_1 Schmieggeraden sind.

Aus D, 10°, S. 7 folgt überdies, dass der Winkel (a, c) fast-recht ist. Ist ausserdem der Abstand AQ ordinär, so sind die beiden Geraden a, c Kreuzgeraden; wären sie nämlich Schmieggeraden, so müssten A und Q nach der obigen Betrachtung Nachbarpunkte sein.

6. Es seien nun a, b senkrecht zu einer Geraden p in zwei Nachbarpunkten A, B (Fig. 3). Jede Transversale c, welche senkrecht auf b steht, schneidet dann die beiden Geraden a, b in zwei Nachbarpunkten P, Q.

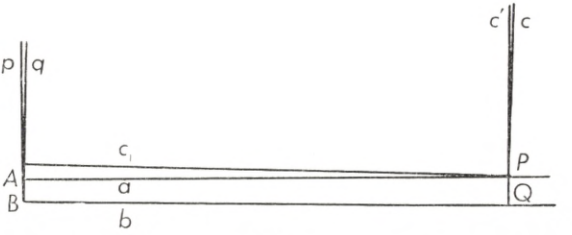

Fig. 3.

Um das zu beweisen, ziehen wir durch A und B eine neue Gerade q und fällen die senkrechte c_1 von P auf q. Durch P ziehen wir ferner die Gerade c' derart, dass $ac_1 = c'c$. Da nun BAc_1 eine involutorische Transformation ist, und da ferner $BA = ba$, so ist

auch $bac_1 = bc'c$ involutorisch, und das bedeutet, dass c' durch den eindeutigen Schnittpunkt Q von b und c geht, dass also die beiden Punkte P und Q zwei verschiedene Verbindungsgeraden c und c' haben, und hiermit ist der Satz bewiesen.

Ähnliche Betrachtungen zeigen umgekehrt, dass ein singulärer Abstand PQ zwischen einem Punkte P und einer Geraden b durch Projektion auf eine beliebige auf b senkrechte Gerade p in einen singulären Abstand übergeht.

Es folgt hieraus, dass zwei Gegenseiten eines dreirechtwinkligen Vierecks entweder beide singulär oder beide ordinär sind.

Ferner ergibt sich, dass zwei Punkte, deren Projektionen auf eine Gerade Fernpunkte sind, selbst Fernpunkte sein müssen.

Ist der Abstand BQ ordinär, so ist die Gerade AQ Schmieggerade von a in A und von b in Q. Durch jeden gemeinsamen Punkt der beiden Geraden AQ und a geht dann eine gemeinsame Normale von a und b (Einl. I, 32). Also:

Haben zwei Nachbargeraden a, b eine gemeinsame Normale, so haben sie unendlich viele gemeinsame Normalen.

§ 4. Die drei Typen der offenen Ebene.

7. Aus Einl. I, 32—36, ziehen wir die folgenden Sätze heran:

Rechtecke existieren in jeder offenen Ebene, wo das Eindeutigkeitsaxiom nicht gilt.

Jedes Rechteck hat zwei Spiegelungsachsen.

Gibt es ein Rechteck $ABCD$, dessen Dimensionen (d. h. die Abstände AB und AD) ordinär sind, so gibt es ein Rechteck mit der Ecke A und mit zwei anderen Ecken X, Y in beliebig gewählten Punkten der beiden Geraden AB und AD.

In diesem Falle soll die Ebene (und ihre Geometrie) singulär heissen.

Auf ähnliche Weise zeigt sich, dass, wenn ein Rechteck $ABCD$ existiert, dessen eine Dimension AB ordinär und die andere Dimension AD singulär ist, dann gibt es ein Rechteck mit der Ecke A und mit zwei anderen Ecken X, Y, von welchen X ein beliebig gewählter Punkt der Geraden AB und Y ein beliebig gewählter Punkt des linearen Elementes $S(A, D)$ ist.

Wenn Rechtecke dieser Art existieren, aber keine Rechtecke, deren Dimensionen beide ordinär sind, soll unsere Ebene (und ihre Geometrie) schwach-singulär heissen.

Wenn hingegen die beiden Dimensionen eines jeden Rechtecks singulär sind, soll die Ebene und die zugehörige Geometrie regulär heissen.

Die Geometrie eines ebenen Elementes ist im allgemeinen schwach-singulär, in besonderen Fällen singulär.

8. Zwei Geraden sollen parallel heissen, wenn sie dasselbe Normalensystem haben.

In der singulären Ebene gibt es parallele Ferngeraden (Fernparallelen) und natürlich auch parallele Nachbargeraden (Nachbarparallelen).

In der schwach-singulären Ebene gibt es Nachbarparallelen aber keine Fernparallelen.

In der regulären Ebene gibt es überhaupt keine Parallelen.

Es liegen nun zwei parallele Nachbargeraden a, a_1 vor (Fig. 4) und es seien b und d zwei ihrer gemeinsamen Normalen, welche a und a_1 in bezw. B, B_1 und A, A_1 schneiden. Von einem beliebig gewählten Punkt D auf d fällen wir das Lot $c = DC$ auf b. Hierdurch entsteht ein 3-rechtwinkliges Viereck $ABCD$ mit rechten Winkeln bei A, B, C. Es lässt sich dann zeigen, dass der vierte Winkel D recht oder fast-recht sein muss.

Die Bewegung aa_1c ist nämlich involutorisch, weil die drei Geraden a, a_1, c senkrecht auf b stehen, und da die Bewegungen aa_1 und AA_1 gleichwertig sind, folgt hieraus, dass auch die Bewegung AA_1c involutorisch ist. Das bedeutet aber, dass eine Gerade d_1 durch A und A_1 senkrecht zu c gelegt werden kann, und hieraus folgt sofort, dass der Winkel (c, d) fast-recht (oder recht) ist, w. z. b. w.

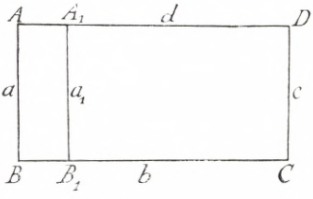

Fig. 4.

Es folgt hieraus zugleich, dass die von einem beliebigen Punkt D der Ebene auf a und b gefällten Lote fast-senkrecht (oder senkrecht) zueinander sind.

Umgekehrt: Hat ein Viereck $ABCD$ ordinäre Seiten AB und BC, rechte Winkel bei A, B, C und einen fast-rechten Winkel bei D, so gibt es eine Nachbarparallele zu a (Fig. 5).

Beweis: Die Normale d_1 von A auf c ist Schmieggerade von d, weil der Winkel (c, d) fast-recht ist. Es sei nun A_1 ein neuer gemeinsamer Punkt von d und d_1, und es sei a_1 die Normale von d in A_1, dann sind die Bewegungen AA_1 und aa_1 gleichwertig und infolgedessen

$$AA_1c = aa_1c,$$

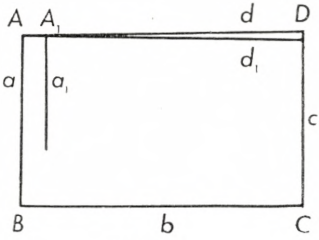

Fig. 5.

also aa_1c involutorisch. Hieraus folgt aber sofort, dass $a_1 \perp b$, d. h. a und a_1 sind parallel.

Es folgt nun ferner, dass die von einem beliebigen Punkt der Ebene auf a und b gefällten Lote fast-senkrecht (oder senkrecht) zueinander sind.

§ 5. Der Mittelliniensatz.

9. Die Mittelpunkte $A', B', C', \cdots$ der Paare entsprechender Punkte in zwei kongruenten geradlinigen Punktreihen $ABC \cdots$ und $A_1B_1C_1 \cdots$ liegen immer auf einer Geraden; speciell können sie in einen einzigen Punkt zusammenfallen.

Beweis: Durch die Punktspiegelung A' wird $ABC \cdots$ in eine Punktreihe $A_1B_2C_2 \cdots$ übergeführt (Fig. 6). Sind die beiden Punkt-

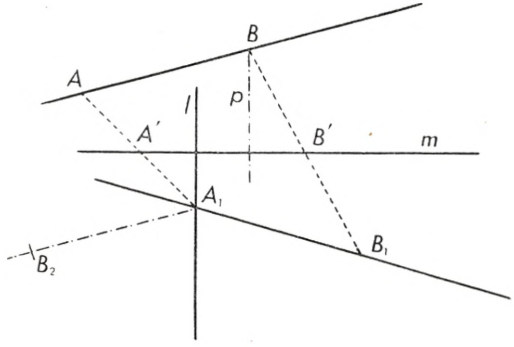

Fig. 6.

reihen $A_1B_2C_2 \cdots$ und $A_1B_1C_1 \cdots$ identisch, so haben wir den genannten Ausnahmefall, wo die Mittelpunkte $A', B', C', \cdots$ in A' zusammenfallen. Anderenfalls betrachten wir die Spiegelungsachse l

der beiden Reihen $A_1B_2C_2 \cdots$ und $A_1B_1C_1 \cdots$ und fällen die senkrechte m von A' auf l. Die Bewegung $A'l$ führt dann die Punktreihe $ABC \cdots$ in $A_1B_1C_1 \cdots$ über. Diese Bewegung ist aber einer anderen pP gleichwertig, wobei p die Normale von B auf m und P einen auf m gelegenen Punkt bezeichnen. Da aber diese Bewegung den Punkt B nach B_1 bringen soll, folgt hieraus, dass P mit dem Mittelpunkt B' von B und B_1 zusammenfällt. Also liegt B' auf m, und die anderen Mittelpunkte ebenfalls.

§ 6. Halbdrehungen.

10. Durch einen Punkt O seien zwei Geraden a, a_1 gelegt, welche nicht senkrecht oder fast-senkrecht zueinander sind. Als Halbdrehung (a, a_1) um O wird dann wie früher diejenige Transformation bezeichnet, bei welcher jedem Punkt P der Mittelpunkt P_1 des Abstands PP' entspricht, wo P' denjenigen Punkt bezeichnet, in welchen P durch die Drehung aa_1 übergeht.

Jede Gerade l mit einer Punktreihe $ABC \cdots$ geht bei der Drehung aa_1 in eine Gerade l' mit der Punktreihe $A'B'C' \cdots$ über, und bei der Halbdrehung (a, a_1) wird also die Punktreihe $ABC \cdots$ in eine Punktreihe $A_1B_1C_1 \cdots$ auf der Mittelgeraden l_1 der beiden kongruenten Reihen $ABC \cdots$ und $A'B'C' \cdots$ übergeführt. Demgemäss definieren wir l_1 als die der Geraden l bei der Halbdrehung (a, a_1) entsprechende Gerade.

Jeder Geraden p durch O entspricht eine Gerade p_1 durch O derart, dass $pp_1 = aa_1$, und jedem Punkt P auf p entspricht seine Projektion P_1 auf p_1.

Die umgekehrte Transformation soll als inverse Halbdrehung $(\overline{a_1, a})$ bezeichnet werden. Bezüglich dieser Transformation muss aber bis auf weiteres beachtet werden, dass sie nicht immer für alle Punkte der Ebene ausführbar ist.

Aus Einl. I, 55 geht hervor, dass zwei Halbdrehungen um denselben Punkt O vertauschbar sind. Dies gilt unabhängig davon, ob die Halbdrehungen direkt oder invers sind, wenn nur in jedem in Betracht kommenden Falle die Punkte, auf welche die Transformationen angewandt werden sollen, wirklich transformierbar sind.

Jede Transformation, welche durch Zusammensetzung einer Folge von direkten oder inversen Halbdrehungen um denselben

Punkt O entsteht, soll als Polarkollineation um O bezeichnet werden. Liegt bei einer solchen Polarkollineation eine gerade Linie durch O fest, so liegen alle gerade Linien durch O fest. Die Transformation wird dann als Polarhomologie um O bezeichnet.

§ 7. Idealpunkte und Idealgeraden.

11. Zwei vorgegebene Ferngeraden a, b bestimmen ein Idealbüschel, d. h. die Gesamtheit aller Geraden c welche mit a und b in Involution sind.

Durch jeden vorgegebenen Punkt C geht eine und nur eine Gerade c des Büschels, welche folgendermassen bestimmt wird (Einl. I, 46):

Von C fällen wir Lote r, s auf a, b mit den Fusspunkten A, B, ferner das Lot t auf die Verbindungsgerade von A und B, und die gesuchte Gerade c wird dann durch die Gleichung $c = rts$ bestimmt.

Wie früher führen wir dann die Redeweise ein, dass das Idealbüschel einen Idealpunkt bestimmt, welcher auf jeder Geraden c des Büschels liegt, und durch welchen jede dieser Geraden geht.

12. Wir gehen nun daran, die so definierten Idealpunkte der offenen Ebene näher zu betrachten.

Zu diesem Zwecke führen wir ein für allemal einen festen Punkt O als Fundamentalpunkt ein, und wir betrachten zunächst nur solche Idealbüschel (Idealpunkte) (a, b), wo a durch O geht, und die von O auf b gefällte Senkrechte a' nicht senkrecht oder fast-senkrecht zu a ist (Fig. 7). In diesem Falle soll das Geradenpaar (das Idealbüschel, der Idealpunkt) regulär heissen; der Abstand OB von O bis zum Schnittpunkt B der beiden Geraden a', b ist der Voraussetzung zufolge ordinär.

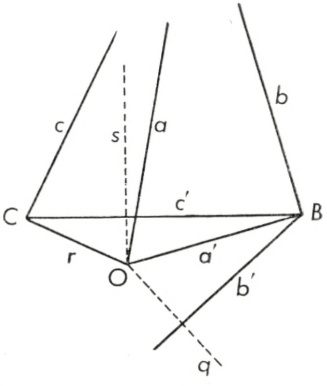

Fig. 7.

Die Halbdrehung (a, a') bringt b nach b' $(a'q = aa', b' \perp q)$.

Es sei nun c eine beliebige Gerade des Büschels (a, b) und r die von O auf c gefällte Senkrechte mit dem Fusspunkt C. Es

sei ferner die Gerade s durch O derart bestimmt, dass $rs = aa'$. Es muss dann die von C auf s gefällte Normale c' durch B gehen, und die Halbdrehung (a, a') führt c in c' über.

Es sei nun d eine neue Gerade des Büschels. Sie wird durch die Halbdrehung (a, a') in ähnlicher Weise in eine Gerade d' durch B transformiert.

Bilden wir die gewöhnliche Fundamentalfigur der Geraden c', d', a', indem wir die Lote von O auf c' und d' fällen, und führen sodann die ganze Figur durch die inverse Halbdrehung $(\overline{a', a})$ wieder in c, d, a mit den Loten von O über, so ergibt sich sofort, dass die Geraden c, d, a in Involution sind. Also ist

$$bca = acb, \quad bda = adb, \quad cda = adc,$$

und hieraus folgt

$$(bca)\,(adb) = (acb)\,(bda),$$

also

$$bcd = dcb,$$

d. h. die Geraden b, c, d sind in Involution.

Nehmen wir eine neue Gerade e des Büschels (a, b), so ergibt sich ebenso, dass die beiden Folgen *ceb* und *deb* involutorisch sind, und da sich schon die Folge *dcb* als involutorisch erwiesen hat, so folgt hieraus, dass auch die Folge *cde* involutorisch ist.

Damit ist gezeigt, dass je drei Geraden des Büschels in Involution sind.

Das ganze Idealbüschel wird durch die Halbdrehung (a, a') in ein Realbüschel mit dem Scheitel B transformiert. Es ist aber nicht zu erwarten, dass jede Gerade dieses Realbüschels durch die inverse Halbdrehung $(\overline{a', a})$ transformierbar ist.

13. Es sei nun ein Idealbüschel (p, q) vorgelegt, wo keine der beiden Geraden p, q durch O geht. Ziehen wir dann durch O die Gerade a, welche dem Büschel angehört, und ist wenigstens eins der beiden Paare a, p und a, q regulär, so lässt sich der vorliegende Fall auf den vorhergehenden zurückführen. Sind aber beide Paare a, p und a, q irregulär, so soll das Büschel (p, q) und somit der Idealpunkt (p, q) irregulär heissen.

Die irregulären Idealpunkte bilden eine besondere Klasse, welche durch alle Halbdrehungen (und Polarkollineationen) um O in sich selbst transformiert wird, d. h. jeder irregulärer Idealpunkt geht durch Halbdrehungen um O in einen irregulären Idealpunkt über.

Die Normalen einer Geraden p bilden ein Idealbüschel. Der zugehörige Idealpunkt P wird als Pol der Geraden p bezeichnet.

Ist die Ebene singulär oder fast-singulär, so ist der Pol P einer Geraden p immer irregulär.

Ist die Ebene regulär, so ist der Pol P einer Geraden p dann und nur dann irregulär, wenn p durch den Fundamentalpunkt O geht oder benachbart zu O ist.

14. Eine Idealgerade wird wie in der elementaren Ebene definiert (Einl. II, 18) als eine Sammlung von eigentlichen und uneigentlichen Punkten, welche durch eine Halbdrehung um den Fundamentalpunkt O in die eigentlichen und uneigentlichen Punkte einer eigentlichen Geraden übergeführt werden können.

Die Pole aller Geraden durch O bilden nach Definition eine besondere Idealgerade, die Fundamentalgerade, die Polare von O.

Der Satz in Einl. II, 19, dass die Pole aller Geraden durch einen beliebigen festen Punkt P auf einer Idealgeraden liegen, gilt hier nur für den Fall, wo P Fernpunkt zu O ist, und wird dann wie früher bewiesen.

§ 8. Ein Hauptsatz über das vollständige Viereck.

15. Es sei ein vollständiges Viereck $ABCD$ (Fig. 8) vorgelegt derart, dass je zwei Ecken Fernpunkte, und je zwei Seiten, welche eine Ecke gemein haben, Kreuzgeraden sind. Es seien ferner von ein und demselben Punkt P die Normalen auf alle sechs Seiten gefällt:

a und a_1 auf AD und BC, b und b_1 auf BD und AC, c und c_1 auf CD und AB.

Wenn dann $bc = c_1b_1$ gilt, so folgt $ca = a_1c_1$ und $ab = b_1a_1$; mit anderen Worten: Die beiden Büschel abc und $a_1b_1c_1$ sind symmetrisch.

Zum Beweise bestimmen wir 6 andere Normalen a', b', c', a'_1, b'_1, c'_1, der Seiten des Vierecks derart, dass

$$Da = a'A, \quad Ac_1 = c'_1B, \quad Bb = b'D, \quad Ca_1 = a'_1B,$$
$$Ab_1 = b'_1C, \quad Dc = c'C.$$

Es folgt hieraus

$$(1) \quad a'c'_1b' = (DaA)(Ac_1B)(BbD) = D(ac_1b)D,$$
$$(2) \quad b'a'_1c' = D(ba_1c)D,$$
$$(3) \quad c'b'_1a' = D(cb_1a)D.$$

Da ferner $bc = c_1b_1$, folgt

$$(Bb'D)(Dc'C) = (Bc'_1A)(Ab'_1C),$$

oder

$$b'c' = c'_1b'_1,$$

woraus man schliesst, dass c'_1 und b'_1 durch den Schnittpunkt P' von b' und c' gehen. Dieser Schnittpunkt P' ist eindeutig be-

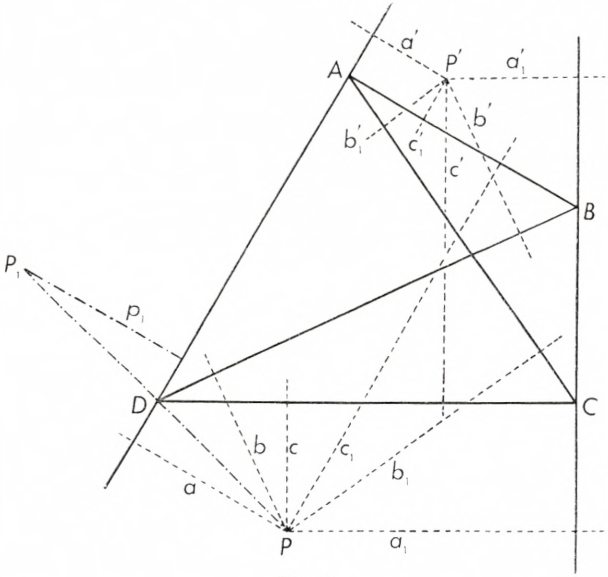

Fig. 8.

stimmt, weil die beiden Normalen BD und CD von b' und c' Kreuzgeraden sind. Derselbe Punkt wird dann auch eindeutig durch die beiden Geraden b' und c'_1 bestimmt, weil diese auf den Kreuzgeraden DB und AB senkrecht stehen.

Auf dieselbe Weise ergibt sich, dass P' durch die Geraden c', b'_1 eindeutig bestimmt wird.

Da nun die auf den rechten Seiten der obenstehenden Gleichungen (1), (2), (3) stehenden Ausdrücke Achsenspiegelungen darstellen, deren Achsen alle durch denjenigen Punkt P_1 gehen, welcher aus P durch Spiegelung an D entsteht, so folgt, dass die

auf den linken Seiten dieser Gleichungen stehenden Spiegelungsfolgen derselben Bedingung genügen. Den obigen Bemerkungen zufolge müssen aber die Achsen der von diesen letzteren Spiegelungsfolgen dargestellten Spiegelungen auch durch P' gehen. Da aber die Punkte P_1 und P' nur eine Verbindungsgerade haben, weil sie auf zwei Fernnormalen p_1 und a' der Geraden DA liegen, so folgt schliesslich, dass die drei in Rede stehenden Achsenspiegelungen identisch sind, also

$$ac_1b = ba_1c = cb_1a,$$

woraus folgt

$$ac_1 = ca_1, \quad ba_1 = ab_1,$$

oder

$$ca = a_1c_1, \quad ab = b_1a_1, \text{ w. z. b. w.}$$

Der Satz gilt auch für reguläre Idealpunkte A, B, C, D, wenn die entsprechenden Bedingungen erfüllt sind, da man dann durch Halbdrehungen um O erzielen kann, dass alle 4 Punkte in Realpunkte übergehen.

§ 9. Die Geometrie der erweiterten Ebene.

16. Fassen wir nun die Gesamtheit der Realpunkte und der regulären Idealpunkte sowie der Real- und Idealgeraden ins Auge, so entsteht eine erweiterte Ebene Ω, deren Geometrie wir im folgenden näher erforschen wollen.

Von den irregulären Idealpunkten kommen dabei nur die Pole der Geraden durch den Fundamentalpunkt O (die zu O konjugierten Punkte), deren Gesamtheit die Fundamentalgerade ω ausmacht, in Betracht. Jede Realgerade hat mit ω einen und nur einen Punkt (Schnittpunkt) gemein. Und dasselbe gilt von jeder regulären Idealgeraden, was daraus hervorgeht, dass diese immer durch Halbdrehungen um O in eine Realgerade transformiert werden kann.

17. Für die Ebene Ω sollen nun die folgenden Redeweisen eingeführt werden:

Zwei Geraden l, m, sollen in Ω parallel heissen, wenn sie die Fundamentalgerade ω im selben Punkt schneiden. Diese Eigenschaft ist bei jeder Halbdrehung um O invariant.

Zu jeder Geraden l kann durch O eine und nur eine Parallele l' gezogen werden. Die zu verschiedenen Geraden $l, m, n, \cdots$ gezogenen Parallelen durch O sollen mit $l', m', n', \cdots$ bezeichnet werden.

Unter dem Winkel (l, m) zweier Geraden l, m in Ω verstehen wir den Winkel (l', m') in der ursprünglichen Ebene.

Zwei Winkel (l, m) und (p, q) sollen in Ω kongruent heissen, wenn die beiden Winkel (l', m') und (p', q') in der ursprünglichen Ebene kongruent sind, d. h. die beiden Systeme (l', m') und (p', q') können durch zwei Spiegelungen deren Achsen durch O gehen, zur Deckung gebracht werden.

l soll dann in Ω senkrecht zu m heissen, wenn $l' \perp m'$ im ursprünglichen Sinne.

Die zu $l, m, n, \cdots$ senkrechten Geraden durch O seien mit $\widehat{l}, \widehat{m}, \widehat{n}, \cdots$ bezeichnet. Der Winkel (l, m) in Ω ist dann mit den beiden Winkeln (l', m') und $(\widehat{l}, \widehat{m})$ in der ursprünglichen Ebene gleichbedeutend.

18. Der Hauptsatz über das vollständige Viereck (15) lässt sich nun als Hauptsatz der Geometrie in Ω in folgender Form aussprechen:

Wenn 4 Punkte A, B, C, D in Ω der Bedingung genügen, dass zwei von ihnen aus den beiden anderen durch kongruente Winkel projiziert werden, dann werden je zwei der vier Punkte aus den beiden anderen durch kongruente Winkel projiziert.

Für die Lage der Punkte und ihrer Verbindungsgeraden gelten dabei dieselben Bedingungen wie früher.

19. Die Fundamentalfigur (Einl. I, S. 24, Fig. 3) lässt sich in folgender Form in die Geometrie der erweiterten Ebene übertragen:

a, b, c seien drei Geraden durch denselben Punkt U derart, dass je zwei von ihnen nur diesen Punkt gemein haben. C sei ein beliebiger Punkt auf c, welcher nicht in U fällt oder Nachbarpunkt von U ist. Es seien ferner $CA = r$ und $CB = s$ die Lote von C auf a und b (in der Ebene Ω). Die Gerade AB sei mit l und das Lot von C auf l mit t bezeichnet. Es wird dann

$$(r, t) \equiv (c, s),$$

d. h. die Winkel (r, t) und (c, s) sind in Ω einander kongruent. Es gelten nämlich in der Ebene Ω die folgenden Kongruenzen:

$$(r, a) \equiv (s, b) \text{ (rechte Winkel in } \Omega),$$

also (dem Viereckssatz zufolge)

$$(a, l) \equiv (c, s).$$

Ferner:

$$(a, l) \equiv (a, r) + (r, l) \equiv (l, t) + (r, l) \equiv (r, t),$$

also

$$(r, t) \equiv (c, s), \text{ w. z. b. w.}$$

20. Durch diese Fundamentalfigur lassen sich analog wie früher Halbdrehungen in Ω, und infolgedessen ähnliche Figuren, d. h. kollineare Figuren, wo entsprechende Winkel stets kongruent sind, definieren.

In Ω lässt sich stets eine Ähnlichkeit so bestimmen, dass zwei vorgegebene Fernpunkte A, B in zwei andere gegebene Fernpunkte A_1, B_1, übergehen. Zu dem Zwecke wählt man zuerst eine Halbdrehung, welche A in A_1 überführt. Hierdurch gehe nun B in B_2 über. Fällt B_2 nicht in B_1, so kann man B_2 immer mittels einer Folge von höchstens 3 Halbdrehungen um A_1 in B_1 überführen. Dass die so hergestellte Ähnlichkeit eindeutig ist, lässt sich folgendermassen einsehen: Man wähle zuerst einen Punkt S derart, dass das Dreieck SAB ordinär ist (d. h. die Seiten und Winkel sind alle ordinär). Der dem Punkt S bei der gesuchten Ähnlichkeit entsprechende Punkt S_1 wird dann als Schnittpunkt der beiden den Geraden SA und SB entsprechenden Geraden bestimmt. Sodann findet man leicht eine eindeutige Konstruktion des einem anderen beliebigen Punkte T entsprechenden Punktes T_1, da wenigstens zwei der Geraden TA, TB, TS einen eindeutigen Schnittpunkt haben.

In dem Spezialfalle, wo AB und A_1B_1 parallel sind, sind je zwei entsprechende Geraden parallel.

21. In der Ebene Ω können wir nun eine erweiterte Art von Symmetrie Σ_a bezüglich einer Geraden a (Spiegelung an a in Ω) einführen, nämlich als eine Kollineation, bei der alle Punkte von a sich selbst entsprechen, während entsprechende Linien l, l_1 stets symmetrische Winkel mit a bilden, d. h. $(l, a) \equiv (a, l_1)$.

Dass eine solche Kollineation existiert, ergibt sich sofort in dem Spezialfalle, wo a durch den Fundamentalpunkt O geht. Die gesuchte Kollineation ist nämlich dann mit der ursprünglich definierten Spiegelung a identisch.

In anderen Fällen, wo die Gerade a nicht durch O geht, braucht man nur eine Spiegelung b der ursprünglichen Ebene, deren Achse b durch O geht, durch eine Halbdrehung in Ω, welche die Gerade b in a überführt, zu transformieren. Die hierdurch entstehende Transformation genügt nämlich der obenstehenden Definition von Σ_a, und ihre Eindeutigkeit folgt aus dieser Definition selbst.

Einander bei Σ_a entsprechende Punkte liegen auf einer Geraden, die in dem für die Ebene Ω eingeführten Sinne auf a senkrecht steht.

22. Schliesslich definieren wir Kongruenztransformationen in Ω als Kollineationen die durch Zusammensetzung von Spiegelungen in Ω entstehen. Dass man hierdurch zu ganz ähnlichen Sätzen wie in der ursprünglichen Ebene gelangt, ist einleuchtend.

Eine Parallelverschiebung soll in Ω als eine Folge von zwei Spiegelungen Σ_a und Σ_b, deren Achsen a, b parallel sind, definiert werden. Bei dieser Transformation geht jede Gerade in eine zu ihr parallele Gerade über, und die auf a und b senkrechte Gerade durch einen beliebigen Punkt P geht durch den entsprechenden Punkt P_1.

Zwei Parallelverschiebungen $P \to A_1$, $P_1 \to P_2$, setzen sich zur Parallelverschiebung $P \to P_2$ zusammen. Dies folgt daraus, dass die Gerade PP_2 in sich selbst verschoben wird.

Sind A, B, C drei Punkte einer geraden Linie, so lässt sich die Parallelverschiebung $A \to C$ aus den beiden Verschiebungen $A \to B$, $B \to C$, zusammensetzen. Hiernach wird die Summe der Abstände (Strecken) AB und BC durch den Abstand (Strecke) AC definiert.

23. Aus den vorhergehenden Entwicklungen geht hervor, dass die erweiterte Ebene Ω eine Ebene vom singulären (euklidischen) Typus darstellt. Wir können deshalb unsere Untersuchung mit einem kurzen Hinweis auf die am Schluss der fünften Mitteilung angegebenen Hilfsmittel abschliessen.

In der Ebene Ω führen wir ein rechtwinkliges Koordinatensystem x_1, x_2 mit dem Anfangspunkt im Fundamentalpunkt O ein. Die Koordinaten (Skalare) werden durch die Punkte der ersten Koordinatenachse x_1 derart repräsentiert, dass O dem Skalar Null (0) und ein anderer, in ordinärem Abstand von O gelegener Punkt e der Achse x_1 dem Skalar 1 (der Einheit), entspricht, und dass ferner zwei Punkte der Achse x_1, die Spiegelbilder bezüglich O sind, stets entgegengesetzten Skalaren (a und $-a$) entsprechen.

Addition der Skalare a und b wird so definiert, dass die Gleichung

$$a + b = c$$

bedeutet, dass die Parallelverschiebung $O \rightarrow c$ durch Zusammensetzung der beiden Parallelverschiebungen $O \rightarrow a$ und $O \rightarrow b$ entsteht. Aus den obigen Betrachtungen folgt dann, dass die gewöhnlichen Gesetze der Addition gültig sind.

Im Falle der homogenen Ebene ist die Summe von zwei singulären Skalaren immer singulär. In der allgemeinen Ebene aber nicht.

Im Falle der graphischen Ebene legen wir die Grössenfolge der Skalare durch die Reihenfolge der Punkte auf der x_1-Achse fest.

Das Produkt zweier Skalare soll durch dieselbe Konstruktion wie in Einl. V, S. 29 ff. definiert werden, und die Beweise der gewöhnlichen Gesetze lassen sich dann wie dort durchführen.

Es ergibt sich so, dass das ganze System von Skalaren einen Ring bildet, in welchem jeder singuläre Skalar einen Nullteiler darstellt.

Die Skalarbezeichungen der Punkte auf der x_1-Achse werden auf die Punkte der x_2-Achse in solcher Weise übertragen, dass jeder Punkt der x_2-Achse durch denselben Skalar bezeichnet wird wie sein auf der x_1-Achse gelegenes Spiegelbild bezüglich einer bestimmten, im voraus gewählten der beiden Spiegelungsachsen von x_1 und x_2.

Jedem Punkt P der Ebene wird sodann ein Skalarpaar (x_1, x_2) zugeordnet, wo x_1 und x_2 diejenigen Skalare sind, welchen die Projektionen von P auf die beiden Koordinatenachsen x_1, x_2 nach obiger Verabredung entsprechen.

Das Skalarpaar (Koordinatenpaar) (x_1, x_2) wird auch als Vektor $x = OP$ bezeichnet, und der Vektor $(-x_2, x_1)$ soll der Quer-

vektor $\widehat{x}$ von x heissen. Dieser entsteht aus x durch eine Drehung um O, welche den Einheitspunkt (1, 0) auf der x_1-Achse in den Einheitspunkt (0,1) auf der x_2-Achse überführt.

24. Im Koordinatensystem x_1, x_2 wird nunmehr jede Gerade g durch eine lineare Gleichung

$$\alpha x_1 + \beta x_2 + \gamma = 0$$

in den laufenden Koordinaten x_1, x_2 dargestellt, wobei α, β, γ (die homogenen Koordinaten von g) Skalare bedeuten, von welchen die zwei ersten nicht beide singulär (Null oder Nullteiler) sind.

Da die Senkrechte von O auf g,

$$-\beta x_1 + \alpha x_2 = 0,$$

Kreuzgerade zu g ist, folgt hieraus, dass die Quadratsumme $\alpha^2 + \beta^2$ ordinär ist.

Da ferner der pythagoreische Lehrsatz nun leicht beweisbar ist (vgl. Einl. V, 43), folgt hieraus erstens, dass die Gleichung $x^2 = -1$ keine Lösung hat, und zweitens, dass der Koordinatenring die fundamentale Eigenschaft besitzt, dass $\sqrt{1+\omega^2}$ für jeden Skalar ω des Ringes existiert, oder in naheliegender Ausdrucksweise:

Der Koordinatenring ist ein pythagoreischer Ring.

25. Wir haben bisher nur Realpunkte und reguläre Idealpunkte in Betracht gezogen. Was die irregulären Punkte anbetrifft, hat man zwei Arten zu unterscheiden: erstens die relativ irregulären Punkte, welche durch veränderte Wahl des Fundamentalpunktes in reguläre Punkte verwandelt werden können, und zweitens die absolut irregulären Punkte, welche bei jeder Wahl des Fundamentalpunktes irregulär bleiben. Die letzteren können nur in den singulären oder schwach-singulären Geometrien auftreten.

26. Es sei nun in einer regulären Ebene eine Schnittpunktsfigur vorgelegt, welche aus einer endlichen Anzahl von Punkten, darunter aber einige relativ irreguläre Punkte U, V, $\cdots$, und Geraden besteht. Durch Halbdrehungen um den vorgegebenen Fundamentalpunkt O kann immer erzielt werden, dass alle Punkte

und Geraden der Figur mit Ausnahme von $U, V, \cdots$ in Realpunkte und Realgeraden übergehen, und durch Halbdrehungen um geeignete neue Fundamentalpunkte können danach auch die irregulären Punkte $U, V, \cdots$ allmählich nacheinander alle in Realpunkte verwandelt werden. Mittels dieses Verfahrens können wir dann in jedem Falle die Schnittpunktsfiguren der regulären Ebene in Figuren überführen, in welchen die in Rede stehenden Punkte sämtlich Realpunkte sind. Es folgt aber hieraus, dass jeder Schnittpunktssatz der gewöhnlichen projektiven Geometrie auch in der hier beschriebenen regulären Geometrie Gültigkeit hat, wenn nur alle der betreffenden Schnittpunktsfigur angehörigen Schnittpunkte und Verbindungsgeraden eindeutig bestimmt sind.

27. Es ergibt sich auch, dass eine Kollineation durch zwei einander entsprechende vollständige Vierecke $ABCD$ und $A_1B_1C_1D_1$ eindeutig festgelegt ist, wenn nur jedes dieser Vierecke ordinär ist, d. h., wenn je zwei Ecken des Vierecks Fernpunkte und je zwei von derselben Ecke ausgehende Seiten Kreuzgeraden sind.

Ferner erhält man, dass zwei projektive Punktreihen durch zwei einander entsprechende Punkttripel ABC und $A_1B_1C_1$ eindeutig bestimmt sind, wenn je zwei Punkte eines jeden dieser Tripel Fernpunkte sind.

28. Auch lässt sich das durch die Realpunkte und ihre absoluten Polaren (sowie die Realgeraden und ihre absoluten Pole) definierte Polarsystem eindeutig auf die ganze Ebene erweitern, und diese absolute Polarität lässt sich durch eine Gleichung der Form

$$xx' = k$$

darstellen, wo x und x' ein beliebiges Paar konjugierter Punkte (x_1, x_2) und (x'_1, x'_2) und k einen konstanten, nicht-singulären Skalar bedeuten.

Die Gruppe der Bewegungen in der ursprünglichen Ebene ist dann die Kollineationsgruppe, welche die durch die obenstehende Gleichung bestimmte absolute Polarität invariant lässt.

29. Im Falle der schwach-singulären oder singulären Geometrie lassen sich die irregulären Punkte nicht durch Halbdrehungen

in Realpunkte überführen, und wir müssen dann bei den projektiven Schnittpunktsfiguren diesen Punkten in anderer Weise Rechnung tragen. Ein Hilfsmittel hierzu haben wir in der analytisch beweisbaren Tatsache, dass ein allgemeines Kennzeichen dafür, dass drei Geraden durch denselben Punkt gehen, die lineare Abhängigkeit ihrer Koordinatentripel $(\alpha_1, \beta_1, \gamma_1)$, $(\alpha_2, \beta_2, \gamma_2)$, $(\alpha_3, \beta_3, \gamma_3)$ ist.

Hiernach bleiben also auch in diesem Falle die Schnittpunktsätze der projektiven Geometrie aufrechterhalten, doch mit dem Vorbehalt, dass alle in Rede stehenden Schnittpunkte und Verbindungsgeraden eindeutig bestimmt sind.

Schlusswort.

Die im vorstehenden entwickelten Hilfsmittel zur Begründung der Kongruenzlehre der offenen Ebene können, wie fast unmittelbar ersichtlich, auch zur Begründung einer analogen Kongruenzlehre der geschlossenen Ebene Verwendung finden. Zu diesem Zwecke sind nur die folgenden naheliegenden Umgestaltungen unseres Axiomsystems notwendig:

1) Im Axiom II muss der letzte Satz ausgelassen werden, d. h. für eine Achsenspiegelung müssen Fixpunkte ausserhalb der Spiegelungsachse zugelassen werden;

2) im Axiom III ist die Aussage über das Senkrechtstehen folgendermassen abzuändern: durch jeden vorgegebenen Punkt P geht eine Gerade a, die auf einer vorgegebenen Geraden b senkrecht steht, die Eindeutigkeit von a wird aber nur verlangt, wenn P auf b liegt;

3) Axiom IV wird durch das folgende ersetzt: Zu zwei Punkten A, B einer Geraden g gibt es immer zwei Mittelpunkte auf g. Durch jeden von diesen geht eine auf g senkrechte Spiegelungsachse von A, B.

Es lässt sich dann beweisen, dass jede Gerade p einen Pol P besitzt, durch welchen alle auf p senkrechten Geraden gehen, und umgekehrt, zu jedem Punkt P gehört eine Polare p, welche alle Geraden durch P senkrecht schneidet. Je zwei Geraden haben wenigstens einen Punkt gemein, und die ganze Lehre von den Idealpunkten braucht uns also hier nicht zu beschäftigen.

Schliesslich lässt sich in analoger Weise wie für die offene

Ebene eine analytische Geometrie vom euklidischen Typus mit Koordinaten, welche einem pythagoreischen Ring angehören, definieren, womit die Begründung erledigt wird.

Was spezielle Anwendungen der in dieser sechsten Mitteilung vorgetragenen Methoden anbetrifft, sei vor allem darauf hingewiesen, dass der elementare Fall, wo das Eindeutigkeitsaxiom als unbedingt gültig angenommen wird, sich nunmehr der älteren Darstellung gegenüber, besonders einfach gestaltet.

Die angegebene axiomatische Transformation der verschiedenen Geometrietypen in eine Geometrie vom euklidischen Typus wird zweifellos bei allen Anwendungen zur Vereinfachung der Probleme beitragen. Auch in der Raumgeometrie erweist sich die analoge Transformation als sehr wertvoll. Und für die Geometrie der Wirklichkeit soll schliesslich eine endgültige Begründung angebahnt werden.

Die hier angekündigten, bemerkenswerten Fragen der Kongruenzlehre sollen in einer späteren Arbeit fertig behandelt werden.

In einer demnächst erscheinenden anderen Arbeit soll ferner gezeigt werden, wie die entsprechenden Erweiterungen der projektiven Geometrie sich vollziehen lassen, und wie diese Erweiterungen dazu beitragen können, über die allgemeinen Grundlagen der Geometrie neues Licht zu verbreiten.

Indleveret til selskabet den 21. januar 1949.
Færdig fra trykkeriet den 19. maj 1949.

DET KGL. DANSKE VIDENSKABERNES SELSKAB
MATEMATISK-FYSISKE MEDDELELSER, BIND XXV, NR. 11

ON THE ENERGY LOSS BY FISSION FRAGMENTS ALONG THEIR RANGE

BY

N. O. LASSEN

KØBENHAVN
I KOMMISSION HOS EJNAR MUNKSGAARD
1949

CONTENTS

Printed in Denmark
Bianco Lunos Bogtrykkeri.

Erratum.

Page 21, note 1: for $P\sigma$ α-particles *read* Po α-particles.

D. Kgl. Danske Vidensk. Selskab, Mat.-fys. Medd. XXV. 11, N. O. Lassen.

INTRODUCTION

From cloud-chamber studies by Bøggild, Brostrøm, and Lauritsen (1) it is known that the curve giving the energy loss by fission fragments along their range differs from the corresponding curve for α-particles. The ionization produced by the fragments is high at the beginning of the path; it decreases along the range, reaching a minimum near the end of the track. In the very end the energy loss per cm is expected to rise again.

According to theoretical considerations regarding the penetration of fission fragments through matter as developed by Bohr (2), the range of the fragments may be divided into two parts over which the stopping mechanisms are essentially different. In the first part, where the fragment velocity is high compared with the orbital velocities of the most loosely bound electrons in the atoms of the stopping material, the energy loss takes place primarily through excitation and ionization of the atoms. In such electronic collisions the fragment with its bound electrons, having a total charge z^*, is assumed to act as a single particle of charge number z^*. The total charge is determined by a balance between capture and loss of electrons from the fragment ion, equilibrium being established when the most loosely bound electron in the fragment ion has an orbital velocity comparable with the translatory velocity v of the fragment. Consequently, the charge decreases as the fragment is slowed down, a phenomenon which has also been verified experimentally (3). Due to this decrease of z^*, the ionization decreases along the range, in contrast to the case of α-particles or protons which exhibit an increasing ionization with decreasing velocity.

When the fragment reaches a velocity of the order of $v_0 = \frac{\varepsilon^2}{\hbar}$ it becomes almost completely neutralized. Moreover, in collisions

with the atoms, the electron structures tend to react adiabatically and, hence, the rate of energy loss in electronic collisions becomes very small. Due to their large mass, the fragments still have a considerable energy of several *MeV* and may thus cover an appreciable distance before being finally stopped. Over this residual part of the range, the energy loss is supposed to take place mainly in nuclear collisions, i. e. in encounters where kinetic energy is imparted to the stopping atom as a whole. From the theory it follows that the energy loss per cm due to such nuclear encounters increases towards the end of the path.

In the cloud-chamber experiments the increase in the number of nuclear collisions along the range was directly observed, but the energy loss per cm was determined in a somewhat indirect way by means of statistical methods. More direct measurements of the specific ionization in the first part of the range were performed by the author. The results obtained for argon have already been briefly reported elsewhere (4). Chapter I of the present paper gives a more detailed account of these experiments, while Chapter II deals with corresponding investigations in other gases. Finally, in Chapter III, an attempt is made to construct the range-velocity curve for the whole range by combining the ionization measurements with the cloud chamber experiments.

CHAPTER I

Specific Ionization in Argon.

§ 1. Experimental arrangement.

The experimental arrangement is shown in Fig. 1. Inside a box, made of a 5″ copper tube with a bottom and a removable lid, is placed a shallow ionization chamber. The collecting electrode is a brass plate mounted on the lid of the box by means of three amber supports (not shown in the figure). The second electrode is a thin foil of aluminum or gold held by a framework of brass, which is also mounted on the lid by means of amber supports. The distance between the two electrodes is 5.0 ± 0.1 mm, the electrodes being as nearly parallel as possible. Inside the box

is furthermore placed a uranium layer, evaporated upon a mica sheet which is fastened to a brass plate. In front of the layer a diaphragm with about 350 openings is mounted; this diaphragm only allows the fission fragments to come out nearly perpendicularly to the surface of the layer. The whole "gun" is mounted on a brass rod which slides in a brass tube, and can be operated from outside; the air-tightening is made by means of a piece of rubber tubing greased with ricinolein. The gun as viewed

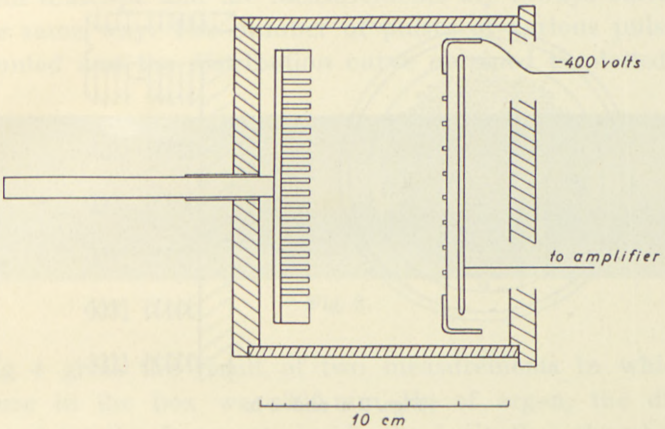

Fig. 1. Experimental arrangement.

from the right side in the picture is shown in Fig. 2a; Fig. 2b gives part of the cross-section *a—a* in enlarged scale. The diaphragm actually consists of nine brass plates, 1 mm thick, and a distance ring, 2 mm thick. The arrangement shown in the figure minimizes the number of fragments reflected from the walls of the channels to the ionization chamber. Later, however, this precaution was found to be unnecessary.

From the geometry described it is easily calculated that the distance traversed by the most obliquely moving fragments is 5 per cent higher than the distance travered by the fragments moving perpendicularly to the surface. When the unavoidable small deviations from planeness of the foil and from parallelism of the electrodes are taken into account, the distances traversed by the various fragments inside the chamber are estimated to be equal within $\pm$ 4 per cent, while the distances traversed on the way to the chamber are equal within $\pm$ 2.5 per cent. Due to

the obliquely moving fragments the average distance traversed by the fragments before observation is 3 per cent higher than the distance between the uranium layer and the middle of the ionization chamber. The corresponding stopping equivalent x is obtained when the pressure of the argon inside the box, measured with a mercury manometer, is taken into account, and when the stopping equivalent of the aluminum foil is added. x can be varied by moving the gun and by varying the pressure. The

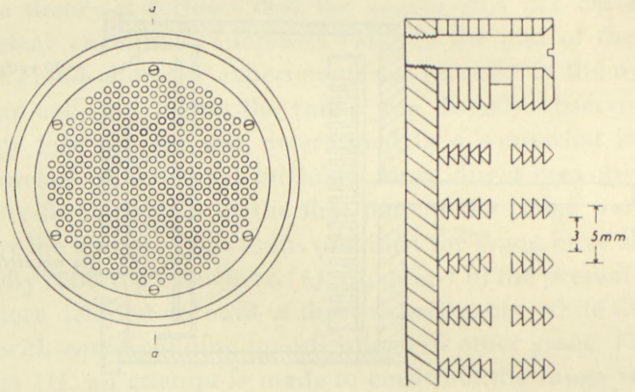

Figs. 2 a and 2 b.

mean thickness of the uranium layer is 0.33 mg/cm^2 as determined by weighing as well as by α-counting and it gives rise only to a small correction to x ($\sim \frac{1}{2} \cdot 0.6$ mm of argon), which has been neglected. The layer is not exactly homogeneous, but the thickness is estimated to vary by less than 20 per cent.

The fission fragments are produced by slow neutrons hitting the uranium layer. The box is placed between the coils of the cyclotron at a distance of about 25 cm from an internal Be-target which is bombarded by deuterons and thus acts as a strong source of neutrons. 3—5 cm of paraffin are inserted between the target and the box which on all sides is surrounded by paraffin.

§ 2. Experimental method.

The ionization chamber is connected to a linear amplifier and a cathode-ray oscillograph whose screen is photographed on a continuously moving film. Fig. 3 shows a piece of a film. The

larger pulses are due to fission fragments, the actual pulses being directed upwards; the peaks going downwards are caused by the amplifier. Pulses due to statistical fluctuations of the background ionization caused by the intense irradiation with γ-rays and fast neutrons also occur. Numerous small pulses, partly separated from each other, are seen on the oscillograph, but on the rather slowly moving film they appear as a considerable broadening of the zero line. The recording films are placed in a small diascope and the measurements are always carried out in the same way. The number of pulses of various pulse sizes is counted and the distribution curve obtained is plotted.

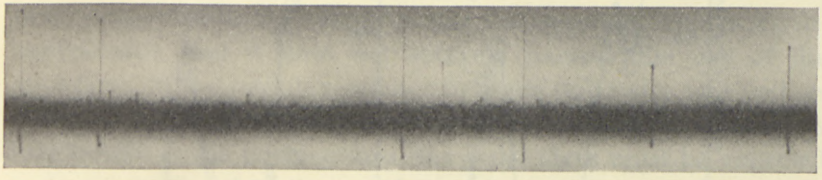

Fig. 3.

Fig. 4 gives the result of two measurements in which the pressure in the box was 300 mm Hg of argon, the distance traversed by the fragments inside the ionization chamber thus corresponding to about 2 mm of argon at atmospheric pressure. The distance x from the uranium layer to the middle of the ionization chamber was equivalent to approximately 10 and 12 mm of argon at atmospheric pressure in the left and right curves, respectively. The curves give the number of pulses plotted against their sizes as measured in relative units (regarding the scale of abscissae, see later). The distribution of pulse sizes for $x = 10$ mm shows the presence of the well-known two groups of fragments. Furthermore, it indicates that a few background pulses are much larger than is indicated by the breadth of the zero line and that some of the pulses due to the heavy group of fragments are smaller than the upper limit for the background pulses while, on the other hand, the light group is completely separated from the heavy group and the background.

From the curve can be determined the values of the abscissae corresponding to the two peaks, i. e. the most frequent sizes of the pulses of the two groups. It is possible approximately to

define what may be denoted as "the upper and lower limits" of the light group and "the upper limit" of the heavy group as the points of intersection between the steepest tangents to the curve and the axis of abscissae. Of course, the limits so obtained

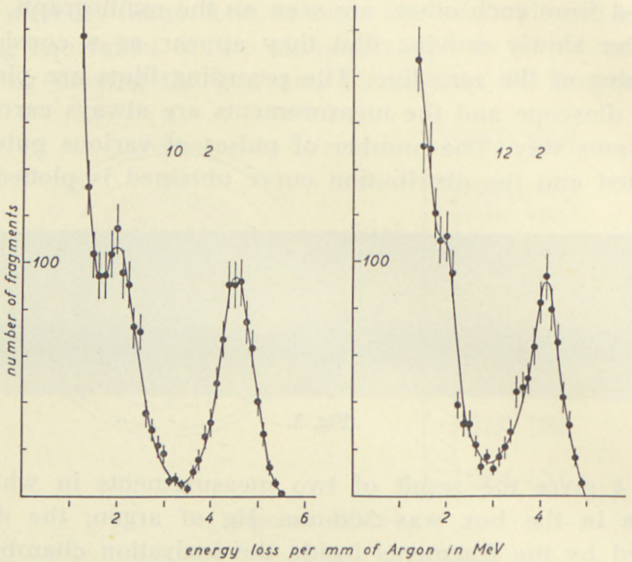

Fig. 4. Distribution of specific ionization by fission fragments having traversed 10 mm of argon (left) and 12 mm of argon (right). Depth of ion chamber corresponds to 2 mm of argon.

are only significant if the spread in pulse size caused by the background is considerably smaller than the width of each of the peaks. This is actually the case, as was shown by means of artificial pulses produced by an apparatus described earlier (5).

The artificial pulses were also used for testing the linearity of the amplifier; during each measurement they were frequently used for checking the amplification which did not remain strictly constant with time. In the various measurements during each series it was furthermore found convenient to use different amplifications of the last stage, and relative measures for the total amplification were obtained by means of the artificial pulses.

§ 3. Investigation of the proportionality between ionization and pulse size.

The magnitude of the background depends on the resolving time of the amplifier. In order to reduce the background to a reasonable amount it was necessary to choose the smallest time constant τ of the amplifier rather low, $\sim 3 \cdot 10^{-5}$ sec. However, while the negative ions were collected in a shorter time, it can easily be calculated from the known ionic mobility of the positive ions that complete collection of the latter required a somewhat longer time than τ, although the field intensity used was rather high, 800 volts/cm. Accordingly, the pulse sizes were found to depend somewhat on the voltage across the chamber. This is an inconvenience, but it does not severely hamper the use of the apparatus. If the interdependence between pulse size and voltage is due solely to the rather small τ in connection with the slow movements of the positive ions, the pulse sizes must be expected to be proportional to the number of ions as long as the voltage and the pressure are kept constant. In fact, for all fragments the conditions in the ionization chamber are nearly identical, the fragments all moving almost parallel to each other. Hence, the collection of the ions will take place quite similarly in the different cases. This means, firstly, that all the negative ions will be collected in a very short time; secondly, that within equal time intervals equal fractions of the total number of positive ions will be collected and, thirdly, that non-collected ions will be displaced by equal lengths. Thus, the shape of the voltage variation with time on the collector plate is the same for each pulse, and the pulse sizes give a relative measure for the ionization. We are, however, unable to perform a calibration by means of α-particles in the usual way, since α-particles moving in the same direction as do the fragments produce too low ionization inside the ionization chamber, and α-particles moving parallel to the plates are unsuitable, since the collection of the ions formed by such particles will take place in a different way.

That the pulse sizes depend on the voltage might also partly be due to lack of saturation and, if this is the case, we shall obtain pulses roughly proportional to $n\,(1 - \alpha n)$, where n is the number of primary ion pairs and α is the coefficient of re-

combination; hence, the larger pulses will be measured relatively too small. Now, since the fragments are moving perpendicularly to the plates, the negative ions have to move through a cloud of positive ions before reaching the collector plate, a fact which tends to increase a possible recombination. Therefore, it is necessary to investigate whether or not the pulse sizes are proportional to the number of primary ions.

The curves in Fig. 4 were obtained with 400 volts across the

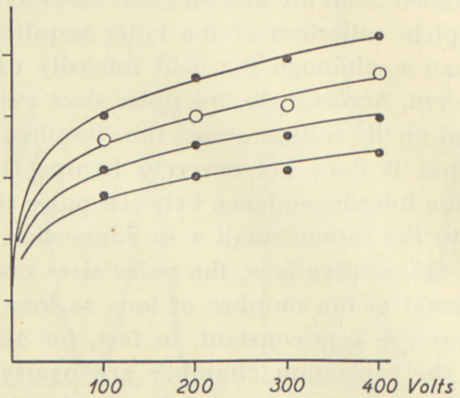

Fig. 5. Abscissa: voltage across the ion chamber. — Ordinates: pulse sizes in relative units. — Open circles correspond to the peak of the light group, full circles to upper and lower limits of the light group and upper limit of the heavy group.

chamber. For $x = 10$ mm similar curves were determined with 300, 200, and 100 volts. In Fig. 5 the values of the pulse sizes are compared. As is seen, a doubling of the voltage corresponds to an increase in pulse size of about 15 per cent. The ordinates of the curves of Fig. 5 have a constant ratio, and the experimentally found points seem to agree fairly well with the assumption of proportionality.

In Table 1 the pulse sizes are given in relative units, the size of the upper limit of the light group being put equal to 1 for each voltage. If recombination takes place the small pulses will be measured relatively too high, an effect which will be the larger, the lower the voltage. Hence, it follows that the figures in the vertical columns should increase downwards, the increase being highest in the last column. In fact, the figures seem to point at a small variation just in this way. However, we conclude that the pos-

Table 1.

Volts	Light group			Heavy group
	Upper limit	Peak	Lower limit	Upper limit
400	1.00	0.88	0.74	0.63
300	1.00	.85	.74	.63
200	1.00	.87	.76	.65
100	1.00	.90	.79	.68

sible recombination can be neglected at 300 or 400 volts and that, for these voltages, the pulse sizes are proportional to the number of primary ions.

§ 4. Distribution of specific ionization for various distances traversed.

From Fig. 4 it can be seen that the pulses are larger for $x = 10$ mm than for $x = 12$ mm. In the latter case, the pulses due to the light group are still clearly separated from the other pulses, while the heavy group has nearly disappeared in the background. For $x = 14$ mm the pulses are further decreased (Fig. 6) and the heavy group cannot be seen any more; the pulses of the light group are also lowered and the separation between the latter and the other pulses is less complete. For $x = 16$, 18, and 20 mm (Fig. 7) the process continues and, in the last case, the light group has also disappeared into the background and can no longer be observed directly. Yet, the distribution curve obtained for $x = 22$ mm (not shown) is slightly steeper than that for $x = 20$ mm and, thus, the presence of fission fragments for $x = 20$ mm can be detected.

The curves of Fig. 8 were obtained with a pressure of 150 mm Hg, the distance traversed by the fragments inside the chamber thus being equal to about 1 mm of argon at atmospheric pressure. The shape of the distribution curve for $x = 10$ mm must, of course, be the same as that shown in Fig. 4 and, in fact, the agreement is satisfactory. The influence of the background seems to be slightly higher at lower pressure but, apart from this, the

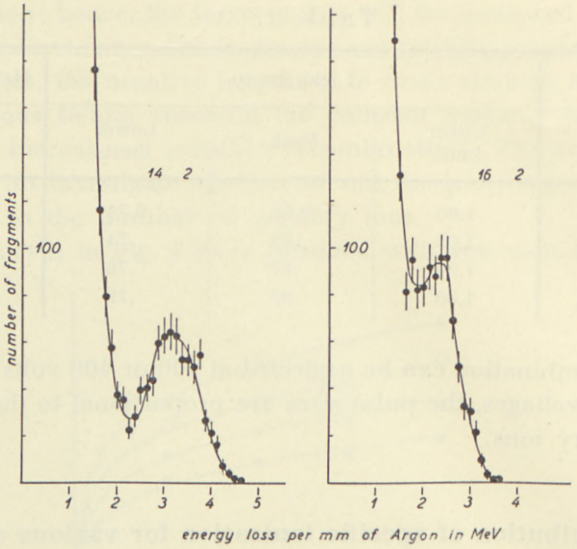

Fig. 6. Specific ionization for $x = 14$ mm (left) and $x = 16$ mm (right). $\triangle x = 2$ mm.

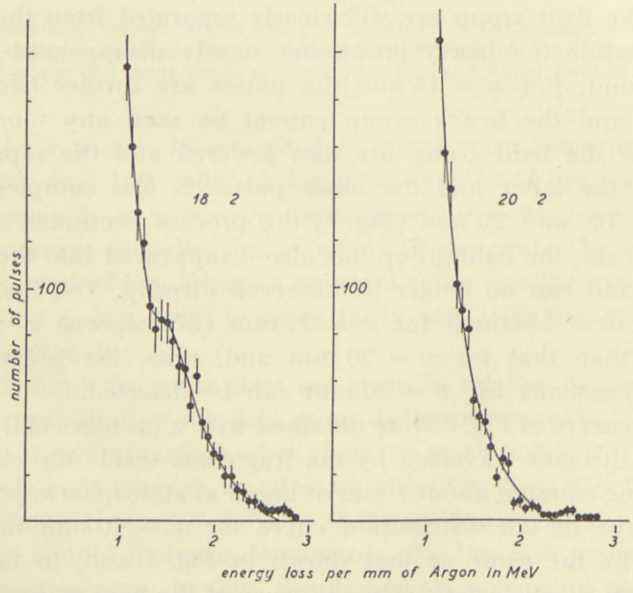

Fig. 7. Specific ionization for $x = 18$ mm (left) and $x = 20$ mm (right). $\triangle x = 2$ mm.

two curves are very similar. The agreement between the absolute values of the abscissae is insignificant, because it is a result of the particular way of determining the scale (see later). Only for measurements performed at the same pressure the pulse sizes can be compared directly. The curves of Fig. 8 for $x = 8$ and $x = 10$ mm indicate that the pulse sizes increase for both groups of fragments when x is lowered. A closer examination of the figure shows that the increase is highest for the heavy group, an obser-

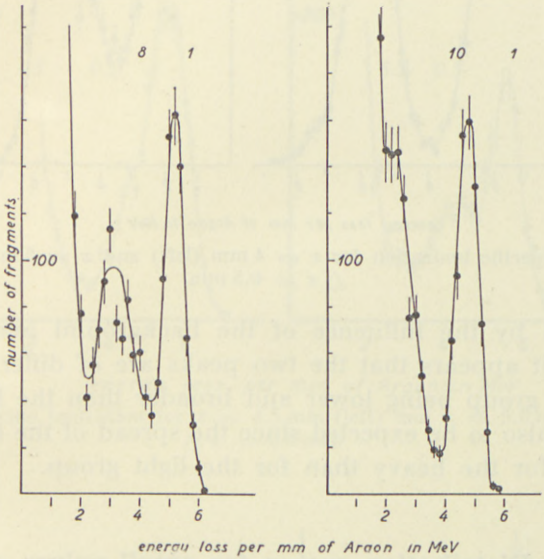

Fig. 8. Specific ionization for $x = 8$ mm (left) and $x = 10$ mm (right). $\triangle x = 1$ mm.

vation which can also be deduced from the change in shape of the distribution curve. The two peaks of the curve have approached each other, which is clearly seen as the valley between the peaks is not so deep for $x = 8$ mm as for $x = 10$ mm.

When x is further decreased the pulse sizes increase further. Fig. 9 shows curves obtained at a pressure of 75 mm Hg. It is clearly seen that the two groups have come still closer to each other for $x = 6$ mm and that they can no longer be separated for $x = 4$ mm. Also the pulse sizes are higher for $x = 4$ mm than for $x = 6$ mm.

Although the peaks on the distribution curves are considerably

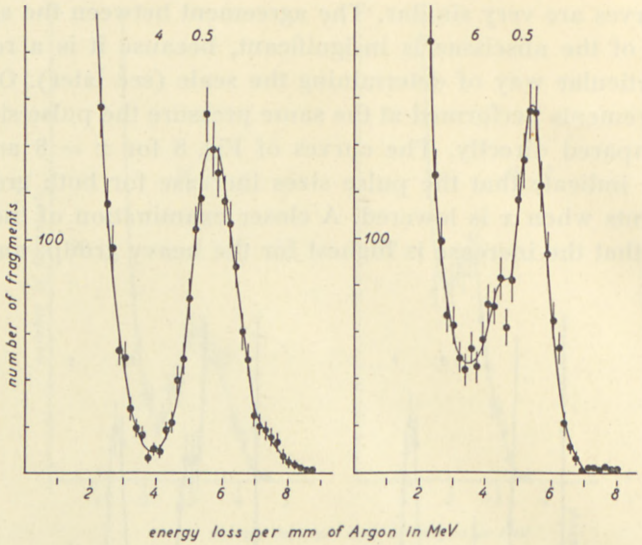

Fig. 9. Specific ionization for $x = 4$ mm (left) and $x = 6$ mm (right). $\triangle x = 0.5$ mm.

broadened by the influence of the background and the finite geometry it appears that the two peaks are of different shapes, the heavy group being lower and broader than the light group. This was also to be expected since the spread of the total energy is higher for the heavy than for the light group.

§ 5. Distribution curves for small values of x.

It is seen that the specific ionization decreases along the path of the fragment and that near the beginning of the path the decrease is higher for the heavy group. This indicates that the curves giving the specific ionization along the range for the two groups will intersect at an x-value of about 4 mm, and the single peak in Fig. 9 may be expected to split up into two peaks again when x is decreased below 4 mm. However, it was desirable to verify this expectation experimentally. This could not be done easily without changing the apparatus because of the rather large thickness of the gun and of the aluminum foil covering the ionization chamber.

An attempt was made to measure the ionization of the frag-

ments immediately outside the uranium layer. In a hemispherical ionization chamber, fission fragments were allowed to come out from a very thin uranium layer in directions diverging less than 60° from the normal. Their paths inside the chamber had the same lengths, corresponding to about 1 mm of argon at atmospheric pressure. The distribution curve for the ionization had only one peak, but this was unsymmetrical, having a hump on

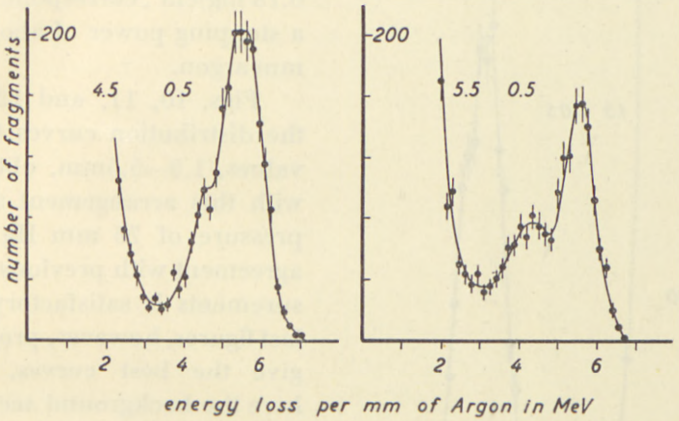

Fig. 10. Specific ionization for $x = 4.5$ mm (left) and $x = 5.5$ mm (right). $\triangle x = 0.5$ mm.

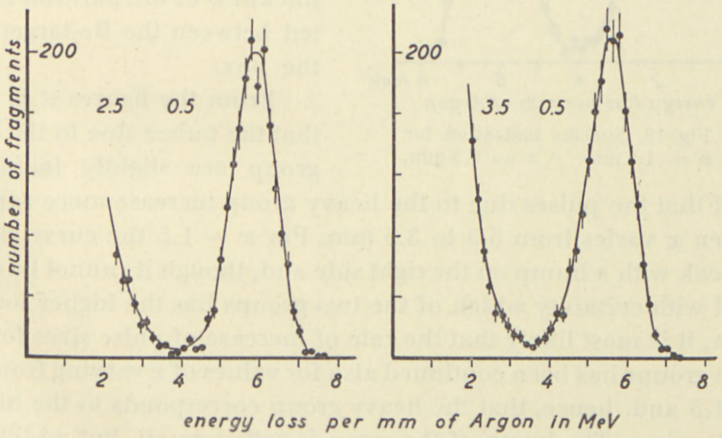

Fig. 11. Specific ionization for $x = 2.5$ mm (left) and $x = 3.5$ mm (right). $\triangle x = 0.5$ mm.

the right side. However, since some amplification took place in the chamber, the measurements were not regarded as sufficiently reliable.

Therefore, after some minor alterations, further measurements were performed with the first arrangement. The gun was provided with a new diaphragm, a 3 mm thick circular aluminum plate with 3000 holes, 1 mm in diameter. The aluminum foil (0.25 mg/cm^2 ∼ 1.7 mm of argon) was replaced by a gold foil, 0.18 mg/cm^2, corresponding to a stopping power of about 0.5 mm argon.

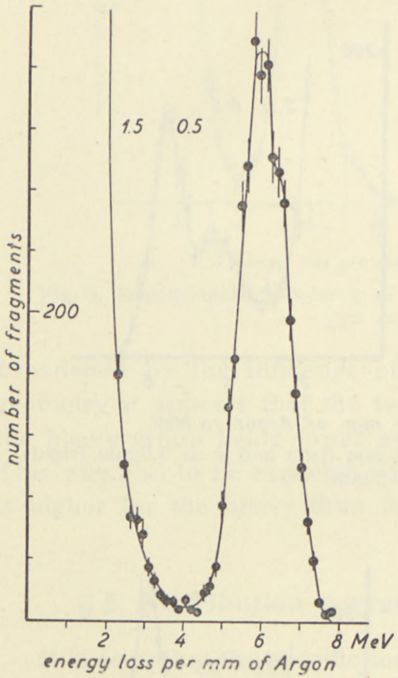

Fig. 12. Specific ionization for $x = 1.5$ mm. $\triangle x = 0.5$ mm.

Figs. 10, 11, and 12 give the distribution curves for x-values, 1.5—5.5mm, obtained with this arrangement and a pressure of 75 mm Hg. The agreement with previous measurements is satisfactory; the last figures, however, probably give the best curves, since here the background seems to be slightly smaller, which may be due to a small change in the position of the box or the thickness of the paraffin inserted between the Be-target and the box.

From the figures it is seen that the pulses due to the light group are slightly increased and that the pulses due to the heavy group increase more rapidly when x varies from 5.5 to 3.5 mm. For $x = 1.5$ the curve shows a peak with a hump on the right side and, though it cannot be decided with certainty which of the two groups has the higher ionization, it is most likely that the rate of increase of pulse sizes for the two groups has been continued also for values of x varying from 3.5 to 1.5 and, hence, that the heavy group corresponds to the higher pulse sizes. The hump of the curve is rather small, but additional indication for its existence was provided by the mentioned mea-

surements with the hemispherical chamber and also by a measurement with the present arrangement at a lower pressure. The latter measurement gave a very similar curve for $x = 1.0$ mm (not shown).

§ 6. Ionization range curves.

In Fig. 13 the ionization values obtained are plotted against the distance x traversed by the fragments before the observation. The pulse sizes are measured in relative units, and for measurements performed at 300 mm Hg, corresponding to x-values of 10—20 mm, the values determined directly are plotted. The values obtained at 150 mm Hg, corresponding to x-values of

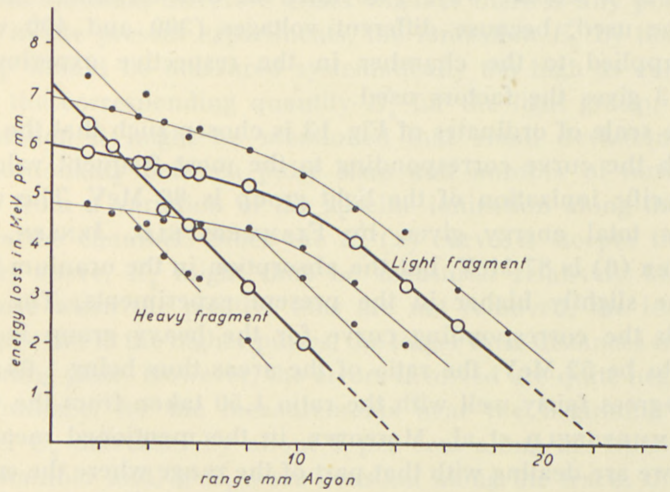

Fig. 13. Ionization range relations for fission fragments in argon. Open circles correspond to the peaks on the ionization distribution curves in the preceding figures, full circles to upper and lower limits. Regarding the scale of ordinates, see text.—When one of the peaks lies near the background the peak will be slightly displaced against the background. Similar phenomena occur when the two peaks lie near together. Small corrections are applied to compensate for this effect.

6—12 mm, are reduced by a suitable factor before plotting and in this way the range-ionization curves are fitted together. The transformation factor was determined by measurements of the ratio between the pulse sizes obtained at 300 mm Hg and at 150 mm Hg, respectively, for x-values of 10 and 12 mm. The

Table 2.

Light group.

	Upper limit	Peak	Lower limit
x = 10 mm	0.77	0.76	0.77
x = 12 -	.81	.83	.81

ratio is given in Table 2, from which the mean value is found to be 0.79.

The measurements performed at a pressure of 75 mm Hg and by means of the first and the second diaphragm have been treated in a similar way. Two different transformation factors must be used, because different voltages (300 and 400 volts) were applied to the chamber in the respective experiments. Table 3 gives the factors used.

The scale of ordinates of Fig. 13 is chosen such that the area beneath the curve corresponding to the most frequent value of the specific ionization of the light group is 86 MeV. The value for the total energy given by FLAMMERSFELD, JENSEN, and GENTNER (6) is 87 MeV, but the absorption in the uranium layer may be slightly higher in the present experiments. The area beneath the corresponding curve for the heavy group is then found to be 52 MeV, the ratio of the areas thus being 1.65; this value agrees fairly well with the ratio 1.50 taken from the work of FLAMMERSFELD et al. Moreover, in the mentioned measurements we are dealing with that part of the range where the energy loss is almost entirely due to electronic collisions. By extrapolating the curves in the way shown they reach the axis of abscissae in

Table 3.

Pressure	Diaphragm	Transformation factor	Range interval
300 mm Hg	No. 1	1.00	10—20 mm
150 - -	- 1	0.79	6—12 -
75 - -	- 1	0.70	4— 8 -
75 - -	- 2	0.63	1.5— 5.5 -

points corresponding to what may be called the extrapolated ranges R_{ex}. Since, as was mentioned in the Introduction, the fragments may traverse a considerable distance after the point where the ionization due to electronic collisions has decreased to zero, the actual ranges R may, however, be somewhat higher than R_{ex} and, hence, the areas beneath the curves drawn do not correspond exactly to the total energies.

These results do not agree with the conclusions of DEMERS (7) based on studies of the density of fission tracks in photographic plates, which point to a higher initial ionization of the light fragment than of the heavy fragment. Similar evidence was also recently obtained by SHERR and PETERSON (8) in an analysis of the shape of pulses from an ionization chamber.

The question therefore arises whether there is any possibility that, in the present experiments, the ionization E_2' by the heavy group should be measured systematically too high as compared with the corresponding quantity E_1' for the light group. In this connection it might be mentioned that small deviations from proportionality between pulse sizes and number of ions might arise from a variation of the specific ionization along the track inside the chamber. Since the $E_2'(x)$ curve is steeper than the $E_1'(x)$ curve, E_2' might thus be measured relatively too high, because when the positive ions are not removed, the ion pairs will give rise to the higher pulses, the larger their distances from the collecting plate. However, the errors involved are quite negligible; for instance, for the measurements near the beginning of the range, E_2' decreases by about 5 per cent along the track inside the chamber and, if E_1' were constant along the track, the error would amount to less than 0.8 per cent.

Another possible source of error is that an ion multiplication occurs in the chamber. Such a multiplication would probably also favorize E_2', because the chance that an electron produces a new ion pair must be assumed to be proportional to the distance traversed by the electron and because the E_2' curve is the steeper one. However, if such a multiplication were present, and if it distorted the results, one should expect the ratio between pulses corresponding to the two groups to vary strongly with the voltage across the chamber, which is not the case. This is proved by Fig. 5 for a pressure of 300 mm Hg. Similar investigations

giving the same result were also performed at lower pressures, 150 and 75 mm Hg.

At first sight, it might seem surprising that the range-ionization curves for the two groups intersect; nevertheless, this is just what should be expected. The heavy group is known to have the lower initial velocity and, since it has the higher initial charge (7), it must also be expected to have the higher initial ionization in agreement with the result of the present experiments. Then, because the heavy group has the shorter range, the curves must intersect.

CHAPTER II

Specific Ionization in Various Gases.

§ 1. Specific ionization in xenon.

Using the apparatus described in Chapter I the specific ionization was measured in several gases.

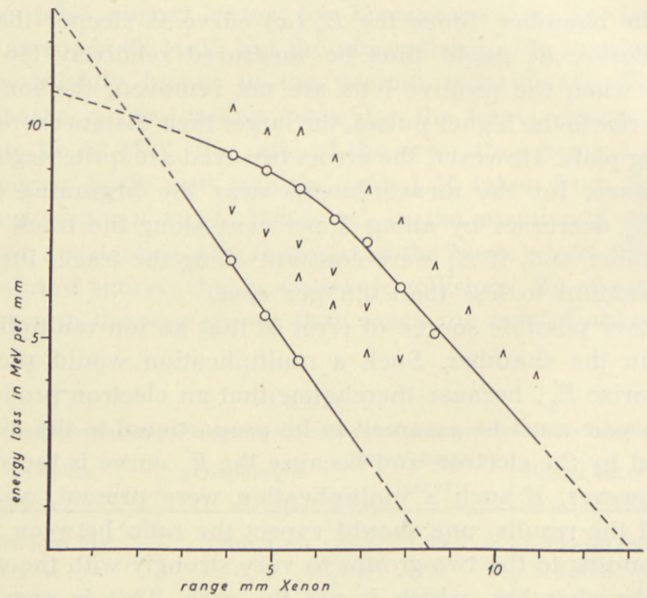

Fig. 14. Ionization range curves in xenon. Open circles correspond to peak values, arrow points to upper and lower limits.

In xenon two series of measurements were performed at a pressure of 115 mm Hg and 38 mm Hg. Since some of the recording films were lost by an accident the transformation factor necessary for a comparison of the two series of measurements could not be determined, but the experimental results were found to be very similar to those in argon, the higher stopping power of xenon of course being taken into consideration. For x-values of 1.9 and 2.9 mm xenon the distribution curves were very similar to those for x-values 3.8 and 5.8 mm of argon (Fig. 9), showing a single, rather symmetrical peak and a peak with a hump on the left side, respectively.

Fig. 14 gives the result of the measurements at a pressure of 115 mm Hg. The extrapolated ranges R_{ex} are found to be 8.5 and 13 mm of xenon, corresponding to 16 and 24 mm of air[1], which is slightly higher than the corresponding values obtained in argon (13.5 and 21.7 mm of air), but the differences are hardly outside the limits of experimental error. The ratio of the areas beneath the two curves is 86:54 = 1.60, in rather good agreement with the value given by FLAMMERSFELD et al.

§ 2. Specific ionization in the light gases.

Preliminary experiments with the first diaphragm and the aluminum foil showed that the ionization distribution curves found in hydrogen, deuterium, and helium were similar to those in argon, the ionization varying along the range in much the same way. However, rather large differences concerning the reduced extrapolated ranges occurred[1]. Also, the magnitude of the background relative to the actual pulses varied from one gas to another; in hydrogen it was slightly higher than in deuterium, and in helium it was considerably higher.

All three gases were used at a pressure of 120 mm Hg (15° C).

[1]) The reduced extrapolated range is here defined by the expression

$$R_{ex}^{air} = R_{ex} \cdot \sigma \cdot \frac{n}{2},$$

σ being the relative stopping power for $P\sigma$ α—particles and n the number of atoms in the molecule.

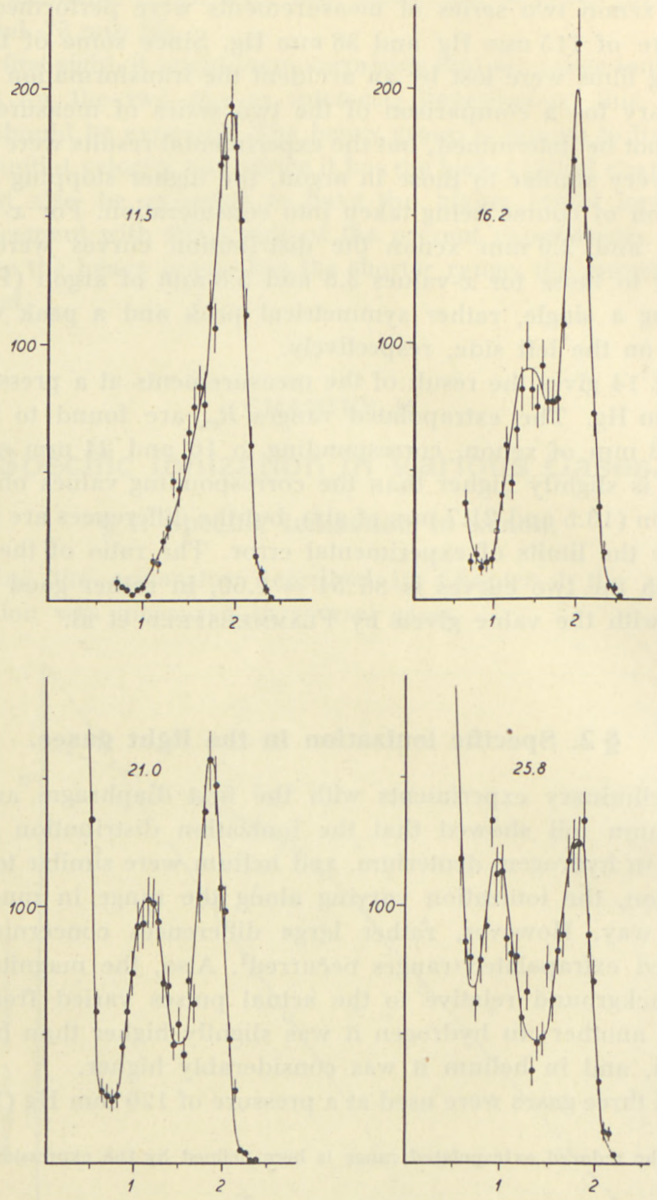

Fig. 15. Ionization distribution curves in deuterium corresponding to distances between uranium layer and ionization chamber ranging from 11.5 to 25.8 mm D_2.—Ordinate: number of fragments.—Abscissa: size of pulses in MeV per mm D_2. (For the calibration of the pulse sizes, see text.)

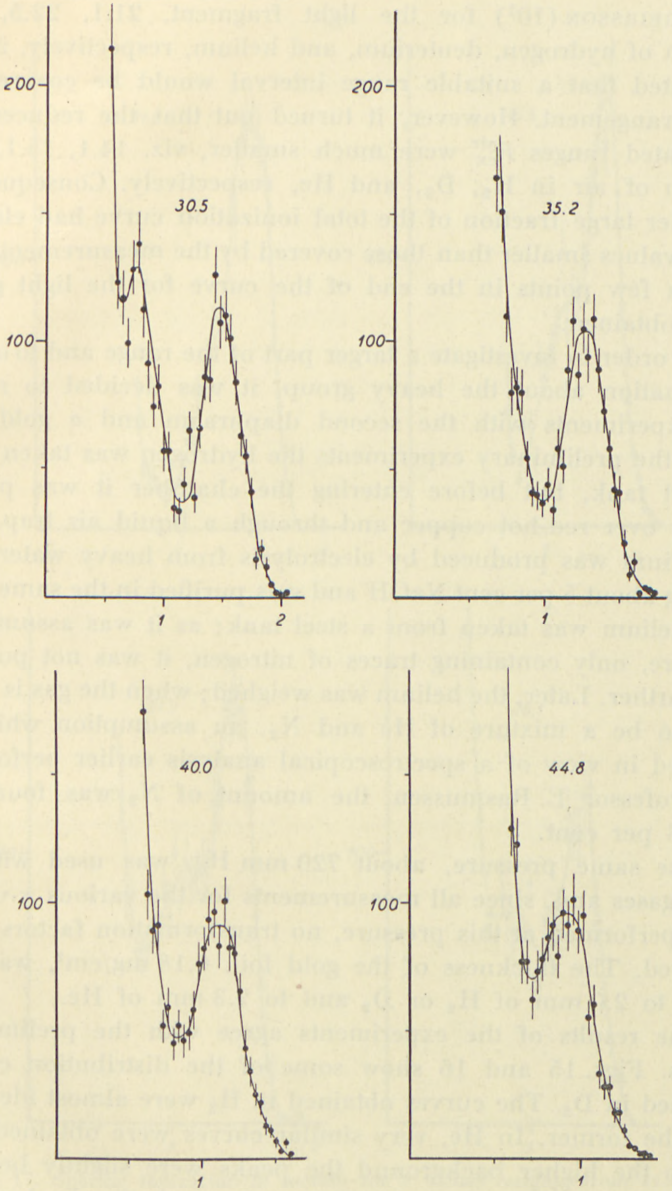

Fig. 16. Specific ionization in deuterium for x values ranging from 30.5 to 44.8 mm.

From the reduced ranges given by Bøggild, Arrøe, and Sigurgeirsson (10[1]) for the light fragment, 21.1, 22.5, and 28 mm of hydrogen, deuterium, and helium, respectively, it was estimated that a suitable range interval would be covered by the arrangement. However, it turned out that the reduced extrapolated ranges R_{ex}^{air} were much smaller, viz. 14.1, 15.1, and 19 mm of air in H_2, D_2, and He, respectively. Consequently, a rather large fraction of the total ionization curve had elapsed for x values smaller than those covered by the measurements and only a few points in the end of the curve for the light group were obtained.

In order to investigate a larger part of the range and to obtain information about the heavy group, it was decided to repeat the experiments with the second diaphragm and a gold foil. As in the preliminary experiments the hydrogen was taken from a steel tank, but before entering the chamber it was passed slowly over red-hot copper and through a liquid air trap. The deuterium was produced by electrolysis from heavy water containing about 5 per cent NaOH and was purified in the same way. The helium was taken from a steel tank; as it was assumed to be pure, only containing traces of nitrogen, it was not purified any further. Later, the helium was weighed; when the gas is assumed to be a mixture of He and N_2, an assumption which is justified in view of a spectroscopical analysis earlier performed by Professor E. Rasmussen, the amount of N_2 was found to be 2.8 per cent.

The same pressure, about 720 mm Hg, was used with all three gases and, since all measurements for the various x-values were performed at this pressure, no transformation factors were required. The thickness of the gold foil, 0.18 mg/cm^2, was put equal to 2.0 mm of H_2 or D_2 and to 2.3 mm of He.

The results of the experiments agree with the preliminary results. Figs. 15 and 16 show some of the distribution curves obtained in D_2. The curves obtained in H_2 were almost identical with the former. In He, very similar curves were obtained, but due to the higher background the peaks were slightly broader and the separation between the peaks and the background was somewhat less complete (cf. Fig. 17).

[1]) In the following cited as B. A. S.

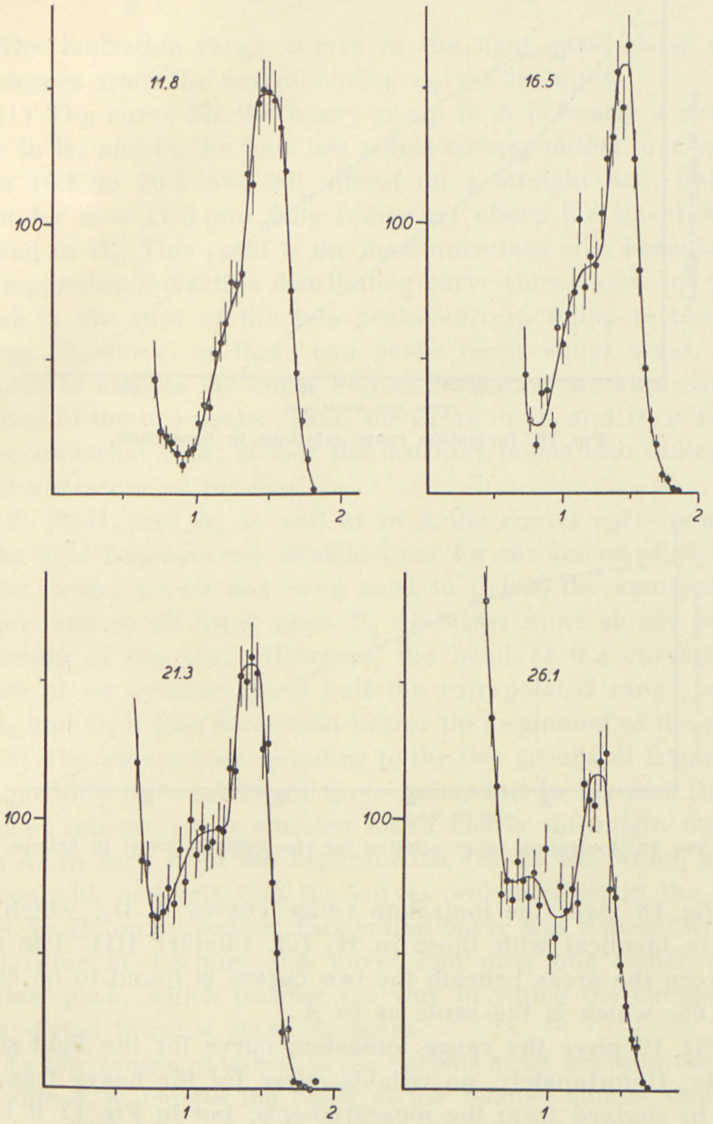

Fig. 17. Specific ionization in helium for x values ranging from 11.8 to 26.1 mm.

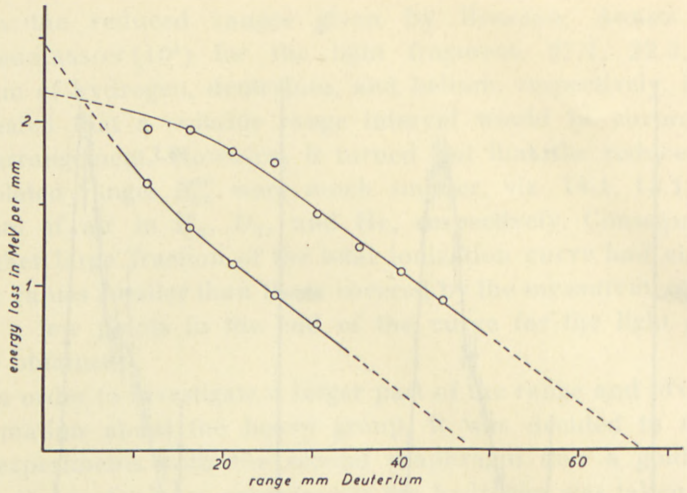

Fig. 18. Ionization range relations in deuterium.

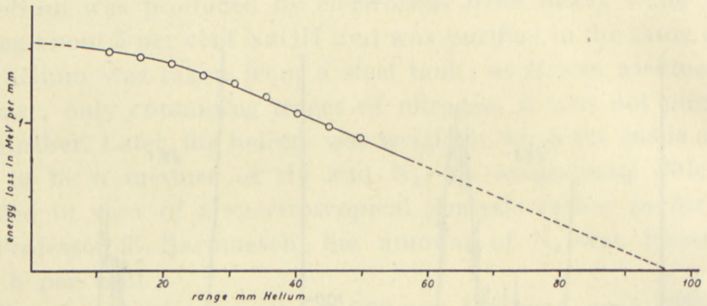

Fig. 19. Ionization range relation for the light fragment in helium.

Fig. 18 gives the ionization range curves in D_2, which are nearly identical with those in H_2 (cf. Chapter III). The ratio between the areas beneath the two curves is found to be 86:52 = 1.65, which is the same as in A.

Fig. 19 gives the range ionization curve for the light group in He. Unfortunately, no reliable curve for the heavy fragment can be derived from the measurements, but in Fig. 17 it is indicated that the point of intersection of the two curves, if any, falls close to the starting point of the fragments.

§ 3. Comparison of various gases.

The ionization range curves in the light gases show some differences from the corresponding curves in argon.

(1) The curve for the heavy group in A is nearly a straight line; in H_2 and D_2 the four last points corresponding to x-values from 16.5 to 30.5 mm fall almost on a straight line, but the point for $x = 11.5$ mm falls somewhat above the line both in H_2 and in D_2. This point is the most uncertain one, because the corresponding ionization distribution curve shows only one peak which is the sum of the two peaks corresponding to the two groups. However, as these two peaks cover equal areas, it is possible to analyse the curve and to determine the approximate position of the two peaks. Thus, the curve in H_2 and D_2 is found to be somewhat bent; in fact, the last four points also indicate a small curvature of the line.

(2) In H_2 and D_2 as well as in A the curves corresponding to the light fragment are straight lines for the intermediate part of the range, which has been used to define the extrapolated ranges, and in all three gases E_1 decreases more slowly in the beginning of the path. However, the bend of the curve in A occurs at an x-value about half the extrapolated range, while in H_2 and D_2 it falls somewhat nearer the beginning of the path.

(3) The curves corresponding to the two groups of fragments will possibly intersect in all three gases, but in H_2 and D_2 the point of intersection is situated much nearer the origin than it is in A; in fact, from the experimental results we cannot at all deduce with certainty that the curves will intersect in the light gases. In H_2 an ionization distribution curve was determined for an x-value of 4.5 mm; this curve had only one rather symmetrical peak, which justifies the way in which the curves are extrapolated towards small x-values.

(4) The ranges obtained in the various gases are summarized in Table 4. σ denotes the value of the relative atomic stopping power used when calculating the reduced extrapolated ranges from the expression $R_{ex}^{air} = R_{ex} \cdot \sigma \cdot \frac{n}{2}$, where n is the number of atoms in the molecules of the gas. In order to compare with the

Table 4.

	σ	Extrapolated ranges (present work)					Ranges given by B. A. S.		
		mm of gas		mm of normal air		$\frac{R_{ex\cdot 2}}{R_{ex\cdot 1}}$	mm of normal air		$\frac{R_2}{R_1}$
		$R_{ex\cdot 1}$	$R_{ex\cdot 2}$	$R^{air}_{ex\cdot 1}$	$R^{air}_{ex\cdot 2}$		R^{air}_1	R^{air}_2	
H_2	0.22	65.5	47.5	14.4 (14.1)[2]	10.5	0.72	21.1	17.7	0.84
D_2	0.22	68	48.5	15.0 (15.1)[2]	10.7	0.71	22.5	18.9	0.84
He[1]	0.395[1]	97		19 (19) [2]			28	23	0.82
A	1.94	22.4	14.4	21.7	14.0	0.65	23.9	19.4	0.81
Xe	3.76	13	8.5	24	16	0.67	23	18	0.81

[1] As the helium gas was a mixture of 97.2 % He and 2.8 % N_2, σ was put equal to $0.35 \cdot 0.972 + 2 \cdot 0.98 \cdot 0.028 = 0.395$; 0.35 and 0.98 being the stopping powers for He and N_2, respectively.

[2] The figures in the brackets are those obtained in the preliminary investigations.

total reduced ranges given by B. A. S. the stopping power for Po α-particles is chosen.

It is seen that the air equivalent of the extrapolated ranges increases monotonically with the atomic number of the stopping

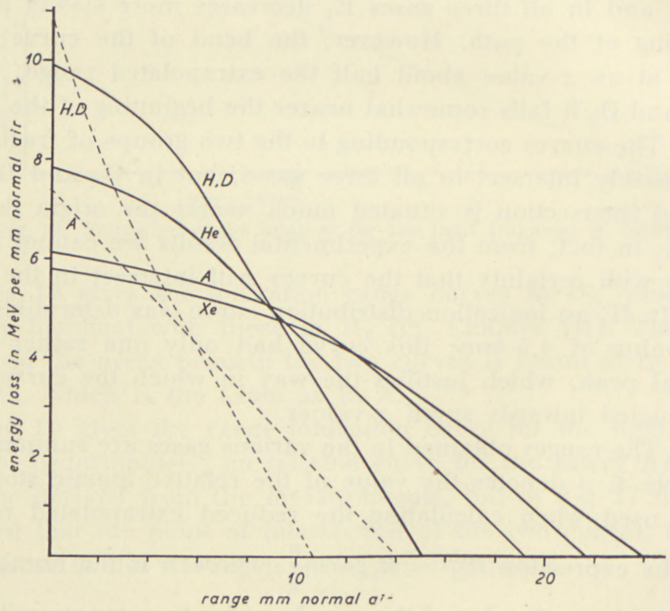

Fig. 20. Ionization range relations in various gases.—The full-drawn curves correspond to the light group, the dotted lines to the heavy group.

gas, in contrast to the total reduced ranges given by B. A. S., which decrease from He through A to Xe. This is by no means a discrepancy, as will be further discussed in Chapter III.

In Fig. 20 are plotted the ionization range curves for the various gases; the abscissae are the distances traversed, reduced to normal air by means of the values for σ given above. Evidently, the small values of the reduced extrapolated ranges in H_2, D_2, and He involve a higher initial ionization per mm of air in these gases than in A, a result which, however, is in agreement with the theory. Moreover, the agreement is not only qualitative. From the figure we find for the ionization per mm of air, i. e. the ionization by fission fragments relative to that by α-particles, that for the light group it is 1.6 times higher in H_2 (D_2) than in A, and 1.2 times higher in He than in A. Assuming the charge to be the same in all gases, Bohr (2) finds the ratios, calculated by means of the theoretical stopping formula, to be 1.5 and 1.2, respectively, in agreement with the experimental values.

§ 4. Measurements in mixtures of gases.

Although the above-mentioned agreement is rather satisfactory, the ionization in H_2 is seen to be slightly higher than

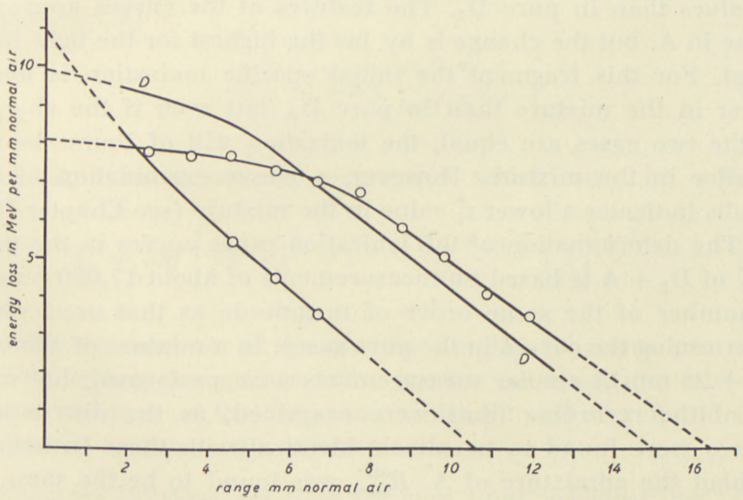

Fig. 21. Ionization range relations in a mixture of 95 per cent deuterium and 5 per cent argon.—The curve *D-D* corresponds to the light group of fragments in pure D_2. The curves for the heavy group in pure D_2 and in the mixture, respectively, are identical.

what corresponds to the calculations. This might indicate that also the charge in H_2 is slightly higher than in the other gases, which would not be difficult to understand from a theoretical point of view. For α-particles the cross-section for electron capture is much smaller in H_2 than in heavier gases and the same should be true for fission fragments. One should thus expect that a small admixture of a heavier gas would cause an increase in the charge and the ionization; measurements of the specific ionization were therefore performed in two gas mixtures.

In a mixture of 564 mm D_2 and 30 mm A the result shown in Fig. 21 was obtained. $R^{air}_{ex\cdot 1}$ is found to be somewhat higher than in pure D_2 (16.4 mm of air against 15.0), but $R^{air}_{ex\cdot 2}$ is unchanged. For a comparison the curves obtained in pure D_2 are shown. The curves for the heavy group are identical, while those for the light group differ markedly. For $x = 2.3$ and 3.2 mm no points are given for the heavy group, since only one peak is seen on each of the corresponding distribution curves and their analysis is rather uncertain, but from the distributions it is obvious that the curves intersect at an x-value near 2. Thus, it is found that the point of intersection has a higher x-value and that the bend of the curve for the light group falls at higher x-values than in pure D_2. The features of the curves approach those in A, but the change is by far the highest for the light fragment. For this fragment the initial specific ionization is much lower in the mixture than in pure D_2, but even if the charges in the two gases are equal, the ionization will of course be the smaller in the mixture. However, a closer examination of the results indicates a lower z_1^* value in the mixture (see Chapter III).

The determination of the ionization range curves in the mixture of D_2 + A is based on measurements of about 17,000 pulses, a number of the same order of magnitude as that used when determining the curves in the pure gases. In a mixture of 560 mm He + 28 mm A similar measurements were performed, but only $^1/_4$ of the recording films were examined, as the distribution curves were found to be almost identical with those in helium without the admixture of A. $R^{air}_{ex\cdot 1}$ was found to be the same in the mixture containing A and in helium, only containing the admixture of N_2 (19.5 and 19.2 mm of air, respectively).

CHAPTER III

Construction of Velocity Range Relations for the whole Range.

§ 1. Energy loss along the range in argon.

The previous measurements of the specific ionization could only yield ionization range curves for the first part of the range since, in the last part of the range, the ionization became too low as compared with the ionization background in the chamber. However, even if the ionization had been measurable, we could not, as in the beginning of the path, expect it to be proportional to the energy loss, since in the end of the path ionization takes place mainly through nuclear collisions and since many of the recoiling atoms might have rather small energies and, hence, produce fewer ion pairs per eV. If for velocities of the fragments smaller than $v_0 = \frac{\varepsilon^2}{\hbar}$ the energy loss due to electronic encounters is neglected in comparison with that due to nuclear collisions, the energy loss may be estimated by the formula (Bohr, ref. 2, formula 5.1,2)

$$-\frac{dv}{dx} = 2\pi N \frac{z^2 z'^2 \varepsilon^4}{m m' v^3} \cdot L_v, \tag{1}$$

where L_v is a logarithmic expression which may be written

$$L_v = log \left\{ z z' \sqrt{z^{2/3} + z'^{2/3}} \cdot \frac{\mu (m + m')}{m m'} \cdot \left(\frac{v_0}{v}\right)^2 \right\}^{-2}. \tag{2}$$

In these expressions, N denotes the number of atoms per cm^3 of the stopping gas, and m and z are the mass and the nuclear charge numbers of the fragment, while m' and z' refer to the gas atoms, and μ is the electronic mass.

Formula (1) does not hold for very small velocities $\left(v < \frac{1}{3} v_0\right)$ for which the logarithmic argument in (2) becomes comparable

with or smaller than unity. For such velocities $-\frac{dv}{dx}$ will vary inversely proportional to v, but in the case of fission fragments this problem affects only the extreme end of the range and is insignificant in the present connection.

Let us consider the "average fragments" to which we ascribe the values $(z_1, m_1) = (39, 95)$ and $(z_2, m_2) = (53, 139)$ (cf. ref. 11). By a numerical integration of (1) we get v and $\frac{dv}{dx}$ as functions of x in the range interval concerned. Fig. 22 shows the result for the light fragment; the point for which $v = v_0$ has been chosen as origin on the axis of abscissae. From these two curves $\frac{dE}{dx} = mv\frac{dv}{dx}$ is calculated and the result is given by curve a in Fig. 23. The end-point for this curve has been chosen to be $x = 2.47$ cm of argon in accordance with the range value given by B. A. S. Curve b of Fig. 23 is the curve from Fig. 13 corresponding to the most frequent values of the specific ionization for the light group, and the full-drawn curve obtained by fitting together a and b in the way shown in the figure may be assumed to represent the $\frac{dE}{dx}$ curve along the whole range for the fragment with $(z_1, m_1) = (39, 95)$. In order to derive this curve, the curves a and b should, strictly speaking, be plotted as functions of the velocity, in which case the contributions from electronic and nuclear collisions could be directly added. However, considering the uncertainty of the whole procedure, it is justified simply to join a and b in a smooth way.

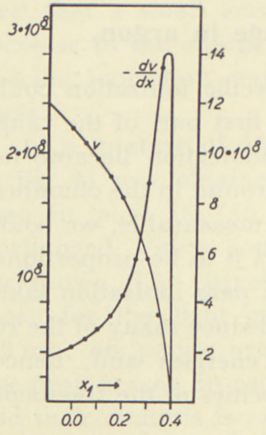

Fig. 22. $v(x)$ (scale to the left) and $-\frac{dv(x)}{dx}$ (scale to the right) for the light fragment in argon. The curves are calculated on the assumption that the energy loss is due entirely to nuclear collisions.

The corresponding curve for the heavy fragment has been obtained in a similar way and is also shown in Fig. 23. The ordinates of the ionization measurements, determined only on a relative scale, have been normalized in such a manner that the area beneath the full-drawn curve for the light fragment is 86 MeV,

representing the initial energy. The area beneath the curve for the heavy fragment is then found to be 55 MeV, corresponding to a ratio 1.56 between the initial energies of the two fragments, in good agreement with the value of 1.50 given by FLAMMERSFELD et al. (6) and the value of 1.49 given by JENTSCHKE (12). It is of interest here to note that the ratio of the areas beneath

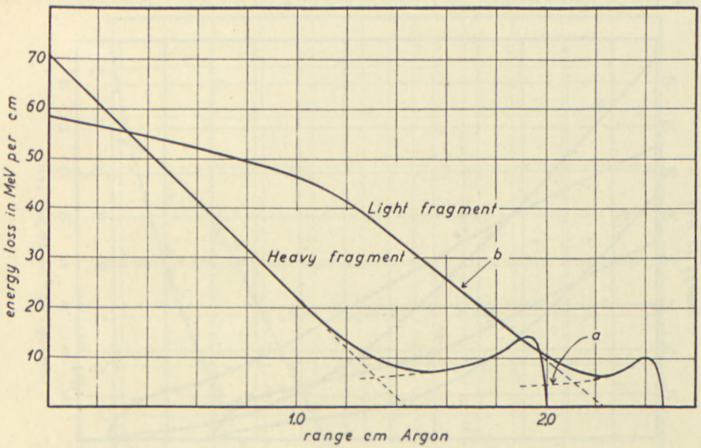

Fig. 23. Energy loss along range in argon.

the two extrapolated ionization curves is 1.65, which is higher than the directly measured ratio of the initial energies and, thus, that we get an improved internal consistency of the empirical data by taking into account the difference between R_{ex} and R.

§ 2. Energy range curves and velocity range curves in argon.

From the $\frac{dE}{dx}$ curves the $E(x)$ curves are obtained by integration. Fig. 24 shows the result for both fragments. The curve for the light fragment may be compared with the curve previously measured in mica (3). Assuming the relative stopping power of argon and mica to be the same for fission fragments as for α-particles of medium velocity, for which 1 cm of argon corresponds to 1.41 mg/cm^2 of mica, we get a very close agreement, the difference between the two curves in the interval from 0 to

2.4 mg/cm² of mica never exceeding 2 MeV. For fragments having traversed 1.04 mg/cm² of mica, corresponding to 0.74 cm argon, E_2 was previously found to be 23 MeV (13), while the corresponding value as taken from Fig. 24 is 19 MeV. Also here it is interesting to note that, if the tail of the $\frac{dE_2}{dx}$ curve had been omitted, we would have obtained an $E_2(x)$ curve giving the value

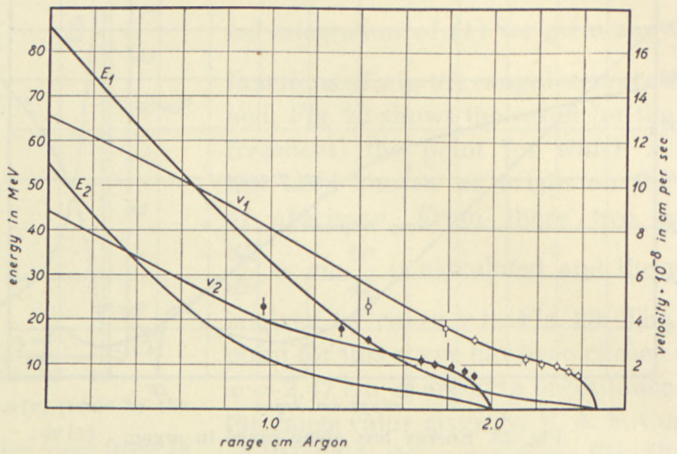

Fig. 24. Energy *vs.* range (scale to the left) and velocity *vs.* range (scale to the right) for fission fragment in argon. Indices 1 and 2 refer to the light and heavy group, respectively. The points are the velocities given by Boggild, Brostrøm, and Lauritsen.

of 12 MeV, which would be in definite disagreement with the measured 23 MeV.

From the $E(x)$ curves also the $v(x)$ curves may be derived. They are shown in the same figure where furthermore are plotted the results obtained by Bøggild, Brostrøm, and Lauritsen (1) who have measured the velocity as a function of the residual range. These authors give mean values for both groups of fragments taken together and, consequently, their data have been compared with the curve for the light fragment (open circles) as well as with the $v_2(x)$ curve (full circles). The points are seen to fall slightly below the $v_1(x)$ curve and slightly above the second curve; thus, the agreement must be considered satisfactory.

§ 3. Energy loss along the range in the light gases.

In complete analogy to the procedure described in § 1 the $\frac{dE}{dx}$ relations have been constructed for H_2 and D_2 by means of the measurements of specific ionization, the nuclear stopping

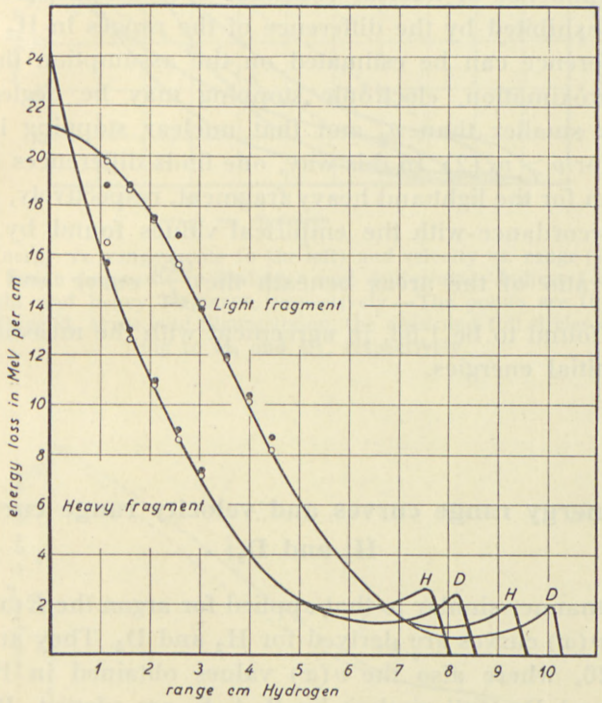

Fig. 25. Energy loss along range in hydrogen and deuterium. The open circles are the experimental values found in H_2, the full circles the corresponding values in D_2.

formula (1), and the range values given by B. A. S. The result is shown in Fig. 25. It should here be remembered that the experimental values are measured only in relative units and, hence, the agreement between the absolute values of the points corresponding to H_2 and D_2 is partly a result of the normalization of the scale, by which the areas beneath the curves for the light fragment in H_2 and D_2 are given the same value. Nevertheless, it is satisfactory to find that the rate of decrease in specific energy loss for the light fragment in the first part of the path is so nearly

the same in the two gases and that also the two curves for the heavy group coincide. This not only checks the reliability of the measurements, but it also confirms the theoretical estimate that the stopping in this part of the range is due to electronic encounters and that nuclear collisions are of negligibly small influence.

The influence of nuclear collisions over the last part of the range is exhibited by the difference of the ranges in H_2 and D_2. This difference can be estimated on the assumption that, as a first approximation, electronic stopping may be neglected for velocities smaller than v_0 and that nuclear stopping is unimportant for $v > v_0$ (2). In this way, one finds differences of 7 mm and 5 mm for the light and heavy fragment, respectively, which is just in accordance with the empirical values found by B. A. S.

The ratio of the areas beneath the $\frac{dE_1}{dx}$ curve and the $\frac{dE_2}{dx}$ curve is found to be 1.53, in agreement with the measured ratio of the initial energies.

§ 4. Energy range curves and velocity range curves in H_2 and D_2.

In a manner similar to that applied for argon the $E(x)$ curves and the $v(x)$ curves are derived for H_2 and D_2. They are shown in Fig. 26, where also the $v(x)$ values obtained in H_2 (open circles) and D_2 (full circles) by B. A. S. are plotted. It is seen that these values fall rather far outside the curves; the discrepancy cannot be explained only by uncertainties in measurements, but seems to represent a systematic deviation. In fact, the points are situated nearly on the straight lines connecting the two ends of the curves (dotted on the figure) and from the preceding procedure it is clear that when representing $v(x)$ by these lines we would find disagreement with the theory as well as with the measurements of the specific ionization.

A possible explanation for the discrepancy might be found in the assumption that the light gases in the cloud-chamber used by B. A. S. were not pure, but contained admixtures of heavier

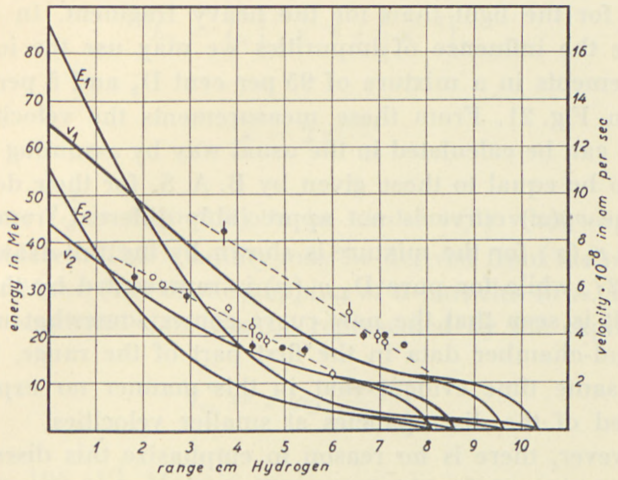

Fig. 26. Energy vs. range (scale to the left) and velocity vs. range (scale to the right) for fission fragments in hydrogen and deuterium.—Indices 1 and 2 refer to the light and heavy fragment, respectively.—The points are the velocities given by Bøggild, Arrøe, and Sigurgeirsson, the open and full circles corresponding to H_2 and D_2, respectively.

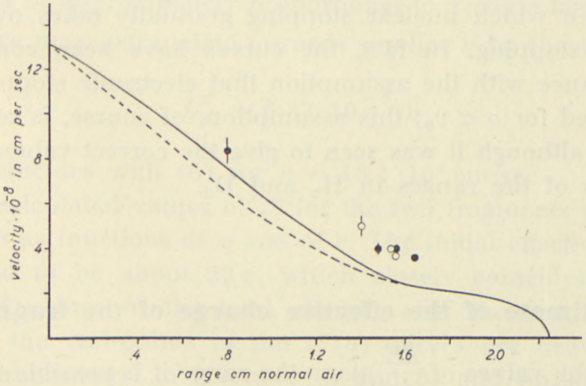

Fig. 27.

gases; in any case, we know that some water vapour was present. As will be seen from Fig. 21, a small contamination of argon in the deuterium gas causes a rather large change of the $\frac{dE_1}{dx}$ curve. The effect is much smaller for the heavy fragment, but in this connection it might also be noted that the deviation of the cloud-chamber data from the curves in Fig. 26 is much

greater for the light than for the heavy fragment. In order to estimate the influence of impurities we may use the ionization measurements in a mixture of 95 per cent D_2 and 5 per cent A, given in Fig. 21. From these measurements the velocity range relation can be calculated in the usual way by assuming the total range to be equal to those given by B. A. S. for their deuterium gas. The $v_2(x)$ curve is not appreciably different from that in Fig. 26; $v_1(x)$ for the mixture is shown by the full-drawn curve in Fig. 27, while for pure D_2 $v_1(x)$ is represented by the dotted curve. It is seen that the new curve comes somewhat nearer to the cloud-chamber data in the first part of the range, but it is at the same time evident that in this manner no explanation si offered of the discrepancies at smaller velocities.

However, there is no reason to emphasize this discrepancy. The cloud-chamber data cannot be expected to have a high accuracy in the velocity region concerned, since they rely on the proton velocity range relation which is not very well known for such small velocities. Moreover, the greatest uncertainty of the constructed velocity range curves falls just in the region in question, in which nuclear stopping gradually takes over from electronic stopping. In fact, the curves have been constructed in accordance with the assumption that electronic stopping may be neglected for $v < v_0$; this assumption, of course, is somewhat arbitrary, although it was seen to give the correct values for the differences of the ranges in H_2 and D_2.

§ 5. Estimate of the effective charge of the fragments.

From the values of $\frac{dE}{dx}$ along the range it is possible to calculate the effective charge z^* of the fragments by means of the electronic stopping formula (Bohr, ref. 2, formula 5.1.2)

$$-\frac{dE}{dx} = 2\pi N \frac{(z^*)^2 \varepsilon^4}{\mu v^2} \cdot L_\varepsilon . \qquad (3)$$

In heavy stopping materials like A the quantity L_ε for fission fragments may be obtained from the relation

$$L_\varepsilon = L_\varepsilon^\alpha \left(\frac{3}{4} \varkappa^{-\frac{1}{3}} + \frac{1}{4} \varkappa^{-1} \right), \tag{4}$$

where

$$\varkappa = 2 z^* \cdot \frac{v_0}{v} \tag{5}$$

and where L_ε^α is a quantity to be used in (3) when α-particles are considered. This quantity may be derived from the measurements of MANO (14) of the stopping of α-particles in A. He finds that the empirical data can be represented by the expression

$$L_\varepsilon^\alpha = z' \log \left(\frac{2 \mu v^2}{\bar{I}} \right)^2 \tag{6}$$

with $\bar{I} = 195\ eV$[1]. MANO's measurements cover only velocities greater than $12 \cdot 10^8$ cm/sec; for considerably smaller values (6) will not hold but, since L_ε^α according to (6) is nearly linear for a large interval of v and since, according to general arguments (2), L_ε^α should be approximately proportional to v over a large velocity region, we may extrapolate towards smaller v by the expression

$$L_\varepsilon^\alpha = 6.33 \cdot 10^{-8} \cdot v \tag{7}$$

which coincides with (6) for $v = 13.1 \cdot 10^8$ cm/sec.

The calculated values of z^* for the two fragments are shown in Fig. 28 as functions of x and of v. The initial effective charges are found to be about $22\,\varepsilon$, which closely coincides with the measured values of the total charges e of the fragments (5). Through the end-points of the $z^*(v)$ curves are drawn dotted curves proportional to v (curves a and b) and proportional to $v^{\frac{1}{2}}$ (curve c). In earlier experiments (3), the total charge e_1 for the light fragment was found to be nearly proportional to $v_1^{\frac{1}{2}}$ in the beginning of the range, and the corresponding quantity e_2 for the heavy fragment was by similar measurements found to decrease somewhat more slowly than v_2. Concerning the present results it is seen that z_2^* varies approximately proportional to v_2,

1) In fact, in deducing the value $\bar{I} = 195$ eV, MANO applied certain corrections to formula (6); in our case, however, these are already included in relation (4).

and that $z_1^*(v)$ decreases more slowly than $z_2^*(v)$, in accordance with the mentioned measurements of the total charges.

A slight discrepancy which definitely cannot be accounted for by experimental uncertainties appears since, according to Fig. 28, we have $z_1^* > z_2^*$ for $x = 0$, while the charge measure-

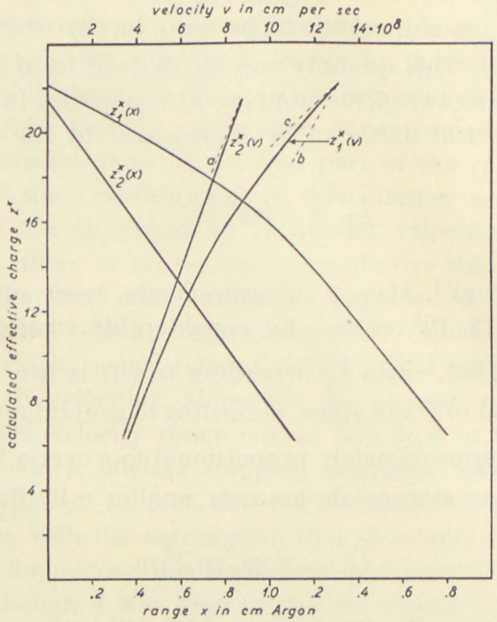

Fig. 28. The effective charge of fission fragments in argon as functions of the distance x traversed (scale of abscissae below) and as functions of the velocity v (scale of abscissae above).

ments (9) have shown that the heavier fragment at the beginning of the range carries a charge about 10 per cent higher than that of the lighter fragment. A possible, though not very probable explanation for this discrepancy might be found in the fact that the measured charge values are those characteristic of the penetration of the fragments through the uranium target, while the values in Fig. 28 correspond to argon. Another explanation would be that the effective charge, as defined by (3), although approximately equal to the total charge of the fragment, still might differ slightly from this quantity.

In the case of hydrogen, the value of L_ε to be introduced in (3) may be written

$$L_\varepsilon = log\left\{\left(\frac{2\,v}{v_0}\right)^4 [\varkappa]^{-2}\left[\varkappa\cdot\frac{v_0}{2\,v}\right]\right\}, \qquad (8)$$

where the square brackets indicate that the quantity in the brackets is to be replaced by unity if smaller than 1. A slightly more

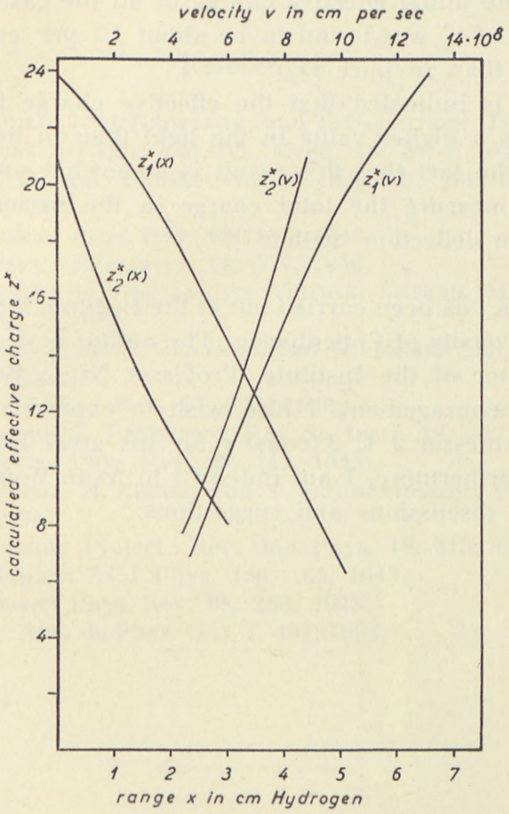

Fig. 29. The effective charge of fission fragments in hydrogen as functions of the distance x traversed (scale of abscissae below) and as functions of the velocity v (scale of abscissae above).

accurate expression is obtained by replacing v_0 by v_H given by $\frac{1}{2}\mu v_H^2 = 16.0$ eV, since expression (8) in the case of fast α-particles for which $\varkappa < 1$ reduces to MANO's semi-empirical formula.

The calculated values of z^* in H_2 are shown in Fig. 29. The curves are similar to those in argon and also here the initial

value of z^* is higher for the light than for the heavy fragment. As is seen, the initial values of z_2^* are approximately equal in the two gases, while z_1^* is slightly higher in H_2 than in A.

Similar calculations for the mixture of 95 per cent D_2 and 5 per cent A lead to the result that the heavy fragment has almost the same initial effective charge in all the gases, while the initial value of z_1^* was found to be about 10 per cent lower in the mixture than in pure D_2.

Thus, it is indicated that the effective charge for the light fragment has a higher value in the light than in heavier gases. In view of the fact that this result is somewhat uncertain it is planned to measure the total charge in the various gases by means of the deflection method*).

This work has been carried out at the Institute for Theoretical Physics, University of Copenhagen. The author is deeply grateful to the Director of the Institute, Professor NIELS BOHR, for his continued encouragement. I also wish to express my heartiest thanks to Professor J. C. JACOBSEN for his great interest in the work and, furthermore, I am indebted to AAGE BOHR, mag. sc., for valuable discussions and suggestions.

*) Note added in proof: As the first results of measurements of the total charge in various gases, the following may be mentioned.

1) In the gases, the light fragment has a higher charge than the heavy fragment, in contrast to the charges as measured in uranium. This result eliminates the discrepancy mentioned on page 40.

2) However, the initial charges are found to be about $15\,\varepsilon$, thus somewhat smaller than the effective charges estimated from the specific energy loss.

3) The charge of the light fragment may be slightly higher in hydrogen than in heavier gases, but the phenomena seem to be more complicated than assumed in the above paragraph.

More detailed information will be given when the experiments are concluded.

References.

1) J. K. Bøggild, K. J. Brostrøm, and T. Lauritsen: D. Kgl. Danske Vidensk. Selskab, Mat.-fys. Medd. **18**; no. 4, 1940.
2) N. Bohr: D. Kgl. Danske Vidensk. Selskab, Mat.-fys. Medd. **18**; no. 8, 1948.
3) N. O. Lassen: Phys. Rev. **69**; 137, 1946.
4) N. O. Lassen: Phys. Rev. **70**; 577, 1946.
5) N. O. Lassen: D. Kgl. Danske Vidensk. Selskab, Mat.-fys. Medd. **23**; no. 2, 1945.
6) A. Flammersfeld, P. Gentner, and W. Jensen: ZS. f. Phys. **120**; 450, 1943.
7) P. Demers: Phys. Rev. **70**; 974, 1946.
8) R. Sherr and R. Peterson: Rev. Sc. Instr. **18**; 567, 1947.
9) N. O. Lassen: Phys. Rev. **68**; 142, 1945.
10) J. K. Bøggild, H. Arrøe, and T. Sigurgeirsson: Phys. Rev. **71**; 281, 1947.
11) The Plutonium Project: Rev. Mod. Phys. **18**; 513, 1946.
12) W. Jentschke: ZS. f. Phys. **120**; 165, 1943.
13) N. O. Lassen: Phys. Rev. **68**; 230, 1945.
14) G. Mano: Ann. de Phys. (11), 1, 407, 1934.

Indleveret til selskabet den 25. februar 1949.
Færdig fra trykkeriet den 31. december 1949.

DET KGL. DANSKE VIDENSKABERNES SELSKAB
MATEMATISK-FYSISKE MEDDELELSER, BIND XXV, NR. 12

TENSIMETRIC AND X-RAY INVESTIGATIONS ON MAGNESIUM CARBONATE TRIHYDRATE AND ITS DEHYDRATION PRODUCTS

BY

AXEL LANNUNG
AND
AKSEL TOVBORG JENSEN

KØBENHAVN
I KOMMISSION HOS EJNAR MUNKSGAARD
1949

CONTENTS

Printed in Denmark
Bianco Lunos Bogtrykkeri

I. Introduction.

In a previous paper (1), we have put forward some observations on the course of dehydration in hydrated salts with special regard to the many conditions for the reversible dehydration of a hydrated salt. In connection with these observations, a detailed knowledge of the dehydration of magnesium carbonate trihydrate and the rehydration of the dehydration products is of considerable interest. The stable end product of the dehydration process, crystalline magnesite, is so hard (H 3.5—4.5) that it can not be expected to be produced at room temperature in the laboratory within a reasonable time. On the other hand, the process

$$\underset{\text{(Nesquehonite)}}{MgCO_3, 3\,H_2O} \rightarrow \underset{\text{(colloidal magnesite)}}{MgCO_3 + 3\,H_2O}$$

is described by geologists as a rapid process. It could therefore be expected that the dehydration of $MgCO, 3\,H_2O$ should be further from the ideal state than the previous studied process $CaCl_2, H_2O \rightarrow CaCl_2 + H_2O$, that thus a study of this process would increase our knowledge of such non-ideal systems, but that it, on the other hand, should not be too slow to measure. This also proved to be the case. By non-ideal dehydration-rehydration systems we understand those in which the thermodynamic properties such as the equilibrium vapour pressure and its temperature coefficient are dependent on the way in which the system is built up; the systems will most often not be completely reversible.

Interest in the process is increased by the fact that comprehensive investigations on the solubility of magnesium carbonates have already been carried out by J. K. Gjaldbæk (2). In his paper, among other peculiarities, it was pointed out that different magnesite preparations have different solubilities; the

explanation for this is now found in the results of our X-ray investigations. With regard to the properties, for example the solubilities of different labile magnesium carbonates, we can also supplement GJALDBÆK's basic work.

Our paper comprises the following main sections:

1) Preparation of the trihydrate, synthetic magnesite and amorphous "active" magnesium carbonates prepared partly by dehydration at two different temperatures and partly by precipitation.

2) Measurements of water vapour and carbon dioxide pressures of systems of magnesium carbonate trihydrate and its dehydration products, in addition to corresponding measurements of systems of amorphous "active" magnesium carbonate and its rehydration products.

3) X-ray examinations of different magnesites, of the "active" magnesium carbonates, of magnesium carbonate trihydrate and also of phases in the systems measured tensimetrically.

The results obtained will be communicated in the first section. After this will follow some general considerations on dehydration-rehydration in non-ideal systems, and then a section on the heats of hydration measured. Finally, a section with experimental details. The many vapour pressure data, the heats of hydration and detailed descriptions of the many systems measured, is appended, because it did not seem unlikely to us that these data could give a more detailed picture of the state in such non-ideal systems than that which we are able to outline at present.

II. Various Solid Systems Consisting of Magnesium Carbonate and Water, their Properties and Mutual Transformations.

The transformation of all known magnesium carbonates to magnesite and water is accompanied by a decrease in the free energy of the system. Nevertheless, it is an experience which our investigations confirm, that well crystallized magnesite can only be prepared by the heat treatment of hydrated magnesium carbonate—preferably in the presence of water—at high temperature.

In systems with no liquid phase, even after heat treatments at temperatures up to about 200°, we were not able in any case to observe even an initial formation of magnesite; this is in agreement with MENZEL, BRÜCKNER and SCHULTZ (3), who only at 320° were able to obtain a small amount of crystalline magnesite in a similar system.

Our synthetic magnesite, produced by heating the trihydrate with water to 175°, gives a powder diagram of the greatest sharpness, which is exactly like a diagram of a coarsely crystalline, calcite-like magnesite, such as the Snarum magnesite, investigated by GJALDBÆK. When GJALDBÆK found that his synthetic magnesite was more easily soluble in water than Snarum magnesite, can we therefore not explain this simply by postulating that the synthetic magnesite is not so well crystallized as Snarum magnesite. The only difference between GJALDBÆK's method of preparation and ours has been that we heated for 20 hours at 175°, while GJALDBÆK reports that the process is complete in 1—2 hours at 160—175°; our crystals were 5—25 μ, while GJALDBÆK states that his crystals were similar to Eubøa magnesite and consequently only 2—3 μ. It is possible that GJALDBÆK has had in his preparation a sufficient quantity of a still finer fraction and this has been responsible for the solubility measured.

Eubøa magnesite, which is stated by GJALDBÆK to crystallize with a particle size of 2—3 μ gives on X-ray investigation too wide lines; this shows that it is not so well crystallized as our synthetic magnesite or as Snarum magnesite. When GJALDBÆK found that this is considerably more soluble than the magnesites, which give sharp powder reflections, this is therefore only as expected. The increase in line width is not especially great, somewhat less than the $\alpha_1\,\alpha_2$ separation. The increase in line width indicates that a considerable part of the substance consists of particles with a size of 800—1000 Å.

What impurities the four magnesites examined have contained, we have not investigated, but they can not all have been pure, since only two of them had the same lattice constants. We have not calculated the absolute values of the lattice constants. This has less interest, since we lack quantitative analyses and detailed information on the sites of origin of the four mineral samples.

On mixing of concentrated equimolar solutions of magnesium

chloride and alkali carbonate a voluminous white precipitate is produced, to which R. ENGEL (4) gives the formula $MgCO_3, 2\ H_2O$ by indirect analysis. This can not stand washing, hence it can not be analyzed directly or used for solubility experiments, and very little is known about the compound except that it is transformed to trihydrate on standing a few hours in its mother liquor. We succeeded in making a powder diagram of the compound before the formation of trihydrate became appreciable. The diagram contained (apart from weak sodium chloride lines from the dried mother liquor) only diffuse rings. The next day, definite crystals of trihydrate could be seen under the microscope. The experiment showed that ENGEL's "dihydrate" is quite amorphous. The water content can not therefore be considered important. The solubility and other properties of the compound will not supposedly differ much from those of other amorphous magnesium carbonates found and described below.

The equilibrium water vapour pressure over a system consisting of magnesite + a magnesium carbonate hydrate is not available for measuring at room temperature on account of the exceptional inertness of magnesite. On the other hand the equilibrium pressure over systems of magnesium carbonate trihydrate + dihydrate, of trihydrate + amorphous "active" magnesium carbonate, of dihydrate + its amorphous dehydration product or of amorphous "active" magnesium carbonate + its amorphous hydration products can be measured. The irreversible "aging" phenomena, which most of the systems mentioned show to some extent, are slow processes compared with the equilibration of the equilibrium vapour pressure.

The starting material for the preparation of all the systems described was a crystalline magnesium carbonate trihydrate prepared according to GJALDBÆK (2).

Rehydration systems.

On heating to 180—210° in a stream of carbon dioxide, the trihydrate changes to an "active" magnesium carbonate, the water content of which decreases within 53 hours to 0.24 moles H_2O per moles $MgCO_3$. According to the X-ray diagram this

Table 1.

Water vapour pressure, carbon dioxide pressure and tensimetric heats of hydration of systems formed by rehydration of amorphous "active" magnesium carbonate, prepared from trihydrate dehydrated at 180—210°.

System No.	$H_2O/MgCO_3$	18°			25°			35°			kcal.	X-ray characteristic
		p_{H_2O}	log r [1]	p_{CO_2}	p_{H_2O}	log r	p_{CO_2}	p_{H_2O}	log r	p_{CO_2}	mole H_2O liq.	
R_1...	0.24	0.08	.71 −3	<0.01								Amorphous
R_2 [2]..	0.33	0.94	.78 −2	0.05	1.26	.725−2	0.06				−3.2	Amorphous
R_3...	0.86	(1.34)	(.941−2)	0.02	(2.15)	(.957−2)	0.02	(4.00)	(.977−2)	0.02	(0.96)	Amorphous
R_4...	1.24	4.29	.443−1	(0.29)	6.12	.411−1	(0.31)	9.32	.344−1	(0.32)	−2.4	Amorphous
R_5a..	1.40	(6.34)	(.612−1)	(0.22)	(8.06)	(.531−1)	(0.23)	(10.38)	(.391−1)	(0.27)	(−5.3)	
R_5b..	1.40	8.92	.761−1	0.13	10.08	.628−1	0.15	11.86	.449−1	0.18	−7.5	16 lines of trihydrate
R_6...	1.94	8.05	.716−1	0.24	8.98	.578−1	0.23	11.05	.418−1	0.23	−7.2	30 lines of trihydrate
R_7...	2.38	11.07	.854−1	0.35	12.64	.726−1	0.43				−7.3	52 lines of trihydrate

[1] r = relative vapour pressure

[2] R_2 : 0°: $p_{H_2O} = 0.40$, $p_{CO_2} = 0.04$

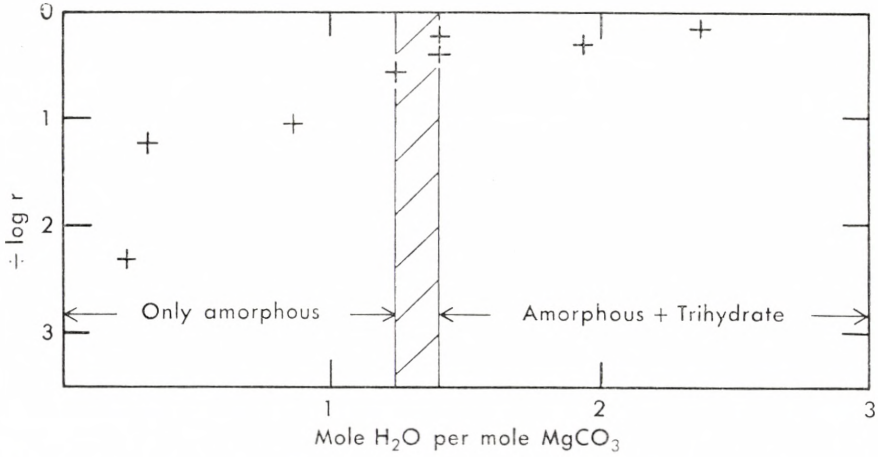

Figure 1. The relative vapour pressure r at 18° as a function of the water content in rehydrated amorphous "active" $MgCO_3$, prepared at about 200°.

preparation is completely amorphous; it gives a pure liquid diagram. It is strongly hygroscopic, on suspension in water it is quickly transformed into a pure crystalline trihydrate. During intermittent measurements of the vapour pressure at 18, 25 and 35° (see table 1) we allowed this "active" magnesium carbonate to take up water. In fig. 1 we have given the relative vapour pressures at 18° as a logarithmic function of the water content. r is the ratio between the vapour pressure of the hydrate system and the vapour pressure of water at the same temperature. Even at a water content of 1.24 moles H_2O per mole $MgCO_3$ it was quite amorphous. Crystallization first begins between 1.24 and 1.40 mole H_2O. The trihydrate is produced. At the same time the water vapour pressure rises to 80 times the initial value. It is remarkable that this "active" magnesium carbonate can remain amorphous with a water content as high as 1.24 moles. On further uptake of water to 2.38 moles H_2O, the vapour pressure only increases 50 %. While the water content rises from 0.24 moles H_2O to 2.38 moles H_2O, the tensimetric heat of hydration—calculated from the temperature coefficient of the vapour pressure—falls from about −2.8 kcal per mole H_2O to −7.5 kcal per mole H_2O.

It is noteworthy that we find negative tensimetric heats of hydration not only for this system, but for several others described in this paper.

In a survey of the literature, positive heats of hydration of the order of a few kcal per mole liquid water will be found in most cases. In a previous paper (5) one of the authors has found positive tensimetric heats of hydration of up to 13.7 kcal per mole H_2O in systems of calcium chloride monohydrate + calcium chloride prepared from the former by dehydration at low temperature. This system contained extremely fine particles, but X-ray analysis showed that the calcium chloride was certainly not amorphous.

Negative heats of hydration are, however, not unknown. Thus H. MENZEL et al. (6) give the vapour pressure at 20 and 25° for a system of $Na_2B_4O_7$, 10 H_2O and its X-ray amorphous dehydration product, from which a tensimetric heat of hydration can be calculated of −4.5 kcal per mole liquid water.

Calculation of the solubility of amorphous magnesium carbonate.

It can be seen from fig. 1 that the tendency of "active" magnesium carbonate to take up the first few hundredths of a mole H_2O is considerable, but it sinks rapidly and is low for the last two moles of water. GJALDBÆK had already found that its reaction with water to form the trihydrate is so rapid that its solubility can not be measured. Numerical calculations of solubility from the vapour pressure are certainly very inexact because we are dealing with a non-ideal system, where we can not be sure of having single homogeneous phases. We will, however, carry through a few calculations to illustrate the information that vapour pressure can give us about the solubility of amorphous magnesium carbonate.

In general it can be said that it must be the most quickly reacting part of the system that determines the vapour pressure. Hence it must for example at the point where the trihydrate is formed, be trihydrate and the most quickly reacting part of the amorphous hydration product nearest to the trihydrate which determine the vapour pressure. This part of the amorphous hydration product must also be considered to be the most readily soluble, so that the water vapour pressure of the system is an

expression of the upper limit for the solubility of the amorphous phase at the given water content.

GJALDBÆK (2) has estimated at 18° the solubility product L_3 and L_5 for trihydrate and pentahydrate, $L_3 = [Mg^{++}]_3\ [CO_3^{--}]_3 = 10^{-5.05}$ and $L_5 = [Mg^{++}]_5\ [CO_3^{--}]_5 = 10^{-4.89}$. The ionic symbols in square brackets with the indices 3 and 5 suffixed, indicate the activity of the corresponding ions in saturated solutions of trihydrate and pentahydrate respectively.

On the basis of vapour pressure measurements of a system, the rehydration system R_5b discussed later, consisting of incompletely crystallized trihydrate and an amorphous phase, which we assume to contain one mole H_2O, we will calculate the solubility product $L_1 = [Mg^{++}]_1\ [CO_3^{--}]_1$ for the supposed monohydrate. The vapour pressure above this system which we designate $p_{1,3}$ was 8.92 mm at 18°.

The transformation of monohydrate to trihydrate: $MgCO_3, H_2O + 2\ H_2O \rightarrow MgCO_3, 3\ H_2O$ can be carried out by evaporating 2 moles H_2O at saturated vapour pressure, p_{H_2O}, expanding to $p_{1,3}$, the vapour pressure over the monohydrate-trihydrate system, and condensing the water vapour on this. By this we gain the work $A_1 = 2RT \ln p_{H_2O}/p_{1,3}$. We can also effect the transformation by dissolving 1 mole $MgCO_3, H_2O$ in the saturated solution of the compound with simultaneous reversible transfer of 1 mole anhydrous magnesium carbonate to a saturated solution of $MgCO_3, 3\ H_2O$ with simultaneous precipitation of 1 mole of the latter. By this we have transformed 1 mole $MgCO_3, H_2O$ to $MgCO_3, 3\ H_2O$, but at the same time diluted the saturated solution of monohydrate with 1 mole H_2O and concentrated the saturated solution of trihydrate by removing 3 moles H_2O by crystallizing out the trihydrate. Since the vapour pressure above the saturated solutions of monohydrate and trihydrate respectively are practically the same and both very near to the vapour pressure over pure water, we can neglect the work of transference for water and obtain for the work of transformation:

$$A_2 = RT \ln \frac{[Mg^{++}]_1\ [CO_3^{--}]_1}{[Mg^{++}]_3\ [CO_3^{--}]_3}.$$

Since $A_1 = A_2$, $\log L_1/L_3 = 2 \log p_{H_2O}/p_{1,3}$ and we find $L_1 = 10^{-4,57}$ for our amorphous monohydrate at 18°.

Table 2.

Water vapour pressure, carbon dioxide pressure and tensimetric heats of hydration of systems formed by dehydration of magnesium carbonate trihydrate at room temperature.

	System No.	$\frac{H_2O}{MgCO_3}$	18°			25°			35°			kcal. / mole H_2O liq.	X-ray characteristic
			p_{H_2O}	log r	p_{CO_2}	p_{H_2O}	log r	p_{CO_2}	p_{H_2O}	log r	p_{CO_2}		
Series 1	D_1. .	2.52	2.50	.208–1	0.35	3.28	.140–1	0.36	4.70	.047–1	0.40	–3.9	34 lines of trihydrate 2 lines of dihydrate
	D_2. .	2.02	(6.01)	(.589–1)	0.20	(7.80)	(.516–1)	0.23	(9.78)	(.365–1)	0.25	(–5.4)	13 lines of trihydrate 6 lines of dihydrate
Series 2	D_3a.	1.88	0.18	.066–2	0.07	0.32	.13–2	0.10	0.73	.238–2	0.16	4.2	
	D_3b.	1.88	0.24	.49–2	0.04	0.43	.26–2	0.05	0.91	.334–2	0.06	3.5	17 somewhat diffuse lines of dihydrate
	D_4. .	1.64	0.04_4	.46–3	0.03	0.08	.53–3	0.04	0.18	.63–3	0.05	4.2	10 diffuse lines of dihydrate
	D_5. .	1.43	0.01_4	.96–4	0.07	0.02_7	.06–3	0.06	0.05_5	.11–3	0.05	3.8	6 diffuse lines of dihydrate
	D_6. .	1.85	(1.90)	(.089–1)	0.21	(2.74)	(.062–1)	0.22	(4.57)	(.035–1)	0.25	(–1.3)	14 lines of trihydrate 9 lines of dihydrate

The difference between the solubility products of the two hydrates, $10^{-5.05}$ and $10^{-4.57}$, is small in proportion to the difference from the crystalline magnesite's solubility product $10^{-8.59}$, a figure we have calculated from GJALDBÆK's data.

The dehydration systems.

It has been shown previously by one of us (5) that the temperature of dehydration in a non-ideal system is determining for the energy state of the dehydration product. In order to investigate the part played by temperature of formation in the properties of the dehydrated trihydrate, another sample of "active" magnesium carbonate was prepared by dehydration of the trihydrate at room temperature over phosphorus pentoxide *in vacuo* for 309 days. The vapour pressures at 18, 25 and 35° were measured at 5 different stages (see table 2). A preparation of the composition $MgCO_3$, 1.43 H_2O was obtained. The rate of

Table 3.

Dehydration of magnesium carbonate trihydrate *in vacuo* over P_2O_5 at room temperature.

Time of dehydration Days	Composition $\frac{\text{mole } H_2O}{\text{mole } MgCO_3}$	Rate of dehydration $\frac{\text{mole } H_2O}{\text{day}}$	System No.
0	3.06	0.09	
0.8	2.99	0.024	
36	2.16	0.020	
50	1.88	0.011	D_3
68	1.69	0.0015	
102	1.64	0.0013	D_4
164	1.56	0.0009	
209	1.52	0.0009	
309	1.43		D_5

dehydration fell in this period from 0.024 moles per day to 0.0009 moles per day (see table 3). Simultaneously with each estimation of vapour pressure an X-ray diagram was made. The lines of the trihydrate disappeared during gradual dehydration, and another line system appeared which we assume to originate from a dihydrate. The supposed dihydrate is identical with a crystalline phase, the existence of which MENZEL et al. (3) have already demonstrated by X-ray analysis in different dehydration products of magnesium carbonate, prepared by them. Our X-ray diagrams show the same lines as those published by MENZEL. MENZEL considered these to be due to a monohydrate. On this point we can not agree. In our diagrams the line system in question is most marked at a water content of a little below 2 moles, at the same time the last trihydrate lines disappear. On further dehydration there is a considerable fall in vapour pressure, and the lines of the new phase decrease in intensity; at a water content of 1.43 moles their intensity has fallen to roughly $^1/_3$ of the maximum. This is not in agreement with the supposition that the new phase is a monohydrate, neither do the diagrams presented by MENZEL et al. support this theory. Their diagram of a preparation with 2 H_2O shows the lines of the new phase most clearly, and another diagram of "magnesium carbonate monohydrate" which they have dehydrated under boiling toluol and according to the data is the completely pure monohydrate, is decidedly the most unsatisfactory of the X-ray diagrams presented by MENZEL.

In our investigations we did not wait for the disappearance of the last dihydrate lines.

A survey of the vapour pressure measurements of the dehydration systems at 18° is given in fig. 2. It can be seen here that the equilibrium pressure of the system dihydrate + trihydrate is rather high. When it is not the same for the two systems, which are later designated system D_1 and D_2, it is because they are not prepared in the same way, but D_2 which contains 2 moles H_2O must according to the method of preparation be considered more nearly a rehydration system. The dihydrate-trihydrate system is a non-ideal system, since the dihydrate is not an easily formed phase. The lines in its powder diagram are markedly diffuse.

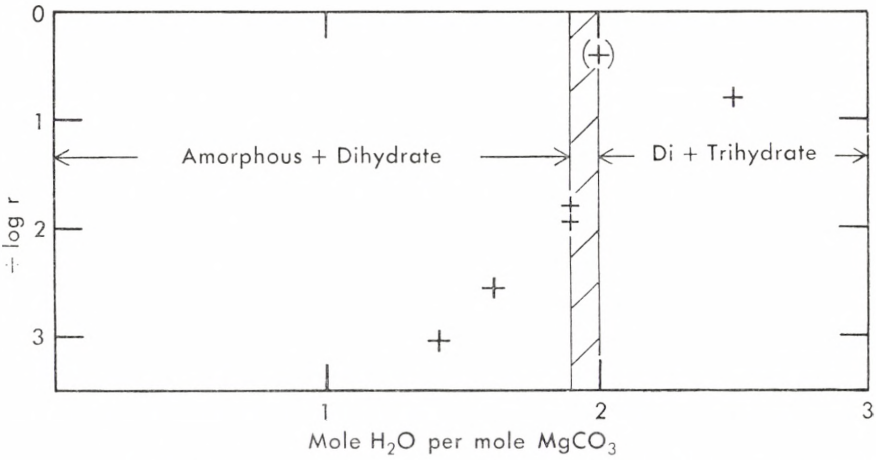

Figure 2. Dehydration of $MgCO_3, 3\,H_2O$ at room temperature. The relative vapour pressure r at 18° as a function of the water content.

In fig. 3 we have given a survey of all the systems investigated. The ordinate expresses the relative water vapour pressure in logarithmic scale, the abscissa, the reciprocals of the absolute temperature. The curves with negative slope thus correspond to systems with negative heats of hydration, the dihydrate-trihydrate system's curves D_1 and D_2 have negative slopes, the calculated tensimetric heats of hydration are of the order of −4 and −5 kcal per mole liquid H_2O.

Comparing the first rehydration systems, R_2 and R_4, with the last dehydration systems, D_3, D_4 and D_5 in fig. 3, it can be seen that the amorphous carbonate, produced by dehydration of the dihydrate at room temperature contains more free energy than the "active" carbonate prepared from the trihydrate by heating to about 200°, although according to the X-ray diagrams both are amorphous.

The amorphous parts of the dehydration systems must contain water. This can be seen from the previously mentioned rate at which the dihydrate's lines vanish as the water content falls; at 1.43 H_2O only 6 lines remain of the original 17, hence the amorphous part supposedly contains at least 1 mole H_2O per mole $MgCO_3$.

After dehydration at room temperature water vapour was led into the system in order to make the regeneration of the dihydrate as complete as possible and so insure that the alleged

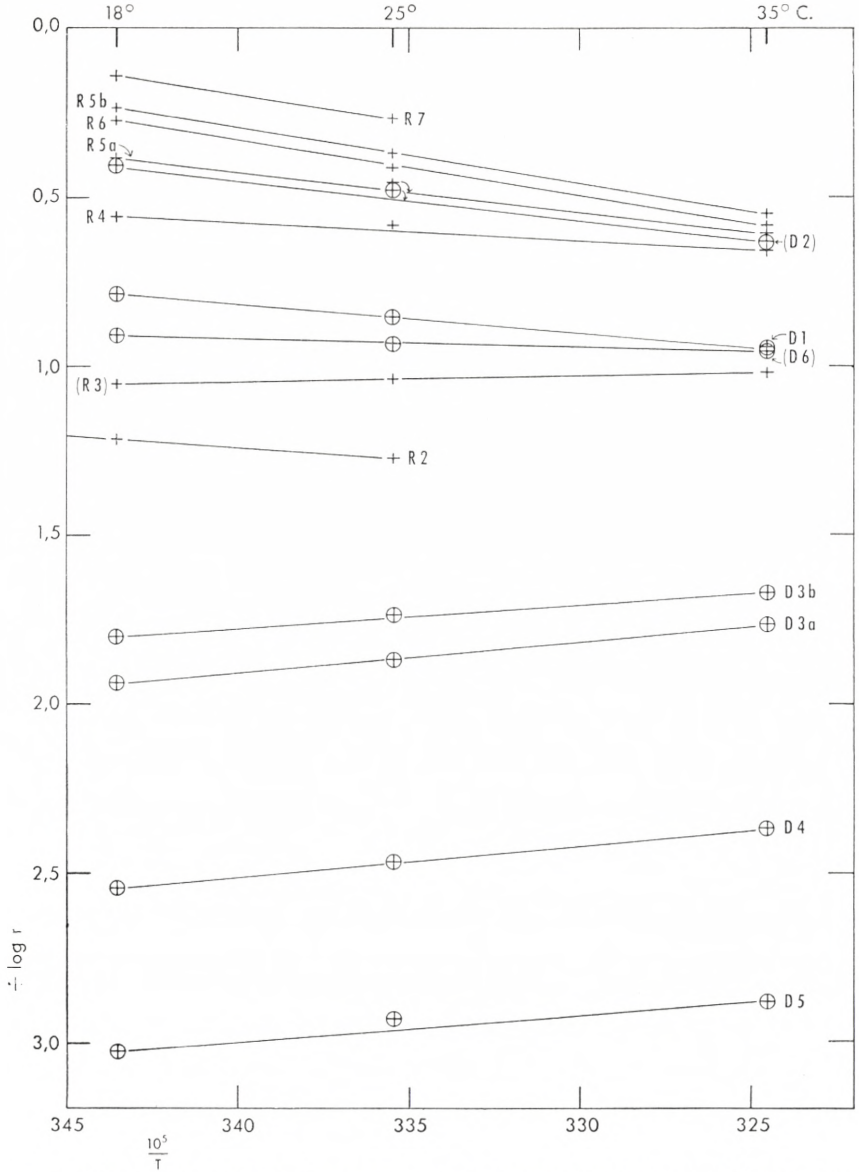

Figure 3. Relative vapour pressure r over rehydration systems (R) and dehydration systems (D) as a function of temperature. The systems R_2—R_7 are formed by gradual rehydration of amorphous "active" magnesium carbonate prepared from trihydrate, that was dehydrated at about 200°.
The systems D_1—D_2 and D_3—D_5 are formed by gradual dehydration of magnesium carbonate trihydrate at room temperature. The system D_6 is formed by partial rehydration of D_5. (Table 3).

dihydrate really contained 2 molecules of water. It appeared, however, that by this procedure trihydrate had already been formed before the system contained 2 molecules of water per molecule of magnesium carbonate. The dihydrate stage did not occur during rehydration. It is described above that the dihydrate stage did not occur during rehydration of "active" magnesium carbonate prepared at high temperature. As already pointed out, crystalline dihydrate is a compound which is produced with difficulty, as is probably consistent with its high solubility (see later), which also explains why the dihydrate is never obtained during precipitation of aqueous solutions at room temperature; instead the less soluble trihydrate is obtained.

Calculation of the solubility of the dihydrate.

We will calculate the solubility product L_2 for the imperfectly crystallized dihydrate. We choose the largest vapour pressure measured at 18°, $p_{2,3} = 6.01$ mm., over the dihydrate-trihydrate system, D_2, as that which refers to the most well crystallized dihydrate. Similarly to the previous example we obtain

$$\log L_2/L_3 = \log p_{H_2O}/p_{2,3}$$

from which we find $L_2 = 10^{-4.64}$ for our dihydrate at 18°.

In table 4 we have summarized the solubility products cal-

Table 4.

Solubility products of magnesium carbonate hydrates and magnesite at 18°.

Preparation	$-\log L_{MgCO_3, mH_2O}$	
	J. K. Gj.	A. L. + A. T. J.
Amorphous monohydrate	..	4.57
Dihydrate	..	4.64
Pentahydrate	4.89	..
Trihydrate	5.05	..
Synthetic magnesite	~ 7.17	..
Eubøa magnesite	~ 7.83	..
Snarum magnesite	~ 8.59	..

culated by GJALDBÆK from experimental data and also the values calculated by us for the amorphous alleged monohydrate and for our incompletely crystallized dihydrate.

Observation on the loss of carbon dioxide.

Small amounts of carbon dioxide are evolved during the slow dehydration of the trihydrate at room temperature and also during rehydration of amorphous "active" magnesium carbonate. The neutral magnesium carbonates are not all stable at very low carbon dioxide pressure. During the vapour pressure measurements it was necessary to correct for this carbon dioxide as later described under section 4, experimental. We did not succeed either in detecting by X-ray diagrams the basic carbonate formed by the carbon dioxide loss, or in indicating the kind of basic carbonate which determined, in connection with the normal carbonate, the carbon dioxide tension measured. The method of dehydration used, where the system apart from short intervals was closed, guarantees, however, that only quite infinitesimal amounts of carbon dioxide are lost during both dehydration and rehydration. It can therefore be assumed that the content of basic carbonate has been very small during the whole period, and has not influenced the water vapour pressure at different stages of dehydration.

GJALDBÆK (2) has shown that magnesium hydroxide in aqueous suspension may change into magnesium carbonate trihydrate, when the carbon dioxide pressure exceeds $10^{-4.54}$ atm. or 0.022 mm. Hg, while it requires a carbon dioxide pressure of 0.2 and 5.5 atm. respectively to bring a granular or fibrous basic magnesium carbonate into equilibrium with the trihydrate.

III. Some Considerations of the Dehydration Processes and Discussion of the Thermodynamic Data.

In our opinion there are three factors which are especially important for the rate, and the greater or lesser reversibility of the dehydration-rehydration processes:

1) The rate and reversibility are promoted by the maintenance of a not too low vapour pressure during dehydration.

2) The probability for reversibility decreases strongly with increasing hardness of the lower hydrate or anhydride, which are produced by the process.

3) The probability for reversibility during dehydration which proceeds to an anhydrous component, is greatest when the ratio, for this compound, between the temperature of dehydration and the melting point in degrees absolute is not too small.

Factor 1) becomes significant in less mobile systems, inert systems, where the processes first proceed with noticeable speed after the system being removed far from the state of equilibrium is brought into a strongly labile state. Compare the observations put forward by us on the kinetics of dehydration processes in an earlier paper (1).

We are not able to define any definite limit for the hardness, at which difficulties with the establishment of equilibrium become perceptible, but there is a strong indication that it lies between 2 and 3 in MOHS's scale. By far the most hydrates are softer than H = 2, while many anhydrous salts are considerably harder; hence the closest approach to reversibility is often found in systems, where the dehydration product is a hydrate.

We will give a few examples to illustrate this. By dehydration in high vacuum at 20 and 40° of $CuSO_4$, 5 H_2O, the hardness of which is rather considerable, although less than 3 (the hardness of calcite), KOHLSCHÜTTER and NITSCHMANN (7) obtain as a dehydration product of constant weight a monohydrate, completely amorphous by X-ray analysis, while dehydration at 100° in air gives a well crystallized monohydrate.

Systems of gypsum, H = 2, and its metastable dehydration product, the X-ray crystalline so-called "soluble anhydrite", shows great difference in energy, varying regularly with the dehydration temperature and sintering temperature and time, as shown in a paper by E. S. NEWMAN and L. S. WELLS (8).

The production of the stable anhydrite, H = 3—3.5, of the "soluble anhydrite" is so slow, in spite of a molar heat of formation of 3 kcal, that even 145 hours of dry heat treatment at 200° does not give a yield demonstrable by X-ray analysis; this, however, is reached after 670 hours. Heating for $1^1/_2$ hours at

170° in the presence of water results, on the other hand, in an anhydrite identical with the natural compound.

Anhydrous calcium chloride, H = 2—3, is rather slowly formed and magnesite, H = 4, simply can hardly be produced by "dry" dehydration of a hydrate. On the other hand, the dehydration of sodium bromide dihydrate even under extreme conditions does not seem to give sodium bromide of abnormal energy. The hardness of anhydrous sodium bromide is also only about 1.5 (1).

G. TAMMANN's (9) observation of recrystallization in the inorganic salts which he investigated, at a temperature of $0.57 \times T_s$, where T_s is the melting point of the salt in degrees absolute, is of special interest in regard to factor 3.

According to the circumstances, one or several of the factors mentioned in dehydration of a hydrate may be of such a size that the dehydration product has such a fine particle size that it is characterized as amorphous. The thermodynamic properties of the system will then differ from those in a corresponding system with well crystallized phases, this can be shown by tensimetric or calorimetric measurements. On dehydration of magnesium carbonate trihydrate we obtain, apart from the dihydrate both at room temperature and at 180—210° amorphous dehydration products. By performing the dehydration in carbon dioxide and heating to 320° for several days, MENZEL et al. (3) have, however, by X-ray analysis, been able to demonstrate the formation of a small amount of magnesite.

Discussion of the thermodynamic data.

We will discuss the energy content of the products, and have in table 5 summarized the tensimetric heats of hydration for all pure rehydration systems produced from the 200°-preparation of amorphous "active" magnesium carbonate. The evolution of heat at the 200°-preparation's uptake of liquid water is seen to be negative during the whole process, but there is a clear difference in its size at different stages of water uptake. It is ca. −3 kcal per mole H_2O in the range from 0.24 H_2O to ca. 1.40 H_2O. From 1.40 H_2O to 2.38 H_2O it is about constant, a good −7 kcal. This is quite a remarkable result. Taking all

Table 5.

Tensimetric heats of hydration of pure rehydration systems formed by rehydration of amorphous "active" magnesium carbonate (dehydrated at about 200°).

System No.	mole H_2O / mole $MgCO_3$	Tensimetric heats of hydration kcal./mole $H_2O_{liq.}$	X-ray characteristic
R_1	0.24	..	Amorphous
R_2	0.33	−3.2	Amorphous
R_4	1.24	−2.4	Amorphous
R_5b	1.40	−7.5	16 trihydrate lines
R_6	1.94	−7.2	30 trihydrate lines
R_7	2.38	−7.3	52 trihydrate lines

the figures together gives the following equation for the whole hydration:

$$\underset{(200°\text{-amorphous})}{MgCO_3,\ 0.24\ H_2O} + 2.76\ H_2O_{liq.} \rightarrow \underset{(cryst.)}{MgCO_3,\ 3\ H_2O} - 14.9\ \text{kcal}\ (1).$$

The figure −14.9 is obviously rather inexact, because we have only a few measurements, the sign and the order of magnitude is, however, reliable.

The heat production on addition of liquid water to anhydrous salts or salt hydrates with crystalline hydrate as reaction product, tends as previously described, to be positive and of the order of magnitude of a few kcal per mole liquid H_2O. Such a heat evolution is—apart from being usually found—reasonable from a kinetic point of view. We find a positive heat evolution, because the water molecules are bound into the lattice and by this loose energy of translation and possibility of orientation.

When, on the other hand, a trihydrate lattice is built up from amorphous magnesium carbonate and liquid water, instead of a few kcal being liberated per mole H_2O some 15 kcal are taken up from the surroundings. Why more than 15 kcal exceeding the normal amount are bound in this hydrate formation is by no means obvious. When the trihydrate is formed from amorphous magnesium carbonate and water, the water molecules doubtless partly displace the carbonate ions from contact with the magnesium ions. The heat absorbed may therefore

have been used to displace the carbonate ions to a distance from the magnesium ions and replace them by water molecules. According to this hypothesis, the carbonate ions are more firmly bound to the magnesium ions than are the water molecules. But this is strange, since the water molecules, all the same, are able to displace the carbonate ions.

It could also be supposed that the amount of heat absorbed is not used to overcome the mutual attraction of the magnesium and carbonate ions, but that it is taken up as heat energy by the trihydrate formed. This would take place, if the possibilities of vibration in the amorphous magnesium carbonate were strictly limited as compared with the crystalline trihydrate. It could be supposed that on hydration a deblocking of the vibrations of the carbonate ions occurred, this being accompanied by a considerable absorption of heat. If something like this occurs, it would not be necessary to assume that the carbonate ions are more firmly bound to the magnesium ions than the water molecules.

Both these assumptions are very unusual and it can therefore be asked whether our tensimetrically estimated heat productions are really identical with the calorimetric heats of production in the processes concerned. There is no doubt but that the vapour pressures, by which the heat absorptions are estimated, are real. They are reproducible and reversible for such large amounts of water, that they can not be explained as equilibrium pressures for the very small amount of water that adheres to the glass walls of the apparatus, or as experimental errors. We also find satisfying that we can calculate the tensimetric heat of hydration of −4.5 kcal per mole liquid water from the data of H. Menzel et al. (6) for sodium borate and its X-ray amorphous dehydration product, as previously mentioned.

It might perhaps be supposed that the reversible hydration that we measure does not lead to the production of the crystalline trihydrate (Nesquehonite), but to an intermediate product which is then irreversibly transformed to the crystalline trihydrate with production of a considerable amount of heat. Such an assumption invalidates the gross equation for the hydration and does not give our amorphous magnesium carbonate with 0.24 H_2O a very low energy content in comparison with the crystalline trihydrate. On the other hand such an assumption gives the hypothetical

intermediate product properties just as unusual as those we had to attribute to the amorphous magnesium carbonate on the supposition that the tensimetric heat of hydration was identical with the calorimetric, and the picture of the formation of the intermediate product from the amorphous magnesium carbonate becomes equally strange.

We can not calculate the heat production in the important process:

$$\underset{\text{(Nesquehonite)}}{MgCO_3, 3\ H_2O} \rightarrow 3\ H_2O + \underset{\text{(Magnesite)}}{MgCO_3} + Q$$

but we can from equation (1) estimate that Q must be positive and large (some kcal greater than 15 kcal).

This can be explained by assuming that magnesium ions and carbonate ions are bound to one another in entirely different ways in the two compounds. In magnesite, the carbonate oxygen touches the magnesium ion, while the water oxygen touches the magnesium ion in magnesium carbonate trihydrate, and Q can scarcely be interpreted in any other way than by difference in strength of magnesium-oxygen bonds in the two cases.

The dehydration systems.

In table 6 we have tabulated the heat productions for hydration of the dehydration systems in different stages. From this we obtain the following equations, valid with the previously mentioned reservations with regard to the tensimetrically estimated heats of hydration,

$$\underset{\text{(20°-amorphous)}}{MgCO_3, 1.43\ H_2O} + 0.57\ H_2O_{liq.} \rightarrow \underset{\text{(cryst.)}}{MgCO_3, 2\ H_2O} + 2.3\ \text{kcal.}$$

Further this equation:

$$\underset{\text{(cryst.)}}{MgCO_3, 2\ H_2O} + H_2O_{liq.} \rightarrow \underset{\text{(Nesquehonite)}}{MgCO_3, 3\ H_2O} - 3.9\ \text{kcal},$$

where we do not need to make reservations with regard to the identity of tensimetric and calorimetric heat production, since X-ray examination shows that we have two crystalline phases. The state of equilibrium is reached slowly, and as expected in a system of two crystalline phases, one of which is rather hard.

Table 6.

Tensimetric heats of hydration of pure dehydration systems formed by dehydration of magnesium carbonate trihydrate at room temperature.

System No.	$\frac{\text{mole } H_2O}{\text{mole } MgCO_3}$	Tensimetric heats of hydration kcal./mole $H_2O_{liq.}$	X-ray characteristic
D_5	1.43	3.8	6 diffuse dihydrate lines
D_4	1.64	4.2	10 diffuse dihydrate lines
D_3b	1.88	3.5	17 diffuse dihydrate lines
D_1	2.52	−3.9	34 trihydrate lines 2 dihydrate lines

On addition of these two equations we obtain:

$$\underset{\text{(20°-amorphous)}}{MgCO_3, 1.43\ H_2O} + 1.57\ H_2O_{liq.} \rightarrow \underset{\text{(Nesquehonite)}}{MgCO_3, 3\ H_2O} - 1.6 \text{ kcal.}$$

The corresponding equation for the formation of Nesquehonite from $MgCO_3$, 1.40 H_2O, produced by rehydration of the amorphous 200°-preparation, gives:

$$\underset{\text{(200°-amorphous, rehydr.)}}{MgCO_3, 1.40\ H_2O} + 1.60\ H_2O \rightarrow \underset{\text{(Nesquehonite)}}{MgCO_3, 3\ H_2O} - 11.7 \text{ kcal}$$

It would be expected that the amorphous system prepared at 20° with 1.40 H_2O should contain more energy than that prepared by rehydration of amorphous $MgCO_{3\,(200°)}$. The difference in energy content of the two systems found, 10 kcal, is of the expected order of magnitude.

IV. Experimental.

Preparation of Magnesium Carbonate Trihydrate, Synthetic Magnesite and Amorphous Magnesium Carbonates.

Magnesium carbonate trihydrate was prepared as described by J. K. Gjaldbæk (2) by mixing 400 cc. of 1 M magnesium sulphate solution with 300 cc. of 1 M sodium carbonate solution and allowing to stand at room temperature for 24 hours, by this procedure the voluminous precipitate first formed became crystalline. The preparation was washed free

from sulphate ion. Under the microscope beautiful well formed needle-shaped crystals were seen in addition to nearly spherical aggregates, which, however, on exposure to the air until next day were for the most part broken. X-ray examination showed only one phase, the trihydrate. For further purification, half the preparation was suspended in 500 cc. of distilled water and dissolved in this on addition of carbon dioxide. Then air was bubbled through the solution, and after a few days only needle-shaped crystals were formed, most of which were free, but a few were in bundles.

The molecular weight of the air dried preparation was determined by dissolving in a slight excess of 0.1 N hydrochloric acid, boiling and back titration with 0.1 N sodium hydroxide, using methyl red as indicator. The molecular weight of the first preparation was 139.4, corresponding to a composition of $MgCO_3$, 3.05 H_2O. The second preparation corresponded to the formula $MgCO_3$, 2.90 H_2O, while a preparation that had been kept in a weighing bottle with a glass stopper for $1^1/_2$ years gave the formula $MgCO_3$, 2.98 H_2O.

Synthetic magnesite was prepared from the trihydrate as described by J. K. GJALDBÆK (2). 1 gm. trihydrate and 5 cc. water were heated in a sealed thick-walled glass tube. To prevent the glass from breaking and in any case to prevent accidents, the sealed glass tube was put with some water into a specially constructed very solid steel bomb with a screw cap and lead washer. The whole was then heated in an electric oven to 175°. After heating for 20 hours the trihydrate had disappeared and rhombohedral crystals 5—25 μ in size appeared; on X-ray examination these gave a very beautiful sharp magnesite diagram.

Amorphous "active" magnesium carbonate was prepared according to J. K. GJALDBÆK (2) by dehydrating the trihydrate in an atmosphere of carbon dioxide at 180—210°. 1.4 gm. trihydrate with the formula $MgCO_3$, 2.90 H_2O were heated in a weighing bottle in the electrical oven to 180° with constant addition of dry carbon dioxide. In the course of 15 hours water corresponding to 2.58 moles per mole $MgCO_3$ had been lost. After the heating had been continued for 4 hours the loss was 2.61 moles, a further 16 hours at 180° increased the loss to 2.62 moles. The product, which was rather hygroscopic at

room temperature, was further heated for 18 hours at 180—210°, whereupon the loss increased to 2.67 moles H_2O. The composition of the preparation after a total of 53 hours heat treatment was calculated from the weight loss observed to be $MgCO_3$, 0.23 H_2O, titration gave the result of $MgCO_3$, 0.24 H_2O. These last 0.24 moles H_2O are thus retained with so much force that they can scarcely be present as a constituent of a crystalline hydrate. X-ray examination also showed the preparation to be completely amorphous.

A sample of the preparation, that on superficial examination had retained the structure of the starting material, when suspended in water changed within a few hours into clear crystalline needles, which microscopically and on X-ray examination proved to consist of pure trihydrate. It was thus confirmed that the loss of carbon dioxide from the carbonate during dehydration had not been considerable.

Amorphous "Active" Magnesium Carbonate Prepared at Room Temperature.

In order to avoid loss of carbon dioxide, the dehydration was carried out by means of phosphorus pentoxide in a closed evacuated system. 1 gm. trihydrate ($MgCO_3$, 3.06 H_2O) was put into a weighed flask, which was connected by a ground glass joint to another flask containing P_2O_5. The system was rapidly evaporated with a mercury vapour pump. Apart from the small amount which served to maintain equilibrium pressure in the flasks, the dehydration can in this way be carried out without loss of carbon dioxide, since the experiment showed that the loss of weight—of water as well of carbon dioxide—during evacuation and the short time of pumping was insignificant.

Table 3 shows the progress of dehydration. After standing *in vacuo* for 18 hours, the loss of water corresponded to 0.07 moles per mole trihydrate. After a little more than a month, the phosphorus pentoxide had absorbed so much water, that the loss reached 0.90 mole. After a further 14 days the total loss was 1.18 moles H_2O per mole trihydrate. After measuring the water vapour and carbon dioxide pressures of this hydrate system (D_3), as described more fully in a following section, several samples—4 mg. in all—were taken for X-ray examination.

The dehydration was then continued as previously, and several systems (D_4 and D_5) with decreasing water content were obtained and measured. For practical reasons the dehydration was not followed for longer than 309 days, by which time it had attained the composition $MgCO_3$, 1.43 H_2O.

Amorphous Magnesium Carbonate Prepared by Precipitation.

According to R. ENGEL (4), magnesium carbonate dihydrate is produced by precipitation of concentrated solutions of magnesium salts by concentrated solutions of alkali carbonates.

We precipitated 3 cc. 3 M magnesium chloride with 2 cc. 3 M sodium carbonate solution at room temperature. The mixture immediately stiffened to a gel forming an almost clear mass, on stirring a whitish suspension appeared. On taking a little up on filter paper, we obtained a damp mass which without washing was taken up on a glass rod for X-ray examination. This showed, as described, that the preparation was completely amorphous, some weak lines were present, originating from sodium chloride which had crystallized out from the mother liquor during the procedure.

Measurements of Water Vapour Pressure and Carbon Dioxide Pressure.

Method.

The vapour pressure measurements were carried out with the previously described KNUDSEN hot-wire manometer (10, 11, 12). For use in the carbon dioxide measurements, the apparatus was connected to a shortened MCLEOD manometer constructed according to M. BRUNNER's (13) description for measurements from 0.01 to 1 mm. Hg. This BRUNNER manometer was constructed so that sufficient pressure was exerted during compression while measuring, that the water vapour present was condensed. The necessary correction for water vapour pressure could then be estimated, when the temperature of the instrument was known. At very low water vapour pressure, however, only the sum of the water vapour and carbon dioxide pressures can be measured; furthermore, this is rather inexact on account of the

adsorption of the water vapour on the glass surfaces. As we shall see below, it is, however, possible in such cases to estimate by means of the hot-wire manometer the ratio between the pressures of water vapour and carbon dioxide in the mixture.

The hot-wire manometer, which was calibrated for measuring water vapour pressures from 0.001 to 20 mm., was in addition calibrated to measure carbon dioxide within the range, 0.01 to 1.20 mm.

Since the measurements of the relatively small carbon dioxide pressure here interested us most as correction to the often many times greater water vapour pressure, we consider the BRUNNER manometer to be sufficiently accurate. It was very practical to use, since it works with a volume of only 2 cc., hence the equilibrium in the water vapour-hydrate systems was not appreciably effected by the measuring.

During measurements of the magnesium carbonate hydrate systems, a reading (s volts) was first taken with the hot-wire manometer, which registered both water vapour and carbon dioxide pressure. By direct reading from the calibration curve for water vapour, we found an approximate value p′ for the water vapour pressure, which was then corrected with half the value, we found at the same time for the carbon dioxide pressure estimated by the BRUNNER manometer. The water vapour pressure p′ read off at once, was corrected with half the carbon dioxide pressure measured, because the p—s calibration curve for water vapour in the range concerned halves the ordinate values for the corresponding curve for carbon dioxide (see fig. 4). Even if this method of correction is not strictly accurate, it can, however, be taken as a very good approximation. The corrections were in general relatively small.

For water vapour pressure that was so small that we could not get the water to condense in the manometer, we estimated an approximate value for the sum of carbon dioxide and water vapour pressures in the BRUNNER manometer. When we then also measured with the hot-wire manometer, we obtained a s-value, which together with the value for the pressure (c) measured in the BRUNNER manometer, were co-ordinates to a point, which lay between the calibration curves for pure water vapour and pure carbon dioxide. Assuming that, corresponding

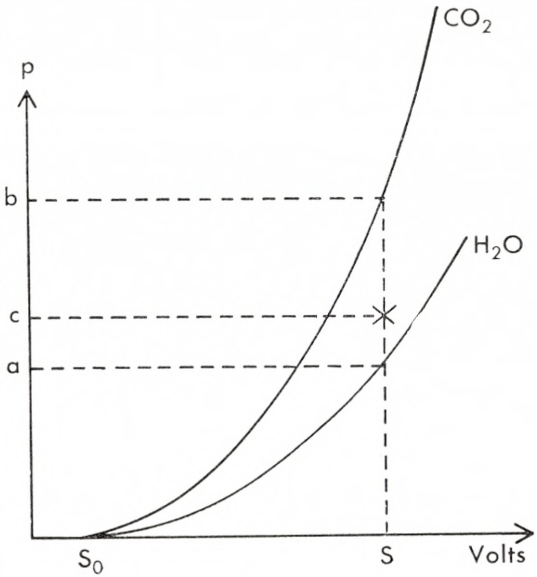

Figure 4. Estimation of the partial pressures of a mixture of CO_2 and H_2O with total pressure c by means of a reading s of the hot-wire manometer potentiometer. — The curves are calibration curves for pure CO_2 and pure H_2O vapour. c and s are co-ordinates to a point lying on a calibration curve for a certain mixture of CO_2 and H_2O vapour.

to the different mixtures of CO_2 and H_2O vapour, there are calibration curves of exactly the same type, lying between the calibration curves for pure water vapour and pure carbon dioxide and dividing the distance linearly in relation to the proportions of the mixtures, the partial pressures can be found from our measurements with the hot-wire manometer, when we know the sum of the pressures. This is most clearly demonstrated in fig. 4. To the s-value found, if this is only due to water vapour pressure, pressure a corresponds, and if only pure carbon dioxide is present, pressure b. We have, however, a mixture with pressure c, hence we calculate

$$p_{H_2O} = a\,\frac{b-c}{b-a} \text{ and } p_{CO_2} = b\,\frac{c-a}{b-a}.$$

Immediately after the pressure measurements, samples were taken out for X-ray examination. When the flask with the preparation was weighed before and after sampling, we could still keep account of the remaining preparation's weight and composition. About 1 mg. of the compound was used for an X-ray specimen.

To just the same extent as in previous papers, the difficulties in vapour pressure measurements are due to the very slow equilibration, occurring in many cases. As criterium for obtainment of equilibrium, we have taken that the same vapour pressure should be reached whether it is approached from a higher or lower vapour pressure. Since we measured at 18, 25 and 35°, it was especially the readings at 25°, that were most valuable in this connection. To illustrate this, we will give some extracts from the records of the measurements of water vapour pressure over two hydrate systems:

a) System R_4, amorphous, 1.24 moles H_2O per mole $MgCO_3$ prepared 25-12-1943 from R_3 (0.86 H_2O) by leading in at room temperature water vapour at 13 mm. pressure in 25 hours, of which 0.0234 gm. $H_2O \sim 0.38$ moles was taken up. Stored until 15-3-44. The alteration in pressure, when the temperature was changed from 18° to 35° is 5 mm., which under the given experimental conditions corresponds to a change of 0.01 mole H_2O in the composition of this system or about 1% of the water content.

Date	Potentiometer reading	Temperature	p_{CO_2} mm	p'_{H_2O} mm	p_{H_2O} mm
16-3-44	9894	18°	..	2.37	..
22-3-44	10422	18°	..	..	..
23-3-44	12188	25°	..	..	..
30-3-44	12650	25°	..	..	..
1-4-44	14801	35°	..	9.20	..
5-4-44	14907	35°	0.24	9.48	9.36
5-4-44	13747	25°	..	6.81	..
17-4-44	13493	25°	0.32	6.33	6.17
19-4-44	12209	18°	..	..	..
21-4-44	12216	18°	0.29	4.43	4.29
22-4-44	13431	25°	..	..	..
24-4-44	13439	25°	0.31	6.27	6.12
25-4-44	14953	35°	..	..	..
27-4-44	14937	35°	0.32	9.58	9.42
1-5-44	13486	25°	..	..	..
3-5-44	13490	25°	0.33	6.33	6.17
4-5-44	12243	18°	..	..	..
6-5-44	12202	18°	0.31	4.43	4.27

b) System D_3b, $MgCO_3$, 1.88 H_2O prepared by dehydration of 0.964 gm. $MgCO_3$, $3H_2O$ at room temperature. Measured after sintering at 35° from 22-9-43 to 8-10-43. The alteration in pressure at temperature change from 18 to 35° is 0.7 mm., corresponding to an alteration of 0.0007 moles H_2O in the composition or 0.037 % of the water content.

Date	Potentiometer reading	Temperature	P_{CO_2} mm	p'_{H_2O} mm	P_{H_2O} mm
8-10-43	2150	18°	..	..	..
13-10-43	3623	18°	..	..	..
14-10-43	3624	18°	0.02	0.21	0.20
20-10-43	4791	25°	..	..	..
20-10-43	4812	25°	0.03	0.41	0.39
22-10-43	6802	35°	..	..	..
22-10-43	6818	35°	0.06	0.94	0.91
23-10-43	5012	25°	..	..	..
25-10-43	5032	25°	0.05	0.46	0.43
27-10-43	3987	18°	0.04	0.26	0.24
2-11-43	3974	18°	..	..	..

The water vapour measurements are by far the most important, since we did not expect that the carbon dioxide pressures were well defined; in any case, we have not been able to detect carbon dioxide pressure determining phases (apart from the $MgCO_3$ hydrates) by X-ray analysis. They may have occurred, but only in very small amounts, we think here in particular of magnesium hydroxide and basic magnesium carbonate.

The measurements were as a rule carried out at 18, 25 and 35°. We were therefore in a position to calculate the heats of hydration q for each system by means of CLAUSIUS-CLAPEYRON's formula:

$$q = R \frac{\ln r_2 - \ln r_1}{\frac{1}{T_1} - \frac{1}{T_2}}$$

in which R is the gas constant, r_1 and r_2, the relative water vapour pressures at absolute temperatures T_1 and T_2, and q the tensimetric heat of hydration valid for 1 mole liquid H_2O. It must be stressed here that the values calculated in each case

are only valid for that part of the system, which has been determining for the vapour pressure. As shown in a previous paper (5), it is not necessarily more than a small part of a system, which is determining the vapour pressure, when one or both phases are inhomogeneous. The tensimetric heats of hydration calculated from the vapour pressure data can under such conditions not be expected to be identical with the mean values obtained by calorimetry.

Measurements of Systems Produced by Rehydration of Amorphous "Active" Magnesium Carbonate.

Rehydration series. Table 1 and figure 3.

System R_1. $MgCO_3$, 0.24 H_2O. The system consisted of the completely amorphous "active" magnesium carbonate prepared by dehydration of the trihydrate in an atmosphere of carbon dioxide at 180—210°. After repeated evacuation to remove all air, the pressure above the system rose in 5 days to 0.08 mm., which, however, was scarcely an equilibrium pressure.

System R_2. $MgCO_3$, 0.33 H_2O. Prepared by leading water vapour at 12 mm. pressure for a few minutes at room temperature into system R_1. Most of the water vapour was taken up within 24 hours, but final equilibrium was not obtained for quite a month. As soon as the water vapour was introduced, the pressure changed immediately, and within short periods almost reproducibly when the temperature was changed, hence the long accomodation time must be due to a slowly progressing alteration in the solid phases of the system, an aging or sintering must have taken place. No samples were collected for X-ray analysis, but the preparation must have been amorphous just as the next and the previous preparations. The heat of hydration was calculated to be −3.2 kcal per mole liquid H_2O.

System R_3. $MgCO_3$, 0.86 H_2O. Water vapour at 15 mm. pressure was led at varying intervals for a total of 131 minutes into R_2, while the flask was kept at 20° to avoid condensation of the water vapour. It was then allowed to stand in the flask for 4 months, after which samples were taken for X-ray analysis. The air was removed by direct evacuation. This caused a certain dehydration, which, in spite of later addition of a little water

vapour, exerted some effect on the measurements which were carried out $1^1/_2$ months later. The water vapour pressures are quite certainly somewhat larger than those in R_2, but the shape of the curve places the system in the dehydration series, since the heat of hydration is positive, 0.96 kcal. These values are therefore put in paranthesis in table 1. X-ray examination showed that the preparation was completely amorphous.

System R_4. $MgCO_3$, 1.24 H_2O. On addition of water vapour at 13 mm. pressure for 25 hours, system R_3 took up 0.38 moles H_2O per mole $MgCO_3$ at room temperature. The system was allowed to stand for $3^1/_2$ months, after this the air present was removed without direct evacuation, but by repeatedly evacuating another part of the apparatus and then opening to the flask containing the preparation. By this procedure the air can be removed without appreciable alterations in the composition of the system. After evacuation of the air, measurements were carried out over a period of 2 months. A considerable increase in the water vapour pressure was noticed. The carbon dioxide pressure is given in parenthesis in table 1, since there was no possibility for analyzing the permanent gas a part of this may have been air. X-ray examination showed the preparation to be quite amorphous. The heat of hydration was negative, −2.4 kcal.

System R_5a and R_5b. $MgCO_3$, 1.40 H_2O. Prepared from R_4 by addition of water vapour as in the previous system, but for 76 hours. After 15 days the first single series was measured from higher to lower temperature, system R_5a. The results are given in the table, but in parenthesis, since it was not proved that equilibrium pressure had been obtained. The system was not investigated by X-ray analysis. By accident, air succeeded in entering the system, this was removed as previously described, and water vapour was introduced for 5 seconds. The measuring of system R_5b, which had practically the same composition as R_5a, was carried out over 3 weeks. On X-ray analysis a diagram was obtained with 16 diffuse magnesium carbonate trihydrate lines. We had previously registered 85 lines in a diagram of well crystallized trihydrate, taken in the same camera. The heat of hydration of system R_5a is given tentatively as −5.3 kcal, that of R_5b is −7.5 kcal.

System R_6. $MgCO_3$, 1.94 H_2O. Prepared from R_5b by ad-

dition of water vapour for 68 hours. The system was not very mobile. The small amounts of water vapour, liberated from or adsorbed by the glass walls of the apparatus outside the thermostat, when the temperature of the laboratory changed considerably during the day on account of lack of fuel, could not be taken up or liberated sufficiently quickly by the hydrate system, and the pressures therefore fluctuated periodically. The measurements of the system were therefore subject to an error of 2—3 %.

The X-ray diagram showed 30 somewhat diffuse lines, all belonging to the trihydrate diagram. No trace of dihydrate was found here, but we assume the system to be like the former, but with more trihydrate. The heat of hydration was of the same order as in the previous system, −7.2 kcal.

System R_7. $MgCO_3$, 2.38 H_2O. Prepared from R_6 by introducing water vapour for 23 hours. On account of the relatively high vapour pressure, the measurements could only be carried out up to 25°. The vapour pressures were somewhat greater than in previous systems. If it is assumed, that the vapour pressure curve in fig. 3 is a straight line, it can be found that it will cut the vapour pressure curve for pure water at a value of 1/T corresponding to 10.4° C. ($\log r = 0$). At about this temperature the system will have the same vapour pressure as the saturated solution of trihydrate, but we do not mean that a transition point is a reality, on the contrary that an irreversible transformation of the amorphous phase to the trihydrate will occur.

The heat of hydration was of the same order as in the previous systems, −7.5 kcal. The X-ray diagram showed 52 trihydrate lines.

Measurements of Systems Produced by Dehydration of Magnesium Carbonate Trihydrate at Room Temperature.

Dehydration series D_1—(D_2) and D_3—D_6.
Table 2 and figure 3.

System D_1. $MgCO_3$, 2.52 H_2O. Prepared by dehydration of trihydrate at room temperature for 9 days. Equilibration of the vapour pressure was very slow, occurring after changes in the temperature only after 5 days, but in a satisfactorily reprodu-

cible way. The heat of hydration was calculated to −3.9 kcal. The X-ray diagram showed 34 trihydrate lines and 2 dihydrate lines.

System D_2. On further dehydration of D_1 for 21 days *in vacuo* in a closed system, the composition was $MgCO_3$, 1.7 H_2O. Since it was especially interesting to obtain a system with as pure dihydrate as possible, water vapour was led in until the composition was $MgCO_3$, 2.02 H_2O. The measurements were carried out after 2 months. According to the method of preparation the system was almost a rehydration system. The relatively high vapour pressure, which is put in parenthesis in table 2, also fits best among the curves of the rehydration systems to R_5a. The X-ray diagram gave a disappointment, since apart from 13 lines of trihydrate it contained only 6 lines from the dihydrate. According to the composition we could scarcely expect to find a trihydrate, but the system must consist of dihydrate, trihydrate and amorphous magnesium carbonate. The heat of hydration was calculated to −4.5 kcal.

System D_3. $MgCO_3$, 1.88 H_2O. The preparation, by dehydration of another portion of well crystallized magnesium carbonate trihydrate at room temperature *in vacuo* in a closed system, is given more fully in a previous section of this paper, where the time of dehydration and its rate for this and the next two systems are tabulated. The measurement of system D_3a was carried out between the 24th and 28th day after the dehydration. In the intermediate period the pressure at 18° was still rising, towards the end, however, extremely slowly. Measurements were therefore also taken at 25 and 35°; these results are given in the table. After measurement at 35° a slow rise in the pressure again occurs. At the end of this last rise, which we consider to be due to an aging or sintering of the solid phases in the system, the measurements which are given for system D_3b, were carried out. The heat of hydration was positive for both systems, 4.2 and 3.5 kcal respectively. The X-ray diagram of the sample removed after the measurements showed only 17 diffuse lines, which originate from the dihydrate, all the trihydrate lines have disappeared. By simple calculation from the width of the lines, the particle size of the dihydrate can be estimated to be of the order of 100 Å.

System D_4. $MgCO_3$, 1.64 H_2O. From D_3b by continued dehydration at room temperature for 52 days. As in the previous system there was a strong sintering effect at 35°. The final measurements were therefore only carried out after 2 months. The small water vapour pressure was remarkable. The heat of hydration was calculated to 4.2 kcal. The X-ray diagram contained 10 diffuse dihydrate lines.

System D_5. $MgCO_3$, 1.43 H_2O. From D_4 by continued dehydration at room temperature for 207 days. Hence the preparation originated by intermittent dehydration of magnesium carbonate trihydrate for a total of 309 days. The sintering effect at 35° was noticed for 14 days, after which the measurements were reproducible at the 3 temperatures. The water vapour pressures at 25 and 18° are so low that no water could condense in the BRUNNER manometer. The measurements in this gave us therefore only the sum of water vapour and carbon dioxide pressures. The partial pressures had therefore to be found from the total pressure by means of simultaneous readings of the hot-wire manometer as described in detail in the previous section. It should be noticed that while the dependance of the water vapour pressure on temperature is normal, this is apparently not so for carbon dioxide pressure. Even if a priori we can not expect any definite correlation, since the carbon dioxide pressure does not need to be defined, it is, however, most reasonable to assume similarity to the previous systems. Errors in carbon dioxide pressures do then not need to be greater than some few 1/100 mm. The errors in the water vapour pressures are probably of the same order. The heat of hydration is calculated from the given water vapour pressures to be 3.8 kcal. X-ray analysis gave us a diagram with 6 very diffuse dihydrate lines.

System D_6 (rehydrated). $MgCO_3$, 1.85 H_2O. In order to obtain a better diagram of the dihydrate and to be able to measure a system produced by rehydration, water vapour was led for 100 hours into system D_5, which then attained the composition $MgCO_3$, 1.85 H_2O. The measurements were carried out after the system had stood for $3^1/_2$ months; they could be well reproduced. The heat of hydration calculated by the usual method is −1.3 kcal. The X-ray diagram, however, showed 14 trihydrate lines and only 9 dihydrate lines although the composition was $MgCO_3$,

1.85 H_2O. This showed that the dihydrate crystallizes so extraordinarily slowly that most of the water vapour enters the trihydrate. The system is of course unstable from a thermodynamic point of view.

It is a pleasure for us to express our best thanks to professor N. Bjerrum for suggesting this work and for his continued interest and valuable criticism during its progress.

For the English translation we are indebted to Cicily Andresen, B. Sc.

Copenhagen. Pharmacy and Chemical Laboratory.
The Royal Veterinary and Agricultural
College.

Literature.

1. A. Tovborg Jensen, Axel Lannung, D. Kgl. Danske Vidensk. Selskab, Mat.-fys. Medd. **XX**, 15 (1943).
2. J. K. Gjaldbæk, D. Kgl. Veterinær- og Landboh. Aarsskr. (1921), 245.
3. H. Menzel, A. Brückner, H. Schulz, Z. Elektrochem. **36** (1930), 188.
4. R. Engel, Compt. rend. **100** (1885), 911.
5. Axel Lannung, D. Kgl. Danske Vidensk. Selskab, Mat.-fys. Medd. **XVII**, 10 (1940).
6. H. Menzel, H. Schulz, L. Sieg, M. Voigt, Z. anorg. Chem. **224** (1935), 1.
7. V. Kohlschütter, H. Nitschmann, Z. physik. Chem. A., Bodenstein-Festbd. (1931), 494.
8. E. S. Newmann, L. S. Wells, Journ. Research Nat. Bureau Stand. **20** (1938), 825.
9. G. Tammann, Z. anorg. Chem. **157** (1926), 321.
10. M. Knudsen, D. Kgl. Danske Vidensk. Selskab, Math.-fys. Medd. **VII**, 15 (1927).
11. Axel Lannung, Z. physik. Chem. A. **170** (1934), 134.
12. — Z. anorg. Chem. **228** (1936), 1.
13. M. Brunner, Helv. chim. act. **13** (1930), 915.

Indleveret til selskabet den 5. januar 1949.
Færdig fra trykkeriet den 8. december 1949.

DET KGL. DANSKE VIDENSKABERNES SELSKAB
MATEMATISK-FYSISKE MEDDELELSER, BIND XXV, NR. 13

ON MODEL ATMOSPHERES FOR THE HIGH-TEMPERATURE STARS

BY

ANNE B. UNDERHILL

KØBENHAVN
I KOMMISSION HOS EJNAR MUNKSGAARD
1950

Printed in Denmark
Bianco Lunos Bogtrykkeri

1. The temperatures of the early-type stars are not known very precisely inspite of a number of investigations to establish the upper end of the temperature scale. This state of affairs is a result partly of the complex and largely unknown relationships existing between the various types of temperature which may be defined, and partly of the observational difficulties. The methods of colour temperature are inconclusive for the high temperature stars because in the *O* and *B* stars most of the flux is emitted at inaccessible wavelengths in the far ultraviolet, hence measurements can only be made on the tail of the energy distribution curve where the gradient is not very sensitive to temperature, and because the spectral distribution of the photographic and visual light received from most *O* and *B* stars is modified by the interstellar material lying between these stars and us. The ionisation temperature scale introduced by FOWLER and MILNE (1) and used extensively by Miss PAYNE (2) and also by PANNEKOEK (3), has been the most useful temperature scale for the early-type stars, but for the earliest types it is somewhat uncertain as it depends entirely upon the spectral type chosen typical of the He^{++} maximum. R. M. PETRIE (4) has discussed critically the existing temperature scales for the early type stars and in particular criticises KUIPER's (5) extrapolated ionisation temperature scale. PETRIE has proposed a more compressed excitation temperature scale, but because his results are based on a single curve of growth for *He I* which is used for all the stars and because of the sensitivity to Stark effect of the lines of *He I* and *He II* which he uses, it is doubtful if the method he has used is very sensitive. In any case it is not clear that ionisation temperature, excitation temperature and effective

temperature should be closely the same for the early type stars. UNSÖLD's (6) investigations of the atmosphere of τSco, a *BO V* star, show the difficulties to be met in trying to establish from observations an exact ionisation or excitation temperature for the early-type stars, and clearly point to the intricate relationship existing in a stellar atmosphere between the various temperatures which may be defined.

In view of the differing observational results that have been obtained, a theoretical determination of the effective temperature of an early-type atmosphere would be valuable. The method of model atmospheres offers a powerful tool for determining effective temperature, for, once an acceptable model atmosphere has been obtained, the integrated net flux emerging from it may be calculated. By definition the integrated net flux determines the effective temperature of the atmosphere. This temperature will be the effective temperature of the spectral type corresponding to the model atmosphere. In this paper, methods for computing model atmospheres for the high temperature stars and for determining the spectra of these atmospheres will be developed and a model atmosphere will be computed. The spectral type of this model atmosphere will be determined by comparison with observations and the emergent flux will be calculated in detail so that the effective temperature of the model atmosphere may be found and a point determined at the upper end of the stellar temperature scale.

Recently the method of model atmospheres has been highly developed by STRÖMGREN (7) and applied by Strömgren and his co-workers to studies of the solar atmosphere and of the atmospheres of stars of neighbouring spectral type, while RUDKJØBING (8) has applied these ideas to the study of the atmospheres of *B*-type stars. We shall proceed in a manner somewhat different in detail from that adopted by Rudkjøbing, who uses the principle of the Rosseland mean absorption coefficient and divides the radiation field into two parts and then works with only the flux at frequencies greater than the Lyman limit to get the structure of his atmosphere, for we shall work with the whole radiation field and we shall use the CHANDRASEKHAR straight mean absorption coefficient (9) which is particularly advantageous for dealing with the effects of radiation pressure on the

mechanical equilibrium of the atmosphere (10). With a view to the extension of the method of model atmospheres to atmospheres of very high effective temperature, we shall consider the effects of radiation pressure in more detail than has been the case in previous investigations. Like Rudkjøbing we shall assume that the opacity in our model atmosphere is given by continuous absorption from hydrogen and helium, which are present in the ratio 85:15 by number, and by electron scattering. We shall go further than Rudkjøbing in that we shall test our model atmosphere for radiative equilibrium by computing the net flux without making any approximations at all. We shall also discuss in detail the question of the *f*-values for the lines of *L-S* coupling multiplets, and will assemble the necessary formulae for computing these *f*-values. The method, due to Strömgren, which we will use for computing the net flux in the atmosphere by solving the Schwarzschild integral equation, provides us with a non-approximate method of calculating the line spectrum of the model atmosphere. A by-product of these calculations is the limb-darkening of the model atmosphere in various wave-lengths.

Numerical methods, such as we will use, give a realistic picture of the stellar atmosphere, for they take account of the actual variation of the quantities in the atmosphere, and make no a priori assumptions about the behaviour of any of these quantities. The model atmosphere is idealised to the extent that it is assumed to be symmetrical with respect to the centre of the star so that the physical parameters vary with depth in the atmosphere only, and it is assumed that the chemical composition is constant throughout the atmosphere. Furthermore the atmosphere is assumed to be in a state of mechanical equilibrium. The dependence of temperature upon the pressure and the electron pressure throughout the atmosphere is then obtained by integrating the differential equation of mechanical equilibrium. The model atmosphere so obtained is said to represent a real stellar atmosphere in radiative equilibrium if it can be shown that an atmosphere with this structure produces a net flux which is constant with increasing optical depth. When a model atmosphere satisfying the two conditions of mechanical equilibrium and constant net flux has been obtained, the line spectrum of the model atmosphere may be calculated and detailed information

about the spectral type of the model atmosphere and the abundance of the elements in the stars may be derived by comparing the computed spectrum with observed spectra.

2. We shall consider an atmosphere of high effective temperature in which the opacity is a result of continuous absorption by hydrogen, neutral helium and ionised helium, and of electron scattering. We shall further assume that the star is a main-sequence star and that the transport of energy by turbulence is not important. The equation for mechanical equilibrium in such an atmosphere is

$$\frac{d\,(p_g + p_r)}{dz} = -g\varrho \tag{1}$$

where p_g is the gas pressure, p_r is the radiation pressure, and ϱ is the density at the level z in the atmosphere. The surface gravity of the star is g. In atmospheres of comparatively low effective temperature the radiation pressure is negligible in comparison to the gas pressure. However, in atmospheres of high effective temperature the radiation pressure is not negligible. In an atmosphere in which the opacity is given by continuous absorption and by electron scattering it may be shown (10) that

$$\frac{dp_r}{dz} = -\frac{\pi}{c}\int_0^\infty (\varkappa_\nu + \sigma)\,\varrho\,F_\nu\,d\nu, \tag{2}$$

where $\varkappa_\nu$ is the monochromatic mass-absorption coefficient in the atmoshpere and σ is the mass-scattering coefficient assumed to be independent of wavelength. In such an atmosphere (11) the gray-body temperature law deduced by CHANDRASEKHAR (9) remains a valid approximation if the optical depth is defined by

$$d\tau = -(\bar{\varkappa} + \sigma)\,\varrho\,dz \tag{3}$$

where

$$\varkappa_\nu = \bar{\varkappa}\,(1 + \delta_\nu), \tag{4}$$

and if $\bar{\varkappa}$ is defined formally in the manner recommended by CHANDRASEKHAR (9), that is if

$$\bar{\varkappa} = \int_0^\infty \varkappa_\nu \frac{F_\nu^{(1)}}{F}\,d_\nu. \tag{5}$$

Here $F_\nu^{(1)}$ is the monochromatic flux in a gray atmosphere in which the opacity is given by continuous absorption and by continuous scattering. In CHANDRASEKHAR's discussion the opacity in the atmosphere is given by absorption only. The quantity δ_ν is a small quantity giving the departure from grayness at any frequency. When we introduce equation (4) into equation (2) we find

$$\frac{dp_r}{dz} = -\frac{\pi}{c}(\bar{\varkappa}+\sigma)\varrho\int_0^\infty F_\nu\,d\nu - \frac{\pi}{c}\bar{\varkappa}\varrho\int_0^\infty \delta_\nu F_\nu\,d\nu. \tag{6}$$

We can be reasonably sure that the second term on the right side of equation (6) is small since the definition of $\bar{\varkappa}$ (eq. [5]) is equivalent to putting

$$\int_0^\infty \delta_\nu F_\nu^{(1)}\,d\nu = 0,$$

and we may expect that the actual monochromatic flux F_ν, is of the same order of magnitude as the gray-body monochromatic flux, $F_\nu^{(1)}$. We shall neglect the second term and write

$$\frac{dp_r}{dz} = -\frac{\pi}{c}(\bar{\varkappa}+\sigma)\varrho\int_0^\infty F_\nu\,d\nu, \tag{7}$$

that is we shall use the radiation pressure gradient of a gray-atmosphere. The definition of effective temperature gives

$$\pi\int_0^\infty F_\nu\,d\nu = \sigma_R T_e^4 \tag{8}$$

where σ_R is the radiation constant, $5{\cdot}67\times10^{-5}$ ergs/cm^2/sec/degree^4. Hence we have

$$\frac{dp_r}{dz} = -(\bar{\varkappa}+\sigma)\varrho\frac{\sigma_R}{c}T_e^4. \tag{9}$$

If we introduce this expression into equation (1) and change to the variable τ, optical depth, we find that the equation for mechanical equilibrium including the effect of radiation pressure is

$$\frac{dp_g}{d\tau} = \frac{g}{\bar{\varkappa}+\sigma} - \frac{\sigma_R}{c}T_e^4. \tag{10}$$

We shall determine the structure of our atmosphere by integrating this equation. The term $(\sigma_R/c)\, T_e^4$ is a constant for any atmosphere. In atmospheres of low effective temperature this term, representing the effect of radiation pressure, is negligible. However, when T_e is greater than 10^4 this term becomes important. This treatment, which is possible only if a straight mean absorption coefficient is used, becomes more accurate as the departures from grayness, δ_ν, become small, and the value of the neglected term approaches zero. This method has the advantage that we use the true surface gravity of the star in integrating our atmosphere rather than an effective surface gravity which is not necessarily constant with depth. That g_{eff} is not necessarily constant with depth may be seen from its usual definition, (12)

$$g_{\text{eff}} = g + \frac{1}{\varrho}\frac{dp_r}{dz}. \tag{11}$$

We have no a priori reason for supposing the term $\varrho^{-1}\, dp_r/dz$ to be constant with depth, and indeed reference to equation (6) will show in general that this term is not constant with depth for $\bar{\varkappa} + \sigma$ and $\bar{\varkappa}$ are not constant with depth. In cases where g_{eff} is very nearly the same as g, the possible variations in g_{eff} are of little account.

In order to integrate equation (10) and obtain the structure of the atmosphere we must know the dependence of $\bar{\varkappa} + \sigma$ on τ. (We shall use the parameter τ as the independent variable in the integration). First we need to know the relation between τ and T, the temperature at any level in the atmosphere, for $\bar{\varkappa}$ depends on T. Analytical studies, (9), (11), have given relations between τ and T which are valid in a gray atmosphere and which should be good approximations in a non-gray atmosphere. However, on integrating a model atmosphere it is immaterial exactly what $\tau - T$ relation we use so long as we obtain an atmosphere which is in mechanical equilibrium and which yields a constant net flux. As a first approximation we shall use the classical relation

$$T(\tau)^4 = T_0^4 \left(1 + \frac{3}{2}\tau\right), \tag{12}$$

where T_0 is the boundary temperature. If the flux from our model is not constant with depth we shall modify this relation in a second approximation.

The opacity of our atmosphere is given by hydrogen, helium and by electron scattering. We assume hydrogen and helium to be present in the proportion 85:15 by number. We can neglect the small amounts of the other elements present, for these elements do not contribute appreciably to the opacity of the atmosphere. The mixture chosen is such that one gram of star material contains 0.585 grams of hydrogen and 0.415 grams of helium. If $k_\nu\,(H)$ is the monochromatic continuous absorption coefficient of hydrogen per gram of neutral hydrogen, $k_\nu\,(He\,I)$ is the monochromatic continuous absorption coefficient of neutral helium per gram of neutral helium, and $k_\nu\,(He\,II)$ is the monochromatic continuous absorption coefficient of ionised helium per gram of once-ionised helium, then the monochromatic continuous absorption coefficient per gram of star material is

$$\begin{aligned}\varkappa_\nu = {} & 0{\cdot}585\,(1-x_H)\,k_\nu\,(H) + 0{\cdot}415\,(1-x_{He\,I}-x_{He\,II})\,k_\nu(He\,I) \\ & + 0{\cdot}415\,x_{He\,I}\,k_\nu(He\,II)\,.\end{aligned} \tag{13}$$

Here x_H is the degree of ionisation of hydrogen, $x_{He\,I}$ gives the fraction of singly ionised helium atoms, and $x_{He\,II}$ gives the fraction of doubly ionised helium atoms. The absorption coefficients $k_\nu\,(H)$, $k_\nu\,(He\,I)$, $k_\nu\,(He\,II)$ depend only on the temperature, or optical depth, whereas the abundance factors, $0{\cdot}585\,(1-x_H)$, etc., depend on the temperature and the electron pressure. These factors may be calculated from the ionisation equation. We have

$$\log\frac{x_H}{1-x_H} = -13{\cdot}53\,\theta + \frac{5}{2}\log T - 0{\cdot}477 - \log p_e, \tag{14}$$

$$\log\frac{N_{He^+}}{N_{He^0}} = \log A = -24{\cdot}46\,\theta + \frac{5}{2}\log T + 0{\cdot}125 - \log p_e, \tag{15}$$

and

$$\log\frac{N_{He^{++}}}{N_{He^+}} = \log B = -54{\cdot}14\,\theta + \frac{5}{2}\log T - 0{\cdot}477 - \log p_e, \tag{16}$$

where we have put $\theta = 5040/T$. Since we define

$$x_{He\,I} = N_{He^+}/N_{He}$$

and

$$x_{He\,II} = N_{He^{++}}/N_{He}$$

where N_{He} is the total number of helium atoms and ions present, it follows that

$$x_{He\,I} = \frac{A}{1 + A\,(1 + B)} \doteq \frac{1}{1 + B} \tag{17}$$

and

$$x_{He\,II} = \frac{AB}{1 + A\,(1 + B)} \doteq \frac{B}{(1 + B)}. \tag{18}$$

The quantities A and B are found from equations (15) and (16). From equations (5) and (13) it follows that

$$\begin{aligned} \bar{\varkappa} = {} & 0{\cdot}585\,(1 - x_H)\,\bar{k}\,(H) + 0{\cdot}415\,(1 - x_{He\,I} - x_{He\,II})\,\bar{k}\,(He\,I) \\ & + 0{\cdot}415\,x_{He\,I}\,\bar{k}\,(He\,II), \end{aligned} \tag{19}$$

where

$$\left.\begin{aligned} \bar{k}\,(H) &= \int_0^\infty k_\nu\,(H)\,\frac{F_\nu^{(1)}}{F}\,d\nu, \\ \bar{k}\,(He\,I) &= \int_0^\infty k_\nu\,(He\,I)\,\frac{F_\nu^{(1)}}{F}\,d\nu, \\ \bar{k}\,(He\,II) &= \int_0^\infty k_\nu\,(He\,II)\,\frac{F_\nu^{(1)}}{F}\,d\nu. \end{aligned}\right\} \tag{20}$$

The coefficient of scattering per gram of star material is $\sigma = \sigma_e \times$ number of electrons per gram of star material where σ_e is the scattering coefficient per electron, $8\,\pi e^4/3\,m^2 c^4$. We find that

$$\sigma = \sigma_e \left[\frac{0{\cdot}585}{m_H} x_H + \frac{0{\cdot}415}{m_{He}} (x_{He\,I} + 2\,x_{He\,II})\right],$$

where m_H is the mass of the hydrogen atom and $m_{He} = 4\,m_H$ is the mass of the helium atom. When the numerical factors are introduced we obtain

$$\sigma = 0{\cdot}397\,\left[0{\cdot}585\,x_H + 0{\cdot}104\,(x_{He\,I} + 2\,x_{He\,II})\right]. \tag{21}$$

The coefficient of scattering per gram of star material depends on the electron pressure and the temperature at any level in the atmosphere. The maximum value σ can reach, ($x_H = 1$, $x_{He\,I} = 0$, $x_{He\,II} = 1$), is 0·315 with the mixture of H and He used.

The monochromatic absorption coefficients for hydrogen and for ionised helium corrected for stimulated emission can readily be found from Kramers law. The development of these formula is discussed for instance by UNSÖLD [(12), p. 117 ff.]. We have

$$k_\nu(H) = \frac{F(H)\,D(H)}{u^3}(1 - e^{-u}), \tag{22}$$

where

$$F(H) = \frac{64\,\pi^4\ me^{10}\ e^{-u_1(H)}}{3\sqrt{3}\ ch^3 m_H (kT)^3}$$

and

$$D(H) = \sum_{1<n}^{n=9} \frac{e^{u_n(H)}}{n^3} + \frac{e^{u_{10}(H)}}{2_{u_1}(H)}.$$

Here we have extended Unsöld's treatment by continuing the summation over all continua up to that from the level $n = 9$, and then have performed an integration. The abreviation $u = h\nu/kT$ is used. The quantity $u_n(H)$ is the value of u at the series limit n,

$$u_n(H) = \frac{1}{n^2}\frac{R_H\,hc}{kT}$$

where R_H is the Rydberg constant for hydrogen. Values of $F(H)D(H)$ for hydrogen at a number of temperatures are given in Table 1. From this information $k_\nu(H)$ may be readily calculated by equation (22) for any temperature and at any wavelength desired.

Since the ionised helium atom is hydrogen-like, we may find the continuous absorption coefficient of ionised helium corrected for stimulated emission in the same way. We have

$$k_\nu(HeII) = \frac{F(HeII)\,D(HeII)}{u^3}(1 - e^{-u}), \tag{23}$$

where

$$F(He\,II) = \frac{64\,\pi^4}{3\sqrt{3}} \frac{me^{10}}{ch^3\,m_{He}} \frac{(2^4)\,e^{-u_1\,(He\,I)}}{(kT)^3}$$

and

$$D(H) = \sum_{1<n}^{n=9} \frac{e^{u_n\,(He\,II)}}{n^3} + \frac{e^{u_{10}\,(He\,II)}}{2\,u^1\,(He\,II)}.$$

The quantity $u_n\,(He\,II)$ is

$$u_n\,(He\,II) = \frac{4}{n^2} R_{He} \frac{hc}{kT}$$

where R_{He} is the Rydberg constant for helium. Values of $F\,(He\,II)$ $D\,(He\,II)$ at a number of temperatures are given in Table 2.

Table 1.

$F(H)\cdot D(H)$ per gram of neutral hydrogen.

T	$0<\lambda<911.6$ A*	$911.6<\lambda<3646$ A*	$3646<\lambda<8204$ A*	$8204<\lambda<14{,}590$ A*
25,200°	1.17×10^{9}	1.81×10^{6}	4.65×10^{5}	2.99×10^{5}
28,000	8.49×10^{8}	2.16	6.20×10^{5}	4.12×10^{5}
30,000	6.96×10^{8}	2.37	7.50×10^{5}	5.14×10^{5}
32,000	5.73×10^{8}	2.62	8.69×10^{5}	6.08×10^{5}
34,000	4.80×10^{8}	2.81	9.90×10^{5}	7.07×10^{5}
38,000	3.42×10^{8}	3.06	1.19×10^{6}	8.74×10^{5}
42,000	2.54×10^{8}	3.22	1.36×10^{6}	1.04×10^{6}
46,000	1.96×10^{8}	3.48	1.61×10^{6}	1.27×10^{6}
50,000	1.52×10^{8}	3.34	1.64×10^{6}	1.33×10^{6}
54,000	1.22×10^{8}	3.42	1.69×10^{6}	1.37×10^{6}
58,000	9.90×10^{7}	3.28	1.73×10^{6}	1.43×10^{6}
62,000	8.15×10^{7}	3.21	1.76×10^{6}	1.46×10^{6}
70,000	5.74×10^{7}	3.08	1.81×10^{6}	1.54×10^{6}
80,000°	3.92×10^{7}	2.76×10^{6}	1.73×10^{6}	1.49×10^{6}

* vacuum wavelengths.

We neglect the Gaunt factors in calculating k_ν, for reference to a review of the question of the values of the Gaunt factors by Chandrasekhar (13) shows that the Gaunt factors are close to unity except near the series limit and in the region $\nu\to\infty$. In the latter region $g\,(\nu, n)\to 0$, but this fact is of little importance for the contribution of k_ν to $\bar{k}$ at the very highest frequencies is

Table 2.

$F(He\ II) \cdot D(He\ II)$ per gram of ionised helium.

T	$0 < \lambda < 228$ A	$228 < \lambda < 912$ A	$912 < \lambda < 2052$ A	$2052 < \lambda < 3646$ A
25,200°	4.74×10^{9}	4.05	4.47×10^{-2}	8.57×10^{-3}
28,000	3.40×10^{9}	19.2	0.312	6.93×10^{-2}
30,000	2.76×10^{9}	48.7	1.18	2.41×10^{-1}
32,000	2.28×10^{9}	1.08×10^{2}	2.70	7.15×10^{-1}
34,000	1.90×10^{9}	2.17×10^{2}	6.54	1.86
38,000	1.36×10^{9}	6.75×10^{2}	27.9	8.95
42,000	9.95×10^{8}	1.65×10^{3}	88.2	31.4
46,000	7.68×10^{8}	3.46×10^{3}	2.29×10^{2}	88.8
50,000	6.93×10^{8}	7.64×10^{3}	6.22×10^{2}	2.60×10^{2}
54,000	4.73×10^{8}	1.01×10^{4}	9.50×10^{2}	4.18×10^{2}
58,000	3.05×10^{8}	1.21×10^{4}	1.31×10^{3}	6.09×10^{2}
62,000	3.14×10^{8}	2.13×10^{4}	2.62×10^{3}	1.28×10^{3}
70,000	2.18×10^{8}	3.67×10^{4}	5.59×10^{3}	2.95×10^{3}
80,000°	1.45×10^{8}	1.03×10^{5}	5.43×10^{4}	6.40×10^{3}

T	$3646 < \lambda < 5698$ A	$5698 < \lambda < 8204$ A	$8204 < \lambda < 11{,}170$ A	$11{,}170 < \lambda < 14{,}590$ A
25,200°	4.02×10^{-3}	2.70×10^{-3}	2.14×10^{-3}	1.85×10^{-3}
28,000	3.51×10^{-2}	2.45×10^{-2}	1.98×10^{-2}	1.74×10^{-2}
30,000	1.27×10^{-1}	9.11×10^{-2}	7.49×10^{-2}	6.61×10^{-2}
32,000	3.93×10^{-1}	2.87×10^{-1}	2.39×10^{-1}	2.13×10^{-1}
34,000	1.05	7.84×10^{-1}	6.59×10^{-1}	5.90×10^{-1}
38,000	5.39	4.13	3.54	3.21
42,000	19.8	15.6	13.5	12.4
46,000	58.3	46.8	41.1	37.8
50,000	1.77×10^{2}	1.45×10^{2}	1.29×10^{2}	1.19×10^{2}
54,000	2.93×10^{2}	2.42×10^{2}	2.19×10^{2}	2.03×10^{2}
58,000	4.34×10^{2}	3.67×10^{2}	3.33×10^{2}	3.10×10^{2}
62,000	9.36×10^{2}	7.96×10^{2}	7.25×10^{2}	6.79×10^{2}
70,000	2.24×10^{3}	1.96×10^{3}	1.80×10^{3}	1.70×10^{3}
80,000°	5.00×10^{3}	4.41×10^{3}	4.09×10^{3}	3.87×10^{3}

negligible, because here the weight function approaches zero. The most serious effect of our neglect of the Gaunt factors is that we have made the continuous absorption coefficient of hydrogen too large just to the violet of the Lyman limit and of the Balmer limit. In practice, however, at the red side of these limits an additional source of pseudo continuous absorption appears owing to the overlap of the wide-spread wings of the higher members of the Lyman and Balmer series. This apparent

continuous absorption is not included in the calculation of the mean continuous absorption coefficient, and its effect on the mean absorption coefficient may be allowed for by neglecting the Gaunt factor. When it is a question of calculating the monochromatic continuous absorption coefficient at any wavelength and working with this, we should closely consider the effect of Gaunt factor and the overlap of the wings of the lines. We neglect both these factors in the ensuing computations, consequently the discontinuity we calculate in the continuous absorption coefficient at the Lyman and Balmer limits will be larger in our model atmosphere than it would be in an actual stellar atmosphere of the same structure. This is because we calculate k_ν too large on the violet side of the limit and too small on the red side. The effects of these approximations on the continuous absorption coefficient of ionised helium are not important for ionised helium is not a major contributor to the opacity of our stellar atmosphere.

To obtain k_ν (*He I*), the monochromatic absorption coefficient for neutral helium per gram of neutral helium corrected for stimulated emission, we must sum the contributions from each of the continua of neutral helium. Atomic absorption coefficients for the continua from the ground level of neutral helium, 1^1S, and from the excited states 2^1S, 2^3S, 2^1P and 2^3P, have been published. However, no value of the atomic absorption coefficient for levels with $n \geq 3$ are available. In order to evaluate the

Table 3.

The continua of the *He I* atom.

Level	*E. P.*	λlimit	source for a_ν
1^1S	0.00 V	504 A	S. Huang, Ap. J. **108**, 354, 1948.
2^3S	19.73	2601	
2^1S	20.53	3112	
2^3P	20.87	3436	L. Goldberg, Ap. J. **90**, 414, 1939, for the *P-D* continua and approximate formulae, privately communicated, for the *P-S* continua.
2^1P	21.13	3682	
$n = 3$	22.88	7710	hydrogen-like formulae.
$n = 4$	23.60	14,020	
$n = 5$	23.92 V	22,030 A	

contribution to the monochromatic absorption coefficient from the continua arising from these levels and from the free-free transitions we assume the helium atom is hydrogen-like, and that Kramer's law can be used. Information about the position of the various series limits and the sources we shall use for a_ν, the atomic absorption coefficient, is given in Table 3. Mean excitation potentials are given for the levels with $n = 3$, 4 and 5.

The contribution to k_ν (*He I*) from any one continuum is $a_\nu \times$ number of atoms in the appropriate level. We assume the excitation is according to Boltzman's law, hence

$$\frac{n_{n,s}}{n_r} = \frac{g_{r,s}}{u_r} e^{-\chi_{r,s}/kT}$$

where $n_{n,s}$ is the number of atoms in the r^{th} state of ionisation excited to the state s which has an excitation energy $\chi_{r,s}$. As usual n_r is the total number of atoms in the r^{th} stage of ionisation, $g_{r,s}$ is the statistical weight of the level s, and u_r is the partition function. We wish to find k_ν (*He I*) per gram of neutral helium, hence $n_r = 1/m_{He}$, where m_{He} is the mass of the helium atom. At any temperature T, the contribution from level s to k_ν (*He I*), corrected for stimulated emission, is

$$k_\nu(s) \frac{g_{1,s}}{m_{He}} e^{-\chi_{1,s}/kT} a_\nu(s) (1 - e^{-h\nu/kT}), \qquad (24)$$

since the partition function for neutral helium is unity. Here $a_\nu(s)$ is the atomic absorption coefficient at frequency ν in the continuum arising from level s. The atomic absorption coefficient, a_ν, for the continua from the 1^1S, 2^1S and 2^3S levels can be found from tables given by Huang (14). We shall use a mean of the values given by Huang for the dipole moment and the momentum interaction. The atomic absorption coefficient for the continua occurring at the limits of the $2^1P - n^1D$ and $2^3P - n^3D$ series can be read from a graph given by Goldberg (15), or computed from the formulae he gives. Dr. Goldberg has privately communicated to me the following approximate formulae for the atomic absorption coefficients in the continua arising at the heads of the $2^1P - n^1S$ and $2^3P - n^3S$ series. In the continuum at the head of the $2^1P - n^1S$ series,

$$a_\nu \sim \frac{1}{2R}\frac{\pi e^2}{mc}\,10^{-15{\cdot}71}\,\nu_{n'}^{4{\cdot}6}\,\nu^{-3{\cdot}6},$$

and in the continuum at the head of the $2^3P - n^3S$ series

$$a_\nu \sim \frac{1}{2R}\frac{\pi e^2}{mc}\,10^{-15{\cdot}80}\,\nu_{n'}^{4{\cdot}3}\,\nu^{-3{\cdot}3}.$$

Here R is the Rydberg constant in frequency units, $\nu_{n'}$ is the frequency of the series limit, and ν is the frequency at which we wish to find the atomic absorption coefficient. When the numerical factors are introduced we have at the head of the $2^1P - n^1S$ series

$$\log a_\nu = 35{\cdot}48 - 3{\cdot}6 \log \nu \tag{25}$$

and at the head of the $2^3P - n^3S$ series

$$\log a_\nu = 31{\cdot}06 - 3{\cdot}3 \log \nu. \tag{26}$$

To find the contributions to k_ν (*He I*) from levels with $n \geq 3$ and from the free-free transitions we must consider the helium atom to be hydrogen-like. According to Kramers law the absorption coefficient per neutral atom at frequency ν for a bound-free transition is

$$a_\nu(n, \infty) = \frac{64\pi^4}{3\sqrt{3}}\frac{Z_{\text{eff}}^4 e^{10} m}{ch^6}\frac{e^{-u_1}}{\nu^3}\sum_{n}'\frac{e^{u_n}}{n^3}, \tag{27}$$

for a hydrogen-like atom of effective nuclear charge Z_{eff}. The summation is carried out over all continua with limits to the red of the frequency being considered. As in the discussion for hydrogen and ionised helium, u_n is the quantity $h\nu_n/kT$, where ν_n is the frequency of the series limit n. The absorption coefficient per neutral helium atom at frequency ν due to free-free transitions is

$$a_\nu(\infty, \infty) = \frac{64}{3\sqrt{3}}\frac{\pi^4 e^{10} m}{ch^6}\frac{2\,e^{-u_1}}{u_1}\frac{1}{\nu^3} \tag{28}$$

since although for free-free transitions $Z_{\text{eff}} = 1$ as in hydrogen, the ratio of the partition functions is $^2/_1$ instead of $^1/_2$ as for hydrogen. Upon combining equations (27) and (28) and in-

tegrating the terms of the sum in equation (27) for values of $n > 5$ (cf. UNSÖLD [12] p. 118), we obtain for the absorption coefficient per atom of neutral helium

$$\left.\begin{aligned} a_\nu(HeI, n\geq 3) = \\ = \frac{64\pi^4 e^{10} m}{3\sqrt{3}\, ch^6} \frac{e^{-u_1}}{\nu^3} \left[Z_{\text{eff}}^4 \left\{ \sum_{3\leq n}^{5} \frac{e^{u_n}}{n^3} + \frac{(e^{u_5}-1)}{2u_1} \right\} + \frac{2}{u_1} \right]. \end{aligned}\right\} \quad (29)$$

The absorption coefficient per gram of neutral helium corrected for stimulated emission is

$$k_\nu(HeI, n\geq 3) = \frac{1}{m_{He}} a_\nu(HeI, n\geq 3)\,(1 - e^{-h\nu/kT}). \quad (30)$$

The total absorption coefficient at any frequency ν of neutral helium per gram of neutral helium corrected for stimulated emission is the sum of the contributions from the individual continua with $n \leq 2$ (eq. [24]), and the contribution from the levels with $n \geq 3$, and from the free-free transitions (eq. [30]).

We must now determine Z_{eff} for the levels $n \geq 3$ of *He I*. For a hydrogen-like level

$$Z_{\text{eff}}^2 = n^2 (R\lambda_n)^{-1} \quad (31)$$

where R is the Rydberg constant, $1{\cdot}097 \times 10^5\ \text{cm}^{-1}$, and λ_n is the wavelength of the series limit n. We have given λ_n in Table 3 for the levels $n = 3$, 4 and 5. From equation (31) we find for $n = 3$, 4 and 5, $Z_{\text{eff}} = 1{\cdot}032$, $1{\cdot}019$ and $1{\cdot}017$ respectively. The mean value of Z_{eff} is 1.023. Since only the levels with $n = 3$, 4 and 5 contribute appreciably to the continuous absorption in the wavelength region in which we are interested, we use the Z_{eff} which gives a mean representation of the energies of these levels.

We have now shown how to obtain $k_\nu(H)$, $k_\nu(He\,I)$ and $k_\nu(He\,II)$ at any temperature corrected for stimulated emission. In this connection it may be remarked that, as RUDKJØBING has shown (8), the coefficient of electron scattering should not be

multiplied by the factor $(1 - e^{-h\nu/kT})$. With this information we can readily find $\bar{k}(H)$, $\bar{k}(He\ I)$ and $\bar{k}(He\ II)$ as functions of the temperature and hence of the optical depth, for the weight functions are tabulated, (9) or (11), as functions of the optical depth.

To obtain the structure of the atmosphere we must integrate the equation of mechanical equilibrium, equation (10), step by step. Since from equations (12), (19), (20) and (21) we can obtain $\bar{\varkappa} + \sigma$ as a function of the election pressure and the optical depth, it is convenient to express p_g in term of p_e and work with τ as the independent variable and p_e as the dependent variable. We have

$$\frac{p_g}{p_e} = \frac{N_H(1 + x_H) + N_{He}(1 + x_{He\,I} + 2\,x_{He\,II})}{N_H x_H + N_{He}(x_{He\,I} + 2\,x_{He\,II})}$$

or inserting numerical values

$$\frac{p_g}{p_e} = \frac{0{\cdot}585\,(1 + x_H) + 0{\cdot}104\,(1 + x_{He\,I} + x_{He\,II})}{0{\cdot}585\,x_H + 0{\cdot}104\,(x_{He\,I} + 2\,x_{He\,II})}. \tag{32}$$

However, for the values of T and p_e of interest in the outer part of the atmosphere p_g/p_e is very close to 2. Hence we explicitly assume $p_g = 2\,p_e$, and find the structure of our atmosphere by integrating numerically the equation

$$\frac{dp_e}{d\tau} = \frac{1}{2}\left[\frac{g}{\bar{\varkappa} + \sigma} - \frac{\sigma_R}{c}\,T_e^4\right]. \tag{33}$$

The presence of the term $(\sigma_R/c)\,T_e^4$ in equation (33) shows that $dp_e/d\tau$ may become quite small. Consequently $dp_g/d\tau$ will become small. If such is the case, convection will set in, for K. Schwarzschild has shown that if the existing temperature and pressure gradients are such in an atmosphere that

$$\left|\frac{d\log T}{d\log p_g}\right| > \left|\left(\frac{d\log T}{d\log p_g}\right)_{\mathrm{ad}}\right|$$

convection will occur. The existing gradient at any level in the atmosphere may be found from

$$\frac{d\log T}{d\log p_g} = \frac{p_g}{T}\left(\frac{dp_g}{d\tau}\right)^{-1}\frac{dT}{d\tau}, \tag{34}$$

and the adiabatic gradient from

$$\left(\frac{d\log T}{d\log p_g}\right)_{\mathrm{ad}} = \frac{4(B+1)p_r/p_g + \left[1+B(5/2+\chi_1/kT)\right]}{4(A+4)p_r/p_g + \left[5/2+A(5/2+\chi_1/kT)\right]} \tag{35}$$

which gives the adiabatic gradient for a mixture of radiation and an ionisable gas, one component of which is being ionised, in thermodynamic equilibrium at temperature T, (10). Here we have

$$p_r = \frac{1}{3}aT^4$$

where a is the Stefan-Boltzman constant, $7{\cdot}55\times10^{-15}$ ergs/cm^3/degree^4. In equation (35) χ_1, is the ionisation energy of the element being ionised,

$$B = \nu_1\left[\frac{1+\bar{x}}{x_1(1-x_1)} + \frac{\nu_1}{\bar{x}}\right]^{-1}$$

and

$$A = B(5/2+\chi_1/kT),$$

where ν_1 is the relative abundance by number of the element being ionised, x_1 is the degree of ionisation of this element, and $\bar{x}$ is the mean degree of ionisation,

$$\bar{x} = \sum \nu_i x_i.$$

A comparison of the results from equations (34) and (35) will show at what depths convection sets in.

In the convective zone the actual temperature gradient will be greater than the adiabatic gradient and less than the radiative gradient, and its exact value will depend upon the relative importance of radiative transport of energy to convective transport. We shall see that in our model the adiabatic gradient is very much the same as the radiative gradient, hence in the convective zone we shall find the structure of our model, that is

the dependence of temperature on pressure, by integrating equation (35). In doing this we do not assume $p_g = 2\,p_e$, but use the exact relation

$$p_g/p_e = (1 + \bar{x})/\bar{x}.$$

The use of equation (35) implies that the radiation field at any level in the atmosphere is that for an enclosed volume in thermodynamic equilibrium at temperature T. Since the convective zone is at some depth in the atmosphere, this approximation is valid. We continue to assume the existence of a state of local thermodynamic equilibrium for the calculation of the ionisation in the atmosphere at any level, as we have done throughout the atmosphere.

3. The numerical results of the integration of a model atmosphere are given in this section. We start from the boundary conditions that $T_0 = 25{,}200°$ and $p_e = 0$, and integrate equation (33) inwards step by step. In the region $0 < \tau < 0{\cdot}10$ we use steps of $\Delta\tau = 0{\cdot}01$, in the region $0.10 < \tau < 1.0$ we use $\Delta\tau = 0{\cdot}10$, and from $1.0 < \tau < 3{\cdot}0$ we use $\Delta\tau = 0{\cdot}20$. In order to find

$$\Delta p_e = \frac{1}{2}\left[\frac{g}{\bar{\varkappa} + \sigma} - \frac{\sigma_R}{c} T_e^4\right] \Delta\tau$$

at any level τ we must know p_e and T at the level τ. The value of T can be found from equation (12) and the value of p_e is found by trial so that

$$\frac{1}{2}\left(\Delta p_{e_{\tau - \Delta\tau}} + \Delta p_{e_\tau}\right) = p_{e_\tau} - p_{e_{\tau - \Delta\tau}}$$

where $\Delta p_{e_{\tau-\Delta\tau}}$ is the increment in p_e calculated at the level $\tau - \Delta\tau$, Δp_{e_τ} is the increment in p_e calculated with the assumed p_e at level τ, and $p_{e_{\tau-\Delta\tau}}$ is the value of the electron pressure at the level $\tau - \Delta\tau$. We take $\log g = 4{\cdot}200$ and we use the value $T_e = 30{,}000°$ which is consistent with the use of the temperature law given in equation (12) and our boundary temperature of $25{,}200°$. The quantities $\bar{k}\,(H)$, $\bar{k}\,(He\,I)$ and $\bar{k}\,(He\,II)$ (cf. eq. [19] and [20]) were computed at the levels $\tau = 0{\cdot}0$, $0{\cdot}20$, $0{\cdot}50$, $1{\cdot}00$, $1{\cdot}40$,

2.00 and graphical interpolation was used to get the $\bar{k}$'s at other optical depths. We used the weight functions tabulated by CHANDRASEKHAR (9) to form the $\bar{k}$'s although strictly speaking this procedure is not quite correct (cf. [11]). We felt justified in doing this because preliminary computations showed that the quantity $\lambda = \bar{\varkappa}/(\bar{\varkappa} + \sigma)$ would be close to unity, and under these circumstances the weight functions tabulated by Chandrasekhar are preferable to those which allow for the effect of electron scattering (11), but make a rather restrictive assumption about the dependence of the Plank function on optical depth. The graphs of the $\bar{k}$'s were extrapolated linearly to $\tau = 3{\cdot}0$, and the model was integrated to this depth step by step. The model atmosphere found is given in Table 4. Log p_g is tabulated rather than log p_e. It will be recalled that we have assumed $p_g = 2\,p_e$ in this region, and that $\theta = 5040/T$.

Table 4.

A model atmosphere with $T_0 = 25{,}200°$, $\log g = 4{\cdot}200$: Radiative zone.

τ	θ	$\log p_g$	$\bar{\varkappa}$	σ	τ	θ	$\log p_g$	$\bar{\varkappa}$	σ
0.00	0.200	2.121	0.802	0.274	0.60	0.170	3.301	3.418	0.275
.01	.199	2.377	1.396	.274	0.70	.167	3.357	3.447	.276
.02	.199	2.489	1.798	.274	0.80	.164	3.407	3.447	.276
.03	.198	2.563	2.033	.274	0.90	.162	3.450	3.526	.277
.04	.197	2.619	2.217	.274	1.00	.159	3.490	3.417	.278
.05	.197	2.665	2.467	.274	1.20	.154	3.549	3.167	.280
.06	.196	2.702	2.568	.274	1.40	.150	3.619	3.136	.282
.07	.195	2.736	2.671	.274	1.60	.147	3.679	3.230	.284
.08	.194	2.765	2.730	.274	1.80	.144	3.731	3.220	.287
.09	.194	2.791	2.896	.274	2.00	.141	3.777	3.168	.290
.10	.193	2.814	2.916	.274	2.20	.139	3.818	3.224	.292
.20	.187	2.926	2.922	.274	2.40	.137	3.856	3.241	.294
.30	.182	3.066	3.253	.274	2.60	.134	3.892	3.070	.297
.40	.178	3.162	3.428	.275	2.80	.132	3.926	3.041	.299
0.50	0.174	3.237	3.467	0.275	3.00	0.131	3.958	3.142	0.300

We must now test this model for stability against convection by computing the radiative gradient $(d \log T/d \log p_g)_{\mathrm{rad}}$ from

equation (34) and comparing it with the adiabatic gradient $(d \log T/d \log p_g)_{\text{ad}}$ at the same temperature and pressure calculated according to equation (35). The results of these calculations are given in Table 5. We see that the atmosphere becomes convectively unstable at about $\tau = 2{\cdot}00$ or $\theta = 0{\cdot}141$. Since the difference between the radiative gradient and the adiabatic gradient is not large, we do not expect any large scale disturbances to occur as a result of the setting in of convection at these levels.

Table 5.

The temperature—pressure gradients in the radiative zone.

τ	$\left(\frac{d \log T}{d \log p_g}\right)_{\text{rad}}$	$\left(\frac{d \log T}{d \log p_g}\right)_{\text{ad}}$	τ	$\left(\frac{d \log T}{d \log p_g}\right)_{\text{rad}}$	$\left(\frac{d \log T}{d \log p_g}\right)_{\text{ad}}$
1.00	0.168	0.230	2.40	0.197	0.188
1.40	0.161	0.200	3.00	0.201	0.197
2.00	0.183	0.188	..	..	..

In order to obtain the structure of the atmosphere at greater depths, higher temperatures, we assume an adiabatic temperature gradient and proceed by integrating equation (35). We assume the ionisation of hydrogen and the first ionisation helium to be complete, and we compute x_1, the second degree of ionisation of helium, from the equation.

$$\log \frac{x_1}{1-x_1} = -54{\cdot}14\,\theta + \frac{5}{2}\log T - 0{\cdot}477 - \log p_e .$$

We note that in this approximation the mean degree of ionisation is

$$\bar{x} = 1{\cdot}00 + 0{\cdot}15\,x_1$$

since the abundance by number of helium is 0·15. The resulting model atmosphere is given in Table 6. Here the assumption $p_g = 2\,p_e$ is not made, and the quantity $\bar{x}$ is not defined.

The model atmosphere given in Tables 4 and 6 may be compared with the model atmosphere with $\theta_0 = 0{\cdot}20$ and log

Table 6.

A model atmosphere with $T_0 = 25{,}200^0$, $\log g = 4{\cdot}200$: Convective zone.

θ	$\log p_g$	$\log p_e$	σ	θ	$\log p_g$	$\log p_e$	σ
0.131	3.958	3.657	0.300	0.0947	4.558	4.286	0.315
.125	4.058	3.780	.305	.0886	4.658	4.386	.315
.119	4.158	3.882	.309	.0830	4.758	4.486	.315
.113	4.258	3.984	.312	.0779	4.858	4.586	.315
.107	4.358	4.085	.313	.0730	4.958	4.686	.315
0.101	4.458	4.186	0.314	.0685	5.058	4.786	.315
..	..	..	..	0.0642	5.158	4.986	0.315

$g_{\text{eff}} = 4{\cdot}20$ computed by RUDKJØBING (8). Rudkjøbing computes the structure of his model using an effective acceleration of gravity, and goes on to estimate that the true acceleration of gravity of his model is $10^{4{\cdot}26}$. In computing our model we have assumed that the actual acceleration of gravity is $10^{4{\cdot}20}$, however, a rough comparison of our models may be made. In the outermost regions of both atmospheres the run of gas pressure with temperature is about the same, but the gas pressure begins to increase more rapidly with increasing temperature in Rudkjøbing's model than in ours and at moderate depths, $\theta \sim 0{\cdot}17$, the gas pressure in Rudkjøbing's model is about 16 percent larger than in the present model. Rudkjøbing finds that convection starts at about the same level, $\theta \sim 0{\cdot}141$, as in the present model atmosphere.

In assessing the behaviour of our model atmosphere it is of interest to find the run with depth of $\log g_{\text{eff}}$, obtained from equations (9) and (11), the quantity $\lambda = \overline{\varkappa}/(\overline{\varkappa} + \sigma)$, the ratio p_g/p_e computed according to equation (32), and the ratio p_r/p_g. We obtain the radiation pressure at any depth τ by integrating the equation, (cf. eq. [9]),

$$\frac{dp_r}{d\tau} = \frac{\sigma_R}{c} T_e^4$$

under the boundary condition that p_r is zero at $\tau = 0$. An

Table 7.

Values of certain quantities in the model atmosphere: Radiative zone.

τ	$\log g_{\text{eff}}$	λ	p_g/p_e	p_r/p_g	$\bar{\varkappa}(H)$	$\bar{\varkappa}(He\,I)$	$\bar{\varkappa}(He\,II)$
0.00	4.152	0.745	1.998	0.000	0.433	0.386	0.001
0.05	4.068	.900	2.000	.166	1.377	1.087	.003
0.10	4.041	.914	2.000	.235	1.690	1.222	.004
0.40	4.009	.926	1.997	.422	2.183	1.228	.017
0.80	4.009	.926	1.991	.480	2.302	1.088	.057
1.20	4.025	.919	1.979	.519	2.144	0.893	.130
1.60	4.017	.919	1.964	.513	2.151	0.808	.271
2.00	4.025	.916	1.945	.512	2.156	0.625	.387
3.00	4.025	0.913	1.913	0.506	2.287	0.373	0.482

abridged table of these quantities is given in Table 7. Also given in Table 7 are $\bar{\varkappa}(H)$, $\bar{\varkappa}(He\,I)$, $\bar{\varkappa}(He\,II)$ the contributions of hydrogen, neutral helium, and ionised helium respectively to the mean absorption coefficient, $\bar{\varkappa}$.

In the convective zone the ratios p_g/p_e and p_r/p_g can be found directly from their definitions. The value of the effective acceleration of gravity is found from the following considerations. We postulate that the model atmosphere must still be in mechanical equilibrium in the convective zone. Consequently we require

$$\frac{dp_g}{dz} + \frac{dp_r}{dz} = -g\varrho \tag{36}$$

in addition to the condition that $d\log T/d\log p_g$ is adiabatic, equation (35). Since in the convective zone we assume that the radiation field is that for an enclosed volume in thermodynamic equilibrium at temperature T we have

$$\frac{dp_r}{dz} = \frac{4}{3}aT^3\frac{dT}{dz}.$$

However

$$\frac{dT}{dz} = \frac{T}{p_g}\left(\frac{d\log T}{d\log p_g}\right)_{\text{ad}}\frac{dp_g}{dz},$$

hence we find

$$\frac{dp_r}{dz} = \frac{4}{3}\frac{aT^4}{p_g}\left(\frac{d\log T}{d\log p_g}\right)_{\mathrm{ad}}\frac{dp_g}{dz}. \tag{37}$$

Remembering that

$$p_r = \frac{1}{3}aT^4$$

and introducing equation (37) into equation (36), we obtain.

$$\frac{dp_g}{dz}\left[1+4\frac{p_r}{p_g}\left(\frac{d\log T}{d\log p_g}\right)_{\mathrm{ad}}\right] = -g\varrho. \tag{38}$$

It follows that

$$g_{\mathrm{eff}} = g\left[1+\frac{4\,p_r}{p_g}\left(\frac{d\log T}{d\log p_g}\right)_{\mathrm{ad}}\right]^{-1}. \tag{39}$$

The values for $\log g_{\mathrm{eff}}$ given in Table 8 were found from equation (39).

From Tables 7 and 8 we see that the effective acceleration of gravity varies with depth in the atmosphere and that the radiation pressure is an appreciable fraction of the gas pressure except in the outermost layers of the stellar atmosphere. Consequently radiation pressure and its effects can not be neglected in an atmosphere such as this. In most of the radiative zone the

Table 8.

Values of certain quantities in the model atmosphere: Convective zone.

θ	$\log g_{\mathrm{eff}}$	p_g/p_e	p_r/p_g	θ	$\log g_{\mathrm{eff}}$	p_g/p_e	p_r/p_g
0.131	4.025	1.91	0.506	0.0947	3.989	1.87	0.552
.125	4.024	1.90	.580	.0886	3.982	1.87	.580
.119	4.016	1.89	.558	.0830	3.978	1.87	.595
.113	4.009	1.88	.542	.0779	3.973	1.87	.601
.107	4.002	1.88	.542	.0730	3.968	1.87	.630
0.101	3.990	1.87	0.548	.0685	3.964	1.87	.648
..	..	..	..	0.0642	3.959	1.87	0.665

ratio p_g/p_e is close to the assumed value of 2·0, but near the beginning of the convective zone this ratio decreases. This is because at the temperatures and pressures of these layers the second ionisation of helium is becoming important. In the radiative zone the quantity λ is sufficiently close to unity to justify the use of CHANDRASEKHAR's weight functions for forming $\bar{\varkappa}$, cf. (11). We see that at all depths hydrogen is the main contributor to the opacity. Neutral helium is an important contributor in the outer regions but at greater depths the second ionisation of helium sets in and then neutral helium decreases in importance as a source of opacity while ionised helium increases in importance. In the convective zone we have assumed that the ionisation of hydrogen and the first ionisation of helium are complete. At the level $\tau = 3{\cdot}0$ we have $1 - x_H = 2{\cdot}77 \times 10^{-6}$ and $N_{\mathrm{He}^+}/N_{He^0} = 5{\cdot}36 \times 10^4$, hence these assumptions are justified.

4. We have constructed a model atmosphere in mechanical equilibrium and we must now compute the net flux at various levels and see if this flux is constant with depth. If this is so we may say that our model atmosphere represents a real stellar atmosphere. The following method of computing the net flux at any level in the atmosphere has been developed by STRÖMGREN (16). The monochromatic equation of transfer for a stellar atmosphere in which the opacity is given by continuous absorption and by electron scattering is

$$\cos\vartheta \frac{dI_\nu}{dt_\nu} = I_\nu - S_\nu \tag{40}$$

where t_ν is the monochromatic optical depth

$$t_\nu = -\int (\varkappa_\nu + \sigma)\, \varrho\, dz, \tag{41}$$

and S_ν is the source function,

$$S_\nu = \lambda_\nu B_\nu + (1 - \lambda_\nu) J_\nu, \tag{42}$$

where

$$\lambda_\nu = \varkappa_\nu/(\varkappa_\nu + \sigma)$$

and $$J_\nu = \frac{1}{2}\int_0^\pi I_\nu \sin\vartheta\, d\vartheta\,.$$

We have

$$J_\nu(t_\nu) = \frac{1}{2}\int_{t_\nu}^{\infty} S_\nu(t'_\nu)\, K_1(t'_\nu - t_\nu)\, dt'_\nu + \frac{1}{2}\int_0^{t_\nu} S_\nu(t'_\nu)\, K_1(t_\nu - t'_\nu)\, dt'_\nu \quad (43)$$

where K_1 is the first exponential integral. If we introduce equation (42) into equation (43) and also define the quantity

$$Y_\nu = J_\nu - B_\nu, \quad (44)$$

we obtain the following functional equation for $Y_\nu(t_\nu)$,

$$\left.\begin{aligned} Y_\nu(t_\nu) = &-B_\nu(t_\nu) + \frac{1}{2}\int_0^{\infty} B_\nu(t'_\nu)\, K_1(|t'_\nu - t_\nu|)\, dt'_\nu \\ &+ \frac{1}{2}\int_0^{\infty}\left[1 - \lambda_\nu(t'_\nu)\right] Y_\nu(t_\nu)\, K_1(|t'_\nu - t_\nu|)\, dt'_\nu\,. \end{aligned}\right\} \quad (45)$$

We now define

$$\overline{B_\nu(t_\nu)} = \frac{1}{2}\int_0^{\infty} B_\nu(t'_\nu)\, K_1(|t'_\nu - t_\nu|)\, dt'_\nu$$

and find $Y_\nu(t_\nu)$ by an iterative process which gives

$$Y_\nu(t_\nu) = Y_\nu^0(t_\nu) + \Delta^1 Y_\nu + \Delta^2 Y_\nu + \cdots$$

where

$$Y_\nu^0(t_\nu) = \overline{B_\nu(t_\nu)} - B_\nu(t_\nu), \quad (46)$$

$$\Delta^1 Y_\nu = \frac{1}{2}\int_0^{\infty}\left[1 - \lambda_\nu(t'_\nu)\right] Y_\nu^0(t'_\nu)\, K_1(|t'_\nu - t_\nu|)\, dt'_\nu, \quad (47)$$

$$\Delta^2 Y_\nu = \frac{1}{2}\int_0^{\infty}\left[1 - \lambda_\nu(t'_\nu)\right] \Delta^1 Y_\nu(t'_\nu)\, K_1(|t'_\nu - t_\nu|)\, dt'_\nu, \quad (48)$$

and in general

$$\Delta^n Y_\nu = \frac{1}{2}\int_0^{\infty}\left[1 - \lambda_\nu(t'_\nu)\right] \Delta^{n-1} Y_\nu(t'_\nu)\, K_1(|t'_\nu - t_\nu|)\, dt'_\nu\,.$$

If the $\Delta^n Y_\nu$ very nearly form a series of constant ratio $(1 - \lambda_\nu)$, we can write

$$Y_\nu(t_\nu) = Y_\nu^0(t_\nu) + \Delta^2 Y_\nu + \lambda_\nu^{-1} \Delta^2 Y_\nu \tag{49}$$

as an approximation. This approximation is quite good when λ_ν is not very small. When λ_ν is small it is better to extend the series to at least $\Delta^3 Y_\nu$ or $\Delta^4 Y_\nu$ before attempting a summation of the remaining correction terms. It follows from equations (44) and (42) that the source function at any level t_ν is

$$S_\nu(t_\nu) = B_\nu(t_\nu) + \left[1 - \lambda_\nu(t_\nu)\right]\left[Y_\nu^0(t_\nu) + \Delta^2 Y_\nu + \lambda_\nu^{-1} \Delta^2 Y_\nu\right], \tag{50}$$

and that the net flux at this level t_ν is given by

$$F_\nu(t_\nu) = 2\int_{t_\nu}^{\infty} S_\nu(t'_\nu)\, K_2(t'_\nu - t_\nu)\, dt'_\nu - 2\int_0^{t_\nu} S_\nu(t'_\nu)\, K_2(t_\nu - t'_\nu)\, dt'_\nu, \tag{51}$$

where K_2 is the second exponential integral. The integrations over the exponential integrals occurring in equations (46), (47), (48), and (51) may be performed by a method of representative points and weights developed by STRÖMGREN (17).

We see that to obtain the source function at any depth we must know the dependence of the Planck function B_ν on t_ν.

Since

$$dt_\nu = \frac{\varkappa_\nu + \sigma}{\bar{\varkappa} + \sigma}\, d\tau \tag{52}$$

we may find t_ν as a function of τ, and thus of temperature, by integrating equation (52) numerically. With this information we can construct tables giving $B_\nu(t_\nu)$. In the convective zone, however, the optical depth, τ, is not defined and the following device must be used to obtain t_ν as a function of temperature. By definition

$$\frac{dt_\nu}{dz} = -(\varkappa_\nu + \sigma)\,\varrho$$

hence from equation (38) we obtain

$$\frac{dt_\nu}{dp_g} = \frac{\varkappa_\nu + \sigma}{g}\left[1 + \frac{4\,p_r}{p_g}\left(\frac{d\log T}{d\log p_g}\right)_{\mathrm{ad}}\right]$$

or $$dt_\nu = \frac{\varkappa_\nu + \sigma}{g}\left[1 + \frac{4\,p_r}{p_g}\left(\frac{d\log T}{d\log p_g}\right)_{\mathrm{ad}}\right] p_g d(\log p_g). \qquad (53)$$

Equation (53) may be integrated numerically to give t_ν as a function of $\log p_g$ and hence of temperature, since in the convective zone we use $\log p_g$ as the independent variable. Using equations (52) and (53) we obtained $B_\nu(t_\nu)$ at a number of wavelengths and then computed tables of $S_\nu(t_\nu)$ according to equation (50). From these tables of the monochromatic source function the net monochromatic flux at any level is readily obtained by evaluating equation (51) by means of STRÖMGREN's tables of representative points and weights (17). I was greatly privileged to use these tables before publication. Without these tables it would have been impossible to have done this work.

We wish to ascertain if the integrated flux

$$F = \int_0^\infty F_\nu \, d_\nu$$

is constant with depth. In order to perform this integration over frequency we divide the continuous spectrum into four regions, λ 504, the 1^1S limit of *He I*, to λ 912; λ 912 to λ 1458; λ 1458 to λ 3646; λ 3646 to λ 8204, the Paschen limit of *H*. The integrated flux in each of these intervals is obtained by finding F_ν at five points equidistant in frequency and summing with the appropriate weights using COTES' formula. The selected wavelengths and the monochromatic fluxes at the depths $\tau = 0.0$, 0.10, 0.60, and 1.00 are given in Table 9. The last line of the table gives the integrated net flux, $F(\tau)$, at each level. The emergent flux in the region λ 228, the Lyman limit of *He II*, to λ 504 was calculated for the level $\tau = 0$, but it was found to be negligible, hence the computations for this region were not carried through to obtain F_ν at other optical depths. Likewise we neglect the flux to the red of the Paschen limit. This flux contributes a very small part to the total flux, and its neglect will not affect our determination of the effective temperature or of the constancy of F with depth.

The mean flux is $F = 33{\cdot}29 \times 10^{12}$ ergs/cm^2/sec which corresponds to an effective temperature of 36,800°. The deviations

Table 9.

The monochromatic flux, F_ν, in the model atmosphere.

λ	$\tau = 0{\cdot}0$	$\tau = 0{\cdot}10$	$\tau = 0{\cdot}60$	$\tau = 1{\cdot}00$
504.3 r	8.05×10^{-4}	9.00×10^{-4}	1.40×10^{-3}	1.69×10^{-3}
567.8	8.42	9.28	1.36	1.72
649.4	8.79	9.64	1.31	1.75
758.7	10.96	11.51	1.31	1.61
911.6 v	15.41×10^{-4}	13.17×10^{-4}	1.20×10^{-3}	1.42×10^{-3}
911.6 r	18.87×10^{-3}	18.48×10^{-3}	18.48×10^{-3}	19.30×10^{-3}
1006	18.18	18.11	18.69	19.01
1122	16.02	16.19	16.69	17.27
1268	14.06	14.01	14.06	14.41
1458	11.69×10^{-3}	11.68×10^{-3}	11.79×10^{-3}	11.77×10^{-3}
1458	11.69×10^{-3}	11.68×10^{-3}	11.79×10^{-3}	11.77×10^{-3}
1716	9.55	9.50	9.33	9.62
2083	7.82	7.81	7.67	7.36
2652	5.47	5.37	5.07	4.68
3646 v	3.41×10^{-3}	3.32×10^{-3}	2.82×10^{-3}	2.36×10^{-3}
3646 r	4.02×10^{-3}	4.02×10^{-3}	3.73×10^{-3}	3.48×10^{-3}
4234	3.01×10^{-3}	2.97×10^{-3}	2.70×10^{-3}	2.44×10^{-3}
5048	2.20×10^{-3}	2.30×10^{-3}	1.87×10^{-3}	1.58×10^{-3}
6251	1.48×10^{-3}	1.43×10^{-3}	1.11×10^{-3}	8.53×10^{-4}
8204 v	8.84×10^{-4}	8.24×10^{-4}	5.22×10^{-4}	3.26×10^{-4}
F	32.72×10^{12}	32.67×10^{12}	33.27×10^{12}	34.49×10^{12}

The units of F_ν are ergs/cm²/sec.

from the mean are $-1{\cdot}7$, $-1{\cdot}9$, $0{\cdot}0$ and $+3{\cdot}6$ percent respectively at the levels $\tau = 0{\cdot}00$, $0{\cdot}10$, 0.60 and $1{\cdot}00$. Thus the constancy of the net flux with increasing depth is highly satisfactory in our model. This result vindicates the use of the straight mean absorption coefficient recommended by Chandrasekhar and the treatment of the effects of radiation pressure which we have employed here. The criticism by UNSÖLD (18) of the Chandrasekhar-mean seems hardly to be justified. It is true as Unsöld points out that in the deeper layers where $S_\nu \simeq B_\nu$ the Rosseland-mean and the Chandrasekhar-mean are equivalent and the Rosseland-mean may be preferred because of the ease of forming

Table 10.

Some values of $(S_\nu - B_\nu)/B_\nu$.

τ	λ 504 v	λ 759	λ 1122	λ 1716	λ 3646 v	λ 4234	λ 8204 v
0.00	0.000	— 0.004	4.98	+ 0.362	— 0.159	— 0.175	— 0.155
0.50	.000	.001	1.12	+ 0.036	.031	.060	.012
1.00	.000	.000	0.568	— 0.026	.014	.037	.004
1.60	.000	.000	0.289	— 0.032	.005	.021	.001
2.20	.000	.000	0.200	— 0.024	.002	.008	.000
3.00	0.000	— 0.000	0.155	— 0.018	— 0.000	— 0.002	— 0.000

it. However, in the upper layers of the atmosphere $S_\nu \neq B_\nu$ and then the use of the Rosseland-mean is subject to criticism. Equation [50] enable us to compute $S_\nu - B_\nu$ at any layer in the atmosphere. A few values of $(S_\nu - B_\nu)/B_\nu$ are given in Table 10 for interest. We see that over much of the spectrum S_ν deviates appreciably from B_ν at depths $\tau < 0{\cdot}50$. In the transparent region, $912 < \lambda < 1500$ A, however, the deviation of S_ν from B_ν extends to great depths. Since most of the emergent radiation passes in this region it seems advisable in computing the structure of the model to use a mean absorption coefficient which allows for the difference of S_ν from B_ν. In order to use a Chandrasekhar-type mean the weight functions F_ν/F must be evaluated in some manner. This procedure involves certain assumptions about the process of radiation transfer in the stellar atmosphere. Chandrasekhar (9) evaluates $F_\nu^{(1)}/F$ in a certain systematic way; Unsöld (18) evaluates these weights in another way. Which way is best, and whether either is better than using the Rosseland-mean can only be proven by model atmosphere computations such as carried through here. The present results support the use of Chandrasekhar's weight functions.

That the flux from the model atmosphere increases slightly with depth is not very significant. This behaviour may be the result of using an adiabatic temperature gradient, which is the minimum gradient expected, in the convective zone. Thereby the flux in the wavelength region $912 < \lambda < 1500$ A, which comes effectively from the convective zone, arises from greater depths than it would if the temperature gradient were larger, for a

decrease of the temperature gradient decreases the monochromatic opacity of the atmosphere. The small percentage reduction of the net flux in the region $912 < \lambda < 1500$ A necessary to make the net flux perfectly constant could easily be obtained by increasing the temperature gradient in the convective zone slightly. Such an increase would be accordant with present concepts of the structure of the convective zone in stellar atmospheres.

Referring to equation (6) we find that

$$\frac{dp_r}{d\tau} = \frac{\sigma_R}{c} T_e^4 + \frac{\pi}{c} \frac{\bar{\varkappa}}{\bar{\varkappa} + \sigma} \int_0^\infty \delta_\nu F_\nu \, d_\nu \tag{54}$$

where

$$\delta_\nu = (\varkappa_\nu / \bar{\varkappa}) - 1 .$$

We have neglected the last term on the right side of equation (54) when integrating our model. Furthermore we have put $T_e = 30{,}000^\circ$, the value corresponding to the boundary temperature $T_0 = 25{,}200^\circ$, according to the classical $T - \tau$ relation, equation (12). We have available the information to evaluate the term

$$\frac{\pi}{c} \frac{\bar{\varkappa}}{\bar{\varkappa} + \sigma} \int_0^\infty \delta_\nu F_\nu \, d_\nu$$

at several values of τ, and we find that it does not vary much with depth and that its mean value is $-2{\cdot}37 \times 10^3$. Using this value and $T_e = 36{,}800^\circ$ we find that the mean value of $dp_r/d\tau$ is $1{\cdot}18 \times 10^3$. The value used in our computations was $1{\cdot}53 \times 10^3$. Fortunately these two quantities are not greatly different. Since

$$g_r = -\frac{1}{\varrho} \frac{dp_r}{dz} = (\bar{\varkappa} + \sigma) \frac{dp_r}{dz}$$

we may readily compute the acceleration due to radiation pressure. At the levels $\tau = 0{\cdot}00$, $0{\cdot}10$, $0{\cdot}60$ and $1{\cdot}00$ it is $1{\cdot}57 \times 10^4$, $3{\cdot}38 \times 10^3$, 3.99×10^3 and 4.10×10^3 cm/sec^2 respectively. For his model with $\log g_{\text{eff}} = 4.20$ and $T_0 = 25{,}200^\circ$, Rudkjøbing estimates that $g_r = 2.35 \times 10^3$ cm/sec^2. His value is less than ours and that is why his model differs from the present model. However, Rudkjøbing's estimate is somewhat uncertain for he neglects some terms. Rudkjøbing estimates g_r from the alternate expression.

$$g_r = \frac{\pi}{c} \int_0^\infty (\varkappa_\nu + \sigma) F_\nu \, d_\nu \, .$$

He evaluates the integral[1] by putting

$$g_r + \frac{\pi}{c} (\bar{k}_1 F_1 + \bar{k}_2 F_2),$$

where $\bar{k}_1$ and $\bar{k}_2$ are harmonic mean absorption coefficients formed in the manner of the Rosseland-mean, F_1 is the integrated flux in the region $\nu_0 < \nu < \infty$, and F_2 is the integrated flux in the region $0 < \nu < \nu_0$. Here ν_0 is the frequency of the Lyman limit of hydrogen. His approximation means that he is writing

$$\varkappa_\nu + \sigma = \bar{k}_1 \left[1 + \delta_1 (\nu)\right], \quad \nu_0 < \nu < \infty,$$

$$\varkappa_\nu + \sigma = \bar{k}_2 \left[1 + \delta_2 (\nu)\right], \quad 0 < \nu < \nu_0.$$

and that he is neglecting the terms

$$\frac{\pi}{c} \bar{k}_1 \int_{\nu_0}^\infty \delta_1 (\nu) F_\nu \, d\nu + \frac{\pi}{c} \bar{k}_2 \int_0^{\nu_0} \delta_2 (\nu) F_\nu \, d_\nu \, . \tag{55}$$

It is not clear that these terms may be neglected, for the definition of a Rosseland-type mean absorption coefficient sets no condition on the vanishing of such integrals in the gray-body or any other approximation. In our case where we have used a Chandrasekhar-type mean absorption coefficient, which implies

$$\int_0^\infty \delta_\nu F_\nu^{(1)} \, d_\nu = 0$$

($F_\nu^{(1)}$ is the monochromatic flux in the gray-body approximation), we have found that

$$\frac{\pi}{c} \int_0^\infty \delta_\nu F_\nu \, d\nu$$

is fairly large.

Rudkjøbing does not give enough data in his paper for us to evaluate (55) directly. However, if we use the flux computed for our model and the values of $\bar{k}_1$, and $\bar{k}_2$ given by Rudkjøbing we find that at the level where $\theta = 0{\cdot}170$, $\log p_g = 3{\cdot}30$, i. e.

[1] Note that Rudkjøbing's F is our πF.

$\tau = 0{\cdot}60$ in the present model, the neglected term is $3{\cdot}13 \times 10^2$ cm/sec^2. Consequently the g_r estimated by Rudkjøbing should be increased to $2{\cdot}66 \times 10^3$. This means that $\log g$ for his model is 4·27. Considering the real difference in the parameter $\log g$ between Rudkjøbing's and the present model, there seems to be no serious difference between our model atmospheres. In order

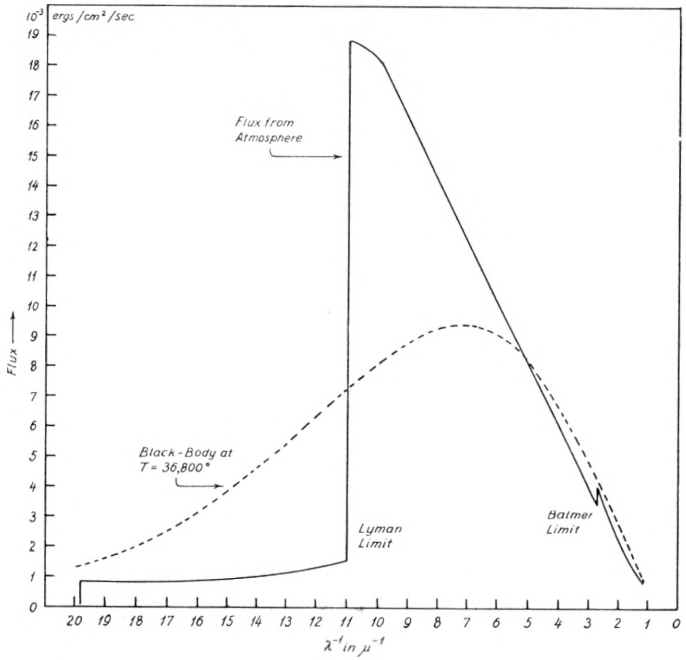

Fig. 1. The emergent flux from the atmosphere as a function of λ^{-1}.

to compute model atmospheres at still higher temperatures and lower surface gravities it would seem preferable to proceed by a method, such as that followed here, which takes account of the effects of radiation pressure directly, rather than the method used by Rudkjøbing, for in these atmospheres the effects of radiation pressure will be important.

The emergent flux is plotted in figure 1 together with B_ν for $T = 36{,}800°$. We see that in the transparent region of the spectrum, $912 < \lambda < 1500$ A, the emergent flux is greatly in excess of the black-body flux, while in the region beyond the Lyman limit the emergent flux is considerably less than that of a black-body at the effective temperature of the star. In the

visual and photographic regions the emergent flux is less than the black-body radiation, but roughly parallels it in intensity distribution. The gradients at any wavelengths in this region are of little meaning, for gradient is not a sensitive indicator of temperature at these high temperatures. The Greenwich gradient, $\lambda\,4100$—$\lambda\,6500$, of our model corresponds to $T > 150{,}000°$. The intensity discontinuities at the Lyman limit, the Balmer limit, and at $\lambda\,504$ for $\tau = 0{\cdot}00$, $0{\cdot}10$, $0{\cdot}60$ and $1{\cdot}00$, are given in Table 11. These discontinuities increase a little with depth.

Table 11.
Discontinuities in the continuous spectrum.

τ	Lyman Limit		Balmer Limit		$\lambda\,504$ Limit	
	$\log \frac{F_r}{F_v}$	Δ mag	$\log \frac{F_r}{F_v}$	Δ mag	$\log \frac{F_r}{F_v}$	Δ mag
		m		*m*		*m*
0.00	1.088	2.72	0.072	0.18	0.270	0.68
0.10	1.147	2.87	0.083	0.21	0.704	1.76
0.60	1.187	2.97	0.122	0.30	..	..
1.00	1.135	2.84	0.168	0.42	..	..

We did not calculate the discontinuities at the 2^1S, 2^3S, 2^1P and 2^3P limits of *He I*. However, this does not mean that small discontinuities are absent here.

According to the work of Barbier and Chalonge (19), the size of the Balmer discontinuity corresponds to spectral type $B1$. However, as we have indicated in our discussion of the continuous absorption coefficient $\varkappa_\nu$, we feel our predicted discontinuities are too large, and it is probable that the model is of earlier spectral type than $B1$. Since the Gaunt factor (13) is 0·88 at $\lambda\,3646\,\mathrm{v}$, we have made $\varkappa_\nu\,(H)$ 12 percent too large at this wavelength. When $\varkappa_\nu\,(H)$ is reduced by this amount and the emergent flux on the violet side of the Balmer limit is recalculated, we find that $F_{3646\,\mathrm{v}}\,(0)$ is $3{\cdot}49 \times 10^{-3}$. Consequently we obtain $\log F_r/F_v = 0{\cdot}061$. This corrected value corresponds more nearly to spectral type $B0$ than the value given in Table 11. If we could estimate the extra pseudo continuous absorption at $\lambda\,3646\,\mathrm{r}$ due to overlap of the broad wings of the higher members of the Balmer series, we could compute a more correct value of $F_{3646\,\mathrm{r}}\,(0)$.

In any case it is evident that our computed value is a maximum value. In comparing our predictions with observation we should also note that the observed quantity D, (cf. BARBIER and CHALONGE [19]), which corresponds to our $\log F_r/F_v$ at the Balmer limit, cannot be so clearly defined as the theoretical quantity. Because of the inherent difficulties in the observation of the quantity D, we should expect the observed value of D to be less than the predicted $\log F_r/F_v$. It seems probable that our model corresponds to about spectral type $B0$.

The observed number of hydrogen lines is an indication of absolute magnitude (20). Since we can compute the electron density at any level in our atmosphere from the election pressure and the temperature, we may readily find n_m, the number of hydrogen lines visible, by the TELLER-INGLIS formula (21). The quantity n_m does not vary rapidly with electron density. If we estimate that the higher members of the Balmer series are formed between the levels $\tau = 0{\cdot}50$ and $\tau = 1{\cdot}00$ we find that the Balmer series will break off at n_m about 15. Reference to the determination of n_m in a number of early type stars by MICZAIKA (22) and to the spectral types by MORGAN, KEENAN and KELLMAN (23) for these stars, shows that for spectral types between $O9$ and $B2$, $n_m = 15$ corresponds about to luminosity class V. There is little doubt that our model atmosphere represents a main-sequence star.

5. From the continuous spectrum and the electron density of our model atmosphere we have estimated that the model corresponds to about spectral type *BO V*. However, it is desirable to confirm this estimate by computing the line spectrum and comparing it to observation. A comparison of the relative strengths of lines arising from atoms in two stages of ionisation will determine the spectral type of the model atmosphere, and a comparison of the absolute strengths of the lines will enable us to derive the abundances of the elements forming the lines. The most prominent lines in the *O* and *B* type stars are those from *H*, *He I* and *He II*. These lines are generally used in classifying the spectra of the earliest type stars (4, 23). However, these lines are strongly affected by Stark effect and the adequate representation of their line-absorption coefficients in a stellar atmosphere is a complex problem. Since it would take a separate lengthy investigation to obtain a detailed form for the line-

absorption coefficient of the lines of *H*, *He I* and *He II* selected by PETRIE as the most sensitive indicators of spectral type in the *O* stars, these lines will not be studied here, but we will attempt to confirm the spectral type of our model by comparing the relative strengths of the combined doublet λ 4267·19 of *C II* and of λ 4187·05 of *C III*, and of the pair of lines λ 4819·74 of *Si III* and λ 4088·86 of *Si IV*. These lines have been selected either because they result from transitions between hydrogen-like levels and hence their *f*-values may be estimated (cf. below), or because an evaluation of the dipole moment matrix element necessary to compute the *f*-value is available.

The method of computing line profiles is straightforward, for the method of obtaining the emergent flux, outlined in the previous section, may be used. Since the lines to be studied arise from levels of high excitation, we shall consider the lines to be formed in absorption. Then the line-absorption coefficient per gram of star material is corrected for stimulated emission and treated as an addition to $\varkappa_\nu$. If F_c is the emergent flux in the continuous spectrum at wavelengths bordering the line, and if F_ν is the emergent flux at any frequency ν in the line, the residual intensity in the line is

$$R_\nu = F_\nu / F_c$$

and the absorption in the line is

$$A_\nu = 1 - R_\nu = \frac{F_c - F_\nu}{F_c}. \tag{57}$$

The line absorption coefficient per gram of star material corrected for stimulated emission is

$$l_\nu = \frac{\sqrt{\pi}\, e^2}{mc} \frac{fN^*}{\Delta\nu_D} H(a, v)\,(1 - e^{-h\nu/kT}), \tag{58}$$

where N^* is the number of atoms of the appropriate type per gram of star material excited to the lower level of the line, and

$$\Delta\nu_D = \frac{\nu_0}{c} \sqrt{\frac{2kT}{m_A}}.$$

Here m_A is the mass of the atom, k is Boltzman's constant, and ν_0 is the frequency of the centre of the line. The function $H(a,v)$ gives the shape of the line absorption coefficient broadened by collisional and radiation damping for atoms in thermal motion. This function has been tabulated by HJERTING (24) for a number of values of a and v. Also recently a series expansion for $H(a,v)$ valid for small values of a has been given by HARRIS (25).

We have

$$H(a,v) = \frac{a}{\pi}\int_0^\infty \frac{e^{-y^2}}{(v-y)^2+a^2}\,dy$$

where

$$v = \frac{\nu-\nu_0}{\Delta\nu_D}$$

and

$$a = \frac{\gamma}{4\pi\Delta\nu_D}.$$

The quantity γ is the damping constant for the line. For radiation damping

$$\gamma = \gamma_m + \gamma_n \tag{59a}$$

where γ_m is the width of the upper level and γ_n is the width of the lower level. It may be shown (cf. for instance, UNSÖLD (12), p. 172) that

$$\gamma_m = \sum_{n<m} A_{nm}(1-e^{-h\nu/kT})^{-1} + \sum_{n'>m} A_{mn'}\frac{2J_{n'}+1}{2J_m+1}(e^{h\nu/kT}-1)^{-1}, \tag{59b}$$

where A_{nm} is the Einstein probability coefficient for spontaneous emission between two levels m and n which have total angular momentum quantum numbers J_m and J_n respectively.

The f-value occurring in equation (58) is the absorption f-value for the line in question. Its value for a line in a multiplet requires some consideration. According to CONDON and SHORTLEY (26) the absorption f-valve is given by

$$f(\alpha j,\alpha' j') = \frac{8\pi^2 m\nu}{3e^2h}\frac{S(\alpha j,\alpha' j')}{2j'+1}, \tag{60}$$

where α is the chief quantum number of the upper level, α' is the chief quantum number of the lower level, and j and j' are the total angular momentum quantum numbers of these levels respectively. The quantity $S(\alpha j, \alpha' j')$ is the theoretical strength of the line, a quantity which is symmetric in the upper and lower levels. For a line designated by

$$\alpha'^{2S+1}L'_{J'} - \alpha^{2S+1}L_J$$

of a multiplet which obeys L-S coupling, explicit forms may be found for the theoretical strength (cf. CONDON and SHORTLEY [26] p. 238). Using these expressions we can write

$$f(\alpha J, \alpha' J') = \frac{8\pi^2 m\nu}{3e^2 h} \left| (\alpha L | P | \alpha' L') \right|^2 \Psi(L, S, J, J'), \qquad (61)$$

where Ψ takes the following values depending in the type of transition.

type of transition	$\Delta L = 1$	$\Delta L = 0$
$J \rightarrow J+1$	$\frac{Q(J)\,Q(J+1)}{4(J+1)(2J+3)}$	$\frac{P(J+1)\,Q(J)}{4(J+1)(2J+3)}$
$J \rightarrow J$	$\frac{P(J)\,Q(J)}{4J(J+1)}$	$\frac{[R(J)]^2}{4J(J+1)}$
$J \rightarrow J-1$	$\frac{P(J)\,P(J-1)}{4J(2J-1)}$	$\frac{P(J)\,Q(J-1)}{4J(2J-1)}$

The table gives $\Psi(L, S, J, J')$.

Here

$$P(J) = (J - S + L)(J + S + L + 1)$$

$$Q(J) = (S + L - J)(J + S - L + 1)$$

$$R(J) = J(J+1) - S(S+1) + L(L+1),$$

and L is the largest of the two L-values occurring while J is the J-value belonging to that term. To obtain the f-value we need

now to evaluate $|(\alpha L|P|\alpha' L')|^2$. For a central field it may be shown (cf. CONDON and SHORTLEY [26], p. 132) that

$$\left|(\alpha L|P|\alpha' L-1)\right|^2 = \frac{e^2}{4L^2-1}\left(R_{\alpha L}^{\alpha' L-1}\right)^2, \qquad (62)$$

where $\left(R_{\alpha L}^{\alpha' L-1}\right)^2$ is the square of the dipole matrix element of the radial part of the wave function. For central fields only transitions with $\Delta L = \pm 1$ are allowed. By combining equations (61) and (62) we find

$$f(\alpha LJ, \alpha' L-1\, J') = \frac{8\pi^2 m\nu}{3h}\left(R_{\alpha L}^{\alpha' L-1}\right)^2 \frac{\Psi(L,S,J,J')}{4L^2-1}. \qquad (63)$$

It may be noted that

$$\left(R_{\alpha L}^{\alpha' L-1}\right)^2 = \left(R_{\alpha' L-1}^{\alpha L}\right)^2.$$

Consequently we may find the f-value for all transitions for which we know $\left(R_{\alpha L}^{\alpha' L-1}\right)^2$. If the energy levels concerned are hydrogen-like we can put

$$\left(R_{\alpha L}^{\alpha' L-1}\right)^2 = \left[R_{\alpha L}^{\alpha' L-1}(H)\right]^2 / Z^2 \qquad (64)$$

where $\left[R_{\alpha L}^{\alpha' L-1}(H)\right]^2$ is the square of the radial matrix element for hydrogen, tabulated for instance by BETHE (27), and Z is the effective charge on the nucleus. Combining equations (61), (62) and (64) we find that the f-value for a line occurring between two hydrogen-like levels is

$$f(\alpha LJ, \alpha' L-1\, J') = \frac{8\pi^2 m\nu}{3h}\frac{\left[R_{\alpha L}^{\alpha' L-1}(H)\right]^2}{Z^2}\frac{\Psi(L,S,J,J')}{4L^2-1}. \qquad (65)$$

Here L is the largest L-value occurring.

In a recent paper (28) BATES and DAMGAARD consider the calculation of the absolute strengths of spectral lines and show that the quantity $\left(R_{\alpha L}^{\alpha' L-1}\right)^2/(4L^2-1)$, which they call σ^2, may be evaluated approximately by neglecting the departure of the potential of an atom or an ion from its asymptotic Coulomb form. They show that this approximation is remarkably good for the

lighter elements, up to *Mg*, and for simple systems which are composed of one electron outside a closed shell, and that it yields useful information for complex systems which have unclosed shells. For many spectral lines of astrophysical interest this evaluation by BATES and DAMGAARD of $\left(R_{\alpha L}^{\alpha' L-1}\right)^2$ is superior to a hydrogenlike approximation.

It is of interest to find the sum of the *f*-values of all components of a multiplet arising from a given sub-level, characterised by J', of the lower term. To find this we evaluate

$$\sum_J f(\alpha J, \alpha' J') = \frac{8\pi^2 m\nu}{3 e^2 h} \frac{1}{2J'+1} \sum_J S(\alpha J, \alpha' J')$$

keeping J' fixed. Reference to CONDON and SHORTLEY (26) p. 238 enables us to evaluate the sum on the right side for the various types of multiplet that occur. In the case $\Delta L = -1$

$$\sum_J f(\alpha LJ, \alpha' L-1 J') = \frac{8\pi^2 m\nu}{3 e^2 h} \left|(\alpha L | P | \alpha' L-1)\right|^2 L(2L+1). \quad (66)$$

In the case $\Delta L = 0$

$$\sum_J f(\alpha LJ, \alpha' LJ') = \frac{8\pi^2 m\nu}{3 e^2 h} \left|(\alpha L | P | \alpha' L)\right|^2 L(L+1), \quad (67)$$

and in the case $\Delta L = +1$

$$\sum_J f(\alpha L-1 J, \alpha' LJ') = \frac{8\pi^2 m\nu}{3 e^2 h} \left|(\alpha L-1 | P | \alpha' L)\right|^2 L(2L-1). \quad (68)$$

Since the lines we shall study belong to the case $\Delta L = -1$ (see Table 12), we shall continue the discussion using only equation (66). Using equation (62) we find that.

$$\sum_J f(\alpha LJ, \alpha' L-1 J') = \frac{8\pi^2 m\nu}{3 h} \frac{L}{2L-1} \left(R_{\alpha L}^{\alpha' L-1}\right)^2. \quad (69)$$

When we compare this expression with the well-known formula for the oscillator strength in a one electron system (cf. for instance BETHE [27] p. 435),

$$f\alpha l - \alpha' l' = \frac{1}{3}\frac{\max(l, l')}{2l'+1}\left(\frac{\nu}{Ry}\right)\left(R^{\alpha' l'}_{\alpha l}\right)^2, \tag{70}$$

where l' is the angular momentum quantum number of the lower state and (ν/Ry) is the frequency of the line in units of the Rydberg frequency, and when we put $l' = L-1$, $l = L$ in equation (70), we find that

$$\sum_J f(\alpha LJ, \alpha' L-1\, J') = f_{\alpha L - \alpha' L-1}. \tag{71}$$

Throughout this paragraph we are implicitly assuming that the frequency of all components of the multiplet arising from the sub-level J' is the same. If this is true then it is apparent that the f-value of any component may be found from the relation

$$\left.\begin{aligned} f(\alpha LJ, \alpha' L-1\, J') &= \frac{f(\alpha LJ, \alpha' L-1\, J)}{\sum_J f(\alpha LJ, \alpha' L-1\, J)} \cdot f_{\alpha L - \alpha' L-1} \\ &= \frac{\Psi(L,S,J,J')}{L(2L+1)} f_{\alpha L - \alpha' L-1}. \end{aligned}\right\} \tag{72}$$

In his paper on τSco, Unsöld (29) effectively uses equation (72) to estimate the f-values of lines in multiplets. However, what he calls "f" is

$$f(\alpha LJ, \alpha' L'J') \cdot \frac{2J'+1}{(2S+1)(2L'+1)}$$

for he combines with the f-value the factor $(2J'+1)/(2S+1)\cdot(2L'+1)$ by which you must multiply

$$N_{r,s} = \frac{g_{r,s}}{u_r} e^{-\chi_{r,s}/kT} \tag{73}$$

to get N^*, the number of atoms excited to the sub-level from which the line arises. Here, as usual, $g_{r,s} = (2S+1)(2L'+1)$, and $\chi_{r,s}$ is the excitation energy of the lower level of the line. Since there is no real advantage to working with the pseudo f-values introduced by Unsöld, and since this procedure may even lead to error if one should take these "f-values" and convert them into Einstein spontaneous emission probabilities by the relation

$$A(\alpha' J', \alpha J) = \frac{8\pi^2 e^2 \nu^2}{mc^3} \frac{(2J'+1)}{(2J+1)} f(\alpha J, \alpha' J'),$$

in order to compute the radiation damping constant of a line according to equations (59a) and (59b), it is preferable to compute the true f-values for the lines of L-S coupling multiplets by equations (63), (65), or (72).

In order to determine the radiation damping constant for the lines studied we shall compute the Einstein spontaneous transition probabilities by the relation

$$A(\alpha' J', \alpha J) = \frac{64\pi^4}{3h} \frac{\nu^3}{c^3} e^2 \left(R_{\alpha L}^{\alpha' L-1}\right)^2 \frac{\Psi(L, S, J, J')}{(4L^2-1)} \frac{(2J'+1)}{(2J+1)}. \quad (74)$$

We shall neglect collision damping. Of the lines chosen, only *Si IV* λ 4089 is sufficiently strong that the exact value of the damping constant is of consequence. For this line RUDKJØBING (8) has shown that collision damping is not important.

The lines studied are given in Table 12 together with the relevant spectroscopic information. The necessary matrix elements, R^2, for obtaining the f-values and damping constants of the *C II*, *C III* and *Si III* lines were obtained by assuming these spectra to be hydrogen-like. The matrix-elements for *Si IV* were found by the method of BATES and DAMGAARD (28). It is to be noted that according to equations (59) the radiation damping constant depends upon the temperature. For the *C II*, *C III* and *Si III* lines γ at 32,000° was used throughout the atmosphere, but for

Table 12.
Lines studied.

Spectrum	Designation	$j' - j$	λ	f	γ at 32,000°
C II	$3d\,^2D$—$4f\,^2F^\circ$	$^3/_2$—$^5/_2$	4267.19	1.11	1.69×10^{10}
		$^5/_2$—$^5/_2$			
		$^5/_2$—$^7/_2$			
C III.....	$4\,^1F^\circ$—$5\,^1G$	3—4	4187.05	1.44	2.22×10^9
Si III	$4f\,^3F^\circ$—$5g\,^3G$	3—3	4819.74	1.25	3.97×10^9
		3—4			
Si IV	$4\,^2S$—$4\,^2P^\circ$	$^1/_2$—$^3/_2$	4088.86	0.751	4.02×10^9

the *Si IV* line γ was calculated at each depth in the atmosphere. In evaluating the damping constant account was taken of all possible transitions to the levels listed by BACHER and GOUDSMIT (30).

The line absorption coefficient per gram of star material corrected for stimulated emission was derived at each level in the atmosphere according to equation (58). The ionisation and excitation equilibria were computed at each level, and account was taken of the temperature dependence of the various partition functions involved. The function $H(a, v)$ was evaluated by the series expansion given by HARRIS (25). The monochromatic continuous absorption coefficient corrected for stimulated emission was also obtained at each level for the central frequency of each line, and then the relative absorption at several points in the line profile was computed by the method outlined above. The results obtained are given in Table 13. These points were plotted and the profile was integrated graphically to give the equivalent widths listed in Table 14. The relative amounts of *C* and *Si* to *H* used, are those found by UNSÖLD (29) for τSco, that is $N(H)/N(C) = 5{\cdot}8 \times 10^3$ and $N(H)/N(Si) = 1{\cdot}6 \times 10^4$.

Table 13.

Computed absorption line profiles*

$\Delta\lambda$	*C II* λ 4267·19	*C III* λ 4187·05	*Si III* λ 4819·74	$\Delta\lambda$	*Si IV* λ 4088·86
0.00 A	0.35	0.30	0.27	0.00 A	0.41
.07	.31	.26	.18	.10	.37
.14	.17	.14	.02	.20	.14
0.21	0.04	0.03	0.00	.40	.05
..	..	..	..	0.80	0.03

* The table gives absorption in the line in terms of the continuous spectrum at the wavelength in question.

The *C II* "line", λ 4267·19, is a blended multiplet of three components. The two components arising from the sub-level with $j = 5/2$ have the same wavelength, hence we form a summed *f*-value for them as in equation (69). This summed *f*-value is the same as that for the one component arising from the level

with $j = 3/2$. We next assume that all components have the mean wavelength 4267·19 A, and find the desired line absorption coefficient by adding the contributions from each component. Since each component has the same damping constant, it follows that l_ν for the combined multiplet is given by formula (58) with f equal to the summed f-value for all components arising from either sub-level $j = 3/2$ or sub-level $j = 5/2$, and that N^* is the number of excited atoms given directly by the Boltzman equation (eq. [73]).

The *C III* and *Si IV* lines are single, consequently the procedure of forming l_ν is straightforward. The *Si III* line is composed of two components which arise from the sub-level $j = 3$ of the lower term. Since these two components have the same wavelength we use a summed f-value, equation (69), and we note that in this case N^* is not given by Boltzman's equation directly; but by $N_{r,s} \times (2J'+1)/(2S+1)(2L'+1)$.

The strength of the lines in the model atmosphere may be compared with measurements made on high dispersion plates of the strengths of the same lines in τ*Sco*, a *BO V* star, by Unsöld (29), and in 10 Lac, an *O* 9 *V* star, by Aller (31).

The observed equivalent widths are given in Table 14 together with the computed equivalent widths. The observed and computed relative intensities *C II*/*C III* and *Si III*/*Si IV* are given in Table 15.

Table 14.

Equivalent widths*.

Line	Computed	τ *Sco BO V* (Unsöld)	10 Lac *O* 9 *V* (Aller)
C II λ 4267	0.099	0.115	0.081
C III λ 4187	0.085	0.065	0.089
Si III λ 4820	0.050	0.071	(<0.050)
Si IV λ 4089	0.209	0.174	0.270

* in equivalent angstroms.

Since Aller does not measure the line λ 4820 in 10 Lac, I estimate that its equivalent width is less than 0·050 E.A. It is not certain that the measurements by Unsöld and by Aller are

on the same scale, for the plates used, although of comparable dispersion, are not taken by the same telescope and spectrograph. This fact should not seriously affect the interpretation of the observed and computed relative intensities *C II/C III* and *Si III/Si IV*, but it will prevent a precise determination of the abundance of carbon and silicon by matching the computed equivalent widths closely to the observed equivalent widths.

Table 15.

Relative intensities.

Ratio	Computed	τ *Sco BO V* (Unsöld)	10 Lac *O* 9 *V* (Aller)
C II/C III	1.17	1.77	0.91
Si III/Si IV	0.24	0.41	($<$0.18)

From the data of Table 15 we conclude that the spectral type of the model atmosphere is definitely earlier than *BO V* and somewhat later than *O* 9 *V*, say *O* 9·5 *V* on the scale of Morgan, Keenan and Kellman (23). R. M. Petrie (4) classifies 10 Lac as an *O* 8·5 star. On his scale the model atmosphere might just be an *O* 9 star. The effective temperature of 36,800° which we have found for the model atmosphere is considerably higher than the excitation temperature of 30,700° found by Petrie for *O* 9 stars from a study of the relative intensities of the *He II* and *He I* lines λ 4542 and λ 4471 respectively, and is also higher than the temperature based on the ionisation scale given by Kuiper (5).

The difference between effective temperature and excitation temperature found here for the *O* 9 stars is in the same direction as that found for later type stars from curve of growth studies. This result occurs because of the rather great transparency of stellar atmospheres to radiation in the range $912 < \lambda < 1500$ A, which tends to increase the integrated emergent flux above that expected for the temperatures indicated by the opacity in the wavelength regions corresponding to the excitation of the commonly studied lines.

The dependence of the monochromatic optical depth, t_ν, on

Table 16.

The monochromatic optical depths, t_ν, at various wavelengths.

τ	λ 314	λ 649	λ 912 v	λ 1006	λ 1458	λ 3646 v	λ 4234	λ 6251
0.00	0.00	0.00	0.00	0.000	0.000	0.000	0.000	0.000
0.10	0.77	0.12	0.32	.013	.014	0.039	0.022	0.040
0.20	1.45	0.24	0.64	.023	.026	0.080	0.044	0.082
0.40	2.56	0.49	1.30	.041	.049	0.17	0.092	0.18
0.60	3.43	0.72	1.93	.059	.074	0.28	0.15	0.30
0.80	4.14	0.96	2.55	.078	.100	0.40	0.21	0.44
1.00	4.71	1.18	3.14	.097	.13	0.53	0.28	0.60
1.40	5.58	1.62	4.31	.139	.19	0.83	0.45	0.98
1.80	6.11	2.06	5.46	.186	.27	1.18	0.67	1.44
2.20	6.66	2.50	6.60	.236	.35	1.59	0.92	1.97
2.60	7.00	2.93	7.73	.289	.44	2.03	1.19	2.55
3.00	7.26	3.35	8.84	0.345	0.53	2.50	1.48	2.97

wavelength in the present model atmosphere is illustrated by the data of Table 16. The emergent monochromatic flux may be roughly evaluated by taking B_ν at the depth $t_\nu = 0{\cdot}60$. It is obvious from the data of Table 16 that the "temperature" of the emergent flux varies considerably with wavelength. In a line, the monochromatic optical depth varies rapidly with wavelength, as is illustrated by the data of Table 17, and it is a question what

Table 17.

t_ν in λ 4267, $N(H)/N(C) = 5{\cdot}8 \times 10^3$.

τ	$\Delta\lambda = 0{\cdot}00$ A	$\Delta\lambda = 0{\cdot}07$ A	$\Delta\lambda = 0{\cdot}14$ A	$\Delta\lambda = 0{\cdot}21$ A
0.00	0.00	0.00	0.000	0.000
0.10	0.55	0.32	0.080	0.031
0.20	1.14	0.66	0.166	0.064
0.40	2.20	1.29	0.34	0.131
0.60	3.10	1.84	0.51	0.20
0.80	3.80	2.31	0.64	0.28
1.00	4.36	2.70	0.81	0.37
1.40	5.13	3.25	1.08	0.56
1.80	5.68	3.68	1.35	0.79
2.20	..	4.08	1.65	1.05
2.60	..	4.46	1.96	1.33
3.00	..	4.82	2.28	1.64

optical depth, or temperature, should be taken as "characteristic" of the whole line, for the level at which $t_\nu = 0{\cdot}60$ occurs differs greatly, depending on the distance from the line centre. The data of Table 17 illustrate nicely that the core of a line is formed in the outermost layers of the atmosphere, while the wings are formed at progressively deeper layers. In any case it is evident that whatever temperature is chosen in order that the actual process of line formation may be represented by line formation in a layer of gas at one temperature and pressure, this temperature will be less than the corresponding temperature for the continuous spectrum in the neighbourhood of the line, and that both of these temperatures will be less than the effective temperature, for the effective temperature is largely determined by the magnitude of the emergent flux in the region $912 < \lambda < 1500$ A, and in this region the "characteristic temperature" is high. Excitation or ionisation temperatures are effectively "characteristic temperatures" for the lines involved and hence bear a complicated relationship to the effective temperature of the atmosphere, which is defined by the integrated emergent flux.

The high effective temperature we have found for the *O* 9·5 *V* stars, which is in accord with the estimate of Rudkjøbing (8) from his study of model atmospheres, means that the *B* stars are spread over a large range of effective temperature, for the effective temperature of *AO V* stars seems to be close to 10,000° (32). The greatest spread in effective temperature probably occurs amongst the early *B*-type stars, for at the temperatures estimated to be characteristic of these atmospheres the peak of the black-body energy distribution curve moves into the range $912 < \lambda < 1500$ A. When this happens an excess of emergent radiation in this critical wavelength range will build up rapidly, and force up the effective temperature. It is difficult to estimate how high the effective temperatures of the absorption-line *O* 5 or *O* 6 stars may be. Consideration of the stability of atmospheres under the effects of radiation pressure (10), indicates that only stars of large surface gravity will have stable atmospheres at very high effective temperatures.

From Table 14 we see that the absolute strengths of the lines in the model atmosphere are intermediate between those observed in τ *Sco*, *BO V*, and in 10 Lac, *O* 9 *V*. This result is in accord

with the spectral type of the model atmosphere being *O* 9·5 *V*, and confirms the assumption that the relative abundances of *C* and *Si* to *H* used are representative of the chemical composition of early-type atmospheres. The actual abundances occurring cannot be far from the chosen abundances, for if the carbon abundance is reduced by a factor 0·4, the absolute strengths of the *C II* and *C III* lines are reduced to 0·069 E.A. and 0·061 E.A. respectively. These values are significantly lower than the observed line strengths. The ratio *C II*/*C III* is nearly unchanged by this change in the carbon abundance, for it becomes 1·13 instead of 1.17. Since hydrogen is the dominant source of opacity in the wavelength range of the lines studied, departure of the real abundance of *He* from the assumed abundance of *He* will not affect the computed line strengths and the relative abundances of *C* and *Si* deduced therefrom by altering the contrast appreciably.

6. The limb-darkening of early type stars is difficult to establish from observations of eclipsing variables in which one or both components are *O* or *B*-type stars, and usually the observations are worked through with estimated values of the coefficient of limb-darkening. Since in the course of the computations for the net flux in the atmosphere we have obtained the monochromatic source function S_ν as a function of the optical depth, we can compute the emergent intensity as a function of the angle of emergence and can thus find the limb-darkening of the model atmosphere in various wavelengths. We have

$$I_\nu(0,\mu) = \mu^{-1} \int_0^\infty S_\nu(t_\nu)\, e^{-t_\nu/\mu}\, dt_\nu, \tag{76}$$

where $I_\nu(0,\mu)$ is the monochromatic intensity emerging at the angle $\cos^{-1}\mu$ to the normal. Here t_ν is the monochromatic optical depth. The limb-darkening is expressed by

$$I_\nu(0,\mu)/I_\nu(0,1) = 1 - u + u\mu, \tag{76}$$

where u is the coefficient of limb-darkening.

The values of $I_\nu(0,\mu)/I_\nu(0,1)$ given in Table 18 were found by integrating equation (75) numerically for values of μ equal to 1·00, 0·50, 0·20 and 0·05. At the limb, $\mu = 0{\cdot}00$, $I_\nu(0,\mu)$

Table 18.

The limb-darkening, $I_\nu(0, \mu)/I_\nu(0, 1)$, of the model atmosphere.

μ	λ 6251	λ 4234	λ 1006	pure scattering
1.00	1.000	1.000	1.000	1.000
0.50	0.892	0.845	0.663	0.688
0.20	0.777	0.726	0.438	0.490
0.05	0.688	0.574	0.373	0.380
0.00	0.561	0.476	0.338	0.331

was put equal to $S_\nu(0{\cdot}0)$. Also given in Table 18 is the limb-darkening computed by CHANDRASEKHAR (33) for an atmosphere scattering according to the Rayleigh phase function, i. e. for electron scattering. The intensity $I_\nu(0,1)$ equals $1{\cdot}57 \times 10^{-3}$, $3{\cdot}17 \times 10^{-3}$ and $24{\cdot}69 \times 10^{-3}$ ergs/cm²/sec respectively at λ 6251, λ 4234 and λ 1006. The wavelength λ 6251 corresponds roughly to the effective wavelength of visual-red observations, while the wavelength λ 4234 corresponds to the effective wavelength of photographic observations. At both these wavelengths hydrogen is the predominant source of opacity in the atmosphere. The limb-darkening was calculated at λ 1006 also, because here electron scattering is the predominant source of opacity, and the

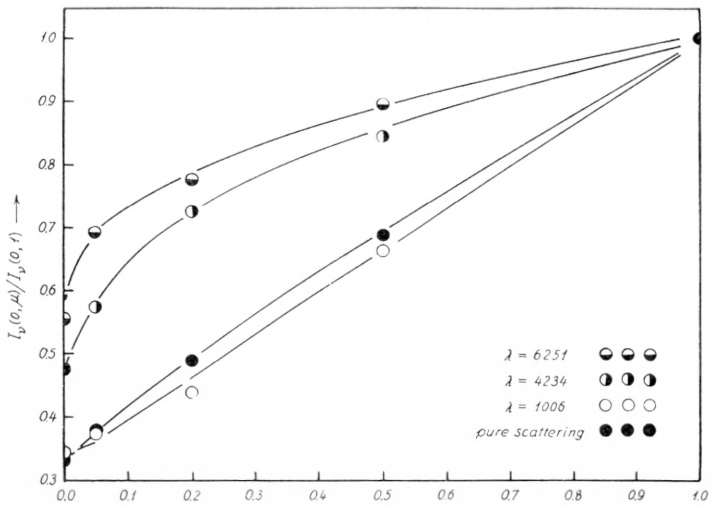

Fig. 2. The limb-darkening of the model atmosphere.

limb-darkening at λ 1006 will be characteristic of electron scattering atmospheres.

The data of Table 18 are plotted in Figure 2 as a function of μ. The limb-darkening at λ 1006 is closely that obtained by Chandrasekhar through exact computations of the limb-darkening expected in an atmosphere scattering according to Rayleigh's phase function. In the present computations the scattering was assumed to be isotropic. At λ 4234 the electron scattering contributes a larger amount to the total opacity than at λ 6251 and the limb-darkening curve is accordingly closer to the limiting curve for pure scattering.

An expression of the form of equation (76) was fitted to the plotted points by the method of least squares, yielding the following coefficients of limb-darkening: $u = 0{\cdot}35$ at λ 6251, 0.44 at λ 4234, 0·65 for pure scattering, and 0·67 at λ 1006. From his study of the light curve of *AO* Cassiopeiae, Frank Bradshaw Wood (34) concludes that the appropriate coefficient of limb-darkening for *O* stars is about 0·6. Since *AO* Cassiopeiae is a pair of *O* 8 supergiants we may expect electron scattering to be predominant even in the photographic and visual spectral regions. The value of the limb-darkening suggested by Wood is consistent with the results of the present computations which show that the limiting value of $u = 0{\cdot}65$ is approached when the opacity is predominantly due to electron scattering.

This investigation was made during the author's tenure of a National Research Fellowship (U. S. A.). The author is most grateful to Professor Bengt Strömgren for many helpful discussions during her stay at the Copenhagen University Observatory and for the friendly welcome she received there.

References.

(1) R. H. Fowler and E. A. Milne, M. N. **83**, 403, 1923 and **84**, 499, 1924.

(2) Cecilia H. Payne, *Stellar Atmospheres*, Harvard Monograph No. 1, 1925.

(3) A. Pannekoek, Ap. J. **84**, 481, 1936.

(4) R. M. Petrie, Pub. Dom. Obs. Vol. 7, No. 21, 1947.

(5) G. P. Kuiper, Ap. J. **88**, 439, 1938.

(6) A. Unsöld, Zs. f. Ap. **21**, 1, 22, 229, 1942.

(7) B. Strömgren, Pub. Cop. Obs. No. 127, 1940 and No. 138. The latter publication gives references to earlier work on model atmospheres by Milne, McCrea, Chandrasekhar, Russell, Unsöld and Pannekoek.

(8) M. Rudkjøbing, Pub. Cop. Obs. No. 145, 1947.

(9) S. Chandrasekhar, Ap. J. **101**, 328, 1945.

(10) A. B. Underhill, M. N. in press.

(11) — Ap. J. **110**, 340, 1949.

(12) A. Unsöld, *Physik der Sternatmosphären* (Berlin: Julius Springer, 1938) p. 141.

(13) S. Chandrasekhar, *An Introduction to the Study of Stellar Structure*, (The University of Chicago Press, Chicago, Illinois, 1939), p. 262.

(14) S. Huang, Ap. J. **108**, 354, 1948.

(15) L. Goldberg, Ap. J. **90**, 414, 1939.

(16) B. Strömgren, A. J. **53**, 107, 1947. The details of his method are unpublished yet.

(17) — A. J. **53**, 107, 1947; Ann. d'Ap. in press.

(18) A. Unsöld, Zs. f. Ap. **25**, 340, 1948.

(19) D. Barbier and D. Chalonge, Ann. d'Ap. **4**, 30, 1941.

(20) O. Struve and A. Unsöld, Ap. J. **91**, 365, 1940.

(21) D. R. Inglis and E. Teller, Ap. J. **90**, 439, 1939.

(22) G. R. Miczaika, Zs. f. Ap. **25**, 268, 1948.

(23) W. W. Morgan, P. C. Keenan, and E. Kellman, *An Atlas of Stellar Spectra*, (University of Chicago Press, Chicago, Illinois, 1943).

(24) F. Hjerting, Ap. J. **88**, 508, 1938.

(25) D. L. Harris III, Ap. J. **108**, 112, 1948.

(26) E. U. Condon and G. H. Shortley, *The Theory of Atomic Spectra*, (Cambridge University Press, 1935), p. 108.
(27) H. Bethe, Hb. d. Phys. **24,1**, 442, 1933.
(28) D. R. Bates and Agnete Damgaard, Trans. Roy. Soc. A, **242**, 101, 1949.
(29) A. Unsöld, Zs. f. Ap. **21**, 22, 1941.
(30) R. F. Bacher and S. Goudsmit, *Atomic Energy States*, (McGraw-Hill Book Company Inc., New York and London, 1932).
(31) L. H. Aller, Ap. J. **104**, 347, 1946.
(32) A. B. Underhill, Ap. J. **108**, 83, 1948.
(33) S. Chandrasekhar, Ap. J. **105**, 435, 1947.
(34) F. B. Wood, Ap. J. **108**, 28, 1948.

Indleveret til selskabet den 8. april 1949.
Færdig fra trykkeriet den 3. juni 1950.

DET KGL. DANSKE VIDENSKABERNES SELSKAB
MATEMATISK-FYSISKE MEDDELELSER, BIND XXV, NR. 14

A THEOREM ON ALMOST PERIODIC FUNCTIONS OF INFINITELY MANY VARIABLES

BY

ERLING FØLNER

KØBENHAVN
I KOMMISSION HOS EJNAR MUNKSGAARD
1950

Printed in Denmark
Bianco Lunos Bogtrykkeri

1. Introduction.

For an almost periodic function $f(x)$ of one variable the following theorem is true: *the function is periodic if and only if the set of all translated functions* $f(x+h)$ *is closed with respect to uniform convergence.* As remarked by B. JESSEN this can easily be proved directly from the structure definition of almost periodicity; also for the corresponding theorem on almost periodic functions $f(x_1, x_2, \cdots, x_m)$ in the m-dimensional space he has shown me such a proof.

The way in which one generalizes the word "periodic" when passing from 1 to m dimensions with this theorem is to what might be called "fully periodic". Let $f(x_1, x_2, \cdots, x_m)$ be a continuous function of $(x_1, x_2, \cdots, x_m)$. A vector $(h_1, h_2, \cdots, h_m)$ is called a period vector of $f(x_1, x_2, \cdots, x_m)$ if $f(x_1 + h_1, x_2 + h_2, \cdots, x_m + h_m) = f(x_1, x_2, \cdots, x_m)$ for all $(x_1, x_2, \cdots, x_m)$. The set of all period vectors of $f(x_1, x_2, \cdots, x_m)$ is obviously a closed module (a module being a set which with two points also contains their sum and difference). This module may consist of $(0, 0, \cdots, 0)$ only, and the function is not periodic at all. If the dimension of the module is equal to the dimension m of the space we call the function *fully periodic.* Our theorem for almost periodic functions of m variables can then be stated, *such a function is fully periodic if and only if the set of all translated functions* $f(x_1 + h_1, x_2 + h_2, \cdots, x_m + h_m)$ *is closed with respect to uniform convergence.*

JESSEN put the problem to decide whether this theorem also holds for almost periodic functions of an infinite number of variables. It will turn out—as a result of this paper—that it does hold in verbally the same formulation, the word "fully periodic" needing of course an appropriate definition. Incidentally, we

shall get another proof in the m-dimensional case than the one referred to above.

JESSEN also remarked that if the almost periodic function $f(x_1, x_2, \cdots)$ in question is limit-periodic, the theorem is true as a simple consequence of a result of H. BOHR [2], [3] obtained in connection with a study of certain classes of almost periodic functions (see **4**, and **6**, p. 12 of the present paper). BOHR's result concerned an infinite system of linear congruences

$$r_{n1} x_1 + r_{n2} x_2 + \cdots + r_{nq_n} x_{q_n} \equiv \theta_n \pmod 1, n = 1, 2, \cdots$$

with infinitely many real variables $x_1, x_2, \cdots$ and rational coefficients. It was later on generalized by BOHR and FØLNER [4] to arbitrary coefficients, and this generalization will be a tool for the proof of the general case of our theorem.

2. Almost Periodic Functions of Infinitely Many Variables.

We start with recalling that an almost periodic function $f(x_1, x_2, \cdots)$ of an infinite number of real variables $x_1, x_2, \cdots$[1] can be characterized as a (complex-valued) function, defined on the space $\mathfrak{R}^\infty$ of points $\boldsymbol{x} = (x_1, x_2, \cdots)$, which can be uniformly approximated by trigonometric polynomials

$$\sum c_n e^{2\pi i (a_1^n x_1 + a_2^n x_2 + \cdots + a_{q_n}^n x_{q_n})}.$$

The space $\mathfrak{R}^\infty$ is topologized in the following way. A sequence of points $\boldsymbol{x}^n$ is said to converge towards $\boldsymbol{x}$, if $x_1^n \to x_1, x_2^n \to x_2, \cdots$. Thus every trigonometric polynomial, and hence also every almost periodic function is continuous on $\mathfrak{R}^\infty$.

The exponent vectors $(a_1^n, a_2^n, \cdots, a_{q_n}^n, 0, 0, \cdots)$ in the trigonometric polynomial above have zeros on all coordinate places from a certain number. We define the space $\mathfrak{R}_\infty$ as the set of all vectors $\boldsymbol{a} = (a_1, a_2, \cdots)$ with zeros on all coordinate places from a certain number (depending on the point), and so the exponent vectors can be said to belong to $\mathfrak{R}_\infty$. The inner

[1] S. BOCHNER [1].

product $a_1x_1 + a_2x_2 + \cdots$ between a vector $\boldsymbol{a} = (a_1, a_2, \cdots)$ from $\mathfrak{R}_\infty$ and a vector $\boldsymbol{x} = (x_1, x_2, \cdots)$ from $\mathfrak{R}^\infty$ is denoted by $\boldsymbol{a} \cdot \boldsymbol{x}$. The trigonometric polynomial above may then be written

$$\sum c_n e^{2\pi i \boldsymbol{a}^n \cdot \boldsymbol{x}} \qquad (\boldsymbol{a}^n \in \mathfrak{R}_\infty, \boldsymbol{x} \in \mathfrak{R}^\infty).$$

To every almost periodic function $f(\boldsymbol{x})$ is associated a unique Fourier series

$$f(\boldsymbol{x}) \sim \sum A_n e^{2\pi i \boldsymbol{a}^n \cdot \boldsymbol{x}}.$$

To the translated function $f(\boldsymbol{x} + \boldsymbol{h})$ is associated the Fourier series

$$f(\boldsymbol{x} + \boldsymbol{h}) \sim \sum A_n e^{2\pi i \boldsymbol{a}^n \cdot \boldsymbol{h}} e^{2\pi i \boldsymbol{a}^n \cdot \boldsymbol{x}}.$$

A necessary and sufficient condition for a sequence of translated functions $f(\boldsymbol{x} + \boldsymbol{h}^1), f(\boldsymbol{x} + \boldsymbol{h}^2), \cdots$ to converge uniformly to the (*eo ipso*) almost periodic function $g(\boldsymbol{x})$ is that the Fourier series of $f(\boldsymbol{x} + \boldsymbol{h}^n)$ converge formally to the Fourier series of $g(\boldsymbol{x})$. Therefore the necessary and sufficient condition for the set of all translated functions $f(\boldsymbol{x} + \boldsymbol{h})$ to be closed is that the set of points

$$\begin{Bmatrix} e^{2\pi i \boldsymbol{a}^1 \cdot \boldsymbol{h}} \\ e^{2\pi i \boldsymbol{a}^2 \cdot \boldsymbol{h}} \\ \cdot \\ \cdot \\ \cdot \end{Bmatrix}$$

where $\boldsymbol{h}$ runs through all vectors in $\mathfrak{R}^\infty$, be closed in $\mathfrak{R}^\infty$ or—what comes to the same thing—that the module of points

$$\begin{Bmatrix} \boldsymbol{a}^1 \cdot \boldsymbol{h} \\ \boldsymbol{a}^2 \cdot \boldsymbol{h} \\ \cdot \\ \cdot \\ \cdot \end{Bmatrix} + i_1 \begin{Bmatrix} 1 \\ 0 \\ \cdot \\ \cdot \\ \cdot \end{Bmatrix} + i_2 \begin{Bmatrix} 0 \\ 1 \\ \cdot \\ \cdot \\ \cdot \end{Bmatrix} + \cdots$$

where $\boldsymbol{h}$ runs through all vectors in $\mathfrak{R}^\infty$ and $i_1, i_2, \cdots$ through all integers, be closed in $\mathfrak{R}^\infty$.

3. Closed Modules and Substitutions in $\mathfrak{R}^\infty$.

Let $f(x_1, x_2, \cdots) = f(\boldsymbol{x})$ be a continuous function on $\mathfrak{R}^\infty$. A vector $\boldsymbol{h} = (h_1, h_2, \cdots)$ is called a period vector of $f(\boldsymbol{x})$ if $f(\boldsymbol{x} + \boldsymbol{h}) = f(\boldsymbol{x})$ for all points $\boldsymbol{x}$. The set of all period vectors of $f(\boldsymbol{x})$ is obviously a closed module in $\mathfrak{R}^\infty$. If it is not contained in any proper vector-subspace (i. e. *closed* linear subset[1]) of $\mathfrak{R}_\infty$ the function $f(\boldsymbol{x})$ is called fully periodic.

As a general example of a fully periodic function we consider an almost periodic function

$$f(\boldsymbol{x}) \sim \sum\nolimits^{\square} A_n e^{2\pi i \boldsymbol{a}^n \cdot \boldsymbol{x}}$$

which is periodic with the period 1 in all the coordinates $x_1, x_2, \cdots$ or—what comes to the same thing—a function which has all integral points as period vectors. Expressed as a property of the Fourier series this means that all the exponent vectors $\boldsymbol{a}^n$ are integral vectors.

In the previously cited paper [4]—and in more detail in [5]—a structure theorem for closed modules in $\mathfrak{R}^\infty$ was obtained. Incidentally, let me remark that this was done by introducing a suitable convergence notion in $\mathfrak{R}_\infty$ to the effect that a duality took place between the closed modules in $\mathfrak{R}^\infty$ and the closed modules in $\mathfrak{R}_\infty$. To formulate the structure theorem we have to introduce the notion of "substitution" in $\mathfrak{R}^\infty$. By this is understood a linear transformation $\boldsymbol{x} = T\boldsymbol{y}$ of the form

$$\begin{aligned} x_1 &= a_{11} y_1 + a_{12} y_2 + \cdots + a_{1 p_1} y_{p_1} \\ x_2 &= a_{21} y_1 + a_{22} y_2 + \cdots + a_{2 p_2} y_{p_2} \\ &\cdots\cdots\cdots\cdots\cdots\cdots\cdots\cdots, \end{aligned}$$

which establishes a one-to-one mapping $\boldsymbol{x} \leftrightarrow \boldsymbol{y}$ of the whole infinite-dimensional space on the whole infinite-dimensional space. It turns out to be the same as a linear, bicontinuous, one-to-one mapping of $\mathfrak{R}^\infty$ onto itself. The structure theorem now runs as follows.

[1] A linear set in $\mathfrak{R}^\infty$ need not be closed as is the case in the m-dimensional space. For instance the points in $\mathfrak{R}_\infty$ form a linear subset of $\mathfrak{R}^\infty$ and its closure is the whole $\mathfrak{R}^\infty$.

Structure theorem. *A closed module in the infinite-dimensional space* $\mathfrak{R}^\infty$ *is a point set* E *which by a substitution can be transformed into a point set of a special form, namely a point set* $[(x_1, x_2, \cdots)]$ *of the following structure: The indices* $1, 2, \cdots, n, \cdots$ *can be divided into three fixed classes* $\{n_r\}$, $\{n_s\}$, $\{n_t\}$, *such that the coordinates* x_{n_r} *independently run through all numbers, and the coordinates* x_{n_s} *independently run through all integers, while all the remaining coordinates* x_{n_t} *are constantly zero. Conversely, each such point set* E *is a closed module.*

The vector-subspaces (i. e. closed linear subsets) of $\mathfrak{R}^\infty$ are of course characterized by an empty class $\{n_s\}$.

That a closed module is not contained in any proper vector-subspace of $\mathfrak{R}^\infty$—as is the demand to the period module of a fully periodic function—means that it has an empty class $\{n_t\}$ or, what is equivalent, that there exists a transformed set which contains all integral points.

If $f(\boldsymbol{x})$ is an almost periodic function on $\mathfrak{R}^\infty$ and we subject $\boldsymbol{x}$ to the substitution $\boldsymbol{x} = T\boldsymbol{y}$, then the transformed function $f(T\boldsymbol{y})$ is an almost periodic function of $\boldsymbol{y}$ in $\mathfrak{R}^\infty$. In fact, a trigonometric polynomial in $\boldsymbol{x}$ will be transformed into a trigonometric polynomial in $\boldsymbol{y}$ by this process, and, to complete the reasoning, $|f(\boldsymbol{x}) - s(\boldsymbol{x})| \leqq \varepsilon$ for all $\boldsymbol{x}$ means the same as $|f(T\boldsymbol{y}) - s(T\boldsymbol{y})| \leqq \varepsilon$ for all $\boldsymbol{y}$. Furthermore, if $f(\boldsymbol{x})$ has the Fourier series

$$\sum' A_n e^{2\pi i \boldsymbol{a}^n \cdot \boldsymbol{x}}, \tag{1}$$

then $f(T\boldsymbol{y})$ has the formally transformed Fourier series

$$\sum' A_n e^{2\pi i \boldsymbol{b}^n \cdot \boldsymbol{y}}, \tag{2}$$

where $\boldsymbol{b}^n$ is determined by $\boldsymbol{a}^n \cdot T\boldsymbol{y} = \boldsymbol{b}^n \cdot \boldsymbol{y}$.[1] To see this, let $s_n(\boldsymbol{x})$ be a sequence of trigonometric polynomials which converges uniformly to $f(\boldsymbol{x})$. It will converge formally to the Fourier series (1), and therefore the sequence $s_n(T\boldsymbol{y})$ of trigonometric

[1] Incidentally we remark that the $\boldsymbol{b}^n$'s are obtained from the $\boldsymbol{a}^n$'s by a "substitution" T^* in $\mathfrak{R}_\infty$, T^* being the "adjoint substitution" of T (see [5]).

polynomials in $\boldsymbol{y}$ converging uniformly to $f(T\boldsymbol{y})$ will converge formally to the series (2), which must therefore be the Fourier series of $f(T\boldsymbol{y})$.

Obviously, a period vector $\boldsymbol{h}$ of $f(\boldsymbol{x})$ is transformed into a period vector $\boldsymbol{k}$ ($\boldsymbol{h} = T\boldsymbol{k}$) of the function $f(T\boldsymbol{y})$.

It follows from what has been said that a necessary and sufficient condition for an almost periodic function $f(\boldsymbol{x})$ to be fully periodic is that there exists a substitution $\boldsymbol{x} = T\boldsymbol{y}$ such that $f(T\boldsymbol{y})$ is periodic with the period 1 in all the coordinates $y_1, y_2, \cdots$, or—what comes to the same thing—that all the Fourier exponent vectors of $f(T\boldsymbol{y})$ are integral.

4. Infinitely Many Linear Congruences with Infinitely Many Variables.

We consider an arbitrary enumerable system of linear congruences with an enumerable number of real variables

$$\begin{aligned} &a_{11}x_1 + a_{12}x_2 + \cdots + a_{1\,n_1}x_{n_1} \equiv \theta_1 \pmod 1 \\ &a_{21}x_1 + a_{22}x_2 + \cdots + a_{2\,n_2}x_{n_2} \equiv \theta_2 \pmod 1 \\ &\cdots\cdots\cdots\cdots\cdots\cdots\cdots\cdots\cdots\cdots \end{aligned} \tag{3}$$

or, briefly written,

$$\begin{aligned} &\boldsymbol{a}^1 \cdot \boldsymbol{x} \equiv \theta_1 \\ &\boldsymbol{a}^2 \cdot \boldsymbol{x} \equiv \theta_2 \\ &\cdots\cdots\cdots, \end{aligned} \tag{3}$$

where every congruence only contains a finite number of variables and the a's and the θ's are arbitrary (real) numbers. By π_1 we denote the module of points $(\theta_1, \theta_2, \cdots)$ in $\mathfrak{R}^\infty$ for which the corresponding infinite system (3) has a solution, and by π_2 the module of points $(\theta_1, \theta_2, \cdots)$ for which any finite subsystem of (3) has a solution. The result of Bohr referred to in **1** was that in case of rational a's *a necessary and sufficient condition on the linear forms* $\boldsymbol{a}^n \cdot \boldsymbol{x}$ *in* (3) *in order that* $\pi_1 = \pi_2$ *is that there exists a substitution* $\boldsymbol{x} = T\boldsymbol{y}$ *in* $\mathfrak{R}^\infty$ *which transforms them into linear forms with integral coefficients.* The generalization in [4] of this result is that without the said restriction of rationality on

the a's *a necessary and sufficient condition on the linear forms in* (3) *in order that* $\pi_1 = \pi_2$ *is that there exists a substitution in* $\mathfrak{R}^\infty$ *which transforms them into a system of linear forms of a certain simple type, denoted by* S. By a system of linear forms *of the type* S we understand a system where certain of the variables (finite or infinite in number) have mere integral coefficients while each of the remaining variables (finite or infinite in number) necessarily becomes 0 if for a sufficiently large m one solves the m first "zero-congruences" corresponding to the linear forms, i. e. the congruences (3) with $\theta_1 = \theta_2 = \cdots = 0$.

By the proof of this theorem the structure theorem for closed modules in $\mathfrak{R}^\infty$ played an important role.

5. Modules in the m-dimensional Space.

The duality between $\mathfrak{R}^\infty$ and $\mathfrak{R}_\infty$ loosely referred to above has its simpler origin in a duality considered by M. Riesz [6] between two m-dimensional spaces $R_m = \{(x_1, x_2, \cdots, x_m)\}$ and $R_m = \{(a_1, a_2, \cdots, a_m)\}$. Since we shall use it in our proof we shall state this duality explicitly[1]. To an arbitrary module M in R_m Riesz considers the point set in (the other space) R_m consisting of all points $\boldsymbol{a} = (a_1, a_2, \cdots, a_m)$ from this latter R_m for which

$$\boldsymbol{a} \cdot \boldsymbol{x} = a_1 x_1 + a_2 x_2 + \cdots + a_m x_m \equiv 0 \pmod 1$$

for every point $\boldsymbol{x} = (x_1, x_2, \cdots, x_m)$ from M. This point set is a closed module in R_m and is called the dual module of M. We denote it by M'. If we repeat the operation of passing to the dual module we get a closed module $M'' = (M')'$ in (the original space) R_m. The relation between M and M'' appears from the following important theorem.

Riesz's theorem. *If* M *is an arbitrary module in* R_m, *the dual* M'' *of its dual module* M' *is the closure* $\overline{M}$ *of* M, *i. e.*

$$M'' = \overline{M}.$$

Before passing to the real proof of our theorem on almost periodic functions of infinitely many variables we shall make a

[1] For the proofs, see [5].

simple, and rather obvious, remark about the type of module M which is obtained by placing subspaces of the same dimension $\nu < m$ through all integral points in R_m and parallel to the same vector-subspace R of dimension ν, i. e. the module obtained by adding to the points in R all integral points in R_m. Our statement is that the largest vector-space contained in M[1] is R. This follows, by an indirect reasoning, from the fact that a usual space of dimension > 0 contains more than an enumerable number of points.

6. Proof of the Theorem.

We repeat the theorem to be proved.

Theorem. *An almost periodic function* $f(\boldsymbol{x}) = f(x_1, x_2, \cdots)$ *of an infinite number of variables is fully periodic*[2] *if and only if the set of translated functions* $f(\boldsymbol{x} + \boldsymbol{h}) = f(x_1 + h_1, x_2 + h_2, \cdots)$ *is closed with respect to uniform convergence.*

It is plain that this theorem contains the analogous theorem on almost periodic functions of a finite number of variables as a special case.

1. The one part of the theorem is easily dealt with. Let $f(\boldsymbol{x})$ be a fully periodic function. In order to show that the set of translated functions $f(\boldsymbol{x} + \boldsymbol{h})$ is closed we choose a substitution $\boldsymbol{x} = T\boldsymbol{y}$ such that the transformed function $f(T\boldsymbol{y}) = g(\boldsymbol{y}) = g(y_1, y_2, \cdots)$ is periodic with the period 1 in all the coordinates $y_1, y_2, \cdots$ (see end of **3**). Let $\boldsymbol{h}^1, \boldsymbol{h}^2, \cdots$ be a sequence of vectors such that $f(\boldsymbol{x} + \boldsymbol{h}^n)$ converges uniformly to a function $d(\boldsymbol{x})$. We have to show that $d(\boldsymbol{x})$ is equal to a translated function $f(\boldsymbol{x} + \boldsymbol{h})$. Let $\boldsymbol{k}^n$ be the corresponding points of $\boldsymbol{h}^n$ by the substitution above, i. e. $\boldsymbol{h}^n = T\boldsymbol{k}^n$. Then $g(\boldsymbol{y} + \boldsymbol{k}^n)$ will converge uniformly to $d(T\boldsymbol{y}) = j(\boldsymbol{y})$. We only have to prove that $j(\boldsymbol{y}) = g(\boldsymbol{y} + \boldsymbol{k})$ for some $\boldsymbol{k}$ since then $d(\boldsymbol{x}) = j(T^{-1}\boldsymbol{x}) = g(T^{-1}\boldsymbol{x} + \boldsymbol{k}) = g(T^{-1}\boldsymbol{x} + T^{-1}\boldsymbol{h}) = f(\boldsymbol{x} + \boldsymbol{h})$, where $\boldsymbol{h}$ is determined by $\boldsymbol{h} = T\boldsymbol{k}$.

The function $g(\boldsymbol{y}) = g(y_1, y_2, \cdots)$ is periodic with the period 1 in all the coordinates, so we may assume that our

[1] The vector-space generated by all vector-spaces contained in M (which on account of the module property must be contained in M).

[2] See **3**.

$\boldsymbol{k}^n$-points are all lying in the "periodicity parallelotope" $0 \leqq y_1 \leqq 1, 0 \leqq y_2 \leqq 1, \cdots$. This point set, however, is compact in the sense that every sequence $\boldsymbol{k}^1, \boldsymbol{k}^2, \cdots$ of points from this set has a subsequence which converges to a point of the set. As our $\boldsymbol{k}$ we may take any such limit-point of the sequence $\boldsymbol{k}^1, \boldsymbol{k}^2, \cdots$, for on account of the continuity of $g(\boldsymbol{y}), j(\boldsymbol{y}) = \lim g(\boldsymbol{y} + \boldsymbol{k}^n) = g(\boldsymbol{y} + \boldsymbol{k})$, q. e. d.

2. We now pass to the more difficult part of the theorem. Let $f(\boldsymbol{x})$ be an almost periodic function for which the set of translated functions $f(\boldsymbol{x} + \boldsymbol{h})$ is closed. Our task is to prove that $f(\boldsymbol{x})$ is fully periodic or, what comes to the same thing, that there exists a substitution $\boldsymbol{x} = T\boldsymbol{y}$ such that the transformed function $f(T\boldsymbol{y})$ has mere integral Fourier exponent vectors (see end of **3**). If

$$f(\boldsymbol{x}) \sim \sum A_n e^{2\pi i \boldsymbol{a}^n \cdot \boldsymbol{x}}, \text{ then } f(T\boldsymbol{y}) \sim \sum A_n e^{2\pi i \boldsymbol{b}^n \cdot \boldsymbol{y}},$$

where the linear forms $\boldsymbol{b}^n \cdot \boldsymbol{y}$ are obtained from the linear forms $\boldsymbol{a}^n \cdot \boldsymbol{x}$ by the substitution $\boldsymbol{x} = T\boldsymbol{y}$. So we have to find a substitution T which transforms the linear forms $\boldsymbol{a}^n \cdot \boldsymbol{x}$ into linear forms with integral coefficients. For this purpose we consider the corresponding system of congruences

$$\begin{aligned} \boldsymbol{a}^1 \cdot \boldsymbol{x} &\equiv \theta_1 \\ \boldsymbol{a}^2 \cdot \boldsymbol{x} &\equiv \theta_2 \\ &\cdots\cdots\cdots\cdots \end{aligned} \tag{4}$$

Let π_1 and π_2 be the modules defined in **4** corresponding to these congruences. Our assumption that the set of translated functions $f(\boldsymbol{x} + \boldsymbol{h})$ is closed is equivalent to π_1 being closed (see **2**).

It is plain that $\pi_1 \subseteqq \pi_2$. Furthermore, the closure $Cl(\pi_1)$ of π_1 contains π_2, $Cl(\pi_1) \supseteqq \pi_2$. For the proof of this let $(\theta_1^0, \theta_2^0, \cdots)$ be an arbitrary point from π_2. In order to approximate $(\theta_1^0, \theta_2^0, \cdots)$ by a point from π_1 we solve the m first congruences in (4) for this choice of $(\theta_1, \theta_2, \cdots)$ and a "large" m. Let $\boldsymbol{x}^0$ be a solution. Then $(\theta_1^0, \theta_2^0, \cdots, \theta_m^0, \boldsymbol{a}^{m+1} \cdot \boldsymbol{x}^0, \boldsymbol{a}^{m+2} \cdot \boldsymbol{x}^0, \cdots)$ from π_1 will be a "good" approximation to $(\theta_1^0, \theta_2^0, \cdots)$ in $\mathfrak{R}^\infty$. Since π_1 closed means $Cl(\pi_1) = \pi_1$, the relations

$$\pi_1 \subseteqq \pi_2 \subseteqq Cl(\pi_1)$$

imply $\pi_1 = \pi_2$. In case $f(\boldsymbol{x})$ is limit-periodic, i. e. all the $\boldsymbol{x}$-vectors are rational, the theorem of BOHR stated in 4 therefore immediately completes the proof.

In the general case we conclude by the theorem of BOHR and FØLNER in 4 that there exists a substitution $\boldsymbol{x} = T\boldsymbol{y}$ which transforms the linear forms into a system of the type S. Our proof will be completed if we can show that the new system has mere integral coefficients. Let the new system of congruences be

$$\begin{aligned} \boldsymbol{b}^1 \cdot \boldsymbol{y} &\equiv \theta_1 \\ \boldsymbol{b}^2 \cdot \boldsymbol{y} &\equiv \theta_2 \\ &\cdots\cdots\cdots\cdots \end{aligned} \tag{5}$$

For an arbitrary m we consider the module of points $(\theta_1, \theta_2, \cdots, \theta_m)$ which is supplied by the m first congruences when $\boldsymbol{y}$ runs through all points in $\mathfrak{R}^\infty$, and we wish to show that this module is closed in R_m. We assume to the contrary that it is not closed. Then there exists a point $(\theta_1', \theta_2', \cdots, \theta_m')$ which belongs to its closure but not to the module itself. We choose a sequence $\boldsymbol{y}^r$ such that $(\boldsymbol{b}^1 \cdot \boldsymbol{y}^r, \boldsymbol{b}^2 \cdot \boldsymbol{y}^r, \cdots, \boldsymbol{b}^m \cdot \boldsymbol{y}^r) \to (\theta_1', \theta_2', \cdots \theta_m')$ (mod 1) and next by the diagonal procedure a subsequence of $\boldsymbol{y}^r$ such that $\boldsymbol{b}^{m+1} \cdot \boldsymbol{y}^r$ modulo 1 converges to a θ_{m+1}', $\boldsymbol{b}^{m+2} \cdot \boldsymbol{y}^r$ modulo 1 converges to a θ_{m+2}', etc., ad inf. The point $(\theta_1', \theta_2', \cdots)$ will then obviously belong to $Cl(\pi_1)$ but not to π_1 (since not even the m first congruences can be fulfilled for this $(\theta_1', \theta_2', \cdots)$). This is a contradiction since $Cl(\pi_1) = \pi_1$. Hence the module $\{(\theta_1, \theta_2, \cdots, \theta_m)\}$ is closed. It will therefore be sufficient to prove that if the system of linear forms in (5) has not mere integral coefficients, then the module cannot be closed for all m.

To fix the matter assume for instance that the first column in our system of linear forms be not integral. The property of a system of linear forms of the type S (see 4) then implies that the variable y_1 necessarily becomes 0 if for a sufficiently large m one solves the m first "zero-congruences" corresponding to the linear forms, i. e. the congruences (5) with $\theta_1 = \theta_2 = \cdots = 0$. Let m be chosen in this way. We shall then show that the module $M = \{(\theta_1, \theta_2, \cdots, \theta_m)\}$ supplied by the m first congruences is not closed. To do this we write the m first congruences in (5) more fully as

$$\begin{aligned} b_{11}y_1 + b_{12}y_2 + \cdots + b_{1n}y_n &\equiv 0_1 \\ b_{21}y_1 + b_{22}y_2 + \cdots + b_{2n}y_n &\equiv 0_2 \\ \cdots\cdots\cdots\cdots\cdots\cdots\cdots\cdots\cdots\cdots & \\ b_{m1}y_1 + b_{m2}y_2 + \cdots + b_{mn}y_n &\equiv 0_m. \end{aligned}$$

The column vectors in this system span a vector-space R of points

$$y_1 \begin{Vmatrix} b_{11} \\ b_{21} \\ \cdot \\ \cdot \\ \cdot \\ b_{m1} \end{Vmatrix} + y_2 \begin{Vmatrix} b_{12} \\ b_{22} \\ \cdot \\ \cdot \\ \cdot \\ b_{m2} \end{Vmatrix} + \cdots + y_n \begin{Vmatrix} b_{1n} \\ b_{2n} \\ \cdot \\ \cdot \\ \cdot \\ b_{mn} \end{Vmatrix},$$

where $y_1, y_2, \cdots, y_n$ run through all numbers. Let its dimension be r. The property that y_1 necessarily becomes zero by solution of the zero-congruences has then as geometrical consequence that the dimension of the lattice of integral points in R is $\leqq r - 1$ (i. e. smaller than the dimension of R), for by the first property all integral points in R have to lie in the vector-subspace

$$y_2 \begin{Vmatrix} b_{12} \\ b_{22} \\ \cdot \\ \cdot \\ \cdot \\ b_{m2} \end{Vmatrix} + \cdots + y_n \begin{Vmatrix} b_{1n} \\ b_{2n} \\ \cdot \\ \cdot \\ \cdot \\ b_{mn} \end{Vmatrix}$$

and the point

$$\begin{Vmatrix} b_{11} \\ b_{21} \\ \cdot \\ \cdot \\ \cdot \\ b_{m1} \end{Vmatrix}$$

has to lie outside this subspace[1]. The module M is obtained by adding to the points in R all integral points in R_m. Denoting the module of integral points in R_m

[1] In fact, if the point lay in the subspace we could even solve the zero-*equations* with an arbitrarily chosen y_1.

$$\begin{pmatrix} i_1 \\ i_2 \\ \cdot \\ \cdot \\ \cdot \\ i_m \end{pmatrix} = i_1 \begin{pmatrix} 1 \\ 0 \\ \cdot \\ \cdot \\ \cdot \\ 0 \end{pmatrix} + i_2 \begin{pmatrix} 0 \\ 1 \\ \cdot \\ \cdot \\ \cdot \\ 0 \end{pmatrix} + \cdots + i_m \begin{pmatrix} 0 \\ 0 \\ \cdot \\ \cdot \\ \cdot \\ 1 \end{pmatrix}$$

by I we may write this

$$M = R + I.$$

In **5** we have seen that the largest vector-subspace in M is R. We now show that the closure $\overline{M}$ of M contains a larger vector-subspace, i. e. a space of dimension $\geqq \nu + 1$. Then $\overline{M}$ must be different from M, and M cannot be closed as we had to prove.

We pass to the dual module M' of M (see **5**) which obviously consists of all integral points $(k_1, k_2, \cdots, k_m)$ in R_m that are orthogonal to R (for $(k_1, k_2, \cdots, k_m) \cdot (\underset{1}{0}, \underset{2}{0}, \cdots, 0, \underset{r}{1}, 0, \cdots \underset{m}{0}) \equiv 0$ means k_r integral, and $(k_1, k_2, \cdots, k_m) \cdot y_r (b_{1r}, b_{2r}, \cdots, b_{mr}) \equiv 0$ for all y_r means $(k_1, k_2, \cdots, k_m) \cdot (b_{1r}, b_{2r}, \cdots, b_{mr}) = 0$).

The vector-space R^* of arbitrary points in R_m which are orthogonal to R has the dimension $m - \nu$. Suppose that the module $M' \subseteq R^*$ had the same dimension; then R could be characterized as the orthogonal vector-space to the module M'. But M' consists of integral points, so in particular a generating system $\boldsymbol{l}^1, \boldsymbol{l}^2, \cdots, \boldsymbol{l}^{m-\nu}$ is integral. Hence R would be the set of points $\boldsymbol{x}$ satisfying

$$\begin{aligned} \boldsymbol{l}^1 \cdot \boldsymbol{x} &= 0 \\ \boldsymbol{l}^2 \cdot \boldsymbol{x} &= 0 \\ \cdots\cdots\cdots\cdots & \\ \boldsymbol{l}^{m-\nu} \cdot \boldsymbol{x} &= 0. \end{aligned}$$

Solving algebraically we should get

$$\boldsymbol{x} = t_1 \boldsymbol{p}^1 + t_2 \boldsymbol{p}^2 + \cdots + t_\nu \boldsymbol{p}^\nu$$

with linearly independent *integral* vectors $\boldsymbol{p}^1, \boldsymbol{p}^2, \cdots, \boldsymbol{p}^\nu$ and $t_1, t_2, \cdots, t_\nu$ running through all numbers; and this contradicts the fact that the lattice of integral points in R has at most the

dimension $\nu - 1$. The argument therefore shows that the lattice M' has at most the dimension $m - \nu - 1$.

To complete the proof we use RIESZ's theorem (see 5) according to which $\overline{M} = (M')'$. Since M' is a lattice of dimension at most $m - \nu - 1$, the largest vector-subspace in $\overline{M}$ has at least the dimension $m - (m - \nu - 1) = \nu + 1$ (for if M' is of dimension s, its orthogonal space is of dimension $m - s$ and this orthogonal space is obviously contained in the dual module $(M')' = \overline{M}$). This proves our theorem.

References.

[1] S. BOCHNER: Beiträge zur Theorie der fastperiodischen Funktionen. II. Teil: Funktionen mehrerer Variabeln. Math. Ann. 96, 383—409 (1927).

[2] H. BOHR: Zur Theorie der fastperiodischen Funktionen. II. Teil: Zusammenhang der fastperiodischen Funktionen mit Funktionen von unendlich vielen Variabeln; gleichmässige Approximation durch trigonometrische Summen. Acta math. 46, 101—214 (1925).

[3] H. BOHR: Unendlich viele lineare Kongruenzen mit unendlich vielen Unbekannten. D. Kgl. Danske Videnskabernes Selskab. Mat.-fys. Meddelelser, Bind VII, 1925.

[4] H. BOHR and E. FØLNER: Infinite systems of linear congruences with infinitely many variables. D. Kgl. Danske Videnskabernes Selskab. Mat.-fys. Meddelelser, Bind XXIV, 1948.

[5] H. BOHR and E. FØLNER: On a structure theorem for closed modules in an infinite-dimensional space. Courant Anniversary Volume 1948.

[6] M. RIESZ: Modules réciproques. Extrait. Congrès International des Mathématiciens Oslo 1936, Tome II, 36—37.

Indleveret til selskabet den 12. september 1949.
Færdig fra trykkeriet den 14. Marts 1950.

DET KGL. DANSKE VIDENSKABERNES SELSKAB
MATEMATISK-FYSISKE MEDDELELSER, BIND XXV, NR. 15

ÜBER ARCHIMEDES' GRÖSSENLEHRE

VON

JOHANNES HJELMSLEV

KØBENHAVN
I KOMMISSION HOS EJNAR MUNKSGAARD
1950

Printed in Denmark.
Bianco Lunos Bogtrykkeri.

1. Wenn man heutzutage die Schriften der alten Mathematiker studiert, fällt es einem bekanntlich sehr schwer, sich gegen den störenden Einschlag des modernen Wissenschaftsmechanismus in den Gedankengang zu wehren. Ein überraschendes Beispiel hierfür meine ich in der herrschenden Auffassung von Archimedes' Grössenlehre gefunden zu haben; es ist nämlich — wie mir scheint — wegen des genannten Umstandes bisher nicht geglückt, ganz auf den Grund von Archimedes' Gedankengang zu dringen.

2. Mit Archimedes, insbesondere mit seiner Schrift über Kugel und Zylinder, beginnt eine neue Epoche der griechischen Grössenlehre. Ganz neue Arten von Grössen wie Längen krummer Linien und Inhalte krummer Flächen werden in den Arbeitsbereich einbezogen, und für diese Grössen werden bestimmte Arbeitsregeln aufgestellt, die in den folgenden Voraussetzungen formuliert sind:

1°. Von allen Linien, die dieselben Punkte verbinden, ist die gerade die kürzeste.

2°. Von zwei konvexen Linien, die dieselben Punkte verbinden und von denen die eine die andere umschliesst, ist die äussere die grösste.

3°. Ein ebenes Flächenstück ist kleiner als jedes krumme Flächenstück mit demselben Rand.

4°. Von zwei konvexen Flächen, die dasselbe Ebenenstück überspannen und von denen die eine die andere umschliesst, ist die äussere die grösste.

5°. Von zwei von einander verschiedenen Grössen derselben Art (Linien, Flächen, Raumstücke) übertrifft die grössere die kleinere um eine Grösse, die hinreichend oft zu sich selbst addiert jede im voraus gegebene Grösse derselben Art übertrifft.

3. Die letzte Annahme 5° (Archimedes' Lemma) soll hier zum Gegenstand einer eingehenden Betrachtung gemacht werden.

Sie enthält das Hilfsmittel für eine Verallgemeinerung der Hauptsätze der uns aus Euklids 5. Buch bekannten, von Eudoxos begründeten Grössenlehre, die ihre Anwendung auch auf die neuen Grössen ermöglicht.

Zunächst werden natürlich aus Eudoxos' Proportionenlehre die einleitenden Definitionen direkt übernommen, in erster Linie

A. Eudoxos' Axiom (Euklid V, Def. 4), das die Grundlage dafür bildet, dass überhaupt von einem Verhältnis zweier Grössen a und b gesprochen werden kann:

Von zwei Grössen wird gesagt, dass sie ein Verhältnis besitzen, wenn sie durch Vervielfachung einander übertreffen können.

$$(a < b, \quad a + a + \cdots + a > b.)$$

Ferner

B. Die Definition der Gleichheit zweier Verhältnisse a/b und c/d:

Für jedes Paar natürlicher Zahlen m, n soll aus $ma \gtreqless nb$ bzw. $mc \gtreqless nd$ folgen.

C. Die Definition der Ungleichheit zweier Verhältnisse:

$a/b > c/d$, wenn es ein Paar natürlicher Zahlen m, n derart gibt, dass $ma > nb$, aber $mc \leqq nd$.

Aus der Proportionenlehre selbst wird in Archimedes' Untersuchungen insbesondere die Hauptregel gebraucht, die besagt, dass aus $a \gtreqless b$ bzw. folgt $a/c \gtreqless b/c$ (oder $c/a \lesseqgtr c/b$). Aber der Beweis dieses Satzes (für das obere Ungleichheitszeichen) erfordert (Euklid V, 8), dass es eine ganze Zahl n derart gibt, dass

$$n(a - b) > c$$

ist. Dies war in der Proportionenlehre von Eudoxos eine direkte Folge seines Axioms, da $a - b$ in dem von ihm betrachteten Bereich stets als Grösse derselben Art wie die gegebenen existiert; innerhalb des neuen Grössenbereichs, mit dem Archimedes nun zu arbeiten hatte, konnte man aber keineswegs ohne weiteres hiervon ausgehen. Was soll man z. B. unter $a - b$ verstehen, wenn a ein Kreisbogen und b eine Strecke ist? Oder wenn a eine Kugelfläche und b ein ebenes Flächenstück ist?

Archimedes wählte den Ausweg, sein Lemma als eine letzte

Voraussetzung über die neuen Grössen, oder, wenn man will, als Bestandteil der Definitionen derselben aufzustellen: Wenn $a > b$ ist, ist die Differenz $a - b$ eine ideale Grösse, für die dieselbe Arbeitsregel gelten soll wie in Eudoxos' Grössenlehre, nämlich dass stets eine ganze Zahl derart existiert, dass $n(a - b)$ grösser ist als eine im voraus gegebene Grösse c von derselben Art wie a und b.

4. Dass Archimedes das so gemeint hat, kommt bereits deutlich in der Vorsicht, man möchte beinahe sagen Ehrfurcht, zum Ausdruck, mit der er in seinen einleitenden Briefen sein Lemma erwähnt (schon in der Schrift über die Quadratur der Parabel, besonders aber in der Schrift über Kugel und Zylinder, wo die eigentliche Grundlage erstmalig aufgestellt ist, und später auch in der Schrift über die Spiralen). Es geht dies aber mit voller Sicherheit aus dem ganzen systematischen Aufbau von Archimedes' Lehre hervor, wie dies im folgenden näher beleuchtet werden soll. Bisher scheint man keinen Blick für die genannte Bedeutung von Archimedes' Lemma gehabt zu haben. Man hat dieses Lemma einfach als gleichbedeutend mit Eudoxos' Axiom aufgefasst, und es ist sogar bekanntlich heutzutage weit verbreiteter mathematischer Sprachgebrauch, Eudoxos' Axiom als Archimedes' Axiom zu bezeichnen[1]. Man hat sogar die Auffassung vertreten, dass Archimedes selbst voraussetzte, dass ein Verhältnis immer als das Verhältnis zweier Strecken dargestellt werden kann. Dass dies ein offensichtliches Missverständnis ist, geht doch bereits aus dem Umstand hervor, dass Archimedes' Lemma danach vollständig überflüssig wäre.

5. Wir gehen nun zu einer näheren Begründung über, indem wir ein konkretes Beispiel einer Beweisführung von Archimedes,

[1] Der Fehler geht zurück auf O. Stolz: Zur Geometrie der Alten, insbesondere über ein Axiom des Archimedes (»Eine Grösse kann so oft vervielfältigt werden, dass sie jede andere ihr gleichartige übertrifft«); Innsbr. Ber. XII, 1882; Math. Ann. 22.

Später wurde er übernommen von G. Veronese: Fondamenti di geometria ..., 1891; deutsche Ausgabe: Grundzüge der Geometrie ..., 1894; Fussnote auf Seite 95: »Stolz ist, soviel wir wissen, der erste gewesen, der die Aufmerksamkeit der Mathematiker auf diesen von ihm mit Recht »Axiom des Archimedes« genannten Satz gelenkt hat ...«.

Schliesslich wurde derselbe Name (»Archimedisches Axiom«) von Hilbert in seinen Grundlagen der Geometrie, 1899 gebraucht.

Zeuthen hat mehrmals gegen diese fehlerhafte Benennung protestiert (u. a. auf dem Heidelberger Kongress 1904).

nämlich für den Satz 2 der Schrift über Kugel und Zylinder durchgehen. Wir beginnen mit einer freien Wiedergabe nach T. L. Heath, The Works of Archimedes, p. 5. Der Satz lautet folgendermassen:

Sind zwei von einander verschiedene Grössen gegeben, so ist es stets möglich, zwei von einander verschiedene Strecken zu finden, für die das Verhältnis (der grösseren zur kleineren) kleiner als das Verhältnis (der grösseren zur kleineren) der gegebenen Grössen ist.

Es mögen AB und D die beiden gegebenen, von einander verschiedenen Grössen symbolisieren, und es sei $AB > D$. Die Differenz $AB - D$ sei durch AC dargestellt, wo also D als BC abgezogen ist. Nach Archimedes' Lemma kann die ganze Zahl n so gross gewählt werden, dass n mal AC die Grösse D übertrifft, also so dass $n \cdot AC = AF$ grösser als CB ist. Auf der Geraden l wählen wir nun die Punkte E, H, G derart, dass GH gleich n mal HE ist. Dann gilt

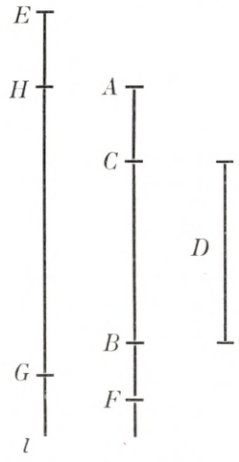

$$EH/HG = AC/AF.$$

Da aber $AF > D$ (oder BC) ist, gilt

$$AC/AF < AC/BC$$

und daher auch

$$EH/HG < AC/BC,$$

also (componendo)

$$EG/GH < AB/D,$$

6. Zu dem wiedergegebenen Beweis fügen wir nun folgende Bemerkungen: Die gegebenen Grössen werden in der Figur durch Strecken (AB und D, $AB > D$) dargestellt (symbolisiert), so dass die Differenz (AC) und zugleich das Vielfache von ihr, das Archimedes' Lemma zufolge D übertrifft, leicht symbolisiert werden können. Dies alles ist aber nur eine symbolische Darstellung, damit man die betreffenden Grössen in Gedanken festhalten kann. Daneben ist eine wirkliche Gerade l dargestellt, auf der die gesuchten Strecken angebracht werden.

Es ist sehr wichtig, dass man beim Studium von Archimedes an dieser Unterscheidung zwischen allgemeinen Grössen und Strecken festhält. Der vorliegende Satz 2 findet eine seiner wichtigsten Anwendungen beim Beweis dafür, dass die Oberfläche O der Kugel gleich dem Vierfachen des Grosskreises c ist (Satz 33). Der Beweis wird indirekt durch den Nachweis geführt, dass O weder grösser noch kleiner als $4c$ sein kann, und zwar beide Male mit Hilfe von Satz 2, wobei die gegebenen Grössen O und $4c$ sind, die durch »dazu proportionale Strecken« zu ersetzen Archimedes natürlich nicht einfällt.

7. Dieser Bemerkung gegenüber steht allerdings die folgende merkwürdige Tatsache:

Der überlieferte griechische Text (Heibergs Archimedes-Ausgabe I, p. 14—15) enthält einen Hinweis auf Euklids Elemente I, 2 in Verbindung mit der in der Figur angegebenen Einführung von Differenzen (in der obigen Figur: AC) der vorgelegten Grössen AB und D, als ob diese etwas mit der in Euklid I, 2 (was übrigens jedenfalls ein Schreibfehler für I, 3 sein muss) angegebenen Konstruktion zu tun hätte! Heiberg führt in einer Fussnote hierzu ein Zitat von Proclus an, aus dem hervorgehen sollte, dass die Archimedes-Texte schon damals denselben Hinweis auf Euklid enthielten. Der Hinweis ist aber jedenfalls vollkommen naiv und muss von einem nicht sachkundigen Abschreiber eingesetzt worden sein.

Dass Zeuthen sich in einer Abhandlung aus dem Jahre 1909[2] durch den genannten Hinweis dazu verleiten liess, allgemein über Archimedes' Grundlagen zu äussern:» Ein Verhältnis kann immer als das Verhältnis zweier Strecken dargestellt werden«, ist ganz unverständlich. Archimedes kann so etwas nicht gedacht haben. Er hat nirgends eine Voraussetzung darüber gemacht, und mit den Voraussetzungen, die er gemacht hat, kann er dies nicht beweisen.

Wenn dem so wäre, hätte er sich die Mühe mit seinen Überlegungen im Beweis von Satz 2 sparen können: Er hätte sich dann nämlich damit begnügen können, darauf hinzuweisen, dass die beiden gegebenen Grössen zu zwei Strecken proportional sind, und danach bloss die grösste von ihnen etwas zu verkleinern.

[2] Über einige archimedische Postulate (Archiv f. d. Gesch. der Naturwissenschaften und der Technik I, 1909).

8. Wir setzen unsere Erörterung des Beweises von Satz 2 fort. Der nächste Punkt, der besprochen werden soll, ist folgender.

Aus $AF > BC$ wird geschlossen, dass $AC/AF < AC/BC$ ist. Wir formulieren die Regel, die hier benutzt wird, mit einfacheren Bezeichnungen so:

Aus $a > b$ folgt $c/a < c/b$.

Sie ist aus Eudoxos' Proportionenlehre übernommen und wird dort, wie früher (3) erwähnt, daraus geschlossen, dass man eine ganze Zahl n derart finden kann, dass $n(a-b) > c$ ist, was aus Eudoxos' Axiom folgt, wenn a und b Grössen sind, deren Differenz sich als Grösse derselben Art wie die gegebenen erweist. Wenn aber a und b allgemeinere Grössen sind wie hier in Archimedes' Grössenlehre, führt diese Bedingung notwendigerweise zur Aufstellung von Archimedes' Lemma.

9. Die letzte, den Beweis von Satz 2 betreffende Frage, auf die wir eingehen wollen, ist der Übergang von der Ungleichung

$$EH/HG < AC/BC$$

zur Ungleichung

$$EG/GH < AB/D$$

oder in einfacheren Bezeichnungen von

$$a/b < c/d$$

zu

$$a + b/b < c + d/d.$$

Für diesen Schluss gibt Archimedes keinen Beweis, und er ist auch nicht in den Elementen erwähnt (bei Euklid findet sich nur der entsprechende Satz mit dem Gleichheitszeichen (V, 18)). In Eutokios' Kommentar findet sich ein Beweis, den wir hier wiedergeben wollen:

Man findet zunächst eine Grösse x derart, dass

$$b/a = d/x \text{ oder } a/b = x/d$$

gilt, woraus nach Euklid V, 18

$$a + b/b = x + d/d$$

folgt. Es ist aber $a/b < c/d$, also $x/d < c/d$, $x < c$, folglich

$$x + d < c + d, \quad x + d/d < c + d/d.$$

Da aber

$$x + d/d = a + b/b,$$

folgt

$$a + b/b < c + d/d \qquad \text{q. e. d.}$$

Ein ähnlicher Beweis findet sich bei Pappos. Zu diesen Beweisen ist indessen zu bemerken, dass sie Archimedes' Zwecken nicht angepasst sind. Sie gründen sich nämlich auf die Existenz der vierten Proportionalen zu drei Grössen b, a, d:

$$b/a = d/x,$$

wenn die Grössen der einen Seite (b und a) Strecken, die der anderen (d und x) aber allgemeine Grössen sind. Die Existenz einer solchen vierten Proportionalen fällt jedoch ganz ausserhalb der von Archimedes gemachten Voraussetzungen und kann aus ihnen nicht gefolgert werden.

Hierdurch wird man auf ähnliche Fragen wie oben geführt, nämlich ob man voraussetzen kann, dass Strecken existieren, die zwei gegebenen allgemeinen Grössen proportional sind, eine Voraussetzung, die Archimedes nicht zur Verfügung hat und die er sich in seiner ganzen Darstellung der allgemeinen Grössenlehre (in der Schrift über Kugel und Zylinder und in späteren Schriften) mit vollem Erfolg zu vermeiden bemüht hat.

Die Beweise von Eutokios und Pappos können also nicht als Kommentare zu Archimedes' letztem Schluss im Beweise von Satz 2 dienen. Bei genauerer Betrachtung sieht man, dass ein Kommentar eigentlich auch überflüssig ist. Der fragliche Satz folgt nämlich direkt aus der Definition der Ungleichheit:

Aus $a/b < c/d$, das heisst $ma < nb$, $mc \geq nd$ folgt nämlich $m(a + b) < (m + n)b$, $m(c + d) \geq (m + n)d$ also

$$a + b/b < c + d/d,$$

womit der Satz bewiesen ist.

Archimedes hat es offensichtlich für überflüssig gehalten, diesen Beweis anzuführen.

10. Um die vorstehend erörterten fundamentalen, das Verständnis von Archimedes' Grössenlehre betreffenden Fragen näher zu beleuchten, wollen wir mit modernen Hilfsmitteln ein arithmetisches Beispiel konstruieren: Wir betrachten eine Koordinatengeometrie mit pythagoreischer Massbestimmung, wo die Koordinaten nicht alle reellen Zahlenwerte, sondern nur die algebraischen annehmen können. In dieser Geometrie kann man eine Grössenlehre aufbauen, in der sämtliche Voraussetzungen von Archimedes gelten. Es gibt aber in dieser Geometrie keine Strecke, die einer Kreisperipherie gleich ist. Hieraus folgt weiter, dass keine zwei Strecken a und b existieren, die einer vorgegebenen Strecke l und einer Kreisperipherie c proportional sind. Sonst würde nämlich die vierte Proportionale der Strecken a, b, l eine Strecke sein, die gleich c ist.

Hiermit ist aber bewiesen, dass Archimedes' Grössenlehre weder explizit noch implizit eine Voraussetzung darüber enthält, dass stets zwei Strecken existieren, die zu zwei gegebenen allgemeinen Grössen proportional sind, oder dass es stets eine vierte Proportionale zu drei gegebenen Grössen gibt.

11. Dass Archimedes innerhalb seiner Grössenlehre die Existenz einer Strecke, die einer vorgelegten Kreisperipherie gleich ist, nicht beweisen kann, folgt ebenfalls aus dem obigen Beispiel. Er hat vielmehr mit Vorbedacht keine Voraussetzung über die Existenz einer solchen Strecke in seine Grössenlehre aufgenommen, was mit grosser Deutlichkeit aus dem Satz 4 der Schrift über die Spiralen hervorgeht:

Sind zwei von einander verschiedene Linien, nämlich eine Strecke und eine Kreisperipherie gegeben, so ist es möglich, eine Strecke zu finden, die kleiner als die grösste und grösser als die kleinste dieser beiden Linien ist.

Der Beweis wird so geführt: Ist c die Kreisperipherie und l die Strecke, und ist $c > l$, so kann l (nach Archimedes' Lemma) in so viele gleich grosse Teile geteilt werden, dass jeder kleiner als die Differenz von c und l ist; danach kann einer dieser

Teile zu l addiert werden, wodurch man gerade eine Strecke der gesuchten Art erhält.

Wäre Archimedes hier davon ausgegangen, dass c gleich einer bestimmten Strecke ist, läge kein Grund dazu vor, den obigen Satz aufzustellen, da seine Aussage dann selbstverständlich wäre.

12. Es ist jedoch interessant zu sehen, wo der Satz später verwendet wird. Dies geschieht bei der Untersuchung der Tangenten der Spirale, in Satz 18, der in moderner Sprache besagt, dass die Polarsubtangente OB im Endpunkt A der ersten Windung OA der Spirale gleich der Peripherie eines Kreises mit dem Radius OA ist. Der Beweis (den wir nicht wiedergeben wollen) läuft darauf hinaus zu zeigen, dass die Polarsubtangente weder grösser noch kleiner als die genannte Kreisperipherie sein kann.

Die Existenz der Spiralentangente, die Archimedes offenbar nicht bezweifelt, hat also die Existenz einer Strecke zur Folge, die der Peripherie eines gegebenen Kreises gleich ist. Es liegt nahe anzunehmen, dass Archimedes von dem Augenblick, wo ihm diese Tatsache bekannt wurde, hierin ein gewisses ergänzendes Fundament gesehen hat, das ihm ermöglicht, weitergehende Untersuchungen über die Rektifikation und Quadratur des Kreises einzuleiten, die dann später in der Schrift über die Kreismessung ausgeführt sind.

Nachdem Archimedes' Methodenlehre 1906 gefunden und gedeutet war, neigten zwar HEIBERG und ZEUTHEN — veranlasst durch eine bestimmte Äusserung darin — im Gegensatz zu früher der Auffassung zu, dass die Schrift über die Kreismessung vor der Schrift über Kugel und Zylinder entstanden sei. Die fragliche Äusserung lautet in Heibergs Übersetzung[3] folgendermassen:

»Durch diesen Lehrsatz, dass eine Kugel viermal so gross ist als der Kegel, dessen Grundfläche der grösste Kreis, die Höhe aber gleich dem Radius der Kugel, ist mir der Gedanke gekommen, dass die Oberfläche einer Kugel viermal so gross ist als ihr grösster Kreis, indem ich von der Vorstellung ausging, dass, wie ein Kreis einem Dreieck gleich ist, dessen Grundlinie die Kreisperipherie, die Höhe aber dem Radius des Kreises gleich,

[3] J. L. HEIBERG und H. G. ZEUTHEN, Eine neue Schrift des Archimedes, Bibl. Math., Dritte Folge, VII, S. 328.

ebenso ist die Kugel einem Kegel gleich, dessen Grundfläche die Oberfläche der Kugel, die Höhe aber dem Radius der Kugel gleich.«

Aber die »Vorstellung«, von der hier die Rede ist, war ja zweifellos zu Archimedes' Zeit so alt — sie muss jedenfalls auf die Studien über die Quadratrix zurückgehen — dass der Umstand, dass sie im oben genannten Zusammenhang erwähnt ist, keinen besonderen Anlass gibt, die Schrift über die Kreismessung gleichzeitig mit oder vor der Methodenlehre zu datieren.

Von grösserem Gewicht dürfte — neben der obigen Betrachtung in der Schrift über die Spiralen — sein, dass nicht nur einige einleitende Sätze über ein- und umbeschriebene Polygone aus der Grössenlehre der Schrift über Kugel und Zylinder (unter Prop. 1 und Prop. 6) in der Schrift über die Kreismessung angewendet werden, sondern dass auch einer dieser Sätze (der letzte unter Prop. 6), »dass es möglich ist, einem Kreis ein Polygon zu umschreiben, dessen Inhalt den Inhalt des Kreises um eine Grösse übertrifft, die kleiner als ein gegebener Flächeninhalt ist«, in beiden Schriften bewiesen ist, und zwar auf einfachere Weise in der Schrift über die Kreismessung. Es kann daher kein Zweifel darüber herrschen, in welcher Reihenfolge diese Beweise gefunden worden sind.

13. Archimedes hat wie gesagt keine Möglichkeit, aus seinen Grössenvoraussetzungen allein die Existenz einer Strecke zu schliessen, die gleich der Peripherie eines gegebenen Kreises ist. Er ist sich aber sicher darüber im Klaren gewesen, dass das Verhältnis zwischen der Peripherie und dem Durchmesser eines Kreises im Gegensatz zum Verhältnis zwischen der Oberfläche und dem Grosskreis einer Kugel, das durch die einfache ganze Zahl 4 ausgedrückt werden konnte, von wesentlich komplizierterer Beschaffenheit ist, so dass es nur mit Hilfe von grösseren und kleineren Zahlen beschrieben werden kann.

Die Untersuchungen, die es ihm mit Hilfe seiner Grössenlehre gelang durchzuführen, stehen den modernen Existenzbeweisen so nahe, dass das fehlende Hilfsmittel nur von formaler Natur ist: eine Erweiterung der eudoxischen Proportionenlehre für Strecken, die auch »unabgeschlossene Strecken« umfasst. Zu diesem Begriff kommt man auf folgende Weise: Wenn auf einer Strecke AB eine Reihe von Strecken AA_1, AA_2, $\cdots$ vorliegt, von

denen jede in der folgenden enthalten ist, und wenn keine Strecke existiert, die von dieser Reihe ausgeschöpft wird, dann definiert die Punktmenge, die sie umfasst, eine »unabgeschlossene Strecke«. Alle abgeschlossenen und unabgeschlossenen Strekken machen einen Grössenbereich aus, für den die ganze eudoxische Proportionenlehre leicht als gültig nachgewiesen werden kann, sobald man die äusserst naheliegenden Definitionen für Summe, Differenz, grösser und kleiner eingeführt hat. Und damit gelangt man direkt von der antiken zur modernen Grössenlehre.

Aber nicht weniger interessant ist es, dass die eudoxisch-archimedische Lehre selbst auf Bereiche angewendet werden kann, die nicht im eigentlichen Sinne stetig sind. In Archimedes' Voraussetzungen liegt ja — wie wir nachgewiesen haben — nicht, dass der Grössenbereich stetig ist, und die Anwendungsmöglichkeiten sind daher keineswegs auf unser gewöhnlich vorgezogenes Kontinuum beschränkt. In einer späteren Arbeit soll gezeigt werden, dass sich die Anwendbarkeit von Archimedes' Lehre mit geringfügigen Änderungen auf die empirische Wirklichkeitsgeometrie (ohne die Voraussetzung der Existenz unbegrenzter Vielfacher oder unbegrenzter Teilbarkeit) und auf die nicht-eudoxische Geometrie ausdehnen lässt.

Indleveret til selskabet den 12. december 1949.
Færdig fra trykkeriet den 4. februar 1950.

DET KGL. DANSKE VIDENSKABERNES SELSKAB
MATEMATISK-FYSISKE MEDDELELSER, BIND XXV, NR. 16

A NEW TYPE OF β-RAY SPECTROGRAPH

BY

O. KOFOED-HANSEN,
J. LINDHARD AND O. B. NIELSEN

KØBENHAVN
I KOMMISSION HOS EJNAR MUNKSGAARD
1950

Printed in Denmark.
Bianco Lunos Bogtrykkeri.

§ 1. Introduction.

In later years several methods of designing magnetic β-spectrographs have been proposed and applied in practice. Among these the most important are the magnetic lens spectrograph used by KLEMPERER (1935) and later on by DEUTSCH, ELLIOTT and EVANS (1944), SIEGBAHN (1943) and others, and the two-directional focusing spectrograph introduced by SVARTHOLM and SIEGBAHN (1946). A modification of the latter spectrograph was built by SNYDER (1948) and used in measurements on protons from nuclear reactions. A spectrograph of the lens type with a special field was recently proposed by RICHARDSON (1949).

It is a common feature of these types of spectrographs that the focusing is obtained only in a first approximation, and since high resolving power is desirable the solid angle of emitted β-particles which could be utilized in the spectrograph had to be small. In fact, there will always be a competition between the resolving power $R = p/\Delta p$ and the effective solid angle, Ω, and the values of these two quantities may for many purposes be taken as a measure of the efficiency of the apparatus, even though other properties like dispersion are of importance. In the best spectrographs one may have, e. g., $1/R \sim 1\,^0/_0$ and $\Omega \sim 1\,^0/_0$ of $4\,\pi$. With refined lens spectrographs it has recently proved possible to attain a further improvement by a factor of 2 (SLÄTIS and SIEGBAHN 1949; see also ZÜNTI 1948, and DU MOND 1949).

The question can now be raised whether it is possible to increase further the transmission by any considerable factor without essential reduction in resolution. This can be brought about only if the β-spectrograph is rather different from the common type, since in principle one must then have exact focusing. It seems reasonable to exclude beforehand spectrographs involving electric fields, since it is much easier to produce

magnetic fields of the order of magnitude demanded in β-spectrographs.

From the experimental point of view the problem of obtaining focusing for a large solid angle is of course always of interest, but it is the more pertinent if one has a β-source of very low intensity. A typical case of this kind arises if one wants to estimate the energy of hard γ-rays from nuclear reactions by measuring the energy of the Compton electrons produced by the radiation. Since the distribution in energy of Compton electrons is comparatively wide, the resolving power need not be very high. On the other hand the intensity is so low that it becomes necessary to focus a considerable fraction of the fast electrons produced.

The present paper is an attempt at solving the problem of focusing for a large solid angle with a magnetic spectrograph. The guiding principles used may be shortly outlined as follows. First of all, it seems natural to demand that the field be cylindrically symmetrical around the line connecting source and focus. We shall further require that each β-particle moves in a plane containing the axis of the spectrograph. The magnetic field must therefore be normal to this plane, which entails that the currents producing the field have component zero perpendicular to the plane. We shall also suppose that the current distribution in a plane containing the axis can be represented by a single closed ringformed current. These requirements make it possible, at least in a first approximation, to build the spectrograph with the use of wedge-shaped pole pieces having plane surfaces, so that the gaps are also wedge-shaped. The edges of the pole pieces will then just correspond to the closed curve describing the associated current. The arrangement of pole pieces and gaps is shown in Fig. 1. With the above conditions the magnetic field will be inversely proportional to the distance from the axis. It may be mentioned that BENDER and BAINBRIDGE[1] have built a spectrograph with one gap, where the magnetic field is inversely proportional to the distance from the centre of the spectrograph. Theoretically, this seems not to give as good possibilities of all-over focusing as the present type.

In the calculation below we shall not in the first instance

[1] We are much indebted to Dr. BAINBRIDGE for information regarding this spectrograph.

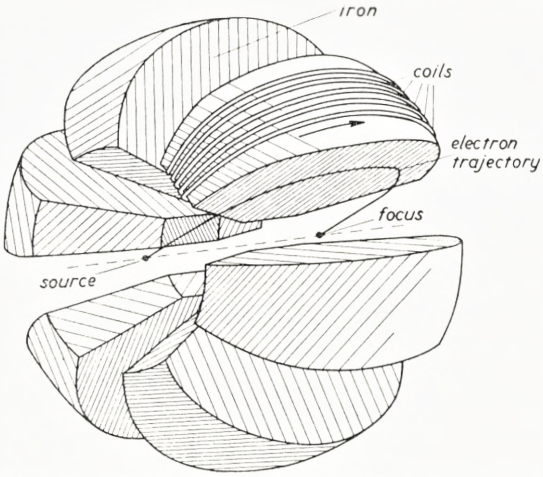

Fig. 1. A schematic illustration of the arrangement of pole pieces and gaps of a symmetrical spectrograph with 6 gaps of opening angle 30°.

discuss the possibilities of constructing magnets giving the desired field. We shall apply instead the idealized picture with a ring current in a plane containing the axis and assume that we can dispose freely of this current and also that it forms no mechanical obstacle to the motion of the β-particles.

It turns out that even with the above limitations there is a great variety of solutions with point focusing for a large solid angle. We have given a detailed description of one particular kind of solution, which besides rotational symmetry shows symmetry with respect to the central plane in the spectrograph. The other types of solutions are accounted for more schematically.

In order to appreciate the advantages or disadvantages of the different solutions it is necessary to obtain estimates of the resolving power of the spectrograph. We have therefore tried to look into the questions of image formation, dispersion and effects of stray fields at the edges of the pole pieces. The above-mentioned symmetrical solution is found to be particularly simple and is the only case with image formation. This is by no means a strong argument against asymmetrical solutions. It seems most important to select only such solutions where the electron trajectories meet the boundary curve at nearly right angles.

A model of the symmetrical spectrograph with only one gap was built, and the focusing and resolution was measured (see

§ 5). This model was found to be in fair accord with theoretical estimates, and as far as the preliminary evidence goes, a spectrograph constructed on these lines can have, e. g., a solid angle $\Omega \sim 20\ ^0/_0$ of $4\,\pi$ and resolving power $1/R \sim 2\ ^0/_0$.

§ 2. The Electron Trajectories.

In this and in the next paragraph the problems of the integration of the equations of motion and the possibilities as to focusing are treated. The discussion is perhaps rather elementary and more detailed than necessary for our purpose. Nevertheless, we considered it of some value to give a comparatively complete account of a treatment which is suited to give the general solution for the kind of spectrograph considered here.

It is convenient to apply cylinder coordinates, where the z-axis passes through source and focus, while r is the distance from the axis, and φ ($0 \leqq \varphi \leqq 2\,\pi$) is the angle of rotation about the axis. As mentioned in the introduction, the current in the z,r-plane is assumed to follow a closed curve, and the component in the direction of φ is zero. In the actual spectrograph this curve describes the boundaries of the pole pieces, in a first approximation at least. The total current in the ring, when integrated over φ, is I e. s. u./sec. It is seen that in the space outside the closed ring the magnetic field is zero and the electrons move in straight lines. Inside the ring the field is

$$H_r = H_z = 0, \quad H = \frac{2\,I}{cr} = \frac{H_1}{r}, \tag{1}$$

where $H_1 = 2\,I/c$ is the field in unit distance from the axis.

Our first step is the integration of the equations of motion for an electron moving in the field given by (1)[1], the motion being confined to the z,r-plane. The radius of curvature of the electron orbits is

$$\left.\begin{aligned} \varrho &= \frac{cp}{eH} = b \cdot r \\ b &= \frac{p \cdot c^2}{2\,eI} \end{aligned}\right\} \tag{2}$$

[1] The motion of electrons in fields of this kind has been treated by Richardson (1947) and applied to β-spectroscopy. However, Richardsons discussion is somewhat different from the present treatment because the application was to a spectrograph similar to the semi-circular type.

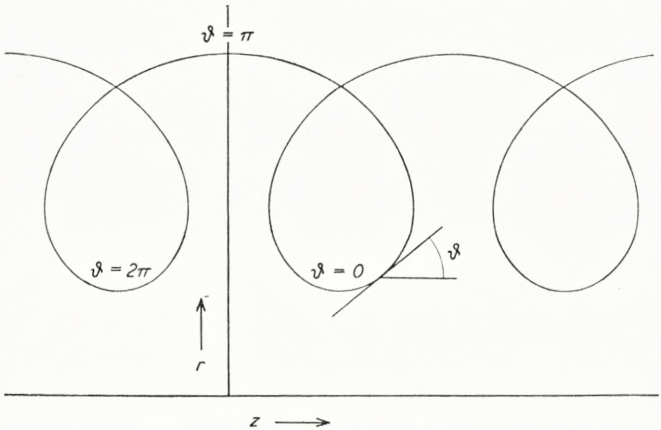

Fig. 2. An electron trajectory in the magnetic field $H = H_1/r$, where the quantity $b = \frac{cp}{eH_1}$ is supposed to have the value 0.6.

and hence ϱ is proportional to r. The constant b depends only on the ratio between the momentum of the electron, p, and the total current, I.

The electron trajectories obey the differential equation

$$\left(1+\left(\frac{dr}{dz}\right)^2\right)^{\frac{1}{2}} = br\frac{d^2r}{dz^2}. \tag{3}$$

This equation is integrated readily and leads to the following expression for z as a function of r

$$z = \int^{r} \frac{\log(y/a)\,dy}{\sqrt{b^2-(\log(y/a))^2}} + z_0. \tag{4}$$

There are two integration constants, a and z_0. In Fig. 2 is shown an electron trajectory, with $b = 0.6$. It is seen that the electrons perform loops, with a drift parallel to the z-axis.

The curves (4) are more conveniently described in a parameter representation with the angle ϑ between the axis and the tangent of the curve as a parameter (see Fig. 2). We write

$$\left.\begin{aligned} z &= ab\,U(b,\vartheta)+z_0 \\ r &= ae^{-b\cos\vartheta} \end{aligned}\right\}, \tag{5}$$

where

$$U(b,\vartheta) = \int_{\pi}^{\vartheta} \cos x\, e^{-b\cdot\cos x}\,dx. \tag{6}$$

We then have $z = z_0$ for $\vartheta = \pi$. It is also seen that the integration constant a simply corresponds to the value of r for $\vartheta = \pi/2$. Moreover, the minimum and the maximum distance from the axis are given by

$$r_{\min} = a \cdot e^{-b}, \quad r_{\max} = a \cdot e^{b}.$$

Therefore, the ratio $r_{\min}/r_{\max}$ is equal to e^{-2b} and does not depend on the constants of integration, but only on the quantity b.

The motion of the electrons was found to be periodic in the direction of the z-axis. From (5) this period is found to be

$$\left.\begin{aligned} z(\vartheta - 2\pi) - z(\vartheta) &= -2\pi\, iab \cdot J_1(ib) = \\ &= 2\pi\, ab^2 (1 + b^2/16 + b^4/192 + \cdots\cdots). \end{aligned}\right\} \quad (7)$$

J_1 is the first order Bessel function of the first kind.

Equation (5) also shows that while b essentially determines the form of the trajectories the integration constant a is a parameter describing a family of curves, similar with respect to the point $z = z_0$ on the z-axis.

The function $U(b, \vartheta)$ defined by (6) can be computed from a suitable series development. For instance, the exponential function in the integrand of (6) may be written as a power series in $b \cos x$, whereby one obtains a rapidly converging series of integrals. However, it seems preferable to use the following series development in Bessel functions

$$\left.\begin{aligned} U(b, \vartheta) &= iJ_1(ib)(\pi - \vartheta) - \\ &- \sum_{n=1}^{\infty} \frac{1}{n} (i)^{n-1} (J_{n-1}(ib) - J_{n+1}(ib)) \sin n\vartheta. \end{aligned}\right\} \quad (8)$$

As will be seen later the values of interest for b will be $b \lesssim 1$. For such values of b it is necessary to retain at most about five or six terms in (8), in order to know U to four decimal places.

In Fig. 3 is shown a set of trajectories, all of them corresponding to the value 1 for b. For all orbits in the figure the maximum value of r corresponds to $z = 0$. This will be called a symmetrical arrangement of orbits all having the same value of b, but different values of a. In Fig. 3 is included only one

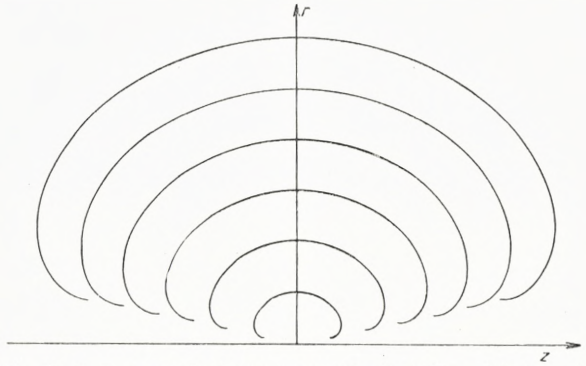

Fig. 3. A symmetrical arrangement of orbits with $b = 1$.

loop in the electron orbits. For obvious reasons the present treatment will be limited to this case, so that $0 \leqq \vartheta \leqq 2\pi$.

Instead of a symmetrical arrangement of orbits we can also pick out a set of orbits for which the z-value corresponding to $r = r_{\max}$ is a function of $r_{\max}$, i. e., a function of a. Any set of orbits of this kind can be characterized by the function

$$\zeta(a) \equiv z(r = r_{\max}). \tag{9}$$

The function $\zeta(a)$ is uniquely defined apart from an arbitrary constant. In the case of a symmetrical arrangement of orbits we may write

$$\zeta(a) = 0. \tag{10}$$

The equations (5) can now be rewritten on the form

$$\left.\begin{aligned} z &= ab\,U(b, \vartheta) + \zeta(a) \\ r &= a\,e^{-b\cos\vartheta}. \end{aligned}\right\} \tag{11}$$

When the function $\zeta(a)$ is chosen the two-parameter family of curves in (5) is replaced by a family depending on only one parameter, a. This representation also corresponds to the point of view to be taken in the following. We choose some one-parameter family of trajectories described by a function $\zeta(a)$ and will then look for the possibilities of obtaining focusing with this family.

§ 3. The Focusing.

Having solved the equations of motion for electrons in the space inside the boundary curve we may proceed to discuss the conditions to be fulfilled by this curve in order that focusing is obtained in a point on the z-axis.

Suppose that β-particles are emitted from a point $z = z_f$ on the z-axis. It is also assumed that we have chosen some one-

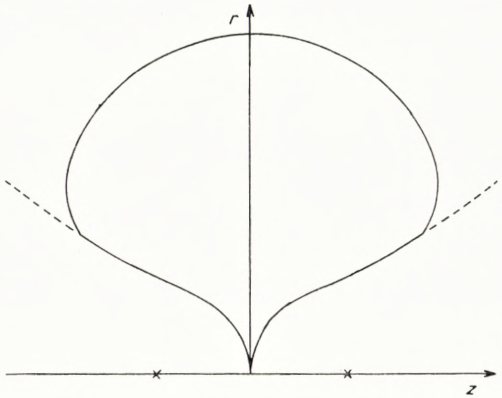

Fig. 4. The figure shows the boundary curve of a symmetrical spectrograph ($z_{f1} = z_{f2}$) with $b = 0.6$. Source and focus are indicated by crosses. Electrons emitted from the source at an angle less than 36° do not meet the boundary curve and can not be focused.

parameter family of curves as described by (11). We then draw the tangents from z_f to each of the curves (11). This is always possible since ϑ varies between 0 and 2π on all curves. Indeed, there will be two tangents for each curve but we choose the tangent on the source side, or the one for which $0 < \vartheta < \pi$. The new curve formed by the touching points of the tangents is just the boundary curve we are looking for, since it corresponds to the edges of the pole pieces of the idealized spectrograph. Inside this curve the magnetic field should be different from zero and the orbits as in (11) while outside we assumed rectilinear motion of the β-particles and a magnetic field equal to zero.

To a point (z, r) is associated a trajectory (11) passing through the point. If the point is to lie on the boundary curve, the tangent

of the trajectory in (z, r) must pass through the source (z_f, o) or

$$\operatorname{tg} \vartheta = \frac{r}{z - z_f}. \tag{12}$$

Together, (11) and (12) therefore give a parameter representation of the boundary curve, and it is most convenient to consider ϑ, and not a, as the parameter. If ϑ is the parameter, we may take (12) as a relation determining a as a function of ϑ; the

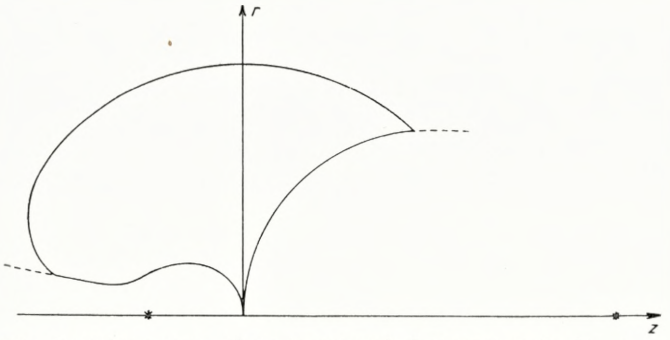

Fig. 5. The boundary curve of an asymmetrical spectrograph ($z_{f1} \neq z_{f2}$) with $b = 1$ and with a symmetrical arrangement of orbits ($\zeta(a) = 0$).

value of a can then be introduced in (11), whereby finally the coordinates (z, r) of the boundary curve are found as functions of ϑ.

Only if $\zeta(a)$ is a simple function will it be easy to give an explicit formula for (z, r). In case $\zeta(a)$ is proportional to a, $\zeta(a) = C \cdot a$, we find

$$\left.\begin{aligned} z &= z_f \cdot \frac{b \cdot U(b, \vartheta) + C}{b \cdot U(b, \vartheta) + C - \cot \vartheta \cdot \exp\{-b \cdot \cos \vartheta\}}, \\ r &= z_f \cdot \frac{\exp\{-b \cdot \cos \vartheta\}}{b \cdot U(b, \vartheta) + C - \cot \vartheta \cdot \exp\{-b \cdot \cos \vartheta\}}, \\ \zeta(a) &= C \cdot a. \end{aligned}\right\} \tag{13}$$

The symmetrical arrangement of orbits corresponds to $C = 0$. As could be anticipated, for $\zeta(a) = C \cdot a$ different values of z_f only lead to boundary curves similar with respect to the origin.

With a given value b it is therefore possible to give once and for all the solution when $\zeta(a) = C \cdot a$, if only the function $U(b, \vartheta)$ is evaluated for this particular value of b. Of course, it holds generally that $U(b, \vartheta)$ is the basic function to be calculated when a boundary curve is desired.

Fig. 4 and 5 show the boundary curves with symmetrical arrangement of orbits in the two cases $b = 0.6$ and $b = 1$. As coordinates are used z/z_f and r/z_f.

Fig. 4 represents a symmetrical arrangement of orbits and the boundary curve is also symmetrical. Evidently, even with the symmetrical arrangement of orbits it is not necessary to have a symmetrical boundary curve. An asymmetrical spectrograph is obtained as soon as the z_f's corresponding to source end and focus end are chosen to be different; this case is illustrated in Fig. 5.

As indicated in Fig.s 3, 4, and 5 only part of the total solid angle can be utilized. If θ is the angle between the positive direction of the z-axis and a straight line through z_f there will be a certain critical angle θ_c defined by the common tangent of the curves (13). Electrons emitted from the source with angles $\theta \leq \theta_c$ can never enter the field and be focused. In the symmetrical case and for b equal to 1 and 0.6, respectively, the critical angles are $\sim 12°$ and $\sim 36°$. This also illustrates the variation of θ_c with b.

Of course, even for angles somewhat larger than θ_c will the trajectories meet the boundary curve at nearly glancing incidence, and it becomes practically impossible to focus the electrons emitted from the source, especially in view of the effects of stray fields occurring at the edges of the pole pieces. This is one of the reasons why in the final spectrograph the cut-off angle must be chosen much larger than θ_c. The angle θ_c will then be of no significance and may be left out of the discussion. We notice that the variation of θ_c with b shows that the larger is chosen the value of b the easier it will be to focus β-rays ejected in backward directions, i. e., with θ small.

In the calculations on the boundary curve we found that there is a large freedom in the choice of the following variables: the distance between source and focus, the boundary curve, the function $\zeta(a)$, the field strength, etc. To put it more definitely we can dispose rather freely of the quantity $b = p \cdot c^2/2\,eI$, the coordinates

of source and focus and at the same time of e. g. the function $\zeta(a)$. The boundary curves at the focus and source end are then determined from these variables. Of course, we may instead choose one of the boundary curves and with this choice find the corresponding function $\zeta(a)$ and the other boundary curve. Finally, the opening angles of the wedge shaped gaps and of the pole pieces are left undetermined so far.

The freedom of choice as expressed by these variables is rather convenient, because the calculations below on focusing and resolving power lead to several restrictions e. g. as regards the form of the boundary curve. Here, the primary condition is that both resolution and effective solid angle are sufficiently large. When these conditions are fulfilled one is still left with several possibilities. The choice between these possibilities will depend on the more technical aspects of the problem.

In the kind of solution considered here the total angular deflection of the orbits is less than 2π. One might also consider solutions where the trajectories perform several loops of the kind shown in Fig. 2 before being focused. The boundary curves will then be somewhat different from those considered here, but they are easily obtained from the present curves. In this connection it may be mentioned that in the present solution many electrons of low energy meeting the boundary curve on the source side may pass through the field performing a number of loops on the way. They will then leave the field in a more or less random direction at the focus end. These electrons, therefore, will give rise to a background, which may be inconvenient. However, spurious effects of this kind can be removed by suitable screening devices.

§ 4. Image Formation, Dispersion and Resolving Power.

In this paragraph we shall treat questions connected with the resolving power of the β-spectrograph. It is well known that in the usual spectrographs with first order focusing there is a very direct competition between the resolving power, R, and the effective solid angle, Ω, utilized in the spectrograph. However, in the type of spectrograph discussed here, with focusing for a large

effective solid angle, the resolution R is more independent of the effective solid angle and can in fact be made quite large. One might say that the spectrograph consists of a number of small spectrographs, each of these corresponding to one of the wedge-shaped gaps so that the possibility of an improvement as regards resolution and solid angle is due to the replacement of one spectrograph by several. As we shall see, such a description can be justified from the fact that while the idealized spectrograph has an infinitely good resolution and corresponds to an infinite number of gaps, the imperfections arise from the number of gaps being limited, whereby the rotational symmetry is violated.

As a preliminary to the discussion of resolution we shall treat the question of image formation. We consider first an electron which, though moving in the z, r-plane, is not emitted from the source point $(z_{1f}, 0)$ but from a point in the immediate neighbourhood of this space point. The variables on the source side of the spectrograph are given the index 1. Let us choose a point (z_1, r_1) on the boundary curve. This point as determined by (11), (13), is a function of ϑ, or, as is convenient in the present case, a function of the parameter a. At the same time, the boundary curve is completely determined from the function $\zeta(a)$ and the value of z_{f1} and b.

Suppose that the electron arrives at (z_1, r_1). If the electrons from the source $(z_{f1}, 0)$ arrive at an angle ϑ_1, the electron considered must pass at a slightly different angle $\vartheta_1 + \delta\vartheta_1$ where $\delta\vartheta_1$ is a function of ϑ_1. Now, since the further motion in the proper trajectory of the electron is described by $\zeta(a)$, as giving the abscissa for the maximum value of r, the slightly changed orbit will be defined by the new ζ-function, $\zeta(a) + \delta\zeta(a)$. We therefore calculate first the change $\delta\zeta(a)$ as a function of $\delta\vartheta_1(\vartheta_1) = \delta\vartheta_1(a)$, remembering that ϑ_1 and a are connected by a one-to-one correspondence. In order to find $\delta\zeta(a)$ we perform a variation calculus in equation (11), varying $\zeta(a)$, a, and ϑ_1, while the point (z_1, r_1) and of course also b are kept fixed. With this procedure we obtain (see Fig. 6)

$$\delta\zeta(a) = \delta\vartheta_1(a) \cdot b \cdot \left(z_{f1} - \zeta(a) + a \cdot \frac{d}{da}\zeta(a) \right) \cdot \sin\vartheta_1 . \qquad (14)$$

Now, we are of course not much interested in the actual values of $\delta\zeta(a)$, since we only want to find the new trajectories in the focus end. Let the variables at the focus end be given the index 2. We shall further use the convention that while the positive direction of the z-axis on the source side is taken from focus to source the positive direction on the focus side is opposite, or from source to focus. This will mean that all formulas between

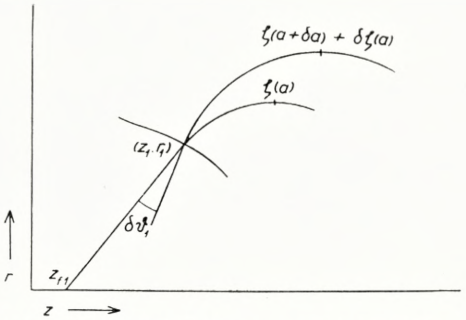

Fig. 6. An illustration of the calculation on image formation. A β-ray entering at an angle $\vartheta + \delta\vartheta_1$ slightly different from that corresponding to focusing. The parameter a and the function $\zeta(a)$, defining the trajectory, are thereby changed.

variables on the focus side are found from those on the source side simple by changing the indices from 1 to 2, and by replacing $\zeta(a)$ by $-\zeta(a)$. This gives immediately the formula corresponding to (14), and the connection between $\delta\vartheta_1(a)$ and $\delta\vartheta_2(a)$ is then

$$\left.\begin{aligned} &\sin\vartheta_2 \cdot \left(z_{f2} + \zeta(a) - a \cdot \frac{d}{da}\zeta(a)\right)\delta\vartheta_2(a) = \\ &-\sin\vartheta_1 \cdot \left(z_{f1} - \zeta(a) + a \cdot \frac{d}{da}\zeta(a)\right)\delta\vartheta_1(a). \end{aligned}\right\} \quad (15)$$

In principle formula (15) describes the new trajectories on the focus side, as corresponding to, e. g., particles coming from a point in the neighbourhood of the source. However, a formula like (15) is rather difficult to handle. In the simplest case, that of the symmetrical spectrograph where $\zeta(a) = 0$, $z_{f1} = z_{f2}$ and $\vartheta_1(a) = \vartheta_2(a)$, it is immediately seen that $\delta\vartheta_1(a) = -\delta\vartheta_2(a)$. This means that there will be first order image formation and the magnification is 1.

The treatment so far relates only to particles moving in the z, r-plane. It is necessary to consider trajectories which are not contained in a plane through the symmetry axis. From conservation of momentum about the axis it follows that a particle passing the axis at a small distance d_1 on the source side, in the focus end will pass at a instance d_2 on the opposite side of the axis, where

$$d_1 \sin \vartheta_1 = d_2 \sin \vartheta_2, \tag{16}$$

ϑ being the angle between the trajectories and the axis. The radial motion of the particle and the connection between ϑ_1 and ϑ_2 remains the same as that described in (15).

Again, in the case of the symmetrical spectrograph where $\vartheta_1 = \vartheta_2$ formula (16) shows that the above mentioned image formation holds true for all directions of emission from a point in the neighbourhood of the source. Moreover, the completely symmetrical spectrograph is the only kind having the property of image formation. We shall not give the proof of this result here; it follows from simple consideration using equations (15) and (16). The property of image formation might seem to imply a special advantage of the symmetrical spectrograph over other types. In how far this property is of importance to the actual spectrograph will be discussed in connection with the resolving power.

In order to find the dispersion of the spectrograph we consider the motion of particles with energies differing slightly from that corresponding to focusing. The effect resulting from a change in energy may also be obtained through a change in the magnetic field, because it only depends on the change δb of the quantity $b = p c^2/2 eI$.

As above the trajectory is supposed to pass through a point (r_1, z_1) at the source end. Keeping z_1, r_1 and ϑ_1 fixed, which means that the particle comes from the source $(z_{f1}, 0)$ the quantities b, a and $\zeta(a)$ in (11), (13) are varied. The variation gives $\delta\zeta(a)$ as a function of δb and a on

$$\left.\begin{aligned} \delta\zeta(a) = -\delta b \Big\{ & ab \cos\vartheta_1 \, U(b, \vartheta_1) + aU(b, \vartheta_1) + \\ & + ab \frac{\partial}{\partial b} U(b, \vartheta_1) + a \cos\vartheta_1 \frac{d}{da} \zeta(a) \Big\}. \end{aligned}\right| \tag{17}$$

From $\delta\zeta\,(a)$ the varied motion in the focus end is calculated in a similar way as in the treatment of image formation. It is then found that the new path through the point (z_2, r_2) on the boundary will leave at the changed angle $\vartheta_2 + \delta\vartheta_2$, given by

$$\left.\begin{aligned}\delta\vartheta_2 \left\{\sin\vartheta_2\, b\frac{d}{da}\zeta\,(b) - b^2\,U\,(b\,,\,\vartheta_2)\sin\vartheta_2 + b\cos\vartheta_2\, e^{-b\cos\vartheta_2}\right\} = \\ = -\delta b\left\{U\,(b\,,\,\vartheta_1) + U\,(b\,,\,\vartheta_2) + bU\,(b\,,\,\vartheta_1)\cos\vartheta_1 + bU\,(b,\,\vartheta_2)\cos\vartheta_2 + \right. \\ \left. + (\cos\vartheta_1 - \cos\vartheta_2)\frac{d\zeta\,(a)}{da} + b\frac{\partial}{\partial b}(U\,(b\,,\,\vartheta_1) + U\,(b,\,\vartheta_2))\right\}.\end{aligned}\right\} \quad (18)$$

It is to be remembered that ϑ_1 and ϑ_2 are the ϑ-values at two points on the two boundary curves, belonging to the same unvaried trajectory. Moreover, the variation δb of b is connected with the variation δp of the momentum through the relation $\delta b/b = \delta p/p$, and this is also approximately equal to $\delta E/E$ if the electrons have relativistic energies.

In the case of the completely symmetrical spectrograph (18) reduces to

$$\delta\vartheta_2 = -\frac{2\,\delta b}{b}\cdot\frac{a}{\sin\vartheta\cdot z_f}\left\{\cos\vartheta\cdot bU\,(b\,,\,\vartheta) + U\,(b\,,\,\vartheta) + b\frac{\partial}{\partial b}U\,(b\,,\,\vartheta)\right\}. \quad (19)$$

One can instead characterize the varied path by the shortest distance δx between the focus and the path. The quantity δx may be called the linear dispersion, and the ratio $\delta x/z_f$ divided by $\delta p/p$ the dispersion factor. The dispersion is easily calculated from (19) and in Table I is tabulated the dispersion factor as a function of ϑ_1 in the case of $b = 0.6$ and for $60° < \vartheta < 150$. This gives a direct illustration of the shift of the trajectory when the energy is changed. For comparison, the corresponding displacement in the semi-circular spectrograph is given by the dispersion factor $f = (\delta x/z_f):(\delta p/p)$ being equal to 2. It is therefore seen that in the present case the dispersion in a reasonably large angular interval is of the order of or larger than that in the semi-circular spectrograph.

So far, we have discussed only image formation and dispersion

Table 1.

The table gives the dispersion factor $f = (\delta x/z_f):(\Delta p/p)$ as a function of ϑ for $b = 0.6$ and $\zeta(a) = 0$. In the same units the dispersion factor of the semicircular spectrograph is $f = 2$.

ϑ	dispersion factor
60°	21
75°	9.1
90°	5,1
105°	3.3
120°	2.8
135°	1.8
150°	.3

in the idealized field. Now, the actual resolution will be determined essentially by two kinds of imperfections.

First, the device for collecting and recording of the β-rays at the focus has a finite extension and will on account of the dispersion registrate particles in a finite energy interval, ε. It is even desirable that particles in a not too small energy interval are counted because the intensity thereby becomes larger. If the dimensions of the collector are $\sim \lambda$ the resolving power resulting from this effect will be of the order

$$R_d = \frac{p}{\Delta p} \sim \bar{f}\frac{\lambda}{z_f} \tag{20}$$

where $\bar{f}$ is an averaged value of the dispersion factor f.

The second imperfection is due to deviations from axial symmetry of the actual field. This gives rise to a finite resolution R_r, and the total resolution will then be a function of R_d and R_r. It is desirable that the comparatively simpler of the two, R_d, gives the smaller contribution to the final resolution, so that

$$R_d \gtrsim R_r \quad \text{and} \quad R \approx R_r .$$

The effects of stray fields on the focusing may be estimated as follows. Suppose that the pole edges are nearly straight lines and that the pole faces are approximately parallel. The extension of the fringing field beyond the edges will then be of the order

of the width of the gap (compare e. g. COGGESHALL 1947) and therefore of the first order in Φ, the opening angle of the gap. The fringing field will have a component parallel to the gap and normal to the boundary curve, besides the component normal to the gap. It will then have mainly two effects on the motion of the β-particles.

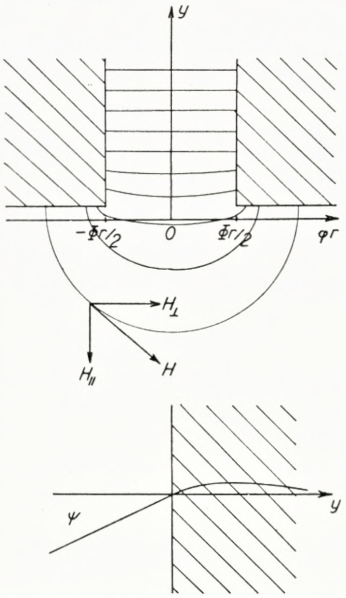

Fig. 7. The effect of the fringing field. The upper figure sketches a section perpendicular to the gap. The distance from the centre of the gap is measured in units φr, r being constant. As illustrated in the lower figure ψ is the angle between the trajectory and the normal of pole boundary.

First, there will be an extra deflection of the β-rays parallel to the plane of the gap. The angular deflection in this plane may be written as (see Fig. 7)

$$\Delta\vartheta = \frac{e}{pc}\int H_{\perp}\, dy \cdot \frac{1}{\cos\psi} = \frac{\alpha \cdot \Phi}{b\cos\psi} \sim \Phi. \qquad (21)$$

Here, ψ is the angle between the trajectory and the normal of the boundary; α is a constant, $\alpha \lesssim 1$, defined by $\int H_{\perp}\, dy = \alpha\, H_0\, r\, \Phi$ where $r\,\Phi$ is the width of the gap. It is noteworthy that

$\Delta\vartheta$ is independent of φ. The effective shift of the boundary curve as estimated in this way $\sim \alpha \cdot r \cdot \Phi$.

The second effect is the deflection normal to the gap, which is brought about by the component of the field parallel to the gap. This deflection is not the same all over the gap, and will be greatest close to the pole faces. We may approximately write $\int H_{||}\, dy = H_0\, r\, \varphi$ and find then for the angular deflection

$$\Delta w = \frac{e}{pc} \int H_{||}\, dy \operatorname{tg} \psi \gtrsim \frac{\varphi\psi}{b}. \tag{22}$$

Since in the gap $\varphi \leq \Phi/2$, the deflection is of the first order in Φ, and at the same time proportional to the angle ψ between the trajectory and the normal of the boundary.

Now, there will be two deflections of this kind, one at either boundary curve, and as a rule these two deflections will be to the same side. This holds for instance in the completely symmetrical spectrograph, if the first deflection is not so large as to bend the trajectory into the other side of the gap.

In order to find the total shift of the trajectory at the focus we may, as in equation (16), find the angular momentum about the axis given to the particle by the deflections. We then find from (22) that the trajectory passes the focus at a distance d from the axis, given by

$$d \sin \vartheta_2 \gtrsim \frac{r_1 \varphi_1 \psi_1 + r_2 \varphi_2 \psi_2}{b} < r\psi\Phi/b\,. \tag{23}$$

At the same time the requirement that a negligible number of the particles e. g. are deflected and hit the pole faces is approximately equivalent to saying that $\psi \ll 1$. From these results it therefore seems most important that ψ is much smaller than 1, i. e., the trajectory should be closely normal to the boundary curve. It is noteworthy that the first order defocusing effect is normal to the axis and not parallel to it. The formulas (22) (23) give a rough estimate of this effect.

In these considerations it was assumed that the fringing field is of small extension. However, it must be remembered that though the fringing field is weak at large distances from the edges

the summed-up effects on the trajectories of the field far from the edges is not completely negligible (COGGESHALL 1947). Moreover, other imperfections as the fringing fields at the outer pole boundaries will entail corrections to the inner boundary curve. We must accordingly expect that the above results as regards defocusing effects can only give an indication of the effect on the trajectories of the opening angle of the gaps being finite.

§ 5. Preliminary Experimental Investigation.

The above theoretical discussion served the following purposes. First, to find the freedom of choice of the variables pertaining to the spectrograph and to make possible approximate calculations of the shape of the pole pieces. Second, through qualitative considerations to obtain an insight in the questions of dispersion, resolving power, etc., in order to have some guidance as regards the choice of the shape of the boundary curve and similar factors.

With the results found in the theoretical treatment one should have a reasonable starting point for the experimental investigation. It was found most profitable to build first a single gap. In this way the theoretical results could be controlled and improved upon. As we shall see, even the one-gap spectrograph shows an appreciable solid angle, and it compares favourably with other spectrographs. Still, it must be remembered that in the case of a single gap the field need not be exactly the same as that in the final spectrograph with many gaps, and some differences may be found at the edges of the pole pieces. With such reservations we shall consider the single gap to give a fair account also of the properties of the spectrograph with many gaps. In particular, the one-gap spectrograph will indicate whether the large value of Ω promised by the theory may be realized.

It was decided to construct a completely symmetrical spectrograph. The form of the boundary curve describing the edges of the pole pieces is then determined by the choice of the value of b. The b-value used was $b = 0.6$. With this values of b and with focusing in the angular interval $75° \lesssim \vartheta \lesssim 135°$ the boundary curve was expected to become nearly perpendicular to the

electron trajectories. The distance between source and focus was chosen to be $2\,z_{f1} = 12$ cm. Two different gaps of the described kind were used; one with an opening angle between the pole pieces of 18°, and the other with opening angle 30°. The maximum solid angle one could hope to utilize in the one-gap models was then 3 % and 5 %, respectively.

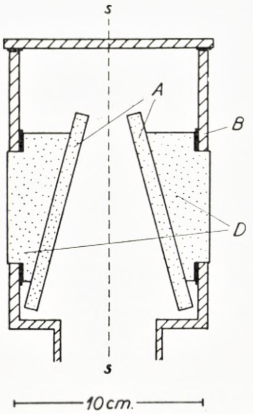

Fig. 8. A section through the 30° one-gap model, perpendicular to the axis.

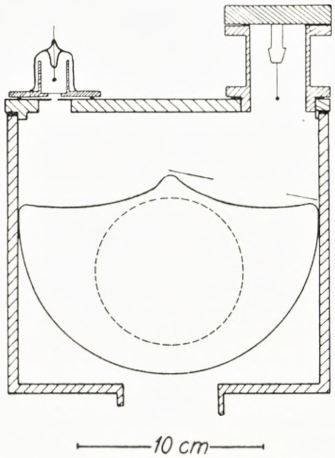

Fig. 9. A section parallel to the axis of the 30° model showing source, focus and one of the pole pieces.

The apparatus is illustrated in Fig.s 8 and 9. As shown in Fig. 8 the pole pieces are two plane parallel iron plates, *A*, of thickness 7 mm. The plates are mounted on two cylindrical iron blocks, *D*, the outer surfaces of which are joined to the pole pieces of an electromagnet. This set-up is placed in a brass vacuum chamber, *B*. In Fig. 8 the angular gap between the pole pieces is seen to be 30°. The model with opening angle 18° is quite similar to the 30°-model illustrated in Fig.s 8 and 9. Fig. 9 shows a cut through the central plane of the chamber, corresponding to the line *s-s* in Fig. 8. At the top of the chamber is an opening, where the source is placed, and at the other end a window corresponding to the focus.

At the bottom is a connection to an oil pump. The pressure is measured by means of a Pirani manometer; the pressures used were of the order of 10^{-2} mm Hg. In Fig. 9 are further

seen the edges of the pole pieces and at the source side a movable aluminium plate with a diaphragm. Since the diaphragm allowed only the passage of limited beams of electrons the focusing for the different trajectories could be measured separately.

The source consisted of a small sample of *Th B* placed on a copper sphere of diameter 1.5 mm. The *F* line of *Th B* of energy 146 keV was used in the measurements. It was possible to focus β-particles of energies up to about 5 MeV. The G.-M. counter was connected to an amplifier, a scale of 32, and a recording arrangement. The source could easily be placed at different points in the neighbourhood of the theoretical source point. The slit at the focus below the counter could also be moved and was in some of the measurements replaced by a small circular hole.

The edges of the pole pieces were formed in accordance with the theoretical boundary curve and without corrections for the effect of the fringing fields, even though such effects could be estimated in a qualitative way.

After the mounting of the apparatus the focusing properties were found by scanning the spectrograph with the *Th B* β-rays by means of the movable aluminum plate with a diaphragm. For each angle, ϑ, of emission of the β-rays was determined the current J', in the coils of the electromagnet giving focusing in the slit placed at the theoretical focus. In this way one found J', as a function of ϑ, as shown by the dotted curve in Fig. 10. Evidently there will be complete focusing only when J', is a constant. From these measurements it was possible to find the corrections to be made on the edges of the pole pieces. In Fig. 11 is seen the profile of a pole piece. The dotted curve is the uncorrected boundary curve, while the full-drawn line corresponds to corrected curve. One might perhaps at first sight expect that the correction should only correspond to a slight upward shift of the boundary curve as a whole, caused by the stray fields extending somewhat beyond the edges. The actual corrections are somewhat different. At the outer edges there is even an addition of iron. The reason for this is that the outermost orbits of the β-particles lie close to the upper edges of the pole pieces and the field is here slightly weaker than the ideal field because of the boundary effects. Further, the inward displacement of the

edges in the middle of the spectrograph is considerable. The main part of this displacement had a special origin, for the surface of the iron blocks holding the pole pieces lies quite close to the boundary curve, as seen from Fig. 9, and therefore the additional stray field between the blocks gave rise to a disturbance. In the model with a gap of 18°, this disturbance was reduced somewhat by removing a part of the blocks, but

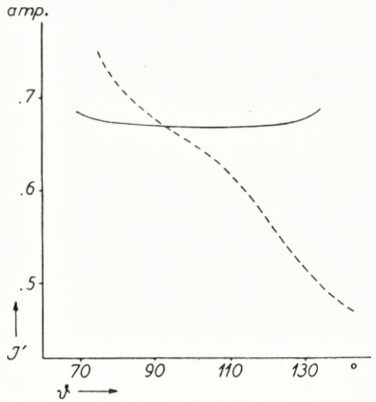

Fig. 10. The current, J', in the electromagnet corresponding to focusing of the *Th B F*-line, as a function of the direction of emission of the β-rays, ϑ. The dotted and the full-drawn lines, respectively, correspond to the uncorrected and the corrected pole pieces.

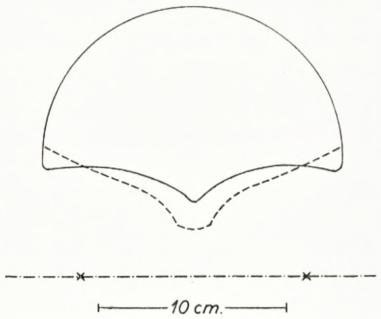

Fig. 11. The figure shows the uncorrected pole pieces (dotted line) and the corrected pole pieces (full-drawn line).

apart from this it was not found worth while to make further corrections of this kind in the preliminary investigation.

With the corrected pole pieces the current J' in the magnet was again found as a function of ϑ. This current is given by the full-drawn curve in Fig. 10 and is very nearly constant in the region $75° \lesssim \vartheta \lesssim 130°$. The corrected pole pieces were therefore considered satisfactory and a more thorough investigation of resolution and focusing was carried through.

In the measurement on resolution the abovementioned diaphragm was so placed as to give a beam of β-particles normal to the edges of the pole pieces. Below the counter at the focus was a slit of width 0.7 mm. The resolution was determined from the width at half peak height of the *F* line of *Th B*. Fig. 12 shows

the β-spectrum of *Th B* in the neighbourhood of this line, as measured with the gap of opening angle 18°. The diaphragm allowed a beam corresponding to 0.7 % of the total solid angle and as seen from Fig. 11 the resolving power was $1/R \sim 1.3$ %. The total gap was estimated to have $\Omega \sim 3$ % and $1/R \sim 4$ %. There seems to be a possibility of considerable improvement of these results, the more so because the pole pieces in the 18°-gap

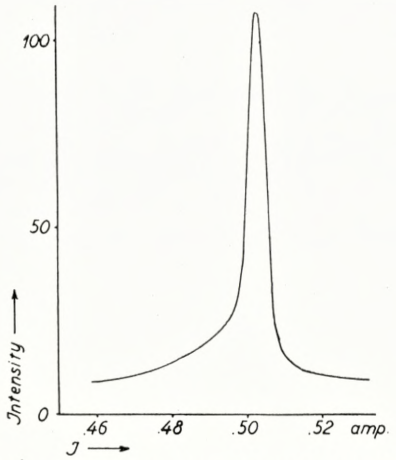

Fig. 12. The *F* line of *Th B* as measured with the 18° one-gap model.

were not corrected in this gap, but were formed as those corrected in the 30°-gap.

With the diaphragm at the source end in the same position the focusing in two directions was investigated. For this purpose the slit at the focus was replaced by a circular diaphragm of diameter 2.5 mm. The diaphragm could be moved perpendicular to the central plane of the gap. For each of a number of positions of the diaphragm was found a curve like that in Fig. 12, giving the intensity of β-particles passing through the diaphragm as a function of the current in the electromagnet. The maximum value of the intensity for each position was determined, and in Fig. 13 these maximum values are plotted as a function of the distance $\Delta_\perp$ between the centre of the diaphragm and the axis of the spectrograph. The different maximum values of intensity were all found to correspond to the same current J' in the elec-

tromagnet. Considering that the diameters of the diaphragm and of the source are 2.5 and 1.5 mm. the curve in Fig. 13 shows that the focusing is good in the direction perpendicular to the central plane of the gap. As expected the spectrograph therefore shows two-directional focusing.

Similar measurements were performed for other sections of the solid angle subtended at the source, and it was found that

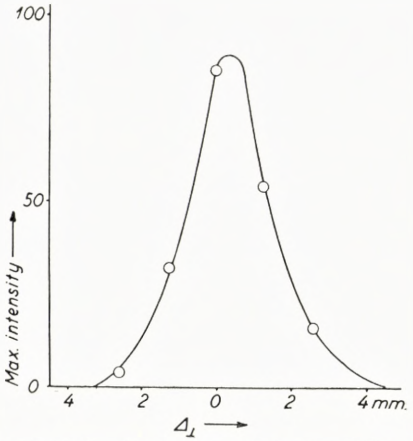

Fig. 13. The focusing perpendicular to the axis in the 18° one-gap model. As abscissa is used Δ_1, the distance from the axis. The ordinate is the maximum intensity through the diaphragm at the distance in question.

in those parts where the trajectories of the β-particles are not perpendicular to the edges of the pole pieces the focusing in the direction normal to the central plane of the gap was markedly inferior. The total width of the curve corresponding to the one in Fig. 13 was in the most unfavourable case as large as ~ 10 mm. According to the considerations in § 4 a pronounced defocusing effect should come in when the trajectories meet the edges of the pole pieces at oblique incidence. Even more quantitatively formula (23) seems in agreement with the defocusing effect measured.

These preliminary measurements indicate that even the very simple one-gap spectrograph can be used to advantage in β-spectroscopy. They also seem promising with respect to the final spectrograph with many gaps. It is planned to build a minor spectrograph of this kind. For instance, it may consist of 6 gaps

of opening angle 18°, which would lead to a maximum solid angle of about 20 %.

Summary.

An axially symmetric β-spectrometer with source and focus outside the magnetic field is discussed, the advantages of the type chosen being large solid angle and a considerable number of different solutions with focusing. The actual spectrograph will contain many gaps between pole pieces with plane faces. With a suitable choice of the boundaries of the pole pieces the effects of fringing fields can be reduced.

The properties of a very crude model with one gap was investigated and it showed agreement with the theory. The final spectrograph with 6 gaps is expected to have a solid angle of about 20 %.

Institute for Theoretical Physics,
University of Copenhagen,
Denmark.

References.

COGGESHALL, N. D., 1947, Journ. Appl. Phys. **18**, 855.

DEUTSCH, M., ELLIOTT, L. G., and EVANS, R. D., 1944, Rev. Sc. Inst. **15**, 178.

DUMOND, J. W. M., 1949, Rev. Sci. Inst. **20**, 160, 616.

KLEMPERER, O., 1935, Phil. Mag. **20**, 545.

RICHARDSON, H. O. W., 1947, Proc. Phys. Soc. London **59**, 791.

RICHARDSON, H. O. W., 1949, Phil. Mag. **40**, 233.

SIEGBAHN, K., 1942, Arkiv f. mat., astr. o. fys. Bd. **28** A, No. 17.

SLÄTIS, H. and SIEGBAHN, K., 1949, Phys. Rev. **75**, 1955.

SNYDER, C. W., 1948, Thesis, California Institute of Technology.

SVARTHOLM, N. and SIEGBAHN, K., 1946, Arkiv f. mat., astr. o. fys. Bd. **33** A, No. 27.

ZÜNTI, W., 1948, Helv. Phys. Acta. **21**, 179.

Indleveret til selskabet den 9. december 1949.
Færdig fra trykkeriet den 21. april 1950.

DET KGL. DANSKE VIDENSKABERNES SELSKAB
MATEMATISK-FYSISKE MEDDELELSER, BIND XXV, NR. 17

ÜBER PROJEKTIVE BÖSCHUNGSLINIEN AUF FLÄCHEN 2. ORDNUNG

VON

FR. FABRICIUS-BJERRE

KØBENHAVN
I KOMMISSION HOS EJNAR MUNKSGAARD
1950

Printed in Denmark.
Bianco Lunos Bogtrykkeri.

EINLEITUNG

In der vorliegenden Arbeit werden wir die sogenannten projektiven Böschungslinien, d. h. diejenigen Raumkurven, deren Tangenten einen gegebenen Kegelschnitt schneiden, untersuchen. Wir beschränken uns jedoch auf die Betrachtung derjenigen projektiven Böschungslinien, die auf einer eigentlichen Fläche 2. Ordnung liegen.

In § 1 behandeln wir einige allgemeine Sätze über die Lage der projektiven Böschungslinien auf der gegebenen Fläche 2. Ordnung. In § 2 untersuchen wir die Zentralprojektionen der Kurven von beliebigen Punkten des Raumes aus. In einer passend gewählten nichteuklidischen Metrik ist die Projektion einer projektiven Böschungslinie eine orthogonale Trajektorie eines Systems von Kreisen, die mit einer zirkularen Kurve 4. Ordnung doppelte Berührung haben. Es ist der Zweck dieses Paragraphen, von projektiven Standpunkt aus einen Überblick über eine Reihe von Sätzen bezüglich der Projektionen von gewöhnlichen Böschungslinien auf Flächen 2. Ordnung, speziell auf Rotationsflächen, zu geben und die Sätze, die W. WUNDERLICH[1] vor kurzem publiziert hat, zu verallgemeinern.

§ 3 enthält eine Untersuchung der geometrischen Örter der Berührungspunkte der Tangenten, die man durch einen gegebenen Punkt an die Zentralprojektionen der Böschungslinien legen kann. In § 4 betrachten wir ausschliesslich projektive Böschungslinien auf konvexen Flächen 2. Ordnung; da sich eine solche Fläche durch eine Kollineation in eine Kugel überführen lässt, kann man sich auf sphärische projektive Böschungslinien be-

[1] »Über die Böschungslinien auf Flächen 2. Ordnung«, Sitz. ber. d. Akad. in Wien, Bd. 155 (1947), p. 309—331, und »Über die Schleppkurven des Kreises«, dieselben Sitz. ber. Bd. 156 (1948), p. 155—173. Diese Arbeiten werden im folgenden mit W I und W II zitiert.

schränken. Diese erweisen sich als orthogonale Trajektorien von gewissen Kreissystemen auf der Kugel. Mit Hilfe dieser Kreissysteme ist es möglich, die Form der sphärischen projektiven Böschungslinien in grossen Zügen zu beschreiben; dadurch erhält man gleichzeitig einen Überblick über den Verlauf der gewöhnlichen Böschungslinien auf einem Ellipsoid, einem zweischaligen Hyperboloid und einem elliptischen Paraboloid.

§ 1. Allgemeine Sätze.

1. Unter einer gewöhnlichen Böschungslinie versteht man bekanntlich eine Raumkurve, deren Tangenten mit einer gegebenen Richtung einen festen Winkel bilden. Der Richtungskegel der Kurve ist ein Rotationskegel, und dieser Kegel und somit auch die Tangentenfläche der Kurve schneidet die unendlich ferne Ebene in einem »Kreis« oder in einem Teil eines Kreises. Durch eine affine oder projektive Abbildung einer solchen Kurve erhält man eine Raumkurve, deren Tangenten einen Kegelschnitt schneiden. Eine solche Raumkurve heisst eine projektive Böschungslinie. Sie heisst speziell affin, wenn der Kegelschnitt in der unendlich fernen Ebene liegt[1].

Im folgenden betrachten wir ausschliesslich projektive Böschungslinien, die auf einer nicht ausgearteten Fläche 2. Ordnung liegen, also Kurven, die durch eine Kollineation in gewöhnliche Böschungslinien auf einer Fläche 2. Ordnung übergeführt werden können.

2. Die gegebene Fläche 2. Ordnung werde mit Φ und der gegebene Kegelschnitt mit a bezeichnet. Die Ebene des Kegelschnittes heisse α und ihr Pol in bezug auf Φ sei A. Wir wollen untersuchen, ob durch einen vorgelegten Punkt P von Φ projektive Böschungslinien gehen. Die Tangentialebene π an Φ im Punkte P hat im allgemeinen 0 oder 2 Punkte mit a gemeinsam. Im ersten Fall geht keine Böschungslinie durch P, im zweiten Fall zwei. Die Tangenten an diese Kurven in P sind die Geraden, die P mit den Schnittpunkten Q_1 und Q_2 von π mit a verbinden. Die Böschungslinie mit der Tangente PQ hat in P eine Schmieg-

[1] Vgl. W. Blaschke, Differentialgeometrie II, Berlin 1923, p. 87.

ebene, die durch PQ und die Tangente in Q an a bestimmt ist, falls diese Geraden verschieden sind.

Wenn π genau einen Punkt mit a gemeinsam hat, d. h. a berührt, muss P auf der Schnittkurve von Φ mit dem Polarkegel Γ von a in bezug auf Φ liegen. Die Kegelfläche hat ihren Scheitel in A, und ihre Schnittkurve mit Φ ist eine Kurve 4. Ordnung und 1. Art, die wir mit C^4 bezeichnen wollen. Falls sie nicht nullteilig ist, trennt sie auf Φ die Gebiete, in denen es projektive Böschungslinien gibt, von den Gebieten, in denen dies nicht der Fall ist. C^4 wird als die zum System der Böschungslinien gehörige Grenzkurve bezeichnet. Liegt P auf der Grenzkurve, so gehen von P zwei Zweige einer Böschungslinie mit gemeinsamer Tangente aus, die P mit dem zugehörigen Punkt Q auf a verbindet. Die Böschungslinie hat daher eine Spitze in P mit PQ als Spitzentangente und der Tangentialebene π als Schmiegebene.

Falls P ein gemeinsamer Punkt von Φ und a ist, können durch P unendlich viele Böschungslinien gehen; dies kann auch eintreffen, wenn die Ebene α die Fläche Φ berührt und P der Berührungspunkt ist.

Wir betrachten nun einen beliebigen Punkt Q auf a und wollen untersuchen, ob es auf Φ Böschungslinien gibt, die Tangenten durch Q schicken. Die Polarebene von Q in bezug auf Φ ist Tangentialebene von Γ und schneidet Φ in einem Kegelschnitt q. Falls q reel ist, geht durch jeden Punkt von q eine Böschungslinie der gewünschten Art. Der Kegelschnitt q hat doppelte Berührung mit C^4, und die Berührungspunkte liegen auf der Erzeugenden, in der die Ebene von q den Kegel Γ berührt. Die Tangente an q in einem beliebigen Punkt P dieses Kegelschnittes und die Gerade QP sind konjugierte Geraden in bezug auf Φ. Daher gilt[1]

Satz 1,1. *Die projektiven Böschungslinien auf Φ, die zu dem Kegelschnitt a gehören, und die Kegelschnitte, die von den Polarebenen der Punkte von a ausgeschnitten werden, bilden konjugierte Kurvensysteme auf der Fläche.*

Mit Hilfe dieses Satzes werden wir im nächsten Paragraphen die Zentralprojektion der projektiven Böschungslinien auf Φ untersuchen und im letzten Paragraphen die projektiven Böschungslinien auf einer konvexen Fläche 2. Ordnung bestimmen.

[1] Vgl. zu diesem Paragraphen W I, p. 310.

§ 2. Die Zentralprojektionen von projektiven Böschungslinien.

3. Wir betrachten nun die Zentralprojektion der in § 1 beschriebenen Figur, die aus der Fläche Φ, dem Kegelschnitte a, der Grenzkurve C^4, dem Kegelschnitt q auf Φ sowie aus der projektiven Böschungslinie σ durch einen Punkt P auf q besteht. Als Projektionszentrum wählen wir einen beliebigen, zunächst nicht auf Φ liegenden Punkt O im Raum und als Projektionsebene eine willkürliche Ebene, die nicht durch O geht.

Die Projektion der Fläche Φ ist ein Gebiet in ω, das von der Kontur φ der Fläche begrenzt wird. Ist ω speziell die Polarebene von O, so ist φ zugleich die Schnittkurve von Φ und ω. Diesen Kegelschnitt wählen wir als absoluten Kegelschnitt einer nichteuklidischen Metrik in der Ebene ω. Ist Φ konvex, so ist die Metrik elliptisch oder hyperbolisch, je nachdem O innerhalb oder ausserhalb Φ liegt; ist dagegen Φ nicht konvex, so ist φ stets ein reeller Kegelschnitt, aber die Projektion der Fläche liegt dann ausserhalb der von φ begrenzten nichteuklidischen Ebene.

Die Projektion $C^{4\prime}$ der Grenzkurve C^4 ist im allgemeinen eine ebene Kurve 4. Ordnung, die φ in vier Punkten berührt und zwei reelle oder imaginäre Doppelpunkte besitzt. Sie wird als nichteuklidische zirkulare Kurve bezeichnet[1].

Die Projektion q' des Kegelschnittes q ist im allgemeinen ein nichteuklidischer Kreis, dessen Mittelpunkt Q' die Projektion von Q ist. Der Kreis q' hat mit $C^{4\prime}$ doppelte Berührung. Der zu dem System der Kreise q' gehörende Deferent, d. h. der geometrische Ort ihrer Mittelpunkte Q', ist die Projektion a' des Kegelschnittes a; und der zugehörige Leitkreis, der sämtliche Kreise q' orthogonal schneidet, ist die Projektion desjenigen Kegelschnittes, in dem die Ebene α die Fläche Φ schneidet[2].

Konjugierte Richtungen durch einen Punkt P auf Φ sind mit den Erzeugenden durch P harmonisch verbunden. Die Erzeugenden gehen bei der Zentralprojektion in Tangenten durch P' an φ über, mithin die konjugierten Richtungen durch P in

[1] Siehe F. Hohenberg, Über zirkulare Kurven in der nichteuklidischen Geometrie. Monatshefte f. Math. u. Phys. Bd. 45 (1937), p. 134.

[2] Hohenberg, l. c. p. 146.

konjugierte Geraden in bezug auf φ d. h. in orthogonale Richtungen in bezug auf die nichteuklidische Metrik. Hieraus folgt, dass die Projektion σ' der Böschungslinie σ den Kreis q' im Punkte P' orthogonal schneidet, also gilt

Satz 2,1. *Die Zentralprojektion einer projektiven Böschungslinie auf einer Fläche 2. Ordnung ist in einer passende nichteuklidischen Metrik im allgemeinen orthogonale Trajektorie eines Systems von Kreisen, die eine zirkulare Kurve 4. Ordnung mit zwei Doppelpunkten doppelt berühren.*

Zu dem durch die Flächen Φ und Γ bestimmten Flächenbüschel mit der Grundkurve C^4 gehören ausser Γ im allgemeinen noch drei Kegel, von denen mindestens einer reell ist. Wählt man das Projektionszentrum O in einem der Scheitelpunkte dieser Kegel, so erhält man als Projektion von C^4 einen Kegelschnitt C^2 statt einer zirkularen Kurve 4. Ordnung; ferner ist in diesem Fall die Projektion σ' von σ orthogonale Trajektorie eines Systems von Kreisen, die den genannten Kegelschnitt doppelt berühren. Die Mittelpunkte dieser Kreise liegen auf der Spur der Ebene α in ω, da die erwähnten Scheitel in der Ebene α liegen. Es gilt also

Satz 2,2. *Die Zentralprojektion einer projektiven Böschungslinie auf einer Fläche 2. Ordnung ist bei passende Wahl des Projektionszentrums orthogonale Trajektorie eines Systems von Kreisen, die einen Kegelschnitt doppelt berühren.*

Wählt man insbesondere O im Scheitel A des Kegels Γ, so bleibt die Projektion von C^4 ein Kegelschnitt, aber die Projektionen der Kegelschnitte q werden nun Tangenten an diesen Kegelschnitt. Da eine orthogonale Trajektorie dieser Tangenten Evolvente des Kegelschnittes ist, gilt

Satz 2,3. *Wird eine, auf einer Fläche 2. Ordnung gelegene projektive Böschungslinie, die zu dem Kegelschnitt a gehört, von dem Pol der Ebene dieses Kegelschnittes aus projiziert, so erhält man eine nichteuklidische Kegelschnittevolvente*[1].

[1] Für gewöhnliche Böschungslinien ist dieser Satz in W I, p. 310 bewiesen worden.

4. Wir gehen nunmehr zur Untersuchung des Falles über, wo das Projektionszentrum O auf der Fläche Φ liegt. Als Projektionsebene ω wählen wir hier eine beliebige Ebene, die O nicht enthält. Der Kegelschnitt φ artet in zwei Punkte aus, und die Metrik in ω wird parabolisch. Insbesondere kann die Metrik euklidisch werden, nämlich wenn Φ eine konvexe Fläche ist und wir stereographisch von einem der Nabelpunkte der Fläche aus projizieren. In diesem Fall wird $C^{4\prime}$ eine bizirkulare Kurve, q' ein gewöhnlicher Kreis, der mit $C^{4\prime}$ doppelte Berührung hat, und σ' wird eine (im gewöhnlichen Sinne) orthogonale Trajektorie des Systems von Kreisen q'. Wir haben also

Satz 2,4. *Die stereographische Projektion einer projektiven Böschungslinie auf einer konvexen Fläche 2. Ordnung von einem der Nabelpunkte der Fläche aus ist eine gewöhnliche orthogonale Trajektorie eines Systems von Kreisen, die eine bizirkulare Kurve 4. Ordnung doppelt berühren.*

Wir wollen nun die Sätze 2,3 und 2,4 kombinieren; zu diesem Zwecke nehmen wir an, dass A auf Φ liegt, d. h. dass die Ebene α Tangentialebene von Φ in A ist, und zugleich, dass A in einen Nabelpunkt fällt. Projiziert man eine zum Kegelschnitt a gehörige, auf Φ gelegene Böschungslinie von A aus, so erhält man in diesem Fall eine gewöhnliche Evolvente eines Kegelschnittes. Es gilt also

Satz 2,5 a. *Falls die Ebene des Kegelschnittes a die Fläche Φ in einem Nabelpunkt A berührt, so wird eine projektive Böschungslinie bezüglich a von A aus stereographisch in eine gewöhnliche Kegelschnittevolvente projiziert.*

Es seien speziell Φ ein elliptisches Paraboloid, die Ebene von a die unendlich ferne Ebene, also A der unendlich ferne Punkt von Φ. Die zu a gehörenden Böschungslinien werden affine Böschungslinien, und die stereographische Projektion wird zu einer Parallelprojektion in der Richtung der Achse auf eine der Kreisschnittebenen der Fläche. Dann erhält man

Satz 2,5 b. *Projiziert man eine auf einem elliptischen Paraboloid liegende affine Böschungslinie parallel in der Richtung der Achse*

auf eine der Kreisschnittebenen, so erhält man eine Kegelschnittevolvente[1].

5. Schliesslich betrachten wir den Fall, dass der Kegelschnitt a die Fläche Φ doppelt berührt. Wir bezeichnen die (reellen oder imaginären) Berührungspunkte mit R_1 und R_2, ihre Verbindungslinie mit r. Der zu a polare Kegel Γ schneidet Φ in zwei Kegelschnitten durch R_1 und R_2; die Kurve C^4 zerfällt somit in diese beiden Kegelschnitte.

Projizieren wir von einem beliebigen Punkt O im Raum auf die Ebene ω, so besteht die Kurve $C^{4\prime}$ aus zwei nichteuklidischen Kreisen C^2 und D^2, und q' ist ein nichteuklidischer Kreis, der die Kreise C^2 und D^2 berührt. Wir sehen, dass in diesem Fall die Brennpunkte des zum Kreissystem q' gehörenden Deferenten die Mittelpunkte von C^2 und D^2 sind.

Projizieren wir speziell von einem Punkt O der Polaren s der Geraden r in bezug auf Φ, so ist die Situation besonders einfach, da die Kreise C^2 und D^2 konzentrisch werden. Der Kegelschnitt a' wird gleichfalls ein nichteuklidischer Kreis und konzentrisch mit C^2 und D^2, da alle drei Kurven den absoluten Kegelschnitt φ in den Projektionen der Punkte R_1 und R_2 berühren. Das Kreissystem q' wird daher im nichteuklidischen Sinne rotationssymmetrisch, d. h. alle Kreise q' werden einander kongruent. Eine orthogonale Trajektorie eines Systems von kongruenten Kreisen ist aber eine Traktrix, die zu der von den Mittelpunkten der Kreise durchlaufenen Kurve gehört. Es ergibt sich also

Satz 2,6. *Hat der Kegelschnitt a doppelt Berührung mit Φ, so ist die Projektion einer zu a gehörigen projektiven Böschungslinie auf Φ von einem Punkt der Polaren der Geraden durch die Berührungspunkte aus eine nichteuklidische Kreistraktrix.*

Bei besonderer Wahl von O auf der Polaren s ergeben sich verschiedene Spezialfälle dieses Satzes. Wählt man etwa O im Schnittpunkt mit der Ebene α, so wird a' eine Gerade, und die Projektion σ' einer projektiven Böschungslinie σ wird eine nichteuklidische Traktrix in bezug auf eine Gerade (Spezialfall von Satz 2,2). Wählt man O im Punkte A, so wird σ' eine nichteuklidische Kreisevolvente (Spezialfall von Satz 2,3).

[1] Für gewöhnliche, nicht affine Böschungslinien auf einem elliptischen Paraboloid ist dieser Satz in W I, p. 312 bewiesen.

In dem Fall, wo R_1 und R_2 (konjugiert) imaginäre Punkte sind, werden die Verhältnisse besonders übersichtlich, wenn man die Fläche durch eine Kollineation derart in eine Rotationsfläche überführt, dass der Kegelschnitt a ein unendlich ferner Kreis wird. Die Gerade r ist dann unendlich fern und die Polare s die Achse der Fläche. Die projektiven Böschungslinien werden gewöhnliche Böschungslinien, deren Tangenten mit der Achse s einen konstanten Winkel bilden. Wählt man zu einem auf s gelegenen Projektionszentrum O eine Projektionsebene ω durch r, d. h. senkrecht auf s, so wird der absolute Kegelschnitt φ ein euklidischer Kreis mit dem Mittelpunkt im Schnittpunkt S von s und ω. Die Kurven C^2, D^2 und a' werden konzentrische euklidische Kreise mit dem Mittelpunkt S, und die oben erwähnte Rotationssymmetrie wird zugleich eine Rotationssymmetrie um S im euklidischen Sinn.

Aus Satz 2,6 und den daraus folgenden speziellen Sätzen erhält man für gewöhnliche Böschungslinien auf Rotationsflächen 2. Ordnung eine Reihe von Sätzen, die sich bei W. Wunderlich[1] finden.

Wir heben besonders hervor, dass die Projektion einer Böschungslinie in bezug auf die unendlich ferne Gerade a' eine nichteuklidische Traktrix wird, wenn es sich um rechtwinklige Projektion in der Richtung der Achse handelt (O ist der unendlich ferne Punkt). Nun ergibt bekanntlich die rechtwinklige Projektion von Böschungslinien einer Rotationsfläche 2. Ordnung auf eine auf der Achse senkrechte Ebene zykloidale Kurven; diese Kurven müssen daher mit nichteuklidischen Traktrizen identisch sein, wenn der absolute Kegelschnitt φ ein Kreis und die entsprechende Linie a' die unendlich ferne Gerade ist.

§ 3. Verallgemeinerungen eines Satzes von C. Juel.

6. In einer Aufgabe im Interméd. math.[2] hat C. Juel auf folgenden Satz aufmerksam gemacht:

Die Berührungspunkte der Tangenten, die von einem Punkt M an eine Epi- oder Hypozykloide gehen, liegen auf der Fusspunkt-

[1] Siehe W II, Satz 3—6.
[2] Interméd. math. I (1894), p. 243.

kurve von M in bezug auf einen Kegelschnitt, also auf einer bizirkularen Kurve 4. Ordnung mit M als Doppelpunkt.

Dreht man die betreffende Zykloide um das zugehörige Zentrum, so zeigt sich, dass die Berührungspunkte der Tangenten von M an die so entstandene Rotationsschar von Zykloiden sämtlich auf derselben bizirkularen Kurve J liegen. Ferner kann die Gültigkeit des Satzes auch für Pseudozykloiden nachgewiesen werden[1].

Auf S. 10 erwähnten wir, dass man durch passende Orthogonalprojektion der Böschungslinien auf einer Rotationsfläche 2. Ordnung zykloidale Kurven erhält. Es liegt daher nahe zu untersuchen, ob der Juelsche Satz auch auf andere Projektionen von Böschungslinien einer Fläche 2. Ordnung übertragen werden kann. Wir wollen damit beginnen, im allgemeinen, dem Satz 2,1 entsprechenden Fall die Kurven zu untersuchen, die aus den Berührungspunkten der Tangenten von einem Punkt M der Ebene an die orthogonalen Trajektorien des in Satz 2,1 genannten Systems von nichteuklidischen Kreisen besteht.

Wir lösen die Aufgabe zunächst durch eine räumliche Betrachtung. Die Tangenten an sämtliche durch den Kegelschnitt a bestimmten projektiven Böschungslinien auf der Fläche Φ, d. h. sämtliche Tangenten von Φ, die a schneiden, bilden eine Geradenkongruenz 4. Ordnung, und die Geraden dieser Kongruenz, die eine beliebig gegebene Gerade m im Raume schneiden, bilden eine geradlinige algebraische Fläche 8. Grades. Diese Fläche berührt Φ längs einer Raumkurve 8. Grades, die wir mit J_1 bezeichnen wollen. Diese Kurve ist offenbar der geometrische Ort derjenigen Punkte auf Φ, für die eine Tangente an Φ sowohl a als auch m schneidet. Die Kurve J_1 muss durch die Schnittpunkte von a und Φ gehen und Doppelpunkte in den Schnittpunkten von m und Φ haben. In einer beliebigen Ebene μ durch m liegen vier Punkt von J_1, nämlich die Berührungspunkt der vier Tangenten, die man von den beiden Schnittpunkten von μ und a an den Kegelschnitt legen kann, in dem μ die Fläche Φ schneidet. Wenn Φ speziell von μ berührt wird, so fallen die vier genannten Punkte alle in den Berührungspunkt, der also

[1] Siehe Wieleitner, Spezielle ebene Kurven, Leipzig 1908, p. 210 und 218.

ein weiterer Doppelpunkt von J_1 ist. Diese Kurve hat daher nicht nur Doppelpunkt in den Schnittpunkten von Φ und m, sondern zugleich in den Schnittpunkten von Φ und der Polaren m_1 von m in bezug auf Φ.

Ist nun m speziell die Gerade, die das Projektionszentrum O mit dem Punkt M der Ebene ω verbindet, so ist die Projektion von J_1 auf ω von O aus gerade die gesuchte Kurve J. Es gilt also folgender

Satz 3,1. *Der geometrische Ort der Berührungspunkte der Tangenten, die man von dem Punkt M an das System von Kurven legen kann, die durch Zentralprojektion aus den zu einem Kegelschnitt gehörigen projektiven Böschungslinien einer Fläche 2. Ordnung entstehen, ist eine algebraische Kurve 8. Ordnung mit vierfachem Punkt in M. Diese Kurve kann als eine nichteuklidische zirkulare Kurve aufgefasst werden; sie berührt sich selbst (und den absoluten Kegelschnitt φ) in den Berührungspunkten der Tangenten von M an φ (der absoluten Tangenten).*

Ohne Übergang zum Raum kann die Kurve J in der folgenden Weise bestimmt werden. Es sei P der Berührungspunkt einer Tangente vom Punkt M an die Projektion σ' einer projektiven Böschungslinie σ. Da σ' nach Satz 2,1 orthogonale Trajektorie eines Systems von Kreisen ist, muss MP Normale des durch P gehenden nichteuklidischen Kreises sein und daher seinen Mittelpunkt enthalten. Man kann also die vier Punkte der Kurve J konstruieren, die auf einer beliebigen Geraden l durch M liegen, indem man l mit der zum Kreissystem gehörigen Deferente a' schneidet. Diese beiden Schnittpunkte sind die Mittelpunkt zweier zum Kreissysteme gehörenden nichteuklidischen Kreise, deren Schnittpunkte mit l die vier gesuchten Punkte ergeben.

Dass M vierfacher Punkt von J ist, kann man folgendermassen einsehen. Sämtliche Kreise durch M, die zu dem zum Kreissystem gehörigen Leitkreis (siehe S. 6) orthogonal sind, bilden zwei Kreisbüschel[1]. Die vier Schnittpunkte der Zentralen dieser beiden Büschel mit dem Deferent sind die Mittelpunkte von vier nichteuklidischen Kreisen, die zu dem betrachteten System gehören und durch M gehen. M ist also vierfacher Punkt von J.

[1] Siehe z. B. Hohenberg, l. c. p. 137.

Wir betrachten nun die Satz 2,2 entsprechenden Zentralprojektion der projektiven Böschungslinien von Φ. Das Projektionszentrum O ist hier ein von dem Scheitel A von Γ verschiedener Scheitel eines der Kegel, die zu dem durch Φ und Γ bestimmten Flächenbüschel gehören. Durch eine harmonische Homologie mit dem Zentrum O und der Homologieebene ω werden die Fläche Φ, der Kegelschnitt a und die Gerade OM in sich übergeführt, was daher auch für die zugehörige Raumkurve J_1 gilt. Die Projektion J von J_1 von O aus ist also in diesem Fall eine Kurve 4. Ordnung mit einem Doppelpunkt in M, die φ in den Berührungspunkten der durch M gehenden absoluten Tangenten berührt. Auch dieses Ergebnis kann man ohne Übergang zum Raum erhalten, da hier von Tangenten an die in Satz 2,2 genannten speziellen orthogonalen Trajektorien die Rede ist. Man verfährt genau wie oben. Wir haben also

Satz 3,2. *Der geometrische Ort der Berührungspunkte der Tangenten, die von einem Punkt M an ein System von projizierten Böschungslinien gehen, ist eine algebraische Kurve 4. Ordnung mit einem Doppelpunkt in M, wenn das Projektionszentrum ein von A verschiedener Hauptpunkt ist. Diese Kurve berührt den absoluten Kegelschnitt in den Berührungspunkten der durch M gehenden absoluten Tangenten.*

In dem Satz 2,3 entsprechenden Fall, wo das Projektionszentrum der Punkt A selbst ist, sind die Projektionen der projektiven Böschungslinien, wie aus dem Satz hervorgeht, nichteuklidische Kegelschnittevolventen. Die Kurve J muss also in diesem Fall die nichteuklidische Fusspunktkurve von M in bezug auf den abgewickelten Kegelschnitt sein. Solche nichteuklidischen Fusspunktkurven für Kegelschnitte sind rationale Kurven 4. Ordnung mit einem Doppelpunkt in M[1]. Wir formulieren dieses Resultat in

Satz 3,3. *Falls die projizierten Böschungslinien nichteuklidische Kegelschnittevolventen sind, liegen die Berührungspunkte der Tangenten von einem Punkt M an diese Kurven auf einer rationalen Kurve 4. Ordnung J mit einem Doppelpunkt in M. Die Kurve J*

[1] Siehe meine Note, Nichteuklidische Fusspunktkurven, Monatshefte f. Math. Bd. 53 (1949), p. 298.

hat ausserdem Doppelpunkte in den Berührungspunkten der absoluten Tangenten durch M.

Wie man sieht, geben die Sätze 3,3, 3,2 und 3,1 schrittweise Verallgemeinerungen des angeführten Juelschen Satzes.

7. Schliesslich betrachten wir den dem Satz 2,4 entsprechenden Fall, wo es sich um die stereographische Projektion der projektiven Böschungslinien auf einer konvexen Fläche 2. Ordnung von einem ihrer Nabelpunkte aus handelt, und wo die projektiven Böschungslinien orthogonale Trajektorien eines Systems von euklidischen Kreisen sind, die eine bizirkulare Kurve 4. Ordnung doppelt berühren.

Es handelt sich hier darum die Raumkurve J_1 von einem ihrer Doppelpunkt aus, nämlich einem der Schnittpunkte der Geraden m mit der Fläche Φ, zu projizieren. Die Projektion J wird daher eine Kurve 6. Ordnung. Die Kurve erhält offenbar Doppelpunkte in M und in den Kreispunkten der Projektionsebene. Wir formulieren das Resultat als einen Satz über ebene Kurven:

Satz 3,4. *Die Berührungspunkte der Tangenten, die man von einem Punkt M an die orthogonalen Trajektorien eines Systems von Kreisen legen kann, die eine bizirkulare Kurve 4. Ordnung doppelt berühren, liegen auf einer bizirkularen Kurve 6. Ordnung mit einem Doppelpunkt in M.*

Wie oben findet man auch dieses Resultat leicht ohne Übergang zum Raume, indem man die im Anschluss an Satz 3,1 besprochene Konstruktion überträgt. Dass der Punkt M hier Doppelpunkt wird, während er oben vierfacher Punkt war, beruht darauf, dass die Kreise eine euklidischen Kreisnetzes, die durch einen gegebenen Punkt gehen, nur ein Kreisbüschel bilden.

Aus Satz 3,4 erhält man spezielle Sätze, wenn die bizirkulare Kurve 4. Ordnung degeneriert. Beispielsweise soll erwähnt werden, dass die Kurve J eine Konkoide ist, wenn das Kreissystem aus kongruenten Kreisen besteht, deren Mittelpunkt eine Gerade durchlaufen, so dass die orthogonalen Trajektorien gewöhnliche Traktrizen sind.

§ 4. Böschungslinien auf konvexen Flächen 2. Ordnung.

8. Bei einer näheren Untersuchung der projektiven Böschungslinien auf einer konvexen Fläche 2. Ordnung ist es bequem, sich diese als Kugelfläche zu denken. Durch eine Homologie kann eine beliebige konvexe Fläche 2. Ordnung in eine Kugelfläche übergeführt werden, wenn man als Homologiezentrum einen der Nabelpunkte der Fläche und als Homologieebene eine Ebene wählt, die die Fläche in einem Kreis schneidet, und, vom Fall einer Rotationsfläche abgesehen, der Tangentialebene im Nabelpunkt nicht parallel ist. Die konvexe Fläche kann dann in die Kugel übergeführt werden, die die gegebene Fläche in dem Nabelpunkt berührt und durch den oben genannten Kreis geht. Durch Zentralprojektion gehen die Böschungslinien der einen Fläche in die der anderen über.

Da konjugierte Kurven auf einer Kugelfläche orthogonal sind, erhält man aus Satz 1,1 unmittelbar

Satz 4,1. *Das System der projektiven Böschungslinien auf einer Kugel Φ, die zu einem gegebenen Kegelschnitt a gehören, besteht aus den orthogonalen Trajektorien des Systems derjenigen Kreise auf Φ, die von den Polarebenen der Punkte von a ausgeschnitten werden*[1].

Die Polarebenen berühren den polaren Kegel Γ von a, der Φ in der von den Kreisen q doppelberührten Grenzkurve C^4 schneidet.

Durch stereographische Projektion von einem Nabelpunkt aus erhält man wieder Satz 2,4. Man sieht somit, dass die Bestimmung der projektiven Böschungslinien auf einer Kugelfläche (oder der gewöhnlichen Böschungslinien auf einer konvexen Fläche 2. Ordnung) mit der Bestimmung der orthogonalen Trajektorien eines Systems von Kreisen, die eine bizirkulare Kurve 4. Ordnung doppelt berühren, gleichbedeutend ist. Nach Belieben kann man dann die Aufgabe in der Ebene oder, mit Hilfe von Satz 4,1, auf der Kugel lösen. Im folgenden wollen wir die Verhältnisse auf der Kugel beschreiben.

[1] Solche Kreissysteme wurden von E. Czuber untersucht in der Arbeit: Die sphärische Kurve 4. Ordnung als Einhüllende von Kreisscharen, Arch. f. Math. u. Phys. (1889), p. 143.

9. Für die genauere Untersuchung ist es bequem, nicht die verschiedenen Lagen der Kegelschnitte a in bezug auf die Kugel zu betrachten, sondern von der Kurve C^4 auszugehen und die verschiedenen Möglichkeiten der Realität und der Lage dieser Kurve auf Φ durchzugehen. Diese Verhältnisse sind bekannt und sollen im folgenden kurz angegeben werden.

Die Kurve C^4 kann elliptisch sein und zwei, einen oder keinen reellen Zweig 4. Ordnung haben, oder sie kann rational sein und einen Doppelpunkt mit reellen oder imaginären Tangenten oder eine Spitze haben.

A. Die Kurve C^4 ist elliptisch.

In dem durch C^4 bestimmten Büschel von Flächen 2. Ordnung gibt es vier Kegelflächen Γ_i mit den Scheiteln A_i ($i = 1, 2, 3, 4$). Die Scheitel bilden die Ecken eines gemeinsamen Polartetraeders der Flächen des Büschels. Die Seitenflächen dieses Tetraeders sollen entsprechend mit α_i bezeichnet werden. Die Punkt A_i und die Seitenflächen α_i heissen die zum Büschel gehörigen Hauptpunkte und Hauptebenen.

Hat die C^4 zwei reelle Zweige, so sind alle Hauptpunkte und alle vier Kegel reell; hat die C^4 einen reellen Zweig, so sind nur zwei der Hauptpunkte und die beiden zugehörigen Kegel reell, und ist endlich C^4 nullteilig, so sind alle Hauptpunkte, aber nur zwei der Kegel reell.

I. Die Kurve C^4 hat zwei reelle Zweige.

Dann ist sie gemeinsame Grenzkurve von vier Systemen von projektiven Böschungslinien auf Φ, die zu den vier polaren Kegelschnitten α_i der Kegel Γ_i gehören. Der Kegelschnitt α_i liegt in der Ebene α_i. Einer der vier Hauptpunkte, z. B. A_1 liegt innerhalb der Kugel, während die drei anderen ausserhalb liegen. Durch eine Homologie, bei der die Kugel in sich übergeht, kann man A_1 in den Mittelpunkt der Kugel überführen; C^4 wird dann ein sphärischer Kegelschnitt. Die Ebene α_1 wird die unendlich ferne Ebene, und das Polartetraeder $A_1 A_2 A_3 A_4$ wird eine dreiseitige Ecke mit dem Scheitel A_1 und drei rechten Winkeln, so dass die Ebenen α_2, α_3 und α_4 die Symmetrieebenen des Büschels werden. Die Kegel Γ_2, Γ_3 und Γ_4 werden Zylinder-

flächen, deren Erzeugende zu den von A_1 ausgehenden Kanten der Ecke parallel sind.

Wir wollen die in den Ebenen α_2, α_3 und α_4 liegenden Grosskreise mit φ_2, φ_3 und φ_4 und die Kegelschnitte, in denen Γ_2, Γ_3 und Γ_4 die genannten Ebenen schneiden, mit c_2, c_3 und c_4 bezeichnen. Eine ganz elementare Betrachtung zeigt dann, dass z. B. c_2 eine Ellipse ist, die ganz innerhalb von φ_2 liegt, c_3 eine Hyperbel, die vier Punkte, aber keine Tangente mit φ_3 gemeinsam hat, und c_4 eine Ellipse, die vier Punkte und vier Tangenten mit φ_4 gemeinsam hat. Hieraus erhält man durch Übergang zu den polaren Kegelschnitten, dass a_2 eine Ellipse ist, die φ_2 umschliesst, a_3 eine Hyperbel, die vier Tangenten, aber keinen Punkt mit φ_3 gemeinsam hat, und a_4 eine Ellipse, die vier Punkte und vier Tangenten mit φ_4 gemeinsam hat.

Wir betrachten nun die vier Fälle.

1) Die zu a_1 gehörigen Böschungslinien auf Φ sind affine Böschungslinien, da a_1 ein unendlich ferner Kegelschnitt ist. Da A_1 der Mittelpunkt der Kugel ist, schneiden die Tangentialebenen an Γ_1 die Kugel in Grosskreisen, und die zugehörigen orthogonalen Trajektorien sind dann sphärische Kegelschnittevolventen. Hiermit ist die Form der Kurven bestimmt. Jede Böschungslinie besteht aus einer Reihe von Bögen, die abwechselnd auf dem einen und auf dem anderen der beiden zu der C^4 gehörigen Zweige zusammenstossen. Da die Tangentenfläche der Böschungslinien die Ebene α_1 im Kegelschnitt a_1 schneidet (der Richtungskegel ist konvex), müssen die Bögen zwischen den Spitzen monoton sein.

Da eine gewöhnliche Böschungslinie auf einem Ellipsoid durch eine Affinität in eine affine Böschungslinie auf einer Kugelfläche übergeführt wird, haben wir hiermit auch die Form der gewöhnlichen Böschungslinien auf einem Ellipsoid bestimmt und gleichzeitig gezeigt, dass sie affine Bilder von sphärischen Kegelschnittevolventen sind[1].

Die orthogonalen Projektionen der Böschungslinien (von A_2 aus) auf die Ebene α_2 liegen in einem ringförmigen Gebiet, das von φ_2 und c_2 begrenzt wird. Die monotonen Bögen werden wieder in monotone Bögen projiziert, da keine Schmiegebene einer Böschungslinie durch A_2 geht. Jede Böschungslinie wird

[1] Siehe W. I., p. 316.

also in eine Kurve projiziert, die aus endlich oder unendlich vielen monotonen Bögen besteht, die den Kreis φ_2 berühren und auf c_2 in Spitzen zusammenstossen. Ist Γ_1 speziell ein Rotationskegel, so geht das Gebiet in einen Kreisring über, und die Projektion der Böschungslinie ist bekanntlich eine Epizykloide, die diesem Ring einbeschrieben ist.

2) Die a_2 entsprechenden Böschungslinien auf der Kugel liegen wieder in dem Gebiet, das von den beiden Zweigen des sphärischen Kegelschnitts begrenzt wird, aber sie sind jetzt orthogonale Trajektorien des Systems der Kreise, die von den Tangentialebenen des elliptischen Zylinders Γ_2 durch C_4 ausgeschnitten werden. Von einem Punkt P der C_4 gehen zwei Zweige einer Böschungslinie aus; jeder dieser Zweige verläuft monoton auf derjenigen von φ_2 begrenzten Halbkugel, die P enthält, windet sich unendlich oft um die Kugel und nähert sich φ_2 asymptotisch.

3) Die zu a_3 gehörigen Böschungslinien auf Φ liegen in demselben Gebiet wie die vorigen. Wie erwähnt hat die Spur c_3 des Zylinders Γ_3 in α_3 vier Punkte mit dem Grosskreis φ_3 gemeinsam; diese sind paarweise diametrale Punkte und sollen mit $M, \overline{M}$ und $N, \overline{N}$ bezeichnet werden. Jede Böschungslinie verläuft dann in einem sphärischen »Rechteck« $MN\overline{M}\overline{N}$, das von den beiden Bögen MN und $\overline{M}\overline{N}$ des Kreises φ_3 und den beiden Bögen $M\overline{N}$ und $\overline{M}N$ des sphärischen Kegelschnittes C^4 begrenzt wird. Betrachtung des Kreissystems, das von den Tangentialebenen an Γ_3 erzeugt wird, lehrt, dass jede Böschungslinie aus monotonen Bögen besteht, die abwechselnd auf den Bögen $M\overline{N}$ und $\overline{M}N$ der C^4 zusammenstossen und sich asymptotisch den Bögen MN und $\overline{M}\overline{N}$ von φ_3 nähern.

4) Die zu a_4 gehörenden Böschungslinien liegen im Gegensatz zu den drei anderen Systemen in den beiden Gebieten der Kugel, die von einem einzelnen Zweig der C^4 begrenzt werden. In jedem dieser Gebiete gibt es zwei »singuläre« Punkte, nämlich die Schnittpunkte S_1 und S_2 der Kugel mit dem Kegelschnitt a_4. Betrachtung des Systems der Tangentialebenen an Γ_4 lehrt, dass jede Böschungslinie von einem Punkt P auf einem der Zweige des sphärischen Kegelschnittes ausgeht und aus zwei monotonen Bögen besteht, von denen der eine P mit S_1 und andere P mit S_2 verbindet. Beide Bögen verlaufen ganz auf einer Seite des Grosskreises φ_4.

II. Die Kurve C^4 hat einen reellen Zweig.

Wie oben erwähnt, gehen durch C^4 zwei reelle Kegel Γ_1 und Γ_2 deren Scheitel A_1 und A_2 ausserhalb der Kugel liegen. C^4 ist also Grenzkurve von zwei Systemen von projektiven Böschungslinien, die zu den Kegelschnitten a_1 und a_2 gehören. Durch eine Kollineation, die die Kugel festlässt, können A_1 und A_2 in unendlich ferne Punkte übergeführt werden, die zwei zu einander orthogonalen Richtungen entsprechen. Die Ebenen α_1 und α_2 werden dann Symmetrieebenen des durch C^4 bestimmten Flächenbüschels, und Γ_1 und Γ_2 werden Zylinderflächen.

Die Zylinderfläche Γ_1 schneide die Ebene α_1 im Kegelschnitte c_1. Man kann dann zeigen, dass c_1 und der in α_1 gelegene Grosskreis φ_1 zwei Punkte und zwei Tangenten gemeinsam haben. Folglich haben auch a_1 und φ_1 zwei Punkte und zwei Tangenten gemeinsam. Die Verhältnisse sind dann genau wie wir sie in 4) beschrieben haben: Man hat ein von dem »Raumoval« C^4 begrenztes Kugelgebiet, in dem es zwei singuläre Punkt gibt, nämlich die genannten Schnittpunkte von φ_1 und a_1. Jede Böschungslinie verläuft dann wie in 4) beschrieben wurde.

Die Zylinderfläche Γ_2 hat in bezug auf die Kugel dieselbe Lage wie Γ_1. Der Kegelschnitt a_2 gibt daher nicht Anlass zu neuen Typen von projektiven Böschungslinien. Es werde jedoch bemerkt, dass die zu a_1 und a_2 gehörenden Böschungslinien in je einem der beiden von C^4 begrenzten Kugelgebiete liegen.

III. Die Kurve C^4 ist nullteilig.

Es gibt vier reelle Hauptpunkte, zwei reelle Kegel Γ_1 und Γ_2 und zwei imaginäre. Wie oben kann man erreichen, dass die Kegel Γ_1 und Γ_2 zu Zylinderflächen mit auf einander senkrechten Erzeugenden werden. Man kann zeigen, dass die Spur c_1 von Γ_1 in der Ebene α_1 eine Hyperbel ist, die vier Tangenten, aber keinen Punkt mit dem Grosskreis φ_1 gemeinsam hat. Daraus folgt, dass der Kegelschnitt a_1 eine Hyperbel ist, die vier Punkte, aber keine Tangente mit φ_1 gemeinsam hat. Die vier Schnittpunkte, die paarweise diametrale Punkte sind, werden wieder mit $M, \overline{M}$ und $N, \overline{N}$ bezeichnet. Man sieht dann, dass durch jeden Punkt P der Kugelfläche zwei projektive Böschungslinien

gehen, die zum Kegelschnitt a gehören; sie sind monotone Bögen, die M und $\overline{M}$ bzw. $\overline{N}$ und N verbinden. Die Böschungslinien verlaufen ganz auf derjenigen von φ_1 begrenzten Halbkugel, die den Punkt P enthält. In gleicher Weise verlaufen die zu dem Kegelschnitt a_2 gehörenden Böschungslinien.

In den letzten fünf Fällen war von sphärischen projektiven Böschungslinien die Rede, für die die Ebene des bestimmenden Kegelschnitts die Kugel schneidet. Denken wir uns die Ebene durch eine Kollineation in die unendlich ferne Ebene transformiert, wobei gleichzeitig der Kegelschnitt a in einen Kreise dieser Ebene übergeht, so sieht man, dass man durch die obige Untersuchung zugleich in groben Zügen die Formen der Haupttypen der gewöhnlichen Böschungslinien auf einem zweischaligen Hyperboloid bestimmt hat.

Nehmen wir an, dass der Asymptotenkegel des Hyperboloids und der zu den Böschungslinien gehörende Rotationskegel denselben Scheitel haben, so entsprechen die beschriebenen fünf Typen $I_{2),\,3),\,4)}$, II und III folgenden Lagen der genannten Kegel: Der Rotationskegel umschliesst den Asymptotenkegel, die Kegel haben vier Tangentialebenen und keine Erzeugende, vier Tangentialebenen und vier Erzeugende, zwei Tangentialebenen und zwei Erzeugenden und keine Tangentialebene und vier Erzeugende gemeinsam.

Wir gehen nun über zu

B. Die Kurve C^4 ist rational.

In diesem Fall berührt die Ebene α die Kugel im Punkt A, so dass der zu dem Kegelschnitt a gehörige Kegel Γ seinen Scheitel A auf der Kugel hat. Die Bestimmung der zu a gehörigen projektiven Böschungslinien ist im wesentlichen durch Satz 2,5a, S. 8 gegeben.

Es gibt drei verschiedene Möglichkeiten, je nachdem der Kegelschnitt a den Punkt A umschliesst, nicht umschliesst oder durch A geht.

Umschliesst a den Punkt A, so hat der Kegel Γ keine Erzeugende in α, und C^4 hat in A einen isolierten Doppelpunkt. Der Kegel Γ schneidet die Kugel in einem Raumoval und die zu a parallele Projektionsebene ω in einer Ellipse. Die Böschungs-

linien ergeben sich durch Zentralprojektion der Ellipsenevolventen auf die Kugel. Jede Böschungslinie hat eine Spitze auf C^4, und jeder der beiden Zweige windet sich unendlich oft um die Kugel und nähert sich A asymptotisch.

Liegt A ausserhalb a, so hat Γ zwei Erzeugende in der Ebene die zu den Tangenten von A an a orthogonal sind. Der Kegel Γ schneidet die Kugel in einer 8-förmigen C^4 und die Ebene ω in einer Hyperbel. Die zu a gehörenden Böschungslinien liegen auf dem ausserhalb der C^4 liegenden Gebiet der Kugel, und jede dieser Kurven entsteht durch Projektion einer Hyperbelevolvente. Jede Böschungslinie besteht also aus einer Reihe monotoner Bögen, die abwechselnd auf jedem der beiden Pseudozweige der C^4 in Spitzen zusammenstossen. Die Bögen nähern sich A asymptotisch.

Geht a durch A, so berührt Γ die Ebene α in einer Erzeugenden, die auf der Tangente von A an a senkrecht steht. Der Kegel Γ schneidet die Kugel in einer C^4 mit einer Spitze in A und die Ebene ω in einer Parabel. Die zu a gehörenden Böschungslinien liegen in demjenigen von C^4 begrenzten Kugelgebiet, das in A den Winkel 360° enthält. Jede Böschungslinie ist die Projektion einer Parabelevolvente auf die Kugel, sie hat eine Spitze auf C^4 und besteht aus zwei monotonen Bögen, die in A enden und a berühren.

Hiermit hat man gleichzeitig einen Überblick über den Verlauf der gewöhnlichen Böschungslinien auf einem elliptischen Paraboloid.

Indleveret til selskabet den 24. november 1949.
Færdig fra trykkeriet den 15. marts 1950.

DET KGL. DANSKE VIDENSKABERNES SELSKAB
MATEMATISK-FYSISKE MEDDELELSER, BIND XXV, NR. 18

A STUDY CONCERNING THE CONGRUENCE SUBGROUPS OF THE MODULAR GROUP

BY

JAKOB NIELSEN

KØBENHAVN
I KOMMISSION HOS EJNAR MUNKSGAARD
1950

Printed in Denmark
Bianco Lunos Bogtrykkeri

Among the subgroups of the modular group the congruence subgroups with respect to a prime have been the chief subject of detailed studies during the initial development of the theory of elliptic modular functions by FELIX KLEIN, ADOLF HURWITZ, WALTER DYCK, GIERSTER and other authors. Most of their papers on this subject are contained in volumes X—XX of the *Mathematische Annalen*. An elaborate exposition has been given in volume I of the *Theorie der elliptischen Modulfunktionen* by F. KLEIN and R. FRICKE (TEUBNER, Leipzig 1890), where more information about the literature on the subject is to be found.

The way in which the question of the congruence groups is approached in these previous investigations contains elements of an arithmetical character, of function theory, non-euclidean geometry, topology, and group theory. It seems worth while to give an introduction to the theory of congruence groups in which the rôle of these separate elements and especially the abstract group-theoretical characteristics are brought out more clearly. For all primes which satisfy a certain arithmetical condition (given in section I) I shall attempt to give such a deduction on the following pages.

I.

Let q be a prime greater than 5. (Without this restriction some special reservations concerning the values 2, 3 and 5 would be necessary in the sequel and, on the other hand, no new facts of interest concerning these cases are obtained. Hence we omit them for simplicity.)

We put $q = 2r + 1$, thus $r = \frac{q-1}{2}$.

All congruences occurring in the sequel are to be understood modulo q unless otherwise stated.

For every residue class $c \not\equiv 0$ the congruence

$$0 \equiv c^{2r} - 1 = (c^r - 1)(c^r + 1)$$

holds, hence

$$c^r \equiv 1 \text{ or } -1,$$

since q is a prime. If r is the least positive exponent satisfying this congruence, we say that c belongs to r.

We restrict q by the condition that 2 belongs to r. No further restriction will be imposed on q.

If c is not the zero class, $c \not\equiv 0$, it possesses a reciprocal class c^{-1} defined by the congruence $cc^{-1} \equiv 1$. Since $-2r \equiv 1$, we get in particular

$$2^{-1} \equiv -r \equiv r + 1, \tag{1}$$

and hence the classes of r and $r+1$ belong to r. Thus the congruence

$$r^{2y} \equiv 1,$$

which is equivalent to

$$r^y \equiv \pm 1,$$

implies

$$y \equiv 0 \text{ modulo } r.$$

Hence the expression r^{2y} yields all quadratic residues exactly once, if y ranges over a complete system of residue classes modulo r.

II.

In this section we define some simple auxiliary functions of an arithmetical character.

II, 1. Let z denote the set of all residue classes ϱ modulo q except the zero class:

$$\varrho \not\equiv 0. \tag{z}$$

This set z forms a group by multiplication. On this set we define a function $\tau(\varrho)$, which is a residue class modulo r, by

(2) $$r^{2\tau(\varrho)} \equiv \varrho^2, \quad \varrho \not\equiv 0.$$

It follows from the last remark in section I that the residue class $\tau(\varrho)$ is uniquely determined by the definition (2). This definition of $\tau(\varrho)$ may also be written

(3) $$r^{\tau(\varrho)} \equiv \pm \varrho.$$

It is immediately inferred that τ has the following properties

$$\left.\begin{array}{ll} (4) & \tau(-\varrho) \equiv \tau(\varrho), \\ (5) & \tau(\varrho_1 \varrho_2) \equiv \tau(\varrho_1) + \tau(\varrho_2), \\ (6) & \tau(\pm 1) \equiv 0. \end{array}\right\} \text{ modulo } r.$$

In consequence of (5) and (6) we get

(7) $$\tau(\varrho) + \tau(\varrho^{-1}) \equiv 0 \text{ modulo } r.$$

In particular

(8) $$\tau(r) \equiv 1 \equiv \tau(-r) \equiv \tau(r+1) \text{ modulo } r$$

and hence for the reciprocal class

(9) $$\tau(2) \equiv -1 \equiv \tau(-2) \text{ modulo } r.$$

II, 2. Let Z denote the set of all "three-sets" $[\varrho, \sigma, \omega]$, where ω denotes a residue class modulo r, and ϱ and σ denote residue classes modulo q with the additional condition that ϱ is an element of z:

(Z) $$[\varrho, \sigma, \omega], \quad \begin{cases} \varrho \not\equiv 0 & \text{modulo } q \\ \sigma \text{ arbitrary} & \text{modulo } q \\ \omega \text{ arbitrary} & \text{modulo } r. \end{cases}$$

Z comprises $\frac{1}{2} q(q-1)^2$ elements. We now put

(10) $$\varphi(\varrho, \sigma) \equiv \varrho(\varrho\sigma - 1)$$

and define on the set Z a function g, which is itself a three-set, by

(11) $$g[\varrho, \sigma, \omega] = [\varrho_g, \sigma_g, \omega_g] \equiv [-\varrho^{-1}, \varphi(\varrho, \sigma), \omega + \tau(\varrho)],$$

τ being the function defined in II, 1; the congruence sign refers to modulus q for the first two numbers in the three-set and to modulus r for the last one. Since $-\varrho^{-1} \not\equiv 0$, the three-set $g[\varrho, \sigma, \omega]$ belongs to Z. We can thus repeat the operation g, and we get

$$g_2[\varrho, \sigma, \omega] = g[\varrho_g, \sigma_g, \omega_g] \equiv [\varrho, \sigma, \omega],$$

since

$$(12)\quad \begin{cases} -(-\varrho^{-1})^{-1} \equiv \varrho, \\ \varphi(-\varrho^{-1}, \varrho(\varrho\sigma - 1)) \equiv -\varrho^{-1}\{-\varrho^{-1}\varrho(\varrho\sigma - 1) - 1\} \\ \quad \equiv \varrho^{-1}\{\varrho\sigma - 1 + 1\} \equiv \sigma, \\ \omega + \tau(\varrho) + \tau(-\varrho^{-1}) \equiv \omega \text{ modulo } r \text{ by (4) and (7).} \end{cases}$$

Hence g is an involutory transformation of the set Z into itself. This transformation leaves no three-set invariant. In particular, the congruences

$$\sigma_g \equiv \sigma \text{ modulo } q$$
$$\omega_g \equiv \omega \text{ modulo } r$$

cannot hold simultaneously.

In fact, if $\varrho \not\equiv \pm 1$, then $\tau(\varrho) \not\equiv 0$ modulo r, and thus

$$\omega_g \equiv \omega + \tau(\varrho) \not\equiv \omega \text{ modulo } r;$$

if $\varrho \equiv \pm 1$, we get from (10)

$$\sigma_g \equiv \sigma \mp 1 \not\equiv \sigma.$$

The elements of Z are thus distributed in pairs by g.

II, 3. Let z' denote the set of all residue classes ϱ modulo q except 0 and -1:

$$(z')\qquad \varrho \not\equiv \begin{cases} 0 \\ -1. \end{cases}$$

On this set z' we define a function $f(\varrho)$, which is itself a residue class modulo q, by

$$(13)\qquad f(\varrho) \equiv -(1 + \varrho^{-1}).$$

In virtue of the condition (z') the class ϱ^{-1} exists, and it is neither 0 nor -1. Hence $f(\varrho)$ is neither 0 nor -1. We can thus repeat the application of f and get

$$f_2(\varrho) = f(f(\varrho)) \equiv -1 + (1+\varrho^{-1})^{-1} \equiv -(1+\varrho)(1+\varrho)^{-1} + \varrho(1+\varrho)^{-1},$$

$$f_2(\varrho) \equiv -(1+\varrho)^{-1}, \tag{14}$$

$$f_3(\varrho) = f(-(1+\varrho)^{-1}) \equiv -1+1+\varrho$$

$$f_3(\varrho) \equiv \varrho. \tag{15}$$

This shows that f is a one-one transformation of order 3 in the set z'.

We may therefore arrange the elements of z' in cyclical subsets of three elements except when invariant under f. We repeat for convenience the general cycle as expressed by (13), (14), and (15):

$$\varrho \to -(1+\varrho^{-1}) \to -(1+\varrho)^{-1} \to \varrho \tag{16}$$

and note the special case, having regard to (1):

$$1 \to -2 \to r \to 1. \tag{17}$$

The latter is not invariant, since we have assumed $q \neq 3$.

It is observed that

$$\varrho \cdot f(\varrho) \cdot f_2(\varrho) \equiv \varrho(1+\varrho^{-1})(1+\varrho)^{-1} \equiv 1. \tag{18}$$

II, 4. Let Z' denote the set of three-sets with the first symbol belonging to z':

$$(Z') \qquad [\varrho, \sigma, \omega], \quad \begin{cases} \varrho \not\equiv 0 \text{ and } -1 & \text{modulo } q \\ \sigma \text{ arbitrary} & \text{modulo } q \\ \omega \text{ arbitrary} & \text{modulo } r. \end{cases}$$

Z' contains $\frac{1}{2} q(q-1)(q-2)$ elements. On this set we define a function G, which is itself a three-set, by

$$G[\varrho, \sigma, \omega] = [\varrho_G, \sigma_G, \omega_G] \equiv [f(\varrho), \varphi(\varrho, \sigma), \omega + \tau(\varrho)]. \tag{19}$$

This three-set belongs to Z', since $f(\varrho)$ belongs to z'. For the same reasons as with Z, this transformation G leaves no three-set invariant; in particular, the second and third symbol are not invariant simultaneously. By repeating this operation we get

$$(20)\quad \begin{cases} G_2[\varrho,\sigma,\omega] = G[\varrho_G,\sigma_G,\omega_G] = [\varrho_{G_2},\sigma_{G_2},\omega_{G_2}] \\ \qquad\qquad \equiv [f_2(\varrho),\varphi_2(\varrho,\sigma),\omega+\tau(\varrho)+\tau(f(\varrho))], \\ \varphi_2(\varrho,\sigma) \equiv f(\varrho)\{f(\varrho)\varphi(\varrho,\sigma)-1\} \\ \qquad\qquad \equiv -(1+\varrho^{-1})\{-(1+\varrho^{-1})\varrho(\varrho\sigma-1)-1\} \\ \qquad\qquad \equiv (1+\varrho)\{(1+\varrho^{-1})(\varrho\sigma-1)+\varrho^{-1}\} \\ \qquad\qquad \equiv (1+\varrho)\{(1+\varrho)\sigma-1\}, \end{cases}$$

and with one more repetition

$$(21)\quad \begin{cases} G_3[\varrho,\sigma,\omega] = G[\varrho_{G_2},\sigma_{G_2},\omega_{G_2}] \equiv [\varrho,\sigma,\omega], \text{ since} \\ \qquad f_3(\varrho) \equiv \varrho \text{ by (15)}, \\ \varphi_3(\varrho,\sigma) \equiv f_2(\varrho)\{f_2(\varrho)\varphi_2(\varrho,\sigma)-1\} \\ \qquad\qquad \equiv -(1+\varrho)^{-1}\{-(1+\varrho)^{-1}(1+\varrho)((1+\varrho)\sigma-1)-1\} \\ \qquad\qquad \equiv (1+\varrho)^{-1}\{(1+\varrho)\sigma-1+1\} \equiv \sigma, \\ \omega+\tau(\varrho)+\tau(f(\varrho))+\tau(f_2(\varrho)) \equiv \omega \text{ modulo } r \text{ by (18), (5) and (6).} \end{cases}$$

Thus G is a one-one transformation of Z' of order 3 without any invariant element, and it distributes the elements of Z' in cycles of three each, the explicit scheme being

$$(22)\quad \begin{aligned} [\varrho,\sigma,\omega] &\to \left[-(1+\varrho^{-1}),\varrho(\varrho\sigma-1),\omega+\tau(\varrho)\right] \\ &\to \left[-(1+\varrho)^{-1},(1+\varrho)\{(1+\varrho)\sigma-1\},\omega+\tau(\varrho)+\tau(1+\varrho^{-1})\right] \\ &\to [\varrho,\sigma,\omega]. \end{aligned}$$

III.

Let $r(q+1)$ simple, oriented polygons be given, each of which has q sides. We intend to combine these polygons into a two-dimensional, closed, orientable manifold Φ by certain identifications of pairs of sides. This is done in an abstract, purely topological way so that (in this section and the next two) no question of metric comes in.

As in section II, the symbol ω denotes residue classes modulo r, while ϱ and σ denote residue classes modulo q. Let r of the polygons

be denoted by $P(\omega)$ and called "central polygons", the remaining qr polygons being denoted by $P(\sigma, \omega)$ and called "peripheric polygons"; here ω ranges over all residue classes modulo r and σ over all residue classes modulo q. Let $s(\sigma, \omega)$ denote the sides of $P(\omega)$, the numbering σ of these sides proceeding in the positive sense of the oriented polygons, and $s(\varrho, \sigma, \omega)$ the sides of $P(\sigma, \omega)$, the numbering ϱ likewise proceeding in the positive sense. With these denotations we define the following identifications:

(A) For all values of σ and ω the side $s(\sigma, \omega)$ of $P(\omega)$ and the side $s(0, \sigma, \omega)$ of $P(\sigma, \omega)$ coincide with opposite senses.

This disposes of all sides of all central polygons and of the sides $s(0, \sigma, \omega)$ of all peripheric polygons. So we are left with all sides $s(\varrho, \sigma, \omega)$, $\varrho \not\equiv 0$, of the peripheric polygons, and these sides thus correspond to the set Z of three-sets. For these sides we define:

(B) The coincidence of these sides in pairs is given by the involutory transformation g: The side $s(\varrho, \sigma, \omega)$ coincides with $s(\varrho_g, \sigma_g, \omega_g)$ with opposite senses.

Since the two last numbers of the three-set are not left invariant simultaneously, no side coincides with a side of the same polygon.

We now establish the cycles of vertices resulting from these identifications by turning around these vertices in the positive sense. Starting in the central polygon $P(\omega)$ we leave it over the side $s(\sigma, \omega)$ and enter across the coinciding side $s(0, \sigma, \omega)$ according to definition (A) into the peripheric polygon $P(\sigma, \omega)$. The preceding side of this polygon is $s(-1, \sigma, \omega)$, which coincides with the side $s(1, \sigma+1, \omega)$ of the peripheric polygon $P(\sigma+1, \omega)$ according to definition (B). The preceding side of this polygon is $s(0, \sigma+1, \omega)$, which coincides with the side $s(\sigma+1, \omega)$ of the central polygon $P(\omega)$, and the preceding side of this polygon is $s(\sigma, \omega)$, with which we started. So we get a cycle of vertices as illustrated by fig. 1.

In this process σ and ω are arbitrary within their range. Therefore all vertices of central polygons are involved. We may also remark that, if we leave an arbitrary peripheric polygon $P(\sigma, \omega)$ by crossing its side $s(-1, \sigma, \omega)$ and turn in the positive sense, we get the cycle of vertices just now established. Likewise, if we leave $P(\sigma, \omega)$ by crossing its side $s(0, \sigma, \omega)$ and

turn in the positive sense, we get a cycle of vertices of the same type, σ being replaced by $\sigma - 1$.

In the remaining cycles of vertices, therefore, only peripheric polygons are involved and, turning always in the positive sense, we have to leave $P(\sigma, \omega)$ by crossing a side $s(\varrho, \sigma, \omega)$, where

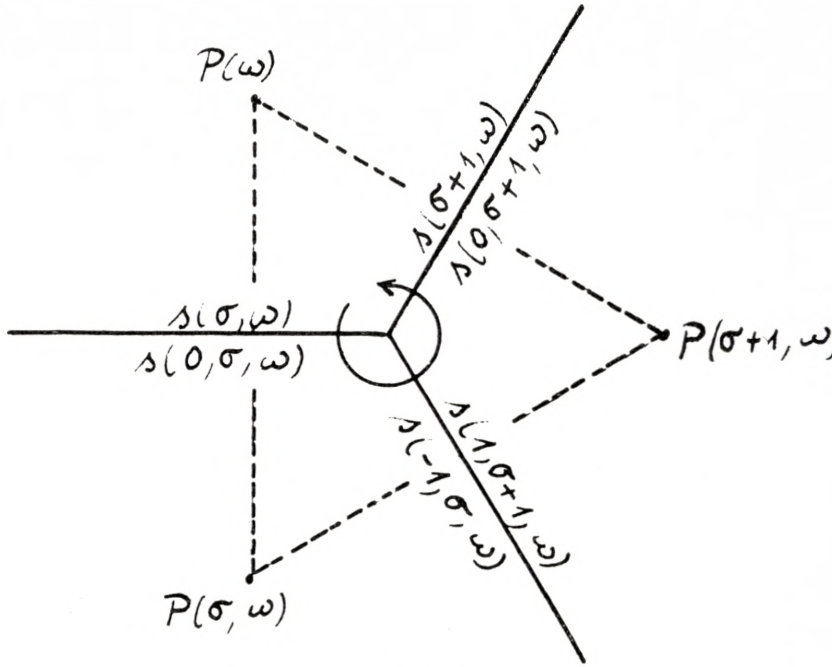

Fig. 1.

ϱ belongs to the set z', ($\varrho \not\equiv 0$ and -1); thus the three-set $[\varrho, \sigma, \omega]$ belongs to Z'. This side coincides with $s(\varrho_g, \sigma_g, \omega_g) = s(-\varrho^{-1}, \varphi(\varrho, \sigma), \omega + \tau(\varrho))$ of $P(\varphi(\varrho, \sigma), \omega + \tau(\varrho))$, and the preceding side of this polygon, which we have to cross in *leaving* the polygon, is

$$s(-\varrho^{-1} - 1, \varphi(\varrho, \sigma), \omega + \tau(\varrho)) = s(\varrho_G, \sigma_G, \omega_G).$$

Therefore we *leave* the next polygon by crossing the side $s(\varrho_{G_2}, \sigma_{G_2}, \omega_{G_2})$, and again we *leave* the next polygon by crossing the starting side $s(\varrho, \sigma, \omega)$ in virtue of (21). So again, we have a cycle of three vertices, as illustrated by fig. 2; compare (22).

In both cases the three polygons arranged round a vertex are different.

It follows from this construction that Φ is a closed surface. Moreover, it is orientable, since the orientation of any two neighbour polygons are in accordance, the common side being oppositely sensed.

We conclude this section by computing the genus p of Φ.

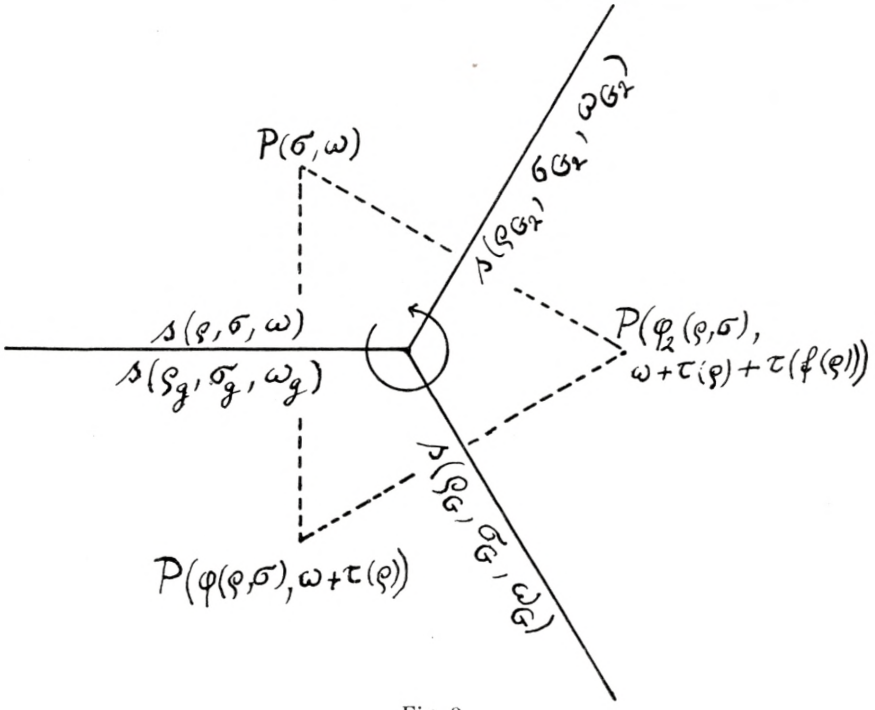

Fig. 2.

The number of polygons is $\alpha_2 = (q+1)\,r$. Thus the number of different sides on Φ is $\alpha_1 = \frac{1}{2}\,q\,(q+1)\,r$, and the number of vertices on Φ is $\alpha_0 = \frac{1}{3}\,q\,(q+1)\,r$. From this we get by Euler's formula

$$2-2p = \alpha_0 - \alpha_1 + \alpha_2 = r\,(q+1)\left(1-\frac{1}{6}\,q\right) = \frac{1}{12}\,(q-1)\,(q+1)\,(6-q)$$

and hence

$$(23) \qquad p = 1+\frac{1}{24}\,(q^2-1)\,(q-6) = \frac{1}{24}\,(q+2)\,(q-3)\,(q-5).$$

We list the smallest values:

$$q = 3 \quad 5 \quad 7 \quad 11 \quad 13 \quad \cdots$$
$$p = 0 \quad 0 \quad 3 \quad 26 \quad 50 \quad \cdots$$

(23) also holds for $q = 3$ and $q = 5$, which might have been included in the preceding considerations by adding a few special remarks. In these cases the structure af Φ is that of a tetrahedron or dodecahedron, respectively.

IV.

In this section we establish by a well-known process[1] the fundamental group (Poincaré group) of Φ by generators and generational relations in a special form derived from the construction of Φ. Inside each polygon we select a representative point, which may be denoted by the same symbol $P(\omega)$ or $P(\sigma, \omega)$ as the polygon itself. From each representative point we draw an oriented path, called "elementary path", to the representative point of each of the q neighbouring polygons and denote it by $a(---)$, the paranthesis including the same symbols as the side $s(---)$ which we cross in leaving the first polygon. So, according to definition (A), $a(\sigma, \omega)$ leads from $P(\omega)$ to $P(\sigma, \omega)$, and $a(0, \sigma, \omega)$ leads from $P(\sigma, \omega)$ to $P(\omega)$. We therefore have

$$a(0, \sigma, \omega) = a(\sigma, \omega)^{-1}. \tag{24}$$

Similarly, for $\varrho \not\equiv 0$, according to definition (B), $a(\varrho, \sigma, \omega)$ leads from $P(\sigma, \omega)$ to $P(\varphi(\varrho, \sigma), \omega + \tau(\varrho))$, and we have for its inverse

$$a(\varrho_g, \sigma_g, \omega_g) = a(-\varrho^{-1}, \varphi(\varrho, \sigma), \omega + \tau(\varrho)) = a(\varrho, \sigma, \omega)^{-1}, \quad \varrho \not\equiv 0. \tag{25}$$

These paths form on Φ a network N of triangles as indicated in fig. 1 and 2 by dotted lines, and this network N is dual to the network of polygons (e.g. the dual of the dodecahedron network is the icosahedron network).

Every path on the network N between two representative points is a chain of elementary paths. We choose the point $P(0)$

[1] See for instance H. Seifert and W. Threlfall, *Lehrbuch der Topologie*, § 46.

as starting point. Next we define for each representative point an individual path on N connecting $P(0)$ with that point in the following way: First, let the point be a $P(\omega)$ and let the path envisaged be called $h(\omega)$. For $\omega = 0$ we take the path $h(0)$ to be empty. Then, by induction, when $h(\omega-1)$ is defined, we put

$$(26)\quad h(\omega) = h(\omega-1)\, a(0,\omega-1)\, a(r,0,\omega-1)\, a(0,r+1,\omega),$$
$$\omega \equiv 1,2,\cdots,r-1 \text{ modulo } r.$$

[To control this, $h(\omega-1)$ leads from $P(0)$ to $P(\omega-1)$, $a(0,\omega-1)$ leads from $P(\omega-1)$ to $P(0,\omega-1)$, $a(r,0,\omega-1)$ leads from $P(0,\omega-1)$ to $P(r+1,\omega)$ by (10) and (8) and, finally, $a(0,r+1,\omega)$ leads from $P(r+1,\omega)$ to $P(\omega)$.] Next, if the representative point is a $P(\sigma,\omega)$, we put for the path $h(\sigma,\omega)$ leading from $P(0)$ to $P(\sigma,\omega)$

$$(27)\qquad h(\sigma,\omega) = h(\omega)\, a(\sigma,\omega)$$

for all values of σ and ω.

The fundamental group of Φ is the group of homotopy classes of closed curves issued from a fixed point, for which we here choose $P(0)$. Every closed path on N issued from $P(0)$ can be composed of certain closed paths depending on the single elementary paths, namely the h_1 leading from $P(0)$ to the starting point of the elementary path a followed by this path a itself and then by the h_2^{-1} leading from its end-point back to $P(0)$. We denote the homotopy class of such a path by $k(---)$ with the same symbols in the parenthesis as for the corresponding elementary path $a(---)$. This finite set of k's then generate the fundamental group.

If a general closed path issued from $P(0)$ is written down as a composition of the a's, then its homotopy class is the product of the corresponding k's, as is seen by inserting between any two consecutive a-factors the corresponding $h^{-1}h$ of their common point. Any equation between the a's therefore yields a relation between the corresponding k's. So we get from (24) and (25) for all values of ϱ,σ,ω, for which these equations hold,

$$(28)\qquad k(\sigma,\omega)\, k(0,\sigma,\omega) = 1,$$

(29) $k(\varrho, \sigma, \omega)\, k(-\varrho^{-1}, \varphi(\varrho, \sigma), \omega + \tau(\varrho)) = 1, \quad \varrho \not\equiv 0,$

the symbol 1 indicating the identity of the fundamental group. (29) may also be written

(29) $$k(\varrho, \sigma, \omega)\, k(\varrho_g, \sigma_g, \omega_g) = 1.$$

The homotopy class derived from the elementary path $a(\sigma, \omega)$ is according to the above definition the homotopy class of the product

$$h(\omega)\, a(\sigma, \omega)\, h(\sigma, \omega)^{-1},$$

$h(\omega)$ and $h(\sigma, \omega)$ being abbreviations for certain products of the a's as defined above. Inserting $h(\sigma, \omega)$ from (27) we find that this reduces to the empty product. Hence

(30) $$k(\sigma, \omega) = 1,$$

and then (28) yields

(31) $$k(0, \sigma, \omega) = 1.$$

Consider the product of a's making up $h(\omega)$. The corresponding product of k's is the homotopy class of

$$h(0)\, h(\omega)\, h(\omega)^{-1},$$

which reduces to the empty product. Thus the product of the k's corresponding to the a's in $h(\omega)$ is 1. (27) together with (30) then shows that this also holds for the $h(\sigma, \omega)$.

This fact together with (30) and (31), when applied to (26), yields the relation $k(r, 0, \omega - 1) = 1$ for the values of ω indicated in (26). We prefer to write this relation

(32) $$k(r, 0, \omega) = 1, \quad \omega \equiv 0, 1, \cdots, r-2 \text{ modulo } r,$$

and we emphasize the fact that the value $\omega \equiv -1$ modulo r is not included in this relation (32).

Finally, the homotopy class derived from the elementary path $a(\varrho, \sigma, \omega)$, $\varrho \not\equiv 0$, is the homotopy class of the product

$$h(\sigma, \omega)\, a(\varrho, \sigma, \omega)\, h(\varphi(\varrho, \sigma), \omega + \tau(\varrho))^{-1}$$

in consequence of the definition (B) of coincidence. This only yields the identical relation $k(\varrho, \sigma, \omega) = k(\varrho, \sigma, \omega)$, since the h's do not contribute.

To these relations we have to add the relations derived from the fact that the cycle of three a's surrounding a vertex of Φ bounds a simply connected piece of Φ and thus belongs to the homotopy class of identity. For a vertex of the type of fig. 1 this yields the relation

$$k(\sigma,\omega)\, k(-1,\sigma,\omega)\, k(0,\sigma+1,\omega) = 1, \tag{33}$$

and for a vertex of the type of fig. 2 the relation

$$k(\varrho,\ \sigma,\omega)\, k(f(\varrho), \varphi(\varrho,\sigma), \omega+\tau(\varrho))\, k(f_2(\varrho), \varphi_2(\varrho,\sigma), \omega+\tau(\varrho) + \tau(f(\varrho)) = 1, \tag{34}$$

in which $\varrho \not\equiv 0$ and -1. With the use of the symbol G this relation reads

$$k(\varrho,\sigma,\omega)\, k(\varrho_G, \sigma_G, \omega_G)\, k(\varrho_{G_2}, \sigma_{G_2}, \omega_{G_2}) = 1. \tag{34}$$

This completes the establishment of the generational relations of the fundamental group. Looking over the result, we see that we may omit the $k(\sigma, \omega)$ and their reciprocals, the $k(0, \sigma, \omega)$, since they are identity according to (30) and (31). Then relation (28) disappears, and (33) reduces to

$$k(-1,\sigma,\omega) = 1, \tag{35}$$

while (29), (32), and (34) remain unaltered. We thus have the following result:

The fundamental group of Φ may be generated by the elements $k(\varrho,\sigma,\omega)$, $\varrho \not\equiv 0$, with (29), (32), (34), *and* (35) *as generational relations.*

One might suggest the elimination even of the $k(r,0,\omega)$ for $\omega \not\equiv -1$ modulo r and of the $k(-1,\sigma,\omega)$ in consequence of (32) and (35), and at the same time of their reciprocals $k(2, r+1, \omega+1)$ and $k(1,\sigma+1,\omega)$. This would, however, destroy the full generality of relation (34), into which some of them enter for special values of ϱ,σ,ω. We therefore prefer to keep them, but we may note

at once the consequences as to the reciprocals. We put them in the form

$$k(2, r+1, \omega) = 1, \quad \omega \not\equiv 0 \text{ modulo } r, \tag{36}$$

$$k(1, \sigma, \omega) = 1. \tag{37}$$

If we put $\varrho \equiv r$, $\sigma \equiv 0$ in (34), we get by (10), (17), (8), and (6)

$$k(r, 0, \omega)\, k(1, r+1, \omega+1)\, k(-2, r, \omega+1) = 1.$$

Here the central factor drops out in virtue of (37). The reciprocal of the last factor is $k(r+1, 0, \omega)$ by (29), (10), (1), and (9). Thus, if $\omega \not\equiv -1$ modulo r, the first factor drops out in virtue of (32), and we get

$$k(-2, r, \omega) = 1, \quad \omega \not\equiv 0 \text{ modulo } r, \tag{38}$$

$$k(r+1, 0, \omega) = 1, \quad \omega \not\equiv -1 \text{ modulo } r. \tag{39}$$

If $\omega \equiv -1$ modulo r, we get

$$k(r, 0, -1) = k(r+1, 0, -1), \tag{40}$$

and for their reciprocals

$$k(2, r+1, 0) = k(-2, r, 0). \tag{41}$$

These last six relations (36) to (41) need not be included in the generational relations of the fundamental group, since they are consequences of the generational relations (29), (32), (34), and (35) established above.

V.

Let F denote the abstract group generated by three elements S, T, U subject to the relations

$$S^q = 1, \qquad T^2 = 1, \qquad U^3 = 1, \qquad STU = 1.$$

Eliminating U by means of the last relation we get for F a representation by two generators S and T with generational relations

(42) $$S^q = 1$$

(43) $$T^2 = 1$$

(44) $$(ST)^3 = 1.$$

We use this latter form and pay attention to relations (42) and (43) by only regarding exponents of S and T as residue classes modulo q or modulo 2, respectively. So (44) is the real working relation and, for convenience, we write it in different, but equivalent forms:

(45) $$(ST)^3 = 1,\ STS = TS^{-1}T,\ TST = S^{-1}TS^{-1},\ (TS^{-1})^3 = 1.$$

As a consequence of (45) we get

(46) $$TS^{-2}T = (TS^{-1}T)^2 = (STS)^2 = STS^2TS.$$

We now take q to mean a prime $q = 2r+1$ subject to the same restrictions as in section I and define the functions $\tau(\varrho)$, $f(\varrho)$ and $\varphi(\varrho, \sigma)$ and the transformations g and G as before. Moreover we introduce a function $\pi(\omega)$ = the smallest non-negative residue of ω modulo r:

$$\pi(\omega) \equiv \omega \text{ modulo } r, \qquad 0 \leq \pi(\omega) < r.$$

We denote by W the following element of F:

(47) $$W = TS^rTS^{-2}TS^r = TS^{r+1}TS^2TS^{r+1},$$

these two products being equal in virtue of (46). We also note the reciprocal of W:

(48) $$W^{-1} = S^{r+1}TS^2TS^{r+1}T = S^rTS^{-2}TS^rT.$$

Regarding as before ϱ and σ as residue classes modulo q and ω as a residue class modulo r, we introduce the subgroup H of F generated by the following elements:

(49) $$k(\varrho, \sigma, \omega) = W^{\pi(\omega)}S^\sigma TS^\varrho TS^{\varrho^{-1}}TS^{-\varphi(\varrho,\sigma)}W^{-\tau(\omega+\tau(\varrho))}, \quad \varrho \not\equiv 0.$$

We set out to prove that these elements satisfy the relations (29), (32), (34), and (35) established in the preceding section for the fundamental group of Φ.

If in (29) we insert the values given by (49), we get

$$W^{\pi(\omega)} S^{\sigma} TS^{\varrho} TS^{\varrho^{-1}} TS^{-\varphi(\varrho,\sigma)} W^{-\pi(\omega+\tau(\varrho))}$$
$$\cdot W^{\pi(\omega+\tau(\varrho))} S^{\varphi(\varrho,\sigma)} TS^{-\varrho^{-1}} TS^{-\varrho} TS^{-\sigma} W^{-\pi(\omega)} = 1.$$

Here we have made use of (12) in the last two factors.

In (32) we have with $\omega \not\equiv -1$ modulo r:

$$k(r, 0, \omega) = W^{\pi(\omega)} TS^{r} TS^{-2} TS^{r} W^{-\pi(\omega+1)} = 1$$

by (8) and (47), for $\pi(\omega+1) = \pi(\omega)+1$, since $\omega \not\equiv -1$ modulo r.

In (34) we get by inserting from (49)

$$W^{\pi(\omega)} S^{\sigma} TS^{\varrho} TS^{\varrho^{-1}} \underline{TS^{-\varphi(\varrho,\sigma)} W^{-\pi(\omega+\tau(\varrho))}}$$
$$\cdot \underline{W^{\pi(\omega+\tau(\varrho))} S^{\varphi(\varrho,\sigma)} T} S^{f(\varrho)} TS^{f(\varrho)^{-1}} \underline{TS^{-\varphi_2(\varrho,\sigma)} W^{-\pi(\omega+\tau(\varrho)+\tau(f(\varrho)))}}$$
$$\cdot \underline{W^{\pi(\omega+\tau(\varrho)+\tau(f(\varrho)))} S^{\varphi_2(\varrho,\sigma)} T} S^{f_2(\varrho)} TS^{f_2(\varrho)^{-1}} TS^{-\sigma} W^{-\pi(\omega)},$$

since by (21)

$$\varphi(f_2(\varrho), \varphi_2(\varrho,\sigma)) = \varphi_3(\varrho,\sigma) \equiv \sigma \text{ modulo } q$$

and

$$\tau(\varrho)+\tau(f(\varrho))+\tau(f_2(\varrho)) \equiv 0 \text{ modulo } r.$$

Here the underlined parts cancel. Moreover we have by (13) and (14) for the exponents of those powers of S which thereby become neighbours

$$\varrho^{-1}+f(\varrho) \equiv \varrho^{-1}-(1+\varrho^{-1}) = -1,$$
$$f(\varrho)^{-1}+f_2(\varrho) \equiv -(1+\varrho^{-1})^{-1}-(1+\varrho)^{-1} \equiv -(1+\varrho)^{-1}(1+\varrho) \equiv -1.$$

We therefore get

$$W^{\pi(\omega)} S^{\sigma} TS^{\varrho} (TS^{-1})^{3} S^{1+f_2(\varrho)^{-1}} TS^{-\sigma} W^{-\pi(\omega)} = 1$$

by using (45) and (14).

Finally, in (35) we find by (45)

$$k(-1, \sigma, \omega) = W^{\pi(\omega)} S^{\sigma} TS^{-1} TS^{-1} TS^{-(\sigma+1)} W^{-\pi(\omega+0)} = 1.$$

The elements (49) therefore also satisfy relations (36)—(41), since these are formal consequences of the four relations just proved. Especially we remark concerning the elements occurring in (40) that by (49) and (1) and (47)

$$(50) \qquad k(r, 0, -1) = W^{r-1} TS^{r} TS^{-2} TS^{r} W^{-\pi(0)} = W^{r}.$$

Thus W^r is an element of H.

VI.

It is inferred from what has just been proved that the subgroup H of F defined in the preceding section is one-one isomorphic either with the fundamental group of Φ or with a factor group of that group. We set out to prove that the first case occurs. This is done by constructing from the group F a set of polygons and of identifications by the $k(\varrho, \sigma, \omega)$ which correspond to the construction of Φ in section III. (This construction is based on a procedure indicated by W. Dyck in a footnote on pages 41—42 of *Mathematische Annalen*, vol. XX. Instead of the pair -2 and r used in the present investigations, Dyck uses a general pair of mutually reciprocal primitive roots α and δ modulo q, thus without imposing any restriction on q.)

Let a triangle stu be given with angles equal to $\frac{\pi}{q}$, $\frac{\pi}{2}$ and $\frac{\pi}{3}$, respectively; see fig. 3. As we assume $q \geq 7$, the triangle is situated in the non-euclidean plane. A reflection in st followed by a reflection in su is a rotation about s through an angle $\frac{2\pi}{q}$ in the positive sense. We denote this rotation by S, and hence S^q is identity. Similarly, T is a half-rotation about t, and U is a third of a full rotation about u, if they are taken to be the product of two analogous reflections. The product of reflections shows that $STU = 1$.[1] Hence S, T, and U generate a group of

[1] A product is read like a composed function: First carry out U, then T, finally S.

motions in the non-euclidean plane, which is our group F, and which we now generate by S and T with relations (42), (43), and (44). The shadowed triangle stu_0 of fig. 3 being derived from stu by reflection at st, the triangle su_0u is a fundamental domain for the group F. In fig. 3 this triangle is inscribed with the symbol of identity. Let the triangle derived from it by an arbitrary element e of F be denoted with the symbol e. If e ranges over the whole of F, these triangles cover the entire non-euclidean plane. This is illustrated by fig. 4 for the case of $q = 7$.[1]

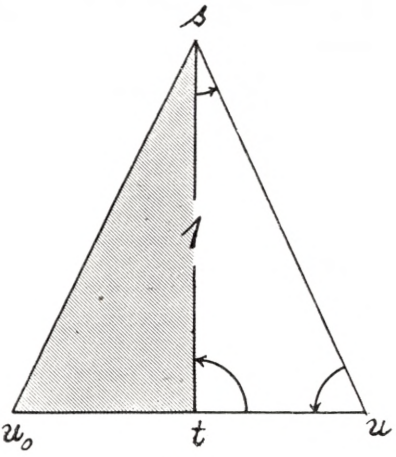

Fig. 3.

The triangles $1, S, S^2, \cdots, S^{q-1}$ form a polygon $P(0)$ with center at the point s, which will also be called the representative point $P(0)$. In the triangle S^σ the side opposite $P(0)$ is called $s(\sigma, 0)$. Then $S^\sigma TS^{-\sigma}$ is a half-rotation about the center of this side, and it carries the "central" polygon $P(0)$ into the "peripheric" polygon $P(\sigma, 0)$, which has its side $s(0, \sigma, 0)$ coinciding with $s(\sigma, 0)$ with opposite senses conforming to the orientation of the plane. The other sides of $P(\sigma, 0)$ are numbered $s(\varrho, \sigma, 0)$ in the positive sense.

This star of $q+1$ polygons, each consisting of q triangles (each triangle being half white, half shadowed) is shown by fig. 5 for $q = 7$.

The triangles of the central polygon $P(0)$ bear the signature S^ϱ, those of $P(0, 0)$ consequently TS^ϱ, and those of $P(\sigma, 0)$ consequently $S^\sigma TS^\varrho$. The side of the latter opposite the center $P(\sigma, 0)$ is $s(\varrho, \sigma, 0)$. The triangle adjacent to $S^\sigma TS^\varrho$ along $s(\varrho, \sigma, 0)$ is $S^\sigma TS^\varrho T$, because the triangle T is adjacent to the triangle 1 along the corresponding side u_0u. In order to make the side $s(-2, r, 0)$ of the peripheric polygon $P(r, 0)$ coincide with the side $s(r+1, 0, 0)$ of the peripheric polygon $P(0, 0)$ with opposite senses we must carry the triangle $S^r TS^{-2} T$ adjacent to $s(-2, r, 0)$

[1] The figures 4 and 5 have been reproduced from KLEIN-FRICKE, *Elliptische Modulfunktionen*, vol. I.

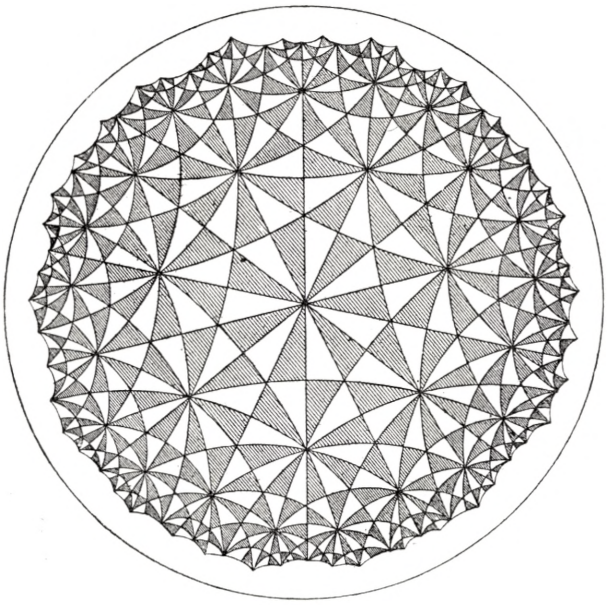

Fig. 4.

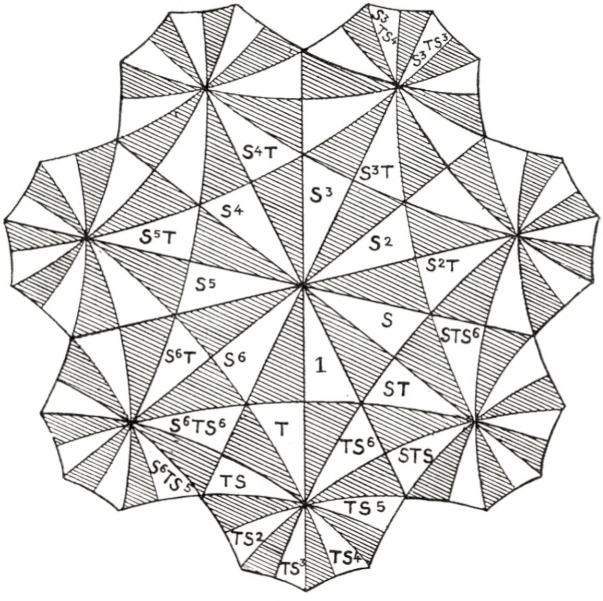
S⁴T
S³
S³T
S⁴
S⁵T
S²
S²T
S⁵
S
STS⁶
S⁶T
S⁶
1
ST
S⁶TS⁶
T
TS⁶
STS
TS
TS⁵
TS²
TS⁴

Fig. 5.

into the triangle TS^{r+1}, and this is done by the motion

$$TS^{r+1}(S^r TS^{-2} T)^{-1} = TS^{r+1} TS^2 TS^{r+1} = W,$$

see (47). The same motion W carries $s(2, r+1, 0)$ into $s(r, 0, 0)$ for analogous reasons:

$$TS^r (S^{r+1} TS^2 T)^{-1} = TS^r TS^{-2} TS^r = W.$$

Thus W can be thought of as a translation sliding the whole star downwards along the vertical diameter of fig. 5 at a distance equal to the length of that diameter. If this displacement is repeated ω times, we get a star composed of a central polygon $P(\omega)$, whose triangles are $W^\omega S^\varrho$, and q peripheric polygons, $P(\sigma, \omega)$, whose triangles are $W^\omega S^\sigma TS^\varrho$. Take $\omega < r$, thus $\omega = \pi(\omega)$. If for $\varrho \not\equiv 0$ we want the side $s(\varrho, \sigma, \omega)$ of this last triangle to coincide with the side $s(\varrho_g, \sigma_g, \omega_g) = s(-\varrho^{-1}, \varphi(\varrho, \sigma), \pi(\omega + \tau(\varrho)))$ of the triangle $W^{\pi(\omega+\tau(\varrho))} S^{\varphi(\varrho,\sigma)} TS^{-\varrho^{-1}}$ with opposite senses, we make the adjacent triangle of the latter, thus $W^{\pi(\omega+\tau(\varrho))} S^{\varphi(\varrho,\sigma)} TS^{-\varrho^{-1}} T$ coincide with the triangle $W^{\pi(\omega)} S^\sigma TS^\varrho$. This is evidently done by the element $k(\varrho, \sigma, \omega)$ defined in (49).

The r stars derived from the first one by W^ω, $\omega = 0, 1, \cdots, r-1$, form a singly connected piece Ω of the plane, bounded by a polygon, whose sides correspond in pairs by those elements $k(\varrho, \sigma, \omega)$ which are not equal to 1. This shows that the construction of the subgroup H of F is a materialization of the fundamental group of the two-dimensional manifold Φ defined in section III by abstract identification. The group H is here realized as a group of motions in the non-euclidean plane, which is a model of the universal covering surface of Φ.

The fundamental domain Ω of H consists of $r(q+1)$ polygons containing q triangles each. This shows that

$$j = r(q+1)\, q = \frac{1}{2} q(q^2-1) \tag{51}$$

is the index of H in F.

If the non-euclidean plane is denoted by D, we may speak of Φ as D modulo H, which means that points of D corresponding by elements of H are considered as identical. In the

same way, D modulo F evidently is a non-euclidean manifold of genus zero, three points of which are singular with respect to the metric, namely those corresponding to s, t, and u. They may be called conical points. D modulo H is a closed manifold, which covers D modulo F with j sheets, and which possesses no conical points. Accordingly, H possesses no elements of a finite order.

VII.

We now want to prove that the covering of D modulo F by D modulo H is regular. This is equivalent to the assertion that H is self-conjugate in F. In order to prove this it is sufficient to prove that the generators $k(\varrho, \sigma, \omega)$ of H are transformed into elements of H by the generators T and S of F.

In preparation for this proof we state the following facts beforehand:

$$TWT^{-1} = W^{-1}. \tag{52}$$

This is immediately seen from (47) and (48). Also the definition of $\pi(x)$ implies:

$$\pi(\pi(x)) = \pi(x), \tag{53}$$

$$\pi(x) + \pi(-x) = \begin{cases} 0 \text{ if } x \equiv 0 \text{ modulo } r \\ r \text{ if } x \not\equiv 0 \text{ modulo } r, \end{cases} \tag{54}$$

$$r^{2\pi(x)} \equiv r^{2x} \text{ modulo } q, \tag{55}$$

since $r^{2r} \equiv 1$.

We now transform $k(\varrho, \sigma, \omega)$ (where it is remembered that $\varrho \not\equiv 0$) by T and get by (49), (52), and (10)

$$\begin{aligned} Tk(\varrho, \sigma, \omega)\, T^{-1} &= TW^{\pi(\omega)} S^{\sigma} TS^{\varrho} TS^{\varrho^{-1}} TS^{-q(\varrho, \sigma)} W^{-\pi(\omega + \tau(\varrho))} T \\ &= W^{-\pi(\omega)} TS^{\sigma} TS^{\varrho} TS^{\varrho^{-1}} TS^{-\varrho(\varrho\sigma - 1)} TW^{\pi(\omega + \tau(\varrho))}. \end{aligned} \tag{56}$$

On the other hand, suppose $\sigma \not\equiv 0$ and $\sigma \not\equiv \varrho^{-1}$ and consider the product

$$k(\sigma, 0, -\omega)\, k(\sigma^{-1}(\varrho\sigma - 1), -\sigma, \tau(\sigma) - \omega)\, k(-\varrho^{-1}(\varrho\sigma - 1)^{-1}, -\varrho(\varrho\sigma - 1), \tau(\sigma) + \tau(\sigma^{-1}(\varrho\sigma - 1)) - \omega)$$

$$= W^{\pi(-\omega)} S^0 TS^{\sigma} TS^{\sigma^{-1}} \underline{TS^{\sigma} W^{-\pi(\tau(\sigma)-\omega)}}$$

$$\cdot \underline{W^{\pi(\tau(\sigma)-\omega)} S^{-\sigma} TS^{\sigma^{-1}(\varrho\sigma-1)} TS^{\sigma(\varrho\sigma-1)^{-1}}} \underline{TS^{\varrho(\varrho\sigma-1)} W^{-\pi(\tau(\sigma)+\tau(\sigma^{-1}(\varrho\sigma-1))-\omega)}}$$

$$\cdot \underline{W^{\pi(\tau(\sigma)+\tau(\sigma^{-1}(\varrho\sigma-1))-\omega)} S^{-\varrho(\varrho\sigma-1)} TS^{-\varrho^{-1}(\varrho\sigma-1)^{-1}}} TS^{-\varrho(\varrho\sigma-1)} TS^0 W^{-\pi(\tau(\sigma)+\tau(\sigma^{-1}(\varrho\sigma-1))+\tau(\varrho^{-1}(\varrho\sigma-1)^{-1})-\omega)}.$$

It should be noted that all reciprocals occurring herein exist owing to the assumptions for ϱ and σ, and the first argument for all three k's is $\not\equiv 0$. Now the underlined parts in the product cancel. Moreover we get for the exponents of the powers of S which thereby become neighbours

$$\sigma^{-1} + \sigma^{-1}(\varrho\sigma - 1) = \sigma^{-1}\varrho\sigma \equiv \varrho,$$
$$\sigma(\varrho\sigma - 1)^{-1} - \varrho^{-1}(\varrho\sigma - 1)^{-1} \equiv (\varrho\sigma - 1)^{-1}(\sigma\varrho\varrho^{-1} - \varrho^{-1}) \equiv (\varrho\sigma - 1)^{-1}\varrho^{-1}(\varrho\sigma - 1) \equiv \varrho^{-1}.$$

Finally, with the use of (5) and (7),

$$\tau(\sigma) + \tau(\sigma^{-1}(\varrho\sigma - 1)) + \tau(\varrho^{-1}(\varrho\sigma - 1)^{-1})$$
$$\equiv \tau\{\sigma \cdot \sigma^{-1}(\varrho\sigma - 1) \cdot \varrho^{-1}(\varrho\sigma - 1)^{-1}\} \equiv \tau(\varrho^{-1}) \equiv -\tau(\varrho) \text{ modulo } r.$$

The above product therefore is equal to

$$W^{\pi(-\omega)} T S^{\sigma} T S^{\varrho} T S^{\varrho^{-1}} T S^{-\varrho(\varrho\sigma-1)} T W^{-\pi(-\omega-\tau(\varrho))}.$$

Comparing this with (56) and slightly reducing the last argument of the third k we get

$$(57)\quad \left\{\begin{aligned} Tk(\varrho,\sigma,\omega)\,T^{-1} = {} & W^{-\tau(\omega)-\pi(-\omega)} \\ & \cdot k(\sigma,0,-\omega) \\ & \cdot k(\sigma^{-1}(\varrho\sigma-1),-\sigma,\tau(\sigma)-\omega) \\ & \cdot k(-\varrho^{-1}(\varrho\sigma-1)^{-1},-\varrho(\varrho\sigma-1),\tau(\varrho\sigma-1)-\omega) \\ & \cdot W^{\pi(\omega+\tau(\varrho))+\pi(-\omega-\tau(\varrho))}. \end{aligned}\right.$$

In consequence of (54) the first factor of the right hand product is either 1 or W^{-r}, and the last one is either 1 or W^{r}. Hence, by (50), the right hand member is an element of H.

We still have to supplement this result by a consideration of the cases $\sigma \equiv 0$ and $\sigma \equiv \varrho^{-1}$, which were excluded in the preceding computation. The two cases exclude each other. Assuming $\sigma \equiv \varrho^{-1}$, we get

$$(57')\quad \left\{\begin{aligned} Tk(\varrho,\varrho^{-1},\omega)\,T^{-1} &= TW^{\pi(\omega)} S^{\varrho^{-1}} T S^{\varrho} T S^{\varrho^{-1}} T S^{0} W^{-\pi(\omega+\tau(\varrho))}\,T \\ &= W^{-\pi(\omega)} T S^{\varrho^{-1}} T S^{\varrho} T S^{\varrho^{-1}} W^{\pi(\omega+\tau(\varrho))} \\ &= W^{-\pi(\omega)-\pi(-\omega)} k(\varrho^{-1},0,-\omega)\, W^{\pi(\omega+\tau(\varrho))+\pi(-\omega-\tau(\varrho))}. \end{aligned}\right.$$

Thus except for powers of W^{r} all the generators of the type $\sigma \equiv \varrho^{-1}$ are transformed by T into all generators of the type $\sigma \equiv 0$. Therefore the inverse is evidently also true. The explicit formula is

$$(57'')\quad Tk(\varrho,0,\omega)\,T^{-1} = W^{-\pi(\omega)-\pi(-\omega)} k(\varrho^{-1},\varrho,-\omega)\, W^{\pi(\omega+\tau(\varrho))+\pi(-\omega-\tau(\varrho))}.$$

We have thus proved that $THT^{-1} = H$.

In order to prove that $SHS^{-1} = H$ we start with generators of the following form:

$$k(r, r^{2\varkappa}, \varkappa) = W^{\pi(\varkappa)} S^{r^{2\varkappa}} TS^r TS^{-2} TS^{-r(rr^{2\varkappa}-1)} W^{-\pi(\varkappa+1)}$$

$$= W^{\pi(\varkappa)} S^{r^{2\varkappa}} WS^{-r^{2(\varkappa+1)}} W^{-\pi(\varkappa+1)}$$

(by (49), (1), (8), and (47)). We form their product for increasing values of $\varkappa$ from $\varkappa = 0$ to $\varkappa = n-1$ and denote this product by $\Psi(n)$:

$$\Psi(n) = k(r, r^{2\cdot 0}, 0)\, k(r, r^{2\cdot 1}, 1) \cdots k(r, r^{2(n-1)}, n-1), \quad n > 0, \tag{58}$$

and remark that $\Psi(0)$ means the empty product. We then get

$$\Psi(n) = SW^n S^{-r^{2n}} W^{-\pi(n)}$$

and from this we get some sort of commutation formula for S and W:

$$SW^n = \Psi(n)\, W^{\pi(n)} S^{r^{2n}}. \tag{59}$$

This is applied to

$$Sk(\varrho, \sigma, \omega) S^{-1} = SW^{\pi(\omega)} S^{\sigma} TS^{\varrho} TS^{\varrho^{-1}} TS^{-\varrho(\varrho\sigma-1)} W^{-\pi(\omega+\tau(\varrho))} S^{-1},$$

and we get for the first two factors of the right hand product

$$SW^{\pi(\omega)} = \Psi(\pi(\omega))\, W^{\pi(\omega)} S^{r^{2\omega}}$$

in consequence of (59), (53), and (55). Similarly, for the last two factors:

$$W^{-\pi(\omega+\tau(\varrho))} S^{-1} = \left[SW^{\pi(\omega+\tau(\varrho))} \right]^{-1} =$$

$$= \left[\Psi(\pi(\omega+\tau(\varrho)))\, W^{\pi(\omega+\tau(\varrho))} S^{r^{2(\omega+\tau(\varrho))}} \right]^{-1},$$

where we note that $r^{2\tau(\varrho)} = \varrho^2$ according to (2). Hence

$$Sk(\varrho, \sigma, \omega) S^{-1} = \Psi(\pi(\omega))\, W^{\pi(\omega)} S^{\sigma + r^{2\omega}} TS^{\varrho} TS^{\varrho^{-1}} TS^{-\varrho^2(\sigma + r^{2\omega}) + \varrho}$$
$$W^{-\pi(\omega+\tau(\varrho))} \Psi(\pi(\omega+\tau(\varrho)))^{-1}$$

$$= \Psi(\pi(\omega))\, k(\varrho, \sigma + r^{2\omega}, \omega)\, \Psi(\pi(\omega+\tau(\varrho)))^{-1}.$$

Since the Ψ's are elements of H defined by (58), this completes the proof of the invariance of H in F. The last formula together with (57), (57'), and (57'') states explicitly the elements of H into which the generators of H are transformed by the generators of F.

VIII.

Let M' denote the set of all matrices

$$(M') \qquad \begin{pmatrix} \alpha & \beta \\ \gamma & \delta \end{pmatrix}, \quad \begin{vmatrix} \alpha & \beta \\ \gamma & \delta \end{vmatrix} = 1,$$

with integer elements and determinant 1. This set M' forms a group by multiplication. The matrices

$$(M'') \qquad E = \begin{pmatrix} 1 & 0 \\ 0 & 1 \end{pmatrix}, \quad -E = \begin{pmatrix} -1 & 0 \\ 0 & -1 \end{pmatrix}$$

constitute a self-conjugate subgroup M'' of M'. The quotient group

$$(M) \qquad M = M'/M''$$

is the modular group, the group of all linear fractional substitutions with integer coefficients.

The (principal) *congruence subgroup modulo* q of M means the set C of elements of M represented by those matrices which modulo q are congruent to an element of M'':

$$(C) \qquad \begin{pmatrix} \alpha & \beta \\ \gamma & \delta \end{pmatrix} \equiv \pm E \text{ modulo } q.$$

It is immediately seen that this set C forms a group and, furthermore, that this group is self-conjugate in M.

Usually, the two matrices

$$S = \begin{pmatrix} 1 & 1 \\ 0 & 1 \end{pmatrix}, \quad T = \begin{pmatrix} 0 & -1 \\ 1 & 0 \end{pmatrix}$$

are taken as generators of M. Since

$$T^2 = -E, \quad (ST)^3 = -E,$$

they satisfy the relations

$$T^2 = 1, \quad (ST)^3 = 1 \tag{60}$$

as generators of M, and it is well known that (60) is a complete set of generational relations for M. Since

$$S^\beta = \begin{pmatrix} 1 & \beta \\ 0 & 1 \end{pmatrix},$$

all powers of S are different in M, but

$$S^q = \begin{pmatrix} 1 & q \\ 0 & 1 \end{pmatrix} = E \text{ modulo } q,$$

and hence S^q belongs to C. The same then is true of the transforms of S^q with arbitrary matrices m from M':

$$mS^q m^{-1} = \begin{pmatrix} \alpha & \beta \\ \gamma & \delta \end{pmatrix} \begin{pmatrix} 1 & q \\ 0 & 1 \end{pmatrix} \begin{pmatrix} \delta & -\beta \\ -\gamma & \alpha \end{pmatrix} = \begin{pmatrix} 1-\alpha\gamma q & \alpha^2 q \\ -\gamma^2 q & 1+\alpha\gamma q \end{pmatrix}. \tag{61}$$

Here α and γ range over all pairs of relatively prime integers, and the resulting matrix does not depend on β and δ.

We can now form a subgroup Q of C, namely the one generated by all elements (61). Evidently Q is self-conjugate in M (and thus also in C), and the quotient group M/Q is obtained by using S and T as generators and adding to the relations (60) of M the single relation

$$S^q = 1.$$

Thus M/Q is one-one isomorphic to the abstract group F of section V, and we write

$$M/Q = F. \tag{62}$$

We now take the modulus q to be a prime subject to the conditions of section I and use the notations introduced in the previous sections. It is remembered that all congruences are understood modulo q unless otherwise stated.

It turns out that (on account of the assumption $q > 5$) the group C contains more elements than its self-conjugate subgroup Q. We want to find a set of generators and generational relations for the quotient group C/Q and to establish the quotient group

of C in M, for which, by a well-known theorem of group theory, we have

$$M/C = \frac{M/Q}{C/Q}.$$

When speaking of matrices $\begin{pmatrix} \alpha & \beta \\ \gamma & \delta \end{pmatrix}$ as representatives of the quotient group M/C, the integers $\alpha, \beta, \gamma, \delta$ may be freely replaced by other members of their residue class modulo q and, moreover, the sign of all four numbers may be changed simultaneously. Under such operations the determinant remains $\equiv 1$ modulo q. We apply this to the following products:

$$S^r = \begin{pmatrix} 1 & r \\ 0 & 1 \end{pmatrix}$$

$$TS^r = \begin{pmatrix} 0 & -1 \\ 1 & r \end{pmatrix}$$

$$S^{-2} TS^r = \begin{pmatrix} -2 & -1-2r \\ 1 & r \end{pmatrix} \equiv \begin{pmatrix} -2 & 0 \\ 1 & r \end{pmatrix}$$

$$TS^{-2} TS^r \equiv \begin{pmatrix} -1 & -r \\ -2 & 0 \end{pmatrix}$$

$$S^r TS^{-2} TS^r \equiv \begin{pmatrix} -1-2r & -r \\ -2 & 0 \end{pmatrix} \equiv \begin{pmatrix} 0 & -r \\ -2 & 0 \end{pmatrix}$$

$$W = TS^r TS^{-2} TS^r \equiv \begin{pmatrix} 2 & 0 \\ 0 & -r \end{pmatrix} \equiv \begin{pmatrix} 2 & 0 \\ 0 & 2^{-1} \end{pmatrix}.$$

Thus modulo q we have for W a diagonal matrix as a representative matrix. For the powers of W we thus get

$$W^n \equiv \begin{pmatrix} 2^n & 0 \\ 0 & 2^{-n} \end{pmatrix},$$

and these are all different for $0 \leqq n < r$ in consequence of the assumption of section I that 2 belongs to r. For $n = r$, however,

$$W^r \equiv \pm E. \tag{63}$$

Thus W^r belongs to C, but no smaller power of W.

In the same way we want to find a matrix representing the product $k(\varrho, \sigma, \omega)$, defined by (49), and we get in turn:

$$S^{\sigma} = \begin{pmatrix} 1 & \sigma \\ 0 & 1 \end{pmatrix}$$

$$S^{\sigma}T = \begin{pmatrix} \sigma & -1 \\ 1 & 0 \end{pmatrix}$$

$$S^{\sigma}TS^{\varrho} = \begin{pmatrix} \sigma & \varrho\sigma - 1 \\ 1 & \varrho \end{pmatrix}$$

$$S^{\sigma}TS^{\varrho}T = \begin{pmatrix} \varrho\sigma - 1 & -\sigma \\ \varrho & -1 \end{pmatrix}$$

$$S^{\sigma}TS^{\varrho}TS^{\varrho^{-1}} \equiv \begin{pmatrix} \varrho\sigma - 1 & -\varrho^{-1} \\ \varrho & 0 \end{pmatrix}$$

$$S^{\sigma}TS^{\varrho}TS^{\varrho^{-1}}T \equiv \begin{pmatrix} -\varrho^{-1} & -\varrho\sigma + 1 \\ 0 & -\varrho \end{pmatrix}$$

$$S^{\sigma}TS^{\varrho}TS^{\varrho^{-1}}TS^{-\varrho(\varrho\sigma-1)} \equiv \begin{pmatrix} -\varrho^{-1} & 0 \\ 0 & -\varrho \end{pmatrix}. \tag{64}$$

Now $k(\varrho, \sigma, \omega)$ arises if we apply the factors $W^{\pi(\omega)}$ in front and $W^{-\pi(\omega+\tau(\varrho))}$ in the rear of (64). But since both W and the element (64) are represented by diagonal matrices when considered as elements of M/C, they are interchangeable, and we therefore multiply (64) by $W^{\pi(\omega)-\pi(\omega+\tau(\varrho))}$. Now

$$\pi(\omega) - \pi(\omega + \tau(\varrho)) \equiv -\tau(\varrho) \text{ modulo } r.$$

Hence, in virtue of (63), we only have to multiply (64) by

$$W^{-\tau(\varrho)} \equiv \begin{pmatrix} 2^{-\tau(\varrho)} & 0 \\ 0 & 2^{\tau(\varrho)} \end{pmatrix} \equiv \begin{pmatrix} (-r)^{\tau(\varrho)} & 0 \\ 0 & (-r)^{-\tau(\varrho)} \end{pmatrix} \equiv \begin{pmatrix} \pm\varrho & 0 \\ 0 & \pm\varrho^{-1} \end{pmatrix}$$

in consequence of (1) and (3). In both places we have the positive sign, or in both places the negative sign. We hereby get

$$k(\varrho, \sigma, \omega) \equiv \pm E. \tag{65}$$

The $k(\varrho, \sigma, \omega)$ are by their definition products of S and T. (65) shows that they belong to C. Together with the generators (61) they generate a certain subgroup C' of C. For this we have

$$M/C' = \frac{M/Q}{C'/Q} = \frac{F}{H}$$

by (62) and the fact that the $k(\varrho, \sigma, \omega)$ generate H when they are considered as elements of F. Thus the index of C' in M is equal to the index j of H in F, which was found in (51).

On the other hand, the index of C in M may be easily established: In a matrix $\begin{pmatrix} \alpha & \beta \\ \gamma & \delta \end{pmatrix}$ of M' the elements α and β cannot both be divisible by q. But take any two numbers α_0 and β_0 which are not both $\equiv 0$ modulo q. Then two numbers a and b exist such that $\alpha = \alpha_0 + aq$ and $\beta = \beta_0 + bq$ are relatively prime. Let γ_0 and δ_0 be so chosen that $\alpha\delta_0 - \beta\gamma_0 = 1$. Then the relation $\alpha\delta - \beta\gamma = 1$ holds for $\gamma = \gamma_0 + v\alpha$, $\delta = \delta_0 + v\beta$ with arbitrary values for v. The choice of residue classes modulo q for α_0 and β_0 admits $q^2 - 1$ combinations. For each of them there are q possible choices of the class of v. Since at least one of α and β are $\not\equiv 0$, the choice of v implies q different residue classes for at least one of the numbers γ and δ. Thus, in all, the matrices fall into $q(q^2-1)$ residue classes modulo q. Taking the simultaneous change of sign for all elements of a matrix into consideration, this corresponds to $\frac{1}{2} q(q^2-1)$ different representative matrices for the elements of M/C. Since this number coincides with the value j in (51), and since C' is known to be a subgroup of C, we infer that $C' = C$.

We can thus generate the congruence subgroup modulo q of M by taking the generators (61) and (65) together. This system reduces to a finite system of generators for C by the matrix m in (61) being made to range over a suitable set of j matrices which are mutually non-congruent modulo q. The usual point of interest is not so much C as $C/Q = H$. This group then is generated by elements $k(\varrho, \sigma, \omega)$, $\varrho \not\equiv 0$, with (29), (32), (34), and (35) as generational relations. The quotient group of C in M, which is at the same time the quotient group of H in F, has S and T as generators, and a system of defining relations is obtained by adding the relations $k(\varrho, \sigma, \omega) = 1$ expressed in S and T to the relations (42), (43), and (44) of F.

This system of relations is, of course, capable of abundant reduction, and no attempt is made here to reduce it to simple forms. It is for instance well known[1] that in the special case of $q = 7$ the step from F to F/H can be carried out by adding one single relation to the relations of F, namely the relation $(S^4 T)^4 = 1$.

[1] See Burnside, *Theory of Groups of Finite Order*, p. 422.

Note.

After the preceding study had been sent to the printer, it came to my knowledge that Mr. HERMANN FRASCH had, in vol. 108 of the *Mathematische Annalen* in 1933, published an article *Die Erzeugung der Hauptkongruenzgruppen für Primzahlstufen*, which had escaped my attention. On examining this earlier article I found a rather far-reaching consonance with my own investigations especially concerning the arithmetical formalism, which I had treated explicitly beforehand in section II, but which is contained implicitly in Frasch's development, and also concerning the choice of generators $k(\varrho, \sigma, \omega)$, which correspond to the $U_{\lambda, \mu, \nu, T}$ in Frasch's notation, and therefore also the relations between these generators. Moreover, Frasch goes into the question of the reduction of this system of relations, which I leave aside.

If, nevertheless, I maintain the publication of my investigations unaltered, I do so on the ground that the chief means of research is different in the two papers. Frasch bases his work on the powerful method of REIDEMEISTER and SCHREIER for the abstract characterization of subgroups of given abstract groups contained in vol. V of the *Abhandlungen aus dem mathematischen Seminar der Hamburgischen Universität.* (By the way, this method would not be necessary for the establishment of a system of generators, since such a system follows directly from formula (9) on page 231 of Frasch's paper). On the other hand, my treatment is based on the most elementary notions of two-dimensional topology without recurrence to Reidemeister and Schreier's method. Upon comparing these two ways of approach I found that they throw some light on each other and that this might justify what could otherwise be called a re-publication of results. For instance, the choice of the $h(\omega)$ and $h(\sigma, \omega)$ in section IV can be taken as an illustration of Schreier's condition (F). The establishment of a complete system of generational relations by simple considerations of surface topology must, in each special case, be simpler than the general mechanism of the Reidemeister-Schreier method, which leads Frasch to rather elaborate calculations. But I am pleased to call attention to Frasch's interesting use of this method, following an earlier paper by Rademacher, the more so as his section 7 hints at more general applications and even touches on the illustration by means of surface topology.

Indleveret til selskabet den 13. december 1949.
Færdig fra trykkeriet den 30. marts 1950.

DET KGL. DANSKE VIDENSKABERNES SELSKAB
MATEMATISK-FYSISKE MEDDELELSER, BIND XXV, NR. 19

A PROOF OF THE SIMPLER PONTRJAGIN DUALITY THEOREMS BY HELP OF THE CONNECTION BETWEEN TWO INFINITE-DIMENSIONAL SPACES

BY

ERLING FØLNER

KØBENHAVN
I KOMMISSION HOS EJNAR MUNKSGAARD
1950

Printed in Denmark
Bianco Lunos Bogtrykkeri

1. Two infinite-dimensional spaces, $\mathfrak{R}^\infty$ and $\mathfrak{R}_\infty$.

In a paper by H. BOHR and the author [1]—and more detailed in [2]—a connection between two infinite-dimensional spaces was established. We shall state explicitly those of the results which will be used in the sequel.

The space $\mathfrak{R}^\infty$ consists of all points $\boldsymbol{x} = (x_1, x_2, \cdots)$ with a countable number of coordinates which are arbitrary real numbers. The convergence notion in $\mathfrak{R}^\infty$ is defined by convergence in each of the coordinates, i. e. $(x_1^n, x_2^n, \cdots) \to (x_1, x_2, \cdots)$ if $x_1^n \to x_1, x_2^n \to x_2, \cdots$. This convergence notion arises from a topology defined by help of neighborhoods $U_{N,\varepsilon}$ of $(0, 0, \cdots)$ where $U_{N,\varepsilon}$ (N positive integer, $\varepsilon > 0$) consists of all $\boldsymbol{x} = (x_1, x_2, \cdots)$ with $|x_i| < \varepsilon$ for $i = 1, 2, \cdots, N$.

The space $\mathfrak{R}_\infty$ consists of all points $\boldsymbol{a} = (a_1, a_2, \cdots)$ with a countable number of real coordinates, but so that they are all zero from a certain step (depending on the point), i. e. $a_n = 0$ for $n \geq N = N(\boldsymbol{a})$. By the topology chosen in $\mathfrak{R}_\infty$—we need not state it here—the module of integral points in $\mathfrak{R}_\infty$, i. e. the points with mere integral coordinates, is discrete.

For an arbitrary closed module M in $\mathfrak{R}^\infty$ we define its *dual module* M' in $\mathfrak{R}_\infty$ as the set of points $\boldsymbol{a}$ in $\mathfrak{R}_\infty$ for which

$$\boldsymbol{a} \cdot \boldsymbol{x} = a_1 x_1 + a_2 x_2 + \cdots \equiv 0 \pmod 1 \text{ for every } \boldsymbol{x} \in M.$$

It is a closed module in $\mathfrak{R}_\infty$ (in the topology only referred to). We also introduce the analogous definition when M is a closed module in $\mathfrak{R}_\infty$.

By a *substitution* $\boldsymbol{x} = T\boldsymbol{y}$ in $\mathfrak{R}^\infty$ we understand a linear transformation of the form

$$\begin{aligned} x_1 &= a_{11} y_1 + a_{12} y_2 + \cdots + a_{1p_1} y_{p_1} \\ x_2 &= a_{21} y_1 + a_{22} y_2 + \cdots + a_{2p_2} y_{p_2} \\ &\cdots\cdots\cdots\cdots\cdots\cdots\cdots\cdots \end{aligned}$$

which establishes a one-to-one mapping of $\mathfrak{R}^\infty$ on (the whole) $\mathfrak{R}^\infty$. It turns out to be the same as a linear, one-to-one, bicontinuous transformation of $\mathfrak{R}^\infty$ onto itself.

The following theorems were proved.

Theorem A. *A closed module in the infinite-dimensional space* $\mathfrak{R}^\infty$ *is a point set* E *which by a substitution can be transformed into a point set of a special form, in the following denoted by* S^∞, *namely a point set* $\{(y_1, y_2, \cdots)\}$ *of the following structure: The indices* $1, 2, \cdots, n, \cdots$ *can be divided into three fixed classes* $\{n_r\}, \{n_s\}, \{n_t\}$, *such that the coordinates* y_{n_r} *independently run through all numbers, and the coordinates* y_{n_s} *independently run through all integers, while all the remaining coordinates* y_{n_t} *are constantly zero. Conversely, each such point set* E *is a closed module.*

Theorem B. *If* M *is a closed module in* $\mathfrak{R}^\infty$ *or in* $\mathfrak{R}_\infty$, *then the dual module* M'' *of its dual module* M' *is the module* M *itself, i. e.*

$$M'' = M.$$

2. The Pontrjagin—van Kampen duality theorems.

Let G be a locally compact abelian group satisfying the second axiom of countability. We use the additive notation for the group. By a continuous character on G we understand (cp. [4], p. 127) a real multi-valued function $\alpha(x)$ uniquely defined modulo 1 on G with the properties

1. $\alpha(x+y) = \alpha(x) + \alpha(y) \pmod 1$.

2. To every $\varepsilon > 0$ can be found a neighborhood U of 0 such that $|\alpha(x)| < \varepsilon \pmod 1$ for $x \in U$.

We organize the set of continuous characters on G so that it becomes a topological group. The sum $(\alpha_1 + \alpha_2)(x)$ of two characters $\alpha_1(x)$ and $\alpha_2(x)$ is defined by $(\alpha_1 + \alpha_2)(x) = \alpha_1(x) + \alpha_2(x)$. With this addition the characters form a group. The zero-element is the character $\alpha(x) = 0$. Corresponding to every $\varepsilon > 0$ and every compact set F in G we define a neighborhood of the zero-character as the set of characters $\alpha(x)$ satisfying

$$|\alpha(x)| < \varepsilon \pmod 1 \text{ for } x \in F.$$

In this way the group of characters becomes a topological group. We call it the character group of G and denote it by $\hat{G}$.

Pontrjagin ([4], p. 128) showed that $\hat{G}$ is also a locally compact group satisfying the second axiom of countability, and furthermore he proved the following two fundamental theorems[1].

Theorem 1. *For a group G of the type mentioned the character group $\hat{\hat{G}}$ of the character group $\hat{G}$ is isomorphic with the group G itself, i. e.*

$$\hat{\hat{G}} \simeq G.$$

The isomorphism between $\hat{\hat{G}}$ and G is realised in the natural way that the element $x \in G$ corresponds to the character $\chi(\alpha) = \alpha(x)$ on $\hat{G}$.

Theorem 2. *Let H be a subgroup of a group G of the type mentioned. If H^* denotes the set of characters on G which are $= 0$ on H, and analogously H^{**} denotes the set of characters on $\hat{G}$ which are $= 0$ on H^* then the set H^{**} by the identification of $\hat{\hat{G}}$ with G is identical with the set H, i. e.*

$$H^{**} = H.$$

The purpose of this paper is to prove the following special case of these theorems by help of the connection between the spaces $\mathfrak{R}^\infty$ and $\mathfrak{R}_\infty$.

Simpler Pontrjagin duality theorems. *For compact and for discrete abelian groups satisfying the second axiom of countability the theorems 1 and 2 are valid. By the operation of passing to the character group, a group of one of the two types is transformed into a group of the other type.*

A group of the first type is in the sequel abbreviatively referred to as a compact group. A group of the second type, i. e. a countable discrete abelian group, is referred to as a discrete group.

By help of these simpler duality theorems and an investigation of the structure of locally compact groups, Pontrjagin and van Kampen obtained the theorems 1 and 2 in the general case.

[1] In this full generality first by van Kampen ([4], p. 126).

3. A realization of a compact group as a factor group inside $\mathfrak{R}^\infty$.

In this section we shall prove a theorem about a concrete way of realizing every compact group. For theorems used in the proof we shall, as before, refer the reader to [4].

Theorem. *Every compact group G is isomorphic to a factor group M/I where I is the module of integral points in $\mathfrak{R}^\infty$ and M is a closed module in $\mathfrak{R}^\infty$ containing I. The topology of M/I is given in the natural way by help of the topology in $\mathfrak{R}^\infty$. Conversely, every factor group M/I of the type mentioned, is a compact group.*

For the proof we take our starting point in the following theorem ([4], p. 46):

Urysohn's lemma. *Let R be a compact regular topological space satisfying the second axiom of countability, and let E and F be two of its non-intersecting closed subsets. Then there exists a continuous function $f(x)$ defined on R such that $0 \leq f(x) \leq 1$ for $x \in R$, $f(x) = 0$ for $x \in E$, and $f(x) = 1$ for $x \in F$.*

Now, let E be a single point a in R and take a countable complete system of neighborhoods of a: $U_1, U_2, \cdots$. For F successively equal to $R - U_1, R - U_2, \cdots$ we construct by Urysohn's lemma the functions $f_1(x), f_2(x), \cdots$. The function

$$g(x) = \sum_{n=1}^{\infty}{}' \frac{f_n(x)}{n^2}$$

is then a continuous function on R with $g(a) = 0$ and $g(x) > 0$ for $x \neq a$.

We may apply this to the compact group G above since the underlying space of a topological group is always regular ([4], p. 56). Let a be chosen as the zero of the group. In this way we get a continuous function $g(x)$ on G with $g(0) = 0$, $g(x) > 0$ for $x \neq 0$.

As a *continuous function on a compact group*, $g(x)$ is uniformly continuous and hence also *almost periodic*. Thus $g(x)$ is a *continuous almost periodic function* on G. We shall use the *unicity theorem* for Fourier series of continuous almost periodic functions

on a topological abelian group. Concerning the fact that we use such a deep-lying theorem we may remark that the main result of the Peter-Weyl theory on continuous functions on compact abelian groups, viz. the possibility of approximating every continuous function on the group by a linear combination of functions $e^{2\pi i\alpha(x)}$, is at the bottom of all proofs of the duality theorems. For a proof of the main results in the theory of almost periodic functions on an abelian group which utilizes the abelian type of the group, see my paper [3]. There no topology was considered, but it is a well-known and obvious fact that if such a topology exists and the almost periodic function $f(x)$ is continuous, then the characters in its Fourier series are all continuous since $C_n e^{2\pi i\alpha_n(x)} = \underset{t}{M}\{f(x-t)e^{2\pi i\alpha_n(t)}\}$ where $f(x)$ is uniformly continuous.

Let our function $g(x)$ above have the Fourier series

$$g(x) \sim \sum_{n=1}^{\infty} C_n e^{2\pi i\alpha_n(x)}.$$

To the arbitrary element h in G we consider the translated function

$$g(x+h) \sim \sum_{n=1}^{\infty} C_n e^{2\pi i\alpha_n(h)} e^{2\pi i\alpha_n(x)}.$$

If $\alpha_n(h) = 0$ for $n = 1, 2, \cdots$, then h must be equal to 0, for on account of the unicity theorem $g(x+h) = g(x)$, in particular $g(h) = g(0) = 0$.

We now map the arbitrary element $h \varepsilon G$ in the points $(\alpha_1(h), \alpha_2(h), \cdots)$ in $\mathfrak{R}^\infty$; these points form a coset in $\mathfrak{R}^\infty$ modulo the integral module I, i. e. an element in $\mathfrak{R}^\infty/I$. Let the image of G in $\mathfrak{R}^\infty$ be (the module) M. Then, G considered as an abstract group is mapped isomorphically on M/I considered as an abstract group. Moreover, this mapping of the topological group G is continuous when the topology in $\mathfrak{R}^\infty/I$ is given in the natural way by the topology in $\mathfrak{R}^\infty$. Since G is compact and M/I is a regular topological space satisfying the second axiom of countability, the mapping is bicontinuous ([4], p. 44). Hence we have an isomorphic mapping of the topological group G on the togological group M/I,

$$G \simeq M/I.$$

As the image of a compact space by a continuous mapping, M/I is closed in $\mathfrak{R}^\infty/I$. This implies that the image M of G in $\mathfrak{R}^\infty$ is closed in $\mathfrak{R}^\infty$ (since otherwise we could choose a sequence in M converging to a point not in M, and the corresponding sequence in M/I would then converge to the corresponding point in $\mathfrak{R}^\infty/I$, a point outside of M/I). Hence M, in the realization of G above, is a closed module in $\mathfrak{R}^\infty$.

Conversely, every factor group M/I, where M is a closed module in $\mathfrak{R}^\infty$ containing the integral module I, is a compact group since a sequence of points in M can be reduced modulo 1 to lie in the compact set $0 \leq x_1 \leq 1, 0 \leq x_2 \leq 1, \cdots$ (the second axiom of countability being obviously fulfilled).

4. Proof of the simpler duality theorems.

Let G be a compact group. We make use of the theorem of the preceding section which states that we can realize G as a factor group M/I inside $\mathfrak{R}^\infty$. By help of this we shall see that the character group $\widehat{G}$ can be realized as a factor group inside $\mathfrak{R}_\infty$.

Let $\alpha(X)$ be a continuous character on M/I where X is a variable coset in M modulo I. We put $\alpha(\boldsymbol{x}) = \alpha(X)$ for every $\boldsymbol{x} \varepsilon X$. In this way we get a continuous character $\alpha(\boldsymbol{x})$ on M. Our first task is to show that

$$\alpha(\boldsymbol{x}) = \boldsymbol{a} \cdot \boldsymbol{x} \text{ where } \boldsymbol{a} \varepsilon \mathfrak{R}_\infty.$$

To see this we choose by theorem **A** a substitution $\boldsymbol{x} = T\boldsymbol{y}$ in $\mathfrak{R}^\infty$ which transforms M into a module $\{(y_1, y_2, \cdots)\}$ of the simple form S^∞. Since M contains I, the class $\{n_i\}$ from theorem A must be empty. By this substitution the continuous character $\alpha(\boldsymbol{x})$ on M is transformed into a continuous character $\beta(\boldsymbol{y}) = \alpha(T\boldsymbol{y})$ on the transformed module $\{(y_1, y_2, \cdots)\} = \{(\text{arbitrary, integral})\}$. Now, let

$$\beta(y_1, 0, 0, \cdots) = b_1 y_1$$
$$\beta(0, y_2, 0, \cdots) = b_2 y_2$$
$$\cdots\cdots\cdots\cdots\cdots\cdots$$

where in case y_n is of "integral" type we may assume b_n reduced modulo 1 to lie in the interval $0 \leq b < 1$. (It has been used here that a continuous character $\gamma(x)$ on the straight line, and on the integers, has the form $\gamma(x) = bx$.) Then

$$\beta(y_1, y_2, \cdots, y_n, 0, 0, \cdots) = b_1 y_1 + b_2 y_2 + \cdots + b_n y_n,$$

but for $n \to \infty$

$$(y_1, y_2, \cdots, y_n, 0, 0, \cdots) \to (y_1, y_2, \cdots)$$

and hence from the continuity of β the sequence

$$b_1 y_1 + b_2 y_2 + \cdots + b_n y_n \tag{1}$$

shall converge modulo 1 for every $(y_1, y_2, \cdots)$ from the transformed module.

Suppose now that b_n was not $= 0$ for $n \geq$ a certain N. Then there would exist a sequence $n_1 < n_2 < \cdots$ such that $b_{n_p} \neq 0$ for $p = 1, 2, \cdots$. To obtain a contradiction we shall indicate a point from the transformed module such that the sequence (1) is not convergent modulo 1. We put $y_n = 0$ if $b_n = 0$. For the n with $b_n \neq 0$, i. e. $n_1, n_2, \cdots$ we choose y_n by induction. y_{n_1} is chosen in accordance with its type (arbitrary or integral). Suppose y_{n_p} chosen. Then we shall determine $y_{n_{p+1}}$ such that the numerical difference modulo 1 between

$$b_{n_1} y_{n_1} + b_{n_2} y_{n_2} + \cdots + b_{n_p} y_{n_p} \tag{2}$$

and

$$b_{n_1} y_{n_1} + b_{n_2} y_{n_2} + \cdots + b_{n_p} y_{n_p} + b_{n_{p+1}} y_{n_{p+1}}$$

is $\geq \frac{1}{4}$, i. e. such that

$$\left| b_{n_{p+1}} y_{n_{p+1}} \right| \geq \frac{1}{4} \pmod 1. \tag{3}$$

If $y_{n_{p+1}}$ is of the "arbitrary" type we only choose $y_{n_{p+1}}$ such that $b_{n_{p+1}} y_{n_{p+1}} = \frac{1}{2}$ which satisfies (3). If $y_{n_{p+1}}$ is of the "integral" type we write $b_{n_{p+1}}$, which is lying in the interval $0 < b < 1$, as a dyadic fraction. Since not all ciphers after the

"point" in the fraction are zero or one we may choose $y_{n_{p+1}}$ as a power of 2 such that the first ciphers after the "point" in $b_{n_{p+1}} y_{n_{p+1}}$ are 01 or 10. Then $b_{n_{p+1}} y_{n_{p+1}}$ reduced modulo 1 to the interval $0 \leq b < 1$ must in the first case lie in the interval $\frac{1}{4} \leq b < \frac{1}{2}$ and in the second case in the interval $\frac{1}{2} < b \leq \frac{3}{4}$. In both cases (3) is satisfied.

For this choice of the point $(y_1, y_2, \cdots)$ from the transformed module it is obvious that (1) cannot converge modulo 1 since the distance modulo 1 between consecutive elements in the subsequence (2) is always $\geq \frac{1}{4}$.

Thus we have seen that

$$\beta(\boldsymbol{y}) = \alpha(T\boldsymbol{y}) = \boldsymbol{b} \cdot \boldsymbol{y} \text{ with } \boldsymbol{b} \in \mathfrak{R}_\infty,$$

and then

$$\alpha(\boldsymbol{x}) = \beta(T^{-1}\boldsymbol{x}) = \boldsymbol{b} \cdot T^{-1}\boldsymbol{x} = \boldsymbol{a} \cdot \boldsymbol{x} \text{ with } \boldsymbol{a} \in \mathfrak{R}_\infty$$

where $\boldsymbol{a}$ is determined by $\boldsymbol{b} \cdot T^{-1}\boldsymbol{x} = \boldsymbol{a} \cdot \boldsymbol{x}$.

On the other hand every function $\alpha(\boldsymbol{x}) = \boldsymbol{a} \cdot \boldsymbol{x}$ with $\boldsymbol{a} \in \mathfrak{R}_\infty$ obviously is a continuous character on M. But in order that it has arisen from a (continuous) character on M/I a necessary and sufficient condition is that

$$\alpha(\boldsymbol{x}) = \boldsymbol{a} \cdot \boldsymbol{x} = 0 \text{ for } \boldsymbol{x} \in I$$

and this means $\boldsymbol{a} \in I'$ where I' is the dual module in $\mathfrak{R}_\infty$ of I, i. e. the module of integral points in $\mathfrak{R}_\infty$ (see 1). Now, however, different $\boldsymbol{a}$'s in I' may determine the same character on M, in fact

$$\boldsymbol{a}_1 \cdot \boldsymbol{x} = \boldsymbol{a}_2 \cdot \boldsymbol{x} \text{ for } \boldsymbol{x} \in M$$

means $\boldsymbol{a}_1 - \boldsymbol{a}_2 \in M'$ where M' is the dual module in $\mathfrak{R}_\infty$ of M (see 1).

Hence, considered as abstract groups, the character group of M/I and the group I'/M' are isomorphic. Furthermore the arbitrary continuous character $\alpha(X)$ on M/I is

$$\alpha(X) = A \cdot X \text{ with } A \in I'/M' \quad (X \in M/I)$$

(the product $A \cdot X$ being defined by help of representatives $\boldsymbol{a}$ and $\boldsymbol{x}$ of A and X).

The topology which is ascribed to the group I'/M' in $\mathfrak{R}_\infty$ is the discrete one since already I' is discrete (see 1). This, however, is also the topology ascribed to it as the character group of a compact group, for if in $\widehat{G}$ we consider the neighborhood of the zero-character determined by $F = G$ and $\varepsilon = \frac{1}{4}$ it consists of the characters α with

$$|\alpha(x)| < \frac{1}{4} \pmod 1 \text{ for } x \in G,$$

and the zero-character is the only such character. In fact, if $\alpha(x') \not\equiv 0$ for an element $x' \in G$ we could find a power 2^N of 2 such that $|\alpha(2^N x')| \geq \frac{1}{4} \pmod 1$ (see top of p. 10).

Hence we have the result that the character group of $G \simeq M/I$ is

$$\boxed{\widehat{G} \simeq I'/M'.}$$

To prove theorem 1 for a compact group G we have to prove that the character group of I'/M' is isomorphic to M/I by the correspondence mentioned in theorem 1. Let $\chi(A)$ be a (continuous) character[1] on I'/M'. For every $\boldsymbol{a} \in A$ we put $\chi(\boldsymbol{a}) = \chi(A)$. Then $\chi(\boldsymbol{a})$ is a character on I'. Assume that

$$\begin{aligned} \chi(1, 0, 0, \cdots) &= x_1 \\ \chi(0, 1, 0, \cdots) &= x_2 \\ &\cdots\cdots\cdots\cdots\cdots. \end{aligned}$$

Then obviously

$$\chi(\boldsymbol{a}) = \boldsymbol{x} \cdot \boldsymbol{a} \text{ with } \boldsymbol{x} = (x_1, x_2, \cdots) \in \mathfrak{R}^\infty.$$

On the other hand every function $\chi(\boldsymbol{a}) = \boldsymbol{x} \cdot \boldsymbol{a}$ with $\boldsymbol{x} \in \mathfrak{R}^\infty$ is a character on I'. But in order that it arises from a character on I'/M' a necessary and sufficient condition is that

$$\chi(\boldsymbol{a}) = \boldsymbol{x} \cdot \boldsymbol{a} = 0 \text{ for } \boldsymbol{a} \in M'$$

which by theorem B means that $\boldsymbol{x} \in M'' = M$. Now, however, different $\boldsymbol{x}$'s in M may determine the same character on I', in fact

$$\boldsymbol{x}_1 \cdot \boldsymbol{a} = \boldsymbol{x}_2 \cdot \boldsymbol{a} \text{ for } \boldsymbol{a} \in I'$$

means $\boldsymbol{x}_1 - \boldsymbol{x}_2 \in I'' = I$.

[1] They are all continuous since the group is discrete.

Hence, considered as abstract groups, the character group of I'/M' and the group M/I are isomorphic. Furthermore an arbitrary character $\chi(A)$ on I'/M' has the form

$$\chi(A) = X \cdot A \text{ with } X \in M/I \ (A \in I'/M').$$

We shall now see that the topology of M/I considered as a character group of I'/M' coincides with the topology of M/I induced by the topology in $\mathfrak{R}^\infty$.

In the first topology a neighborhood of zero is determined by an $\varepsilon > 0$ and a compact set F from I'/M', and since I'/M' is discrete F consists of a finite number of elements $A_1, A_2, \cdots, A_N$ from I'/M'. The neighborhood consists of all $X \in M/I$ with

$$|X \cdot A_n| < \varepsilon \pmod 1, \quad n = 1, 2, \cdots, N. \tag{4}$$

We now consider an arbitrary neighborhood of zero in the other topology. It consists of the $X \in M/I$ for which a representative $\boldsymbol{x} = (x_1, x_2, \cdots)$ satisfies

$$\begin{aligned} &|x_1| < \varepsilon \pmod 1 \\ &|x_2| < \varepsilon \pmod 1 \\ &\cdots\cdots\cdots\cdots \\ &|x_N| < \varepsilon \pmod 1 \end{aligned} \tag{5}$$

where $\varepsilon > 0$, and N is a positive integer. In order to find a neighborhood (4) in the first topology contained in this neighborhood (5) we use the same ε and N in (4) as in (5) and choose for $A_1, A_2, \cdots, A_N$ the (not necessarily different) cosets with the respective representatives $(1, 0, 0, \cdots)$, $(0, 1, 0, \cdots)$, $\cdots$, $(0, 0, 0, \cdots, 0, 1, 0, 0, \cdots)$. In fact, for this choice the neighborhood (4) will coincide with (5).

Conversely, given an arbitrary neighborhood (4) it is possible to choose ε and N in (5) such that the neighborhood (5) is contained in the neighborhood (4). This is true since the A_n have integral $\boldsymbol{a}_n$ as representatives in $\mathfrak{R}_\infty$.

Hence the two topologies are equivalent, and we have the result that the correspondence from theorem 1 is an isomorphism

$$\boxed{\hat{\hat{G}} \simeq G.}$$

This proves theorem 1 for a compact group G.

Theorem 1 for the case of a discrete group which is written in the form $\hat{G}$ where G is compact, follows from the result above. In order to prove theorem 1 for an arbitrary discrete group it is therefore enough to prove that every such group is the character group of a compact group, a fact which is also stated in the "simpler theorems" on p. 5. This is easily done. Let G be an arbitrary countable discrete group. We choose a system of generators $a_1, a_2, \cdots$ of G (for instance all elements in G). An arbitrary element $a \in G$ may be written

$$a = a_1^{n_1} a_2^{n_2} \cdots. \tag{6}$$

We map a in the set of integral points $(n_1, n_2, \cdots)$ of $\mathfrak{R}_\infty$ for which (6) holds good. Let 0 by this procedure be mapped in the module M_1. Then obviously

$$G \simeq I'/M_1.$$

Hence, from the result on p. 11 and theorem B, the group G is the character group of the compact group M_1'/I.

This proves theorem 1 for compact and discrete groups.

We now pass to the proof of theorem 2 for compact and discrete groups. Let G be a compact group and H a subgroup. By the isomorphism

$$G \simeq M/I$$

the set H corresponds to the set N/I where N is a closed module in $\mathfrak{R}^\infty$, $I \subseteq N \subseteq M$. As found on pp. 10—11, the character group of M/I is I'/M' and an arbitrary continuous character $\alpha(X)$ on M/I is of the form

$$\alpha(X) = A \cdot X \quad (A \in I'/M', X \in M/I).$$

We shall now pick out the characters which are $= 0$ on N/I, i. e. for which

$$A \cdot X = 0 \text{ for } X \in N/I,$$

but this means (by the definition of dual module, p. 3) that the A's from I'/M' shall be taken from the subset N'/M'.

We repeat the procedure. As found on p. 12, an arbitrary character $\chi(A)$ on I'/M' has the form

$$\chi(A) = X \cdot A \quad (X \in M/I,\ A \in I'/M'),$$

and we have to pick out the characters which are $= 0$ on N'/M', i. e. for which

$$X \cdot A = 0 \text{ for } A \in N'/M',$$

but this means (by the definition of dual module, p. 3) that the X's from M/I shall be taken from the subset N''/I which by theorem B is equal to N/I, q. e. d.

Since $\widehat{G} \simeq I'/M'$ is an *arbitrary* discrete group and $H^* \simeq N'/M'$ is an *arbitrary* subgroup of $\widehat{G} \simeq I'/M'$, the theorem 2 is also proved for a discrete group.

References.

[1] H. Bohr and E. Følner: Infinite systems of linear congruences with infinitely many variables. D. Kgl. Danske Vidensk. Selskab. Mat.-fys. Medd. XXIV, 12 (1948).

[2] H. Bohr and E. Følner: On a structure theorem for closed modules in an infinite-dimensional space. Courant Anniversary Volume 1948, pp. 45—62.

[3] E. Følner: A proof of the main theorem for almost periodic functions in an abelian group. Annals of Mathematics, Vol. 50, pp. 559—569 (1949).

[4] L. Pontrjagin: Topological groups. Princeton University Press. 1946.

Indleveret til selskabet den 12. september 1949.
Færdig fra trykkeriet den 22. marts 1950.

DET KGL. DANSKE VIDENSKABERNES SELSKAB
MATEMATISK-FYSISKE MEDDELELSER, BIND XXV, NR. 20

A THEOREM ON THE MEAN MOTIONS OF ALMOST PERIODIC FUNCTIONS

BY

HANS TORNEHAVE

KØBENHAVN
I KOMMISSION HOS EJNAR MUNKSGAARD
1950

Printed in Denmark
Bianco Lunos Bogtrykkeri

INTRODUCTION

Let $f(t)$, $-\infty < t < \infty$ be a complex-valued almost periodic function satisfying a condition $|f(t)| \geqq k > 0$, and let arg $f(t)$ denote a continuous argument of $f(t)$. According to a theorem by H. BOHR[1] we have

$$\arg f(t) = ct + g(t)$$

where c is a real constant and $g(t)$ is an almost periodic function. The constant c is called the mean motion of $f(t)$.

The mean motion is unchanged if $f(t)$ is multiplied by an arbitrary complex constant. The function $\frac{1}{f(t)}$ will have the mean motion $-c$. If we have a relation $f(t) = f_1(t) f_2(t)$, where $f_1(t)$ and $f_2(t)$ are almost periodic functions satisfying the conditions $|f_1(t)| \geqq k > 0$, $|f_2(t)| \geqq k > 0$, then $c = c_1 + c_2$, where c_1 and c_2 are the mean motions of $f_1(t)$ and $f_2(t)$.

These trivial examples suggest that a relation between almost periodic functions $f_1(t), \cdots, f_n(t)$, where $|f_\nu(t)| \geqq k > 0$, may imply a relation between the corresponding mean motions $c_1, \cdots, c_n$.

The first not trivial result in this direction was proved by B. JESSEN[2] and we shall state his theorem in the following form:

If $f_1(t)$ and $f_2(t)$ are almost periodic functions satisfying the conditions $|f_1(t)| \geqq k > 0$, $|f_2(t)| \geqq k > 0$, and further satisfying a linear relation

$$\alpha_1 f_1(t) + \alpha_2 f_2(t) = \beta,$$

[1] H. BOHR: Kleinere Beiträge zur Theorie der fastperiodischen Funktionen 1. D. Kgl. Danske Vidensk. Selskab, Mat.-fys. Medd. X 10 (1930). Über fastperiodische ebene Bewegungen. Comment. math. helv. 4 (1932).

[2] B. JESSEN: Über die Säkularkonstanten einer fastperiodischen Funktion. Math. Ann. 111 (1935).

where α_1 and α_2 are $\neq 0$, then the corresponding mean motions c_1 and c_2 will satisfy a relation

$$r_1 c_1 + r_2 c_2 = 0,$$

where r_1 and r_2 are rational numbers and $(r_1, r_2) \neq (0, 0)$.

The author[1] has recently proved the following generalization of Jessen's theorem:

If $f_1(t), \cdots, f_n(t)$ are almost periodic functions satisfying the conditions $|f_1(t)| \geqq k > 0, \cdots, |f_n(t)| \geqq k > 0$, and further satisfying a linear relation

$$\alpha_1 f_1(t) + \cdots + \alpha_n f_n(t) = \beta,$$

where $\alpha_1, \cdots, \alpha_n$ are $\neq 0$, then the corresponding mean motions will satisfy a relation

$$r_1 c_1 + \cdots + r_n c_n = 0,$$

where $r_1, \cdots, r_n$ are rational numbers and $(r_1, \cdots, r_n) \neq (0, \cdots, 0)$.

This theorem is an immediate corollary of the following result:

If $f_1(t), \cdots, f_n(t)$ are almost periodic functions satisfying the conditions $|f_1(t)| \geqq k > 0, \cdots, |f_n(t)| \geqq k > 0$, and with rationally independent mean motions $c_1, \cdots, c_n$ (i. e. with mean motions $c_1, \cdots, c_n$, which do not satisfy any linear relation $r_1 c_1 + \cdots + r_n c_n = 0$, where $r_1, \cdots, r_n$ are rational numbers and $(r_1, \cdots, r_n) \neq (0, \cdots, 0)$), *and if further $v_1, \cdots, v_n$ are arbitrary real numbers and ε is an arbitrary positive number, then there exists a real number t^*, such that we have simultaneously*

$$|\arg f_\nu(t^*) - v_\nu| \leqq \varepsilon; \quad \nu = 1, \cdots, n$$

for convenient choice of the arguments.

The author was further able to prove another generalization of Jessen's theorem concerning three almost periodic functions $f_1(t)$, $f_2(t)$, $f_3(t)$, satisfying a relation

$$\alpha_1 f_1^2 + \alpha_2 f_2^2 + \alpha_3 f_3^2 + \beta_1 f_2 f_3 + \beta_2 f_3 f_1 + \beta_3 f_1 f_2 = k.$$

Also in this case the mean motions will satisfy a linear relation $r_1 c_1 + r_2 c_2 + r_3 c_3 = 0$, and the theorem follows immediately from

[1] H. TORNEHAVE: On a Generalization of Kronecker's Theorem. D. Kgl. Danske Vidensk. Selskab, Mat.-fys. Medd. XXIV 11 (1948).

the fact that it is possible to choose φ_1, φ_2 and φ_3 such that $\alpha_1 e^{2i\varphi_1}$, $\alpha_2 e^{2i\varphi_2}$, $\alpha_3 e^{2i\varphi_3}$, $\beta_1 e^{i(\varphi_2+\varphi_3)}$, $\beta_2 e^{i(\varphi_3+\varphi_1)}$ and $\beta_3 e^{i(\varphi_1+\varphi_2)}$ and $-k$ are situated in the same half-plane.

All theorems mentioned so far have been proved by an investigation of the arguments of almost periodic functions with rationally independent mean motions, and the behaviour of their absolute values has not been taken into account. The absolute values, however, are also subject to quite important restrictions, and one might therefore expect that much stronger theorems would hold. In the present paper we shall prove a generalization of this type, dealing with more general relations between two almost periodic functions. Our principal result will be the following theorem.

Theorem 1. *Let $F(z_1, z_2)$ be an integral function, which is not identically zero. If $f_1(t)$ and $f_2(t)$ are almost periodic functions satisfying the conditions $|f_1(t)| \geqq k > 0$, $|f_2(t)| \geqq k > 0$, and further satisfying the relation*

$$F(f_1(t), f_2(t)) = 0, \quad -\infty < t < \infty,$$

then the corresponding mean motions c_1 and c_2 will satisfy a relation

$$r_1 c_1 + r_2 c_2 = 0 \tag{1}$$

where r_1 and r_2 are rational numbers and $(r_1, r_2) = (0, 0)$.

A careful examination of our proof will show that the function $F(z_1, z_2)$ need not be integral. Let M denote the closure of the set of all points $(f_1(t), f_2(t))$, $-\infty < t < \infty$, and let $U_1, \cdots, U_n$ be open domains in the (z_1, z_2)-space, such that M is contained in $U_1 + \cdots + U_n$. Let $F_\nu(z_1, z_2)$; $\nu = 1, \cdots, n$ be analytic and not identically zero in U_ν. If then

$$F_\nu(f_1(t), f_2(t)) = 0; \quad \nu = 1, \cdots, n$$

for all values of t, for which $(f_1(t), f_2(t))$ belongs to U_ν, we have the relation (1).

The zeros of $F(z_1, z_2)$ will form a two-dimensional manifold S in four-dimensional real space, and we may consider $z_1 = f_1(t)$, $z_2 = f_2(t)$ as an almost periodic movement on S. Almost periodic

movements on two-dimensional surfaces were studied by FENCHEL and JESSEN[1], who proved that an almost periodic movement on a two-dimensional surface admitting the non-Euclidean plane as universal covering can be transformed continuously into a periodic movement. If the manifold of zeros of the function $F(z_1, z_2)$ of Theorem 1 is a surface of this kind, Theorem 1 will follow from Fenchel's and Jessen's theorem. The manifold of zeros may, however, consist of several surfaces intersecting each other, and the theorem of Fenchel and Jessen can not be applied in that case. We are going to prove Theorem 1 by a method very different from the one applied by Fenchel and Jessen; in fact, our proof will be based on the analytic properties of the manifold of zeros, while the proof of Fenchel and Jessen was based on topological properties of the surfaces.

Our proof will be indirect. We shall assume from the start that Theorem 1 is wrong and most of our considerations will therefore be based on the following (false) assumption:

A. *There exist an integral function* $F(z_1, z_2)$, *which is not identically zero, and two almost periodic functions* $f_1(t)$ *and* $f_2(t)$ *satisfying the conditions* $|f_1(t)| \geqq k > 0$, $|f_2(t)| \geqq k > 0$. *The mean motions* c_1 *and* c_2 *of* $f_1(t)$ *and* $f_2(t)$ *are rationally independent and we have identically*

$$F(f_1(t), f_2(t)) = 0.$$

In § 1 we shall bring the assumption A on a more convenient form. For this purpose we need a few well-known results concerning almost periodic functions. These results are briefly outlined in the earlier paper by the author, quoted above[2]. In § 2 we shall prove that the functions $f_1(t)$ and $f_2(t)$ in the assumption A can be replaced by differentiable functions. The proof of Theorem 1 follows in § 3 and § 4. Our proof will be based on the special properties of analytic manifolds in four-dimensional space, and it admits no obvious generalizations to the case of relations involving more than two almost periodic functions.

[1] W. FENCHEL und B. JESSEN: Über fastperiodische Bewegungen in ebenen Bereichen und auf Flächen. D. Kgl. Danske Vidensk. Selskab, Mat.-fys. Medd. XIII 6 (1935).

[2] H. TORNEHAVE, loc. cit.

§ 1.

An almost periodic function $f(t)$ can be written on the form

$$f(t) = \Phi(\beta_1 t, \beta_2 t, \cdots),$$

where $\beta_1, \beta_2, \cdots$ are real numbers satisfying the condition that $\beta_1, \cdots, \beta_n$ are rationally independent for every value of n, while $\Phi(x_1, x_2, \cdots)$ is a so-called limit periodic function with limit period 2π, i. e. to $\varepsilon > 0$ corresponds a continuous function $P(x_1, \cdots, x_n)$ periodic in each variable with a period which is an integral multiple of 2π, such that $|\Phi(x_1, x_2, \cdots) - P(x_1, \cdots, x_n)| \leqq \varepsilon$ for all values of $x_1\ x_2, \cdots$. The function $\Phi(x_1, x_2, \cdots)$ is called a spatial extension of $f(t)$, and it is uniquely determined by $f(t)$ and the basis $\beta_1, \beta_2, \cdots$. A finite number of almost periodic functions will possess a common basis, and this basis can be chosen such that it contains a previously given sequence of rationally independent numbers. Let us choose a common basis $\beta_1, \beta_2, \cdots$ for the functions $f_1(t)$ and $f_2(t)$ of the assumption A, and let us choose $\beta_1 = c_1$, $\beta_2 = c_2$. Let $\Phi_1(x_1, x_2, \cdots)$ and $\Phi_2(x_1, x_2, \cdots)$ be the spatial extensions. We have

$$\begin{aligned} \arg \Phi_1(x_1, x_2, \cdots) &= x_1 + \Psi_1(x_1, x_2, \cdots) \\ \arg \Phi_2(x_1, x_2, \cdots) &= x_2 + \Psi_2(x_1, x_2, \cdots), \end{aligned}$$

where $\Psi_1(x_1, x_2, \cdots)$ and $\Psi_2(x_1, x_2, \cdots)$ are limit periodic functions with limit period 2π. The relation $F(f_1(t), f_2(t)) = 0$ implies

$$F(\Phi_1(x_1, x_2, \cdots), \Phi_2(x_1, x_2, \cdots)) = 0 \tag{2}$$

for all values of $x_1, x_2, \cdots$.

To bring this relation in a more convenient form we introduce the analytic function

$$H(s_1, s_2) = H(\sigma_1 + it_1, \sigma_2 + it_2) = F(e^{s_1}, e^{s_2})$$

which is periodic with period $2\pi i$ in each variable. If we further put

$$\begin{aligned} \varphi_1(x_1, x_2) &= \log |\Phi_1(x_1, x_2, 0, 0, \cdots)| \\ \varphi_2(x_1, x_2) &= \log |\Phi_2(x_1, x_2, 0, 0, \cdots)| \\ \psi_1(x_1, x_2) &= \Psi_1(x_1, x_2, 0, 0, \cdots) \\ \psi_2(x_1, x_2) &= \Psi_2(x_1, x_2, 0, 0, \cdots) \end{aligned}$$

the relation (2) takes the form

$$(3)\quad H(\varphi_1(x_1, x_2)+i(x_1+\psi_1(x_1, x_2)), \varphi_2(x_1, x_2)+i(x_2+\psi_2(x_1, x_2))) = 0$$

in other words, the surface with the parametric representation

$$(4)\quad \begin{cases} \sigma_1 = \varphi_1(x_1, x_2); & t_1 = x_1+\psi_1(x_1, x_2) \\ \sigma_2 = \varphi_2(x_1, x_2); & t_2 = x_2+\psi_2(x_1, x_2) \end{cases}$$

is situated on the manifold of zeros of the analytic function $H(s_1, s_2)$. It is important for our proof that the four functions $\varphi_1(x_1, x_2)$, $\varphi_2(x_1, x_2)$, $\psi_1(x_1, x_2)$ and $\psi_2(x_1, x_2)$ have the limit period 2π. Hence these four functions are continuous and to $\varepsilon > 0$ corresponds an integer N, such that we have

$$|\varphi_1(x_1+2\pi\nu N, x_2)-\varphi_1(x_1, x_2)| \leqq \varepsilon$$
$$|\varphi_1(x_1, x_2+2\pi\nu N)-\varphi_1(x_1, x_2)| \leqq \varepsilon$$

for all real values of x_1 and x_2 and for all integral values of ν, and the same condition is satisfied by the functions $\varphi_2(x_1, x_2)$, $\psi_1(x_1, x_2)$ and $\psi_2(x_1, x_2)$.

§ 2.

Let ε be a given positive number. It is easy to prove the existence of a function $\varphi_1^*(x_1, x_2)$ with limit period 2π in each variable and satisfying the condition

$$|\varphi_1(x_1, x_2)-\varphi_1^*(x_1, x_2)| \leqq \varepsilon$$

for all real values of x_1 and x_2 and we can further choose $\varphi_1^*(x_1, x_2)$ such that its partial derivatives are bounded and continuous. We may e. g. define $\varphi_1^*(x_1, x_2)$ as a convenient Féjér sum of the Fourier series of $\varphi_1(x_1, x_2)$. If, however, we apply this process on each of the functions φ_1, φ_2, ψ_1 and ψ_2, the surface

$$\sigma_1 = \varphi_1^*(x_1, x_2); \quad t_1 = x_1+\psi_1^*(x_1, x_2)$$
$$\sigma_2 = \varphi_2^*(x_1, x_2); \quad t_2 = x_2+\psi_2^*(x_1, x_2)$$

will not always be situated on the manifold of zeros of $H(s_1, s_2)$. We must therefore choose $\varphi_1^*(x_1, x_2)$ and $\psi_1^*(x_1, x_2)$ and afterwards determine $\varphi_2^*(x_1, x_2)$ and $\psi_2^*(x_1, x_2)$ such that (3) still holds, i. e. such that

$$(5)\quad H(\varphi_1^*+i(x_1+\psi_1^*), \varphi_2^*+i(x_2+\psi_2^*)) = 0.$$

We can change φ_1 and ψ_1 into φ_1^* and ψ_1^* by a continuous transformation, e.g. by means of the continuous families $\varphi_t = (1-t)\varphi_1 + t\varphi_1^*$ and $\psi_t = (1-t)\psi_1 + t\psi_1^*$ and we may choose $(s_1(t), s_2(t))$ on the manifold of zeros of $H(s_1, s_2)$ such that the functions $s_1(t)$ and $s_2(t)$ are continuous for fixed (x_1, x_2), and such that $s_1(t) = \varphi_t + i(x_1 + \psi_t)$. If $(s_1(t), s_2(t))$ never passes through a singular point on the manifold of zeros, we may put $s_2(1) = \varphi_2^* + i(x_2 + \psi_2^*)$ and the functions φ_2^* and ψ_2^* thus obtained will be continuos and differentiable and satisfy (5). The trouble is that the manifold of zeros usually possesses some singularities and the curve $(s_1(t), s_2(t))$ must occasionally pass through a singular point. We must therefore more carefully study the singularities on the manifold of zeros and take them into account in our considerations.

Let (a_1, a_2) be a zero of $H(s_1, s_2)$. In a certain neighbourhood of (a_1, a_2) we have according to Weierstrass' preparation theorem

$$H(s_1, s_2) = H^*(s_1, s_2)\ P(s_1, s_2),$$

where $H^*(s_1, s_2)$ is an analytic function without zeros, while $P(s_1, s_2)$ is a so-called pseudopolynomial, i. e. a function of the form

$$P(s_1, s_2) = A_0(s_1)(s_2 - a_2)^p + A_1(s_1)(s_2 - a_2)^{p-1} + \cdots + A_p(s_1).$$

By convenient choice of $H^*(s_1, s_2)$ we have $A_0(s_1) = (s_1 - a_1)^q$, and for $\nu \geq 1$ we have $A_\nu(s_1) = A_\nu^*(s_1)(s_1 - a_1)^q$, where $A_\nu^*(s_1)$ is analytic in the neighbourhood of a_1 and $A_\nu^*(a_1) = 0$.

The pseudopolynomial $P(s_1, s_2)$ has coefficients from the integral domain of functions of one variable, analytic in a neighbourhood of a_1. An element $u(s_1)$ of this integral domain is a unity, if and only if $u(a_1) \neq 0$, and the only prime elements are the functions $u(s_1)(s_1 - a_1)$. Every function of the integral domain can in a certain neighbourhood of a_1 be written on the form $u(s_1)(s_1 - a_1)^p$ and this representation is unique. But we have then according to a well-known theorem from the algebra a unique factorization also in the integral domain of pseudopolynomials, i. e. every pseudopolynomial can in exactly one way be written as a product

$$(6) \qquad P(s_1, s_2) = (s_1 - a_1)^q (P_1(s_1, s_2))^{q_1} \cdots (P_l(s_1, s_2))^{q_l}$$

where $P_1(s_1, s_2), \cdots, P_l(s_1, s_2)$ are irreducible pseudopolynomials. The representation (6) holds in a certain bicylinder

$$|s_1 - a_1| \leqq \varrho; \quad |s_2 - a_2| \leqq \varrho. \tag{7}$$

The zero (a_1, a_2) is called a normal zero of $H(s_1, s_2)$, if all factors of the product (6) are identical, i. e. if $P(s_1, s_2)$ is a power of some irreducible pseudopolynomial. The zeros, which are not normal, are called critical. We shall prove that the number of critical zeros in the bicylinder (7) is finite. Let $R_{\mu\nu}(s_1)$ denote the resultant of $P_\mu(s_1, s_2)$ and $P_\nu(s_1, s_2)$, when $\mu \neq \nu$, and let $R_{\nu\nu}(s_1)$ denote the discriminant of $P_\nu(s_1, s_2)$. As the pseudopolynomials $P_\nu(s_1, s_2)$ are irreducible and different, the functions $R_{\mu\nu}(s_1)$ are analytic and not identically zero. If a zero (b_1, b_2), where $b_1 \neq a_1$, is critical, then the product $\prod_{\mu,\nu=1}^{l} R_{\mu\nu}(s_1)$ must vanish, when $s_1 = b_1$. This, however, will happen only for a finite set of values of b_1. Obviously the zeros (a_1, b_2), where $b_2 \neq a_2$, are normal. Hence the number of critical zeros inside the bicylinder (7) is finite and it follows that the critical zeros are isolated. In the following we shall consider $H(s_1, s_2)$ only inside a certain fixed tube $\sigma_1^2 + \sigma_2^2 \leqq C^2$ and, taking into account that $H(s_1, s_2)$ is periodic, we conclude that there exists a positive constant d, such that the distance between two arbitrary critical points is $\leqq d$.

Accordingly we may arrange all critical points on the manifold of zeros of $H(s_1, s_2)$ inside a fixed tube which contains the surface (4) in a sequence $(a_1^{(\nu)}, a_2^{(\nu)})$; $\nu = 1, 2, \cdots$. Let η be a positive number, and let U_ν denote a neighbourhood of $(a_1^{(\nu)}, a_2^{(\nu)})$ consisting of all points on the manifold of zeros of $H(s_1, s_2)$ that satisfies

$$0 > |s_1 - a_2^{(\nu)}| > \eta$$

and all points on the manifold of zeros of $H(s_1, s_2)$ that satisfies

$$|s_2 - a_2^{(\nu)}| < \eta; \; s_1 = a_1^{(\nu)}.$$

From the representation $P(s_1, s_2) = 0$ of the manifold of zeros follows that we can choose η so small that the distance from $(a_1^{(\nu)}, a_2^{(\nu)})$ to an arbitrary point of the neighbourhood U_ν is $< \frac{\varepsilon}{3} < \frac{d}{3}$ and, as $H(s_1, s_2)$ is periodic, we can even choose η so small that this condition holds simultaneously for all values of ν.

Let M_ν denote the set of points in the (x_1, x_2)-plane, for which

$$s_1 = \varphi_1(x_1, x_2) + i(x_1 + \psi_1(x_1, x_2)); \quad s_2 = \varphi_2(x_1, x_2) + i(x_2 + \psi_2(x_1, x_2))$$

is a point of the neighbourhood U_ν. As φ_1, φ_2, ψ_1 and ψ_2 are continuous there exists a number Δ, such that the distance between M_μ and M_ν is $\geqq \Delta$, when μ and ν are arbitrary positive integers. The complementary set of $M_1 + M_2 + \cdots$ is divided in two open sets N_1 and N_2, where N_1 consists of points (x_1, x_2) corresponding to points (s_1, s_2) in the neighbourhood of which the manifold of zeros of $H(s_1, s_2)$ has the form $s_2 = h(s_1)$, while N_2 consists of points (x_1, x_2) corresponding to points (s_1, s_2) in the neighbourhood of which the manifold of zeros has the form $s_1 = \text{constant}$. The sets N_1 and N_2 are separated by $M_1 + M_2 + \cdots$, but they need not be connected and one of them may be empty.

We choose a positive number $\delta < \frac{d}{3\sqrt{2}}$, such that the oscillation of each of the functions $\varphi_1 + i(x_1 + \psi_1)$ and $\varphi_2 + i(x_2 + \psi_2)$ is $\leqq \frac{\varepsilon}{2\sqrt{2}}$ on every square with its side $\leqq \delta$. We divide the (x_1, x_2)-plane in squares with side δ by means of straight lines parallel to the axes. Let M'_ν denote the sum of all squares that contain a point of M_ν or its boundary in their interior. The boundary of each set M'_ν consists of a number of closed broken lines, but we replace it by a curve differentiable an infinity of times by replacing each corner on the boundary by a small arc similar to the arc

$$e^{-\frac{1}{x_1^2}} + e^{-\frac{1}{x_2^2}} = 1; \quad x_1 \geqq 0, \quad x_2 \geqq 0.$$

If the corner is convex, we choose the arc so small that no part of M_ν is cut away, but if the corner is concave, we let the arc join the midpoints of the adjoining square. A corner, where two squares of M'_ν have one common angle is treated as two concave corners. If we count the curvature positive, when the curve is concave, the new boundary will possess a finite maximal curvature corresponding to a definite radius of curvature ϱ. Let M^*_ν denote the set, into which M'_ν is changed by our modification of the boundary, and let M^{**}_ν denote the set of all points with distance $\leqq \frac{\varrho}{2}$ from M^*_ν. The set M^{**}_ν is bounded by a curve

parallel to the boundary of M_ν^* and differentiable everywhere an infinity of times. Let N_1^* and N_2^* denote the parts of N_1 and N_2 outside M_ν^{**}.

Let $S_1(x_1, x_2)$ and $S_2(x_1, x_2)$ denote exponential sums satisfying

$$(8)\quad \begin{cases} |\varphi_1(x_1, x_2)+i\psi_1(x_1, x_2)-S_1(x_1, x_2)| \leqq \operatorname{Min}\left(\dfrac{\varepsilon}{6\sqrt{2}}, \dfrac{\eta}{2}\right) \\ |\varphi_2(x_1, x_2)+i\psi_2(x_1, x_2)-S_2(x_1, x_2)| \leqq \operatorname{Min}\left(\dfrac{\varepsilon}{6\sqrt{2}}, \dfrac{\eta}{2}\right). \end{cases}$$

We define

$$(9)\quad \begin{cases} \varphi_1^*(x_1, x_2)+i\psi_1^*(x_1, x_2) = S_1(x_1, x_2) & \text{in } N_1^* \\ \varphi_2^*(x_1, x_2)+i\psi_2^*(x_1, x_2) = S_2(x_1, x_2) & \text{in } N_2^* \\ \left.\begin{aligned} \varphi_1^*(x_1, x_2)+i(x_1+i\psi_1^*(x_1, x_2)) &= a_1^{(\nu)} \\ \varphi_2^*(x_1, x_2)+i(x_2+i\psi_2^*(x_1, x_2)) &= a_2^{(\nu)} \end{aligned}\right\} & \text{in } M_\nu^*. \end{cases}$$

If we put $(0 \leqq t \leqq 1)$

$$(10)\qquad \varphi_1^{(t)}+i\psi_1^{(t)} = (1-t)(\varphi_1+i\psi_1)+t(\varphi_1^*+i\psi_1^*) \quad \text{in } N_1^*$$

there exists a uniquely determined function

$$\varphi_2^{(t)}(x_1, x_2)+i\psi_2^{(t)}(x_1, x_2),$$

continuous as a function of t, x_1 and x_2, when $0 \leqq t \leqq 1$ and (x_1, x_2) belongs to N_1^* and satisfying

$$H(\varphi_1^{(t)}+i(x_1+\psi_1^{(t)}),\ \varphi_2^{(t)}+i(x_2+\psi_2^{(t)})) = 0$$

and

$$\varphi_2^{(0)}+i\psi_2^{(0)} = \varphi_2+i\psi_2.$$

In fact, it follows from (8), (9) and (10) that

$$|(\varphi_1^{(t)}+i(x_1+\psi_1^{(t)}))-(\varphi_1+i(x_1+\psi_1))| \leqq \frac{\eta}{2}$$

and according to the definition of the neighbourhoods U_ν this implies that $(\varphi_1^{(t)}+i(x_1+\psi_1^{(t)}),\ \varphi_2^{(t)}+i(x_2+\psi_2^{(t)}))$ will never reach any of the critical points $(a_1^{(\nu)}, a_2^{(\nu)})$. We define

$$\varphi_2^*(x_1, x_2)+i\psi_2^*(x_1, x_2) = \varphi_2^{(1)}(x_1, x_2)+i\psi_2^{(1)}(x_1, x_2) \quad \text{in } N_1^*.$$

We have

$$|(\varphi_2^* + i\psi_2^*) - (\varphi_2 + i\psi_2)| \leqq K\frac{\varepsilon}{6},$$

where K is the maximum value of the derivative of the function $s_2 = h(s_1)$ representing the manifold of zeros at all points inside the tube and outside the neighbourhoods U_ν. According to the periodicity of $H(s_1, s_2)$ the constant K will be finite. We define

$$\varphi_1^*(x_1, x_2) + i\psi_1^*(x_1, x_2) = \varphi_1(x_1, x_2) + i\psi_1(x_1, x_2) \text{ in } N_2^*.$$

The function

$$E(t) = \frac{e^{-\frac{2t-1}{t(t-1)}}}{1 + e^{-\frac{2t-1}{t(t-1)}}}$$

is differentiable an infinity of times in the interval $0 \leqq t \leqq 1$, if we define $E(0) = 0$ and $E(1) = 1$, and we have

$$E^{(\nu)}(0) = E^{(\nu)}(1) = 0; \quad \nu = 1, 2 \cdots.$$

Let $r(x_1, x_2)$ denote the distance from (x_1, x_2) to the boundary of M_ν^*. We define

$$(11)\quad \begin{cases} \varphi_1^*(x_1, x_2) + i(x_1 + \psi_1^*(x_1, x_2)) = \\ = a_1^{(\nu)} + (S_1(x_1, x_2) + ix_1 - a_1^{(\nu)})\, E\left(\dfrac{2\, r(x_1, x_2)}{\varrho}\right) \end{cases}$$

in all components of $M_\nu^{**} - M_\nu^*$, which separate M_ν^* and N_1^*, and

$$\varphi_2^*(x_1, x_2) + i(x_2 + \psi_2^*(x_1, x_2)) =$$
$$= a_2^{(\nu)} + (S_2(x_1, x_2) + ix_2 - a_2^{(\nu)})\, E\left(\frac{2\, r(x_1, x_2)}{\varrho}\right);$$
$$\varphi_1^*(x_1, x_2) + i\psi_1^*(x_1, x_2) = \varphi_1(x_1, x_2) + i\psi_1(x_1, x_2)$$

in all components of $M_\nu^{**} - M_\nu^*$, which separate M_ν^* and M_2^*. From (11) and (8) follows that

$$\varphi_1^* + i(x_1 + \psi_2^*) \neq a_1^{(\nu)}$$

in the first kind of components of $M_\nu^{**} - M_\nu^*$, and we can therefore in exactly one way determine two continuous functions $\varphi_2^*(x_1, x_2)$ and $\psi_2^*(x_1, x_2)$ satisfying

$$H(\varphi_1^* + i(x_1 + \psi_1^*),\ \varphi_2^* + i(x_2 + \psi_2^*)) = 0.$$

We have now defined the functions $\varphi_1^*(x_1, x_2)$, $\psi_1^*(x_1, x_2)$, $\varphi_2^*(x_1, x_2)$ and $\psi_2^*(x_1, x_2)$ for all values of x_1 and x_2, and they are obviously differentiable an infinity of times everywhere. We cannot prove that they are limit periodic, but we can obviously choose the numbers η, ε and δ so small that the difference $|\varphi_1 - \varphi_1^*|$ and the analogous differences are smaller than $\frac{\varepsilon_0}{3}$, where ε_0 is a previously given positive number. There will then exist an integer N, such that we have

$$|\varphi_1^*(x_1 + 2\pi\nu N, x_2) - \varphi_1^*(x_1, x_2)| \leqq \varepsilon_0$$
$$|\varphi_1^*(x_1, x_2 + 2\pi\nu N) - \varphi_1^*(x_1, x_2)| \leqq \varepsilon_0$$

for all real values of x_1 and x_2 and all integral values of ν, and the three other functions will satisfy the analogous inequalities. It is further easy to prove that there exists a constant K_0, such that the four functions φ_1^*, ψ_1^*, φ_2^* and ψ_2^* and their partial derivatives of the first order are $\leqq K_0$ in absolute value.

§ 3.

In the neighbourhood of every normal point of the manifold of zeros of $H(s_1, s_2)$ the manifold of zeros is a two-dimensional surface defined by an equation

$$s_2 = h(s_1) = h_1(\sigma_1, t_1) + ih_2(\sigma_1, t_1)$$

or by two real equations

$$(12) \quad \begin{cases} \sigma_2 = h_1(\sigma_1, t_1) \\ t_2 = h_2(\sigma_1, t_1) \end{cases}$$

where the functions h_1 and h_2 satisfy the Cauchy-Riemann differential equations

$$(13) \quad \begin{cases} \dfrac{\partial h_1}{\partial \sigma_1} = \dfrac{\partial h_2}{\partial t_1}, \quad \dfrac{\partial h_1}{\partial t_1} = -\dfrac{\partial h_2}{\partial \sigma_1}. \end{cases}$$

We can solve the equations (12) on the form

$$(14) \quad \begin{cases} t_1 = U(\sigma_1, \sigma_2) \\ t_2 = V(\sigma_1, \sigma_2), \end{cases}$$

if the condition

$$D = \begin{vmatrix} \frac{\partial h_1}{\partial t_1} & 0 \\ \frac{\partial h_2}{\partial t_1} & -1 \end{vmatrix} = -\frac{\partial h_1}{\partial t_1} = \frac{\partial h_2}{\partial \sigma_1} \neq 0$$

is satisfied.

Let us first assume that $\frac{\partial h_1}{\partial t_1}$ is not identically zero. The functional determinant D will then vanish only along a certain analytic curve on the surface $h_2 = h(s_1)$. In the neighbourhood of all other points of the surface $h_2 = h(s_1)$ we can represent this surface by the equations (14), and we have according to (12) and (13)

$$\frac{\partial h_1}{\partial \sigma_1} - \frac{\partial h_2}{\partial \sigma_1}\frac{\partial U}{\partial \sigma_1} = 0 \qquad -\frac{\partial h_2}{\partial \sigma_1}\frac{\partial U}{\partial \sigma_2} - 1 = 0$$

$$\frac{\partial h_2}{\partial \sigma_1} + \frac{\partial h_1}{\partial \sigma_1}\frac{\partial U}{\partial \sigma_1} - \frac{\partial V}{\partial \sigma_1} = 0 \qquad \frac{\partial h_1}{\partial \sigma_1}\frac{\partial U}{\partial \sigma_2} - \frac{\partial V}{\partial \sigma_2} = 0,$$

hence

$$\frac{\partial U}{\partial \sigma_1} = \frac{1}{D}\frac{\partial h_1}{\partial \sigma_1} \qquad \frac{\partial U}{\partial \sigma_2} = -\frac{1}{D}$$

$$\frac{\partial V}{\partial \sigma_1} = \frac{1}{D}\left(\left(\frac{\partial h_1}{\partial \sigma_1}\right)^2 + \left(\frac{\partial h_2}{\partial \sigma_1}\right)^2\right) \qquad \frac{\partial V}{\partial \sigma_2} = -\frac{1}{D}\frac{\partial h_1}{\partial \sigma_1},$$

and it follows that

$$\frac{\partial U}{\partial \sigma_1} = -\frac{\partial V}{\partial \sigma_2}$$

and

$$\frac{\partial U}{\partial \sigma_1}\frac{\partial V}{\partial \sigma_2} - \frac{\partial U}{\partial \sigma_2}\frac{\partial V}{\partial \sigma_1} = 1.$$

It follows that the mapping (14) of the real plane on the imaginary plane leaves the area unchanged.

If D is identically zero, we have

$$\operatorname{Im}\frac{dh}{ds_1} = \frac{\partial h_2}{\partial \sigma_1} = 0,$$

hence

$$\frac{dh}{ds_1} = c,$$

where c is a real constant. In this case the surface of zeros is

$$s_2 = cs_1 + a,$$

where a is a complex number. The surface of zeros is a plane, perpendicular on both the real and the imaginary plane, and the projections on the real and the imaginary plane of an area situated in such a part of the manifold of zeros will have measures equal to zero.

If a bounded surface is situated on the manifold of zeros, it follows generally that the areas of its projections on the real and the imaginary plane are identical.

§ 4.

We shall now again consider the surface given by the parametric representation

$$(15)\quad \begin{cases} \sigma_1 = \varphi_1^*(x_1, x_2); & t_1 = x_1 + \psi_1^*(x_1, x_2) \\ \sigma_2 = \varphi_2^*(x_1, x_2); & t_2 = x_2 + \psi_2^*(x_1, x_2). \end{cases}$$

Let A denote a part of the surface (15), determined by the conditions

$$(16)\qquad 0 \leqq x_1 \leqq 2\pi N, \quad 0 \leqq x_2 \leqq 2\pi N.$$

The projection of A on the real plane will have the area

$$A_r = \int_0^{2\pi N} \int_0^{2\pi N} \left(\frac{\partial \varphi_1^*}{\partial x_1} \frac{\partial \varphi_2^*}{\partial x_2} - \frac{\partial \varphi_1^*}{\partial x_2} \frac{\partial \varphi_2^*}{\partial x_1} \right) dx_1 dx_2$$

or, if B denotes the boundary of the rectangle (16), according to Gauss' formula

$$A_r = \int_B \varphi_1^* \left(\frac{\partial \varphi_2^*}{\partial x_1} dx_1 + \frac{\partial \varphi_2^*}{\partial x_2} dx_2 \right) =$$

$$= \int_0^{2\pi N} \left(\varphi_1^*(2\pi N, x_2) \frac{d\varphi_2^*(2\pi N, x_2)}{dx_2} - \varphi_1^*(0, x_2) \frac{d\varphi_2^*(0, x_2)}{dx_2} \right) dx_2$$

$$- \int_0^{2\pi N} \left(\varphi_1^*(x_1, 2\pi N) \frac{d\varphi_2^*(x_1, 2\pi N)}{dx_1} - \varphi_1^*(x_1, 0) \frac{d\varphi_2^*(x_1, 0)}{dx_1} \right) dx_1.$$

Denoting these integrals A_r' and A_r'', we have

$$A_r' = \int_0^{2\pi N} (\varphi_1^*(2\pi N, x_2) - \varphi_1^*(0, x_2)) \frac{d\varphi_2^*(2\pi N, x_2)}{dx_2} dx_2$$
$$+ \int_9^{2\pi N} \varphi_1^*(0, x_2) \frac{d(\varphi_2^*(2\pi N, x_2) - \varphi_2^*(0, x_2))}{dx_2} dx_2$$

and we obtain by partial integration

$$A_r' = \varphi_1^*(0, 2\pi N)(\varphi_2^*(2\pi N, 2\pi N) - \varphi_2^*(0, 2\pi N))$$
$$- \varphi_1^*(0, 0)(\varphi_2^*(2\pi N, 0) - \varphi_2^*(0, 0))$$
$$+ \int_0^{2\pi N} (\varphi_1^*(2\pi N, x_2) - \varphi_1^*(0, x_2)) \frac{d\varphi_2^*(2\pi N, x_2)}{dx_2} dx_2$$
$$- \int_0^{2\pi N} (\varphi_2^*(2\pi N, x_2) - \varphi_2^*(0, x_2)) \frac{d\varphi_1^*(0, x_2)}{dx_2} dx_2,$$

hence, if we according to the remarks at the end of § 2 choose $2\pi N$ as a translation number of φ_1^*, ψ_1^*, φ_2^* and ψ_2^*, we have

$$|A_r'| \leq 2K\varepsilon_0 + 4\pi N K_0 \varepsilon_0.$$

We get a similar estimate for A_r'', so that we finally obtain

$$|A_r| \leq 4K_0\varepsilon_0(2\pi N + 1) < 16\pi N K_0 \varepsilon_0. \tag{17}$$

The projection of A on the imaginary plane will have the area

$$A_i = \int_B (x_1 + \psi_1^*)\left(\frac{\partial \psi_2^*}{\partial x_1} dx_1 + \left(1 + \frac{\partial \psi_2^*}{\partial x_2}\right) dx_2\right) =$$
$$= \int_B x_1 dx_2 + \int_B \psi_1^* dx_2 + \int_B x_1 \left(\frac{\partial \psi_2^*}{\partial x_1} dx_1 + \frac{\partial \psi_2^*}{\partial x_2} dx_2\right)$$
$$+ \int_B \psi_1^* \left(\frac{\partial \psi_2^*}{\partial x_1} dx_1 + \frac{\partial \psi_2^*}{\partial x_2} dx_2\right).$$

For the two first integrals we obtain immediately

$$\int_B x_1 dx_2 = 4\pi^2 N^2,$$

$$\left| \int_B \psi_1^* dx_2 \right| \leq 4\pi K_0 N.$$

For the third integral we obtain

$$\int_B x_1 \left(\frac{\partial \psi_2^*}{\partial x_1} dx_1 + \frac{\partial \psi_2^*}{\partial x_2} dx_2 \right) =$$

$$= \int_0^{2\pi N} x_1 \frac{\partial \psi_2^*(x_1, 0)}{dx_1} dx_1 + 2\pi N \int_0^{2\pi N} \frac{d\psi_2^*(2\pi N, x_2)}{dx_2} dx_2 - \int_0^{2\pi N} x_1 \frac{d\psi_2^*(x_1, 2\pi N)}{dx_1} dx_1 =$$

$$= 2\pi N(\psi_2^*(2\pi N, 0) - \psi_2^*(2\pi N, 2\pi N))$$
$$+ 2\pi N(\psi_2^*(2\pi N, 2\pi N) - \psi_2^*(2\pi N, 0))$$
$$+ \int_0^{2\pi N} (\psi_2^*(x_1, 2\pi N) - \psi_2^*(x_1, 0)) dx_1,$$

hence

$$\left| \int_B x_1 \left(\frac{\partial \psi_2^*}{\partial x_1} dx_1 + \frac{\partial \psi_2^*}{\partial x_2} dx_2 \right) \right| \leq 2\pi N \varepsilon_0.$$

For the last integral we have obviously the estimate (17) hence

$$|A_i| \geq 4\pi^2 N^2 - 4\pi N K_0 - 2\pi N \varepsilon_0 - 16\pi N K_0 \varepsilon_0,$$

and it follows that

$$|A_i| > |A_r|,$$

when N is great enough. But this is contradictory to the result derived in § 3. This completes the proof of Theorem 1.

Indleveret til selskabet den 13. januar 1950.
Færdig fra trykkeriet den 3. juni 1950.